Progress in Landslide Research and Technology

Biljana Abolmasov
Irasema Alcántara-Ayala
Željko Arbanas
Kazuo Konagai
Matjaž Mikoš
Kyoji Sassa
Shinji Sassa
Binod Tiwari
Veronica Tofani *Editors*

Progress in Landslide Research and Technology, Volume 4 Issue 1, 2025

OPEN ACCESS

Springer

Progress in Landslide Research and Technology

Now accepted in SCOPUS.

The Open Access book series of the International Consortium on Landslides (ICL) aims to be the common platform for the publication of recent progress in landslide research and technology for practical applications and the benefit of society contributing to the Kyoto Landslide Commitment 2020, which is expected to continue to 2030 and beyond for the global promotion of understanding and reducing landslide disaster risk, as well as the 2030 Agenda Sustainable Development Goals, the New Urban Agenda and the Paris Climate Agreement. The contributions include original and review articles, case studies, activity reports and teaching tools for the promotion of understanding and reducing landslide disaster risks.

Society and Partnerships:

International Consortium on Landslides (ICL)
https://www.landslides.org/book-series-of-klc-2020/
Landslides: Journal of the International Consortium on Landslides
https://link.springer.com/journal/10346

Biljana Abolmasov • Irasema Alcántara-Ayala
Željko Arbanas • Kazuo Konagai
Matjaž Mikoš • Kyoji Sassa • Shinji Sassa
Binod Tiwari • Veronica Tofani
Editors

Progress in Landslide Research and Technology, Volume 4 Issue 1, 2025

Springer

Editors
Biljana Abolmasov
Faculty of Mining and Geology
University of Belgrade
Belgrade, Serbia

Željko Arbanas
Faculty of Civil Engineering
University of Rijeka
Rijeka, Croatia

Matjaž Mikoš
Faculty of Civil & Geodetic Engineering
University of Ljubljana
Ljubljana, Slovenia

Shinji Sassa
National Institute of Maritime, Port and Aviation
Technology, Port and Airport Research Institute
Yokosuka, Japan

Veronica Tofani
Department of Earth Sciences
University of Florence
Florence, Italy

Irasema Alcántara-Ayala
Institute of Geography
Natl Autonomous University of Mexico
Ciudad De Mexico, Estado de México, Mexico

Kazuo Konagai
International Consortium on Landslides
Kyoto, Japan

Kyoji Sassa
International Consortium on Landslides
Kyoto, Japan

Binod Tiwari
California State University
Placentia, CA, USA

ISSN 2731-3794 ISSN 2731-3808 (electronic)
Progress in Landslide Research and Technology
ISBN 978-3-031-89835-8 ISBN 978-3-031-89836-5 (eBook)
https://doi.org/10.1007/978-3-031-89836-5

This work was supported by International Consortium on Landslides.

Cover illustration: A catastrophic landslide occurred on October 18, 2020, in Quang Tri Province, Vietnam. It killed 22 soldiers in barracks. The landslide volume was approximately 180,000 m3. (Photograph taken by Le Hong Luong, Pham Van Tien)

This Springer imprint is published by the registered company Springer Nature Switzerland AG
The registered company address is: Gewerbestrasse 11, 6330 Cham, Switzerland

Editorial Board of the Book Series

Qunli Han, Co-chair of the Global Promotion Committee of the International Programme on Landslides and Kyoto Landslide Commitment 2020.
Nicola Casagli, Immediate Past President of the International Consortium on Landslides.
Peter Bobrowsky, Past President of the International Consortium on Landslides.

Advisory Members for KLC2020
Abou Amani, Director, Division of Water Sciences, Secretary, Intergovernmental Hydrological Programme (IHP), UNESCO.
Soichiro Yasukawa, Chief of Disaster Risk Reduction Unit, UNESCO.
Sonia Talwar, Director General, Geological Survey of Canada, Natural Resources Canada, Canada.
Hassina Mouri, President of the International Union of Geological Sciences (IUGS).
John LaBrecque, Chair of IUGG GeoRisk Commission, Center for Space Research, University of Texas at Austin, USA.
Vassilis Marinos, President of the International Association for the Engineering Geology and the Environment (IAEG).
Paolo Canuti, past president of the International Consortium on Landslides (ICL), Italy.
Sàlvano Briceño, First chair of the Global Promotion Committee of the International Programme on Landslides.
Badaoui Rouhban, IPL Advisor and Moderator of ISDR-ICL Sendai Landslide Partnerships 2015–2025 Session of third WCDRR in 2015.

KLC2020 Official Promoters

Host Organization
Željko Arbanas, International Consortium on Landslides (ICL).

Public Sectors: KLC2020 Official Promoters—Public
International Unions/Associations, Governmental Organizations, Universities, and Research Institutes

- Hassina Mouri, The International Union of Geological Sciences (IUGS)
- Chris Rizos, The International Union of Geodesy and Geophysics (IUGG)
- Vassilis Marinos, The International Association for the Engineering Geology and the Environment
- John Kraus, International Geosynthetics Society (IGS)
- Sonia Talwar, Geological Survey of Canada, Natural Resources Canada, Canada
- Matjaž Mikoš, Faculty of Civil and Geodetic Engineering, University of Ljubljana, Slovenia
- Huiming Tang, China University of Geosciences, Wuhan, China
- Qiang Xu, The State Key Laboratory of Geohazard Prevention and Geoenvironment Protection, Chengdu University of Technology, Sichuan, China
- Louis Ge, Department of Civil Engineering, National Taiwan University, Chinese Taipei
- Josef Stemberk, Institute of Rock Structure and Mechanics, the Czech Academy of Sciences
- Wei Shan, Institute of Cold Regions Science and Engineering, Northeast Forestry University, China

Private Sectors: KLC2020 Official Promoters—Private
Companies and Corporation

- Marui & Co. Ltd., Japan
- Nippon Koei Co., Ltd., Japan
- Ellegi srl, Italy

Global Promotion Committee of the International Programme on Landslides and Kyoto Landslide Commitment 2020

A Commitment to the Sendai Framework and the Sustainable Development Goals

Chair
Matjaž Mikoš, Faculty of Civil and Geodetic Engineering, University of Ljubljana.

Co-Chairs
Qunli Han, Integrated Research on Disaster Risk, IRDR.
Soichiro Yasukawa, Programme Specialist on Disaster Risk Reduction, UNESCO, Paris.
Hiroshi Kitazato, International Union of Geological Sciences, IUGS.
John LaBrecque, Chair of IUGG GeoRisk Commission.

Secretary
Kyoji Sassa, IPL World Centre, Director.

Members of the IPL-KLC Global Promotion Committee

ICL Full Members
Geotechnical Engineering Office, Hong Kong, China; The State Key Laboratory of Geohazard Prevention and Geoenvironment Protection (SKLGP), Chengdu University of Technology, China; UNESCO Chair for the Prevention and the Sustainable Management of Geo-hydrological Hazards—University of Florence, Italy; Faculty of Civil and Geodetic Engineering, University of Ljubljana (ULFGG), Slovenia; and other members (total 59 members from 27 countries/regions).

ICL Supporting Organizations
UNESCO, UNDRR, WMO, FAO, UNU, ISC, WFEO, IUGS, IUGG.

KLC2020 Official Promoters Host Organization

Host Organization
Željko Arbanas, International Consortium on Landslides (ICL).

Public Sectors: KLC2020 Official Promoters—Public

- Hassina Mouri, The International Union of Geological Sciences (IUGS)
- Chris Rizos, The International Union of Geodesy and Geophysics (IUGG)
- Vassilis Marinos, The International Association for the Engineering Geology and the Environment (IAEG)
- John Kraus, International Geosynthetics Society (IGS)

- Sonia Talwar, Geological Survey of Canada, Natural Resources Canada, Canada
- Matjaž Mikoš, Faculty of Civil and Geodetic Engineering, University of Ljubljana, Slovenia
- Huiming Tang, China University of Geosciences, Wuhan, China
- Qiang Xu, The State Key Laboratory of Geohazard Prevention and Geoenvironment Protection (SKLGP), Chengdu University of Technology, China
- Louis Ge, Department of Civil Engineering, National Taiwan University, Chinese Taipei
- Josef Stemberk, Institute of Rock Structure and Mechanics, the Czech Academy of Sciences
- Wei Shan, Institute of Cold Regions Science and Engineering, Northeast Forestry University, China

Private Sectors: KLC2020 Official Promoters—Private

- Marui & Co. Ltd., Japan
- Nippon Koei Co., Ltd., Japan
- Ellegi srl, Italy
- IDS GeoRadar s.r.l., Italy
- Chuo Kaihatsu Corporation, Japan
- Godai Kaihatsu Corporation, Japan
- Kiso-Jiban Consultants Co., Ltd., Japan
- Kokusai Kogyo Co., Ltd., Japan
- OSASI Technos, Inc., Japan

IPL World Centre

IPL World Centre (IWC) was established in 2006 by the Tokyo Action Plan to serve, as it does, as the secretariat of IPL,GPC/IPL as well as of UNITWIN UNESCO-KU-ICL Programme. IWC also serves as the secretariat of KLC2020. IWC is a part of the legal body (NPO-ICL registered in Kyoto, Japan) of ICL. The Council of the IWC consists of advisors from Ministry of Education, Sports, Science and Technology, Ministry of Agriculture, Forestry and Fisheries, Ministry of Land, Infrastructure and Tourism of the Government of Japan, UNESCO, and of members from ICL Headquarters, chairs of GPC/IPL-KLC, and presidents and officers of ICL.

Secretariat of GPC/IPL-KLC Secretary

Kyoji Sassa.
International Consortium on Landslides.
138–1 Tanaka-Asukai cho, Sakyo-ku, Kyoto 606–8226, Japan Tel: +81 (75) 7230640.
Fax: +81 (75) 9500910.
E-mail: Secretariat@landslides.org
URL: https://www.landslides.org/; https://www.landslides.org/ipl-info/

Contents

IPL/WCOE/KLC2020

ICL Landslide Teaching Tools

Technical Notes and Case Studies

World Landslide Reports

Characteristics of Earthquake-Induced Landslides—Case Studies from the 2011 Tōhoku and 2015 Gorkha Earthquakes

Binod Tiwari

Abstract

Ground shaking due to earthquakes or similar seismic activities is one of the major triggers of landslides globally. It is important to document the characteristics of landslides triggered by earthquakes with different characteristics so that precautions can be taken for future co-seismic landslides. This will help to protect people and reduce potential damage to the infrastructure resulting from such landslides. As such, studying, in parallel, the characteristics of the earthquakes and corresponding co-seismic landslides is critical for infrastructure planning. In particular, this is necessary to develop relationships between the earthquake magnitude or peak ground acceleration and the total area or number of landslides triggered as well as between the maximum distance to landslide observations from the epicenter or fault rupture. In this study, the co-seismic landslides triggered by two major earthquakes in 2010s—the 2011 Tōhoku Earthquake and the 2015 Gorkha Earthquake are separately presented. In addition, comparisons are made among the co-seismic landslides. Comparisons are also made with 35 historical earthquake events from 1920 to 2015 focusing on how the co-seismic landslides triggered by these two events compare with the data obtained from other historical earthquake events.

Keywords

Landslides · Earthquake · Tōhoku earthquake · Gorkha earthquake · Rockslide · Cyclic failure

B. Tiwari (✉)
Department of Civil and Environmental Engineering, California State University, Fullerton, Fullerton, CA, USA
e-mail: btiwari@fullerton.edu

1 Background

Globally, landslides cause approximately 11,500 fatalities per year between 2004 and 2016 (United Nations Office for Disaster Risk Reduction, UNDRR 2019). It is important to note that the number of fatalities can vary greatly depending on the severity and location of the landslide. For example, the risk of deaths from landslides increases in highly mountainous regions in proximity to dense neighborhoods (Tiwari and Ajmera 2017). In particular, the highest mortality risks appear in Asia near the Himalayas and in South America by the Andes.

In addition to the fatalities, landslides can cause extensive damage to buildings, roads, and other infrastructure. The associated economic impact can be significant. For example, in the United States, landslides cost an average of $1–2 billion annually in direct costs and indirect economic losses (Tiwari and Ajmera 2017).

Other impacts caused by landslides that cannot be captured quantitatively also exist. For example, landslides can have long-lasting effects on the environment. They can alter landscapes, destroy vegetation, and disrupt ecosystems. The sediment and debris carried by landslides can also affect rivers and streams, leading to water pollution and affecting aquatic habitats. The disturbance they cause to communities can lead to the displacement of residents, loss of livelihoods, and social and economic instability. Infrastructure damage can hamper transportation, communication, and access to essential services, affecting the overall well-being of the impacted areas.

One of the major causes of landslides is seismic activity and as a result, earthquake-induced landslides have been the focus of many studies that have turned to small- and large-scale physical modelling, numerical analyses, or the examination of the characteristics of landslides induced during recent earthquakes to better understand the triggering factors and consequences of these landslides (Tiwari and Ajmera 2017). Keefer (1984) complied data from 40 historical earth-

B. Abolmasov et al. (eds.), *Progress in Landslide Research and Technology, Volume 4 Issue 1, 2025*, Progress in Landslide Research and Technology, https://doi.org/10.1007/978-3-031-89836-5_1

quakes occurring between 1811 and 1980 and developed relationships between the magnitude of the earthquake, distance from the epicenter, and the total area affected by the landslides. Rodríguez et al. (1999) expanded the database developed by Keefer (1984) to include an additional 36 earthquakes from 1980 to 1994. They developed slightly different correlations between the earthquake magnitude and the total landslide area based on the expanded database. The work by Keefer (1984) and Rodríguez et al. (1999) made several important contributions to the understanding of the characteristics of earthquake-induced landslides. However, the most notable is probably the relationships between the seismic ground shaking, specifically the magnitude of the earthquake, and number of landslides and the area affected by the landslides in addition to the relationship between the magnitude of earthquake and the maximum distance of landslide observations from the epicenter in different geological, topographical, and climatic conditions. In both studies, the peak ground acceleration, which is a better indicator of the intensity of shaking, was not incorporated. Later, Tiwari and Ajmera (2017) developed the relationship between peak ground acceleration (PGA) as well as the magnitude of the earthquake and number of observed landslides in the areas within diverse geological, topographical, and climatic conditions.

The 2011 Tōhoku and the 2015 Gorkha Earthquakes were two large events that occurred in 2010s and were responsible for a significant loss of lives and property in Japan and Nepal, respectively. While the death toll with Tōhoku Earthquake was significantly large, majority of the fatalities were due to the tsunami triggered by the earthquake. However, the death toll due to the Gorkha Earthquake was mainly due to several causes including landslides, rockfalls, debris flows, avalanches, and building collapses. Presented in this paper are summaries of the landslides triggered by these two large earthquakes and their comparison with each other as well as with the observations from the historic earthquakes. These case studies will provide a database for landslide researchers regarding the characteristics of co-seismic landslides.

2 Case Study 1—Landslides Triggered by 2011 Tohoku Earthquake

The M_w 9.0 Tōhoku Earthquake (also referred to as the Great East Japan Earthquake) struck the northeast region of Japan on March 11, 2011 at 05:46 UTC (14:46 local time). It killed more than 20,000 people, injured more than 5000 people, and displaced more than 130,000 people. The earthquake damaged over 332,000 buildings, more than 2000 roads, 56 bridges and 26 railway tracks, resulting in more than $300 billion in damages (Wartman et al. 2013; Tiwari et al. 2013; Pradel et al. 2011, 2013a, b). The majority of the death toll was due to a devastating tsunami triggered by the earthquake. However, in excess of 20 people were reported to be dead due to landslides triggered by this major earthquake and its aftershocks.

Thousands of aftershocks followed the main shock, with four of them exceeding M_w 7.0. Although the main quake and the largest aftershocks occurred offshore, many significant aftershocks occurred inland, i.e., in close proximity to populated areas, such as the M_w 6.6 strong aftershock of April 11, 2011 that hit the Fukushima area. The ground rupture and motions from the April 11th aftershock caused structural damage to temples, roads and buildings, as well as numerous shallow landslides and rockfalls (Towhata et al. 2011; Wartman et al. 2013; Tiwari et al. 2013; Pradel et al. 2011, 2013a, b). This section of the paper covers the area impacted by the 2011 Tohoku earthquake and its aftershocks due to co-seismic landslides. The study area includes the zone covered between Ibaraki to Sendai area (Fig. 1). Additional detailed information regarding these landslides is

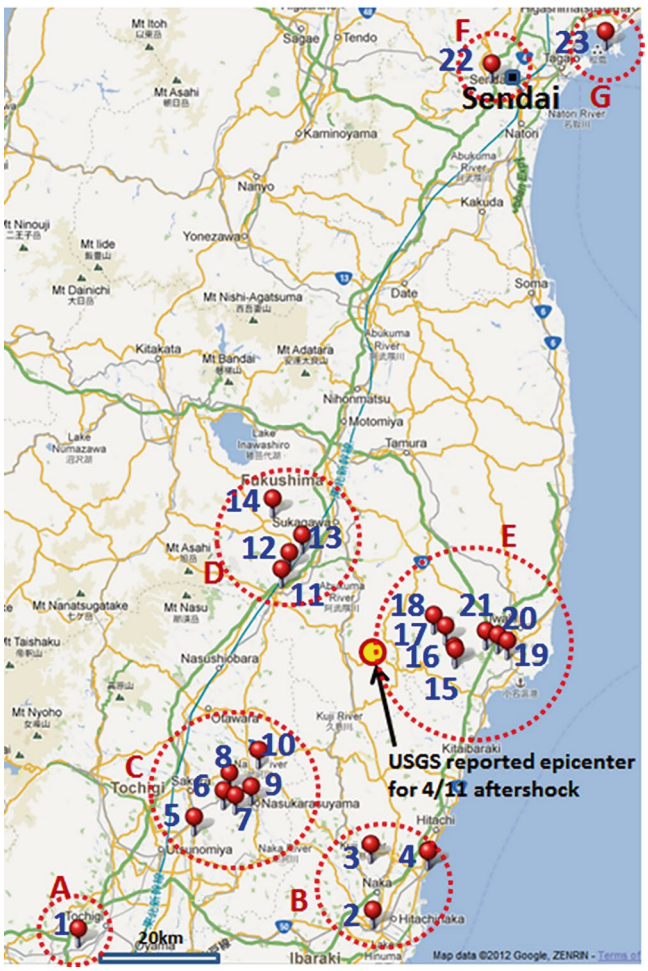

Fig. 1 Location map of the study area (numbers are the location numbers of the visited sites, as indicated in Table 1 and letters are geological divisions)

available in Wartman et al. (2013), Tiwari et al. (2013), and Pradel et al. (2011, 2013a, b).

2.1 Geology of the Study Area

The study area for this case study is divided into seven different geological settings—A through G, as presented in Fig. 1. The geological characteristics of these regions are described below and are also presented in detail in Wartman et al. (2013), Tiwari et al. (2013), and Pradel et al. (2011, 2013a, b).

2.1.1 Sano-Simotsuga Area

Sano-Simotsuga area (Area A in Fig. 1) of Tochigi prefecture has rocks of Ryoko Belt. Sandstone and alteration of sandstone and mudstone and chert of Triassic-Jurassic age are the main lithologies of Sano-Simotsuga area. Unconsolidated gravel, sand and mud deposits are common in river valleys and flood plains.

2.1.2 Mito-Hitachi Area

Mito-Hitachi area (Area B in Fig. 1) has mainly volcanic ash deposits (Kanto Loam Formation) of Pleistocene. It also has thin layers of semi-consolidated sand, iron sand and pumice grains of Ishizaki Formation along with gravel, sand, silt and clay of Ibaraki Clay, Ryugasaki and Miwa Formations. Hitachi is situated to the north of Mito and also has the similar bed rock geology. However, the southern coastal part (south of Kuji River) of Hitachi has Holocene Dune Deposit. The Hitachi plain consists of same Pleistocene volcanic ash deposit of Kanto Loam Formation. In the western hills of Hitachi, intercalation of meta-volcanic rocks, sheared granite, slate and phyllite, amphibole schist, mica schist, quart schist, serpentine with patches of limestone are major rock units. The northwestern part of Hitachi has plutonic rocks and granite is the major lithological unit. On the left bank of Kuji River at Hitachiomiya, sandy siltstone and siltstone (Zuiryu and Sakachi Formations) of Miocene are the major lithologies, whereas the right bank of same river has same volcanic ash deposit of Kanto Loam Formation. Miocene accretionary wedge deposit consists of pumaceous volcanic tuff, volcanic sandstone, andesitic volcanic breccia alternatively deposited with sandstone, siltstone and conglomerate that are well distributed in the upper stream area of Kuji River near Hitachiomiya.

2.1.3 Nasukarasuyama-Otawara Area

Within the Nasukarasuyama-Otawara area (Area C in Fig. 1), sandy mudstone, alteration of sandstone, mudstone, and conglomerate of Miocene are major rock types in the Nasukarasuyama and Naka River areas. Triassic-Jurassic sandstone, chert and shale are also found in western part of Nasukarasuyama City. In Sakura, Pleistocene volcanic sand, pumaceous sand and pumaceous tuff deposits are equally distributed with Holocene gravel, sand and mudstone deposits. The northeast area of Utsunomiya basically consists of volcanic ash underlain by Triassic-Jurassic sandstone and mudstone. Likewise, Triassic-Jurassic sandstone and shale are major rock units of Nakagawa area. Otawara area has unconsolidated Holocene mudstone, sandstone and gravel beds. They belong to the flood plain and natural levee deposits. Pleistocene volcanic ash (Tawara, Takaragi, Housakuji Loams) and pumice tuff deposit are also found in Otawara area. Nasushiobara (northwest of Otawara) also has same Pleistocene volcanic ash and Holocene sand and gravel deposits.

2.1.4 Shirakawa-Fukushima Area

Within the Shirakawa-Fukushima area (Area D in Fig. 1), Shirakawa city is situated on the unconsolidated Holocene sand and gravel deposits. Early Pleistocene Dacite Pyroclastic Rocks (Shirakawa Formation) are found in the hills around Shirakawa city. Volcanic debris deposit, volcanic ash and andesitic lava are common rocks of southern part of Shirakawa. When travelling from Shirakawa to Sukagawa, cretaceous granite and Pleistocene Dacite Pyroclastic Rocks are encountered as the major lithology of the area. In Yabuki area, granite, dacite ash flow deposit, tuffaceous sandstone and conglomerate are underlain by recent sand and gravel beds. Pleistocene pyroclastic sediments (Shirakawa Formation) are widely distributed in Sukagawa area. On the right bank of Sukagawa area, metamorphic rocks are found. Fukushima Airport is situated on hillocks of Pre-Tertiary crystalline schist and gneiss which are overlain by dacite ash flow deposit. In Kubo-Yashiki area (road connecting to Lake Inawashiro), the dacite pyroclastic sediments and Miocene rhyolite and quart porphyry are the primary bedrock.

2.1.5 Iwaki Area

Zone E consists of Iwaki area (Area E in Fig. 1). Conglomerate, mudstone, medium to coarse sandstone and tuffaceous sandstone of Miocene belonging to Yunagaya, Takaku and Taga groups are major lithologies of Onahama area. In the western part of Iwaki, schist (green, black, psammatic, pelitic, basic, and ambhibole) and gneiss of Pre-Tertiary age are major rock units. They are well distributed in Shirahata and Takashiba dam at Itozawa area. Within this metamorphic sequence, Miocene sandstone and Pre-Tertiary granite are also found in the western part of Takashiba dam.

2.1.6 Sendai Area

Sendai area (Area F in Fig. 1) basically has semi-consolidated sedimentary rocks of Pliocene and Quaternary age. Few bands of consolidated sandstone, mudstone and shale of Miocene are also found in the southern part of the city. Marine and beach sand with widely distributed mud and peat

are found in eastern part of city as well as in and around the Sendai Airport.

2.1.7 Matsushima Bay Area

Within the Matsushima Bay area (Area G in Fig. 1), Matsushima Islands mainly consist of the Miocene sedimentary rocks (tuffaceous sandstone, pumice tuff, siltstone, sandstone, conglomerate, and cross bedded sandstone), which strike in the NW-SE direction. Similarly, Matsushima Hill is mainly composed of the Miocene Matsushimawan Group, which strike the NW-SE direction. Matsushima Bay is underlain primarily by Holocene marine clay sediments, which directly cover the Miocene bedrocks. In southern part of Matsushima, Miocene dacite lava and volcanic breccia are also found as intercalated sequence with sandstone and conglomerate.

2.2 Landslides Observed in the Study Area

Wartman et al. (2013) conducted a comprehensive study to understand the characteristics and spatial distribution of coseismic landslides triggered by 2011 Tōhoku Earthquake and its aftershocks in eastern Honshu region of Japan. Using the high-resolution satellite imagery released by Google Earth right after the earthquake and field reconnaissance, the authors developed a geo-spatial database consisting of nearly 3500 landslides, each landslide with an area larger than 4 m^2, within the studied region encompassing nearly 29,000 km^2. The landslides were uniformly distributed across the study area. Majority of the landslides were disrupted or lateral spread landslides. Coherent landslides were distributed mostly along the Neogene Sedimentary. Over 80% of the landslides were developed along younger (Neogene) rock units and Quaternary sediments.

This paper discusses the various geotechnical hazards observed in the study area which includes fault ruptures, large-scale landslides, slope failures, rock falls, damages to urban areas, damages induced by the tsunami, dam collapse, and damages to levees. Shown in Fig. 1 is the area covered in this study, where red pinned points show key locations described in the paper. The letters in Fig. 1 indicate the geological regions of the studied sites, as already described above. Geographic coordinates, types of failures, elevations, and recorded ground accelerations of some selected sites during the main shock and April 11 aftershock are presented in Table 1. Tiwari et al. (2013) elaborates on each of these sites, while this paper will focus on the damages associated with the majority of these sites. The descriptions of the sites are made based on Keefer (1984)'s classification. It is noted that the majority of the damages associated to the slopes and embankments, presented here were due to the March 11 main shock.

The observed disasters include all types of slope related disasters associated with the main shock (Table 1), e.g. rock slides/fall/avalanche (Iwafune, Naka, Matsushima), embankment failures (Sorihata, Highway 245 near Hitachi Bay, Oridate Residential Area in Sendai City), soil slope/slump/avalanche (three slides in the Kashiwasaki Landslide Area, Arakawa Landslide, Kanaya Landslide, Hanokidaira Landslide, Kitanoiri Landslide, Daishin Nakashinjo Landslide, Yabeya Landslide, Kamenashi Landslide, and Hanokidaira Landslide), retaining wall failure (shrine in Mito City) and Fujinuma dam failure. The characteristics of some of these damages will be explained in detail in the subsequent sections. As presented in Table 1, the recorded PGAs at the rock fall/slide/avalanche sites identified in these locations ranged from 0.16g to 0.68g with majority of the sites (two locations) having a PGA greater than 0.4g. Likewise, the soil slide/slump/avalanche sites identified in these locations were recorded with PGAs ranging from 0.32g to 0.68g with majority (six locations) having PGAs higher than 0.6g.

2.3 Ground Ruptures Associated with April 11 Aftershock

Continuous ground ruptures were clearly visible (Tiwari et al. 2013) at two locations. The first rupture was observed at Kantokuji Shrine (location ID 20 in Fig. 1 and Table 1) in Iwaki City of the Fukushima Prefecture. The observed fault, locally named as Yunodake Fault, was approximately 1 km long (Fig. 2). A vertical drop of 0.7 m was observed near the shrine (Fig. 3). As the rupture passed through the Kantokuji shrine and all the way down from the Iwaki Ishikawa bypass road, it completely damaged the shrine and approximately 30 m length of the road. A location with continuous ground rupture is shown in Fig. 4.

Approximately 11 km away from the Yunodake fault rupture area, there was an approximately 8.3 km long continuous fault rupture (Fig. 2). As presented in Fig. 5, the first rupture with a clear vertical drop of 1.5 m was observed along Highway 14, i.e. Gosaisho Highway (location ID 17 in Fig. 1). The detailed geographic location and elevation of this location are presented in Table 1. This fault continues in southeast direction to the junction of Prefectural Highways 71 and 34 through the playground of the Tabito Junior High School (location ID 16 in Fig. 1). A continuous rupture, as presented in Fig. 4, was observed on the ground, which passes through the junior high school and highway 34, damaging approximately 5 m length of the road at two locations. No damage was observed in the junior high school. A drop of 1.5 m was observed along the road close to the junction of highways 71 and 34 (Location ID 15 in Fig. 1), as presented in Fig. 6 and Table 1. This fault had been recorded in an old geological map as the Itozawa

Table 1 Geographic coordinates, elevation and recorded PGAs of the studied sites

Location	Site ID (Fig. 1)	Type of failure	Latitude	Longitude	Elevation (m)	Main shock PGA (x g)	PGA of April 11 Aftershock (x g)
Iwafune Rock Avalanche	1	Rock Avalanche	36°19′54.2″N	139°38′56.1″E	41	0.16	0.08
Naka Rock Slide	3	Rock Block Slide	36°31′12.9″N	140°28′5.5″E	47	0.68	0.28
Saibachi Rock Slide	17	Rock Slide	37°0′43.2″N	140°40′34″E	248	0.28	0.36
Matsushima Island	23	Rock Fall/Rock Slide	38°20′5.7″N	141°6′59.4″E	39	0.40	0.08
Slide near Hitachi Bay	4	Soil Falls	36°30′22.2″N	140°37′44.8″E	25	0.40	0.20
Kamenashi Landslide	5	Soil Slump	36°34′59.2″N	139°58′29″E	162	0.60	0.16
Kashiwazaki Landslide	6	Soil Slump	36°38′38.8″N	140°3′18.3″E	170	0.60	0.16
Daishin Nakashinjo Landslides	13	Soil Slump	37°12′52.4″N	140°16′35.7″E	378	0.44	0.36
Nishigo Iwasaki Area	19	Soil Slump	36°58′46.4″N	140°51′28″E	22	0.28	0.24
Watanabe Landslide	21	Soil Slump	37°0′ 2.8″N	140°47′24.9″E	114	0.28	0.28
Oridate Residential Area	22	Soil Slump	38°15′33.3″N	140°48′26″E	142	0.32	0.08
Arakawa Landslide	8	Soil Avalanche	36°40′50.7″N	140°4′22.6″E	127	0.56	0.16
Kanaya Landslide	9	Soil Avalanche	36°39′0.1″N	140°7′59.6″E	131	0.64	0.20
Hanokidaira Landslide	11	Soil Avalanche	37°8′18.4″N	140°13′3.1″E	402	0.68	0.32
Kitanoiri Landslide	12	Soil Avalanche	37°10′28.4″N	140°14′22.2″E	367	0.60	0.32
Yabeya Landslide	12	Soil Avalanche	37°10′33.1″N	140°14′19.5″E	412	0.56	0.32
Kaiya Landslide	18	Soil/Rock Avalanche	37°2′7.8″N	140°38′38.6″E	226	0.32	0.40
Slides along Fuji River Bank	10	Soil Falls	36°45′42.6″N	140°8′19.7″E	121	0.48	0.16
Retaining Wall Collapse, Mito City	2	Retaining Wall Failure	36°22′19.4″N	140°28′21.8″E	26	0.56	0.24
Sorihara Road Slide	7	Embankment Failure	36°37′48.5″N	140°5′21″E	182	0.68	0.20
Fujinuma Dam Failure	14	Dam Failure	37°18′6.6″N	140°11′45″E	433	0.20	0.20
Tabito Junior High School	16	Fault Rupture	36°57′53.4″N	140°42′5.8″E	194	0.28	0.32
Junction of Highways 71 and 34	15	Fault Rupture	36°57′30.9″N	140°42′14.5″E	187	0.28	0.32
Kantokuji Shrine	20	Fault Rupture	36°59′26.8″N	140°49′23.4″E	42	0.28	0.28

Fault. According to local experts, this fault has not been active for the past 2000 years. However, it is to be noted that the epicenter of April 11 aftershock was recorded at the location identified by a circle in Fig. 1 (USGS), which is approximately 20 km west of the fault that was observed in the field. Crib wall of some houses near the junction of highways 71 and 34 were broken but the houses were not affected.

2.4 Damages Associated with April 11 Aftershock

As explained earlier, two different fault ruptures were observed. Major damages were observed near the Yunodake Fault Rupture area—Watanabe Landslide and slides in the residential area at Nishigo Iwasaki (Fig. 1 and Table 1), as presented in Fig. 7. Figures 8 and 9 show the damages at these two locations. Major slope related failures observed near the Itozawa Fault Rupture were a rock fall along Highway 14, i.e., Gosaisho Highway and Kaiya Landslide (Figs. 10, 11, 12 and 13). Characteristics of these failures will be explained in detail in the subsequent sections. As presented in Table 1, the recorded PGA at the rock fall/slide/avalanche site identified in these locations was 0.36g. Likewise, the PGAs at the soil slide/slump/avalanche sites identified in these locations were ranged from 0.28g to 0.40g, which were higher than the PGAs recorded at those sites during the main shock.

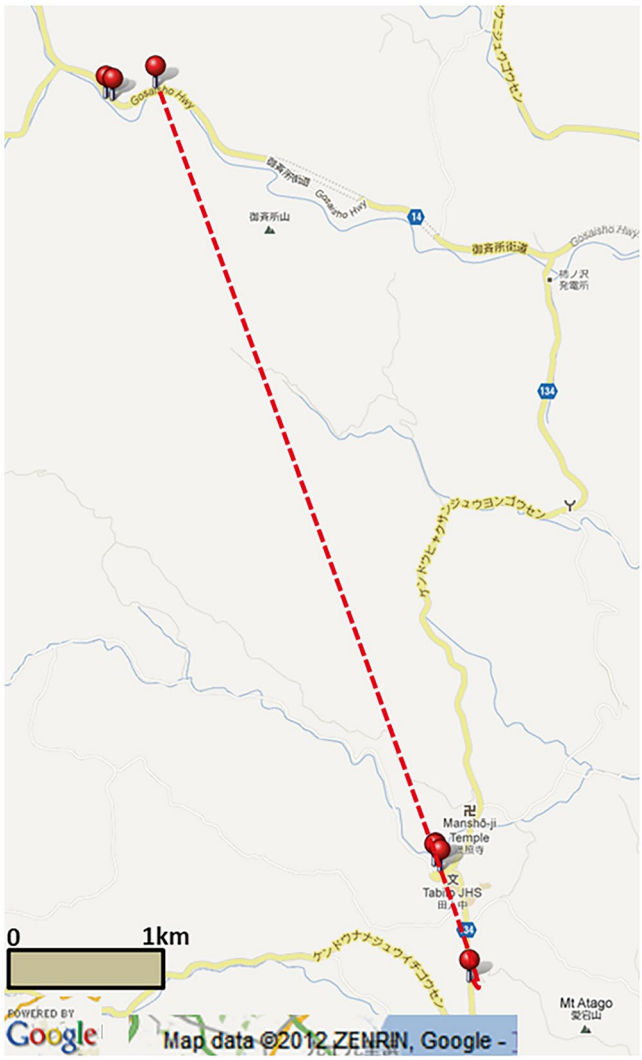

Fig. 2 Ground rupture observed at Itozawa Fault area

Fig. 3 Fault rupture at Kantokuji Shrine

Fig. 4 Ground rupture near Tabito Junior High School, Location b in Fig. 2

Fig. 5 Photograph at the location a, Gosaisho Highway in Fig. 2

Fig. 6 Photograph rupture at junction of Highways 71 and 34, location c in Fig. 2

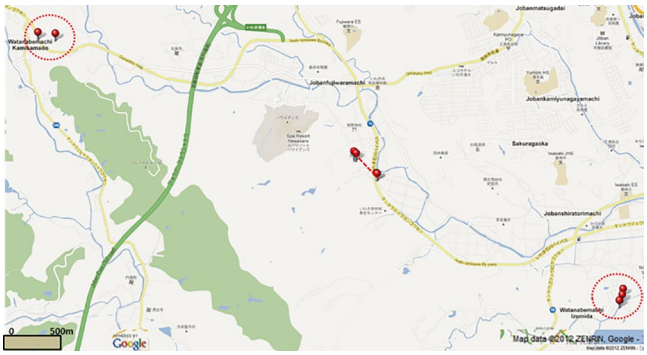

Fig. 7 Watanabe Landslide (a) and Nishi Iwasaki landslide (b) located near the Yunodate fault rupture area

Fig. 8 Watanabe Landslide located near the Yunodate fault rupture area

Fig. 9 Nishi Iwasaki Landslide located near the Yunodate fault rupture area

2.5 Characteristics of Landslides

The majority of the slope failures observed during this study area were located along the alignment of the Tohoku Express Highway and the Tohoku Shinkansen Tracks/Tunnel, both of which run relatively close to each other (zones A, C, D, F and G in Fig. 1). This roughly North-South oriented alignment coincides with a localized area of fault ruptures—a zone where the bedrock would be in its natural condition, intensely sheared and fractured. Volcanic ash deposits were the dominating sliding mass in the majority of these slides (Pradel et al. 2011; Tiwari et al. 2013). Two large landslides blocked nearby rivers/streams. Moreover, Fujinuma dam (location ID 14 in Fig. 1) collapsed. There were several massive rock falls scattered throughout the study area. The characteristics of a few failures are presented here.

2.5.1 Landslides Along Volcanic Ash Deposits

Earthquake-induced landslides that resulted in a significant damage were triggered in areas with loose volcanic ash deposits. Unique characteristics of these landslides included: similar type and density of the soil mass, long run-out distances and sliding along preexisting and well-defined slickenside surfaces. Characteristics of some of the major slides are described below.

2.5.2 Landslides Along Highway Embankments

Several soil slumps/slides were observed along highway embankments (Fig. 14). One of them was the Kamenashi Landslide, a soil slide that occurred near Goshaisho Highway (location ID 5 in Fig. 1). The soil mass that slid was classified as loam by local experts. A portion of slid mass blocked an irrigation channel completely (Fig. 15) with repair work underway within a month after the earthquake. Likewise, approximately 150 m length of a pavement collapsed in Sorihata of Nasukarasuyama City (location ID 7 in Fig. 1), as shown in Fig. 16. A vertical drop of approximately 30 m was observed at the head scarp. The soil mass, also identified as a loam, slid at an angle of 30°. As shown in Fig. 17, a landslide inclined at approximately 25° in loam soil was also

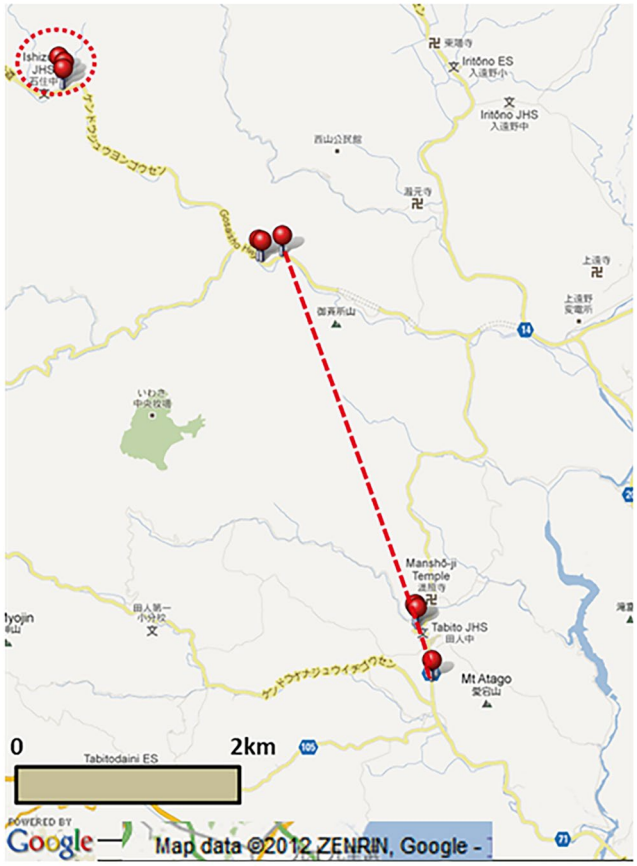

Fig. 10 Location of Saibachi Rock fall (a) and Kaiya landslide (b) located close to the Itozawa Fault Rupture area

Fig. 11 Damage at the Saibachi Rock fall

observed along highway near Daishin Nakashinjo area (location ID 13 in Fig. 1). This landslide blocked a Prefectural highway. All of these failures occurred after the March 11 main shock. As presented in Table 1, the recorded PGAs at Kamenashi, Shorihara, and Daishin Nakashinjo areas in

Fig. 13 Flow path of debris at Kaiya Landslide

Fig. 12 Damage at Kaiya Landslide

March 11, 2011 event were 0.6g, 0.68g, and 0.44g, respectively. These ground accelerations are relatively large.

2.5.3 Kanaya Landslide

A photograph of Kanaya Landslide is shown in Fig. 18. The repair work was underway during the reconnaissance visit undertaken in April 2011. The slide mass consists of volcanic ash materials, which are locally classified as loam. Several rock outcrops composed of weathered to highly weathered mudstone and tuff were also observed in the failure area. Although this landslide occurred in a sparsely populated area, it still killed three people, damaged several properties and completely destroyed one home. Two houses along the edges of the slide path were filled with the landslide debris (Fig. 19). The sliding mass separated into two directions, as can be observed in Fig. 18. According to the local people, the first slide was triggered right after the main

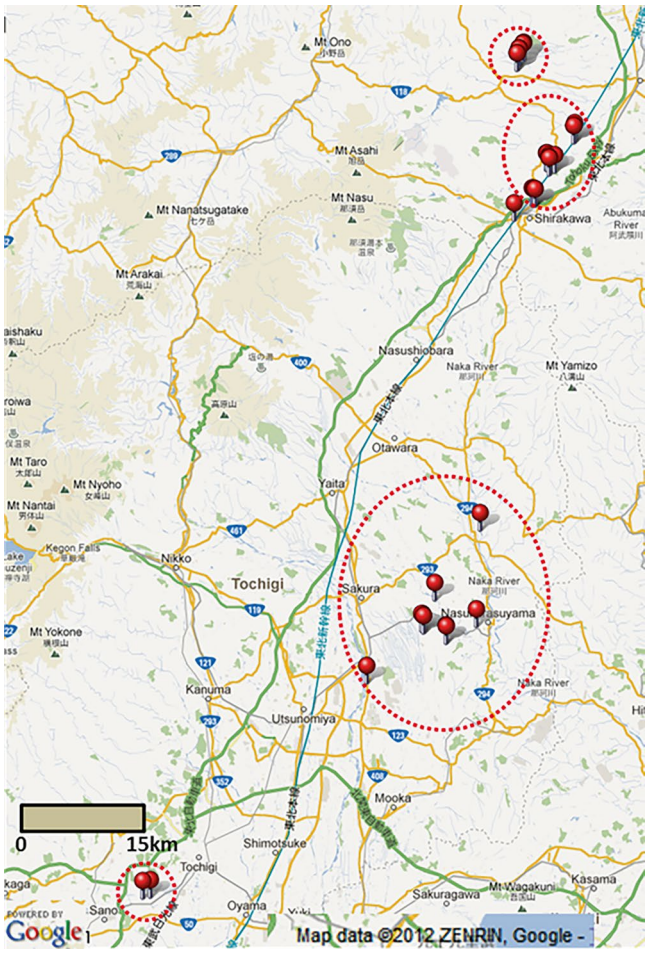

Fig. 14 Landslides that occurred near major highways—Daishin Nakashinjo area (a), Sorihata area (b) and Gosaisho Highway (c)

Fig. 15 Landslide that occurred at Gosaisho Highway

shock during the March 11 earthquake. The sound of ground breaking was heard when the first slide was triggered. Two minutes after the first slide, another landslide was triggered.

Fig. 16 Landslide in the Sorihata area

Fig. 17 Landslides in the Daishin Nakashinjo area

The peak ground acceleration recorded near the landslide site after March 11 earthquake was 0.64g (Table 1).

2.5.4 Hanokidaira Landslide

An overall view of Hanokidaira Landslide, located in Shirakawa City (location ID 11 in Fig. 1) is presented in Figs. 20 and 21. This landslide also occurred in volcanic ash materials (locally classified as loam) and was the reactivation of a preexisting landslide. According to the geological map, alternate layers of mudstone and sandstone in the landslide area were overlain by 7–8 m deep weathered volcanic ash. The triggered landslide mass had an inclination of 27° at the top and the debris came to rest at an average angle of 8°. This landslide damaged 11 residential and commercial buildings. A total of 13 people were killed. The landslide was approximately 250 m long and 120 m wide. The difference in elevation from top to the bottom of the landslide was about 48 m. The estimated depth of landslide was 10 m. Thus, the

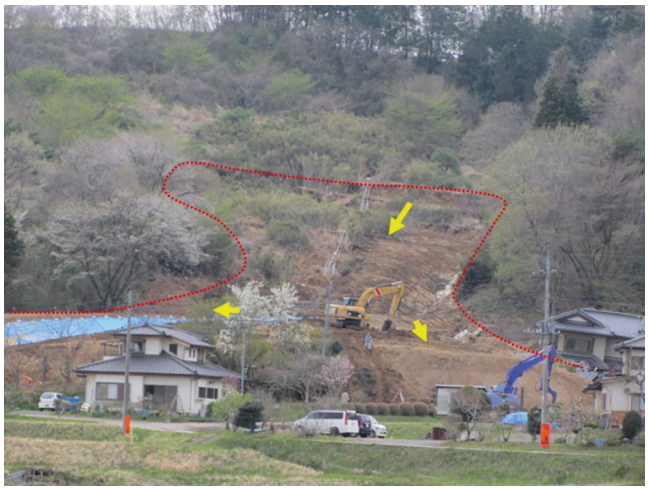

Fig. 18 Overall view of Kanaya Landslide from the toe

Fig. 21 View of Hanokidaira Landslide from the toe

Fig. 19 A house filled with landslide debris at Kanaya Landslide

Fig. 22 Slickensides observed in the slid mass at Hanokidaira Landslide

Fig. 20 View of Hanokidaira Landslide from top

approximate volume of the landslide material, calculated from the topographic map was 31,000 m^3. Slickensides, as presented in Fig. 22 were observed at numerous locations along the exposed sliding planes. According to the eye witnesses, the lower part of the slope, approximately 175 m above the existing road slid first after the main shock during March 11 earthquake and then the upper part, located 100 m above the lower part, moved down. A peak ground acceleration of 0.68g was recorded near this location during the March 11 earthquake (Table 1) whereas a PGA of 0.32g was observed in this area during the April 11 aftershock.

2.5.5 Kitanoiri Landslide

As explained earlier, several long run-out type landslides, such as Kitanoiri Landslide (location ID 12 in Fig. 1) were observed along the Tohoku Shikansen Tunnel. This landslide is pictured in Figs. 23 and 24. The top 110 m long and 40 m

Fig. 23 View of Kitanoiri Landslide from the bottom

Fig. 24 View of Kitanoiri Landslide from the top

wide section slid first during the March 11 earthquake and then travelled approximately 150 m downwards at an inclination of 18°. Depth of the head scarp was approximately 25 m. Estimated depth and volume of the sliding mass were 10 m and approximately 49,000 m^3, respectively. This landslide also occurred in volcanic ash, locally classified as loam. As can be observed in Figs. 23 and 24, this landslide also reactivated preexisting landslides. As shown in Fig. 25, this landslide exhibited slickensides along the sliding planes. The PGA recorded at this site during the March 11 main shock was 0.6g, whereas a PGA of 0.32g was recorded during the April 11 aftershock (Table 1).

2.5.6 Yamabe Landslide

The Yamabe Landslide (location ID 12 in Fig. 1) is also located along the Tohoku Shinkansen Tunnel. The landslide

Fig. 25 Slickenside surface observed in the slid mass of the landslide

mass was similar to the one observed in the Kitanoiri Landslide. The landslide also occurred in a preexisting landslide area. Similar slickensides as in Kitanoiri Landslide, but with more moisture were observed during the field visit. A 150 m long and 60 m wide portion of landslide slid at the top of the slope and then travelled a distance of approximately 400 m (Fig. 26) at an inclination of 15°. Slickenside surface observed during the field visit and toe of the sliding mass are presented in Figs. 27 and 28, respectively. Estimated depth of slide was 10 m, while the estimated volume of the landslide was 35,000 m^3. An outcrop of weathered green tuff was observed at several locations. The PGA recorded at this site during the March 11 main shock was 0.56g, whereas a PGA of 0.32g was recorded during the April 11 aftershock (Table 1).

2.5.7 Watanabe Landslide

Watanabe Landslide (location ID 21 in Fig. 1) is located in Iwaki City, proximate to the location of fault rupture described above. This landslide was triggered after the April 11 aftershock. Unlike, the previously described landslides the sliding surface was developed on highly weathered mudstone surfaces (although some weathered tuffs were also observed within the slide mass). The main portion of the landslide was about 300 m long and 60 m wide with a head scarp height of 20 m. The average slope of the landslide was 22° (Figs. 29 and 30). This landslide blocked approximately 100 m of the Gosaisho Highway. The road cut along the toe of the slide resulted in withdrawal of lateral support and likely contributed to the observed failure. The recorded PGA near this area during the April 11 aftershock was 0.28g, whereas a PGA of equal magnitude was also recorded near this area during the March 11 earthquake (Table 1).

Fig. 26 View of Yamabe Landslide from top

Fig. 29 Overall view of Watanabe Landslide

Fig. 27 Slickenside surface observed along a sliding plane

Fig. 30 Head scarp of Watanabe Landslide

Fig. 28 Toe of Yamabe Landslide

2.6 Landslides Triggered in Embankments and Fills

Numerous fill slopes failed during the Tōhoku Earthquake and affected residential neighborhoods. Some of those landslides, observed along the roads, were presented above. Details of several other landslides are presented below.

2.6.1 Landslide in Kashiwazaki Residential Area

Several soil slumps were observed in a residential area at Kashiwazaki (location ID 6 in Fig. 1). Several houses including a shrine were affected by these landslides (Figs. 31 and 32). The commonalities between these two locations are the long run-out distance exceeding 400 m and a sliding mass containing mixtures of organic soil with loam. Over 30 houses were threatened by these landslides. The repair work

Fig. 31 Landslide damage at location ID 1 in the Kashiwazaki Residential Area

Fig. 33 Google Earth images of the Oritate Residential Area prior to and after the earthquake (locations a and b are the locations of photographs in Figs. 34 and 35)

Fig. 32 Landslide damage at location ID 2 in the Kashiwazaki Residential Area

Fig. 34 Cracks on the road surface (location a) at Oritate Residential Area

was ongoing in both landslides within a week after the earthquake. The PGA recorded near these locations during the March 11 main shock and April 11 aftershock were 0.6g and 016g, respectively (Table 1).

2.6.2 Oridate Residential Area

One of the landslides that caused significant damage occurred in Oritate, near Sendai City (location ID 22 in Fig. 1). This landslide, which occurred during the March 11 main shock, damaged numerous residential buildings constructed on compacted fills. The buildings either collapsed or were severely tilted (Figs. 33, 34 and 35). Over 43 buildings were red tagged while at least another eight were yellow tagged. This landslide can be attributed to the effect of strong ground shaking in the compacted fill. According to the local residents, a fill was placed on the existing ground prior to the development of this residential area. The bedrock is located approximately 8 m below the ground level. The fill material was borrowed from the excavated earthwork while leveling the slope. Ground water table was observed at depths of approximately 3 m. Also shown in Fig. 33 is the effect of movement in a northeast direction towards the adjacent Oritate Elementary School. The average length and width of the landslide were 230 m and 170 m, respectively. Collapse of this mass would inevitably cause damage to the elementary school. PGAs of 0.32g and 0.08g were recorded near this site during March 11 main shock and April 11 aftershock, respectively (Table 1). Please note that this landslide was not unique to the area. In particular, another landslide located approximately 4 km away resulted in the collapse of

Fig. 35 Collapsed building in Oritate Residential Area (location b)

Fig. 36 Collapse of buildings constructed on fills near Sendai City

four buildings and the red tagging of four houses after March 11 event (Fig. 36).

2.7 Landslides that Caused Natural Damming

Two landslides—Kaiya Landslide and Arakawa Landslide—both triggered during March 11 earthquake, caused damming of the natural streams. Additional details about both failures are presented below.

2.7.1 Kaiya Landslide

Kaiya Landslide (location ID 18 in Fig. 1; Figs. 12 and 13) is located in Ishizumi Kaiya of Iwakishi Tabito Cho. Four people were killed and three buildings were completely destroyed due to this landslide. As described earlier, a 75 m long and 60 m wide sliding mass originally inclined at 27° was triggered.

Fig. 37 Stream that was blocked by Kaiya Landslide

This mass travelled a distance of 125 m and blocked a stream located 100 m south of the sliding mass near the toe of the slope (Fig. 37). A total difference in elevation from the head to the toe of the slide was 160 m, of which approximately 100 m difference in elevation was observed across the triggered mass and the remaining 60 m was associated with the sliding mass. According to the local people, 3 min after they felt the aftershock of April 11, they heard a sound of a landslide triggered at the top of the slope. The natural dam, according to them, was breached artificially (Fig. 37) to reduce the risk of damming a larger sized river, which is located 100 m south of the sliding mass. Analysis of historic images show that construction of a hiking track between 2006 and 2009 caused a significant loss of vegetation cover increasing the vulnerability to potential slope failures. The recorded PGAs near the Kaiya Landslide during the March 11 main shock and April 11 aftershock were 0.32g and 0.4g, respectively (Table 1), both sufficiently strong to trigger the landslide.

2.7.2 Arakawa Landslide

The Arakawa Landslide is located in Fujitsu-Nasukarasuyama (location ID 8 in Fig. 1). A 200 m long and 200 m wide mass of soil, mainly composed of volcanic ash (locally classified as loam) slid down during the March 11 earthquake and blocked the Arakawa River. Shown in Fig. 38 is the image of the landslide prior to the March 11 earthquake. Figures 39 and 40 contain photographs of Arakawa Landslide after the earthquake. According to the local people, the landslide dam was quickly breached artificially (Fig. 40) to avoid the potential for overtopping and downstream flooding. This could damage more than 150 houses as well as a bridge located at less than a kilometer downstream.

There were several vertical collapses observed along Fuji River. Locations of these failures are presented in Fig. 1

Fig. 38 Image of the Arakawa Landslide prior to the earthquake

Fig. 39 Photograph of the Arakawa Landslide taken after the earthquake

Fig. 40 Landslide dam formed at the Arakawa Landslide after the earthquake

(location ID 10). Those collapses are not described in this paper.

2.8 Rock Falls

There were several rock falls triggered by both the March 11 main shock and April 11 aftershock. Some of them include Saibachi Rock Fall (location ID 17 in Fig. 1), Iwafune Rock Slide (Fig. 41, location ID 1 in Fig. 1), Naka Rock Fall (Fig. 42, location ID 3 in Fig. 1). Saibachi Rockslide is located 100 m away from the Itozawa Fault. This rock slide resulted in the collapse of a house and one fatality. Iwafune Rock Slide is an interesting slide as the entire mountain was separated, as shown in Figs. 41 and 42. According to a report published by the Japan Landslide Society, the mountain was not separated prior to the March 2011 earthquake. Recorded PGAs near this location during the March 11 main shock and April 11 aftershock were 0.16g and 0.08g, respectively

Fig. 41 Separation observed in the mountain at Iwafune from the west side

Fig. 42 Separation observed in the mountain at Iwafune observed from the east side

(Table 1), which are not as high as the shaking intensities observed in other locations.

The Naka Rock Fall damaged three buildings, as shown in Fig. 43. It appears that the rock mass slid from an existing landslide surface, which could have been developed during the time of excavation associated with the construction of those houses. The recorded PGAs near this location at the time of March 11 main shock and April 11 aftershock were 0.68g and 0.28g, respectively (Table 1). The rock fall can be attributed to such strong shakings.

Several rockslides were observed in Matsushima area of Tohoku Prefecture (location ID 23 in Fig. 1). The recorded PGAs near this location at the time of March 11 main shock and April 11 aftershock were 0.40g and 0.08g, respectively (Table 1). These rock falls will be described later. The other soil/rock slump, which caused major damage to the highway was a road slide observed along the Hitachi Bay (location ID 4 in Fig. 1). This landslide collapsed a 4.5 m section of the highway (Figs. 44 and 45). The recorded PGAs near this location at the time of

Fig. 43 Rock slide that damaged three buildings in the Naka area

Fig. 44 Coastal landslide observed near Hitachi Bay

Fig. 45 Coastal landslide observed near Hitachi Bay

Fig. 46 Typical rockfall observed in Matsushima Island

March 11 main shock and April 11 aftershock were 0.40g and 0.20g, respectively (Table 1). During the field visit, toe of the landslide was protected by a buttress wall. Width of the slide at the head was 40 m. There was a drop of 0.6 m at the head scarp.

2.9 Damage in Matsushima Island

Major features of the disaster observed in the Matsushima Island were rockfall and tsunami disasters (location ID 23 in Fig. 1). The island was not open to public for over a month after the earthquake. Pictured in Fig. 46 is a typical rockfall observed in the Matsushima Island.

2.10 Damage in the Urban Area

In addition to the damages sustained on slopes and embankments, several houses were cracked, and retaining walls were collapsed (Fig. 47). Roads were also damaged in Mito City (ID 2 in Fig. 1).

Fig. 47 Damage of retaining wall of a shrine observed in Mito City

Fig. 49 Collapsed saddle dam portion of the Fujinuma Dam after the earthquake

Fig. 48 Collapsed main dam portion of the Fujinuma Dam after the earthquake

Fig. 50 Damage sustained at the downstream due to the collapse of Fujinuma Dam

2.11 Fujinuma Dam Collapse

The main shock collapsed the Fujinuma Dam (Fig. 48, ID 14 in Fig. 1) and caused a rapid drawdown type failure in the Fujinuma saddle dam (Fig. 49). The failure of the dam caused a significant loss of lives and properties. The damage sustained on the downstream side is presented in Fig. 50. The detailed discussion and analysis pertinent to Fujinuma Dam failure are presented in Pradel et al. (2012).

2.12 Overall Observation

As discussed earlier, majority of the landslides and rockslides were triggered by the March 11 earthquake. However, the aftershock of April 11 also caused significant damage near the vicinity of the fault. Majority of the landslides triggered after the March 11 earthquakes were localized along the alignment of Tohoku Shinkansen/Tunnel and Tohoku Highway. They were also observed at the contact of bedrock

Table 3 Monthly precipitation recorded in four different cities during the respective years of major earthquake

Place	Year	Jan	Feb	Mar	Apr	May	June	July	Aug	Sept	Oct	Nov	Dec	Total
Kobe	1995	***37.5***	14.0	59.0	106.0	348.0	80.0	342.5	12.5	46.0	85.5	51.5	8.0	1190.5
Niigata	2004	203.0	110.0	84.0	111.5	192.5	132.5	222.5	178.0	109.0	***237.5***	193.0	193.0	1917.5
Sendai	2008	10.0	21.5	40.0	127.5	149.5	***101.5***	73.5	444.0	95.5	191.0	60.0	35.0	1349.0
Shirakawa	2011	9.5	71.5	***38.0***	119.0	108.0	98.0	221.5	132.0	446.5	118.0	61.0	16.5	1439.5

Table 2 Comparison of three major recent earthquakes in Japan with the 2011 Tōhoku Earthquake

Earthquake	Day	Month	Year	Depth (km)	Magnitude	Max. PGA (x g)	Number of deep-seated landslides	Number of Landslide Dams
Hyogoken Nanbu	17	January	1995	17	6.8	0.80	Few	0
Niigata	23	October	2004	16	6.8	1.02	>1000	>50
Iwate-Miyagi	14	June	2008	10	6.9	1.02	>4100	>3
Tōhoku	11	March	2011	30	9.0	2.93	<100	1

(mainly mudstone and green tuff) and loose volcanic ash overtopping those rocks, exhibiting highly polished slickensides with long travel distances.

Presented in Table 2 is the information regarding four recent earthquakes that caused significant damages in Japan. Among these four earthquakes, the 2004 Niigata Earthquake and 2008 Iwate-Miyagi Earthquake triggered thousands of landslides including several landslide dams (Table 2). More than 1000 deep seated landslides and an incredible number of slope failures were recorded after the 2004 Niigata Earthquake (Yamagishi and Iwahashi 2007). Moreover, over 50 landslide dams were identified among which 12 of them had the volumes in excess of million m^3. Likewise, more than 3000 landslides were identified within an area of 300 km^2 after the 2008 Iwate-Miyagi Earthquake. A landslide dam with more than 67 m^3 debris volume was observed in Aratozawa River (Yagi et al. 2009). Considering the significantly high magnitude as well as maximum peak ground acceleration during the 2011 Tōhoku earthquake compared to the prior earthquakes, a large number of landslides could be expected. However, to surprise of the author, the number of landslides triggered by this earthquake were significantly low. It should be noted that Hyogoken Nanbu Earthquake (also known as Kobe Earthquake) did not trigger many landslides (Sassa et al. 1995) in comparison to the 2004 Niigata and 2008 Iwate-Miyagi Earthquakes although the magnitudes of all three events were comparable.

The significantly lower number of landslides observed during the 2011 Tohoku Earthquake compared to the 2004 Niigata and 2008 Iwate-Miyagi Earthquake can be attributed to the fact that the Hyogoken Nanbu Earthquake occurred in January (dry season) whereas the Niigata and Iwate-Miyagi Earthquakes both occurred during the rainy season. The 2004 Niigata earthquake occurred 3 days after the area received more than 100 mm of rainfall due to the Typhoon 23. According to the data obtained from the Japan Meteorological Association, an annual precipitation of 1439.5 mm was recorded in the Shirakawa City (station no. 47597) in 2011, of which the amount of rainfall recorded in March and April was 38 mm and 119 mm, respectively (Table 3). Occurrence of this earthquake 3 months later (i.e. in June 2011) could have caused significant damages. For comparison purpose, monthly precipitation of Kobe, Niigata, Sendai, and Shirakawa during the corresponding earthquake years is presented in Table 3. Presented in bold and italics are the months corresponding to the associated earthquake. The data shows that the monthly rainfall during 1995 Kobe and 2011 Tōhoku Earthquake were both approximately 38 mm, more than six times lower than the precipitation observed in Niigata in the month when earthquake occurred. Nevertheless, the number of fatalities and the volume of landslides, as presented above, were significant. This shows that the occurrence of this earthquake during or after the rainy season could be significantly devastating, not only due to the fatalities and damage to buildings; this would be further exacerbated by the blockade of roads, which could significantly impact the rescue operations as observed in 2004 Niigata Earthquake.

The length, width, volume, and damages caused by the major landslides are presented in Table 4. Although the length, volume and run-out distance of all nine landslides were significantly large, only three landslides caused significant damages to houses and lead to fatalities. This can be attributed to the fact that there was no residential area along the travel route of the six landslides that did not cause significant damages despite their size. Had residential areas been located below these landslides, they could have caused more damage and fatalities than the other three failures. Moreover, looking at the nature of slides, all types of failures including rock falls/avalanche, soil slide/slump/avalanche and embankment failures were observed throughout the study area. The PGAs that caused failure in those locations ranged from 0.3g to 0.68g, but in the majority of cases was higher than 0.6g. The occurrence of this earthquake during the rainy season would have required significantly lower PGAs to cause slopes to slide. Table 2 shows that the maximum PGA during

Table 4 Geometry of major landslides and associated damages (landslides with * were triggered during April 11 aftershock and rest of the landslides were triggered during the March 11 main shock)

Location	Site ID (Fig. 1)	Triggering length (m)	Run-out length (m)	Width (m)	Slide volume (m^3)	Damage	Human fatality	Area below the slide
Kashiwazaki Landslide	6	30	400	25	15,000	Trees	0	Vegetation
Watanabe Landslide*	22	300	50	60	48,000	Road	0	Road/houses
Arakawa Landslide	8	200	150	200	40,000	River	0	River/houses
Kanaya Landslide	9	150	170	30	29,000	4 houses	3	Houses
Hanokidaira Landslide	12	190	60	120	31,000	11 houses	13	Houses
Kitanoiri Landslide	13	110	150	40	49,000	Trees	0	Rice fields
Yabeya Landslide	13	150	400	60	35,000	Trees	0	Forest
Kaiya Landslide*	19	75	125	60	24,000	3 houses	4	River
Oridate Residential Area	23	230	Small	170	25,000	50 houses	0	School

the 2011 Tōhoku Earthquake was approximately three times greater than the maximum PGAs recorded during 2004 Niigata and 2008 Iwate-Miyagi Earthquakes. The most common characteristic of the landslides triggered by the 2011 Tōhoku earthquake was large run-out distances. This could cause significant damages if the landslides occurred in the heavily populated areas.

3 Case Study 2—Landslides Triggered by 2015 Gorkha Earthquake

The M_w 7.82015 Gorkha Earthquake struck Nepal on 25 April 2015 at 06:11:26 UTC (11:56:26 local time). The epicenter was located at Barpak, Gorkha, approximately 80 km northeast of Kathmandu. The hypocenter was at the depth of 8.2 km. There were two aftershocks of M_w 6.6 and larger within 48 h of the main shock, followed by hundreds of aftershocks located east of the hypocenter. The magnitude of the aftershocks decayed with time until the largest aftershock with Mw 7.3 occurred 17 days after the main shock on 12 May 2015 (referred to as the aftershock throughout this paper). Over 400 aftershocks, between M_w 4.0 and M_w 5.0, were recorded within a year after the main shock. The earthquake killed over 9000 people, injured over 22,000 people, resulted in a financial loss of over $7 billion, and left over 3.5 million people homeless. The earthquake fully or partially damaged approximately 1.1 million houses (Government of Nepal Disaster Risk Reduction Portal 2016).

The main shock and aftershocks triggered thousands of co-seismic landslides that damaged many buildings and hydropower stations, temporarily obstructed transportation networks throughout the region and temporarily blocked the natural flow of rivers. Reports indicate that landslides were the direct cause of over 400 fatalities during and after the earthquake. The features and damages made by the main shock and associated aftershocks are available in the Geotechnical Extreme Events Reconnaissance (GEER) report (Hashash et al. 2015; Moss et al. 2015), United States Geological Survey (USGS) open file report (Collins and Jibson 2015; Collins 2015), and Tiwari et al. (2017a, b, c). Seismological details of this earthquake are available in Avouc et al. (2015), Bilham (2015), Elliott et al. (2016), Gardin et al. (2015), Liang and Zhou (2016), and Lindsey et al. (2015).

Tiwari et al. (2017a, b, c) performed comprehensive study to characterize the landslides triggered by the 2015 Gorkha Earthquake and its aftershocks. Their study area expands from 84°20′ to 86°30′ E longitude and 27°20′ to 28°40′ N latitude, i.e., a few kilometers west of the epicenter of the main shock to a few kilometers east of the epicenter of the Mw 7.3 aftershock. The study area covers 11 districts including Gorkha, Rasuwa, Dhading, Nuwakot, Lalitpur, Kathmandu, Bhaktapur, Makawanpur, Sindhupalchowk, Dolakha, and Ramechhap out of a total of 76 districts in Nepal. The study area begins in the Gorkha district in the west and extends to the Ramechhap district in the east.

Total length, width, and area of the study area are approximately 238 km, 110 km, and 26,200 km^2, respectively. The study area extends from the elevation of 60 m in south to 8387 m in the north within a north–south distance of approximately 100 km. The ground slope ranges from very flat terrains to stiff cliffs. Majority of the study area consists of medium to steep relief, bisected by thousands of small or medium sized streams and hundreds of rivers. The study area also parallels the estimated major fault rupture surface, which is roughly rectangular in shape (Collins and Jibson 2015).

3.1 Geology of the Study Area

As summarized in Tiwari et al. (2017a, b, c), the Himalayan Range was formed as a result of collision between the Indian

plate and Eurasian plate about 50 mya (Copley et al. 2010). The collision led to a large crustal shortening, resulting into the development of the Himalaya, where the mountain-building process is still ongoing (Hagen 1969). This youngest mountain range in the world is southward convex and extends for over 2400 km in the east–west direction. The Himalayan range and its south margin can be broadly divided into a number of longitudinal tectonic divisions. The 2015 Gorkha earthquake-affected region of central Nepal consists of the Lesser Himalayan Sequence, Higher Himalayan Crystallines, and the Tibetan–Tethyan Sediments (Gansser 1964; Dhital 2015). These major geologic divisions are further classified into various lithostratigraphic units. Tiwari et al. (2017a, b, c) elaborated the geology of the study area in more detail.

3.2 Climatic and Meteorological Conditions of the Study Area

Tiwari et al. (2017a, b, c) summarized the climatic and meteorological conditions of the study area. Nepal experiences four different seasons. Spring ranges from March to May, whereas summer, autumn, and winter typically span from June to August, September to November, and December to February, respectively. Low land in Terai experiences warm and humid sub-tropical climate temperature ranging from 22 to 27 °C and 10 to 15 °C in summer and winter, respectively. In contrast, the high-altitude experiences alpine climate with summer and winter temperatures ranging from 5 to 15 °C and less than 0 °C, respectively.

The annual precipitation of the country ranges from 500 to 5000 mm, with the national average annual precipitation of approximately 1400 mm. Southern Terai region experiences 1000–2500 mm of annual precipitation, whereas the central hilly region experiences 1700–3000 mm of annual precipitation. Almost 80% of the annual precipitation occurs within the 4 months of the monsoon season, spanning from June to September. Tiwari et al. (2017a, b, c) presented the monthly precipitation data prior to the Gorkha earthquake and 30-year mean and standard deviation for the same period for several stations within the study area. According to Tiwari et al. (2017a, b, c), the minimum, average, and maximum precipitation values for a year prior to the earthquake event at nine rain gauge stations that are spread throughout the study area were 566, 1464, and 2117 mm, respectively (Nepal Department of Hydrology and Meteorology 2016). The 30-year minimum, average, maximum precipitation values within the same stations and same period were 555, 2035, and 3825 mm, respectively. Likewise, 3-month antecedent rainfall in those stations prior to the Gorkha Earthquake and the 30-year mean were 94 and 123 mm, respectively. Similarly, the average 4-month monsoon precipitation (June to September 2014) prior to Gorkha earthquake and 30-year average were 1147 and 1661 mm, respectively. This clearly shows that the slopes were not exposed to relatively high amounts of precipitation prior to the earthquake. This implies that the number of landslides could increase significantly if the antecedent precipitation or the monsoon precipitation would have been similar to the 30- year mean precipitation.

3.3 Seismic Ground Shaking from the Main Shock

The earthquake occurred as a low-angle subduction event along the interface of the Indian plate and overriding Eurasian plate to the north. Strong shaking was felt throughout the study area during the earthquake event. Ground motion intensity in terms of horizontal PGA, presented by the USGS, was considered in this study as this ground motion parameter that most closely corresponds to the initiation of landslides on shallow and loose soil deposits throughout the study area. The PGA from the main shock varied in the study area from ~0.09 to ~0.76g and from ~0.04 to ~0.86g for the aftershock (Tiwari et al. 2017a, b, c). While there was a general attenuation of ground motion induced by the main shock towards the east, the intensity of shaking was not uniform and localized high intensity zones were found near the Gorkha, Dhading, and Sindhupalchowk districts. The intensity of shaking from the aftershock was strongly localized in a high intensity zone near the Dolakha district. Distributions of the PGAs (modified from USGS) within the study area due to the M_w 7.8 2015 Gorkha earthquake and M_w 7.3 major aftershock are presented in Tiwari et al. (2017a, b, c).

3.4 Methodology for Data Collection and Analysis

Tiwari et al. (2017a, b, c) developed the landslide database during the post-earthquake field reconnaissance effort using ground- and helicopter-based surveys and also by examining the high-resolution images from Digital Globe, US Department of State Geographer, CNES/Astrium, and Landsat in a Google Earth platform. A multi-team field reconnaissance of the meizoseismal region took place in three phases—from 6 to 31 May 2015, 2 to 12 August 2015, and 14 to 21 August 2015. Automobile and foot surveys were performed in Kathmandu, Lalitpur, Bhaktapur, Dhading, Gorkha, Kabhre, Nuwakot, Rasuwa, Dolakha, and Sindhupalchowk districts in addition to a total of 32 h that were spent for aerial surveys using helicopters throughout the study area and beyond. The Google Earth platform was used in this study due to the ease, rapidness, and effective-

ness to promptly and accurately identify disaster areas to focus post-earthquake rescue efforts. The co-seismic landslides identified through the high-resolution Google Earth images of the study area were verified with the data obtained from the field or helicopter surveys.

Tiwari et al. (2017a, b, c) identified 14,670 total landslides of which 3400 were larger than 100 m^2 in size. While the details of the distribution of those landslides throughout the study area—triggered separately by mainshock and aftershock—and their correlations with various topographical, geological, and seismological factors are available, in Tiwari et al. (2017a, b, c), this paper only describes the characteristics of some of those landslides. It is noteworthy that during some isolated occasions prior to this event, a single landslide killed over 100 people. For example, Jure Landslide that occurred on August 5, 2014 due to heavy rainfall blocked the Sunkoshi River and killed more than 168 people.

Although landslides in Nepal typically occur during the monsoon season, there are some recorded earthquake induced landslide events in the past such as the Okharpauwa landslide, Tigaun Landslide, and Ilam Landslide. The 2015 Gorkha earthquake occurred 2 months prior to the monsoon season and did not trigger as many landslides as expected. However, the April 29, 2015 main shock and May 12 aftershock did trigger some devastating landslides that killed hundreds of people, blocked several roads, buried villages, and dammed natural rivers. Presented below are the characteristics of the co-seismic landslides triggered by the 2015 Gorkha Earthquake and its aftershocks.

Fig. 51 Landslides along river back opposite from Prithivi Highway

Fig. 52 Landslide along an irrigation channel located opposite to the Prithivi Highway

3.5 Landslides Along Highways

There were several highways impacted by the earthquake-induced landslides, while others were not affected much. For example, Prithivi Highway, that connects Kathmandu with a touristic town of Pokhara along which the epicenter of the 2015 Gorkha Earthquake mainshock lies almost at the mid-length, did not experience large landslides during the event. However, there were isolated rockslide cases along the slopes of a few riverbanks and irrigation channel alignments (Figs. 51 and 52). On the other hand, another highway, the Araniko Highway that connects Kathmandu to the China border at Kodari in the east, experienced large earthquake shakings both during the main shock and aftershocks, suffered among the most severe landslide damages. Typical first-time landslide triggered along the road is presented in Fig. 53. Translational landslides and rock falls blocked the road in numerous locations (Fig. 54). Several riverbank failures, downslope of the roads, threatened to undermine the stability of the road (Fig. 55). As this highway traversed north along the Sunkoshi River, the roadway was increasingly damaged by rock slides resulting from joint plane failures, emanating from steeper and higher slopes along the roadway (Fig. 56).

Fig. 53 Typical co-seismic landslide along the Araniko Highway

The town of Kodari was destroyed by large rockfalls from the near vertical slopes that sent boulders up to 4 m in diameter through the buildings and vehicles along the narrow roadway. Some of the landslides along the highway are reactivated landslides (Fig. 57). The major issue identified along

Fig. 54 Typical disrupted landslides that blocked the Araniko Highway at multiple locations

Fig. 55 Typical failure along Araniko Highway due to river undercutting and earthquake shaking

Fig. 56 Typical joint plane failure that threatened to block the Araniko Highway

Fig. 57 Typical reactivated landslide along the Kodari Highway that threatened to dam the Sunkoshi River

this road sector is the potential of large landslides and slope failures triggered on top of the ridge that may not only block and damage the road, but also have the potential to block the natural flow of Sunkoshi River (Fig. 58).

Another highway that was significantly affected by many rockslides and rockfalls was the Lamosangu-Manthali Highway that passes through the access road of the largest water supply project of the country—the Melamchi Water Supply Project. This highway was impacted mainly by the M_w 7.3 aftershock as the epicenter was located in close proximity to this highway. The boulders that slid down were very large in size (Figs. 59 and 60) and caused massive destruction. A large-scale rockslide was observed that could potentially

Fig. 58 Landslides along the top of the ridge that are threatening Araniko Highway and Sunkoshi River

Fig. 61 Fresh rockfall observed at the Melamchi Access Road during field visit

Fig. 59 Typical size of the bolder observed after the 2015 Gorkha Earthquake along the Melamchi Road

Fig. 60 Typical rockfall that blocked Melamchi Road at multiple locations

block the river since its head scarp goes to the top of the mountain several hundred meters above the road (Fig. 61). On the other hand, the access road of Upper Tamakoshi Hydropower Project, the largest hydropower project in the country, specifically along the Singati-Lama Bagar Sector (Fig. 62), was disrupted at multiple locations with several landslides. The project was non-functional for several months following the earthquake. Majority of the road alignment along this road section was lost due to the landslides. As the road is narrow and was constructed in very steep topography, the 2015 Gorkha Earthquake and its May 12 aftershock caused serious damage. Moreover, alignments of several rural roads were also affected by seismically induced landslides (Fig. 63). Likewise, the Kathmandu—Dhunche—Rasuwagadi Road sector that connects to the Chinese border, had many dry landslides triggered by the earthquake (Fig. 64) especially along the sector from Niwakot to Rasuwagadi. Many of those landslides fully or partially blocked the Trishuli River and its tributaries (Fig. 65) and also affected some villages (Fig. 66).

3.6 Landslides Along Riverbanks

Several locations near Kathmandu Valley were affected by earthquake-induced landslides along the river bank (Fig. 67). Similarly, there were several locations along the Trishuli River near the Kathmandu-Rasuwagadi Road, up to the Nepalese border with China, where massive landslides fully or partially blocked the Trishuli River (as previously shown in Fig. 65). Landslides were also observed at both sides of the Langtang River, enhancing the possibility of blocking the river during monsoon season (Fig. 68). A significant amount of loose sediment was observed upstream of the Langtang River as well as in the mountains near Kyamgjon Kharka and the Yala Peak (Fig. 69). Moreover, loose debris/sediments were also observed along the tributaries of the Langtang River, especially at or near the top of the peaks throughout Langtang and Kyamgjong Kharka and beyond. This showed

Fig. 62 Damages sustained by the Upper Tamakoshi Hydropower Project Access Road due to the 2015 Gorkha Earthquake

Fig. 63 Typical landslides triggered by the 2015 Gorkha Earthquake along the rural road alignments

the potential of another debris flow event as the snow melted or during the rainy season. Likewise, there were many large-scale landslides observed along the Tributaries of Marshyangdi River including Daraudi River as well as near Dhawa, Baluwa, and Barpak areas that threatened not only the river, but also some hydropower stations located along the river (Fig. 70).

A massive dry landslide occurred on May 24, 2015 on Kali Gandaki River in Myagdi District, nearly 100 km west from the epicenter. The landslide buried a village with 25 houses but, fortunately, did not cause any human casualties. The area was evacuated right before the landslide occurred when several signs of landslides were observed after the April 25 main shock and its subsequent aftershocks. The landslide blocked the Kali Gandaki River creating a landslide dam with nearly 150 m deep water impoundment extending over a kilometer in length. The water started overtopping the dam 16 h after the landslide without causing major damage or casualties in the downstream towns (Hashash et al. 2015).

3.7 Landslides Near Hydropower Stations

Both upstream and downstream areas from the dam site of the Upper Tamakoshi Hydropower Project were affected by multiple rock fall events (Fig. 71). The sizes of the boulders that rolled downslope and travelled over 100 m distance shows that the ground shaking level at this location was high (Fig. 72). However, ground motion observation data was not available in this area. Likewise, several hydropower projects

Fig. 64 Typical landslides triggered by the 2015 Gorkha Earthquake along the Nuwakot-Dhunche-Rasuwagadi Road

Fig. 66 Typical landslides triggered by the 2015 Gorkha Earthquake along the Dhunche Road that was threatening the community

Fig. 67 Typical landslides triggered by the Gorkha Earthquake along rivers near Kathmandu Valley

Fig. 65 Typical landslides triggered by the 2015 Gorkha Earthquake along the Dhunche Road that has partially blocked the Trishuli River

Fig. 68 Typical landslides triggered by the 2015 Gorkha Earthquake along the banks of Langtang River

Fig. 69 Loose debris observed along the Langtang River catchment

Fig. 72 Typical size of boulders dislodged by the earthquake from the slopes near the Upper Tamakoshi Hydropower Project

Fig. 70 Typical landslides triggered by the 2015 Gorkha Earthquake along the Maryangdi River

Fig. 71 Typical rockslide observed at Upper Tamakoshi Hydropower Station triggered by the Gorkha Earthquake

such as Chilime Hydropower project, Rasuwagadi Hydropower project and Trishuli Hydropower project were seriously affected by the landslides (Hashash et al. 2015).

3.8 Landslides Along Community

There were several large-scale landslide fissures that were observed at Ramkot and other areas in the vicinity of Kathmandu Valley (Fig. 73). A continuous fissure with more than 15 cm wide cracks that was triggered by the earthquake posed threaten to the settlement below the ridge. Likewise, a few villages were observed either above or below the earthquake-triggered landslides at the Syaprubesi-Rasuwagadi aerial route. Their reactivation during the monsoon could significantly affect those villages (Hashash et al. 2015).

3.9 Debris Avalanche

Right after the main shock of the Gorkha Earthquake, a large debris avalanche buried over 400 people in the Langtang Village located at N 28° 12′ 55.43″, E 85° 30′ 8.95″ and alt 3297 m amsl (Fig. 74). The estimated length and width of the debris deposits was 900 m and 400 m, respectively (Fig. 75). The estimated amount of debris volume based on the aerial observation is 2.5 million m^3, sourced approximately 3 km above the current debris depositional area with an elevation difference of approximately 1800 m (Fig. 76).

Part of Langtang Village, a village well known among the trekkers, that was distributed over an area of 600 m × 200 m, was buried under the debris. The remaining part of the village was destroyed by the debris flow induced winds. The wind completely uprooted and flattened the trees of the left

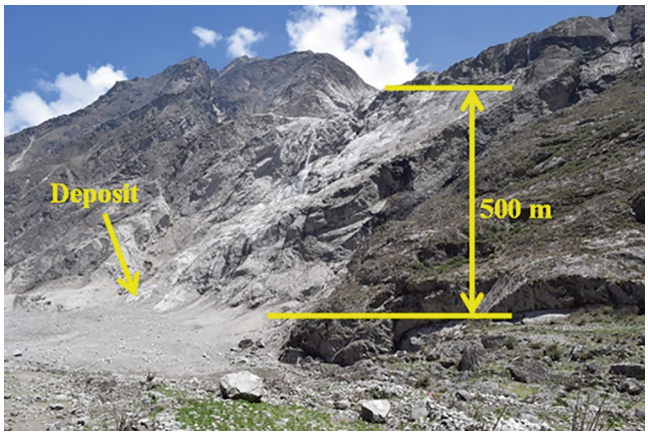

Fig. 74 Aerial view of the Langtang Debris Avalanche

Fig. 73 A long crack observed along the mountain ridge at Ramkot Village near Kathmandu

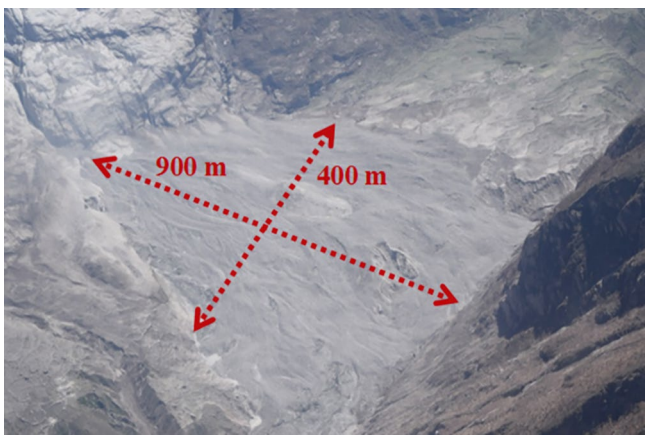

Fig. 75 Accumulated debris mass of the Langtang Debris Flow

bank of the river along the flow direction (Fig. 77). Likewise, the buildings along the left side of the debris avalanche area were also blown away. The debris mass blocked the Langtang

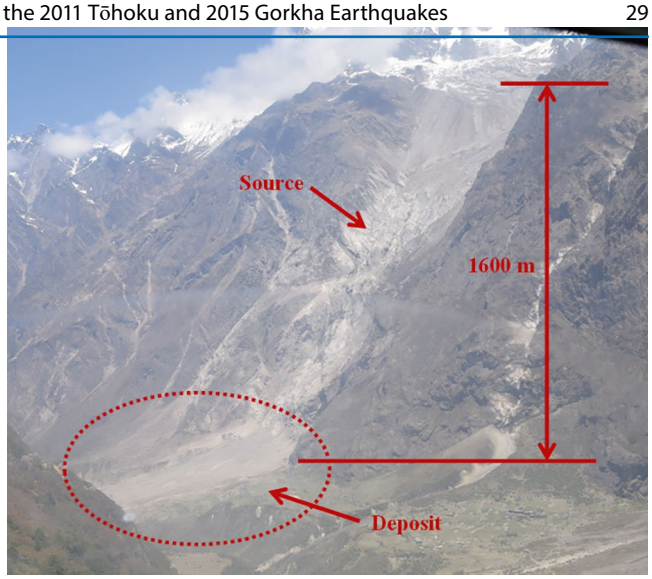

Fig. 76 Source of Landslide Debris Avalanche

Fig. 77 Trees along the left bank of Langtang River flattened due to airborne pressure initiating from the debris avalanche

River completely although the river could pass under the debris mass preventing the ponding of water (Fig. 75). Several cracks were still observed on the left bank of the river, which had potential to slide down in future. The debris materials were very loose and wet at the time of the field visit. More than 95% of the debris materials were finer than 0.5 m. The details of this avalanche are available in Tiwari et al. (2017a, b, c).

3.10 Landslide Dams

There were several landslide dams observed throughout the study area. Those dams are listed in Tiwari et al. (2017a, b, c), but a few are presented in this article. One among those landslide dams was observed near Barpak (Fig. 78). Several landslide dams were observed along Besisahar-Manang-

Fig. 78 Typical landslide dam triggered by the Gorkha Earthquake

Fig. 79 Loose sediments along the river banks near Manang

Fig. 80 Landslides along the river bank damming the streams

Fig. 81 Loose debris and multiple landslides along the watershed threatening to block the river near Lake Tilicho, Manang

Fig. 82 Landslides observed along the Budi Gandaki River, near Pork

Pork route. Manang area, especially at the altitude higher than at Chame Village, is composed of very loose sediments even in the mountain slope (Fig. 79). The 2015 Gorkha Earthquake dislodged some of those sediments and caused a blockade of Marshayngdi River a few kilometers upstream of Higde Airport (Fig. 80).

Very loose debris masses with the potential to slide down and block the Marshangdi River were observed along the route to Lake Tilicho (Fig. 81). Likewise, many landslides were observed along the banks of Budi Gandaki River towards Prok (Fig. 82). Those landslides partially blocked the river and damaged the local road connecting Arughat to Arukhet at several locations (Fig. 83). There were many large-scale landslides between Arukhet to Prok that partially blocked the Budi Gandaki River (Fig. 84). A tributary of Budi Gandaki River near Prok was blocked at several locations by the landslide mass triggered by the 2015 Gorkha earthquake (Fig. 85). A medium-scale landslide dam was observed at Pandise in Sertung Village of the Dhading District (Fig. 86). The landslides occurred at Ankhu Khola, a tributary of the Budi Gandaki River. Slope of the tributary was approximately 30–35°. Big boulders slid down along the tributary of Ankhu Khola right after the main shock and blocked the river for about a week (Fig. 87). The landslide dam was naturally breached.

Fig. 83 Landslide mass blocking roads and threatening to block stream flow

Fig. 84 River blocked by the landslide debris

Fig. 85 A portion of the river blocked by landslide debris

3.11 Landslides Along Mountain Ridges

Mountains at the ridges of the Sunkoshi River are highly fractured exhibiting the possibility of large landslides during the monsoon season, which had potential to block Sunkoshi River and its tributaries. Some of those landslides have large size boulders vulnerable to slide any time during a wet season or any large earthquake event. Several of those boulders threatened buildings either below or above the landslide area.

Fig. 86 Landslide dam created at Pandise area along the Aankhu Khola

Fig. 87 Landslide debris responsible to block Aankhu Khola and trigger the Pandise Landslide Dam

3.12 Landslides at the Epicenter

A landslide scarp was observed at the north-east edge of Barpak village (Fig. 88), which is the epicenter of the 2015 Gorkha Earthquake. Similar scarps were observed at the south-west edge of the village. Although these landslides did not pose significant threats to Barpak Village at the time of the earthquake, failure of these steep slopes may affect the village in future.

3.13 Lokanthali Ground Failure

During the Gorkha Earthquake, severe seismic damage was experienced at a site locally known as Lokanthali, which is located about 1 km east of Tribhuvan International Airport in Kathmandu, Nepal (27°40′28.1″ N, 85°21′44.6″ E). Evidence of ground failure was observed along a ridge (consisting of recent lacustrine terrace deposits) for a distance of about 1 km, consisting of fissures (up to 2-m deep) and large tension cracks (with vertical offsets up to 1.4 m) along the top of the small ridge (Figs. 89, 90 and 91). Of particular interesting about Lokanthali that prompted the additional investigation is that a ground failure with landslide features occurred in a gentle sloping terrain environment, with an average inclination of 4°, during an earthquake that produced only relatively moderate ground accelerations.

The site was investigated by several post-earthquake reconnaissance teams including Geotechnical Extreme Events Reconnaissance (GEER), Hashash et al. (2015), that mapped the relatively narrow zone of deformation along the ridge. The vertical displacements were typically on the order of 1 m and horizontal displacements were about 0.5 m. Moss et al. (2015) and Tiwari and Pradel (2017) described the site conditions in more detail. Due to the elongated nature of the zone of ground failure (i.e., narrow and longitudinally constrained), the site was studied as a possible trace of the Himalayan Frontal Thrust Fault after the Gorkha earthquake. Interferometric Synthetic Aperture Radar, ground observations, and aftershock, revealed that the observed features along the ridge were not consistent with deep-seated tectonic displacements, but were instead, most likely the result of local site conditions and ground shaking.

Based on the lack of evidence for liquefaction and the observation that the slip surface extended into weak clays, Hashash et al. (2015) initially concluded that Lokanthali was likely affected by cyclic failure, i.e., the structural breakdown of clay particles (Moss et al. 2015). Field investigations, laboratory test, and numerical simulation of this ground failure site by Tiwari et al. (2017a, b, c) showed that the site was most likely affected by seismically induced landslide movements. Results of the study is presented in detail in Tiwari et al. (2017a, b, c).

Fig. 88 Several long landslide scarps observed at the ridge above Barpak after the 2015 Gorkha Earthquake

Fig. 89 Deformation of Araniko Highway at Lokanthali due to Gorkha Earthquake

Fig. 90 Cracks observed along the Lokanthali ground failure area

4 Comparison of Landslides Triggered by the Two Events with Database of Historical Co-Seismic Landslides

As described in detail in previous sections, the 2011 Tōhoku Landslide triggered a large number of disrupted landslides and lateral spreads as well as a reasonably large number of coherent landslides. However, majority of the landslides triggered by 2015 Gorkha Earthquake were disruptive landslides

Fig. 91 Tilted buildings along the main scarp of the Lokanthali ground failure site

in the form of rockfall, rock slump and dry soil slump. The size of the landslides triggered by the Tōhoku Earthquake were significantly larger than that triggered by the 2015 Gorkha Earthquake. This can be attributed to the magnitude and larger peak ground accelerations of the Tōhoku Earthquake. One of the characteristics that was observed on the landslides triggered by the Tohoku Earthquake and was not observed on landslides triggered by the Gorkha Earthquake were large run-out distances and slickensides. This can be attributed to the type of soil in the area and reactivation of old landslides as well as the significantly larger shaking intensity of the Tōhoku Earthquake.

Tiwari and Ajmera (2017) performed an extensive study on landslides triggered by earthquakes from 1920 to 2015. Using 35 co-seismic landslide inventories reported in the literature, they developed correlations between—(a) areas affected by the co-seismic landslides and earthquake magnitude, (b) areas affected by the co-seismic landslides and maximum peak ground acceleration recorded for the earthquake, (c) number of co-seismic landslides triggered and earthquake magnitude, (d) number of co-seismic landslides—overall and larger than 100 m^2 size—triggered and recorded maximum peak ground acceleration. Tiwari and Ajmera (2017) emphasized that the best correlation is established with the maximum peak ground acceleration and not the magnitude of the earthquake.As presented in Fig. 92, the area affected by Gorkha earthquake fits fairly well with the relationship in Keefer (1984) with magnitude of the earthquake. However, the reported area is significantly lower for the 2011 Tōhoku Earthquake. This can be attributed to the fact that the Wartman et al. (2013) data does not cover the entire region affected by the earthquake or include small

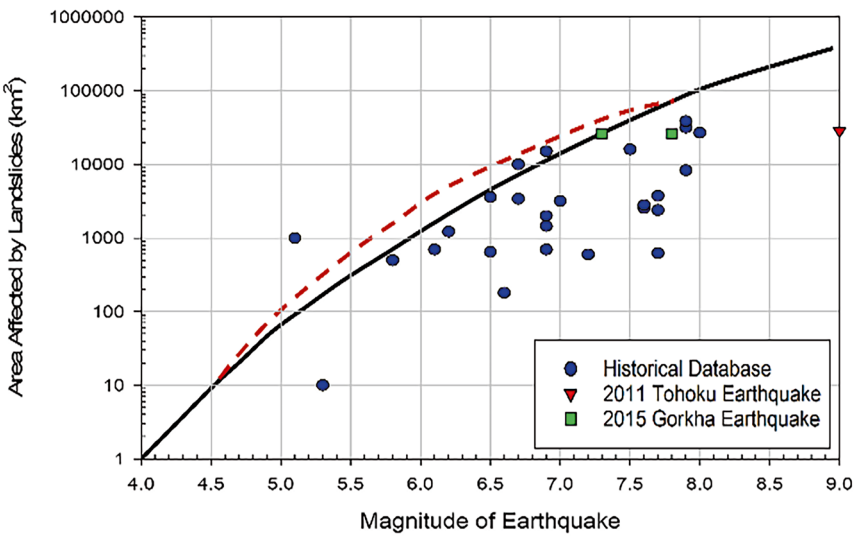

Fig. 92 Relationship between the total area affected by the earthquake-induced landslides and the magnitude of the earthquake; Solid line is the relationship proposed by Keefer (1984) and dashed line is the revision to the relationship proposed by Rodríguez et al. (1999). (Modified from Tiwari and Ajmera (2017))

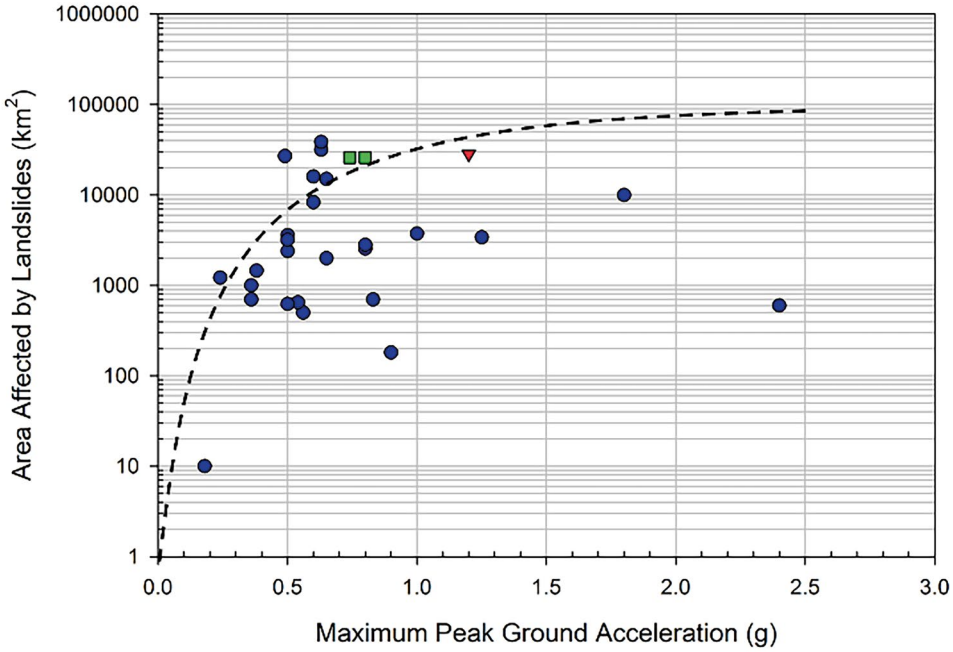

Fig. 93 Relationship between the total area affected by the earthquake-induced landslides and the peak ground acceleration. (Modified from Tiwari and Ajmera (2017))

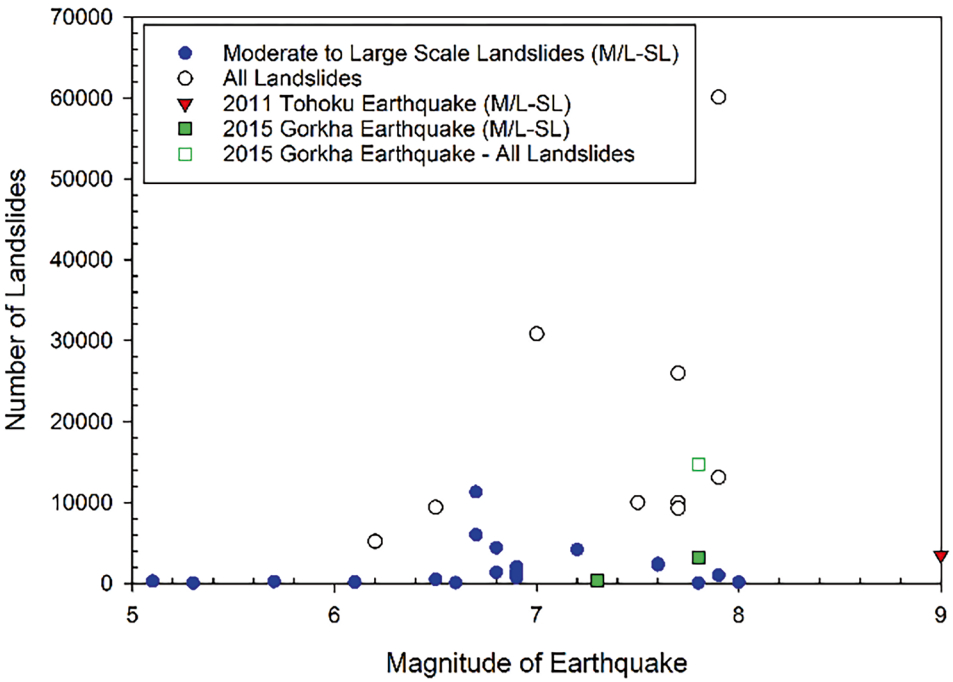

Fig. 94 Relationship between the number of landslides triggered and the earthquake magnitude. (Modified from Tiwari and Ajmera (2017))

sized landslides. As presented in Fig. 93, the total area affected by the landslides triggered by the 2015 Gorkha Earthquake fits well with the relationship developed by Tiwari and Ajmera (2017) between the affected area and the maximum peak ground acceleration. However, for the same reasons explained earlier, the affected area recorded for the landslides triggered by the 2011 Tōhoku Earthquake was significantly lower than the predicted area. Likewise, as presented in Fig. 94, the number of landslides triggered by both earthquakes fit well when compared to the magnitude of the earthquake, although the relationship was not clearly defined. Figure 95 shows that the best relationship was developed between the number of co-seismic landslides and maximum recorded peak ground acceleration due to the earthquake. The number of landslides from the Gorkha Earthquake fit well with the correlation while that from the Tōhoku Earthquake were well below for the reason discussed earlier.

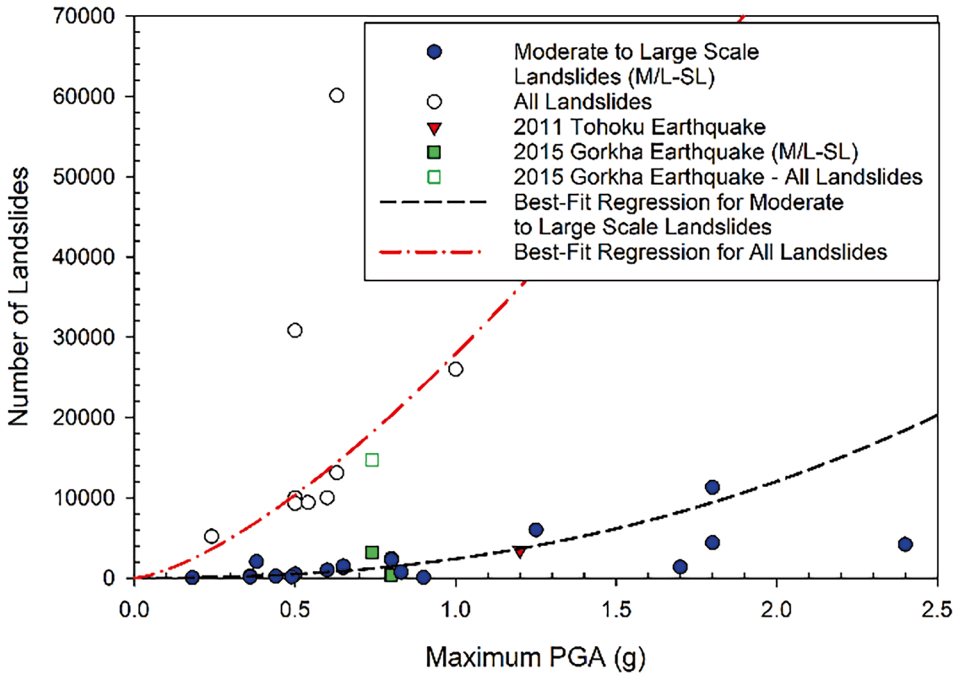

Fig. 95 Relationship between the number of landslides triggered and the peak ground acceleration. (Modified from Tiwari and Ajmera (2017))

5 Conclusions

While landslides are triggered by several factors, earthquakes are considered among the frequent causes. The area impacted by, economic impacts, and human casualties due to earthquake-induced landslides can be significantly large in comparison to landslides triggered by isolated rainfall incidences. However, the impact can significantly larger if the earthquake occurs during or right after the rainy season. This paper explains in detail about the negative impact of coseismic landslides, correlation between magnitude as well as maximum peak ground acceleration and total area as well as number of triggered landslides. The number of landslides triggered by the Gorkha Earthquake, both landslides of all sizes and those landslides larger than 100 m^2 size, fit well with the relationships developed by Tiwari and Ajmera (2017). However, as the database developed from Wartman et al. (2013) only partially covers the area affected by the 2011 Tōhoku Earthquake, the number and area of the triggered landslides are slightly lower than predicted by Tiwari et al. (2017a, b, c).

As the magnitude and maximum peak ground acceleration associated with the 2011 Tōhoku Earthquake were both high and the shaking occurred in relatively young geological formations, it triggered significant number of disrupted, coherent, and lateral spread type landslides. However, due to the smaller magnitude and peak ground accelerations as well as the affected geological formation, majority of the landslides triggered by the 2015 Gorkha Earthquake were disruptive landslides despite the fact both earthquakes occurred in dry season. The Gorkha earthquake did not reactivate existing landslides whereas Tōhoku Earthquake reactivated many, including several fatal landslides. The Tōhoku Earthquake triggered many long-run out landslides in volcanic depositional areas, exhibiting clear slickenside surfaces, which was not the case for the Gorkha Earthquake. While the property loss due to both landslides was significantly high, human casualties due to landslides in Gorkha Earthquake was significantly larger in comparison to those from the Tōhoku Earthquake. Despite the large magnitude and high ground acceleration of the Tōhoku earthquake, the number of landslides triggered in the studied area were significantly low in comparison to three past major earthquakes in the vicinity. This can be attributed to the fact that the earthquake occurred during the dry season, 3 months prior to the rainy season. Had this earthquake occurred 3 months later, it could trigger a significant number of landslides and other slope related disasters. This is true for the Gorkha Earthquake as well. Although the earthquake triggered a significantly large number of disrupted landslides, the number and size of the landslides could be significantly large if the earthquake have occurred 3 months later. The information presented in this paper will be valuable to understand the characteristics of earthquake induced landslides.

This review paper is developed based on the extensive work of the author and his co-authors in numerous papers. As such, the full credit for this manuscript goes to his co-authors on various publications including but not limited to: Dr. Joseph Wartman (University of Washington), Dr. Daniel Pradel (Ohio State University), Dr. Beena Ajmera (Iowa State University), Dr. Youssef M.A. Hashash (University of Illinois Urbana Champion), Dr. Robb E. S.

Moss (California Polytechnic University, San Luis Obispo), Dr. Domniki Asimaki (California Institute of Technology), Mr. Kevin B. Clahan (Lettis Consultants International, Inc.), Dr. D. Scott Kieffer (Graz University of Technology), Ms. Amy Macdonald (Thornton Tomasetti), Mr. Chris M. Madugo (Pacific Gas and Electric), Dr. H. Benjamin Mason (Oregon State University), Dr. Menzer Pehlivan (MPERA Group), Dr. Deepak Rayamajhi (Oregon State University), Dr. Indra Acharya (Tribhuvan University) and Dr. Basanta Adhikari (Tribhuvan University).

Additional detailed information about this manuscript is available in: Pradel et al. (2011, 2012, 2013a, b), Tiwari et al. (2012, 2013, 2017a, b, c, 2018), Wartman et al. (2013), Hashash et al. (2015), Moss et al. (2015), Tiwari and Pradel (2017), and Tiwari and Ajmera (2017).

Acknowledgements The author would like to acknowledge the support from the following organizations or individuals during the post-earthquake reconnaissance visits of which he was a member or was a lead/co-lead of the team: (a) American Society of Civil Engineers (ASCE) Geo-Institute, (b) Japan Landslide Society, (c) Professor Keijo Ugai, Professor Wakai, Dr. Sai, and Dr. Yamada (Gunma University), (d) Professor Higaki (Hiroshaki University), (e) Professor Miyagi (Tohoku Gakuin University), (f) Professor Chiba (Sendai Polytechnic University), (g) Dr. Ranjan Kumar Dahal (Tribhuvan University), (h) Brian D. Collins (USGS), (i) Randall Jibson (USGS), (j) Eric M. Thompson (USGS), (k) Sachindra Dahal (University of Illinois, Urbana-Champaigh, UIUC), (l) Diwakar Khadka (MT), (m) Sital Uprety (UIUC), (n) Maja Bitenc (TUGraz), (o) Mirjam Ziselsberger (TUGraz), (p) Sanjib Basnet (TU), (q) Sangita Rai (TU), (r) Surendra Awasthi (TU), (s) Gerhard Lauk (TUGraz), (t) Smriti Dhital, and (u) Geotechnical Extreme Event Reconnaissance (GEER).

References

Avouc J-P, Meng L, Wei S, Wang T, Ampuero J-P (2015) Lower edge of locked Main Himalayan thrust unzipped by the 2015 Gorkha earthquake. Nat Geosci 8:708–711

Bilham R (2015) Raising Kathmandu. Nat Geosci 8:582–584

Collins BD (2015) Video data files to accompany USGS OFR 2015-1142—assessment of existing and potential landslide hazards resulting from the April 25, 2015 Gorkha, Nepal earthquake sequence. U.S. Geol Surv Data Release. https://doi.org/10.5066/F7X928BN

Collins BD, Jibson RW (2015) Assessment of existing and potential landslide hazards resulting from the April 25, 2015 Gorkha, Nepal Earthquake Sequence. U.S. Geological Survey Open-File Report 2015-1142. https://doi.org/10.3133/ofr20151142

Copley A, Avouac J-P, Royer J-Y (2010) India–Asia collision and the Cenozoic slowdown of the Indian plate: implications for the forces driving plate motions. J Geophys Res 115:B03410

Dhital MR (2015) Geology of the Nepal Himalaya. Regional perspective of the classic orogeny. Springer, Cham. 498 pages

Elliott JR, Jolivet R, González PJ, Avouac J-P, Hollingsworth J, Searle MP, Stevens VL (2016) Himalayan megathrust geometry and relation to topography revealed by the Gorkha earthquake. Nat Geosci 9:174–180

Gansser A (1964) Geology of the Himalayas. Interscience, New York

Gardin R, Vallée M, Satriano V, Lacassin R, Klinger Y, Simoes M, Bollinger L (2015) Rupture process of the Mw = 7.9 2015 Gorkha earthquake (Nepal): insights into Himalayan megathrust segmentation. Geophys Res Lett 42:8373–8382

Government of Nepal Disaster Risk Reduction Portal (2016). http://drrportal.gov.np/. Last accessed 22 Apr

Hagen T (1969) Report on the geological survey of Nepal. Volume 1: preliminary reconnaissance. Denkschiiften der Schweizerischen Naturforschenden Gesellschaft, Band LXXXVI/1

Hashash YMA, Tiwari B, Moss RES, Asimaki D, Clahan KB, Kieffer DS, Dreger DS, Macdonald A, Madugo CM, Mason HB, Pehlivan M, Rayamajhi D, Acharya I, Adhikari B (2015) Geotechnical field reconnaissance: Gorkha (Nepal) Earthquake of April 25 2015 and related shaking sequence. Geotechnical Extreme Event Reconnaissance GEER Association Report No. GEER-040. Version 1.1

Keefer DK (1984) Landslides caused by earthquakes. Geol Soc Am Bull 95:406–421

Liang G, Zhou N (2016) Background and reflections on Gorkha earthquake of April 25, 2015. Nat Hazards 81:1385–1392

Lindsey EO, Natsuaki R, Xu X, Shimada M, Hashimoto M, Melgar D, Sandwell DT (2015) Line of sight displacement from Alos-2 interferometry: Mw 7.8 Gorkha earthquake and Mw 7.3 aftershock. Geophys Res Lett 42:6655–6661

Moss R, Thompson EM, Kieffer DS, Tiwari B, Hashash YMA, Acharya I, Adhikari B, Asimaki D, Clahan KB, Collins BD, Dahal S, Jibson RW, Khadka D, Macdonald A, Madugo CLM, Mason HB, Pehlivan M, Rayamajhi D, Uprety S (2015) Geotechnical effects of the 2015 magnitude 7.8 Gorkha. Nepal Earthquake and Aftershocks, Seismological Research Letters, Seismological Society of America, 86

Nepal Department of Hydrology and Meteorology (2016). http://www.dhm.gov.np/. Last accessed 22 Apr 2016

Pradel D, Tiwari B, Wartman J (2011) Landslides triggered by 2011 Tohoku Pacific Earthquake. Geostrata 2011(September/October):28–32

Pradel D, Wartman J, Tiwari B (2012) Failure of Fujinuma Dam during the 2011 Tohoku Earthquake. In: 9th International conference on urban earthquake engineering/4th Asia conference on earthquake engineering, Japan

Pradel D, Wartman J, Tiwari B (2013a) Failure of the Fujinuma dams during the 2011 Great East Japan Earthquake. Geotechnical Special Publication, ASCE 231(1):1566–1580

Pradel D, Wartman J, Tiwari B (2013b) Impact of anthropogenic changes in liquefaction along Tone River during the 2011 Tohoku Earthquake. Natural Hazards Review, ASCE 15(1):13–26

Rodríguez CE, Bommer JJ, Chandler RJ (1999) Earthquake-induced landslides: 1980–1997. Soil Dyn Earthq Eng 18:325–346

Sassa K, Fukuoka H, Scarascia-Mugnozza H, Irikura K, Okimura T (1995) Landslides triggered by the Hyogoken-Nanbu Earthquake. Landslide News 9:2–5

Tiwari B, Ajmera B (2017) Landslides triggered by earthquakes from 1920 to 2015. Advancing Culture of Living with Landslides, Springer Nature 2(1):5–15

Tiwari B, Pradel D (2017) Ground deformation at Lokanthali, Kathmandu due to Mw 7.8 2015 Gorkha Earthquake. Geotechnical Special Publication, ASCE 278:333–342

Tiwari B, Pradel D, Wartman J (2012) Performance of slopes and dams in the Mw 9.0 Tohoku, Japan, earthquake. In: Second international conference on performance based design in earthquake geotechnical engineering, Italy

Tiwari B, Wartman J, Pradel D (2013) Slope stability issues after Mw9.0 Tohoku earthquake. Geotechnical Special Publication, ASCE 231(1):1594–1601

Tiwari B, Ajmera B, Dhital S (2017a) Characteristics of moderate to large scale landslides triggered by the Mw8 Gorkha earthquake and its aftershocks. Landslides, Springer Nature 14(4):1297–1318

Tiwari B, Ajmera B, Dhital S (2017b) Geological, topographical and seismological control on the co-seismic landslides triggered by the 2015 Gorkha Earthquake. Geotechnical Special Publication 278, ASCE:234–243

Tiwari B, Ajmera B, Dhital S, Sitoula NR (2017c) Landslides induced by the 2015 Gorkha Earthquake. Advancing Culture of Living with Landslides, Springer Nature 2(2):819–827

Tiwari B, Pradel D, Ajmera B, Yamashiro B, Diwakar K (2018) Landslide movement at Lokanthali during the 2015 earthquake in Gorkha, Nepal. J Geotech Geoenviron Eng ASCE 144(3):05018001 1-12

Towhata I, Goto H, Kazama M Kiyota T, Nakamura S, Wakamatsu K, Wakai A, Yasuda S, Yoshida N (2011) On gigantic Tohoku Pacific Earthquake in Japan. Earthquake News, Bulletin of the International Society for Soil Mechanics and Geotechnical Engineering 5, 2, April, 2011

UNDRR (2019) Global assessment report on disaster risk reduction 2019. United Nations Office for Disaster Risk Reduction

Wartman J, Tiwari B, Pradel D (2011) Japan earthquake/tsunami reconnaissance team 2 reports. ASCE

Wartman J, Dunham L, Tiwari B, Pradel D (2013) Landslides in Eastern Honshu induced by the 2011 Tōhoku Earthquake. Bull Seismol Soc Am 103(2B):1503–1521

Yagi H, Sato G, Higaki D, Yamamoto M, Yamasaki T (2009) Distribution and characteristics of landslides induced by the Iwate-Miyagi Nairiku earthquake in 2008 in Tohoku District, Northeast Japan. Landslides 6:335–344

Yamagishi H, Iwahashi J (2007) Comparison between the two triggered landslides in Mid-Niigata, Japan by July 13 heavy rainfall and October 23 intensive earthquakes in 2004. Landslides 4:389–397

From Sky to Safety: Unmanned Aerial Vehicles and Geomorphological Insights to Local-Scale Household Landslide Exposure

Maryjose Sánchez-Rojo, Ricardo J. Garnica-Peña, and Irasema Alcántara-Ayala

Abstract

Disasters associated with slope instability are a growing concern globally, particularly in regions like Mexico's Sierra Norte de Puebla (SNP), where natural and anthropogenic factors converge. This chapter examines the intersection of geomorphological hazards and socio-economic vulnerabilities, focusing on mass movement processes that pose significant risks to human settlements. Drawing on a case study from Tlatlauquitepec, Puebla, an Unmanned Aerial Vehicle (UAV) technology was employed to generate high-resolution aerial imagery, enabling a comprehensive assessment of landslide exposure. A detailed exposure map was created, classifying 358 properties into high, medium, and low-risk categories. The study revealed that 45.5% of the properties fall into the medium-risk category due to their location on or near steep slopes with a history of instability. The application of UAV technology and advanced 3D modelling, including developing Digital Surface Models (DSM) and Red Relief Image Maps (RRIM), highlighted the value of remote sensing tools in disaster risk assessment. This research underscores the need for targeted disaster risk management strategies, integrating technological innovations and socio-economic considerations to mitigate future hazards and improve resilience in vulnerable communities.

Keywords

Landslide exposure · Landslide awareness · Landslide disaster risk management · UAV technology · Local context

1 Introduction

Disasters associated with natural phenomena are complex processes that occur globally and have significantly impacted societies due to the presence of goods, services, and communities settled in high-risk areas.

In the global context, in just the last 50 years, factors such as urban and population growth, changes in the dynamics of human activities, climate change, and the worsening of issues like poverty and inequality have led to an exponential increase in both the occurrence and intensity of disasters (Kirsch-Wood et al. 2022).

In this sense, disaster risk associated with slope instability is a severe problem in Mexico and worldwide. According to data from EM-DAT (2024) and UNDRR (2013), mass movement processes are considered the second most significant geomorphological hazard in causing global deaths and the second leading cause of economic losses in the country.

These phenomena have also been classified as socio-natural hazards. Although slope instability can occur due to inherent conditions and factors of the natural landscape, it has also been exacerbated by human intervention and transformation of the environment, such as the construction of inadequate infrastructure and the drastic alteration of the landscape due to poor planning (Alcántara-Ayala et al. 2023).

This, combined with the creation of social inequalities and the dynamic and complex development of the social strata, has led to the establishment of conditions that make certain communities vulnerable to any hazard present in their environment and to the increase in areas highly susceptible to mass movement processes (Garnica-Peña and Alcántara-Ayala 2021).

M. Sánchez-Rojo
Faculty of Philosophy and Letters, Geography College, National Autonomous University of Mexico (UNAM), Mexico City, Mexico

R. J. Garnica-Peña · I. Alcántara-Ayala (✉)
Institute of Geography, National Autonomous University of Mexico (UNAM), Mexico City, Mexico
e-mail: garnica@geografia.unam.mx; ialcantara@geografia.unam.mx

B. Abolmasov et al. (eds.), *Progress in Landslide Research and Technology, Volume 4 Issue 1, 2025*, Progress in Landslide Research and Technology, https://doi.org/10.1007/978-3-031-89836-5_2

Currently, various territories and international organisations have addressed the problem related to disaster risk through an integrated approach that enables the development of strategies and action plans aimed not only at understanding and containing the hazard but also at generating information that allows for the identification of the factors that create risk and the implementation of prospective and corrective measures.

Disasters are defined as significant disruptions to the functioning of a community or society at any scale. These disruptions occur due to hazardous events interacting with factors like exposure, vulnerability, and capacity. As a result, disasters can lead to various impacts, including human, material, economic, and environmental losses.

In this regard, various authors have identified vulnerability and exposure as the primary factors to consider for the assessment and reduction of disaster risk, as the occurrence of a disaster is directly related to the impact a hazard may have on a population with varying degrees of vulnerability, occupying an area exposed to the effects of that hazard (Alcántara-Ayala et al. 2023).

The most recent terminology updated band adopted by the UN General Assembly (2016) defines vulnerability as "the conditions determined by physical, social, economic, and environmental factors or processes that increase the susceptibility of an individual, a community, assets, or systems to the impacts of hazards" (p. 25). However, vulnerability is also the result of historical causes that have led specific communities to develop vulnerabilities due to factors such as discrimination, inequity, race, gender, corruption, and even language (Alcántara-Ayala et al. 2023).

On the other hand, exposure is defined as "the situation of people, infrastructure, housing, production capacities, and other tangible human assets located in hazard-prone areas" Measures of exposure can include the number of individuals or types of assets situated in these risk-prone areas (UN General Assembly 2016, p. 19). This is closely linked to vulnerability, as factors such as poverty or even institutional deficiencies and development plans have encouraged illegal occupation of risk zones due to necessity or lack of information.

The study of exposure is vital in disaster risk assessment, as it identifies elements such as population, infrastructure, and services located in areas susceptible to hazards. Evaluating these regions should also involve assessing the populations and assets at risk due to their locations. This understanding enables the formulation of strategies aimed at preventing and mitigating human and material losses.

Additionally, exposure is closely intertwined with vulnerability, as factors like poverty and inadequate planning frequently lead to the illegal occupation of hazardous areas, often driven by necessity or misinformation.

In the case of Mexico, the state of Puebla is one of the entities with the highest slope instability in its territory (Domínguez et al. 2016). The mountainous region of the Sierra Norte de Puebla (SNP) has been particularly affected by mass movement processes, as its lithological, geomorphological, and hydrological characteristics, along with the socio-economic characteristics of its population, have created conditions that make it a territory susceptible and exposed to disaster occurrences associated with this type of hazard (Fig. 1) (Alcántara-Ayala, et al. 2017).

The October 1999 disaster in Puebla is one of the most well-known examples in the region, as well as in Mexico. It affected several states and municipalities in the Sierra Norte de Puebla (SNP) after a series of landslides were triggered by the heavy rains brought by Tropical Depression 11 (Fig. 2).

However, some municipalities within the SNP, such as Tlatlauquitepec, which have previously been affected by mass movement processes, have had little study regarding landslide disaster risk. To such an extent, they do not even possess the primary tool for territorial evaluation and planning, their own Municipal Risk Atlas.

Under this context, technological development has created new methodologies for analysing the various elements and processes occurring in a given area due to the multicausality involved in disaster risk construction.

In recent decades, the use of unmanned aerial vehicles (UAVs) in fields of knowledge related to spatial analysis has increased thanks to the ability to obtain precise geographical information of the territory at more detailed scales.

In disaster risk assessment, the products obtained from these tools have allowed various disciplines to identify, characterise, and analyse different risk components and to participate in tasks related to disaster risk management, such as monitoring the behaviour and evolution of specific hazards

Fig. 1 Landslide in Pahuatlán, Puebla—2006. (Photo courtesy of Ricardo J. Garnica-Peña)

Fig. 2 Damage following the rainfall events of October 1999 https://laruleta.com.mx/la-tragedia-que-marco-a-los-serranos/

and evaluating exposed populations; supporting and monitoring during emergencies, and assessing and evaluating post-disaster damage (Giordan et al. 2017).

According to Garnica-Peña and Alcántara-Ayala (2021), drones have been a recurrent tool for analysing and monitoring the dynamics of slopes and exposed populations in slope movement research.

The acquisition of aerial photographs and the analysis of the territory using UAVs has been a significant advantage in the study of landslide disaster risk, as it not only allows the gathering of information on the characteristics of the study area, the slope movements, or surface changes, but also enables the creation of potential scenarios, the design of strategies, and the issuance of early warnings to prevent the occurrence of a disaster and the generation of new risk conditions (Carrero 2021).

2 Studied Area

Tlatlauquitepec is a municipality that forms part of the Sierra Nororiental of Puebla and is situated in a transition zone between the Sierra Madre Oriental and the Trans-Mexican Volcanic Belt (Fig. 3). The municipality's geographical location, along with its lithological, geomorphological, and hydrological characteristics, creates contrasts and contact boundaries in its materials that can lead to slope instability (Borja-Baeza 2012).

Its lithology is diverse; however, most of the municipality of Tlatlauquitepec is composed of volcanic materials and sedimentary rocks of marine origin (Fig. 4). These materials, combined with the presence of tropical climates, are often susceptible to landslides due to their high permeability, low resistance to erosion, and high water infiltration, which generates pore pressure (Capra et al. 2003; Lugo-Hubp et al. 2005; Borja-Baeza 2012).

Nevertheless, to the northeast of the town centre, there are formations of metamorphic rocks such as Palaeozoic schists that act as the basement for the sedimentary rocks (Borja-Baeza 2012), as well as contact zones between schists and granites on low mountains and ancient alluvial hills. Due to the characteristics of these units, they have been the scene of gravitational processes such as landslides and flows, as factors such as their texture, folding, inclination, permeability, and fracturing tend to destabilise more easily (Lugo-Hubp et al. 2005).

The relief of the SNP is predominantly mountainous and composed of volcanic and sedimentary rocks. Volcanic mountain systems have low and slightly inclined reliefs, unlike those where sedimentary materials predominate, in which the slopes tend to be abrupt and with a high presence of river currents that erode slopes and their bases, generating conditions of instability (Fig. 5). The territory of Tlatlauquitepec includes low mountains in the southern portion, composed of volcanic rocks, and elevations of steep slopes in the north, these made of sedimentary materials.

Moreover, the municipality of Tlatlauquitepec belongs to the Tuxpan-Nautla hydrological region (92.01%) and the Balsas region located in the extreme south (7.99%) (INEGI 2010). The courses of its fluvial system mostly follow the direction of the region's slope, which, along with the presence of ignimbritic materials, has favoured erosive action and sediment accumulation due to their low resistance and the creation of surface streams (Borja-Baeza 2012).

Factors such as the proximity to the Gulf of Mexico promote constant rainfall throughout the year across most of the municipality, especially in the central and northern areas. The region experiences its highest rainfall between May and October, with a range of precipitation from 600 to 4100 mm, according to INEGI (2010), and an average annual precipitation of 1435 mm.

Most municipal territory, particularly in the south, has been designated for agricultural use (INEGI 2021). According to Mejía and Castellanos (2018), potato cultivation has become one of the municipality's primary agricultural activities.

The original vegetation of the municipality has decreased in percentage due to land use changes for agricultural purposes, deforestation, and the illegal sale of plots (Cerón-Carpio et al. 2006; Borja-Baeza 2012), which have contributed to land degradation and erosion, thereby increasing the susceptibility of the slopes.

In addition to the municipality's physical and geographical factors, the Tlatlauquitepec Municipal Development Plan (PDM 2022) 2021–2024 and the Institute for Municipal Management, Administration, and Linkage (IGAVIM 2020) have indicated that approximately 16.54% of the population lives in areas with high landslide susceptibility.

Furthermore, the municipality faces socio-economic challenges, such as a high percentage of the population living in poverty (67.34%), low incomes, rapid housing growth, and

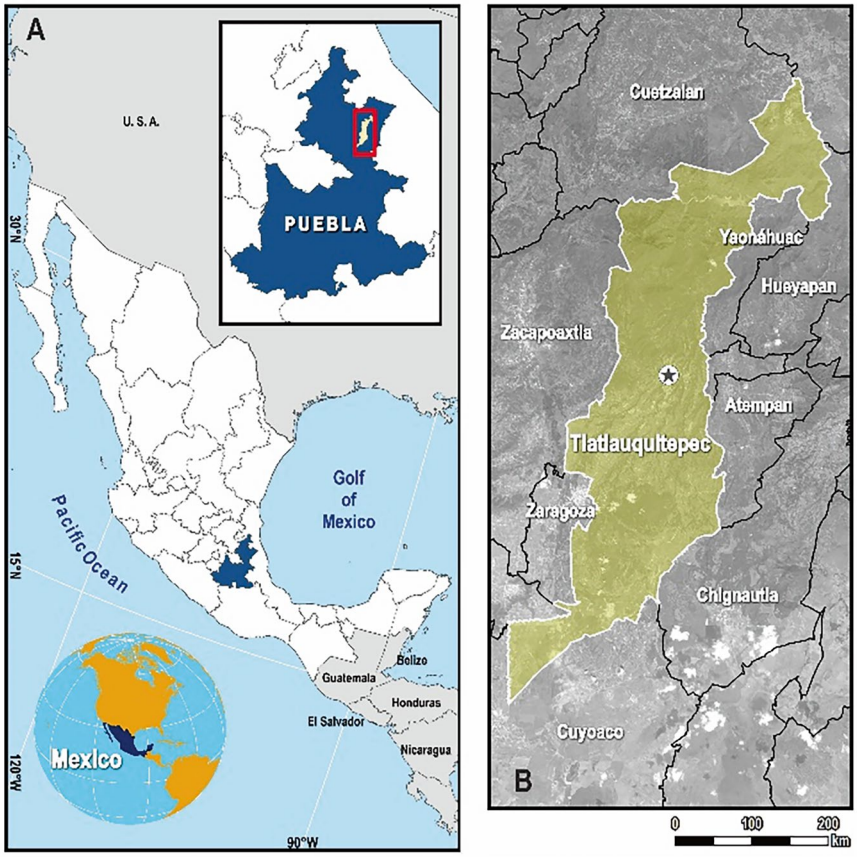

Fig. 3 Location of the municipality of Tlatlauquitepec, Puebla, Mexico. (**a**) The State of Puebla at the centre of Mexico. (**b**) Tlatlauquitepec located at north of Puebla

environmental degradation issues resulting from land use changes and economic activities (PDM 2022).

The municipality of Tlatlauquitepec lacks sufficient research and inventories related to landslide disasters. According to data from INEGI (2020), approximately 312 mass movement processes have been recorded, primarily triggered by meteorological phenomena and prolonged rainfall. Although there is no exact record of the loss of human lives and affected population, these events have particularly impacted the municipality's infrastructure and communication routes, such as roads and rural paths.

According to EM-DAT (2024) data, 1999 was the year with the highest recorded losses and those affected by landslide disasters. This was due to the October 1999 Sierra Norte de Puebla event. During this event, Tlatlauquitepec experienced significant impacts on its communication routes, which were constructed around the slopes.

Another significant event in the municipality was the one that occurred in October 2005 due to Hurricane Stan (Fig. 6). The landslides triggered by the heavy rains resulted in the deaths of three people, an estimated loss of 917.3 million pesos, and more than 25,000 people displaced in the Sierra Norte and Sierra Nororiental of Puebla. Tlatlauquitepec was one of the most affected municipalities due to the destruction of service infrastructure and communication routes (Borja-Baeza 2006).

With the recent passage of Tropical Depression Chris in July 2024, a series of landslides occurred in the municipality of Tlatlauquitepec, causing trees to fall, rocks to slide, and earth movements that affected the electrical infrastructure and obstructed roads in various areas of the municipality (Olán, 2024).

3 Methodology

3.1 Site Selection and Flight Plan

During a visit to the municipality of Tlatlauquitepec, an interview was held with the authorities, particularly with members of Civil Protection who recognised that the western portion of the town's centre had been affected by landslides and flooding (Fig. 7). The event most remembered by the authorities is the one that occurred in October 1999, when several landslides occurred in the area studied here.

Based on that information, a strategy was designed to carry out a flight plan to acquire aerial photographs with a UAV, process them, and prepare an exposure map of the homes located in the selected site so that the images' coverage would reach the homes and properties closest to the headwaters or edges of the slopes (Fig. 8).

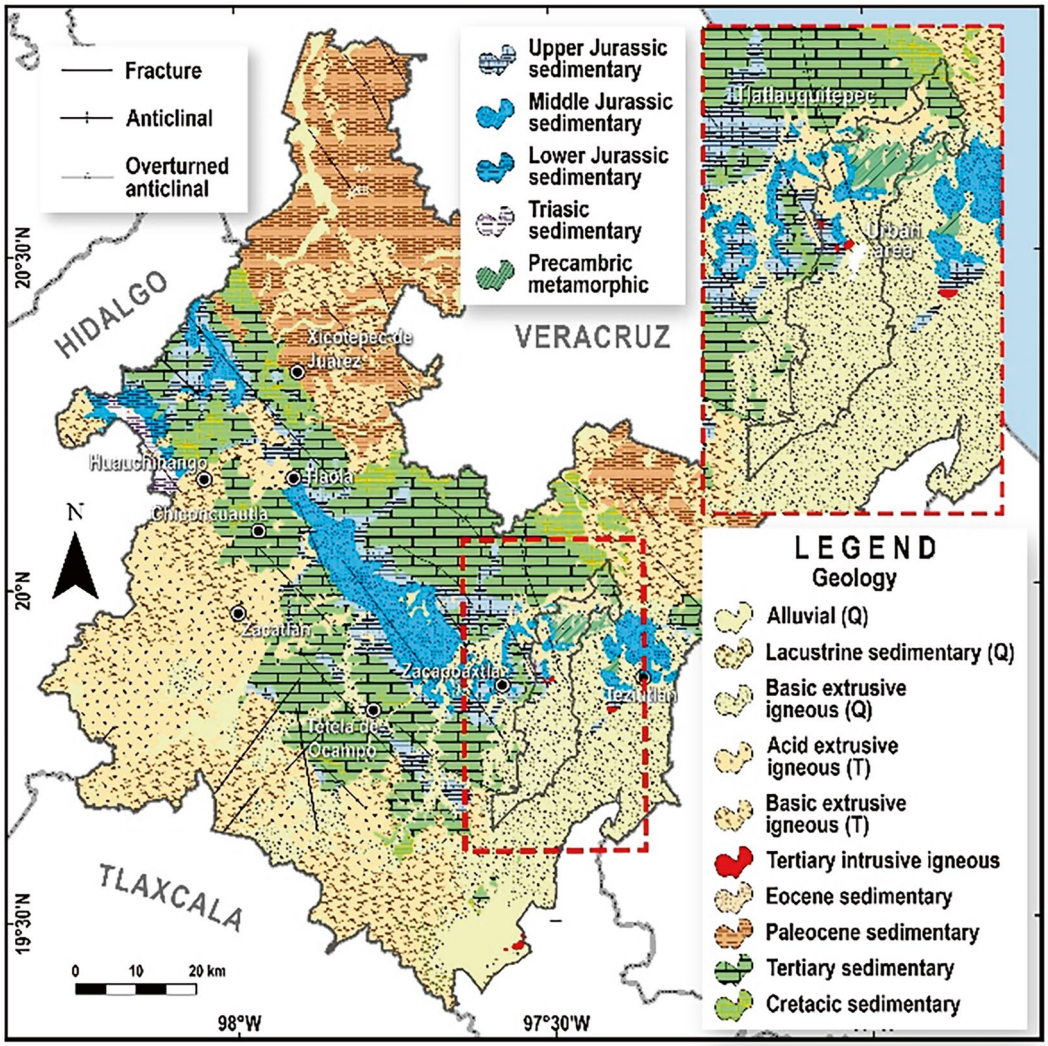

Fig. 4 Geological map of the studied area. (Source: Padilla y Sánchez et al. 2013)

The flight plan was prepared using the Map Pilot Pro application (Maps Made Easy), establishing the limits of the study area and the flight height (depending on the number of batteries available). In this way, two projects were drawn with different flight orientations, north/south—east/west, with a spatial resolution of 4 cm in each of the shots.

Once in place, a take-off base large enough to allow visual monitoring and an excellent transmission signal was established (Fig. 9). The equipment utilised was a DJI Phantom 4 Pro drone with a 1″ and 20-megapixel sensor and a flight range of approximately 25 min per battery. The drone covered 92.52 ha using nine batteries, and 1270 images of the study area were acquired.

3.2 Image Processing

The iTwin Capture Modeler software (Bentley) was used to process images. This software allows three-dimensional reconstruction from images from various sensors and sources.

In a very general way, the process consisted of determining each shot's exact location and orientation (considering its position and ground control points) and the characteristics of the drone sensor. Subsequently, once the photographs were oriented, the reconstruction process was carried out, which allowed, later, to generate the digital surface model (DSM), the orthophoto, and a cloud of points (with x, y, z values), said products, inputs for the analysis and interpretation of landslide susceptibility, and the exposure of the infrastructure.

Based on the point cloud, a digital terrain model was created by classifying the points and defining three main classes: ground, buildings, and vegetation. This allowed the generation of a model that only considered the base level of the terrain to identify possible landslides or susceptible areas. The model was also used to generate other derivatives, such as the slope model and the Topographic Wetness Index (TWI).

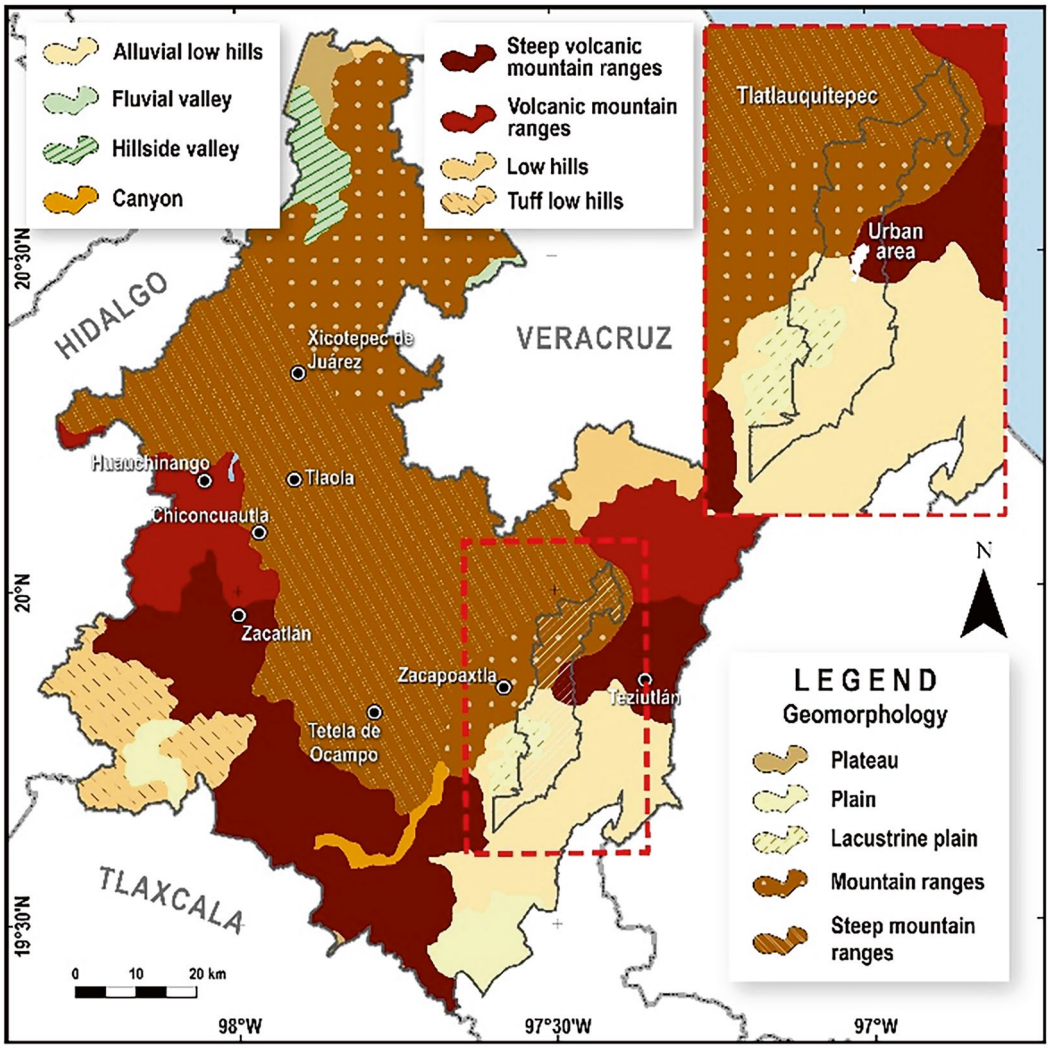

Fig. 5 Geomorphological map of Tlatlauquitepec. (Source: INEGI 2001)

Fig. 6 Debris flow occurred after Stan/Tlatlauquitepec—2006. (Photo courtesy of Ricardo J. Garnica-Peña)

3.3 Preparation of the Preliminary Landslide Exposure Map

The orthophoto and the digital surface model (DSM) were used as base inputs to prepare the preliminary landslide exposure map. From these inputs, three products were generated: a Red Relief Image Map, based on the works of Yokoyama et al. (2002) and Chiba et al. (2008); the Topographic Wetness Index (TWI); and a slope map, which was prepared based on the synthesis of the FAO (2009) classification of soil profiles across six sections, ranging from 0% to more than 55% slope. Additionally, support for three-dimensional visualization of the 3D model was provided using anaglyph glasses, allowing for the identification of landslides and areas with the most significant exposure (Fig. 10).

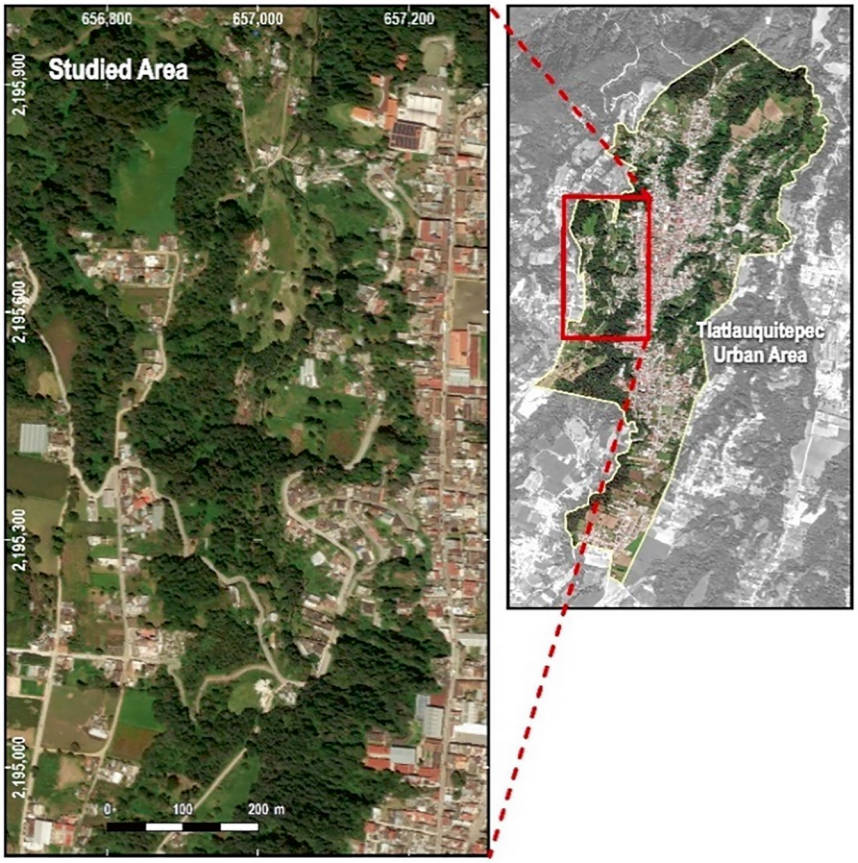

Fig. 7 Location of the research area

The Red Relief Image Map image allowed the identification of the geometry of the slopes by combining the slope levels and the shape of the terrain (concave or convex), indicating the presence of ancient landslides. On the other hand, the topographic humidity index was used to identify the areas of the terrain in which the water that descends from the slopes tends to concentrate or accumulate, thus defining areas susceptible to landslides.

Three primary risk levels were determined. A high degree of exposure: constructions and elements located near containment works and in areas that show signs of mass removal processes. Medium degree of exposure: houses or constructions located directly on the slopes and that have a high degree of slope and that, added to factors such as the material of the region, the geometry of the slopes, as well as the water characteristics, etc., represent an essential threat factor. Low exposure represents buildings far from the slopes, flat areas, or valleys.

3.4 Field Visit to Validate the Map

Finally, a field visit was carried out to validate the results obtained in the landslide exposure map. This tour included visits to the sites where representative elements of previously occurring landslides had been identified and to the properties and homes considered in the medium and high exposure levels.

During the visit, it was confirmed that the landslides that occurred have the particular characteristic that they originated on the edges of the ravine under study, in the highest portion of the slopes, on the limits with the flat area that includes the plateau on which the city of Tlatlauquitepec is located. Likewise, it was possible to recognise some elements or symptoms that denoted instability or areas with potential for landslides. It is worth highlighting areas in which retaining walls were built by the inhabitants to try to stop the movement of the slope or the fall of its materials, as well as depressed areas in the terrain that were associated with sites in which the landslides originated or were displaced.

Regarding the housing properties or infrastructure, a significant number (approximately 198) are located on the slope or slope change limits. The case of the "Elvira Cabañez de Flores" school stands out. It was affected by a landslide that occurred in 1999, and its facilities still show signs of displacement or loss of material on the slope on which they sit. This represents high exposure and risk for staff and students (Fig. 11).

Fig. 8 Applied methodology

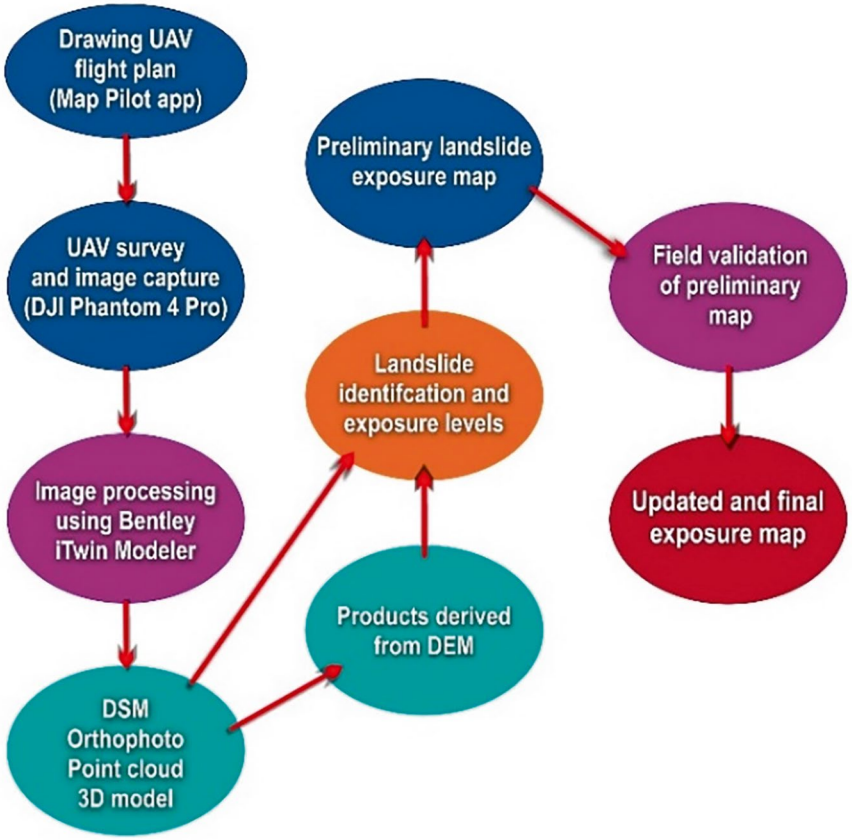

Fig. 9 Making flight plans in Tlatlauquitepec, 2023. (Photo courtesy of Brenda Neri Ruiz)

Likewise, two houses stand out (Fig. 12). They surround the crown of an old landslide that only attempted to stabilize the slope by using liquid concrete to prevent erosion in the highest part of the slope.

In this same area, on the road connecting Independencia Avenue with the road to Huaxtla, three properties are in the crown of a landslide. The neighbours and authorities tried to contain the surface's displacement and erosion. On the way to Huaxtla some walls try to contain the fall of material from the slopes to avoid blocking the road.

On the western slope, in the town of Huaxtla, elements of instability or the occurrence of landslides could be observed. However, the area does not have a high presence of houses or a change in the slope's edge. The area is better preserved and has less vegetation loss due to urban expansion, which is why it is considered that the homes in this area have less exposure.

4 Results

Based on the information obtained through the work carried out with the drone images and the field visit, 358 properties were considered for preparing the exposure map. These were selected based on the terrain's characteristics, proximity to steep slopes, symptoms of instability, and signs of ancient mass removal processes (Fig. 13).

Due to its proximity to the City of Tlatlauquitepec, located east of the study area, there is a higher concentration of human settlements in this region. According to the slope map, the predominant slopes in this area range from 0% to 13%, which indicates that the land is mostly flat or only slightly inclined. However, there are specific areas with steep escarpments. More than half of the identified properties or buildings are situated in steep areas or areas transitioning in slope. At the same time, human settlements tend to be smaller and are primarily found in slightly inclined or flat regions.

In the study area, specific locations are characterised by pronounced scarps with inclines exceeding 55%. These steep

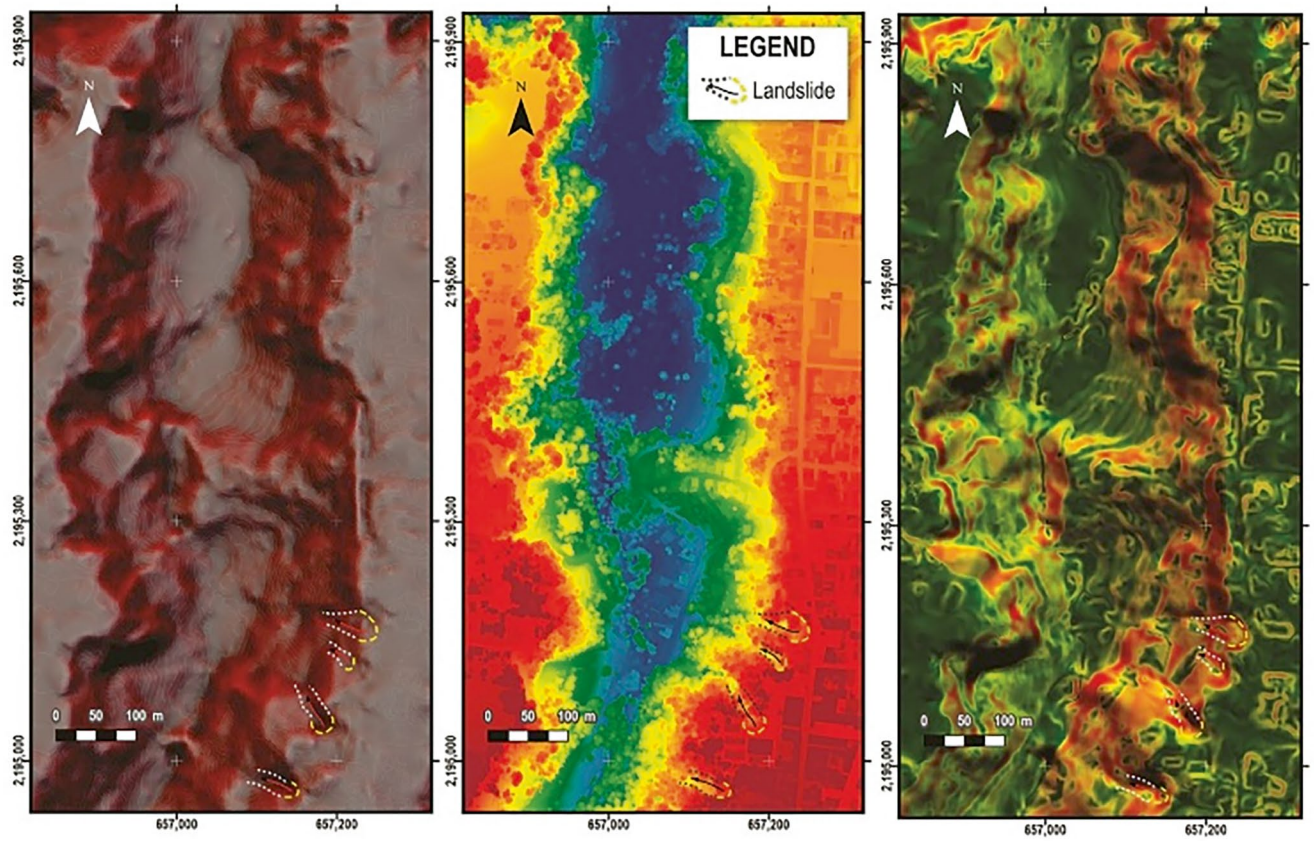

Fig. 10 Red Relief Image Map, Topographic Wetness Index and slope maps used as inputs to prepare the preliminary landslide exposure map

Fig. 11 Shows that "Elvira Cabañez de Flores" school is in a high-risk landslide area in 2023. Drawn lines indicate the main scarp and flanks of the past landslide. (Photo courtesy of Ricardo J. Garnica-Peña)

Fig. 12 Homes with shotcrete walls, 2023. Drawn lines indicate the main scarp and flanks of the past landslide. (Photo courtesy of Ricardo J. Garnica-Peña)

areas are predominantly found in the extreme west of the region, where there is a lower concentration of human settlements. However, more than half of the identified properties or buildings are situated in steep areas or transition zones, with inclines ranging from 13% to 25%. In contrast, human settlements are less common in slightly inclined or flat areas.

According to the calculation of the study area's topographic humidity index (TWI), the areas with greater inclination present a more significant accumulation of humidity and runoff, so they may present more intense erosion processes due to this factor, leading to slope instability. It should be noted that it is in these areas where the main signs of

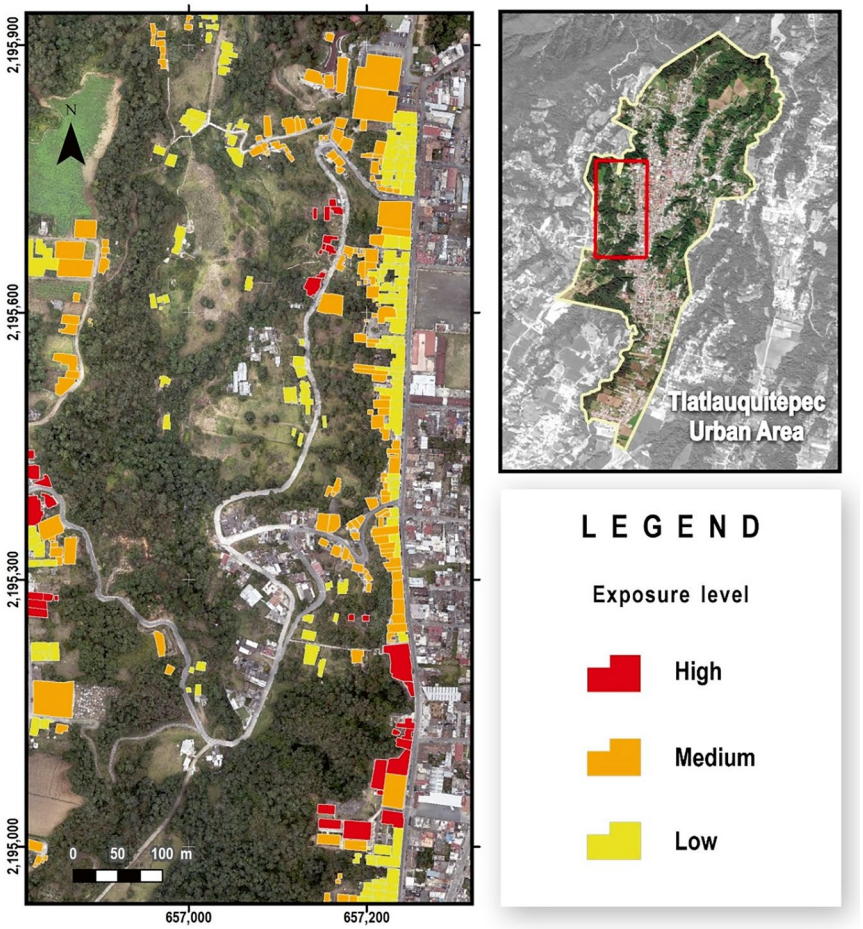

Fig. 13 Map of landslide exposure

instability identified in the area are found, the barriers and containment work, and signs of old landslides.

On the other hand, based on the red relief image map (RRIM), slopes with concave geometry predominate in the study area, mainly those with greater inclination and a greater tendency to accumulate moisture.

Some primary containment works, such as the one near the Elvira Cabañez de Flores Secondary School, are located on slopes with these characteristics, which present water and topographic instability factors.

The results obtained during the field visit helped to identify 358 properties which were classified according to previously defined exposure levels.

The high level of exposure represents the lowest percentage in the study area (9.8%). Thirty-five sites were classified as more likely to be affected by mass removal processes because the land on which they sit has already presented instability. This is reflected in the terrain, with symptoms of instability such as erosion and cracking, landslides such as those in 1999, and works and containment barriers built to contain the movement of the slopes.

The clearest example of this level of exposure is that of the Elvira Cabañez de Flores Secondary School, where one of the primary containment works identified during the tour is located. According to the information obtained by the school authorities, this containment work was built due to a landslide that occurred in 1999. However, it has not received maintenance since then, showing signs of decadency and cracks that represent a danger.

On the other hand, most of the constructions identified in the study area are in a medium degree of exposure (45.5%). This is because they are located on slopes with steep slopes or in transition zones. In turn, these areas have been extensively modified for the construction of homes or businesses and for the construction of roads and highways that surround or are located directly on the slopes.

With medium exposure, these properties do not present apparent symptoms of instability, both in the land and the homes. However, as they are located in areas with steep slopes, in conjunction with the physical characteristics of the study area (geology and hydrology), they represent risk factors due to the slopes' characteristics and the imbalance that has been generated on them.

Finally, 160 buildings (44.7%) were classified as having low exposure. These buildings are located in areas with

gentle or practically flat slopes, so the risk of mass removal processes due to the slope's characteristics is lower.

In this sense, although these constructions were classified within an area of low exposure to slope landslides due to their topographic characteristics, this should not be considered zero exposure since the occurrence of unexpected and high-magnitude processes can generate adverse effects on the population that lives in these homes due to factors such as falling debris, loosening of materials on the slopes, and erosion, among others.

4.1 Concluding Remarks and Future Steps

This study highlights the urgent issue of landslide risk in regions such as the Sierra Norte de Puebla, where the interaction between natural hazards and socio-economic vulnerabilities significantly increases disaster susceptibility. The use of UAVs in assessing landsliding proved to be highly effective, providing detailed, high-resolution data that facilitated the development of exposure maps. Classifying properties into high, medium, and low-risk categories illustrates that areas on steep slopes or near historical landslide zones are particularly exposed. These findings underline the importance of detailed terrain analysis and risk mapping in regions prone to geomorphological hazards.

In addition to geographical factors, the research also emphasises the socio-economic dimensions of disaster vulnerability. Communities in or near slope instability areas are often socio-economically marginalised, lacking the resources necessary for adequate infrastructure and safety measures. The case of Tlatlauquitepec, specifically the "Elvira Cabañez de Flores" school, illustrates that institutional neglect, such as the failure to maintain containment structures, exacerbates long-term susceptibility and exposure. This case reflects a broader issue: socio-economic disparities and infrastructural deficiencies deepen disaster risk.

The findings of this research underscore the importance of adopting data-driven approaches to disaster risk management. UAV technology and advanced three-dimensional modelling techniques present significant advantages in accurately identifying and monitoring landslide-prone areas. These tools enable the production of precise exposure maps, which can assist authorities in assessing the hazard levels and formulating targeted mitigation strategies. Policymakers should prioritise investment in such technologies to enhance the reliability of disaster risk assessments.

Moreover, the study highlights the need for a more integrated approach to disaster risk reduction. Effective landslide risk management should extend beyond hazard control to address the underlying socio-economic vulnerabilities exacerbating disaster risk. Factors such as poverty, inadequate housing, and the illegal occupation of high-risk areas must be considered when developing prevention strategies. Policies integrating infrastructure development with social welfare programmes and equitable land-use planning are essential for reducing risk and fostering long-term resilience.

The research also stresses the importance of prospective infrastructure maintenance. Regular monitoring and timely repairs of existing containment structures and drainage systems are critical to mitigating landslide risks. The example of the school in Tlatlauquitepec illustrates that a lack of maintenance can render even well-constructed containment measures ineffective, thereby increasing a community's exposure to hazards. Long-term policy frameworks should incorporate plans for maintaining critical infrastructure to ensure that safety measures remain effective.

Community engagement and public education are additional components and crucial pillars of disaster risk management. Populations residing in high-risk areas must be adequately informed about the dangers of living near unstable slopes and empowered to take preventative action. Public awareness campaigns and education on safe construction practices can equip communities with the knowledge to reduce their vulnerability. Hence, policy frameworks should not just include community involvement and education provisions but prioritise them as integral components of disaster risk management strategies.

Finally, the study underlines the necessity of long-term policy planning. As urbanisation and climate change are expected to increase landslide risks, policies must anticipate these challenges by enforcing strict zoning regulations and integrating climate adaptation strategies into land-use planning. Governments should embed climate resilience into their disaster risk management frameworks to prepare for and mitigate the heightened risks posed by environmental and developmental changes.

Acknowledgements Thanks to DGAPA-UNAM for providing financial support to conduct landslide risk research through Project PAPIIT IN300823 and a scholarship to Maryjose Sánchez Rojo.

References

Alcántara-Ayala I, Garnica-Peña RJ, Coll-Hurtado A, Gutiérrez de MacGregor MT (2017) Inestabilidad de laderas. Factores inductores del riesgo de desastre. Investigaciones Geográficas. https://doi.org/10.14350/sc.05

Alcántara-Ayala I, Gómez C, Chmutian K, Niekerek D, Raju E, Marchezini V, Rom-Cadag J, Galliard JC (2023) Disaster risk. Routledge, London. https://doi.org/10.4324/9781315469614

Borja-Baeza RC (2006) Inestabilidad de laderas en Tlatlauquitepec, Sierra Norte de Puebla: Análisis y modelación en materiales sedimentarios. Tesis de maestría. Facultad de Filosofía y Letras. UNAM, México City. http://132.248.9.195/pd2006/0605736/0605736.pdf

Borja-Baeza RC (2012) Diseño de un sistema de alerta temprana para mitigar el impacto generado por inestabilidad de laderas: Tlatlauquitepec, Sierra Norte de Puebla. Tesis de doctorado, Facultad de Filosofía y Letras. UNAM, México City. http://132.248.9.195/ptd2012/febrero/0677538/0677538_A1.pdf

Capra L, Lugo-Hubp J, Borselli L (2003) Mass movement in tropical volcanic terrains: the case of Teziutlán (México). Eng Geol 69:359–379. https://doi.org/10.1016/S0013-7952(03)00071-1

Carrero J (2021) Importancia de los drones en la gestión del riesgo de desastres en Colombia. Revista del Consejo Colombiano de Seguridad, Protección & Seguridad (400). https://ccs.org.co/portfolio/importancia-de-los-drones-en-la-gestion-del-riesgo-de-desastres-en-colombia/

Cerón-Carpio AB, Arreguín-Sánchez ML, Fernández-Nava R (2006) Listado con anotaciones de las pteridofitas del municipio de Tlatlauquitepec, Puebla, México y distribución de las especies en los diferentes tipos de vegetación. Polibotánica 21:45–60

Chiba T, Kaneta S, Suzuki Y (2008) Red relief image map: new visualization method for three-dimensional data. Int Arch Photogramm Rem Sens Spatial Inf Sci 37(Part B2):1071–1076

Domínguez et al (2016) Análisis de umbrales de lluvia que detonan deslizamientos y sus posibles aplicaciones en un sistema de alerta temprana por inestabilidad de laderas. CENAPRED. https://www1.cenapred.unam.mx/COORDINACION_ADMINISTRATIVA/SRM/FRACCION_XLI_A/23.pdf

EM-DAT (2024) Clasificación de Desastres. Bélgica: Centre for Research on the Epidemiology of Disasters-CRED, Université catholique de Louvain. Recuperado el 18 de enero de 2024, de https://public.emdat.be/data

FAO (2009) Guía para la descripción de suelos. https://openknowledge.fao.org/server/api/core/bitstreams/b54d0348-dfce-413c-bd5d-142b3a14a049/content

Garnica-Peña RJ, Alcántara-Ayala I (2021) The use of UAVs for landslide disaster risk research and disaster risk management: a literature review. J Mt Sci 18:482–498. https://doi.org/10.1007/s11629-020-6467-7

Giordan D, Manconi A, Remondino F, Nex F (2017) Use of unmanned aerial vehicles in monitoring application and management of natural hazards. Geomat Nat Haz Risk 8(1):1–4. https://doi.org/10.1080/19475705.2017.1315619

IGAVIM (2020) Población susceptible por deslizamiento de laderas en los municipios del Estado de Puebla. http://igavim.org/Documentos%20Generados/Documentos%20Generales/2020%20Poblacion%20Susceptible.pdf

INEGI (2001) Sistema de topoformas. Datos vectoriales. Escala 1:1,000,000

INEGI (2010) Compendio de información geográfica municipal 2010. Tlatlauquitepec, Puebla. https://www.inegi.org.mx/contenidos/app/mexicocifras/datos_geograficos/21/21186.pdf

INEGI (2020) Inventario nacional de fenómenos geológicos. Escala 1(250):000. https://www.inegi.org.mx/app/biblioteca/ficha.html?upc=889463842767

INEGI (2021). Uso de suelo y vegetación, 1:250,000 serie VII. Continuo Nacional. http://geoportal.conabio.gob.mx/metadatos/doc/html/usv250s7gw.html

Kirsch-Wood J, Katsanakis R, Hieber Girardet L, Kumar A, Mena R, Cook R, Delpech F, Elsworth J, Langella F, Alcántara-Ayala I et al (2022) Global assessment report 2022. United Nations Office for Disaster Risk Reduction, Geneva. 237 pp

La ruleta (2023) A 24 años de la tragedia que marcó a los Serranos. https://laruleta.com.mx/la-tragedia-que-marco-a-los-serranos/

Lugo-Hubp J, Zamorano-Orozco JJ, Capra L, Inbar M, Alcántara-Ayala I (2005) Los procesos de remoción en masa en la Sierra Norte de Puebla, octubre de 1999; Causas y efectos. Revista Mexicana de Ciencias Geológicas 22(2):212–228

Mejía G, Castellanos JA (2018) Costos de producción y rentabilidad del cultivo de la papa en Zacapoaxtla, Puebla. Revista Mexicana de Ciencias Agrícolas 9(8):1651–1661. https://doi.org/10.29312/remexca.v9i8.1721

Olán (2024). Afectaciones en Tlatlauquitepec tras paso de Chris. https://www.e-consulta.com/nota/2024-07-02/municipios/afectaciones-en-tlatlauquitepec-tras-paso-de-chris

Padilla y Sánchez RJ, Domínguez Trejo I, López Azcárraga AG, Mota Nieto J, Fuentes Menes AO, Rosique Naranjo F, Germán Castelán EA, Campos Arriola SE (2013) Tectonic Map of Mexico GIS Project, American Association of Petroleum Geologists GIS Open Files series National Autonomous University of Mexico

PDM (2022) Tlatlauquitepec. Plan de Desarrollo Municipal 2021–2024. https://planeader.puebla.gob.mx/pdf/Municipales2021/Tlatlauquitepec_PMD%202021-2024.pdf

UN General Assembly (2016) Report of the open-ended intergovernmental expert working group on indicators and terminology relating to disaster risk reduction. United Nations General Assembly, New York, 41p

UNDRR (2013) Mexico disaster database. https://www.desinventar.net/DesInventar/profiletab.jsp?countrycode=mex&continue=y

Yokoyama R, Shirasawa M, Pike R (2002) Visualizing topography by openness: a new application of image processing to digital elevation models. Photogramm Eng Remote Sens 68(3):257–265

Interweaving Systems of Knowledge: Leveraging Transdisciplinary Research to Strengthen Landslide Disaster Risk Reduction

Irasema Alcántara-Ayala

Abstract

The unprecedented pace and complexity of global change, driven by climate change, environmental degradation, demographic transitions and inequities, necessitate reevaluating traditional approaches to disaster risk reduction (DRR). This chapter examines transdisciplinary research (TDR) as a critical approach for advancing landslide risk management in this context. Landslides (LS), as multifactorial phenomena, arise from an intricate interplay of natural processes and anthropogenic activities, with their impacts exacerbated by the accelerating dynamics of global change. The chapter posits that an integrated approach to LS-DRR underpinned by TDR is essential for addressing the compounded vulnerabilities and exposures characterising socio-environmental systems. It argues for a paradigm shift that transcends disciplinary silos, advocating for the co-production of knowledge through the collaborative engagement of scientists, policymakers, practitioners, local communities and diverse actors. The chapter delineates TDR's principles, methodologies, and tools, illustrating their application in the context of LS-DRR. By critically assessing the implications of TDR for policy and practice, the chapter underscores its potential to enhance resilience, equity, and sustainability in the face of escalating global challenges.

Keywords

Landslides · Integrated Landslide Disaster Risk Management (ILDRiM) · Transdisciplinary research · Landslide preparedness · Co-production of knowledge · Community participation · Disaster risk reduction

1 Introduction

In a world increasingly defined by rapid and profound transformations, global change stands at the forefront of society's collective challenges. Defined by sweeping shifts in key socioenvironmental processes, global change encompasses the dynamic interplay of these factors as they reshape our planet. The relevance of global change has never been more pressing as the world grapples with these multifaceted issues. Global change encompasses critical phenomena such as climate change, environmental degradation, rapid urbanisation, and shifts in population dynamics, all of which have profound implications for the planet's ecosystems and human societies (Steffen et al. 2005). These changes are not isolated events but are deeply intertwined, creating complex challenges that affect the stability and resilience of natural systems and the well-being of communities worldwide.

Understanding and addressing global change is crucial for developing effective strategies to reduce disaster risks, adapt to new conditions, and promote sustainable development (UN/GA 2015). As these global shifts unfold, their impact on disaster risk, resource management, and socio-environmental systems underscores the urgent need for coordinated and innovative solutions to safeguard the planet's future.

Understanding and addressing global changes is mandatory due to their profound impacts on socio-environmental systems, which are increasingly vulnerable to disasters and associated risks (UNISDR 2015). As climate change intensifies weather patterns, deforestation accelerates environmental degradation, and urbanisation expands into hazardous areas, communities' abilities and ecosystems' resilience are severely tested. These global changes exacerbate existing vulnerabilities and create new risks, leading to more frequent and severe socially constructed disasters (Oliver-Smith et al. 2016; Kelman 2024).

Award Memorial Article: Varnes Medal 2023

I. Alcántara-Ayala (✉)
Institute of Geography, National Autonomous University of Mexico (UNAM), Mexico City, Mexico
e-mail: ialcantara@geografia.unam.mx

B. Abolmasov et al. (eds.), *Progress in Landslide Research and Technology, Volume 4 Issue 1, 2025*, Progress in Landslide Research and Technology, https://doi.org/10.1007/978-3-031-89836-5_3

Socio-environmental systems, which include the interactions between human societies and their natural environments, face the dual challenge of adapting to rapidly evolving conditions while managing the compounded risks of disasters. This complexity is heightened by socio-economic inequities, where marginalised communities often bear a disproportionate burden of disaster impacts and have fewer resources for effective adaptation and recovery. Addressing these challenges requires a comprehensive approach that integrates sustainable development, disaster risk reduction, and climate adaptation, ensuring that interventions are inclusive and equitable to the multifaceted pressures of global change (Peduzzi 2019).

Landslides have far-reaching impacts globally, leading to loss of life, extensive damage to infrastructure, and significant economic disruption. Recent examples, such as the 2021 landslide in the Indian state of Uttarakhand, where a rock avalanche in the Raunthi glaciated valley triggered a large debris flow, leading to flash floods in the Rishiganga and Dhauliganga rivers, causing significant damage to hydropower projects and infrastructure and resulted in many fatalities (Martha et al. 2021), highlight the grave consequences of these disasters.

The causes of landslides are often intricate and multifaceted, encompassing natural factors like geological instability, weather patterns, and human activities (Highland and Bobrowsky 2008). Risk drivers such as deforestation, urban expansion, and poor land-use practices destabilise slopes and mount susceptibility and exposure to landslides. Climate change further complicates the situation by intensifying extreme weather events, such as heavy rains and storms, which can trigger landslides in vulnerable and exposed areas. These intertwined causes and risk drivers underscore the urgent need for integrated landslide risk management (ILDRiM) strategies that address both environmental and human factors to mitigate the impacts of landslides and increase community resilience (Alcántara-Ayala 2021).

An integrated approach to landslide disaster risk reduction is essential for effectively managing the multifaceted challenges posed by landslides. This approach should integrate various dimensions, including hazard assessment, vulnerability and exposure reduction, to address the complexities of landslide risk (Smith 2013) (Fig. 1).

Combining scientific research with practical interventions contributes to advancing and including all aspects of risk, ranging from understanding the geodynamic factors that trigger landslides to incorporating engineering solutions that mitigate localised landslide risks and implementing land-use policies (Puente-Sotomayor et al. 2021). Furthermore, this comprehensive approach involves engaging with local communities, actors, stakeholders, and policymakers to develop context-specific strategies that enhance resilience and adaptability (Sultana and Tan 2021). It also should include continuous monitoring and early warning systems to provide timely alerts and reduce response times (Casagli et al. 2024). This holistic perspective is crucial for minimising the immediate impacts of landslides and fostering long-term resilience and sustainable development in vulnerable regions (Alcántara-Ayala and Geertsema 2023).

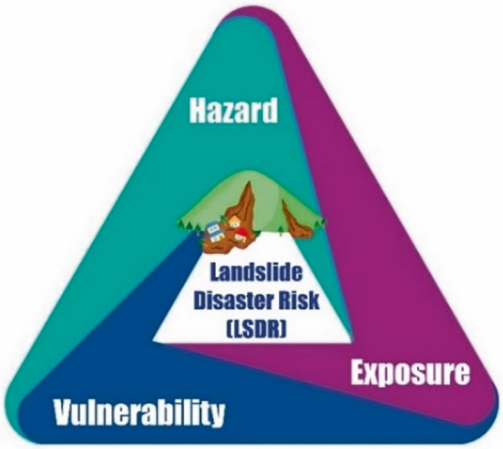

Fig. 1 Triangle illustrating the main components of landslide disaster risk (LSDR): Hazard (trigger), Vulnerability (propensity to damage), and Exposure (presence of people and assets in areas potentially affected by hazards). (Source: The author, 2024)

Transdisciplinary research (TDR) is pivotal in integrating knowledge and perspectives from various disciplines, stakeholders, and sectors. TDR transcends traditional academic boundaries, fostering collaboration between scientists, policymakers, practitioners, and communities to address complex environmental and societal challenges (Lawrence et al. 2022).

TDR is particularly valuable for reducing landslide disaster risk by combining geological and environmental sciences with engineering, urban planning, social sciences, and the knowledge provided by other actors. This integration facilitates a comprehensive understanding of landslide causes and impacts, enabling the development of effective, context-specific risk reduction strategies. By involving diverse stakeholders, TDR encourages local knowledge, social dynamics, and policy considerations to be incorporated into solutions, enhancing their relevance and efficacy. Additionally, TDR supports the co-production of innovative practices and adaptive measures, leading to more resilient approaches for managing landslide risks and other intricate environmental challenges (Matsuura and Razak 2019).

This chapter is structured to comprehensively explore how TDR can enhance landslide disaster risk reduction (LS-DRR). It begins with an introduction, followed by the methodology, and sets the stage by outlining the significance of integrating diverse perspectives and approaches in LS-DRR. The chapter then delves into understanding landslide disaster risk, examining the nature of landslides, their

causes, and the factors contributing to vulnerability and exposure. The subsequent section, TDR, discusses its principles and benefits, emphasising its role in bridging scientific research and practical application gaps. The chapter continues with the co-production of knowledge, highlighting the importance of collaborative efforts among researchers, actors, stakeholders, and communities in developing effective DRR strategies. Methodologies and Tools for TDR LS-DRR provides a detailed overview of the techniques and technologies used to support TDR in landslide risk management. Finally, the chapter concludes with policy and practice implications and concluding remarks summarising key insights and offering recommendations for policy and practice to improve landslide DRR through transdisciplinary approaches.

2 Methodology

The methodology for this research integrates a comprehensive review of secondary literature with practical fieldwork knowledge to investigate landslide disaster risk reduction. The literature review examines the multifaceted drivers of landslides, including environmental degradation, urbanisation, climate change, and governance challenges, alongside best practices in disaster risk management. Field insights are derived from extensive landslide risk research in developing countries and stakeholder engagements, including interviews and community workshops, to capture grounded perspectives on vulnerabilities and risk reduction strategies. By synthesising scientific, local, and indigenous knowledge, the study demonstrates how transdisciplinary research fosters collaborative approaches essential for addressing the compounded risks and inequities that define socio-environmental systems in a rapidly changing world.

3 Understanding Landslide Disaster Risk

Understanding landslide disaster risk involves a detailed analysis of several interconnected dimensions, including the geodynamics of landslides, people's vulnerability to such events, and their exposure to them. This holistic approach seeks to foster comprehensive and effective risk management strategies (Winter 2014).

Pardeshi et al. (2013) emphasised the importance of integrating multiple techniques to improve the accuracy and reliability of landslide hazard assessments. They also discussed the challenges in predicting landslides and the need for continuous technological advancements and methods to understand better and mitigate landslide risks. Evaluating landslide hazards entails thoroughly analysing environmental and geological conditions contributing to slope instability. Precise geological surveys ascertain soil and rock composition and structure, aiding in locating areas with inherent weaknesses (Soeters and van Westen 1996).

Geomorphological studies examine landscape dynamics, including slope angles, landforms, and erosion patterns, all influencing landslide potential (Carrara et al. 2003). Hydrological investigations are equally important as they focus on the impact of rainfall, snowmelt, and groundwater flow on soil saturation and their role in triggering landslides. Special attention should also be given to precipitation thresholds (Segoni et al. 2018).

Furthermore, human activities such as mining, construction, and deforestation destabilise slopes and alter natural drainage patterns (Glade 2003). By comprehending these factors, it becomes feasible to generate intricate hazard maps that identify areas of susceptibility and exposure and, along with vulnerability analysis, can contribute to formulating science-based effective mitigation strategies (Lacasse et al. 2009).

The vulnerability analysis examines how various socio-economic and demographic factors impact a community's capacity to endure and rebound from landslides. Such assessment encompasses evaluating the quality of housing and infrastructure, such as the structural integrity of buildings, landslide resilience and positioning on stable ground. Socio-economic factors like income levels, poverty, marginalisation, inequality, access to education, and resources significantly contribute to vulnerability (Cutter et al. 2012).

Socioeconomic conditions exert a significant influence on the vulnerability to landslides. Communities with limited financial resources often inhabit high-risk areas due to affordable land or inadequate housing options. These populations may lack the means to invest in landslide-resistant construction or implement necessary protective measures (Fig. 2). Economic disparities can impact access to early warning systems, emergency response services, and recovery assistance, compounding vulnerability. The analysis should consider how poverty, income inequality, and economic instability contribute to the vulnerability of individuals exposure and communities to landslides (Carvalho et al. 2022).

Communities with limited financial resources may encounter difficulties implementing effective protective measures or conducting timely evacuations during emergencies. Moreover, the social cohesion within a community, comprising the strength of social networks, local knowledge, and institutional support, can influence overall resilience. Marginalised populations, specifically those residing in informal settlements, are not only highly exposed; they often encounter more significant hardships in preparing for and recovering from landslides (Sultana and Tan 2021).

Fig. 2 Houses on unstable slopes illustrate how low-income communities often live in high-risk areas due to affordable land and limited housing options. (Source: The author, 2024)

Fig. 3 Urban expansion and land use changes in hilly areas susceptible to landsliding increase exposure, placing more people and assets at risk. (Photo courtesy of Ricardo J. Garnica-Peña)

Social structures and institutional frameworks enormously influence vulnerability to hazards such as landslides. Communities exhibiting strong social networks and local knowledge are better positioned to prepare for and respond to these events. Conversely, marginalised groups with limited social capital may need help accessing crucial information, resources, and support.

Furthermore, institutional factors play a critical role, including the efficacy of local governance, land-use regulations, and the implementation of disaster risk reduction policies (Alam and Ray-Bennett 2021). Analysing the impact of these factors on community resilience aids in identifying deficiencies and opportunities for enhancing landslide risk management.

The political context and power dynamics can impact vulnerability by influencing decision-making processes and resource allocation. Inequities in political representation and power can result in the neglect of high-risk areas, insufficient regulation enforcement, and unequal resource distribution (Blaikie et al. 2014). The analysis should explore how political factors, such as governance structures, policy decisions, and corruption, affect the ability to address landslide risks and support vulnerable populations.

Humanitarian crises, such as conflict, the loss of Indigenous knowledge, and historical injustices, can significantly increase landslide risks. Conflicts lead to population displacement, forcing communities into unstable areas with poor infrastructure. The loss of Indigenous knowledge undermines effective land use and hazard awareness, while historical injustices limit access to safe land and resources. These factors increase landslide vulnerability and reduce community resilience (Ahmed 2021).

Cultural attitudes and behaviours can significantly influence vulnerability. A community's perception of risk, historical landslide experiences, and traditional practices shape how people respond to landslide hazards (Nathan 2008). Understanding these cultural and behavioural factors is crucial for devising effective risk communication strategies and engaging communities in disaster preparedness and mitigation efforts.

Exposure refers to how landslides can impact people, property, infrastructure, livelihoods, and the environment based on location. This aspect involves mapping and analysing the spatial distribution of populations and assets in areas prone to landslides. High exposure occurs when significant development, such as residential, commercial, and critical infrastructure, is situated in or near hazardous zones (Pellicani et al. 2014).

Factors like urban expansion, changes in land use, and infrastructure development can increase exposure by putting more people and assets at risk (Fig. 3). Effective exposure management involves implementing land-use planning and zoning regulations that restrict development in high-risk areas and ensuring that new construction meets safety standards (Cascini et al. 2005).

Additionally, incorporating risk reduction measures into infrastructure planning, such as strengthening retaining walls, improving drainage systems, and designing structures resistant to landslides, can help reduce the impact of landslides on exposed assets (Choi and Cheung 2013).

The evaluation of landslide risk underscores the necessity of adopting an integrated approach that extends beyond merely considering hazard geodynamics. This involves examining the social, economic, political, cultural, and institutional aspects that shape vulnerability and exposure. By addressing these factors, more effective and equitable strategies for reducing landslide risk can be developed, enhancing community resilience and minimising the impacts of landslides.

4 Transdisciplinary Research

Transdisciplinary research (TDR) is an integrative approach that seeks to address complex societal issues by combining insights, methods, and perspectives from multiple academic disciplines and non-academic stakeholders. It transcends traditional disciplinary research by focusing on real-world problems and involving diverse participants, including practitioners, policymakers, community members, and other relevant stakeholders (Cronin 2008; Lawrence et al. 2022).

In TDR, the research process involves the collaborative production of knowledge, where all participants work together in the design, execution, and application of the research. This collaborative effort strives for the knowledge produced to be relevant and applicable to society. Thus, the approach should be context-sensitive, considering the specific cultural, social, economic, institutional, and environmental conditions in which the research is conducted, thereby helping tailor solutions to local needs and realities (Schneider et al. 2022). In the realm of transdisciplinary research, the process encompasses three vital stages aimed at tackling intricate societal challenges: the collaborative framing of problems, the co-creation of solution-oriented knowledge, and the integration and application of the resulting knowledge (Lang et al. 2012) (Fig. 4).

In the collaborative problem-framing phase, clear goal establishment and competent project management lay the foundation for effective resource utilisation and focused direction (Norström et al. 2020). Engaging diverse actors and stakeholders throughout fosters inclusivity and ensures the relevance of research outcomes, facilitated by collaboration and partnership among stakeholders (Buser 2021).

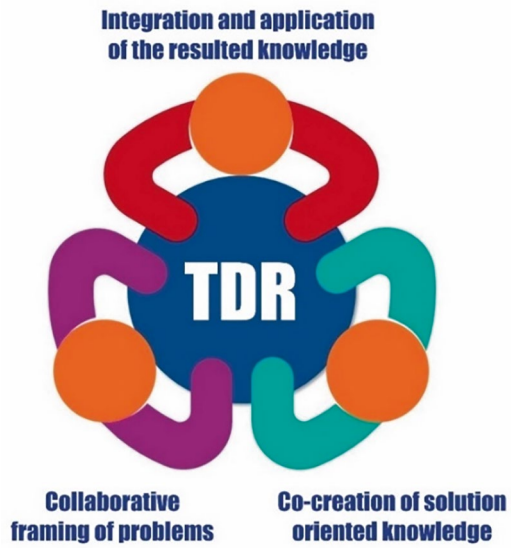

Fig. 4 Stages of transdisciplinary research (TDR). (Adapted from Lang et al. 2012) (Source: The author, 2024)

Coherent framing of the problem integrates diverse perspectives, guiding research activities with a shared understanding of complexity and nuance (Brandt et al. 2013; Lang 2020).

Moving to the co-creation stage, a problem-oriented approach centres research efforts on identified challenges in the co-production of knowledge, ensuring practical and applicable outcomes (Brandt et al. 2013; Jorgenson 2021). Acknowledging the complexity and heterogeneity of problems and perspectives informs context-sensitive solutions adaptable to diverse needs and dynamics (Bergmann et al. 2021).

Negotiation and mutual learning promote collaboration, enriching problem-solving and decision-making processes (Klein 2001; Walter et al. 2007). Capacity building and empowerment enable stakeholders to make sustainable decisions underpinned by ethical considerations that ensure participant welfare and research integrity (Jacobi et al. 2022). Resource optimisation supports the implementation of research outcomes in the integration and application phase, while communication and dissemination strategies promote knowledge sharing and public engagement (Hoffmann et al. 2019). Evaluation and feedback mechanisms drive continuous improvement, ensuring the relevance and effectiveness of research activities (Stokols et al. 2003; Klein 2008). Innovation and creativity foster transformative change while addressing power dynamics and promoting equity within partnerships (Bréthaut et al. 2019), fostering inclusivity and representation (Barth et al. 2023).

Despite its suitability for solving the most pressing societal problems, TDR's development faces several challenges. TDR is inherently complex due to the collaboration it demands across diverse disciplines and with non-academic stakeholders. This type of research requires the integration of different forms of knowledge—scientific, practical, and local—each of which comes with its language, methods, and expectations. These differences can create significant challenges in communication and collaboration. Researchers and stakeholders may struggle to understand each other's perspectives and priorities, leading to misunderstandings, conflicts, and inefficiencies. Building a shared understanding and maintaining clear, open lines of communication are essential but often difficult to achieve.

Another one of TDR's main challenges is managing the diversity of participants. Bringing together academic researchers, policymakers, community members, and industry professionals can be daunting. Each group brings its values, experiences, and knowledge systems, which must be harmonised to create a cohesive research approach. However, this integration is only sometimes smooth. Power imbalances can emerge, where the voices of some stakeholders, particularly those with less formal education or institutional power, may be marginalised.

Ensuring all participants are equally heard, and their contributions are valued is not just a goal but a necessity. This requires careful facilitation and a steadfast commitment to equity in the research process. In TDR, balancing scientific rigour with practical relevance is a significant challenge. Academic researchers prioritise methodological rigour and theoretical contributions, while external stakeholders focus on applying research to real-world problems. Bridging these two priorities requires flexibility and adaptation without compromising quality and integrity, leading to difficulties in meeting academic and practical criteria.

Institutional barriers further complicate TDR. Traditional academic structures and funding mechanisms are often not designed to support transdisciplinary work's time-intensive and resource-heavy nature. Funding agencies may prioritise more conventional, discipline-specific research, leaving TDR projects underfunded. Additionally, the academic reward system, which often emphasises publication in discipline-specific journals and rapid outputs, may not align with TDR's slower, more iterative process. As a result, researchers may find it challenging to pursue transdisciplinary projects without facing career risks, including reduced chances for promotion or tenure.

Finally, sustaining engagement from all stakeholders throughout the research process to ensure scalable and durable outcomes, aligning research efforts with broader societal goals and aspirations, thereby enhancing the coherence and impact of the research outcomes, poses a significant challenge in TDR (Table 1). However, these processes are not without their tensions, contractions and power asymmetries that must also be carefully negotiated (Bréthaut et al. 2019).

Stakeholders often operate on different timelines, levels of interest, and competing commitments, resulting in uneven participation and a loss of momentum over time. Maintaining stakeholder involvement requires continuous communication, flexibility, and occasionally adjusting research goals to preserve their investment. This is particularly crucial in long-term projects where immediate benefits may only be apparent to some participants. Ensuring sustained engagement is indispensable for the success of TDR, as it depends on the active contribution and collaboration of all involved parties to achieve its goals.

The core principles of transdisciplinary research form the ethical and practical foundation for coordinated problem-solving efforts and community betterment. Collaborative, iterative processes foster the collective effort needed to address complex challenges, while inclusivity ensures that diverse perspectives are valued and integrated throughout the research process (Klein 2008; Kok et al. 2021). Ethical conduct upholds integrity and trust, safeguarding the rights and well-being of all involved parties (Cockburn and Cundill 2018). Sustained engagement underscores the commitment to long-term relevance, quality and positive impact. It harnesses diverse perspectives to ensure solutions align with stakeholders' needs and values, enhancing credibility and effectiveness to address complex societal challenges responsibly (Polk 2015) (see Fig. 5).

5 Co-Production of Knowledge

Co-production of knowledge is a complex and challenging process involving stakeholders such as researchers, policymakers, and local communities in creating and applying knowledge. This collaborative approach is essential for addressing complex societal and environmental issues by combining diverse perspectives, expertise, and experiences to generate more relevant and impactful solutions (Polk 2015; Kruijf et al. 2022).

The process of co-producing knowledge with stakeholders begins with collaboratively framing the issues. This initial step is crucial as it ensures that all relevant voices are heard and that the research agenda addresses the concerns and priorities of those directly affected by the issue. Techniques for joint problem-framing include participatory workshops, focus groups, and community meetings where stakeholders can share their views, experiences, and expectations (Schmidt et al. 2020). These interactions help define the scope and objectives of the research, ensuring that it is context-specific and aligned with the community's needs.

Data collection in co-production combines traditional scientific methods with participatory approaches. Researchers utilise surveys, interviews, and field observations while also integrating community-led data-gathering techniques such as participatory mapping, citizen science, and local monitoring initiatives (Hicks et al. 2019). This combination of methods enriches the available data, resulting in a more comprehensive understanding of the topic at hand.

In co-production analysis, stakeholders collaborate to interpret data and gain insights. This may involve joint workshops where researchers and community members analyse findings together, ensuring that interpretations are based on local realities and experiences. Collaborative analysis validates results and enhances stakeholder credibility and acceptance (Bieluch et al. 2017).

Sharing co-produced knowledge is a collaborative endeavour that involves making the results accessible to all stakeholders through appropriate channels. This can be achieved through various techniques such as community presentations, policy briefs, interactive websites, and social media campaigns. The ultimate goal is to ensure the generated knowledge is widely disseminated and translated into practical actions and policies that benefit the community (Adler et al. 2018).

The co-production of knowledge presents various challenges, with one significant hurdle being managing power

Table 1 Key dimensions and core principles of the fundamental stages of transdisciplinary research

Key dimensions	I. Collaborative problem framing	II. Co-creation of solution-oriented and transferable knowledge	III. Integration and application of produced knowledge
Problem-oriented approach	Focus research efforts on addressing specific challenges identified by stakeholders, considering local contexts.	Adopt problem-oriented approaches that integrate traditional knowledge and respect cultural norms and values.	Apply research outcomes to solve identified problems in culturally sensitive and contextually appropriate ways.
Clear goals establishment	Establish clear, shared research objectives and goals.	Align research activities with established goals.	Monitor implementation and assess alignment with project objectives.
Context sensitivity and adaptability	Adapt research approaches to diverse contextual needs, including cultural and traditional contexts.	Enhance applicability through adaptation to various cultural contexts, respecting local customs and traditions.	Adapt research outcomes to diverse cultural contexts, responding sensitively to local norms and values.
Coherent framing	Develop a shared understanding of the problem among stakeholders, integrating diverse cultural perspectives.	Guide research activities with coherent framing that incorporates local and traditional knowledge.	Synthesise findings to develop a cohesive narrative informed by cultural norms and values.
Participation of stakeholders, users, and decision-makers (entire process)	In problem-framing, engage diverse stakeholders, including local communities and traditional knowledge holders.	Involve stakeholders in all stages of knowledge co-creation, including traditional, local and tacit knowledge holders.	Collaborate with stakeholders, incorporating local and traditional knowledge, in implementing research outcomes.
Integration of diverse perspectives and methods	Engage stakeholders, including traditional communities, to define the problem using diverse research methods and integrating local knowledge and values.	Collaborate across disciplines and cultures, integrating traditional and scientific knowledge for innovative solutions that respect diverse values and norms.	Synthesise findings, ensure alignment with local values and sustain engagement for implementation—Utilise diverse methods for ongoing evaluation.
Collaboration, cooperation, partnership	Foster collaboration among stakeholders, including local communities and traditional knowledge holders.	Facilitate interdisciplinary collaboration and integration, incorporating diverse cultural perspectives.	Work collaboratively with stakeholders, respecting cultural norms and values, to achieve the desired impact.
Stakeholders' engagement	Engage stakeholders, including practitioners and communities, to define the problem collaboratively, integrating traditional and local knowledge for a comprehensive understanding.	Collaborate with stakeholders to develop solutions, integrating traditional and local knowledge alongside scientific insights for relevance and ownership.	Involve stakeholders in synthesising knowledge, ensuring cultural alignment for effective implementation and ongoing refinement.
Reflexivity and iterative learning	Engage stakeholders, integrate traditional knowledge, and foster reflexivity for a nuanced understanding of the problem.	Co-create solutions, integrating traditional knowledge with scientific insights, and continuously refine based on feedback.	Reflect on outcomes, align with local values and iterate solutions for cultural sensitivity and effectiveness.
Complexity and heterogeneity	Address the complexity and diversity of stakeholder perspectives, including local and traditional knowledge.	Embrace complexity to develop contextually relevant solutions that respect cultural diversity.	Account for complexity in applying research findings in ways that honour cultural norms and values.
Negotiation, mutual learning	Facilitate dialogue and mutual learning among stakeholders, promoting cross-cultural understanding.	Promote knowledge exchange and mutual learning, fostering respect for diverse cultural perspectives.	Engage in dialogue and negotiation with stakeholders, valuing diverse viewpoints and cultural insights.
Communication and dissemination	Develop effective communication strategies for research findings that are culturally sensitive and accessible.	Communicate research findings in ways that respect cultural diversity and promote meaningful engagement.	Disseminate research outcomes in culturally appropriate formats, fostering community ownership and understanding.
Evaluation and feedback	Implement mechanisms for ongoing evaluation and feedback that prioritise community input and participation.	Solicit feedback from stakeholders, including local communities, to assess research impact and relevance.	Evaluate the impact of research outcomes on addressing community needs and priorities and honouring cultural contributions.

(continued)

Table 1 (continued)

Key dimensions	I. Collaborative problem framing	II. Co-creation of solution-oriented and transferable knowledge	III. Integration and application of produced knowledge
Innovation and creativity	Foster a culture of innovation and creativity that embraces diverse cultural perspectives and traditions.	Encourage innovative thinking that draws inspiration from local and traditional knowledge systems.	Promote innovative approaches honouring cultural heritage and empowering communities to address their challenges.
Transdisciplinary learning for transformative change	Engage stakeholders in defining the problem inclusively, integrating traditional, local knowledge, values, and norms for transformative change.	Co-create solutions across disciplines and cultures, integrating traditional knowledge with scientific insights for transformative change.	Synthesise knowledge, aligning with local values and norms for culturally sensitive and effective solutions for transformative change.
Capacity building and empowerment for sustainable decision-making	Build stakeholder capacity for informed decision-making, incorporating traditional knowledge systems.	Empower stakeholders to apply research outcomes in ways that preserve and promote cultural heritage and values.	Support stakeholders in evidence-based decision-making that respects and integrates local and traditional knowledge.
Power dynamics and equity	Address power dynamics and promote equity within research partnerships, ensuring the representation of diverse voices.	Foster inclusive decision-making processes that respect and amplify marginalised cultural perspectives.	Promote equitable participation and representation in research activities, empowering marginalised communities.
Socially Robust Orientations (SoROs)	Ensure research outcomes contribute to socially robust orientations that respect cultural diversity.	Promote socially robust orientations that reflect and celebrate diverse cultural norms, values, and traditions.	Integrate socially robust orientations into decision-making processes, fostering cultural inclusivity and equity.
Competent project management	Ensure effective project management and resource allocation.	Manage project resources and timelines efficiently.	Collaborate with stakeholders to translate research findings into action.
Resource allocation	Optimise resource allocation to support research activities that respect and integrate traditional knowledge.	Efficiently manage resources to support culturally sensitive research activities and community engagement.	Allocate resources to sustain and scale research outcomes in ways that support cultural preservation and empowerment.
Long-term sustainability	Consider the long-term sustainability of research outcomes in ways that preserve and promote cultural heritage.	Plan for sustainability and scalability of research interventions that respect and support cultural traditions.	Ensure research outcomes contribute to lasting cultural resilience and empowerment, fostering intergenerational continuity.
Collaborative iterative process			
Ethics			
Trust building			
Inclusivity			
Flexibility			
Sustained Engagement			

Adapted from Klein (2001, 2008), Stokols et al. (2003), Walter et al. (2007), Lang et al. (2012), Brandt et al. (2013), Polk (2015), Scholz and Steiner (2015), Bréthaut et al. (2019), Hoffmann et al. (2019), O'Rourke and Crowley (2020), Lang (2020),Norström et al. (2020), Bergmann et al. (2021), Buser (2021), Kok et al. (2021), Jorgenson (2021), Barth et al. (2023), Scholz and Renn (2024) (Source: The author, 2024)

dynamics between researchers and stakeholders (Zurba et al. 2022). Ensuring equitable participation demands ongoing efforts to foster trust, respect, and mutual understanding. Furthermore, co-production can be time-consuming and resource-intensive, requiring sustained commitment from all parties involved. Addressing differing stakeholder priorities and expectations may also pose challenges, emphasising the need for effective facilitation and conflict resolution strategies (Lang et al. 2012).

Adhering to best practices in co-production involves cultivating transparent communication, nurturing enduring partnerships, and prioritising capacity building. Establishing clear-cut roles and responsibilities is fundamental while maintaining flexibility and adaptability.

Regular feedback loops are crucial in maintaining stakeholder engagement and ensuring the co-production process remains relevant and responsive. These feedback loops facilitate the adaptive integration of new ideas and strategies by allowing stakeholders to assess progress and suggest improvements continuously. This iterative approach helps refine and evolve the project's architecture and ensures the process stays aligned with all involved parties' evolving needs and perspectives. According to Morton et al. (2015), such dynamic and interactive processes are essential for fostering sustained collaboration and achieving successful outcomes in co-production efforts.

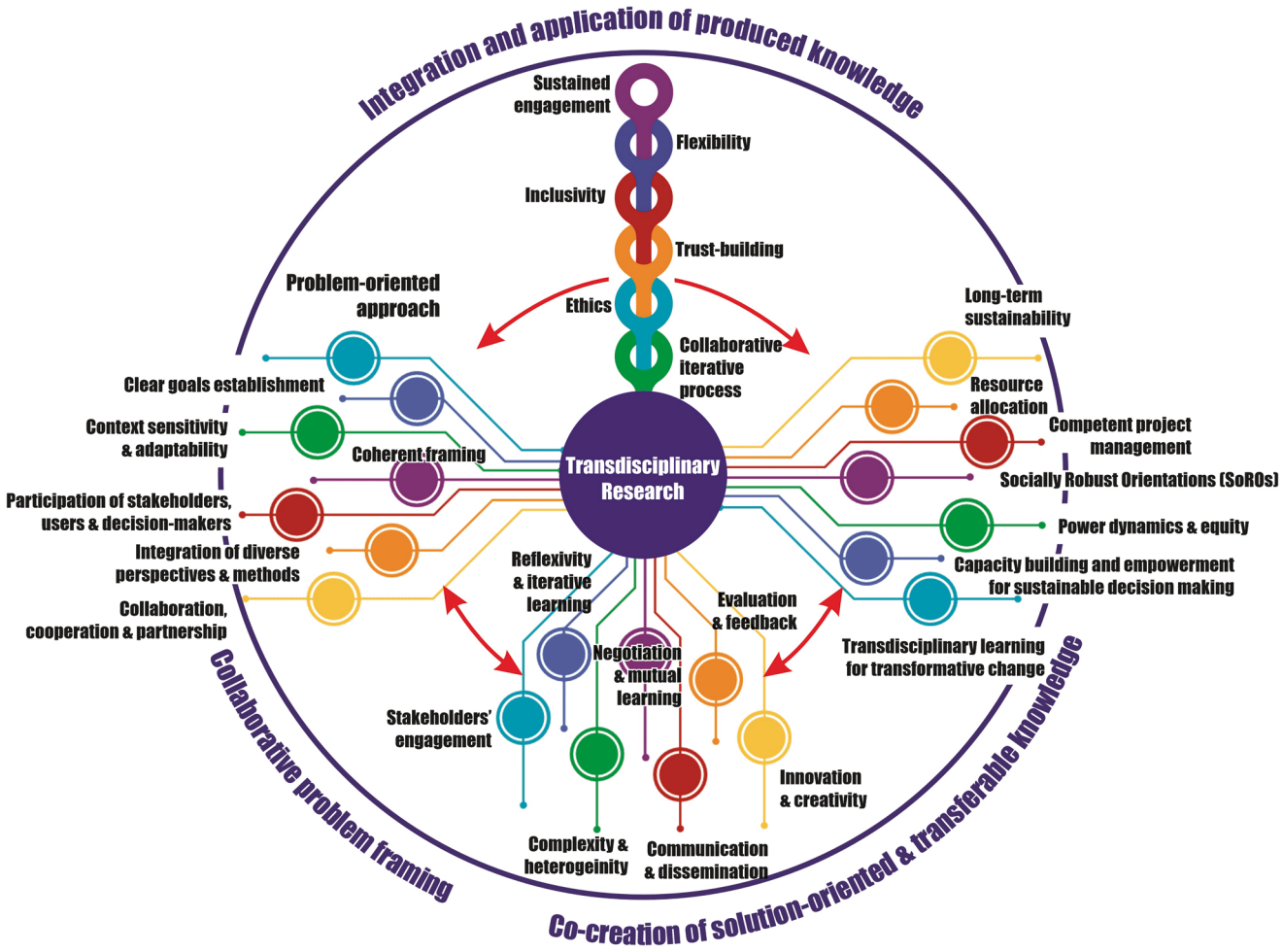

Fig. 5 Comprehensive framework representing key dimensions and core principles of transdisciplinary research. This figure encapsulates the essential elements of transdisciplinary research, which should be incorporated throughout the fundamental stages of the entire process (Collaborative Problem Framing, Co-creation of Solution-Oriented and Transferable Knowledge, and Integration and Application of Produced Knowledge). It underscores its character through a collaborative, iterative process, ethical practices, trust-building, inclusivity, flexibility, and sustained engagement as core principles. (Source: The author, 2024)

6 Methodologies and Tools for Transdisciplinary Landslide DRR (TDR-LSDRR)

The traditional methodologies and tools for landslide disaster risk reduction (DRR) are comprehensive and diverse (Alcántara-Ayala 2018). They can be adjusted to integrate scientific research, local knowledge, and collaborative efforts among communities and stakeholders to mitigate landslide risks effectively from a TDR perspective.

6.1 Community-Based Landslide Mapping and Hazard Assessment

Community-based landslide mapping and hazard assessment involve local populations in identifying, documenting, and assessing landslide-prone areas by combining local knowledge with scientific expertise. This helps develop a comprehensive understanding of landslide risks and enhances community preparedness and resilience. Geospatial data and community insights are used to produce detailed hazard

maps, highlighting areas susceptible to landslides based on factors such as slope instability, soil composition, land use patterns, and historical occurrences of landslides.

Such efforts can be combined with more technical elements, including advanced technologies like remote sensing and GIS. These are crucial for creating detailed hazard maps by identifying landscape changes indicating landslide activity (Nithya and Prasanna 2010). Likewise, field surveys can validate remote sensing and gather site-specific data, while geotechnical investigations involve soil sampling to determine slope stability. Monitoring using instruments provides real-time landslide trigger data (Duncan et al. 2014) that are highly valuable for landslide warnings.

6.2 Incorporating Local Knowledge

Local knowledge is essential in landslide DRR as it provides context-specific insights that may be overlooked by scientific approaches alone. Involving local communities in participatory mapping exercises allows residents to contribute their historical knowledge of landslide events, areas of frequent occurrence, and local risk factors.

Additionally, focus group discussions and community workshops can reveal socio-cultural factors influencing vulnerability and resilience, such as traditional land-use practices, local governance structures, and community coping mechanisms (Dasanayaka and Matsuda 2022) (Fig. 6).

Comprehensive case studies and ethnographic research enable a profound comprehension of how local communities perceive and address landslide risks (Nathan 2008; Alam 2020). These methodologies can unveil the intricacies of community dynamics, power relations, and resource access, which are fundamental for devising inclusive and effective strategies for disaster risk reduction (DRR).

Fig. 6 Socio-cultural factors affecting vulnerability and resilience revealed through community workshops. (Photo courtesy of Ricardo J. Garnica-Peña)

6.3 Vulnerability and Exposure Assessment

Evaluating vulnerability and exposure encompasses examining the socio-economic and demographic characteristics influencing a community's resilience to and recovery from landslides.

Gathering data on household income, education levels, health status, and housing conditions through surveys and resident interviews and then analysing these factors helps pinpoint the most vulnerable populations and their specific challenges.

Spatial analysis tools can map the distribution of vulnerable populations in landslide hazard zones. Social vulnerability indexing involves combining various socio-economic indicators into a composite index that quantifies levels of vulnerability across different regions (Murillo-García et al. 2015). This can help prioritise areas for intervention and resource allocation.

6.4 Risk Communication and Community Engagement

Efficient risk communication is crucial for ensuring that all stakeholders comprehend and implement the outcomes of hazard and vulnerability assessments. Visual tools such as hazard maps, infographics, and 3D models can facilitate the comprehension of intricate scientific data. Additionally, interactive platforms and mobile applications can deliver real-time information and alerts to vulnerable communities.

Public meetings and training programs foster dialogue between scientists, policymakers, and community members, facilitating a shared understanding of risks and preparedness measures (Alcántara-Ayala and Moreno 2016; Raška 2019). Moreover, role-playing simulations and scenario-based exercises are valuable tools for communities to practice emergency response actions and enhance readiness (Suharini and Baharsyah 2020).

6.5 Landslide Early Warning Systems (LEWS)

Traditional early warning systems integrate various monitoring technologies to identify signs of potential landslides and issue timely alerts. Rain gauges, ground sensors, and satellite data monitor rainfall intensity, soil moisture, and ground deformation. This data is then analysed to establish thresholds that prompt warning notifications (Intrieri et al. 2012).

International initiatives like Early Warnings for All focus on integrating disaster risk knowledge, hazard detection, and effective warning dissemination with preparedness and response efforts. This comprehensive approach helps develop

inclusive multi-hazard early warning systems, promoting timely action and reducing vulnerabilities to mitigate disaster impacts better (WMO 2024).

Effective Early Warning Systems (EWS) rely on robust communication networks to disseminate alerts. This can involve mobile phone alerts, community sirens, radio broadcasts, and social media channels. Community-based monitoring networks, where residents are trained to observe and report early warning signs, further enhance the effectiveness of EWS (Macherera and Chimbari 2016). Nonetheless, from a transdisciplinary approach, EWS should be co-designed with at-risk communities and other actors and stakeholders.

6.6 Structural and Non-structural Measures

Mitigation strategies consist of structural and non-structural measures to reduce landslide risks. Structural measures involve engineering solutions, such as retaining walls, slope stabilisation techniques, and improved drainage systems. These interventions seek to alter the landscape physically to prevent or mitigate landslide occurrences.

Non-structural measures encompass ecosystem-based approaches such as reforestation, stabilising slopes through root reinforcement, and agroforestry, which integrates trees and crops to mitigate soil erosion. Effective land-use planning and zoning regulations are crucial to restrict development in high-risk areas and promote sustainable land management practices (Alcántara-Ayala and Geertsema 2022).

6.7 Decision Support Systems

Decision support systems (DSS) are advanced tools that integrate various data sources and analytical models to assist in making well-informed decisions. DSS can simulate different scenarios, assess the potential impacts of mitigation measures, and optimise resource allocation.

Multi-criteria decision analysis is a widely used technique in DSS to evaluate multiple factors and criteria in decision-making processes comprehensively. Considering a range of objectives and stakeholder preferences aids in identifying the most effective and feasible strategies for landslide DRR (van Westen et al. 2021).

6.8 Capacity Building and Education

Capacity building entails training community members, local officials, and stakeholders in risk assessment, emergency response, and mitigation planning. Workshops, drills, and educational programs heightened awareness and knowledge, strengthening communities' ability to take prospective measures.

Establishing collaborative networks and partnerships among government agencies, non-governmental organisations, academic institutions, and local communities is crucial for enhancing the sustainability of DRR efforts. This facilitates knowledge exchange and technical assistance from experts, further strengthening local capacities (Bobrowsky and Highland 2013).

6.9 Monitoring and Evaluation

Continuous monitoring and evaluation are crucial to ensure that DRR strategies remain effective and adaptable to changing conditions. Monitoring includes regular data collection on hazard indicators, vulnerability factors, and the effectiveness of implemented measures. Evaluation processes assess the outcomes of DRR initiatives, identify areas for improvement, and facilitate sharing of best practices (Sarabia et al. 2020).

Adaptive management is an iterative approach integrating feedback and learning into the DRR process. It involves continuously adjusting strategies based on new information and changing conditions to ensure that DRR efforts remain relevant and effective over time (Paton and Buergelt 2019).

In transdisciplinary landslide disaster risk reduction (TDR LS-DRR), various methodologies and tools offer a comprehensive and multifaceted approach to addressing landslide hazards. While these tools and methods are traditionally employed in scientific research for landslide disaster risk assessment, their application extends beyond conventional boundaries. They facilitate the integration of scientific inquiry with local knowledge and collaborative input from diverse actors and stakeholders.

This integrative framework enhances the effectiveness of LS-DRR by combining empirical data with contextual insights and experiential knowledge. As a result, the methodologies support a more nuanced understanding of landslide risks and contribute to the development of robust, context-sensitive strategies for risk mitigation and management (Fig. 7).

7 Policy and Practice Implications

TDR for LS-DRR adopts a comprehensive approach that integrates scientific knowledge, local insights, and collaborative practices to address the multifaceted nature of landslide risks. This is a cardinal course for ILDRiM (Fig. 8). ILDRiM, like any other integrated disaster risk management process, focused on diverse hazards, should be an integral part of

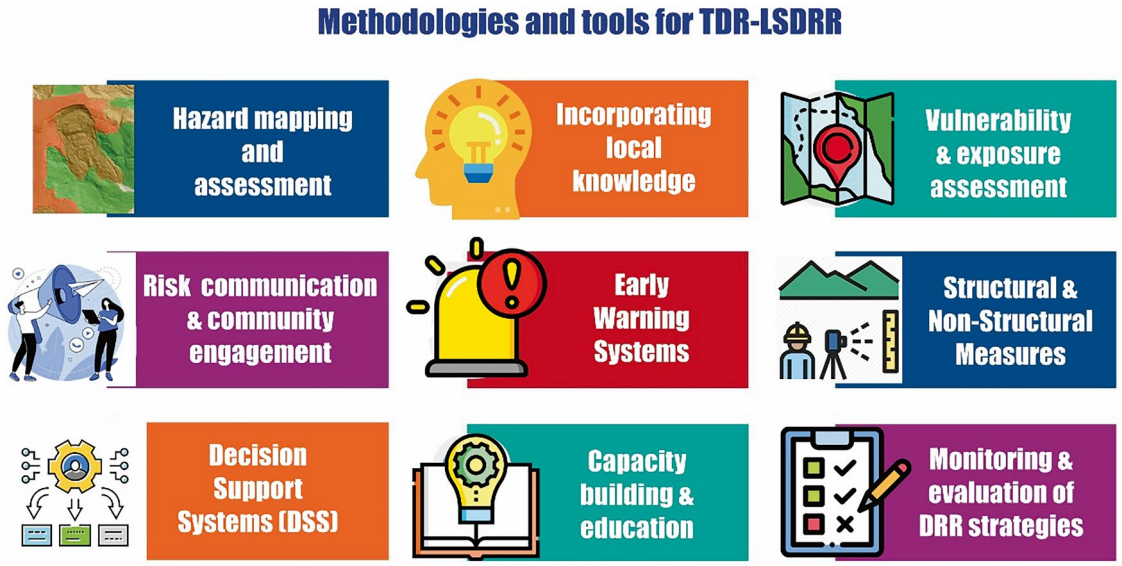

Fig. 7 Essential methodologies and tools that can be used for (TDR-LSDRR). (Source: The author, 2024)

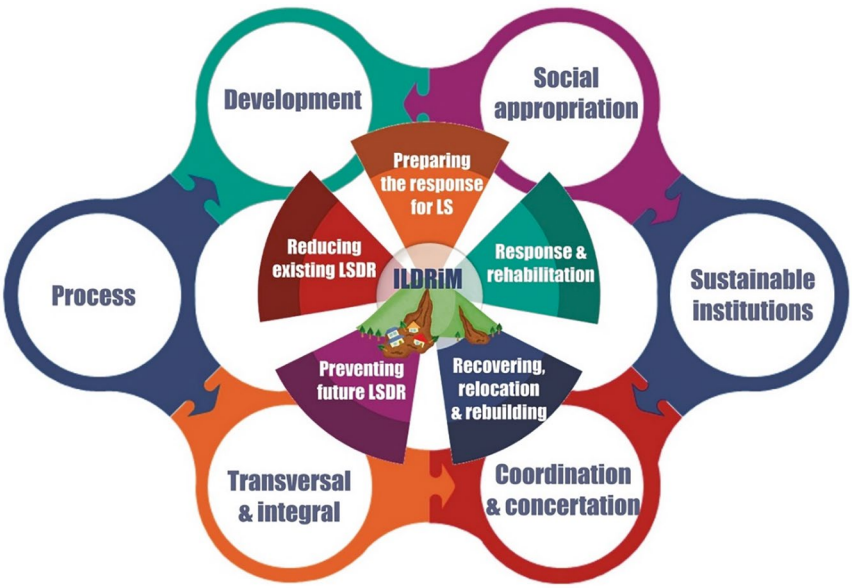

Fig. 8 Characteristics of optimal risk management within an integrated landslide disaster risk management framework, highlighting key processes: risk identification and assessment, prevention and mitigation, preparedness planning, response, recovery, and learning for continuous improvement. (Adapted from Narvéz et al. 2009) (Source: The author, 2024)

development, aiming to integrate with sustainable processes and ensure ongoing sustainability (Narvéz et al. 2009).

Likewise, landslide risk evaluation requires active participation for legitimacy and belonging, strengthening social actors in decision-making, where ownership is crucial. A fundamental principle in integrating risk management with development is to avoid creating new institutions. Instead, risk concerns can be addressed by integrating them into existing development institutions, requiring an overarching coordinating body to work through established organisations.

Furthermore, effective ILDRiM requires coordination and monitoring at the local level and integration with higher hierarchical levels, including subregional, regional, national, and international levels. Local risks are interconnected with social and territorial processes that extend beyond local boundaries, emphasising the need for integration within a broader territorial framework.

ILDRiM should be regarded as a comprehensive practice encompassing prevention, mitigation, preparedness, response, rehabilitation, and reconstruction. It aims to address the evolving nature of landslide disaster risk by reducing or anticipating it (Narvéz et al. 2009) (Fig. 8).

This complex endeavour has significant implications for policy and practice, as TDR can bridge the gap between theoretical research and practical applications, ensuring that

DRR strategies are both effective and sustainable (Matsuura and Razak 2019).

7.1 Informing Policy and Practice with TDR Findings

TDR findings can profoundly inform policy and practice by comprehensively understanding landslide risks, including environmental and socio-economic dimensions (Schneiderbauer et al. 2023). Scientific data on geological conditions, rainfall patterns, and land use can be combined with local knowledge about historical landslide events and community vulnerabilities. This integrated perspective ensures that policies and practices are grounded in thoroughly understanding all relevant factors.

For instance, hazard maps created through TDR can inform land-use planning and zoning regulations, helping to prevent development in high-risk areas. Vulnerability assessments can identify communities or individuals who are particularly at risk, enabling targeted interventions such as relocation assistance, housing improvements, and social safety nets. Policymakers can use these findings to prioritise investments in infrastructure, early warning systems, and community preparedness programs, ensuring that resources are allocated efficiently and effectively.

TDR also facilitates the development of context-specific policies tailored to different communities' unique needs and capacities. By involving local stakeholders in the research process, TDR ensures that policies are scientifically sound, culturally appropriate, and socially acceptable. This enhances effective implementation and sustainability. For instance, Smith et al. (2022) studied participatory landslide risk management in informal Latin American settlements, emphasising community-government collaboration and academia's role in effective co-production.

7.2 Strategies for Translating Research into Actionable Policies and Interventions

Translating TDR findings into actionable policies and interventions necessitates strategic efforts to ensure effective communication and implementation of research insights (West et al. 2019). One key strategy involves fostering continuous dialogue among researchers, policymakers, and community stakeholders. Regular workshops, policy briefings, and collaborative platforms can facilitate this dialogue, allowing stakeholders to discuss research findings, explore their practical implications, and co-design interventions (Pipere and Lorenzi 2021).

Developing decision-support tools is a fundamental strategy. These tools can incorporate TDR findings and offer policymakers user-friendly platforms to visualise different scenarios, evaluate the impacts of various policy options, and make well-informed decisions. For instance, GIS-based platforms can overlay hazard maps with socio-economic data, assisting planners in identifying high-risk areas and prioritising interventions (Castro and Rifai 2021).

Pilot projects and demonstration sites are practical avenues for translating TDR findings into action. By implementing research-informed interventions in specific communities or regions, these initiatives can demonstrate the effectiveness of TDR approaches and provide valuable insights for scaling up. They also function as testing grounds for refining strategies based on real-world experiences, ensuring that interventions are both practical and impactful.

Capacity-building initiatives are vital for effectively translating research into practice. Training programs, workshops, and knowledge exchange forums can equip policymakers, practitioners, and community members with the essential skills and knowledge to apply TDR findings (O'Donovan et al. 2022). This includes training in risk assessment techniques, emergency response planning, and community engagement strategies.

7.3 Building Institutional Capacity for Transdisciplinary Approaches

Developing institutional capacity for transdisciplinary approaches entails establishing an environment that fosters and promotes collaboration across various disciplines and sectors. This necessitates implementing organisational and systemic changes to cultivate a culture of integration and partnership (O'Donovan et al. 2022).

Institutions should establish frameworks and mechanisms to foster collaboration among scientists, policymakers, practitioners, and communities. This can be achieved by creating interdisciplinary research centres, developing partnerships between academic institutions and government agencies, and promoting collaborative networks that unite diverse stakeholders. These structures provide the institutional support needed to sustain transdisciplinary research efforts and ensure their incorporation into policy and practice (Lang et al. 2012).

Adapting funding mechanisms is essential for supporting TDR. Funding agencies and donors should prioritise projects involving multiple disciplines and stakeholders. Providing long-term support for iterative learning and adaptation is crucial. Flexible funding arrangements can enable researchers and practitioners to respond to emerging challenges and opportunities, ensuring the relevance and responsiveness of TDR (Cundill et al. 2019).

Education and training programs are crucial in establishing institutional capacity for transdisciplinary approaches.

By incorporating TDR principles into curricula and providing hands-on learning opportunities, educational institutions can effectively equip future researchers, policymakers, and practitioners with the skills to collaborate across disciplinary boundaries.

Participating in professional development courses and workshops can facilitate the acquisition of the necessary competencies for current practitioners and policymakers to engage in effective transdisciplinary work (Matsuura and Razak 2019).

Policy frameworks should embrace the principles of TDR, which involve incorporating requirements for stakeholder engagement, collaboration, and knowledge integration into DRR policies and guidelines. By embedding these principles into policy frameworks, we can ensure the systematic application of transdisciplinary approaches and achieve benefits on a broader scale (Whelchel et al. 2018).

7.4 Enhancing Resilience Through Integrated Policies

Integrated policies that integrate scientific, technical, and local knowledge are indispensable for enhancing landslide resilience. These policies can address the root causes of vulnerability, such as poverty, inadequate infrastructure, and environmental degradation while implementing effective risk-reduction measures (Alcántara-Ayala et al. 2017). For instance, integrated policies could encompass structural measures, such as slope stabilisation and improved drainage systems, and non-structural measures, such as land-use planning, community education, and social protection programs (Alcántara-Ayala and Geertsema 2022).

Furthermore, comprehensive policies should support adaptive management practices that facilitate continual learning and adjustments. This includes consistently monitoring and assessing the effectiveness of disaster risk reduction (DRR) interventions, integrating new knowledge and experiences, and making essential modifications to strategies and plans. Adaptive management guarantees that DRR initiatives remain effective and adaptable to evolving conditions and emerging risks (Roux et al. 2017).

7.5 Strengthening Community Engagement and Ownership

Community engagement serves as a cornerstone for effective TDR and DRR. Prioritising community participation in policies and practices can enhance the relevance and sustainability of risk reduction efforts. Involving communities in the research process ensures that local knowledge and priorities are considered and fosters a sense of ownership and empowerment. As a result, this can lead to a more substantial commitment from the community to implement and sustain DRR measures (Takeuchi et al. 2024).

Implementing effective community engagement strategies involves participatory risk assessments, community-driven monitoring systems, and inclusive decision-making processes. These strategies foster trust and collaboration among communities, researchers, and policymakers, ultimately leading to more effective and sustainable DRR outcomes.

7.6 Facilitating Knowledge Exchange and Learning

It is essential to recognise that knowledge exchange and continuous learning play a vital role in the success of transdisciplinary approaches. Platforms and networks that enable sharing knowledge, experiences, and best practices are instrumental in helping stakeholders learn from one another and enhance their disaster risk reduction efforts (Roux et al. 2017). These platforms may include conferences, workshops, online forums, and collaborative research initiatives.

Knowledge exchange platforms can foster a culture of learning and innovation and support the development of new tools, methodologies, and strategies for landslide DRR. Moreover, these platforms provide valuable opportunities for stakeholders to establish relationships and partnerships essential for effective collaboration and integration (Beckett and Vachhrajani 2017).

7.7 Promoting Policy Coherence and Integration

Effective landslide disaster risk reduction DRR requires policy coherence and integration. This means aligning DRR policies with broader development, environmental, and social policies. For instance, incorporating DRR considerations into urban planning, infrastructure development, and environmental conservation policies can address the underlying drivers of landslide risk and foster sustainable development (Acuña et al. 2021).

Facilitating coordination and collaboration across diverse government departments, sectors, and levels of governance is essential to advancing policy coherence. This can be accomplished by establishing inter-agency working groups, developing integrated policy frameworks, and integrating DRR as a pivotal consideration in all relevant policy domains (Collins et al. 2017).

8 Challenges for TDR-ILDRiM

Transdisciplinary research is valuable for addressing complex issues, such as integrated landslide disaster risk management. However, this collaborative approach encounters challenges stemming from the need for strong collaboration, methodological innovation, and sustained engagement.

Integrating knowledge from various disciplines poses a significant challenge in managing landslide disaster risk. Due to their distinct methodologies and terminologies, it is not easy to incorporate insights from geology, engineering, urban planning, sociology, and environmental science. Furthermore, involving non-academic stakeholders such as local communities, policymakers, and emergency responders adds further complexity, necessitating intellectual flexibility and a deep understanding of each field's principles.

Collaboration and communication are essential for successful transdisciplinary research in disaster risk management, but they pose significant challenges. Language barriers, specialised terminology, and differing communication styles often impede effective communication across disciplines. Coordinating diverse participants necessitates strong leadership, clear communication, and the establishment of a shared vision, which can be challenging to achieve in practice.

Methodological challenges are prevalent in transdisciplinary research on landslide risk management. New or adapted existing methods are often necessary to address unique and complex questions. This involves integrating quantitative data, such as slope stability analysis, with qualitative insights from community-based risk assessments. Synthesising data from various sources and formats and ensuring robust and applicable findings further complicates the research process.

Institutional and structural barriers can impede collaboration in transdisciplinary research. For example, researchers focusing on landslide risk management may struggle to secure funding from discipline-specific funding agencies. Additionally, career advancement in interdisciplinary work may be hindered by traditional academic evaluation criteria.

The time and resource intensity of transdisciplinary research in landslide risk management cannot be underestimated. These projects often require extended timeframes due to the need for iterative collaboration, data integration, and the engagement of diverse stakeholders. The resource demands are also significant, as successful projects typically require access to a wide range of expertise, extensive stakeholder involvement, and the development of complex methodologies. These factors can make transdisciplinary research more resource-intensive and challenging to sustain than traditional, discipline-specific approaches.

Evaluating the success and impact of transdisciplinary research is challenging. Traditional academic metrics may not fully capture the real impact of research focused on disaster risk management, which prioritises practical solutions and real-world change. Recognising and rewarding participating researchers in collaborative projects is also complex.

Transdisciplinary research in disaster risk management presents ethical and political challenges. Stakeholder involvement can lead to power imbalances, conflicting interests, and the need for careful navigation to balance local knowledge and scientific standards.

Another significant challenge is maintaining long-term engagement and collaboration across disciplines and sectors. In landslide risk management, maintaining collaboration over time can be difficult, particularly when faced with team member turnover, stakeholder priority shifts, or funding availability changes. Ensuring that the knowledge generated through transdisciplinary research is effectively transferred to and utilised by stakeholders, such as through the implementation of early warning systems or the development of new land-use policies, requires ongoing effort and engagement beyond the formal conclusion of the research project.

Finally, cultural and societal factors play a crucial role in the success of transdisciplinary research in landslide risk management. Engaging with communities from diverse cultural backgrounds requires a deep understanding of and sensitivity to different worldviews and local practices. This is particularly important in areas where traditional knowledge and local practices are integral to disaster risk management. Balancing scientific rigour with the need to produce socially relevant and actionable outcomes can create tension between academic and societal expectations, further complicating the research process.

9 Concluding Remarks

Understanding landslide disaster risk requires a multifaceted approach that goes beyond the hazards. It examines the socio-economic, social, political, and cultural dimensions contributing to vulnerability and exposure. This multidimensional perspective enables the development of targeted strategies that address the complexities of landslide risks, including underlying factors and risk drivers, and enhance communities' resilience. By considering the interplay between natural hazards, human factors, and spatial exposure, it becomes possible to design effective risk reduction

measures that decrease the likelihood and impact of landslides, safeguarding lives and property.

ILDRiM necessitates a transdisciplinary, integrated, and collaborative approach involving governments, non-governmental organisations, the private sector, and communities. This implies integrating scientific knowledge, technological advancements, experience from successful practice, local knowledge and traditional practices to manage landslide risk effectively. ILDRiM aims to create safer, more resilient communities capable of understanding, withstanding and recovering from landslide disasters by prioritising the reduction of vulnerability and exposure within this comprehensive framework (Alcántara-Ayala 2021).

Against this background, innovative and constructive approaches need to be employed. TDR integrates academic and non-academic expertise to address complex societal challenges. It stresses applying knowledge in real-world scenarios, the fusion of multiple disciplines, the involvement of diverse stakeholders, and the collaborative production of knowledge. TDR is contextually sensitive and iterative, fostering mutual learning, systems thinking, and reflexivity among all participants (Lang et al. 2012).

Engaging stakeholders in the collaborative production of knowledge is a dynamic process that enriches the relevance and impact of research. Co-production ensures that the knowledge generated is context-specific and actionable by involving stakeholders in problem framing, data collection, analysis, and dissemination. While this approach poses challenges, implementing best practices can lead to more equitable and effective outcomes, ultimately developing more resilient and sustainable communities (Weichselgartner and Pigeon 2015).

Methodologies and tools for transdisciplinary landslide disaster risk reduction encompass a broad spectrum of activities (Thiery et al. 2017). These activities integrate scientific and local knowledge, facilitate effective risk communication, support collaborative planning, and build capacity among stakeholders. By utilising these diverse approaches, it is possible to develop comprehensive, context-specific strategies that enhance community resilience and reduce the impacts of landslides.

Transdisciplinary research has substantial implications for reducing the risk of landslide disasters. Integrating diverse forms of knowledge and engaging various stakeholders can provide comprehensive and context-specific insights (Alcántara-Ayala 2018). These insights can inform more effective and equitable policies and interventions.

Under such account, regarding policy and practice applications, a transdisciplinary research approach is essential for bridging the gap between theoretical insights and practical application in addressing landslide disaster risk. Research outcomes can effectively translate into actionable policies and interventions by leveraging TDR findings to inform policy and practice.

Building institutional capacity for transdisciplinary approaches involves creating an enabling environment that supports collaboration, adapting funding mechanisms, enhancing educational and training programs, and promoting policy coherence and integration. Through these efforts, transdisciplinary research can contribute to developing more resilient and sustainable communities better prepared to manage and reduce the risks of landslides.

Integrating policies that enhance resilience addresses both immediate and long-term risk management needs while strengthening community engagement ensures that local knowledge and perspectives are integral to the process.

While transdisciplinary research holds significant promise for advancing integrated landslide disaster risk management, it is accompanied by many challenges. These range from the complexities of integrating diverse knowledge systems and navigating interdisciplinary communication to institutional barriers, ethical considerations, and the demands of long-term collaboration. Addressing these challenges requires careful planning, a commitment to innovation, and a sustained effort to bridge the gap between academic research and practical, real-world applications.

Nonetheless, we concur with Ismail-Zadeh et al. (2017), who emphasised the necessity for a transdisciplinary approach that integrates natural, engineering, and social sciences with active involvement from diverse stakeholders and policymakers. This approach aims to generate practical research to inform disaster risk reduction and resilience strategies, particularly in the context of climate change and increasing societal vulnerabilities.

Transdisciplinary education, hands-on learning opportunities, and mentorship programs should be promoted to equip the next generation to tackle global future challenges. These initiatives will help develop practical skills and foster a community of transdisciplinary thinkers across the science, policy, and society interface (Alcántara-Ayala et al. 2024).

In closing, research can be transformed into action by bridging disciplines and engaging diverse actors and stakeholders; only with community agency will it be possible to work towards protecting society's future by understanding and addressing the mounting challenges of disaster risks, climate change and the unsustainable world we have shaped (Fig. 9).

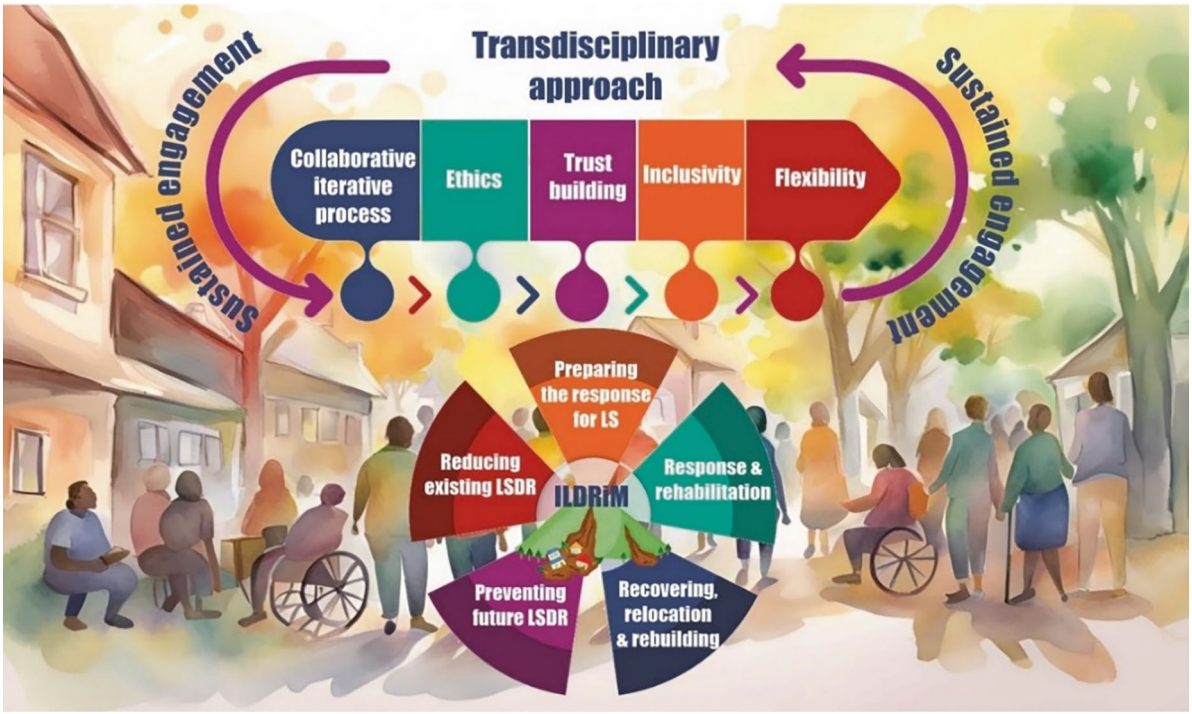

Fig. 9 Transdisciplinary research in integrated landslide disaster risk management involves key processes such as risk assessment, prevention, preparedness, response, recovery, and continuous improvement. It requires adherence to core principles: collaborative, iterative processes, ethics, trust building, inclusivity, flexibility, and sustained engagement, ensuring the research is both scientifically sound and practically effective

Acknowledgements Thanks to DGAPA-UNAM for providing financial support to conduct landslide risk research through Project PAPIIT IN300823.

References

Acuña V, Roldán F, Tironi M, Juzam L (2021) The geo-social model: a transdisciplinary approach to flow-type landslide analysis and prevention. Sustainability 13(5):2501

Adler C, Hirsch Hadorn G, Breu T, Wiesmann U, Pohl C (2018) Conceptualizing the transfer of knowledge across cases in transdisciplinary research. Sustain Sci 13:179–190

Ahmed B (2021) The root causes of landslide vulnerability in Bangladesh. Landslides 18:1707–1720

Alam E (2020) Landslide hazard knowledge, risk perception and preparedness in Southeast Bangladesh. Sustainability 12(16):6305

Alam E, Ray-Bennett NS (2021) Disaster risk governance for district-level landslide risk management in Bangladesh. Int J Disaster Risk Reduct 59:102220

Alcántara-Ayala I (2018) On the multi-dimensions of integrated research on landslide disaster risk. In: Landslides and engineered slopes. Experience, theory and practice. CRC Press, pp 155–168

Alcántara-Ayala I (2021) Integrated landslide disaster risk management (ILDRiM): the challenge to avoid the construction of new disaster risk. Environ Hazards 20(3):323–344

Alcántara-Ayala I, Geertsema M (2022) Landslides. In: Routledge handbook of environmental hazards and society. Routledge, pp 49–70

Alcántara-Ayala I, Geertsema M (2023) Construction of disaster risk in mountain systems and its integrated management. In: Montology palimpsest: a primer of mountain geographies. Springer International Publishing, Cham, pp 335–355

Alcántara-Ayala I, Moreno AR (2016) Landslide risk perception and communication for disaster risk management in mountain areas of developing countries: a Mexican foretaste. J Mt Sci 13:2079–2093

Alcántara-Ayala I, Murray V, Daniels P, McBean G (2017) International Council for Science (ICSU)—on the future challenges for the integration of science into international policy development for landslide disaster risk reduction. In: Advancing culture of living with landslides: volume 1 ISDR-ICL Sendai partnerships 2015–2025. Springer International Publishing, pp 143–154

Alcántara-Ayala I, Vogel C, Kotani M, Mooney C, Singh SM, Leal de Moraes OL (2024) Towards pathways to sustainable futures: the role of transdisciplinary approaches to weather, climate, water and related environmental and social sciences. In: Stuart S, Pusch C, Bhasin I, Gallo I (eds) United in Science 2024: a multi-organization high-level compilation of the latest weather, climate, water and related environmental and social sciences for the future. World Meteorological Organisation, Geneva

Barth M, Jiménez-Aceituno A, Lam DP, Bürgener L, Lang DJ (2023) Transdisciplinary learning as a key leverage for sustainability transformations. Curr Opin Environ Sustain 64:101361

Beckett RC, Vachhrajani H (2017) Transdisciplinary innovation: connecting ideas from professional and user networks. J Ind Integr Manag 2(04):1750016

Bergmann M, Hirsch Hadorn G, Metag J (eds) (2021) Conceptualising transdisciplinarity—origins, approaches and challenges. Springer Nature

Bieluch KH, Bell KP, Teisl MF, Lindenfeld LA, Leahy J, Silka L (2017) Transdisciplinary research partnerships in sustainability science: an examination of stakeholder participation preferences. Sustain Sci 12:87–104

Blaikie P, Cannon T, Davis I, Wisner B (2014) At risk: natural hazards, people's vulnerability and disasters. Routledge

Bobrowsky P, Highland L (2013) The landslide handbook-a guide to understanding landslides: a landmark publication for landslide education and preparedness. Springer, Berlin/Heidelberg, pp 75–84

Brandt P, Ernst A, Gralla F, Luederitz C, Lang DJ, Newig J et al (2013) A review of transdisciplinary research in sustainability science. Ecol Econ 92:1–15

Bréthaut C, Gallagher L, Dalton J, Allouche J (2019) Power dynamics and integration in the water-energy-food nexus: learning lessons for transdisciplinary research in Cambodia. Environ Sci Pol 94:153–162

Buser T (2021) Transdisciplinary research as boundary work: facilitating collaboration between disciplines and with society. Springer Nature

Carrara A, Crosta G, Frattini P (2003) Geomorphological and historical data in assessing landslide hazard. Earth Surface Process Landf 28(10):1125–1142

Carvalho C, Del Campo AG, de Carvalho Cabral D (2022) Scales of inequality: the role of spatial extent in environmental justice analysis. Landsc Urban Plan 221:104369

Casagli N, Canuti P, Sassa K, Tofani V (2024) The Sixth World Landslide Forum (WLF6), Florence, 2023. Landslides 21(6):1161–1172

Cascini LCJRJO, Bonnard C, Corominas J, Jibson R, Montero-Olarte J (2005) Landslide hazard and risk zoning for urban planning and development. In: Landslide risk management. CRC Press, pp 209–246

Castro CV, Rifai HS (2021) Development and assessment of a web-based national spatial data infrastructure for nature-based solutions and their social, hydrological, ecological, and environmental co-benefits. Sustain For 13(19):11018

Choi KY, Cheung RW (2013) Landslide disaster prevention and mitigation through works in Hong Kong. J Rock Mech Geotech Eng 5(5):354–365

Cockburn J, Cundill G (2018) Ethics in transdisciplinary research: reflections on the implications of 'Science with Society'. In: The Palgrave handbook of ethics in critical research, pp 81–97

Collins A, Tatano H, James W, Wannous C, Takara K, Murray V et al (2017) The third global summit of research institutes for disaster risk reduction: expanding the platform for bridging science and policy making. Int J Disaster Risk Sci 8:224–230

Cronin K (2008) Transdisciplinary research (TDR) and sustainability. Overview report prepared for the Ministry of Research, Science and Technology

Cundill G, Harvey B, Tebboth M, Cochrane L, Currie-Alder B, Vincent K et al (2019) Large-scale transdisciplinary collaboration for adaptation research: challenges and insights. Global Chall 3(4):1700132

Cutter SL, Boruff BJ, Shirley WL (2012) Social vulnerability to environmental hazards. In: Hazards vulnerability and environmental justice. Routledge, pp 143–160

Dasanayaka U, Matsuda Y (2022) Role of social capital in local knowledge evolution and transfer in a network of rural communities coping with landslide disasters in Sri Lanka. Int J Disaster Risk Reduct 67:102630

Duncan JM, Wright SG, Brandon TL (2014) Soil strength and slope stability. Wiley

Glade T (2003) Landslide occurrence as a response to land use change: a review of evidence from New Zealand. Catena 51(3–4):297–314

Hicks A, Barclay J, Chilvers J, Armijos MT, Oven K, Simmons P, Haklay M (2019) Global mapping of citizen science projects for disaster risk reduction. Front Earth Sci 7:226

Highland LM, Bobrowsky P (2008) The landslide handbook-a guide to understanding landslides (No. 1325). US Geological Survey

Hoffmann S, Klein JT, Pohl C (2019) Linking transdisciplinary research projects with science and practice at large: introducing insights from knowledge utilization. Environ Sci Pol 102:36–42

Intrieri E, Gigli G, Mugnai F, Fanti R, Casagli N (2012) Design and implementation of a landslide early warning system. Eng Geol 147:124–136

Ismail-Zadeh AT, Cutter SL, Takeuchi K, Paton D (2017) Forging a paradigm shift in disaster science. Nat Hazards 86:969–988

Jacobi J, Llanque A, Mukhovi SM, Birachi E, von Groote P, Eschen R et al (2022) Transdisciplinary co-creation increases the utilization of knowledge from sustainable development research. Environ Sci Pol 129:107–115

Jorgenson AJ (2021) The transdisciplinary turn in environmental sociology. Routledge

Kelman I (2024) Choosing or avoiding disaster. Geography 109(1):36–39

Klein JT (2001) The discourse of transdisciplinarity: An expanding global field. In: Klein JT, Häberli R, Scholz RW, Bill A, Welti M (eds) Transdisciplinarity: Joint problem solving among science, technology, and society: An Effective Way for Managing Complexity (pp. 35–44). Birkhäuser Basel, Basel

Klein JT (2008) Evaluation of interdisciplinary and transdisciplinary research: a literature review. Am J Prev Med 35(2):S116–S123

Kok KP, Gjefsen MD, Regeer BJ, Broerse JE (2021) Unraveling the politics of 'doing inclusion' in transdisciplinarity for sustainable transformation. Sustain Sci 16:1811–1826

Kruijf JVD, Verbrugge L, Schröter B, den Haan RJ, Cortes Arevalo J, Fliervoet J et al (2022) Knowledge co-production and researcher roles in transdisciplinary environmental management projects. Sustain Dev 30(2):393–405

Lacasse S, Nadim F, Lacasse S, Nadim F (2009) Landslide risk assessment and mitigation strategy. In: Landslides–disaster risk reduction. Springer, Berlin, pp 31–61

Lang DJ (2020) Opening up the future(s)—transdisciplinarity as freedom. Sustain Sci 15(5):1363–1374

Lang DJ, Wiek A, Bergmann M, Stauffacher M, Martens P, Moll P et al (2012) Transdisciplinary research in sustainability science: practice, principles, and challenges. Sustain Sci 7:25–43

Lawrence MG, Williams S, Nanz P, Renn O (2022) Characteristics, potentials, and challenges of transdisciplinary research. One Earth 5(1):44–61

Macherera M, Chimbari MJ (2016) A review of studies on community based early warning systems. Jàmbá: J Disaster Risk Stud 8(1)

Martha TR, Roy P, Jain N, Vinod Kumar K, Reddy PS, Nalini J et al (2021) Rock avalanche induced flash flood on 07 February 2021 in Uttarakhand, India—a photogeological reconstruction of the event. Landslides 18(8):2881–2893

Matsuura S, Razak KA (2019) Exploring transdisciplinary approaches to facilitate disaster risk reduction. Disaster Prev Manag Int J 28(6):817–830

Morton LW, Eigenbrode SD, Martin TA (2015) Architectures of adaptive integration in large collaborative projects. Ecol Soc 20(4)

Murillo-García F, Rossi M, Fiorucci F, Alcántara-Ayala I (2015) Population landslide vulnerability evaluation: the case of the indigenous population of Pahuatlán-Puebla, Mexico. In: Engineering geology for society and territory-volume 2: landslide processes. Springer International Publishing, pp 1793–1797

Narvéz L, Lavell A, Pérez Ortega G (2009) La gestión del riesgo de desastres: un enfoque basado en procesos. In: La gestión del riesgo de desastres: Un enfoque basado en procesos, pp 102–102

Nathan F (2008) Risk perception, risk management and vulnerability to landslides in the hill slopes in the city of La Paz, Bolivia. A preliminary statement. Disasters 32(3):337–357

Nithya SE, Prasanna PR (2010) An integrated approach with GIS and remote sensing technique for landslide hazard zonation. Int J Geo Geosci 1(1):66–75

Norström AV, Cvitanovic C, Löf MF, West S, Wyborn C, Balvanera P et al (2020) Principles for knowledge co-production in sustainability research. Nat Sustain 3(3):182–190

O'Donovan C, Michalec A, Moon JR (2022) Capabilities for transdisciplinary research. Res Eval 31(1):145–158

Oliver-Smith A, Alcántara-Ayala I, Burton I, Lavell A (2016) Forensic investigations of disasters (FORIN): a conceptual framework and guide to research. Integrated Research on Disaster Risk, Beijing

O'Rourke M, Crowley S (2020) Philosophy of transdisciplinarity. Oxford University Press
Pardeshi SD, Autade SE, Pardeshi SS (2013) Landslide hazard assessment: recent trends and techniques. Springerplus 2:1–11
Paton D, Buergelt P (2019) Risk, transformation and adaptation: ideas for reframing approaches to disaster risk reduction. Int J Environ Res Public Health 16(14):2594
Peduzzi P (2019) The disaster risk, global change, and sustainability nexus. Sustainability 11(4):957
Pellicani R, Van Westen CJ, Spilotro G (2014) Assessing landslide exposure in areas with limited landslide information. Landslides 11:463–480
Pipere A, Lorenzi F (2021) The dialogical potential of transdisciplinary research: challenges and benefits. World Futures 77(8):559–590
Polk M (2015) Transdisciplinary co-production: designing and testing a transdisciplinary research framework for societal problem solving. Futures 65:110–122
Puente-Sotomayor F, Egas A, Teller J (2021) Land policies for landslide risk reduction in Andean cities. Habitat Int 107:102298
Raška P (2019) Contextualizing community-based landslide risk reduction: an evolutionary perspective. Landslides 16(9):1747–1762
Roux DJ, Nel JL, Cundill G, O'farrell P, Fabricius C (2017) Transdisciplinary research for systemic change: who to learn with, what to learn about and how to learn. Sustain Sci 12:711–726
Sarabia MM, Kägi A, Davison AC, Banwell N, Montes C, Aebischer C, Hostettler S (2020) The challenges of impact evaluation: attempting to measure the effectiveness of community-based disaster risk management. Int J Disaster Risk Reduct 49:101732
Schmidt L, Falk T, Siegmund-Schultze M, Spangenberg JH (2020) The objectives of stakeholder involvement in transdisciplinary research. A conceptual framework for a reflective and reflexive practise. Ecol Econ 176:106751
Schneider F, Llanque-Zonta A, Andriamihaja OR, Andriatsitohaina RNN, Tun AM, Boniface K et al (2022) How context affects transdisciplinary research: insights from Asia. Afr Latin Am Sustain Sci 17(6):2331–2345
Schneiderbauer S, Pisa PF, Shroder JF, Szarzynski J (eds) (2023) Safeguarding mountain social-ecological systems, vol. 1: a global challenge: facing emerging risks and adapting to changing environments. Elsevier
Scholz RW, Renn O (2024) Codes of conduct for collaboration as social rule systems for transdisciplinary processes. Syst Pract Action Res 37(1):81–101
Scholz RW, Steiner G (2015) The real type and ideal type of transdisciplinary processes: part I—theoretical foundations. Sustain Sci 10:527–544
Segoni S, Piciullo L, Gariano SL (2018) A review of the recent literature on rainfall thresholds for landslide occurrence. Landslides 15(8):1483–1501
Smith K (2013) Environmental hazards: assessing risk and reducing disaster. Routledge
Smith H, Garcia Ferrari S, Medero GM, Rivera H, Coupé F, Mejía Escalante ME et al (2022) Exploring appropriate socio-technical arrangements for the co-production of landslide risk management strategies in informal neighbourhoods in Colombia and Brazil. Int J Urban Sustain Dev 14(1):242–263
Soeters R, van Westen CJ (1996) Slope instability recognition, analysis, and zonation. In: Landslides, investigation and mitigation. National Academy Press, pp 129–177
Steffen W, Sanderson RA, Tyson PD, Jäger J, Matson PA, Moore B III et al (2005) Global change and the earth system: a planet under pressure. Springer Science & Business Media
Stokols D, Fuqua J, Gress J, Harvey R, Phillips K, Baezconde-Garbanati L et al (2003) Evaluating transdisciplinary science. Nicotine Tob Res 5(Suppl_1):S21–S39
Suharini E, Baharsyah M (2020) Learning about landslide disaster mitigation based on a role-playing method assisted by the disaster education pocket book. Rev Int Geogr Educ Online 10(4):618–638
Sultana N, Tan S (2021) Landslide mitigation strategies in Southeast Bangladesh: lessons learned from the institutional responses. Int J Disaster Risk Reduct 62:102402
Takeuchi K, Mangada L, Inoue M, Kikuiri K, Tsukahara K, Katsuhama Y, Ishiwatari M (2024) Challenges of transdisciplinary approach in disaster recovery management. Nat Hazards:1–19
Thiery Y, Reninger PA, Lacquement F, Raingeard A, Lombard M, Nachbaur A (2017) Analysis of slope sensitivity to landslides by a transdisciplinary approach in the framework of future development: the case of La Trinité in Martinique (French West Indies). Geosciences 7(4):135
UN/GA (United Nations General Assembly) (2015) Transforming our world: the 2030 Agenda for Sustainable Development, A/RES/70/1. United Nations
UNISDR (United Nations International Strategy for Disaster Reduction) (2015) Sendai framework for disaster risk reduction 2015–2030
van Westen CJ, Fonseca F, Van Den Bout B (2021) Challenges in analyzing landslide risk dynamics for risk reduction planning. In: 13th International symposium on landslides
Walter AI, Helgenberger S, Wiek A, Scholz RW (2007) Measuring societal effects of transdisciplinary research projects: Design and application of an evaluation method. Evaluation and Program Planning, 30(4), 325–338.
Weichselgartner J, Pigeon P (2015) The role of knowledge in disaster risk reduction. Int J Disaster Risk Sci 6:107–116
West S, Van Kerkhoff L, Wagenaar H (2019) Beyond "linking knowledge and action": towards a practice-based approach to transdisciplinary sustainability interventions. Policy Stud 40(5):534–555
Whelchel AW, Reguero BG, van Wesenbeeck B, Renaud FG (2018) Advancing disaster risk reduction through the integration of science, design, and policy into eco-engineering and several global resource management processes. Int J Disaster Risk Reduct 32:29–41
Winter MG (2014) A strategic approach to landslide risk reduction. Int J Lands Environ 2(1):14–23
WMO (2024) FACTSHEET. Available at: https://wmo.int/sites/default/files/2024-06/Early-Warnings-for-All_Factsheet_EN.pdf
Zurba M, Petriello MA, Madge C, McCarney P, Bishop B, McBeth S et al (2022) Learning from knowledge co-production research and practice in the twenty-first century: global lessons and what they mean for collaborative research in Nunatsiavut. Sustain Sci 17(2):449–467

Role of Land Cover and its Changes in Triggering Rainfall-Induced Shallow Landslides in Central Italy

Stefano Luigi Gariano, Maria Teresa Brunetti, Massimo Melillo, Elisabetta Napolitano, Eleonora Gioia, Marco Lazzeri, Gabriella Speranza, and Silvia Peruccacci

Abstract

A regional analysis of the role of land cover and its changes on landslide occurrence is carried out. Using a comprehensive dataset of shallow landslides that occurred from 2002 to 2020 in the Marche region (central Italy), hourly rainfall measurements, and different land cover maps, we evaluate how the triggering rainfall conditions change on different land covers. The impact of temporal changes in land cover on the occurrence of landslides is also studied. We find a relevant increase in landslide density in urban areas, a different seasonal distribution of landslides in areas with different land cover, and differences in rainfall thresholds for the initiation of slope failures. More rainfall is needed to trigger landslides in agricultural and forested areas than on artificial surfaces, as a sign of worsening stability conditions due to human activity. Forested areas are characterized by higher values of cumulated rainfall required to trigger landslides, an indication of the slope stabilizing effect of vegetation. Different rainfall triggering conditions are observed in different types of agricultural areas, indicating how agricultural practices can influence slope instability. The findings of this work are useful for territorial planning and landslide risk assessment, also in view of ongoing climate and environmental changes.

Keywords

CORINE land cover · Rainfall thresholds · Landslide distribution · Shallow landslides · Marche

1 Introduction

Land cover, and their changes, influence the occurrence, distribution, and frequency of landslides (Sidle and Ochiai 2006). They act as predisposing factors for landslides and also affect the distribution of the vulnerable elements, thus influencing both landslide hazard and risk. Changes in land cover can reduce slope stability in some cases—e.g. deforestation or cutting of slopes for road or building construction—or increase it in others—e.g. new vegetation reducing soil erosion and increasing stabilizing forces through root reinforcement (Masi et al. 2021; Pacheco Quevedo et al. 2023). Furthermore, unsustainable agricultural practices characterized by heavy mechanization, such as tillage, can cause soil instabilization (Volpe et al. 2022). Therefore, evaluating the role of land cover, and its change, in the initiation of rainfall-induced landslides is relevant for landslide risk analysis and management.

The role of land cover/use on landslide occurrence has been addressed in works, considering both observed and projected changes (Glade 2003; Alcàntara-Ayala et al. 2006; Beguería 2006; Reichenbach et al. 2014; Pisano et al. 2017; Gariano et al. 2018; Shu et al. 2019; Knevels et al. 2020; Ávila et al. 2021; Hürlimann et al. 2022; Pacheco Quevedo et al. 2023). Almost all works focused on evaluating the influence of land cover/use changes on landslide susceptibility assessment at the basin scale. A regional-scale analysis of the influence of land cover and its changes on rainfall

Award Memorial Article: ICL Book Article Award

S. L. Gariano (✉) · M. T. Brunetti · M. Melillo · E. Napolitano · S. Peruccacci
CNR IRPI, Perugia, Italy
e-mail: stefanoluigi.gariano@cnr.it; mariateresa.brunetti@cnr.it; massimo.melillo@cnr.it; elisabettanapolitano@cnr.it; silvia.peruccacci@cnr.it

E. Gioia
Marche Polytechnic University, Ancona, Italy
e-mail: e.gioia@univpm.it

M. Lazzeri · G. Speranza
Civil Protection Office of Marche Region, Ancona, Italy
e-mail: marco.lazzeri@regione.marche.it; gabriella.speranza@regione.marche.it

B. Abolmasov et al. (eds.), *Progress in Landslide Research and Technology, Volume 4 Issue 1, 2025*, Progress in Landslide Research and Technology, https://doi.org/10.1007/978-3-031-89836-5_4

triggering conditions of shallow landslides is missing. Such an analysis can provide significant insights into this complicated relationship, useful for landslide risk mitigation and territorial planning and management.

In this work, we consider land cover, i.e. the biological and physical materials on the Earth's surface comprising both natural elements and surfaces modified by humans, rather than land use, i.e. the socio-economic occupation of the land (Herold et al. 2006), to evaluate both natural and anthropogenic influences on landslide triggering. We use a comprehensive dataset of shallow landslides that occurred in the Marche region (central Italy) from 2002 to 2020 and different maps of land cover to evaluate whether the landslide-triggering rainfall conditions change in areas with different land cover. The effect of temporal changes in land cover on the occurrence of landslides is also assessed.

2 Data

2.1 Landslide and Rainfall Records

We use a catalogue of 1221 rainfall-induced shallow landslides that occurred between 2002 and 2020 in the Marche region, located in the eastern part of central Italy. Figure 1 shows the distribution of landslides in the regional territory. Slope failures are homogenously distributed in both the hilly and mountainous areas of the region.

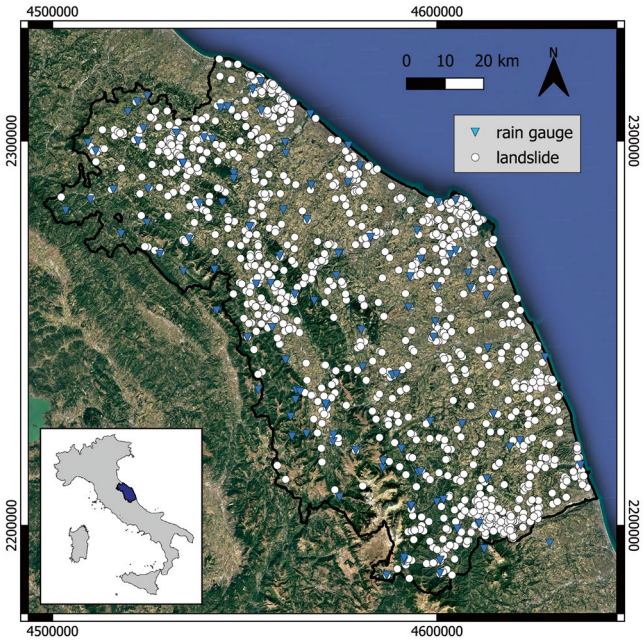

Fig. 1 Distribution of the 1221 rainfall-induced shallow landslides and the 149 rain gauges in Marche region. The inset shows the location of the region within the Italian peninsula. Background from Bing. EPSG: 3035

All landslides are mapped as points and for each record several information is known, including: source of information, landslide type (if available), geographic coordinates, location and municipality, day and approximate or exact time of occurrence, classes of spatial and temporal accuracy. Information is gathered mostly from local and national newspapers (mainly online) and technical reports from Fire Fighters. Almost all landslides (97%) are classified as generic shallow movements, with only a few mud flows, earth flows and rock falls (1% each) (Hungr et al. 2014). More than 40% of the landslides (492) are localized with a high mapping accuracy (uncertainty <1 km^2) while 692 movements (57%) are mapped with a medium accuracy (uncertainty <10 km^2). Only 37 records (3%) are mapped with a low accuracy (uncertainty between 10 and 100 km^2). For half of the landslides (619 out of 1221) the exact time of occurrence is known; for 147 landslides (12%) the part of the day and for 455 landslides (37%) only the day is known. Regarding the monthly distribution, landslides occurred mostly in spring (530 records, 43%, in March–April-May) and winter (298, 24%, in December–January-February). Only 21% and 12% of the records occurred in autumn (251 landslide) and summer (142), respectively. The average number of landslides per year is 64, with a peak in 2013 and 2014 with 206 and 246 records, respectively (Fig. 2).

The landslide records are included in the ITAlian rainfall-induced LandslIdes Catalogue (ITALICA), an extensive and spatially and temporally accurate catalogue of 6312 rainfall-induced landslides that occurred in Italy between 1996 and 2021 (Peruccacci et al. 2023). The ITALICA catalogue is freely downloadable from Zenodo (Brunetti et al. 2023).

To reconstruct the rainfall responsible for the initiation of each landslide, we use the hourly rainfall data recorded by

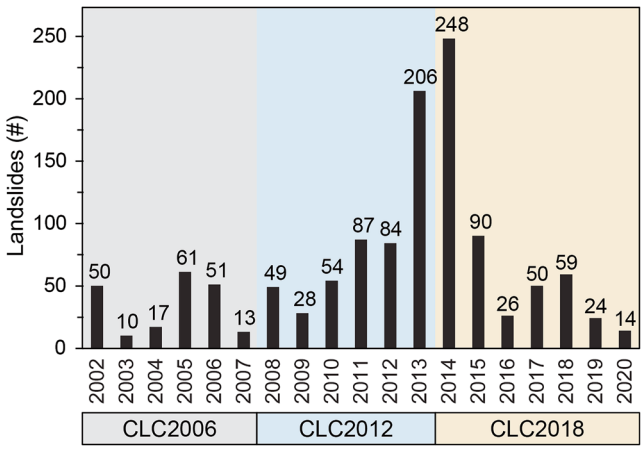

Fig. 2 Annual distribution of the analyzed landslides and scheme used for the association of the CLC classes from three Corine releases to the landslide records

Table 1 Percentage of area per CLC class in the region. The percentages for wetlands and water bodies are not reported

CLC class (level 1)	Percentage of regional area (%)		
	CLC 2006	CLC 2012	CLC 2018
Artificial surfaces	4.7	4.8	4.9
Agricultural areas	64.4	63.8	63.7
Forested areas	30.8	31.3	31.3

149 rain gauges in the regional network managed by the regional Civil Protection Office (triangles in Fig. 1).

2.2 Land Cover Maps

We use three releases of the Corine (Coordination of Information on the Environment) Land Cover (CLC) maps, for the years 2006, 2012, and 2018 (namely CLC2006, CLC2012, and CLC2018). CLC is a vector-based dataset of 44 land cover/use classes, derived from different satellite missions, providing information at a pan-European scale, with a minimum mapping unit of 25 hectares and updates every six years (Corine Land Cover 2021).

We consider the first and the second levels of the maps, which include five and 15 fields, respectively. For each CLC release, Table 1 lists the percentages of regional areas covered by the three first-level land cover classes, i.e., artificial surfaces (AS), agricultural areas (AA) and forested areas (FA). The variations in the percentages of the three first-level classes are minimal in the CLC releases +0.2% for AS, −0.7% for AA and + 0.5% for FA).

3 Methods

3.1 Attribution of Land Cover to Landslides

Each landslide in the catalogue is associated with a land cover class according to its spatial and temporal features. An overlay between the landslide points and the CLC maps is made according to the year of occurrence of the landslides. To consider the land cover of the year closest to the year of occurrence, landslides between 2002 and 2007 are assigned to CLC2006, those between 2008 and 2013 to CLC2012, and those between 2014 and 2020 to CLC2018 (Fig. 2).

Landslide points are converted into circles depending on their mapping accuracy. The radius of the circles is set to 0.6 km, 1.8 km and 5.6 km (corresponding to circular areas equal to 1 km^2, 10 km^2, and 100 km^2) for landslides mapped with a high, medium and low accuracy, respectively. The landslides are then intersected with the CLC class layers and the proportion of each CLC class within each buffer is calculated. A CLC class is attributed to each landslide if it covers at least 75% of the area (Peruccacci et al. 2017).

The number and density of landslides in each class are evaluated for the time intervals associated with CLC2006, CLC2012 and CLC2018. All landslides associated with each CLC class are grouped to assess monthly and seasonal variations in landslide occurrence as a function of land cover. Finally, we reconstruct and analyze the rainfall conditions that triggered the landslides in the different CLC classes.

3.2 Evaluation of Rainfall Triggering Conditions

To automatically reconstruct the rainfall conditions responsible for landslide initiation and to calculate rainfall thresholds, we use CTRL-T (Calculation of Thresholds for Rainfall-induced Landslides—Tool) introduced by Melillo et al. (2018). Using continuous rainfall measurements, rain gauge and landslide locations, and landslide triggering time, CTRL-T (1) identifies the representative rain gauges, (2) reconstructs the triggering conditions (in terms of rainfall duration D and cumulated event rainfall E), and (3) calculates frequentist rainfall thresholds and their associated uncertainties.

Rainfall thresholds at different non-exceedance probabilities are defined adopting the frequentist method (Brunetti et al. 2010), which assumes a power law curve linking D (in h) and E (in mm) in the equation:

$$E = \left(\alpha \pm \Delta\alpha\right) D^{(\gamma \pm \Delta\gamma)} \quad (1)$$

where, α is a scaling constant (the intercept), γ is the shape parameter (that defines the slope), and Δα and Δγ are the uncertainties of α and γ, respectively. Uncertainties associated with the threshold parameters are calculated using a "bootstrap" non-parametric statistical technique (Peruccacci et al. 2012) and depend on the number and distribution of the empirical data points. As an example, the threshold at 5% non-exceedance probability leaves 5% of the (D,E) points below itself.

4 Results

4.1 Spatial and Temporal Variations of Landslides

Figure 2 shows the number of landslides per year divided into the time intervals associated with CLC2006, CLC2012 and CLC2018. In total there are 202 landslides for CLC2006, 508 for CLC2012 and 511 for CLC2018. Two maxima with more than 200 landslides are visible in the years 2013 and

2014. Table 2 lists the number of landslides in each CLC class (AS, AA and FA) based on the maps released in 2006, 2012, 2018.

Fig. 3a shows the percentage of landslides in the three CLC classes, and Table 2 lists the number of landslides per CLC class for the 2006, 2012 and 2018 Corine releases. In all periods, more than 65% (806) of the recorded landslides take place in agricultural areas, and about 20% (238) and 15% (177) in artificial surfaces and forested areas, respectively. No significant percentage changes in the three main CLC classes are observed between the different releases, apart from a slight increase in AS and a slight decrease in FA. The density of landslides per class (number of landslides per 100 km^2), shown in Fig. 3b, exhibits a huge increase in all CLC classes from 2006 to 2012. In particular, landslide density in AA and FA more than doubled, while almost tripled in AS. From 2012 to 2018, landslide density did not change significantly across the three CLC classes.

Table 2 Number of landslides per CLC class

CLC class (level 1)	Landslides (#)		
	CLC 2006	CLC 2012	CLC 2018
Artificial surfaces	35	102	101
Agricultural areas	136	328	342
Forested areas	31	78	68

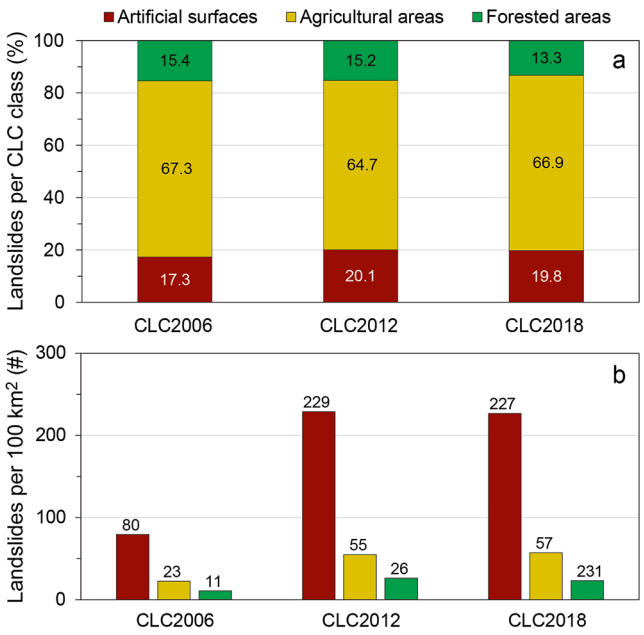

Fig. 3 (**a**) percentage of landslides per CLC class, first level, related to the Corine maps released in 2006, 2012, and 2018; (**b**) number of landslides per 100 km^2 in each CLC class

Figure 4 shows the monthly distribution of landslides and Table 3 lists seasonal number of landslides in AS, AA and FA, respectively. The monthly distribution of landslides varies in the three classes: in AS, landslides occur mainly in March, and December; in AA, landslides take place primarily in early spring (March and May) and secondarily in autumn (September, November, December). In FA, slope failures occur mainly in December and May. Overall, most landslides occur in the spring season (MAM) regardless of CLC class (Table 3).

4.2 Changes in Landslide-Triggering Rainfall Conditions

Using CTRL-T, a triggering rainfall condition is calculated and associated with 703 landslides. The triggering conditions are reconstructed using rain gauges located at an average distance of 6.2 km from the landslides, with a maximum distance of 20 km. The landslide-triggering rainfall conditions have duration D ranging between 1 h and 306 h and cumulated rainfall E values between 5.4 mm and 446.0 mm (with a mean value of 71.6 mm). The corresponding mean

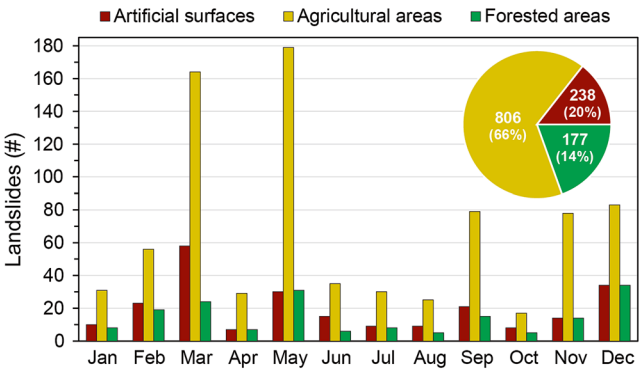

Fig. 4 Monthly number of landslides in the three first-level CLC classes. The pie chart in the inset shows the total number and percentage of landslides in the three classes

Table 3 Seasonal distribution of the landslides in the three CLC classes (first level). Key: DJF, December–January-February; MAM, March–April-May; JJA, June–July-August; SON, September–October-November

CLC class (level 1)	Landslides (#)			
	DJF	MAM	JJA	SON
Artificial surfaces	36	59	17	26
Agricultural areas	95	217	50	94
Forested areas	32	41	13	22

rainfall intensity values range between 0.2 mm/h and 41.2 mm/h (mean value 3.4 mm/h).

For 518 landslides, it was not possible to reconstruct a rainfall condition for various reasons: (1) unlikely amount of rainfall to justify triggering the landslide movement (i.e., cumulated rainfall values too low and inconsistent with the information source), or (2) malfunctioning rain gauges or unreliable rainfall measurements. It is possible that several landslides are triggered by the same rainfall event and reconstructed using the same representative rain gauge. In order to keep only the first triggered landslides and to avoid duplicates, such records were excluded from the analysis.

Overall, 138, 456, and 109 rainfall conditions are reconstructed and associated with landslides that occurred in AS, AA and FA, respectively.

Figure 5 shows the box-and-whiskers plots of the duration and cumulated event rainfall of the rainfall conditions that have triggered landslides the three CLC classes. The landslides that occurred in AA are characterized by a lower rainfall duration median value, while those in FA are triggered by longer rainfall conditions. On the other hand, the cumulated rainfall needed to trigger landslides on AS is on average lower than in AA and FA.

Similar results can be seen by looking at Fig. 6, which shows the kernel density distribution of the *ED* rainfall conditions that induced landslides in the three main CLC classes. In general, landslides occurring in urbanized areas are trig-

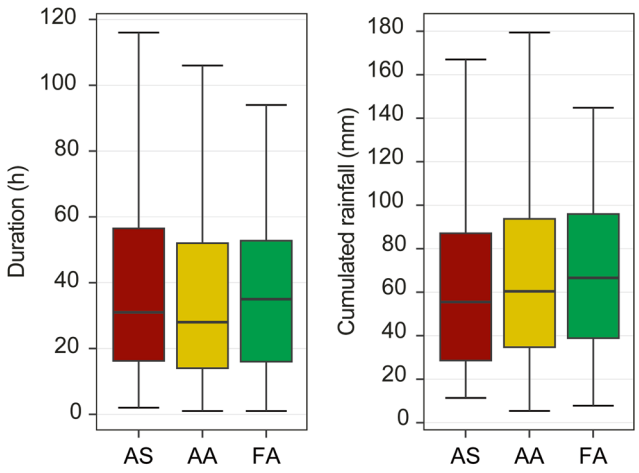

Fig. 5 Box-and-whiskers plots of duration (h) and cumulated event rainfall (mm) of the rainfall conditions that have triggered landslides in artificial surfaces, agricultural areas, and forested areas. Graphs show the median values (horizontal lines inside the boxes), the 25th and 75th percentiles (bottom and top of rectangular boxes), and the value range of 1.5 times the interquartile range (whiskers)

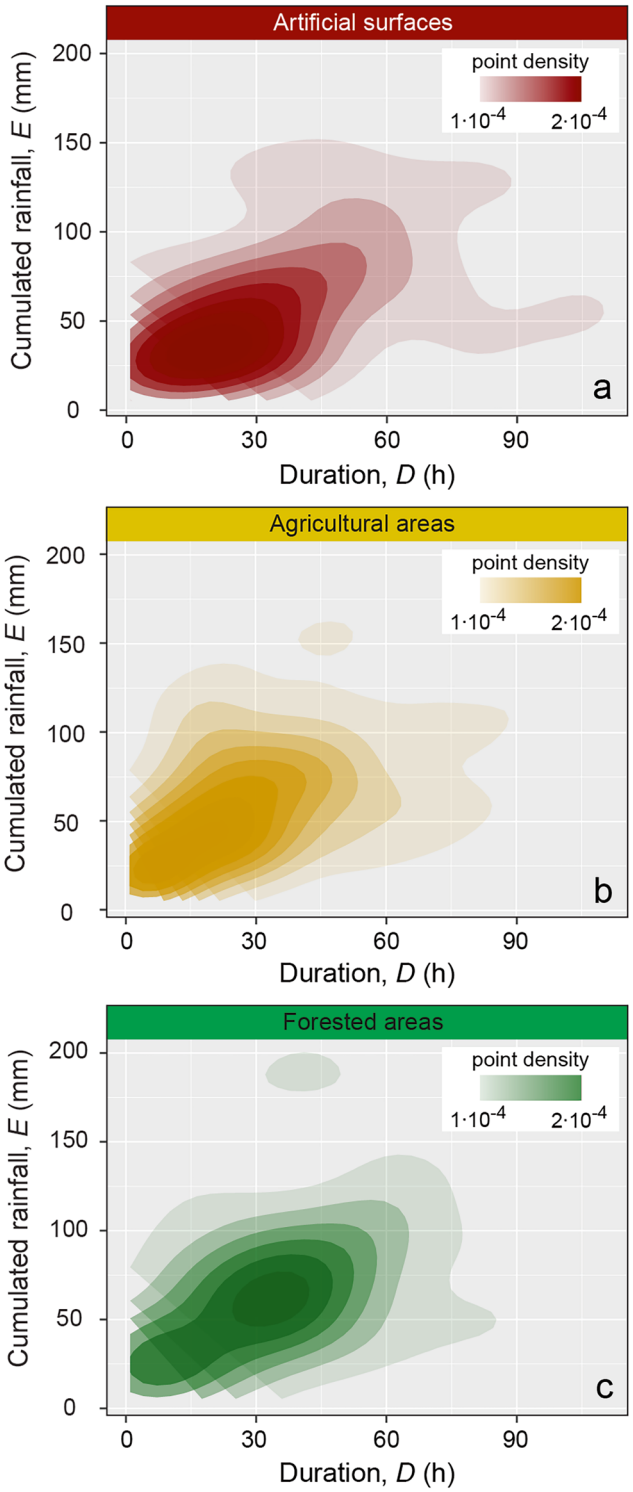

Fig. 6 Kernel density distributions of the cumulated rainfall-duration (*ED*) conditions that triggered landslides in (**a**) artificial surfaces, (**b**) agricultural areas, and **c** forested areas

gered by significantly shorter and less intense rainfall conditions than those localized in vegetated areas. On the other hand, longer and wetter conditions are required to trigger landslides in forested areas.

4.3 Changes in Rainfall Thresholds

Figure 7 shows the cumulated rainfall-rainfall duration (*ED*) conditions that have resulted in landslides in AS (Fig. 7a), AA (Fig. 7b) and FA (Fig. 7c), and the corresponding frequentist thresholds at 5% non-exceedance probability level (T_{AS}, T_A, T_{FA}), according to Eq. 1. The threshold equations are listed in Table 4.

The thresholds allow a quick comparison between the rainfall conditions that are likely to trigger a landslide in each land cover area. It can be observed that less rainfall is required to trigger a landslide on AS than on AA. The threshold for FA is less steep than that for AA, meaning that for longer duration ($D > 24$ h) a landslide can be triggered with less rainfall in forests than in agricultural areas.

The number of landslide records collected allows a more detailed analysis of the role of land cover in the rainfall conditions that can trigger landslides. Therefore, further analysis is carried out at the second and third levels of the CLC (Corine Land Cover 2021). Here we report the results only for those fields where enough landslides are found. In AS, almost all landslides occur in areas classified as *discontinuous urban fabric* (CLC code 1.1.2, 119 movements). In AA, they are found mostly on arable land (code 2.1 in CLC) and heterogenous agricultural areas (code 2.4). In even more detail, several landslides occur in areas classified as *non-irrigated arable land* (code 2.1.1 in CLC, 191 landslides), *complex cultivation patterns* (code 2.4.2, 156 landslides) and *land principally occupied by agriculture* (code 2.4.3 in CLC, 103 points). In FA, most landslides occur in *broad-leaved forests* (CLC code 3.1.1, 71 landslides). Threshold equations are listed in Table 4.

Given the number of *ED* conditions, the thresholds for discontinuous urban fabric ($T_{C1.1.2}$) and forests ($T_{C3.1.1}$) are quite similar to the corresponding thresholds for artificial surfaces and forested areas (T_{AS} and T_{FA}). On the

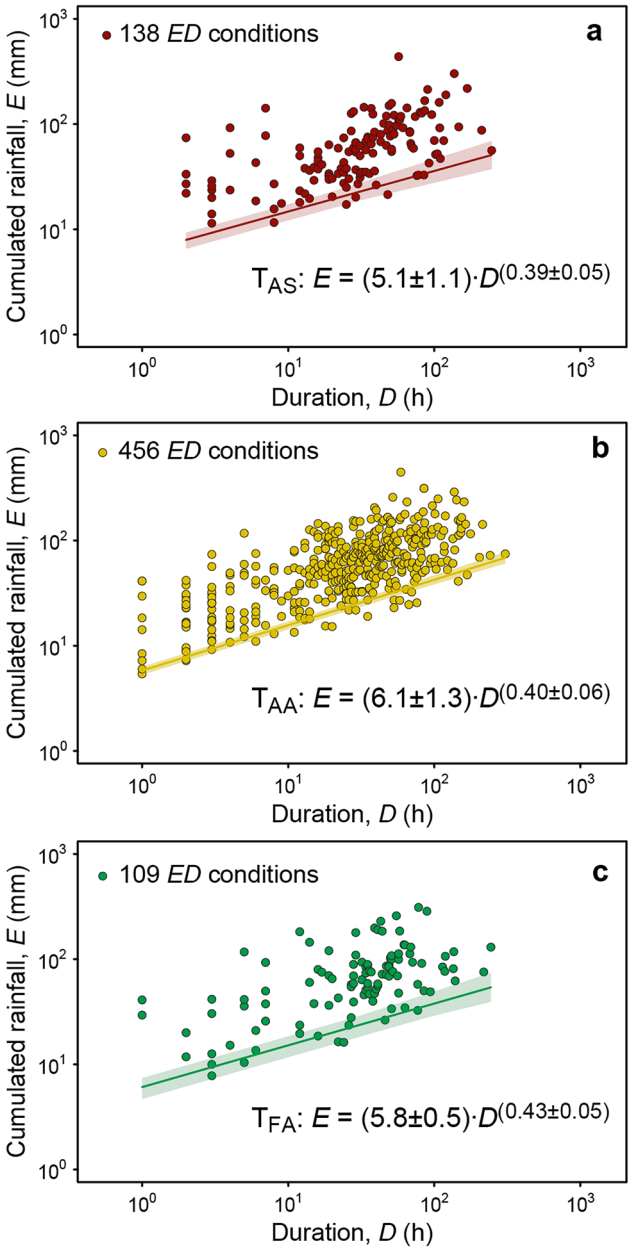

Fig. 7 *ED* conditions that have resulted in landslides in (**a**) artificial surfaces (T_{AS}), (**b**) agricultural areas (T_{AA}), and (**c**) forested areas (T_{FA}), and corresponding frequentist thresholds at 5% non-exceedance probability level, according to Eq. 1. Shaded areas show uncertainty of the thresholds. Data shown in logarithmic coordinates

Table 4 Parameters (Eq. 1) of the *ED* rainfall thresholds for the possible initiation of landslides in areas with different CLC classes (third level). The thresholds are defined for durations in hours and cumulated event rainfall in mm. Key: #, number of rainfall conditions used to calculate the thresholds; T_{AS}, threshold for *artificial surfaces*; T_{AA}, threshold for *agricultural surfaces*; T_{FA}, threshold for *forested areas*; $T_{C1.1.2}$, threshold for *discontinuous urban fabric* CLC1.1.2; $T_{C2.1.1}$, threshold for *non-irrigated arable land* CLC2.1.1; $T_{C2.4.2}$, threshold for *complex cultivation patterns* CLC2.4.2; $T_{C2.4.3}$, threshold for and *land principally occupied by agriculture* CLC2.4.3; $T_{C3.1.1}$, threshold for *broad-leaved forests* CLC3.1.1

		Threshold parameters				
Label	#	α	Δα	γ	Δγ	*D* range (h)
CLC first level						
T_{AS}	138	5.1	1.1	0.39	0.05	2–247
T_{AA}	456	6.1	1.3	0.40	0.06	1–306
T_{FA}	109	5.8	0.5	0.43	0.05	1–244
CLC third level						
$T_{C1.1.2}$	119	5.0	1.0	0.38	0.05	2–247
$T_{C2.1.1}$	191	6.3	0.9	0.42	0.04	1–204
$T_{C2.4.2}$	156	6.4	0.8	0.40	0.05	1–306
$T_{C2.4.3}$	103	4.5	0.8	0.50	0.05	1–204
$T_{C3.1.1}$	71	5.9	1.6	0.41	0.07	2–244

other hand, significant differences are found among the thresholds defined for the three third-level agricultural classes. The thresholds for classes 2.1.1 and 2.4.2 (*non-irrigated arable land* and *complex cultivation patterns*) are similar, while the threshold defined for the class 2.4.3 (*land principally occupied by agriculture*) is lower and steeper.

5 Discussion and Conclusions

Using a comprehensive catalogue of rainfall-induced shallow landslides in the Marche region, hourly rainfall measurements and three releases of Corine land cover maps, we observe differences in the distribution of landslides at different land cover levels and in landslide triggering conditions.

A high landslide density in urban areas is observed in the examined period (Table 2, Fig. 3). This result has relevant implications for landslide risk assessment. In general, the link between urbanization and landslide risk is known, but poorly quantified (Ozturk et al. 2022). Human modifications to slopes (e.g., slope cutting for building construction, vegetation removal, changes in hydrogeological conditions due to poor drainage or leaking pipes) can increase their instability. On the other hand, it should be acknowledged that landslides information in urban areas may be more frequent and easier to obtain than in agricultural and forested areas, often non urbanized (Peruccacci et al. 2023).

Various seasonal distributions are observed in the CLC classes (Table 3, Fig. 4). Almost all landslides occurring in agricultural areas are concentrated in spring, while the slope failures occurring in forested areas are distributed between late autumn and mid spring. The information available in the catalogue does not allow an evaluation of the relationship between the land cover and the type of landslide movement. It is worth noting that this analysis was previously done for an event landslide inventory for about two thousand landslides that occurred in the Marche region after an extraordinary rainfall event in September 2022 (Donnini et al. 2023). In that case, almost all the landslides classified as falls and three quarters of those classified as flows occurred in forested areas, while most slides occurred in agricultural areas. The results of such different analyses made with different datasets could (and should) be combined to provide information on the occurrence of landslides of different types are expected in different land covers.

Relevant differences in the rainfall conditions able to trigger shallow landslides in the study area are also found. In detail, more rainfall is needed to trigger a landslide in agricultural and forested areas than on artificial surfaces (Fig. 5). Again, human modifications to natural environments may have worsened the stability conditions of the terrains covered by artificial surfaces. Forested areas are characterized by the higher values of cumulated rainfall needed to trigger landslides, particularly for duration longer than 24 h (Figs. 6 and 7). This is linked to the stabilization action played by vegetation on the slopes, mainly due to: (1) reduction of effective rainfall and infiltration, by interception and evapotranspiration; (2) increase in shear strength and additional soil cohesion due to root reinforcement; (3) changes in soil suction through root water uptake; (4) stabilization of the shallowest soil layers (Schmaltz et al. 2017; Masi et al. 2021).

Looking in more detail, different landslide-triggering conditions are observed in three agricultural areas. Less rainfall is needed to initiate a landslide in areas classified as *land principally occupied by agriculture* than in areas defined as *non-irrigated arable land* and *complex cultivation patterns* (Table 4). This could be an indication of some agricultural practices that may favor soil degradation and shallow slope instability (Tarolli and Straffelini 2020; Volpe et al. 2022).

The evaluations and the outcomes of this work will be even more relevant in a climate change context. In addition to the evident worldwide rise in temperature, global warming may increase extreme rainfall events due to an enhanced atmospheric moisture retention and consequently affect land cover, for example by changing agricultural and forestry practices. These changes have a direct and indirect impacts on slope stability and landslide occurrence (Sidle and Ochiai 2006; Gariano and Guzzetti 2016).

The results of this work are of interest for regional land-use planning and landslide risk assessment in the short and long term. The findings can also be used for a future evaluation of changes in landslide triggering conditions in response to projected land cover changes. The addition of new records to the landslide catalogue will allow further analysis at the second and third Corine levels to evaluate more specific differences in landslide triggering conditions in various types of crops and different forest species. Finally, the release of a new CLC map will allow new temporal analyses to look for recent most changes and trends in the density and distribution of the landslides.

Acknowledgments Work supported by the Collaboration Agreement between the Marche Region and the National Research Council—Research Institute for Hydrogeological Protection, for the definition of rainfall conditions for landslide triggering, the implementation of a regional landslide early warning system for the triggering of rain-induced landslides, and the definition of soil moisture estimation products.

References

Alcàntara-Ayala I, Esteban-Chavez O, Parrot JF (2006) Landsliding related to land-cover change: a diachronic analysis of hillslope instability distribution in the sierra Norte, Puebla. Mexico Catena 65(2):152–165. https://doi.org/10.1016/j.catena.2005.11.006

Ávila FF, Alvalá RC, Mendes RM, Amore DJ (2021) The influence of land use/land cover variability and rainfall intensity in triggering landslides: a back-analysis study via physically based models. Nat Hazards 105:1139–1161. https://doi.org/10.1007/s11069-020-04324-x

Beguería S (2006) Changes in land cover and shallow landslide activity: a case study in the Spanish Pyrenees. Geomorphology 74(1–4):196–206. https://doi.org/10.1016/j.geomorph.2005.07.018

Brunetti MT, Melillo M, Gariano SL, Guzzetti F, Bartolini D, Brutti F, Bianchi C, Calzolari C, Denti B, Gioia E, Luciani S, Martinotti ME, Palladino MR, Pisano L, Roccati A, Solimano M, Vennari C, Vessia G, Viero A, Peruccacci S (2023) ITALICA (ITAlian rainfall-induced LandslIdes CAtalogue). Zenodo. https://doi.org/10.5281/zenodo.8009366

Corine Land Cover (2021) CORINE land cover product user manual (version 1.0). European Environment Agency (EEA), Copenhagen

Donnini M, Santangelo M, Gariano SL, Bucci F, Peruccacci S, Alvioli M, Althuwaynee O, Ardizzone F, Bianchi C, Bornaetxea T, Brunetti MT, Cardinali M, Esposito G, Grita S, Marchesini I, Melillo M, Salvati P, Yazdani M, Fiorucci F (2023) Landslides triggered by an extraordinary rainfall event in Central Italy on September 15, 2022. Landslides 20:2199–2211. https://doi.org/10.1007/s10346-023-02109-4

Gariano SL, Guzzetti F (2016) Landslides in a changing climate. Earth-Sci Rev 162:227–252. https://doi.org/10.1016/j.earscirev.2016.08.011

Gariano SL, Petrucci O, Rianna G, Santini M, Guzzetti F (2018) Impacts of past and future land changes on landslides in southern Italy. Reg Environ Chang 18:437–449. https://doi.org/10.1007/s10113-017-1210-9

Glade T (2003) Landslide occurrence as a response to land use change: a review of evidence from New Zealand. Catena 51:297–314. https://doi.org/10.1016/s0341-8162(02)00170-4

Herold M, Latham JS, Di Gregorio A, Schmullius CC (2006) Evolving standards in land cover characterization. J Land Use Sci 1:157–168. https://doi.org/10.1080/17474230601079316

Hungr O, Leroueil S, Picarelli L (2014) The Varnes classification of landslide types, an update. Landslides 11:167–194. https://doi.org/10.1007/s10346-013-0436-y

Hürlimann M, Guo Z, Puig-Polo C, Medina V (2022) Impacts of future climate and land cover changes on landslide susceptibility: regional scale modelling in the Val d'Aran region (Pyrenees, Spain). Landslides 19:99–118. https://doi.org/10.1007/s10346-021-01775-6

Knevels R, Petschko H, Proske H, Leopold P, Maraun D, Brenning A (2020) Event-based landslide modeling in the Styrian Basin, Austria: accounting for time-varying rainfall and land cover. Geosciences 10(6):217. https://doi.org/10.3390/geosciences10060

Masi EB, Segoni S, Tofani V (2021) Root reinforcement in slope stability models: a review. Geosciences 11:212. https://doi.org/10.3390/geosciences11050212

Ozturk U, Bozzolan E, Holcombe EA, Shukla R, Pianosi F, Wagener T (2022) How climate change and unplanned urban sprawl bring more landslides. Nature 608(7922):262–265. https://doi.org/10.1038/d41586-022-02141-9

Pacheco Quevedo R, Velastegui-Montoya A, Montalván-Burbano N, Morante-Carballo F, Korup O, Daleles Rennó C (2023) Land use and land cover as a conditioning factor in landslide susceptibility: a literature review. Landslides 20:967–982. https://doi.org/10.1007/s10346-022-02020-4

Peruccacci S, Brunetti MT, Luciani S, Vennari C, Guzzetti F (2012) Lithological and seasonal control of rainfall thresholds for the possible initiation of landslides in Central Italy. Geomorphology 139–140:79–90. https://doi.org/10.1016/j.geomorph.2011.10.005

Peruccacci S, Brunetti MT, Gariano SL, Melillo M, Rossi M, Guzzetti F (2017) Rainfall thresholds for possible landslide occurrence in Italy. Geomorphology 290:39–57. https://doi.org/10.1016/j.geomorph.2017.03.031

Peruccacci S, Gariano SL, Melillo M, Solimano M, Guzzetti F, Brunetti MT (2023) The ITAlian rainfall-induced LandslIdes CAtalogue, an extensive and accurate spatio-temporal catalogue of rainfall-induced landslides in Italy. Earth Syst Sci Data 15:2863–2877. https://doi.org/10.5194/essd-15-2863-2023

Pisano L, Zumpano V, Malek Z, Rosskopf CM, Parise M (2017) Variations in the susceptibility to landslides, as a consequence of land cover changes: a look to the past, and another towards the future. Sci Total Environ 601–602:1147–1159. https://doi.org/10.1016/j.scitotenv.2017.05.231

Reichenbach P, Busca C, Mondini AC, Rossi M (2014) The influence of land use change on landslide susceptibility zonation: TheBriga catchment test site (Messina, Italy). Environ Manag 54:1372–1384. https://doi.org/10.1007/s00267-014-0357-0

Schmaltz EM, Steger S, Glade T (2017) The influence of forest cover on landslide occurrence explored with spatio-temporal information. Geomorphology 290:250–264. https://doi.org/10.1016/j.geomorph.2017.04.024

Shu H, Hürlimann M, Molowny-Horas R, González M, Pinyol J, Abancó C, Ma J (2019) Relation between land cover and landslide susceptibility in Val d'Aran, Pyrenees (Spain): historical

aspects, present situation and forward prediction. Sci Total Envion 693:133557. https://doi.org/10.1016/j.scitotenv.2019.07.363
Sidle RC, Ochiai H (2006) Landslides: processes, prediction, and land use. Water Resour Monogr 18:312. https://doi.org/10.1029/WM018
Tarolli P, Straffelini E (2020) Agriculture in hilly and mountainous landscapes: threats, monitoring and sustainable management. Geogr Sustain 1:70–76. https://doi.org/10.1016/j.geosus.2020.03.003
Volpe E, Gariano SL, Ardizzone F, Fiorucci F, Salciarini D (2022) A heuristic method to evaluate the effect of soil tillage on slope stability: a pilot case in Central Italy. Land 11(6):912. https://doi.org/10.3390/land11060912

Amplification of Landslide Hazards Due to Terrain Modification in Jintian Village During the Ms 6.2 Jishishan Earthquake

Jian Guo and Yifei Cui

Abstract

Terrain modifications significantly influence landslide formation and dynamics. On December 18, 2023, a catastrophic landslide struck the Jintian Village in Gansu Province, China. While triggers such as earthquakes and irrigation are well-studied, the impact of terrain modifications, particularly the extraordinary runout and the severe damage it caused, remains less explored. This study integrates field investigations, remote sensing analysis, and numerical simulations to reconstruct the landslide's dynamics and assess how terrain changes affect its behavior. Our findings reveal that land reclamation, which involved valley infilling to create flat areas, altered regional hydrology by raising groundwater levels. This elevation promoted soil liquefaction and increased terrain instability, heightening the susceptibility to seismic activity. Additionally, the distinctive throat-like terrain regulated the volume and flow rate of landslide material, controlling the disaster's scale. Although check dams initially restrained the flowing mass, their eventual failure amplified the landslide's volume and potential energy, extending its reach and worsening its impact. The results underscore the need for regions with loess, particularly those prone to earthquakes and groundwater fluctuations, to carefully evaluate the detrimental effects of terrain modifications. Furthermore, the structural integrity of check dams should be reexamined to mitigate the risk of similar disaster chains.

Keywords

Jintian Village landslide · Liquefied landslide · Throat-like terrain · Dam failure · Disaster chain · 12.18 Jishishan earthquake

1 Introduction

At 23:59 on December 18, 2023, a Ms 6.2 earthquake struck Jishishan County in Linxia, Gansu Province (N35.70°, E102.79°), with a focal depth of 10 km and a maximum intensity of VIII. The earthquake triggered a large-scale landslide in Jintian Village, Zhongchuan Town, leading to the destruction of 51 houses and resulting in 20 fatalities (Fig. 1a, b). The event garnered significant attention from the landslide researchers, with some scholars drawing comparisons to the renowned disaster at the Lajia archaeological site, located just 3.5 km away. The Lajia event, which occurred 3850 years ago, may have involved a combination of prehistoric earthquakes, landslides, and floods (Fig. 1a) (Shi et al. 2024).

The Jintian village landslide, similar to other historically documented earthquake-induced events, exemplifies the typical long-runout landslide chains characteristic of loess regions. For instance, the 1920 Haiyuan Ms 8.5 earthquake triggered the liquefaction and flow of loess deposits over a 9-km-long and 1.5-km-wide area in Shibeiyuan, Ningxia, burying two villages and resulting in over 400 fatalities (Fig. 1c). The earthquake also caused a massive landslide in Dangjiacha, with an estimated volume of 200 million cubic meters, which led to the formation of a large landslide-dammed lake. Similarly, the 2018 Palu Ms 7.5 earthquake in Indonesia, which claimed 4340 lives, triggered numerous low-angle liquefied landslides (Fig. 1d), causing extensive

Award Memorial Article: Best Paper Award for Journal Landslides 2022

J. Guo
Key Laboratory of Land Surface Pattern and Simulation, Institute of Geographic Sciences and Natural Resources Research, Chinese Academy of Sciences (CAS), Beijing, China

State Key Laboratory of Hydroscience and Engineering, Tsinghua University, Beijing, China

Y. Cui (✉)
State Key Laboratory of Hydroscience and Engineering, Tsinghua University, Beijing, China
e-mail: yifeicui@mail.tsinghua.edu.cn

B. Abolmasov et al. (eds.), *Progress in Landslide Research and Technology, Volume 4 Issue 1, 2025*, Progress in Landslide Research and Technology, https://doi.org/10.1007/978-3-031-89836-5_5

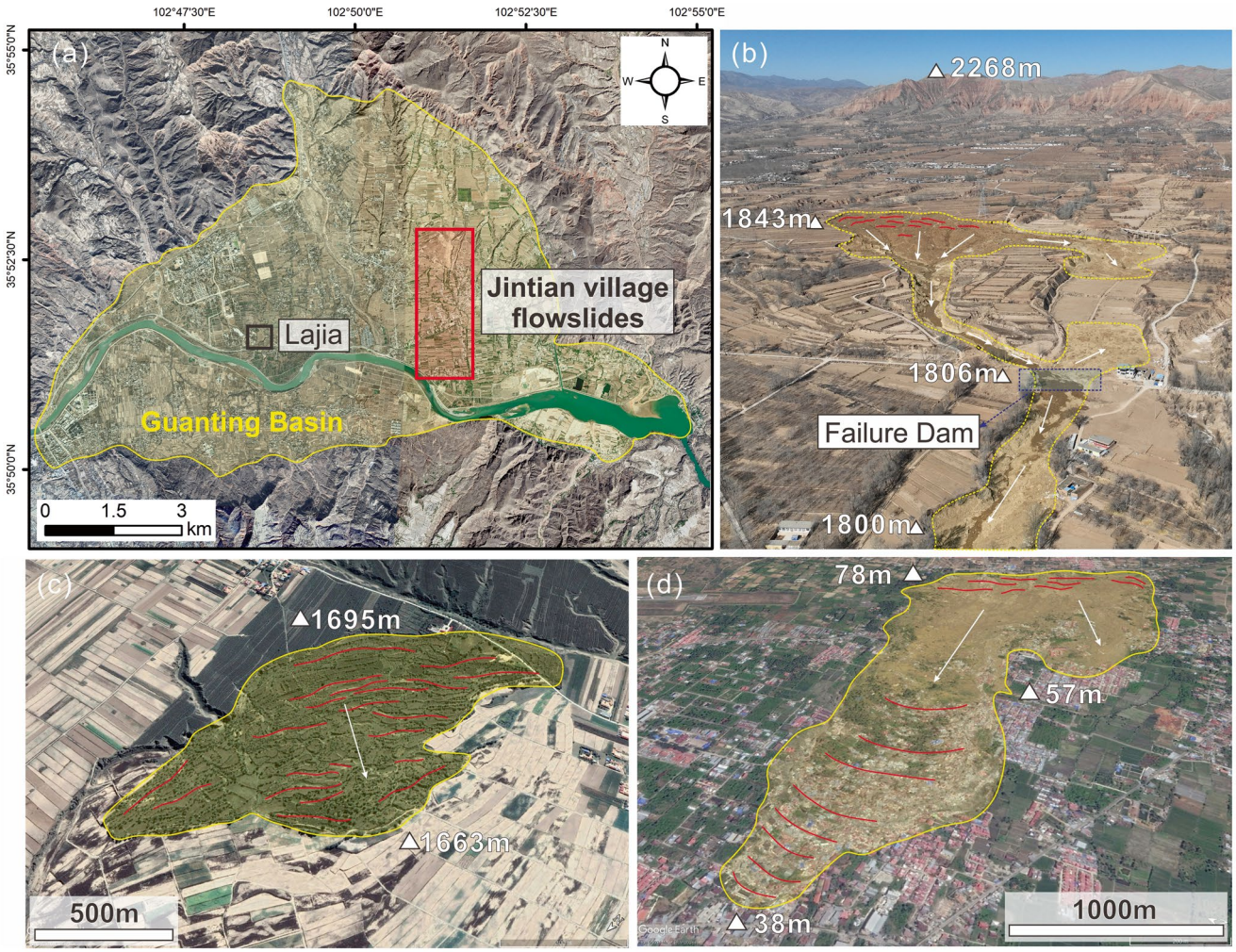

Fig. 1 Overview of the Study Area. (**a**) Location of the study area in the Guanting Basin. The Jintian Village landslide (**b**), along with similar high-mobility landslides such as (**c**) the Southern sliding zone of Shibeiyuan, Ningxia, (**d**) Petobo earth flows in Palu. (**a**, **c**, **d** are sourced from Google Earth Pro, while **b** is from UAV imagery taken after the Jintian Village landslide)

damage to houses and roads. These highly mobile, flow-like landslides are often associated with soil liquefaction, typically triggered by earthquakes or irrigation, enabling the landslides to travel considerable distances, even in regions with very gentle slopes (Zhao 2024).

Researchers have thoroughly examined the factors contributing to the formation of the Jintian Village landslide, focusing on triggers such as seismic activity, irrigation, groundwater, and the properties of loess (Liu et al. 2024; Wang et al. 2024; Xu et al. 2024). However, the exceptional mobility of the landslide has not yet received significant attention in related studies. According to local villagers, the earthquake and landslide occurred almost simultaneously. The landslide had traveled 2.0 km from its source and buried nearby houses within approximately 10 min. Based on this timeline, the average velocity of the landslide is estimated at around 3.3 m/s. This observation raises an question that how did the landslide achieve such a high velocity in a gently sloping valley with a gradient of just 1.9°.

The Jintian village landslides exhibited a distinct multi-phased, chain-like progression. Human activities had significantly modified the terrain in the affected area, and the topography along the landslide's path changed multiple times, segmenting its dynamic processes into distinct phases. Due to the complexity of this process, traditional empirical methods are inadequate for accurately capturing the variations in velocity. It remains unclear whether these terrain alterations enhanced or hindered the landslide dynamics, limiting our understanding of the event and impeding future prevention efforts. As a result, this study focuses on simulating the landslide's dynamic process to assess how terrain modifications influenced the disaster's behavior and impact

zones. The findings aim to provide valuable insights for improving landslide prevention and mitigation strategies.

2 Methods

2.1 Numerical Simulation Method

In this study, the dynamic process of the landslide was reconstructed using a depth-integrated method, as described by Savage and Hutter (1989) and George and Iverson (2014). The landslide model is based on a Cartesian coordinate system (as show in Fig. 2), where the X-axis represents the primary sliding direction, and the Z-axis is oriented vertically, perpendicular to the XOY plane, indicating the depth of the landslide mass. The computational domain is divided into grids across the landslide area in the XOY plane. Within each grid, the landslide mass thickness (h) varies over time (t) and spatial coordinates (x, y), and is calculated using a finite difference algorithm. The model conceptualizes the landslide mass as a series of vertical soil columns, each subjected to four forces: gravity (W), lateral pressure (P), support force (N), and frictional force (S).

In the Eulerian coordinate system, and neglecting erosion and deposition, the continuity equation for the control volume is expressed as follows:

$$\frac{\partial h}{\partial t}+\frac{\partial Q_x}{\partial x}+\frac{\partial Q_y}{\partial y}=0 \tag{1}$$

In Eq. (1), h represents the thickness of the landslide within the soil column control volume, while $Q_x = v_x h$ and $Q_y = v_y h$ denotes the flow rates of the soil mass through the column in the X and Y directions per unit time, respectively.

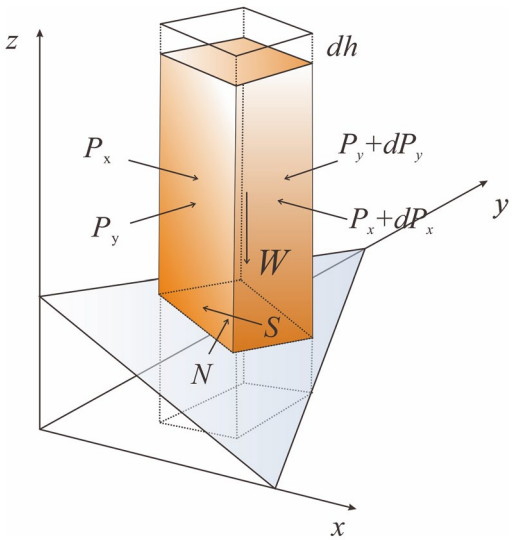

Fig. 2 The soil column unit in a landslide moving on a sloping ground and its force analysis

To analyze the forces acting on the soil column and determine the impact of each force on its acceleration, the momentum equations in the X and Y directions are derived following Sassa et al. (2010) as follows:

$$\frac{\partial v_x}{\partial t}+v_x\frac{\partial v_x}{\partial x}+v_y\frac{\partial v_x}{\partial y}= (Ag+B)\frac{\tan\alpha}{1+G}-\mathrm{kg}\frac{\partial h}{\partial x}- \frac{D_x}{\sqrt{1+G}}\left((Ag+B)(1-\lambda)\tan\varphi_\alpha+\frac{c}{\rho h}(1+G)\right) \tag{2}$$

$$\frac{\partial v_y}{\partial t}+v_x\frac{\partial v_y}{\partial x}+v_y\frac{\partial v_y}{\partial y}= (Ag+B)\frac{\tan\beta}{1+G}-\mathrm{kg}\frac{\partial h}{\partial y}- \frac{D_y}{\sqrt{1+G}}\left((Ag+B)(1-\lambda)\tan\varphi_\alpha+\frac{c}{\rho h}(1+G)\right) \tag{3}$$

where:

$A=k\frac{\partial h}{\partial x}\tan\alpha+k\frac{\partial h}{\partial y}\tan\beta+1$ represents the combined effects of lateral pressure and gravity on the support force.

$B=\frac{C_x}{\cos\alpha}\left(\frac{V_x}{\cos\alpha}\right)^2+\frac{C_y}{\cos\beta}\left(\frac{V_y}{\cos\beta}\right)^2$ represents the effects of centrifugal and centripetal forces.

$G=\tan^2\alpha+\tan^2\beta$ denotes intermediate parameters related to the slip surface topography.

$D_x=\frac{-V_x}{\sqrt{V_x^2+V_y^2+V_z^2}}$ and $D_y=\frac{-V_y}{\sqrt{V_x^2+V_y^2+V_z^2}}$, represent the projections of velocity in the XOZ and YOZ planes, respectively.

The detailed derivation of the governing equations can be found in Shen et al. (2018) and Guo et al. (2022a) In the model, the parameter λ represents the pore water pressure ratio, which indicates the degree of liquefaction of the bed material, with values ranging from 0 (dry) to 1 (fully saturated). The generation and dissipation of pore water pressure are influenced by particle expansion and hydraulic diffusion rates. Due to the complexity involved in pore water pressure evolution, a uniform λ is adopted for simplification, as suggested by Ouyang et al. (2017).

2.2 Terrain Restoration and Reconstruction

Historical remote sensing images of the study area were obtained from Google Earth and used to assess changes in

vegetation types, land use, and other environmental factors, providing insights into the long-term evolution of the landslide surroundings. Additionally, pre-disaster digital elevation models (DEMs) with a 15-meter resolution were sourced from Google Earth. After the disaster, on-site drone surveys with fixed-wing measurements were conducted, producing orthophotos and DEMs with an accuracy of 0.3 m based on aerial imagery. Given the study area's location on the Yellow River terrace, characterized by minimal vegetation cover and minor terrain changes, drone data effectively calibrated the elevation of the disaster region, yielding reliable results. The calibrated pre- and post-disaster images were then utilized to delineate the landslide's initiation, movement, and deposition areas. This, combined with the DEM data, allowed for accurate calculation and description of the landslide's volume and movement process.

Accurate pre-disaster channel topography and slip surface data are essential for numerical simulations of landslides. To obtain these data, field investigations were conducted, and borehole and groundwater data from related studies were referenced (Wang et al. 2024).

During the simulation, the potential failure of the soil dam was also taken into account. To account for the terrain's impact, we reconstructed the soil dam located 600 m from the initiation site. Contours of the area were first generated using DSM from post-disaster drone surveys. Subsequently, the damaged dam was reconstructed based on another earth dam situated in a parallel trench, 50 m away. The reconstruction was facilitated by the presence of a hardened road that traversed both dams and the similarity in their construction times and techniques. Consequently, the two dams had similar height, width, slope, and shape of contours. Using these modified contours, a high-precision digital elevation file was re-generated to represent the pre-disaster terrain accurately.

While commonly used dam breach models are based on hydrodynamic erosion, there is no mature theoretical model for soil dam instability induced by landslide impacts (Zhuang et al. 2020). Interviews with local villagers indicated that the soil dam became unstable very rapidly. Therefore, in our simulation, we simplified the breach process by assuming that the dam would fail and move with the landslide mass once the deposit thickness at the rear edge of the landslide reached the height of the dam. This approach streamlines the simulation process while minimizing its impact on the overall results.

2.3 Numerical Setup

The simulation requires the input of physical indicators and strength parameters for the landslide. Field investigations revealed that the soil in the top 2 m of the destabilized slide consisted of arable soil and red clay, while the 2–20 m depth primarily comprised sandy powdery clay, which was the predominant soil type for the slide. For simplicity, the specific properties of the topsoil were not modeled separately; instead, the simulation used the physical indices of the powdery clay for the entire slide. Laboratory test results indicated that the density of the slide body is 1.570 g/cm^3, with a water content of 24%, cohesion of 200 kPa, and an angle of internal friction of 17°. These parameters were used as the basic indicators for the soil in the model.

Two sets of simulations were conducted. In the first set, we varied the pore water pressure ratio λ (ranging from 0 to 1.0 in increments of 0.1) while keeping constant slip surface and topography in the source zone. This variation allowed us to investigate how changes in pore water pressure ratio affect landslide initiation and to explore the influence of throat-like terrain on the flow rate and initial volume of the landslide. In the second set of simulations, we evaluated the impact of a check dam on the landslide's movement. By comparing scenarios with and without the check dam, we analyzed the landslide's speed, runout distance, and the mechanism through which the deposition of landslide material affects subsequent dynamic characteristics.

Since our study focuses on the influence of topography on landslide evolution and motion, we do not address the complex formation process of slide surface, which requires more detailed research. At the start of the simulation, we assumed a predefined sliding surface, inferred from high-precision post-disaster and pre-disaster DEMs, as well as the depth of the sliding surface. The dam was modeled as rigid, without considering its deformation or interaction with the landslide, treating it instead as a fixed component of the terrain. During the simulation, we replaced the bottom boundary of the model and incorporated the dam's volume into the running landslide, by which we accounting for the effects of the dam breach indirectly. Finally, by inputting data on the slide's thickness and velocity distribution at various times, we reconstructed the full motion trajectory of the landslide.

3 Results

3.1 The Effects of Ditch Filling

Figure 3 presents remote sensing images from March 26, 2014 (Fig. 3a) and November 9, 2016 (Fig. 3b). A significant change is visible in the red area of Fig. 3a. In 2014, this area displayed prominent gully formations, whereas, by 2016, it had been transformed into light yellow due to land reclamation efforts, which involved filling the original gullies with loess to create new farmland.

In Fig. 3, the blue lines represent the surface runoff paths. Local runoff flows from the northern watershed towards the southern Yellow River, influenced by the topography.

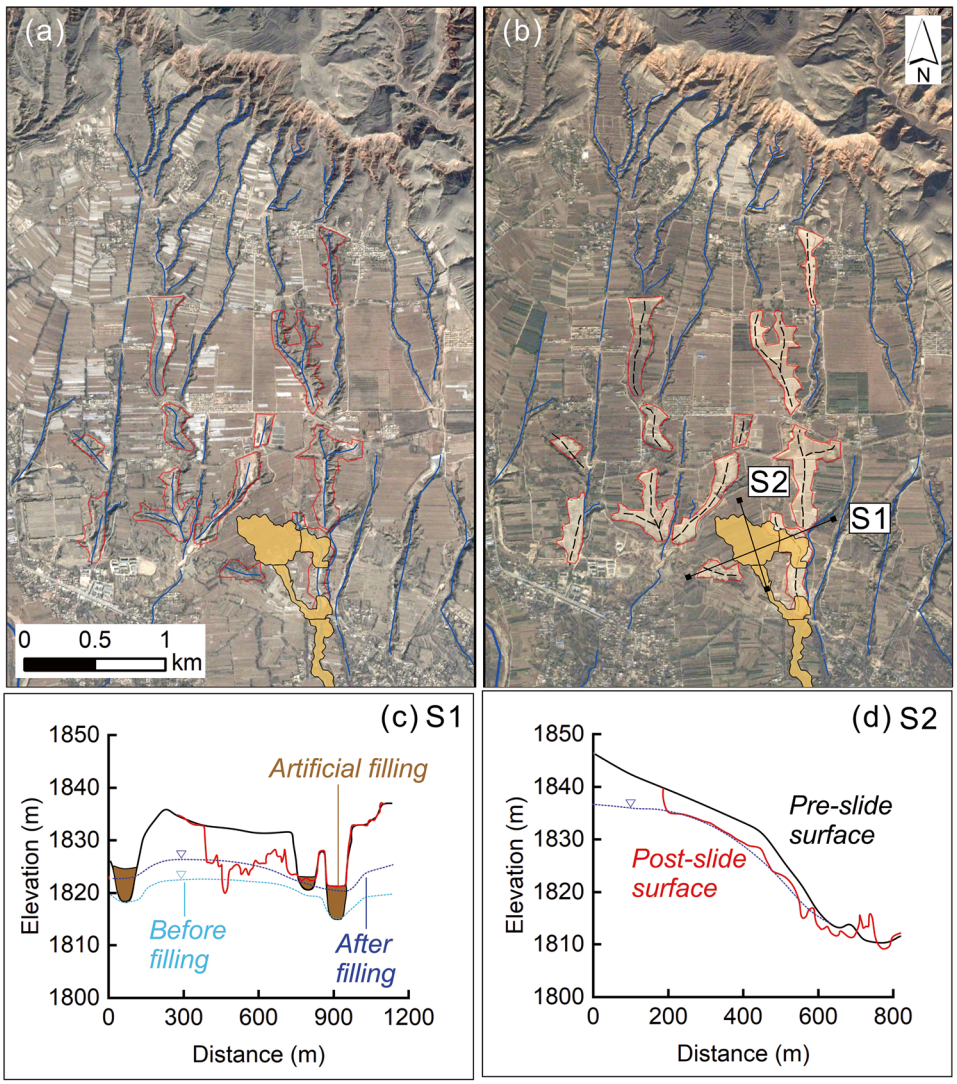

Fig. 3 Comparison of Remote Sensing Images in the Landslide Source Area. (**a**) and (**b**) display Google Earth images taken before (March 26, 2014) and after (November 9, 2016) human-induced terrain modifications. (**c**) and (**d**) present topographic profiles extracted from (**b**), with groundwater levels inferred from site investigations (the blank and red line represent the surface before and after the landslide)

Located on the Yellow River terrace, the area has a high groundwater level, as indicated by numerous surface water ponds. It was observed that in the reclaimed areas, surface runoff has shifted to subsurface runoff, which may have altered groundwater distribution in this region.

The terrain in the landslide source area is bordered by fill areas on the east, west, and north sides. Figure 3c presents a topographic cross-section in the east-west direction. The brown areas indicate changes in topography resulting from the filling of previously deeper gullies for the purpose of agricultural development. According to the unsaturated soil theory, negative pore pressures generated in soils due to matrix suction, resulting in upward seepage of groundwater along the soil pores (Fredlund et al. 1978). As a result, a high groundwater table in the center and low on both sides will be formed. The groundwater in central would naturally drained through the gullies in both two sides. However, as fill occurs, the water table, both in platforms and gullies, will rise due to matrix suction. While the soil stability in the east-west direction remains intact, issues have arisen on the southern side. Figure 3b shows that groundwater levels on the northern side have increased due to filling, whereas the southern gully area remains unfilled. With generally elevated groundwater levels, surface water may have emerged on the southern side. Figure 8b illustrates a pond, approximately 900 m^2 in area, located at the end of Zone 3, which is replenished solely by the water from the landslide source area.

The artificial modification of the terrain led to changes in groundwater distribution, causing groundwater levels to rise and the region to eventually reach a new stable state. However, on December 18, 2023, the Ms 6.2 earthquake disrupted this stability. The intense, high-frequency vibrations induced widespread liquefaction of the saturated loess over an area of 149,000 m^2. As a result, the upper landslide mass began to exhibit characteristics of floating, leading to a typical failure type of spread (Hungr et al. 2014). Additionally, a series of tension cracks developed at the rear end of the source area.

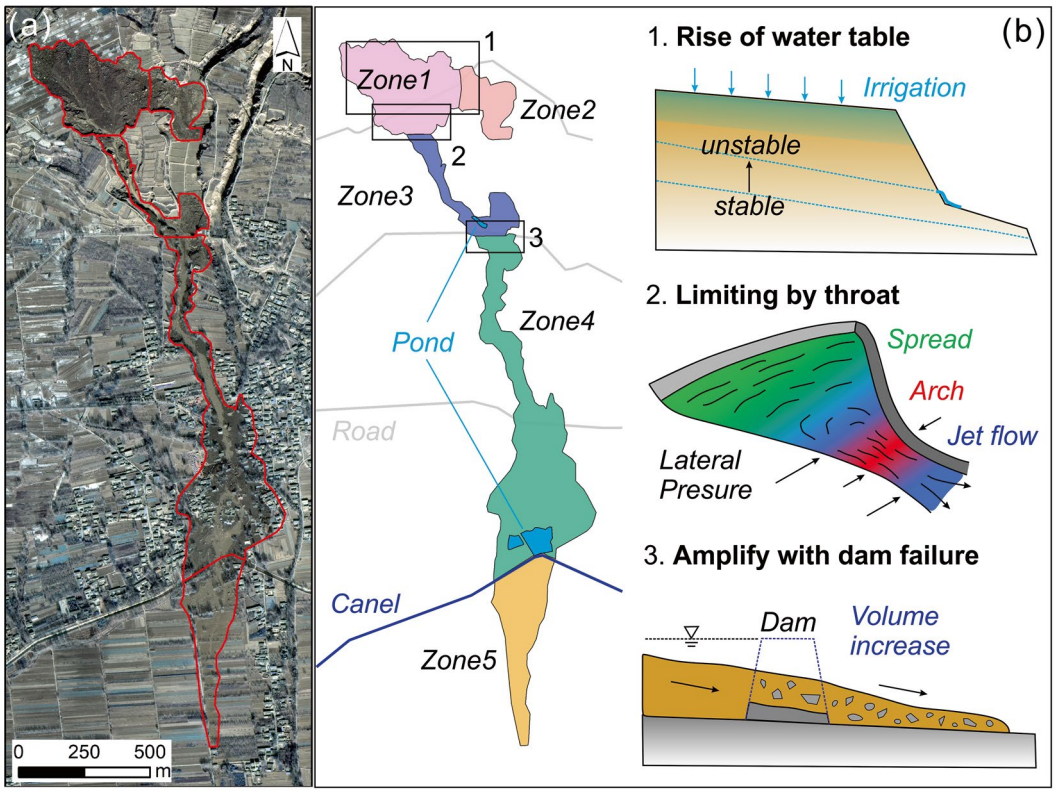

Fig. 8 Overview of the Landslide Event. (**a**) Post-disaster image, (**b**) Schematic diagram illustrating the disaster zones and key physical mechanisms affecting each location

3.2 The Effects of the Throat Region

The landslide source area measures up to 500 m wide at its rear and narrows to 70 m at the shear outlet, forming a throat-like region (Guo et al. 2022b). High-density electrical resistivity testing and borehole data indicated that the groundwater level was approximately 12.5 m below the surface (Wang et al. 2024). Due to the gentle slope of less than 5°, the landslide mass moved as flow because of the liquefaction toward the outlet. At this stage, the extent of soil liquefaction influenced both the volume of material flowing through the constriction and the changes in flow rate.

By varying the pore water pressure ratio (λ) in the numerical model, the results indicate that as λ increases, the volume of soil flowing out of the constriction rises rapidly before stabilizing (Fig. 4a). When λ is less than 0.7, the impact of the constriction on the total outflow volume is minimal, with volumes ranging from 20 to 35 × 10^4 m^3, stabilizing within the first 50 s. This phenomenon suggests that once the landslide becomes unstable, the marginal portion quickly destabilizes and moves, but the majority of the soil mass remains in the source area due to constraints imposed by the lateral topography and earth pressure. When λ exceeds 0.7, the outflow volume increases continuously, with material flowing through the constriction for a longer duration. As shown in Fig. 4c, the volume of material transforming into flowslide reaches nearly four times the amount observed with lower saturation when λ is greater than 0.7.

The flow rate at the constriction outlet was calculated based on the volume changes. As illustrated in Fig. 4b, the flow rate through the constriction initially increases rapidly before gradually decreasing. When λ is below 0.7, the flow rate drops to 0 m^3/s within 100 s, indicating that soil with a lower pore water pressure ratio significantly reduced mobility. In contrast, when λ exceeds 0.7, the flow rate decreases more gradually, suggesting that liquefied soil continues to flow out. Statistical analysis shows that the peak flow rate increases exponentially with the rising pore water pressure ratio.

Figure 4 illustrates the significant influence of bed liquefaction (λ) on the scale of the disaster. At lower saturation levels, the constriction topography severely restricts soil movement within the source area, resulting in reduced landslide mobility and a smaller disaster scale. Conversely, higher saturation levels alleviate topographic constraints on the source material, leading to increased soil mobility, higher peak flow rates, and a substantially larger disaster scale. The results indicate that topography plays a crucial role in modulating the disaster scale by affecting the mobility of the source material.

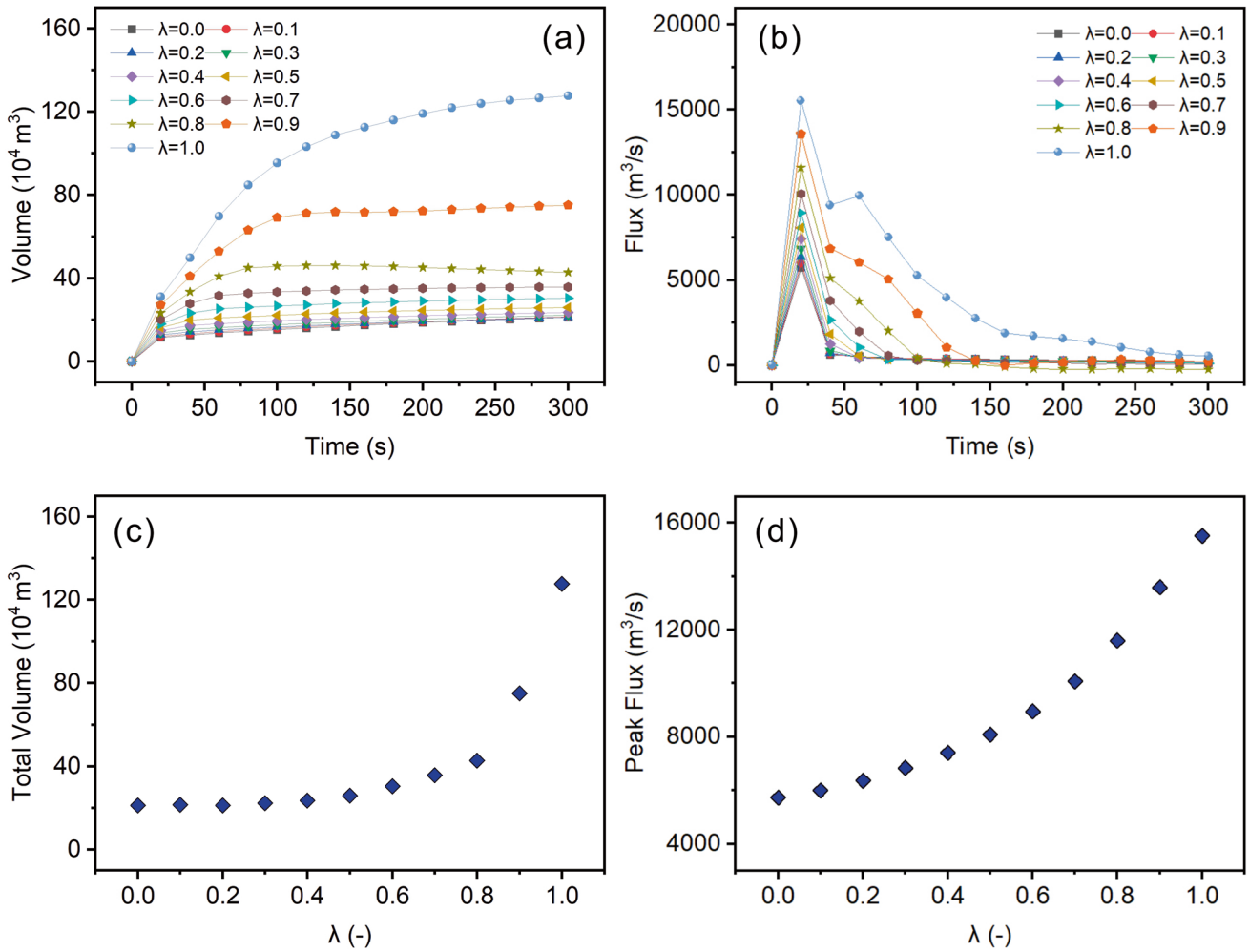

Fig. 4 Impact of Liquefaction on Flow Rate Changes in the Source Area. (**a**) Changes in the volume of soil flowing out from the constriction under different λ. (**b**) Variation in flow rate with different λ. (**c**) Changes in the total outflow volume as a function of λ. (**d**) Changes in peak flow rates with varying λ

3.3 The Effects of Dam Failure

At the confluence of the channels, a soil dam was originally located 600 m from the exit of the landslide's source area. Post-disaster surveys indicated that this dam was destroyed during the event. To assess the dam's impact, two simulations were performed by altering the bed topography. The results of these simulations are presented in Fig. 5.

Figure 5 illustrates the impact of the dam on landslide behavior. At t = 150 s, the landslide continues to advance along the ditch when without the dam. With the dam in place, most of the soil is retained behind the dam (Fig. 5b). By t = 800 s, part of the landslide mass overflows from the dam, which aligns closely with field investigation results. Comparing Fig. 5c, d, it is evident that the presence of the dam increases the affected range and movement distance of the landslide, particularly when dam failure is considered.

Fig. 6 presents the kinematic indices related to the landslides extracted from the simulation results. Figure 6a indicates that without the dam, the landslide rapidly increased its movement distance, reaching over 2000 m within approximately 700 s. In contrast, with the dam in place, the landslide's maximum distance was constrained. At 600 m from the source, a significant portion of the landslide material was retained behind the dam. Although some material did overflow the dam due to the terrain, the runout distance increase was minimal due to the reduced speed. Following dam failure, the movement distance significantly increased, with the landslide traveling over 2300 m, an additional 300 m compared to the scenario when without the dam. Furthermore, the movement duration extended by about 300 s. The impact area of the disaster displayed a similar pattern. Initially, the impact area was consistently larger without the dam. However, the impact area with the dam exceeded that of the no-dam scenario in around 550 s,.

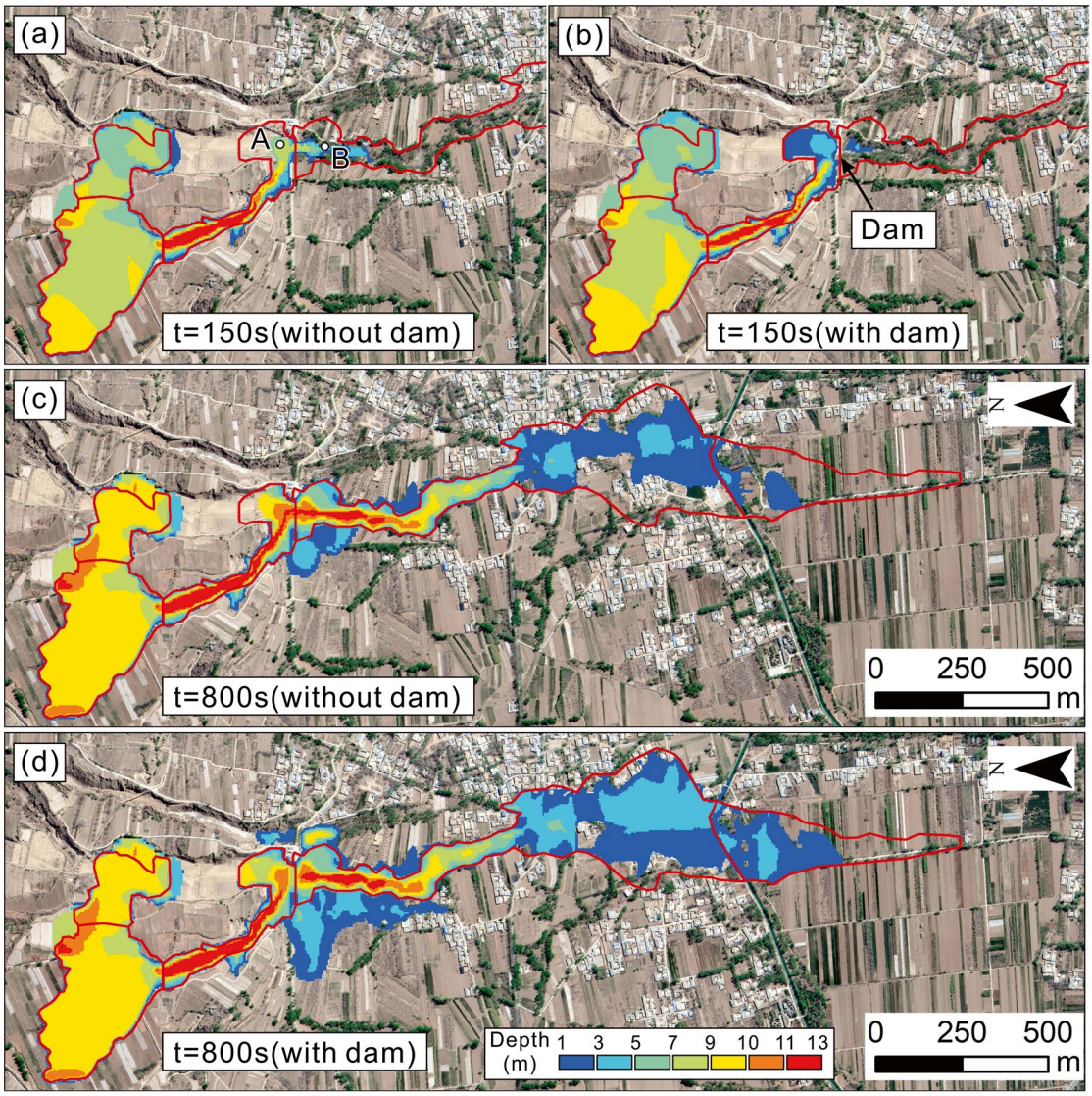

Fig. 5 Results of the Numerical Simulations. (**a**) and (**b**) Deposition depth of the landslide when it reaches the dam at t = 150 s, both with and without the dam. (**c**) and (**d**) Depth of the landslide at t = 800 s, with and without the dam

Figure 6c illustrates that the presence of the dam accelerated the accumulation of sediment thickness at Point A in Fig. 5a, reflecting the sedimentation process behind the dam. After the dam failure, the sediment depth behind the dam initially decreased due to the outflow and then increased as the incoming flow. Despite these fluctuations, the final sediment depth after the disaster was similar to that observed in the scenario without the dam. Figure 6d indicates that without the dam, the velocity at Point A quickly reached a peak of 7 m/s before gradually decreasing. In contrast, the dam significantly reduced the peak velocity at Point A, which then increased slowly to 2.3 m/s. Notably, after 350 s, the influence of the dam on the landslide velocity diminished.

Fig. 6d also reveals that at monitoring Point B, downstream of the dam, sediment accumulation steadily increased throughout the simulation without the dam. With the dam in place, sediment accumulation at Point B was delayed by approximately 200 s. The depth change exhibited a small peak around 450 s, followed by stabilization, reflecting the dam's failure. The final sediment thickness at Point B with the dam was slightly less than that without the dam, possibly due to fluctuations caused by the dam's failure, which allowed more material to be transported to the front, extending the runout distance.

Velocity monitoring at Point B reveals that without the dam, the peak velocity reached approximately 2.7 m/s at 150 s, gradually decreasing to 0.7 m/s over time. The peak

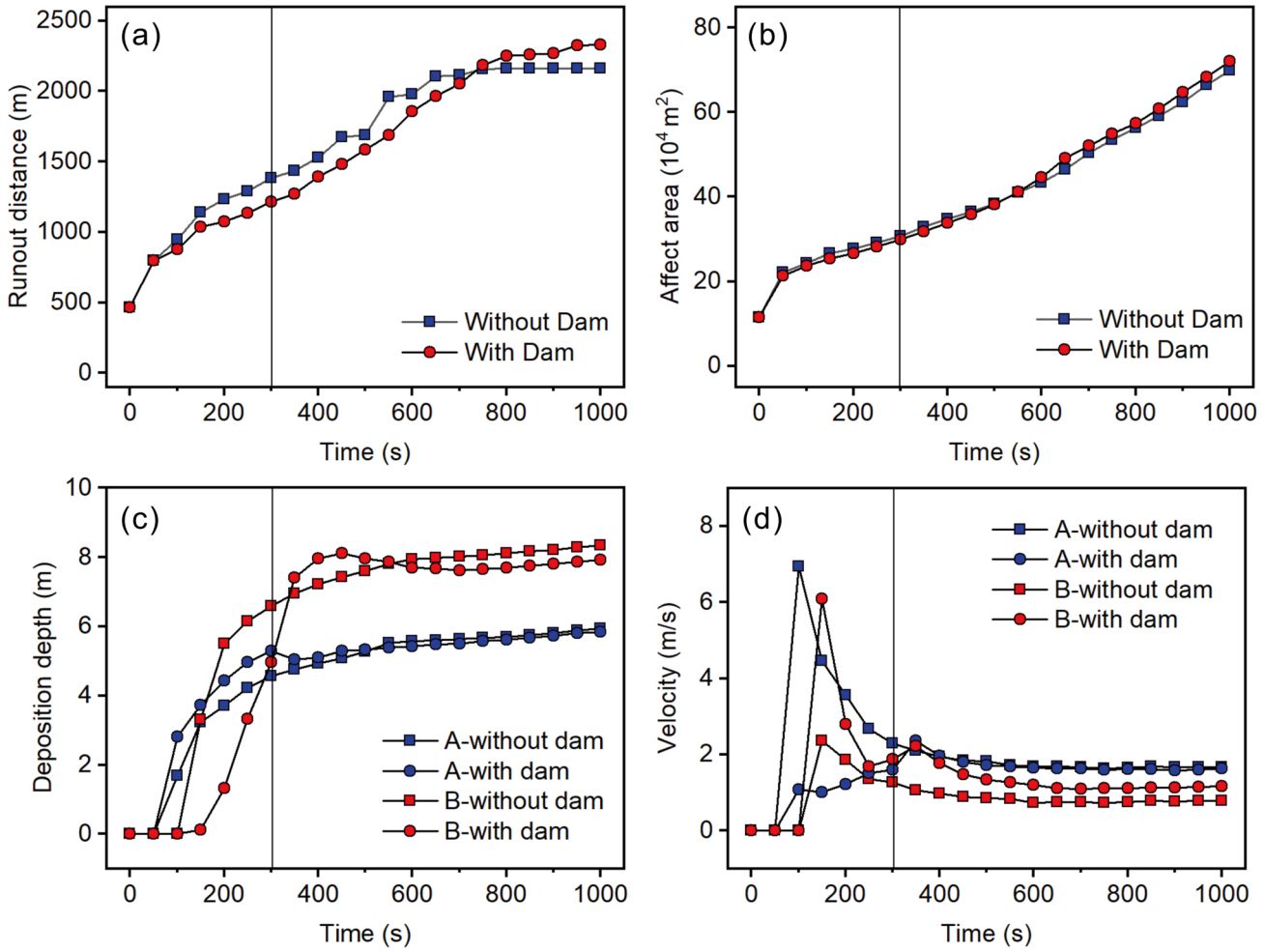

Fig. 6 The Impact of the Dam on Landslide Dynamics. (**a**) Runout distance of the landslide. (**b**) Area affected by the landslide. (**c**) the depth and (**d**) velocity at upstream and downstream monitoring points relative

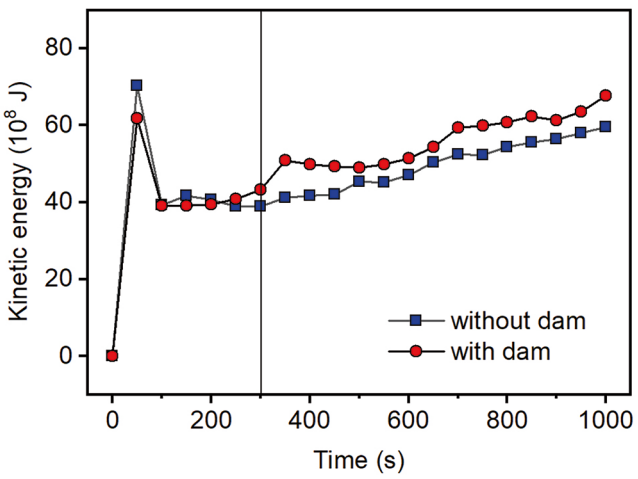

Fig. 7 Variation of the kinetic energy of the disaster over time under different conditions

velocity was raised to 6 m/s when the dam was present, however, it decreased rapidly afterward. Following the dam's failure, the velocity at Point B slightly increased before tapering off again. This suggests that the dam's presence led to a higher stable velocity at Point B, while its failure further increased the landslide's mobility.

Figure 7 presents the variation in kinetic energy, E_k=0.5$\sum mv^2$, of the landslide mass over time. The results indicate that the kinetic energy rises significantly during the initial stages of the landslide and then decreases due to terrain constraints. The kinetic energy of material flowing out of the source area remains stable until the check dam fails. Without the dam, the kinetic energy increases at a slower rate, while with the dam, the increase becomes more pronounced after the dam breach. This phenomenon implies that the failure of the dam enhances the kinetic energy of the landslide, amplifying its destructive potential.

4 Discussion

Based on the previous analysis and field investigation results, the evolution of the landslide can be summarized as follows. Since 2014, land reclamation activities involving valley infill have significantly altered the groundwater distribution in the area. The original surface runoff transitioned into subsurface flow, leading to a generalized rise in groundwater levels around the landslide source. However, the unmodified southern terrain provided a natural groundwater discharge path and served as a free face (Fig. 8b). Despite these changes, the region remained stable for nearly a decade. The equilibrium was abruptly disturbed by the Ms 6.2 earthquake. Seismic activity induced the gradual liquefaction of the highly saturated loess, resulting in the formation of a continuous liquefied layer at depth (Ni et al. 2024). The soil near the southern free face, already vulnerable due to groundwater conditions, was the first to destabilize and move along the channel. Simultaneously, the middle and rear sections of the landslide mass were driven towards the outlet by the terrain.

The throat-like region, characterized by a wide rear and a narrow front (Zone 2), exerted increased lateral pressure on the soil near the constriction, limiting the movement of the sliding material (Fig. 8b). The constraint hindered the fully mobilization of the rear portion at the source region, leading to the formation of numerous tension cracks perpendicular to the movement direction in Zone 1, which is a common feature in low-angle landslides (Fang et al. 2024). Upon reaching Zone 3, an artificial soil dam obstructed the landslide's downstream progression, causing the material to backfill. However, the dam quickly became unstable and failed within a short time (Fig. 8b). As a result, the accumulated material, along with the large volume of soil previously held back by the dam, was reactivated and continued moving downstream for 2 km, destroying numerous houses and causing widespread damage.

The results suggest that land reclamation projects involving gully filling contributed to the occurrence of the landslide. Similar reclamation activities are currently underway in other regions of the Loess Plateau, such as Lanzhou and Yan'an. This event underscores the critical importance of monitoring hydrological changes caused by large-scale terrain modifications. It also highlights the need for comprehensive risk assessments of potential disasters, particularly under extreme conditions such as earthquakes or heavy rainfall (Li et al. 2014; Arran et al. 2016, 2022).

The simulation results also demonstrate that the failure of the check dam may increase the landslide's runout distance, hazard range, and overall disaster scale. In the Loess Plateau, siltation dams are frequently built in gullies to mitigate soil erosion. However, this study highlights the need to reassess the design criteria for these structures. It is crucial to account for the potential disaster amplification that could occur if dams fail, to prevent cascading effects that may worsen the impact of future landslides (Fu et al. 2017; Arran et al. 2023).

This study employed numerical simulations to analyze the movement dynamics of the Jintian Village landslide. However, it is important to recognize that our simulations did not encompass all factors affecting the disaster's behavior. Specifically, we did not account for the influence of the pond situated in front of the dam on the physical properties of the landslide material. Additionally, the model excluded the large water pond located at the boundary between Zone 4 and Zone 5. In reality, as the landslide mass interacted with this pond, a substantial volume of water was displaced, which may facilitated the transport of debris mass over greater distances.

In summary, the Jintian Village landslide progressed through multiple stages, with material redistribution, water availability, and variations in seismic forces playing pivotal roles in determining the disaster's trajectory and impact area. To fully understand the mechanisms behind the rapid and extensive movement of the loess landslide-debris flow, further research is needed. Future research should focus on the intricate interactions among these factors to provide a comprehensive understanding of such complex events.

5 Conclusion

This study presents a comprehensive analysis of the Jintian Village landslide's dynamics through numerical simulations, the conclusions are as follows: The extensive gully modifications for agricultural purposes altered the terrain by raising groundwater levels. Although these changes maintained regional stability for nearly a decade, the Ms 6.2 earthquake in December 2023 disrupted the situation and initiated the Jintian village landslide. The simulations demonstrate that the pore water pressure ratio (λ) affects landslide behavior. Increased saturation will enhance the mobility of landslide materials, thereby amplifying the scale of the disaster. The throat-like terrain further limits material movement, resulting in pronounced spread patterns. The failure of the check dam in the landslide path increased its runout distance and enlarged its impact area. To some extent, it increases the harm of disasters. In conclusion, attention should be paid to the disaster impact of human topographic reconstruction in the loess area.

Acknowledgments The authors gratefully acknowledge the financial support provided by the National Natural Science Foundation of China (Grant No. 42307194, 42120104002) and the China Postdoctoral Science Foundation through the Postdoctoral Fellowship Program Grade B (Grant No. 2022 M721771, GZB20230325). We also extend our heartfelt thanks to our colleagues and collaborators who provided valuable insights and feedback throughout this study.

References

Arran MI, Mangeney A, De Rosny J et al (2016) Characteristics of groundwater flow field after land creation engineering in the hilly and gully area of the loess plateau. Arab J Geosci 9:646

Arran MI, Mangeney A, De Rosny J et al (2022) Subsidence monitoring and influencing factor analysis of mountain excavation and valley infilling on the Chinese loess plateau: a case study of yan'an New District. Eng Geol 297:106482

Arran MI, Mangeney A, De Rosny J et al (2023) Response of soil erosion to vegetation restoration and terracing on the loess plateau. Catena 227:107103

Fang K, Jia S, Tang H, Zhou R, Kong Z, Fu Y et al (2024) Arching effect in slopes under excavation: classification and features. Eng Geol 337:107563

Fredlund DG, Morgenstern NR, Widger RA (1978) The shear strength of unsaturated soils. Can Geotech J 15(3):313–321

Fu B, Wang S, Liu Y et al (2017) Hydrogeomorphic ecosystem responses to natural and anthropogenic changes in the loess plateau of China. Annu Rev Earth Planet Sci 45:223–243

George DL, Iverson RM (2014) A depth-averaged debris-flow model that includes the effects of evolving dilatancy. II. Numerical predictions and experimental tests. Proc R Soc A 470:20130820

Guo J, Cui Y, Xu W et al (2022a) A novel friction weakening-based dynamic model for landslide runout assessment along the Sichuan-Tibet railway. Eng Geol 306:106721

Guo J, Cui Y, Xu W et al (2022b) Numerical investigation of the landslide-debris flow transformation process considering topographic and entrainment effects: a case study. Landslides 19:773–788

Hungr O, Leroueil S, Picarelli L (2014) The Varnes classification of landslide types, an update. Landslides 11:167–194

Li P, Qian H, Wu J (2014) Environment: accelerate research on land creation. Nature 510:29–31

Liu C, Liang K, Wang X (2024) Cause analysis of disaster chain of soil flow in Dashagou Basin in Jishishan Ms 6. 2 magnitude earthquake area (in Chinese). Geol Rev 70:960–974

Ni X, Ma J, Zhang F (2024) Mechanism of the variation in axial strain of sand subjected to undrained cyclic triaxial loading explained by DEM with non-spherical particles. Comput Geotech 165:105846

Ouyang C, Zhou K, Xu Q et al (2017) Dynamic analysis and numerical modeling of the 2015 catastrophic landslide of the construction waste landfill at Guangming, Shenzhen, China. Landslides 14:705–718

Sassa K, Nagai O, Solidum R et al (2010) An integrated model simulating the initiation and motion of earthquake and rain induced rapid landslides and its application to the 2006 Leyte landslide. Landslides 7:219–236

Savage SB, Hutter K (1989) The motion of a finite mass of granular material down a rough incline. J Fluid Mech 199:177–215

Shen W, Li T, Li P, Guo J (2018) A modified finite difference model for the modeling of flowslides. Landslides 15:1577–1593

Shi P, Liu F, Meng X et al (2024) Recent Jishishan earthquake ripple hazard provides a new explanation for the destruction of the prehistoric Lajia settlement 4000a B.P. Sci Rep 14:11630

Wang L, Xu S, Wang P et al (2024) Characteristics and lessons of liquefaction-triggered large-scale flow slide in loess deposit during Jishishan M6.2 earthquake in 2023. Chin J Geotech Eng 46:235–243

Xu Q, Peng D, Fan X et al (2024) Characteristics and initiation mechanism of Zhongchuan town Flowslide triggered by Jishishan Ms 6.2 earthquake in Gansu Province (in Chinese). Geomatics and Information Science of Wuhan University, pp 1–18

Zhao B (2024) Climatological and geological controls on seismic earthflows in coastal areas. Catena 235:107692

Zhuang Y, Yin Y, Xing A, Jin K (2020) Combined numerical investigation of the Yigong rock slide-debris avalanche and subsequent dam-break flood propagation in Tibet, China. Landslides 17:2217–2229

A Novel Fluid-Solid Coupling Model for Landslide-Induced Tsunami Simulation

Wang Lu, Wengang Zhang, Luqi Wang, Kaiqiang Zhang, and Songlin Liu

Abstract

Landslides are a common type of geological hazard. When a landslide collides with a water body, it can generate secondary waves, the destructive potential of which may exceed that of the landslide itself, highlighting the necessity for research on landslide-generated tsunamis. This catastrophic disaster represents a typical fluid-solid coupling process, and the interactions among the two phases significantly complicate the study of this issue. This research proposes an innovative approach to efficiently and effectively simulate this disaster using multi-layer nested grids and a flexible selection of various governing equations. The method couples the progressive landslide model (Ls-Rapid), developed by the International Consortium on Landslides, with the Cornell Multi-grid Coupled Tsunami Model; data conversion between the two models was implemented in Fortran. The effectiveness of this method at different computational scales was validated through case studies of the Gongjiafang landslide in the Three Gorges Reservoir area in 2008 and the 1946 Aleutian tsunami. The simulated results align well with field survey data, demonstrating the promising application prospects of this method in predicting and mitigating landslide-generated tsunamis.

Keywords

Landslide-induced tsunami · Progressive landslide model · COMCOT · Fluid-solid coupling model

1 Introduction

Landslides are significant geological hazards that can generate impulse waves, posing severe risks to coastal communities and infrastructure. Historical events such as the Vaiont landslide in Italy (Dykes and Bromhead 2018, 2022) and the 1964 Prince William Sound earthquake-triggered tsunamis (Suleimani et al. 2009) underline the potential devastation these phenomena can cause. The ICL journal *Landslides* recently published its inaugural Virtual Thematic Issue titled "Landslides and Tsunamis: Multi-Geohazards" (Sassa 2023), involving coastal and submarine landslides, river landslides, reservoir landslides, lake landslides, and fjord landslides. The origins of these events vary widely, attributed to factors such as earthquakes, volcanoes, intense rainfall, rising water levels, among others. Notable contributions in this Virtual Thematic Issue include highly cited papers focusing on landslide and tsunami occurrences as multi-geohazards, such as the 2018 Indonesia Sulawesi earthquake and tsunami disasters (Sassa and Takagawa 2019) and the landslides and tsunamis in the Three Gorges Reservoir region during the twenty-first century (Yin et al. 2015). The interaction between land movement and water bodies results in complex wave dynamics that demand a thorough investigation to predict their impact accurately. Understanding the dynamics of landslides and their multi-phased physics is essential for a rational comprehension and prediction of tsu-

W. Lu · K. Zhang · S. Liu
School of Civil Engineering, Chongqing University, Chongqing, China
e-mail: 202116131374@cqu.edu.cn; 20231601146g@stu.cqu.edu.cn; songlinl@cqu.edu

W. Zhang
School of Civil Engineering, Chongqing University, Chongqing, China

National Joint Engineering Research Center of Geohazards Prevention in the Reservoir Areas, Chongqing University, Chongqing, China
e-mail: zhangwg@cqu.edu.cn

L. Wang (✉)
School of Civil Engineering, Chongqing University, Chongqing, China

Chongqing Field Scientific Observation Station for Landslide Hazards in Three Gorges Reservoir Area, Chongqing University, Chongqing, China
e-mail: wlq93@cqu.edu.cn

B. Abolmasov et al. (eds.), *Progress in Landslide Research and Technology, Volume 4 Issue 1, 2025*, Progress in Landslide Research and Technology, https://doi.org/10.1007/978-3-031-89836-5_6

nami waves resulting from landslides, as highlighted in the global panel discussion on understanding and mitigating the disaster risks associated with landslide-induced tsunamis (Sassa et al. 2022).

Recent advances in research have propelled our understanding of wave generation, propagation, and run-up associated with landslide events. Laboratory experiments and numerical simulations have become pivotal in modeling these processes, allowing for the exploration of key variables influencing wave characteristics. Walder et al. (2003) conducted a series of laboratory experiments to predict the amplitude and shape of near-field water waves generated by landslides. Their findings highlighted that key parameters, including water depth, slide volume, and the duration of submerged landslide motion, significantly influence wave characteristics. Additionally, Ataie-Ashtiani and Nik-Khah (2008) conducted 120 laboratory tests to investigate impulse waves generated by subaerial landslides. Their study examined the effects of several key parameters on wave characteristics. The results indicated that while the wave pattern remained consistent across all cases, variations in amplitude and period were observed. Specifically, wave height was significantly influenced by factors such as bed slope angle, landslide impact velocity, thickness, and the shape of the landslide. Notably, the use of different numerical models has improved simulation accuracy for large-scale events, enhancing disaster preparedness strategies. Some researchers have treated the effects of landslide motion as either initial or boundary conditions for the water surface (Harbitz et al. 1993; Shi et al. 2012), which overlooks the reciprocal response of the water body to the landslide. More sophisticated modeling techniques have emerged recently that integrate the strengths of discrete element modeling (DEM) and computational fluid dynamics (CFD). DEM effectively simulates landslide motion, while CFD accurately captures fluid behavior. The coupling of DEM and CFD yields improved simulation accuracy and enhanced model visualization (Bilal et al. 2021; Hu et al. 2021; Yang et al. 2024). Although the DEM-CFD model is favored for simulating landslide-generated waves, it significantly increases computational demands due to the complexity of accounting for the entire processes of wave generation, evolution, and run-up.

Despite notable progress in laboratory research and the validation of numerical models, the inherent complexity of wave generation from landslides remains a challenge. Understanding the triggering mechanisms, energy dissipation, and intricate wave dynamics is essential for accurate prediction and risk mitigation in affected regions. This study aims to enhance methodologies for predicting impulse waves from landslides by integrating theoretical insights with empirical data, thereby contributing to improved safety measures and disaster response strategies in vulnerable coastal and reservoir areas. The workflow of this paper is presented in Fig. 1.

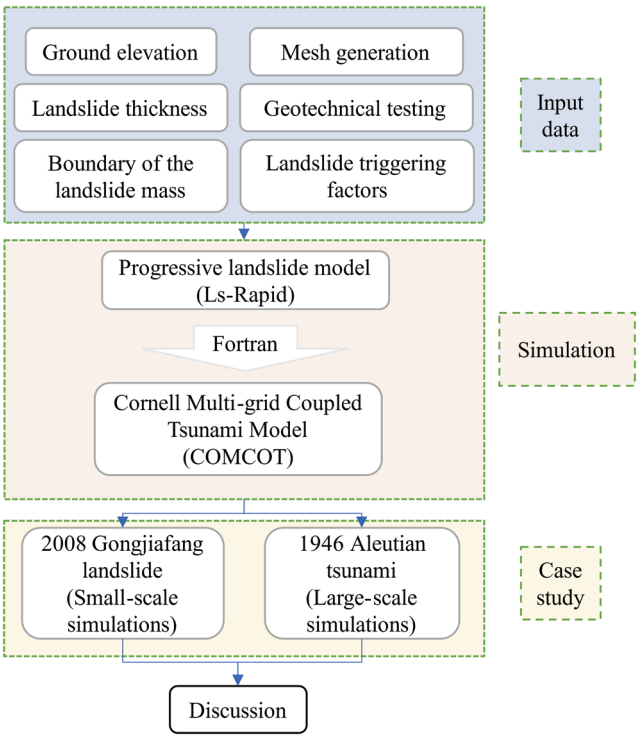

Fig. 1 Technical Flowchart

2 Methodology

2.1 Progressive Landslide Model

Limit equilibrium stability analysis methods typically assume that when a landslide is on the verge of failure, the entire sliding surface will fail simultaneously. However, subsequent research has shown that in large-scale landslides, the weak zone within the landslide initiates failure first, leading to an expansion of the failure area before the entire landslide ultimately fails and begins to move (Miao et al. 2017). Progressive failure has been widely acknowledged in related studies (Miao et al. 2011; Yin et al. 2022).

Sassa et al. (2004) developed a three-dimensional model, known as Ls-Rapid, based on progressive failure to simulate the initiation and motion of landslides triggered by rainfall and earthquakes. Ls-Rapid employs a grid-based approach grounded in Newton's second law. In this model, the geometric representation is divided into rectangular grids on the horizontal plane, effectively segmenting the geographic model into columns. By analyzing the forces acting on each column, the accelerated velocity of the sliding mass can be determined to describe its movement.

The following factors primarily influence each column: (1) the self-weight of the soil column (W); (2) the vertical seismic force (F_v) and the horizontal seismic forces (F_x and F_y); (3) the lateral pressure (P) exerted on the side of the

column unit; (4) the shear force (R) at the bottom of the column unit; (5) the support force (N) at the base of the column unit; and (6) the pore water pressure (U) at the bottom of the column unit. The acceleration resulting from the net forces acting on the column unit can be expressed as:

$$ma = \left(W + F_v + F_x + F_y\right) + \left(\frac{\partial P_x}{\partial x}\Delta x + \frac{\partial P_y}{\partial y}\Delta y\right) + R \quad (1)$$

Equation 1 is projected onto the horizontal plane in the x-direction:

$$\frac{\partial M}{\partial t} + \frac{\partial}{\partial x}\left(u_0 M\right) + \frac{\partial}{\partial y}(v_0 M = gh\left\{\frac{\tan\alpha}{q+1}\left(1+Kv\right) + Kx\cos^2\alpha\right\}$$

$$-\left(1+Kv\right)kgh\frac{\partial h}{\partial x} - \frac{g}{\left(q+1\right)^{\frac{1}{2}}}\cdot\frac{u_o}{\left(u_0^2+v_0^2+w_0^2\right)^{\frac{1}{2}}}\{h_c\left(q+1\right)$$

$$+\left(1-r_u\right)htan\phi_a\} \quad (2)$$

and in the y direction:

$$\frac{\partial N}{\partial t} + \frac{\partial}{\partial x}\left(u_0 N\right) + \frac{\partial}{\partial y}\left(v_0 N\right) = gh\left\{\frac{\tan\beta}{q+1}\left(1+Kv\right) + Ky\cos^2\beta\right\}$$

$$-\left(1+Kv\right)kgh\frac{\partial h}{\partial y} - \frac{g}{\left(q+1\right)^{\frac{1}{2}}}\cdot\frac{v_o}{\left(u_0^2+v_0^2+w_0^2\right)^{\frac{1}{2}}}\{h_c\left(q+1\right)$$

$$+\left(1-r_u\right)htan\phi_a\} \quad (3)$$

Assuming that the total mass of the landslide remains constant throughout the motion, we obtain the following:

$$\frac{\partial h}{\partial t} + \frac{\partial M}{\partial x} + \frac{\partial N}{\partial y} = 0 \quad (4)$$

where h is the height of the soil column within a grid; g is the acceleration due to gravity; α and β are the angles of the ground surface relative to the X-Z plane and Y-Z plane, respectively. The velocities of a column in the X, Y, and Z directions are denoted by u_0, v_0, and w_0; the velocity in the vertical direction is disregarded as there is no soil discharge occurring vertically. M and N represent the soil discharge per unit width in the X and Y directions, respectively. The lateral pressure coefficient (k) is defined as the ratio of horizontal compressive stress to vertical compressive stress. The apparent friction coefficient of the sliding surface during motion is represented by $\tan\phi_a$, while h_c denotes soil cohesion expressed per unit height. ρ indicates soil density, $q = tan^2\alpha + tan^2\beta$, $w_0 = -(u_0\ tan\ \alpha + v_0\ tan\ \beta)$, and the seismic coefficients in the X, Y, and Z directions are represented by K_v, K_x, and K_y, respectively. Finally, r_u represents the pore pressure ratio.

2.2 Cornell Multi-Grid Coupled Tsunami

COMCOT employs a leap-frog time-differencing scheme to efficiently solve the shallow water equations, enabling the simulation of the entire life cycle of tsunamis. During model execution, all physical variables within the subgrid are calculated simultaneously, significantly reducing computation time and enhancing operational efficiency. The governing equations are derived from the Navier-Stokes equations, making them suitable for modeling tsunami waves. COMCOT incorporates various wave-triggering mechanisms, including earthquakes, faults, submarine landslides, and artificial waves. Additionally, both linear and nonlinear shallow water wave equations are integrated, which enhances the model's versatility. Researchers have utilized COMCOT to simulate historical tsunami events (Syamsidik et al. 2017). In this study, we adopt COMCOT version 1.7, which has undergone continuous improvements and updates.

The COMCOT model can flexibly utilize linear or nonlinear shallow water equations in either spherical or Cartesian coordinates, with four types of governing equations applicable to different scenarios. For deep-sea tsunamis, where the amplitude of water waves is considerably smaller than the sea depth, a linear shallow water equation in a spherical coordinate system can be employed, as follows:

$$\frac{\partial \eta}{\partial t} + \frac{1}{Rcos\varphi}\left\{\frac{\partial P}{\partial \psi} + \frac{\partial}{\partial \varphi}\left(\cos\varphi Q\right)\right\} = -\frac{\partial h}{\partial t} \quad (5)$$

$$\frac{\partial P}{\partial t} + \frac{gh}{Rcos\varphi}\frac{\partial \eta}{\partial \psi} - fQ = 0 \quad (6)$$

$$\frac{\partial Q}{\partial t} + \frac{gh}{R}\frac{\partial \eta}{\partial \varphi} + fP = 0 \quad (7)$$

Linear shallow-water equations become inadequate as tsunami waves approach the coastline. As these linear waves propagate into shallower waters, their wavelength decreases while their amplitude increases. In this context, the Coriolis force and dispersion effects due to Earth's rotation can be disregarded, while friction and convective inertial forces become increasingly significant. Therefore, it is appropriate to utilize a nonlinear shallow water equation in the spherical coordinate system, as demonstrated below:

$$\frac{\partial \eta}{\partial t} + \frac{1}{Rcos\varphi}\left\{\frac{\partial P}{\partial \psi} + \frac{\partial}{\partial \varphi}\left(\cos\varphi Q\right)\right\} = -\frac{\partial h}{\partial t} \quad (8)$$

$$\frac{\partial P}{\partial t} + \frac{1}{Rcos\varphi}\frac{\partial}{\partial \psi}\left\{\frac{P^2}{H}\right\} + \frac{1}{R}\frac{\partial}{\partial \varphi}\left\{\frac{PQ}{H}\right\} + \frac{gH}{Rcos\varphi}\frac{\partial \eta}{\partial \psi} - fQ + F_x = 0 \quad (9)$$

$$\frac{\partial Q}{\partial t}+\frac{1}{Rcos\varphi}\frac{\partial}{\partial \psi}\left\{\frac{PQ}{H}\right\}+\frac{1}{R}\frac{\partial}{\partial \varphi}\left\{\frac{Q^2}{H}\right\}+\frac{gH}{R}\frac{\partial \eta}{\partial \varphi}+fP+F_y=0 \quad (10)$$

In Eqs. 5–10, η is the height of water waves above sea level, P is the volume flux along the longitude, Q represents the volume flux along latitude, φ represents latitude, ψ represents longitude, R is the radius of the earth, g is gravitational acceleration, h is the depth of still water, H is the sum of η and h, f represents the coefficient of Coriolis force caused by earth rotation, F_x and F_y represent the bottom friction force in the x or y direction respectively, and n is the Manning coefficient. If necessary, the shallow water equations can be derived in a Cartesian coordinate system through minor mathematical manipulation.

Shallow water equations are commonly employed to simulate the flow of both oceanic and atmospheric systems, making them suitable for analyzing free surface flows where the horizontal scale greatly exceeds the vertical scale. Generally, when the dispersion effect—measured by the ratio of water depth to tsunami wavelength—is less than 1/20, the shallow water equations are considered sufficient for studying tsunami evolution (Glimsdal et al. 2013). Compared to the Navier-Stokes equations from which they are derived, SWEs reduce one spatial dimension, significantly enhancing computational efficiency.

3 Landslide-Induced Tsunami in Reservoir Area

3.1 Gongjiafang Landslide

On November 23, 2008, the Gongjiafang landslide occurred, displacing a significant volume of material into the Yangtze River and generating a substantial impulse wave. This landslide is located 4 km downstream from Wushan County in Chongqing Municipality, China (Fig. 2). The estimated volume of the collapsed rock mass was approximately 3.79×10^5 m^3, with the resulting impulse waves reaching a run-up height of around 10 m on the opposite bank.

The Gongjiafang landslide took place following an experimental impoundment of the Three Gorges Dam, which raised the reservoir water level to an altitude of 173 m. Researchers have suggested that this impoundment may have triggered landslides in the vicinity of the Three Gorges Reservoir (Tang et al. 2019; Wang et al. 2008). The slope at Gongjiafang is characterized as an anaclinal, layered rocky formation composed of hard limestone at the top and a softer rock toe. The presence of developed fissures and significant weathering has resulted in numerous discontinuities within the shale slope. Additionally, the slope toe has experienced

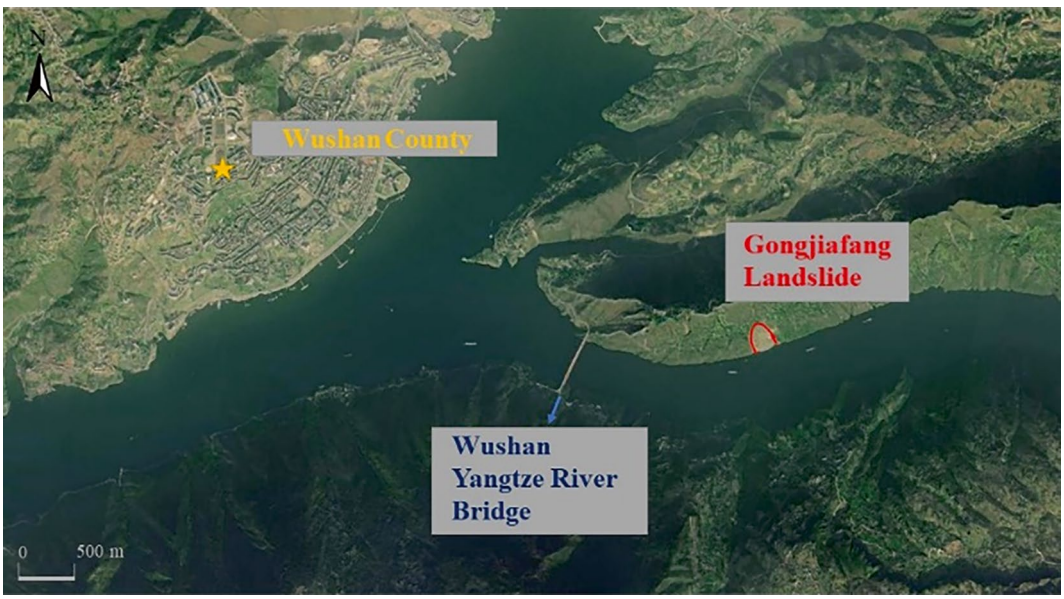

Fig. 2 Location of Gongjiafang landslide

severe erosion due to fluctuations in the reservoir water level. It is believed that the toppling deformation and minor failure of the slope toe contributed to the occurrence of the Gongjiafang landslide. For detailed information regarding the failure mechanisms of the Gongjiafang landslide, refer to Gu and Huang (2016).

3.2 Simulation of Gongjiafang Landslide-Induced Tsunami

On November 23, 2008, the Gongjiafang landslide occurred, di Based on prior research (Huang et al. 2014; Xiao et al. 2015; Gu and Huang 2016; Huang et al. 2023), the degradation of the slope toe due to river erosion and severe weathering, coupled with variations in pore water pressure resulting from impoundment, significantly contribute to the collapse of the Gongjiafang landslide. The mechanical parameters of submerged rock masses are primarily influenced by river erosion, while those of subaerial rock masses are predominantly affected by weathering. Consequently, the simulation model of the Gongjiafang landslide divides the sliding area into two distinct sections: the submerged grid and the subaerial grid. These two components have different parameter settings, which are informed by previous studies (Huang et al. 2012; Huang et al. 2014; Xiao et al. 2015), as detailed in Table 1.

The initiation and movement process of the Gongjiafang landslide was simulated using LS-Rapid. The landslide is highlighted within a pink circle, while the red spheres represent the flow of geological materials, as illustrated in Fig. 3.

The front portion of the landslide is approximately 120 m above sea level, while the trailing edge is around 400 m high. During the failure process, the toe section of the landslide experienced localized collapse; however, the upper portion remained stable. The fractured rock mass moved downward and impacted the riverbed. As the pore water pressure ratio continued to increase, the rock mass in the upper section of the landslide lost support from the toe, leading to movement in the upper half after 5 s. At 15 s, the two slip masses coalesced and began to move as a single unit, with the higher slip mass colliding with the deposits that had collapsed during the initial failure stage. By 58 s, the slip mass came to a halt and settled in the riverbed, with the morphology of the deposition reflecting findings from field surveys.

Based on the results of the landslide simulation, secondary tsunami events were further modeled. The time variation of ground elevation was generated using LS-Rapid, and these data files were normalized in FORTRAN to facilitate their compatibility with the COMCOT model for topographic analysis. In simulating the Gongjiafang landslide's impact, transient riverbed motion patterns and nonlinear shallow water equations were employed. This approach is justified given that the duration of the landslide event is relatively short in comparison to the duration of the resulting impulse waves. Furthermore, the nonlinear characteristics of the bank slope were considered crucial for accurately capturing the dynamics of the tsunami generation and propagation.

The run-up and wave propagation of the Gongjiafang impulse waves are illustrated in Fig. 4 at various time intervals. During the initiation phase, the slip mass interacts with the water body, generating arched water waves that propagate outward. By 28 s, these waves spread along the river channel and reach the opposite bank, achieving a maximum run-up height of 15 m. As the impulse waves travel, they reflect off surfaces and interact, with the superimposed waves persisting for a duration of 90 s before arriving at the Wushan Yangtze River Bridge. After 230 s, the water wave reaches Wushan County town with an amplitude of 0.09 m. By 1500 s, the wave has extended throughout the entire length of the river; however, its amplitude has diminished significantly due to dissipation and spreading effects. This simulation highlights the complex interactions between landslide-induced waves and their subsequent impact on surrounding areas.

Table 1 Selection of parameters for Gongjiafang landslide simulation modeling

Submerged rock			Subaerial rock		
Parameters	Symbols	Values	Parameters	Symbols	Values
Lateral pressure ratio	k	0.5	Lateral pressure ratio	k	0.5
Effective friction within the landslide	$\tan\phi_i$	0.54	Effective friction within the landslide	$\tan\phi_i$	0.63
Effective friction on the sliding surface	$\tan\phi_m$	0.62	Effective friction on the sliding surface	$\tan\phi_m$	0.45
Shear stress at the steady state	τ_{ss}	30 kPa	Shear stress at the steady state	τ_{ss}	50 kPa
Pore pressure generation rate	B_{ss}	1	Pore pressure generation rate	B_{ss}	0
Unit weight of mass	γ	15.2 kN/m^3	Unit weight of mass	γ	25 kN/m^3
Pore pressure ratio	r_u	0.15	Pore pressure ratio	r_u	0.15

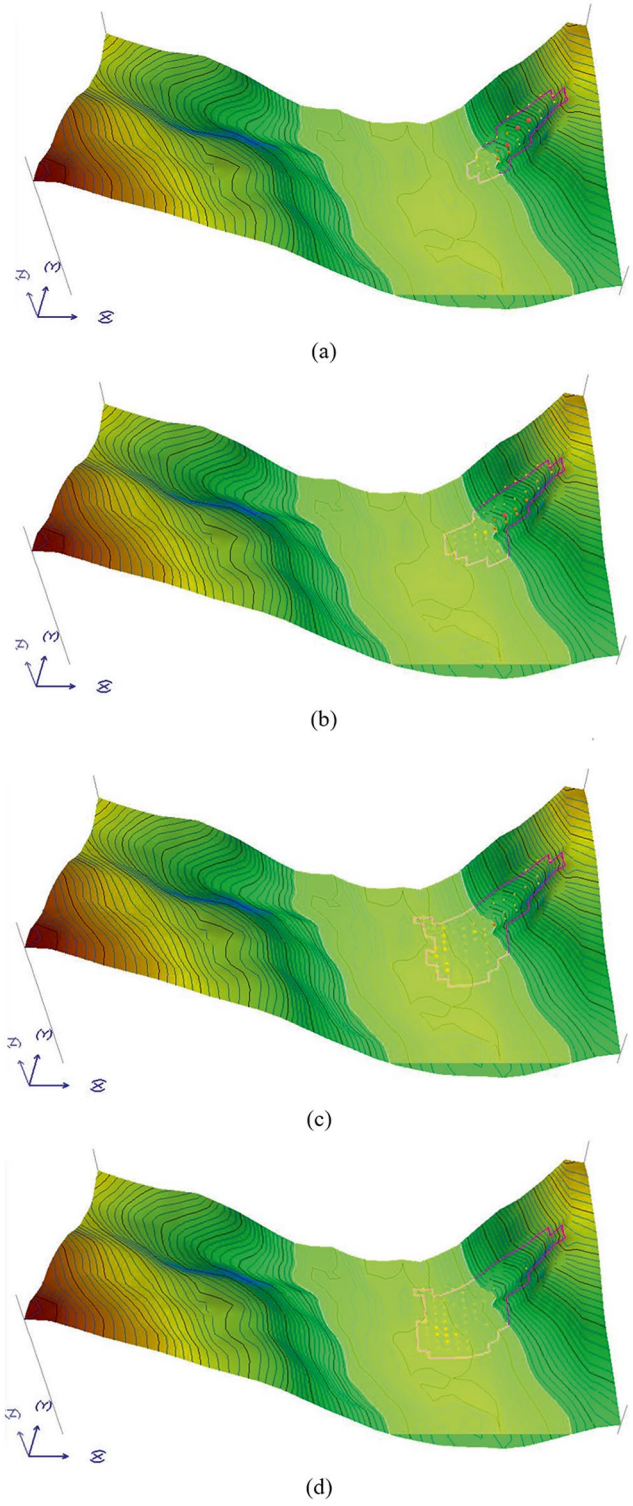

Fig. 3 Motion process of Gongjiafang landslide: (**a**) t = 1 s; (**b**) t = 5 s; (**c**) t = 15 s and (**d**) t = 58 s

4 Submarine Landslide-Induced Tsunami

4.1 1946 Aleutian Tsunami

On April 1, 1946, an unprecedented seismic event and the resulting tsunami impacted the Aleutian Islands, located on the western side of the Alaska Peninsula. This event was described by researchers as "a very unusual earthquake," characterized by a surface wave magnitude (M_s) of only 7.4, yet it generated an exceptionally powerful tsunami with a tsunami magnitude (M_t) of 9.3 (Abe 1979). The tsunami's run-up height exceeded 30 m on Unimak Island, leading to the destruction of the Scotch Cap lighthouse and resulting in the fatalities of five individuals. The tsunami subsequently propagated across the Pacific Ocean and struck the Hawaiian Islands, claiming the lives of 159 people (Lander 1989). As illustrated in Fig. 5, the tsunami inundated the building outlined in white, with the maximum run-up observed at location 3, indicated by the black arrow.

The 1946 Aleutian earthquake, although relatively moderate in magnitude, generated one of the largest trans-Pacific tsunamis ever recorded. This unusual phenomenon prompted extensive research. Kanamori (1972) proposed that the earthquake had a significant effective moment sustained over an extended duration. Furthermore, the faulting mechanism exhibited a substantial dip-slip component, leading to the generation of devastating tsunamis despite the earthquake's modest size; such events are commonly termed "tsunami earthquakes." However, subsequent studies challenged the view that the 1946 Aleutian tsunami was solely the result of underthrusting (Johnson and Satake 1997; Sykes 1971). Okal et al. (2003) conducted a comprehensive field investigation on Unimak and Sanak Islands, compiling a dataset that included wave arrival times, run-up heights, their distribution, and anecdotal reports of local increases in water depth following the quake. Their findings indicated that the tsunami's generation mechanism was linked to one or more significant submarine landslides triggered by the earthquake. Among the notable candidates was the Ugamak Slide, identified through side-scan sonar imagery as shown in Fig. 5 (Fryer et al. 2004). Fryer et al. (2004) thoroughly examined the distinctive features of the 1946 Aleutian tsunami, noting that while the run-up reached an extraordinary 42 m at Scotch Cap, it rapidly diminished with distance. For example, at Sanak Village, located 126 km from Scotch Cap, the run-up height measured only 6 m. This pattern is consistent with typical characteristics of landslide-generated tsunamis

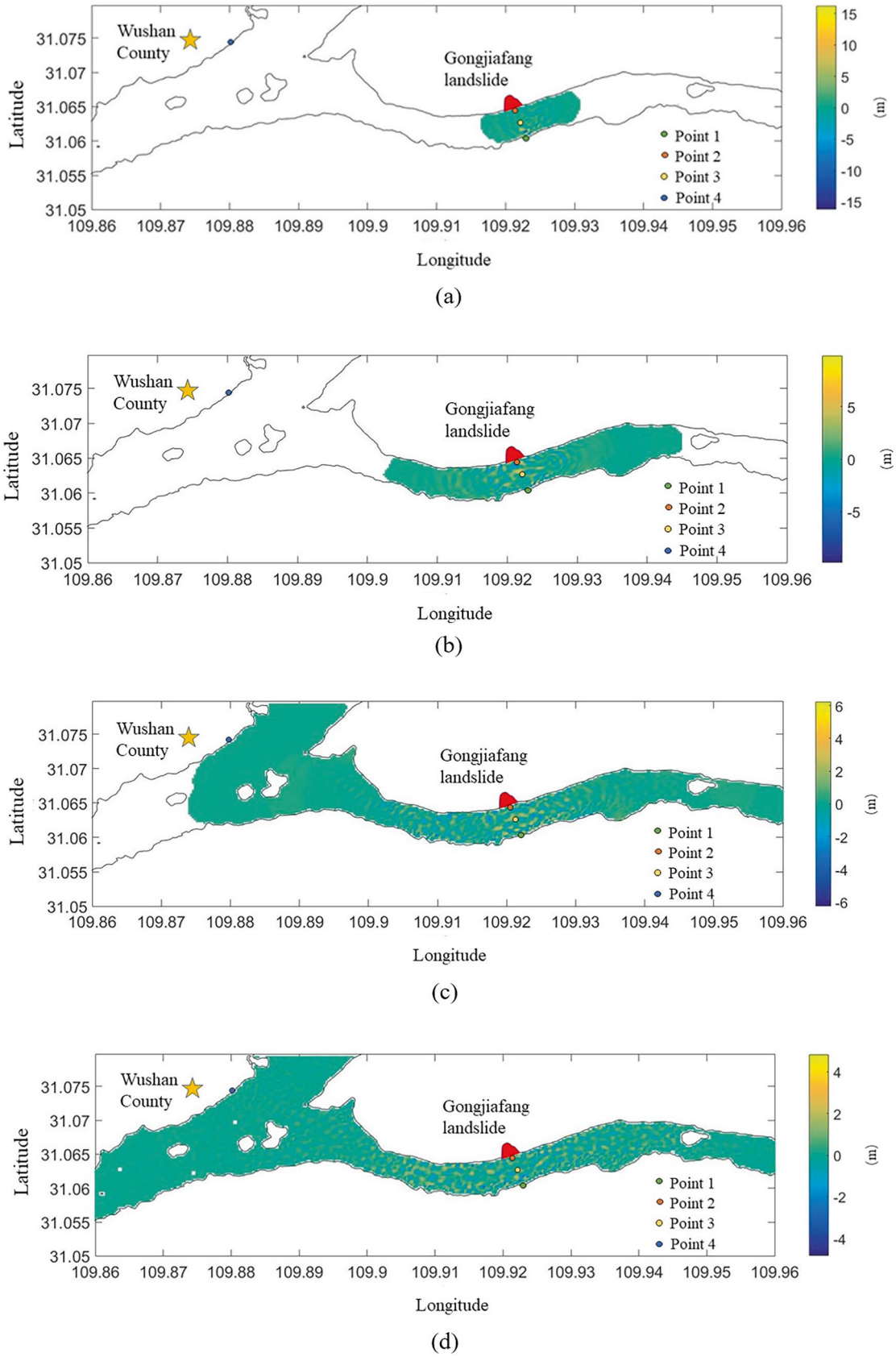

Fig. 4 Propagation process of landslide-induced tsunami: (**a**) t = 28 s, (**b**) t = 90 s, (**c**) t = 230 s and (**d**) t = 1500 s

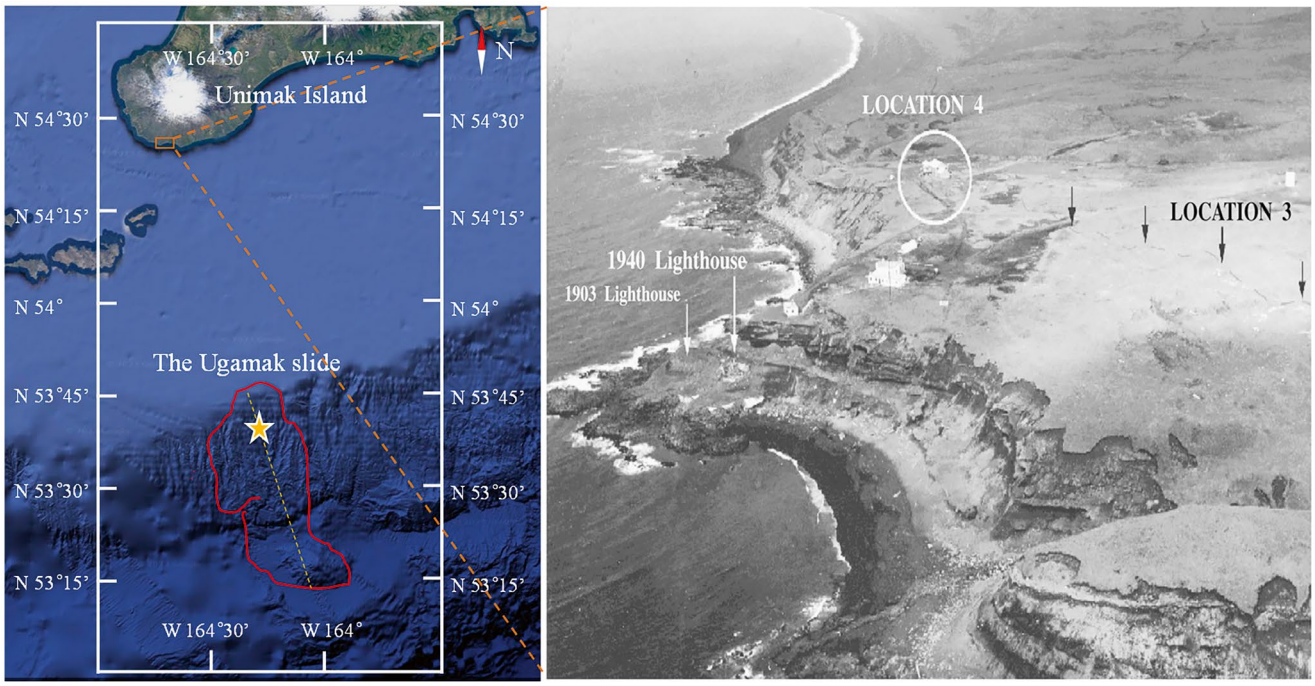

Fig. 5 The study area: (**a**) aerial view of Unimak Island and the Ugamak slide (modified from Google Earth) and (**b**) ruins of Scotch Cap lighthouse (Okal et al. 2003)

(Hidayat et al. 1995). Additionally, global bathymetry data indicated a significant failure event at the location of the Ugamak Slide.

Based on previous studies, the proposed model was utilized to simulate the 1946 Aleutian tsunami, which is believed to have been triggered by a landslide.

4.2 Simulation of 1946 Aleutian Tsunami

In the landslide simulation process, elevation data from the SRTM1 DEM (Lee and Lee 2018), established in the WGS1984 geodetic coordinate system, were utilized for geometric modeling. In Ls-Rapid, we employed ArcMap 10.6 software to convert the original DEM elevation data into the WGS_1984_UTM_Zone_3N projection coordinate system, using an input grid size of 925 m × 925 m. Taking into account the landslide's location, measured data from the Alaska coast, and findings from previous experiments (Sassa et al. 2014; Suleimani and Freymueller 2020; Suleimani et al. 2009), the input parameters for the Aleutian tsunami landslide are presented in Table 2.

The definition of the timestep (Δt) enhanced the accuracy of the calculations. It is expressed as Δt = dx/(N/v), where N represents the number of calculation iterations, dx is the grid size (in meters), and v is the grid velocity. Consequently, the timestep becomes a variable in the computation.

Table 2 Selection of parameters for Aleutian landslide simulation modeling

Parameters	Symbols	Values
Lateral pressure ratio	k	0.5
Effective friction within the landslide	$\tan\phi_i$	0.6
Effective friction on the sliding surface	$\tan\phi_m$	0.7
Shear stress at the steady state	τ_{ss}	45 kPa
Pore pressure generation rate	B_{ss}	1
Unit weight of mass	γ	18.5 kN/m^3
Pore pressure ratio	r_u	0.3

In Ls-Rapid, the dynamic movement of the submarine landslide is visually represented using red spheres, as illustrated in Fig. 6. In Fig. 6a, only 4.1 s after the initiation of the landslide, the lower section of the sliding mass propelled the upper portion, resulting in coordinated movement. At this stage, the slide body maintained a semi-ellipsoidal shape, with a maximum thickness of approximately 348 m. However, as the sliding mass continued to advance and reached 250.5 s, the lower segment began to disperse rapidly, causing the upper part to lose its cohesive movement and fragment into two distinct sections, as shown in Fig. 6b. As the slide body progressed to approximately 530 s, it predominantly moved in two directions until it encountered a level

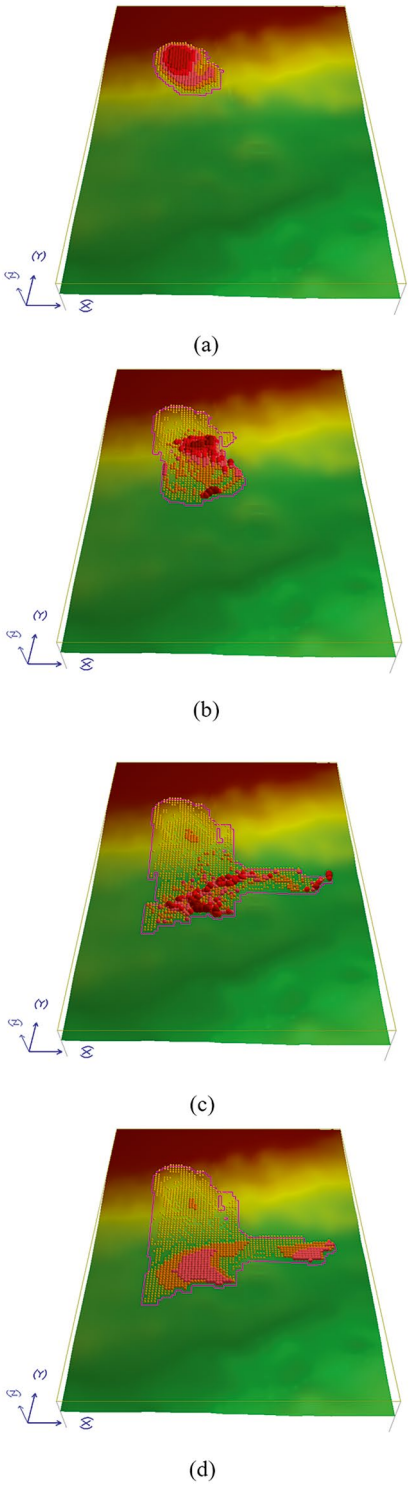

Fig. 6 Motion process of submarine landslide: (**a**) t = 4.1 s; (**b**) t = 250.5 s; (**c**) t = 530.6 s and (**d**) t = 2365.5 s

terrain, as depicted in Fig. 6c. Due to frictional forces, the slide body eventually came to rest, aligning itself into two distinct orientations. This entire process lasted for a total of 2365.5 s, culminating in the configuration shown in Fig. 6d. Notably, the maximum velocity attained during this process reached an impressive 86.7 m/s.

The submarine landslide was identified as the triggering factor for the catastrophic Aleutian tsunami. To enhance the accuracy of large-scale simulations, we employed the bilinear interpolation method to increase the density of the DEM elevation data. The entire duration of the tsunami, spanning 3600 s, was comprehensively simulated. Notably, the progressive landslide model produced a distinctive wave shape characterized by two nested arcs. Figure 7 visually illustrates the genesis and progression of tsunami waves triggered by submarine landslides at various time intervals. After 600 s of landslide motion, the sliding mass began to disintegrate from its initial semi-ellipsoidal shape, sliding toward the southeast and southwest regions of the Pacific Ocean. This movement resulted in the propagation of tsunami waves with two central sources, leading to overlapping water waves that collided and formed higher waves, as depicted in Fig. 7a. By the 1800-second mark, the central waves had gradually dissipated, causing the wave height to stabilize; however, the waves continued to disperse in a circular arc pattern. It is noteworthy that the circular diffusion waves in the southwest exceeded those in the southeast, consistent with simulation findings indicating greater deposition in the southeast direction. At this point, the tsunami had reached Scotch Cap, featuring an initial wave height of 0.89 s, as shown in Fig. 7b. After 3600 s of landslide movement, the water waves extended into the distant sea, crossing Unimak Bay and reaching the northern shoreline of Unimak Island; however, the overall wave amplitude had significantly attenuated by this stage.

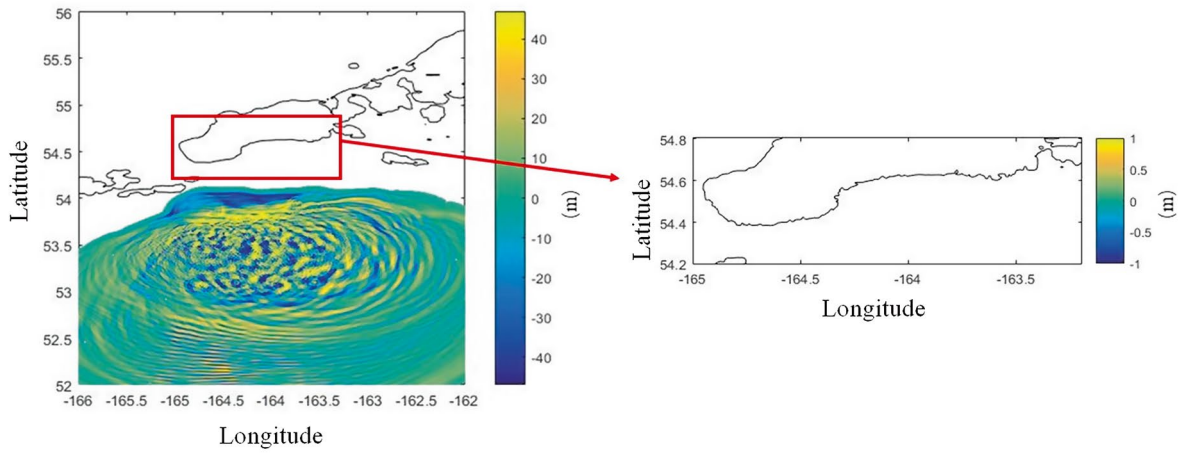

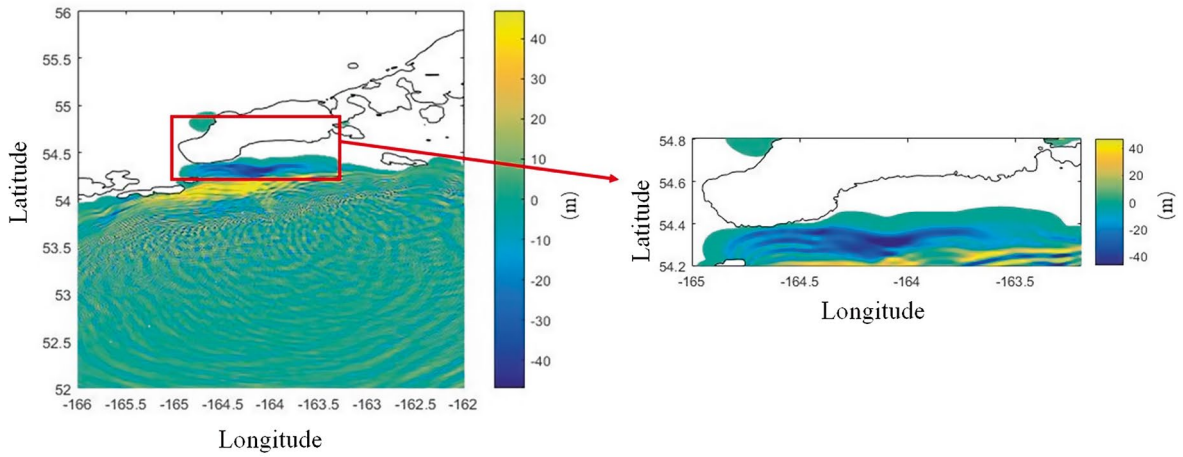

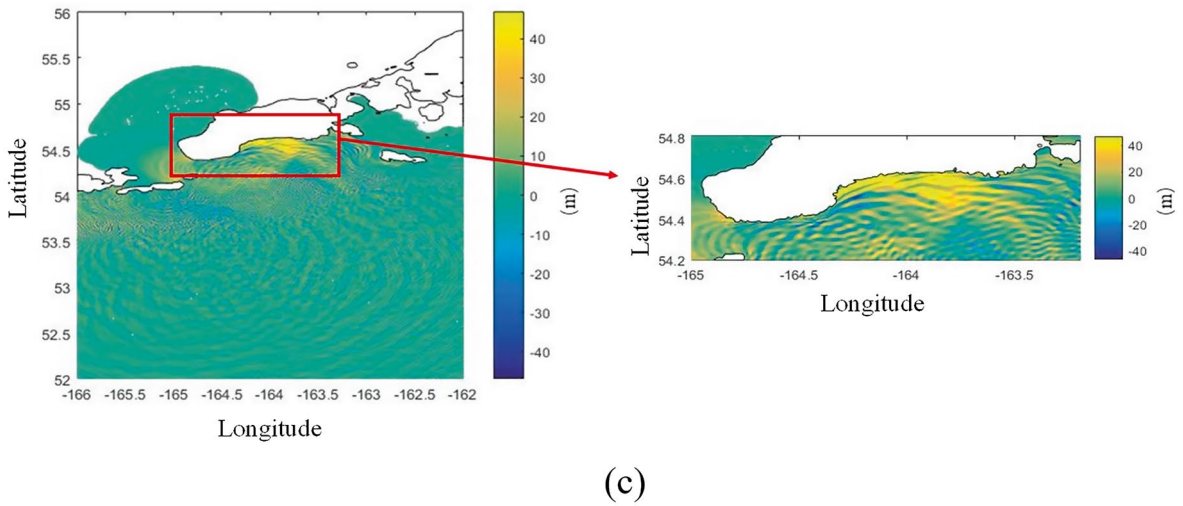

Fig. 7 Propagation process of 1946 Aleutian tsunami: (**a**) t = 600 s, (**b**) t = 1800s, and (**c**) t = 3600 s

5 Discussion

Comparing the results of numerical simulations with field observations of tsunamis serves as a means to validate the accuracy of the model. In this section, we evaluate the effectiveness of the proposed method for both landslides in reservoir areas and underwater landslides, followed by relevant discussions and analyses.

5.1 Model Performance in a Limited Computational Domain

Field surveys conducted by researchers have investigated the impact of Gongjiafang impulse waves (Huang et al. 2012; Huang et al. 2014; Xiao et al. 2015). By analyzing the trails of wave run-up along the river course and gathering information from eyewitness accounts, observed wave heights were recorded. These observed values are compared with simulated results to validate the accuracy of the proposed approach, as illustrated in Fig. 8.

The maximum wave run-up on the inshore side of the landslide is estimated to be approximately 13 m, while the maximum wave run-up on the opposite side is estimated to be about 15 m. When compared to the observed values, the calculated wave run-up demonstrates a strong correlation, with a maximum discrepancy of around 2 m noted on the opposite side. Overall, the model's calculated values align closely with the observed data, falling within an acceptable error range. This comparison highlights the model's performance in replicating real-world conditions, providing insights into its reliability and effectiveness.

5.2 Model Performance in a Large Computational Domain

The calculations of maximum tsunami wave height were plotted along the longitudinal axis, with points representing observed values marked for comparison, as shown in Fig. 9.

The results indicated a high degree of consistency between the calculated and observed values. Notably, there was a gradual increase in wave height from west to east along the longitudinal axis. At Scotch Cap Island, the maximum computed tsunami wave height reached 43.9074 m, closely approximating the observed value of 42 m. Along the eastern coast of Unimak Island, significant fluctuations in wave height occurred due to collisions and extrusions caused by sediment accumulation in the southeast direction. While the calculated values were slightly higher than the observed ones, they still exhibited a satisfactory overall fit. In summary, the proposed model demonstrates a close alignment with the characteristic behavior of submarine landslides, further reinforcing its suitability for simulating such events.

Comparing the simulation results of reservoir landslides and submarine landslides reveals that the proposed model demonstrates higher accuracy when simulating wave surges caused by reservoir bank landslides. In complex topographies typical of reservoir areas, wave surges are prone to colliding and interacting with riverbanks, which allows for highly accurate calculations using nonlinear shallow water equations. Conversely, the simulation accuracy for underwater landslides is not as high as that for reservoir landslides, primarily due to the greater challenges associated with simulating wave surges over large computational domains. As a result, considerations regarding computational costs necessitate some sacrifices in accuracy. In these larger com-

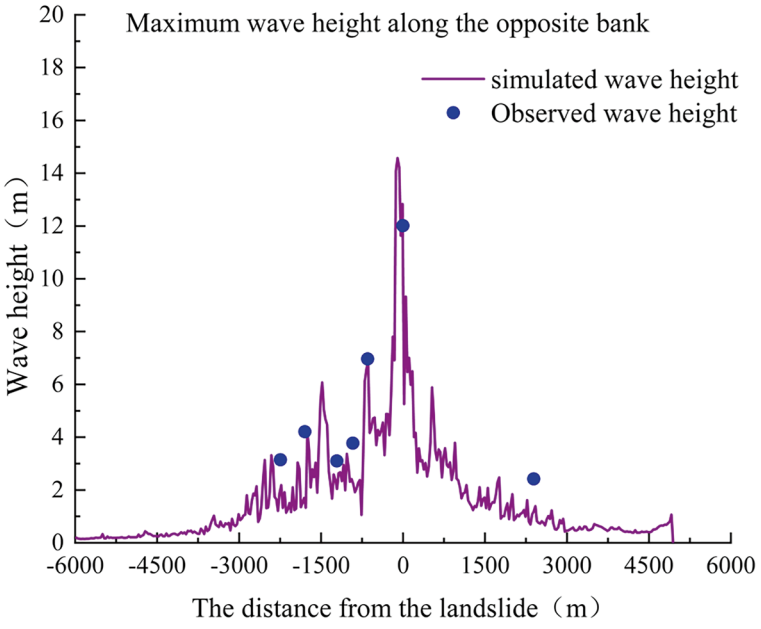

(a)

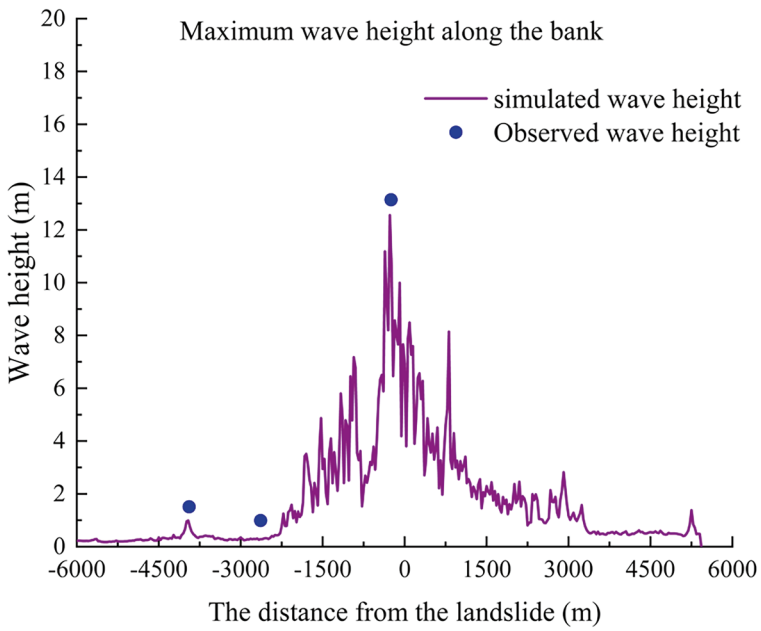

(b)

Fig. 8 Maximum wave height along the river course: (**a**) cross-shore run-up, (**b**) inshore run-up

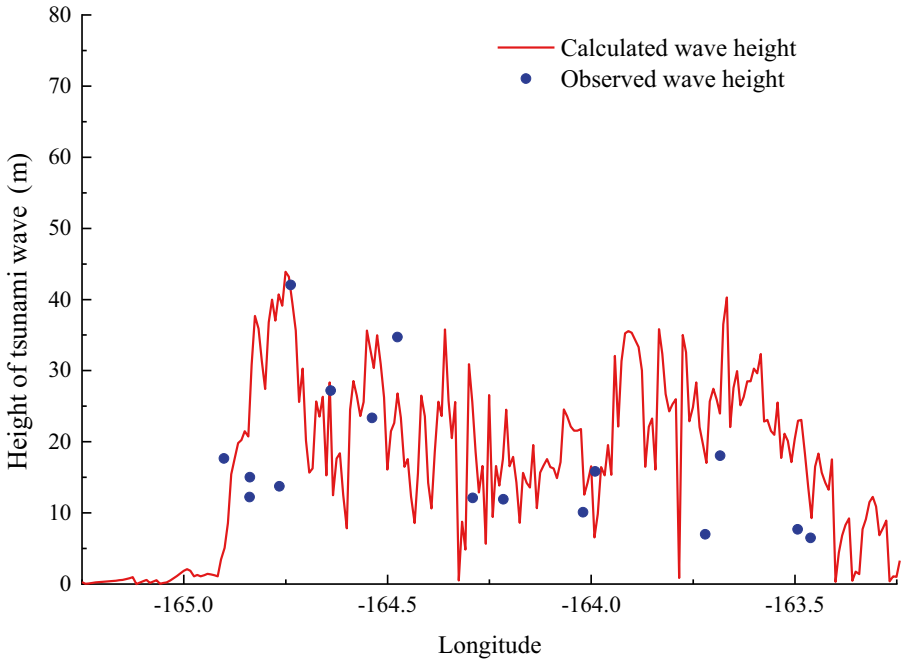

Fig. 9 Calculated tsunami height and observed tsunami height

putational domains, a combined approach utilizing both linear and nonlinear shallow water equations is typically employed.

6 Conclusion

The dynamic simulation of landslides and the resulting tsunamis constitutes a pioneering effort in the assessment of geological hazards. Simulating tsunamis generated by landslides presents complex challenges involving multiple phases and processes, making accurate simulations particularly demanding. The proposed methodology, strike an effective balance between accuracy and efficiency by leveraging the advantages of progressive landslide model alongside shallow water equations. This approach has been validated through case studies on the Gongjiafang landslide and the Aleutian tsunami.

The dynamics of landslides have a profound impact on the characteristics of subsequent tsunami waves. Modifications to the landslide model lead to significant variations in wave generation, propagation, runup, and maximum wave height. Therefore, accurately reproducing landslide motion is essential. Furthermore, when compared to submarine landslides, the proposed method demonstrates superior performance in simulating reservoir landslide-generated waves. Notably, in larger computational domains, a combined approach that integrates both linear and nonlinear shallow water equations is commonly employed. However, the constitutive equations themselves may contain inherent errors, and the accumulation of errors from numerical approximations can further contribute to a decline in accuracy. Further applications across diverse scenarios could further validate its reliability and precision from multiple perspectives.

The proposed model demonstrates significant practicality in engineering applications by efficiently simulating the complete lifecycle of tsunami waves within a short timeframe, thereby providing valuable support for tsunami warning systems. Furthermore, the model's ability to replicate historical tsunami events serves as an essential resource for engineers and researchers investigating this natural disaster.

Importantly, there is some ambiguity in the model establishment process. The topography of the study area was derived from SRTM1 DEM data; however, its accuracy requires enhancement. Additionally, the lack of a site investigation presents a significant challenge, as conducting a submarine geological survey is complicated by limitations in available equipment and high costs. The input data for the model is based on related research, but the uncertainties inherent in the model necessitate further clarification. More detailed geological survey data would be highly beneficial to improve the reliability of the model.

An even more significant concern pertains to the determination of parameters associated with the analytical model, rather than merely selecting appropriate models. This process requires a comprehensive integration of engineering expertise, financial resources, exploration techniques, and data-sharing considerations.

References

Abe K (1979) Size of great earthquakes of 1837–1974 inferred from tsunami data. J Geophys Res Solid Earth 84:1561–1568

Ataie-Ashtiani B, Nik-Khah A (2008) Impulsive waves caused by subaerial landslides. Environ Fluid Mech 8:263–280

Bilal M, Xing A, Zhuang Y, Zhang Y, Jin K, Zhu Y, Leng Y (2021) Coupled 3D numerical model for a landslide-induced impulse water wave: a case study of the Fuquan landslide. Eng Geol 290:106209
Dykes AP, Bromhead EN (2018) New, simplified and improved interpretation of the Vaiont landslide mechanics. Landslides 15:2001–2015
Dykes AP, Bromhead EN (2022) Hazards from lakes and reservoirs: new interpretation of the Vaiont disaster. J Mt Sci 19:1717–1737
Fryer GJ, Watts P, Pratson LF (2004) Source of the great tsunami of 1 April 1946: a landslide in the upper Aleutian forearc. Mar Geol 203:201–218
Glimsdal S, Pedersen GK, Harbitz CB, Løvholt F (2013) Dispersion of tsunamis: does it really matter? Nat Hazards Earth Syst Sci 13:1507–1526
Gu D, Huang D (2016) A complex rock topple-rock slide failure of an anaclinal rock slope in the Wu gorge, Yangtze River, China. Eng Geol 208:165–180
Harbitz CB, Pedersen G, Gjevik B (1993) Numerical simulations of large water waves due to landslides. J Hydraul Eng 119:1325–1342
Hidayat D, Barker JS, Satake K (1995) Modeling the seismic source and tsunami generation of the December 12, 1992 Flores Island, Indonesia, earthquake. Pure Appl Geophys 144:537–554
Hu Y-X, Zhu Y-G, Li H-B, Li C-J, Zhou J-W (2021) Numerical estimation of landslide-generated waves at Kaiding slopes, Houziyan reservoir, China, using a coupled DEM-SPH method. Landslides 18:3435–3448
Huang B, Yin Y, Liu G, Wang S, Chen X, Huo Z (2012) Analysis of waves generated by Gongjiafang landslide in Wu gorge, three gorges reservoir, on November 23, 2008. Landslides 9:395–405
Huang B, Yin Y, Wang S, Chen X, Liu G, Jiang Z, Liu J (2014) A physical similarity model of an impulsive wave generated by Gongjiafang landslide in three gorges reservoir, China. Landslides 11:513–525
Johnson JM, Satake K (1997) Estimation of seismic moment and slip distribution of the April 1, 1946, Aleutian tsunami earthquake. J Geophys Res Solid Earth 102:11765–11774
Kanamori H (1972) Mechanism of tsunami earthquakes. Phys Earth Planet Inter 6:346–359
Lander JF (1989) United States tsunamis: (including United States possessions): 1690–1988. In: Lockridge PA (ed) U.S. Dept. of commerce, National Oceanic and Atmospheric Administration, National Environmental Satellite, data, and information service. National Geophysical Data Center, Boulder, Colo
Lee S, Lee C-W (2018) Analysis of the relationship between volcanic eruption and surface deformation in volcanoes of the Alaskan Aleutian Islands using SAR interferometry. Geosci J 22:1069–1080
Miao H, Yin K, Li D (2011) Mechanical analysis for progressive failure of debris landslide. J Mt Sci 8:328–335
Miao F, Wu Y, Xie Y, Yu F, Peng L (2017) Research on progressive failure process of Baishuihe landslide based on Monte Carlo model. Stoch Env Res Risk A 31:1683–1696
Okal EA, Plafker G, Synolakis CE, Borrero JC (2003) Near-field survey of the 1946 Aleutian tsunami on Unimak and Sanak Islands. Bull Seismol Soc Am 93:1226–1234
Sassa S (2023) Landslides and tsunamis: multi-Geohazards. Landslides 20:1335–1341
Sassa S, Takagawa T (2019) Liquefied gravity flow-induced tsunami: first evidence and comparison from the 2018 Indonesia Sulawesi earthquake and tsunami disasters. Landslides 16:195–200
Sassa K, Wang G, Fukuoka H, Wang F, Ochiai T, Sugiyama M, Sekiguchi T (2004) Landslide risk evaluation and hazard zoning for rapid and long-travel landslides in urban development areas. Landslides 1:221–235
Sassa K, Dang K, He B, Takara K, Inoue K, Nagai O (2014) A new high-stress undrained ring-shear apparatus and its application to the 1792 Unzen–Mayuyama megaslide in Japan. Landslides 11:827–842
Sassa S, Grilli ST, Tappin DR, Sassa K, Karnawati D, Gusiakov VK, Løvholt F (2022) Understanding and reducing the disaster risk of landslide-induced tsunamis: a short summary of the panel discussion in the world tsunami awareness day special event of the fifth world landslide forum. Landslides 19:533–535
Shi F, Kirby JT, Harris JC, Geiman JD, Grilli ST (2012) A high-order adaptive time-stepping TVD solver for Boussinesq modeling of breaking waves and coastal inundation. Ocean Model 43-44:36–51
Suleimani E, Freymueller JT (2020) Near-field modeling of the 1964 Alaska tsunami: the role of splay faults and horizontal displacements. J Geophysical Res Solid Earth 125:e2020JB019620
Suleimani E, Hansen R, Haeussler PJ (2009) Numerical study of tsunami generated by multiple submarine slope failures in Resurrection Bay, Alaska, during the MW 9.2 1964 earthquake. Pure Appl Geophys 166:131–152
Syamsidik T, Meutia A, Al'ala M, Fahmi M, Meilianda E (2017) Numerical simulations of impacts of the 2004 Indian Ocean tsunami on coastal morphological changes around the Ulee Lheue Bay of Aceh, Indonesia. J Earthq Tsunami 11:1740005
Sykes LR (1971) Aftershock zones of great earthquakes, seismicity gaps, and earthquake prediction for Alaska and the Aleutians. J Geophys Res 1896–1977(76):8021–8041
Tang H, Wasowski J, Juang CH (2019) Geohazards in the three gorges reservoir area, China—lessons learned from decades of research. Eng Geol 261:105267
Walder JS, Watts P, Sorensen OE, Janssen K (2003) Tsunamis generated by subaerial mass flows. J Geophys Res Solid Earth 108:1
Wang F, Zhang Y, Huo Z, Peng X, Araiba K, Wang G (2008) Movement of the Shuping landslide in the first four years after the initial impoundment of the three gorges dam reservoir, China. Landslides 5:321–329
Xiao L, Ward SN, Wang J (2015) Tsunami squares approach to landslide-generated waves: application to Gongjiafang landslide, three gorges reservoir, China. Pure Appl Geophys 172:3639–3654
Yang X, Feng J, Li G, Li R, Li Z, Li H (2024) Transport behavior of particles and evolution of plugging zones in rough fractures: insights from a novel coupled CFD-DEM model. Comput Geotech 173:106553
Yin Y-P, Huang B, Chen X, Liu G, Wang S (2015) Numerical analysis on wave generated by the Qianjiangping landslide in three gorges reservoir, China. Landslides 12:355–364
Yin Y, Wang L, Zhang W, Zhang Z, Dai Z (2022) Research on the collapse process of a thick-layer dangerous rock on the reservoir bank. Bull Eng Geol Environ 81:109

Rock Avalanches of North-Eastern Transbaikalia (Russia)

Oleg V. Zerkal and Olga S. Barykina

Abstract

North-Eastern Transbaikalia is characterized by contrasting relief, high tectonic activity and seismicity. In the Quaternary period, the region was covered by glaciers during the cooling epochs, and during the warming epochs extensive paleolakes repeatedly appeared in the intermountain depressions. The Angarakan-Okuyakan and Parama clusters of large-scale rockslides and rock avalanches have been described in the North-Eastern Transbaikalia. Eight large-scale rockslides and rock avalanches have been identified within the Angarakan-Okuyakan landslide cluster and six—within the Parama landslide cluster. The largest Ugrum-1 rockslide has a volume > 1.5 km^3. Four rockslides and rock avalanches are characterized by volumes of several hundred million cubic meters. Most of the described rock avalanches in North-Eastern Transbaikalia belong to the frontally confined rock avalanches. The coefficient H/L from 0.28 to 0.34 is typical for them. Several large-scale rockslides and rock avalanches have formed landslide dams that blocked the river flow. All the described large-scale rock avalanches and rockslides distributed in North-Eastern Transbaikalia are characterized by their proximity to zones of active, seismogenic (up to M = 7.6 + 0.3) faults. It is concluded that all the described large-scale rock avalanches and rockslides are seismogenic.

Keywords

Rock avalanche · Baikal rift system · North-eastern Transbaikalia · Landslide activity · Paleolake

O. V. Zerkal (✉) · O. S. Barykina
Lomonosov Moscow State University, Geological Department, Moscow, Russia
e-mail: zerkalov@geol.msu.ru; barykina@geol.msu.ru

1 Introduction

North-Eastern Transbaikalia is a vast mid-mountain region located in the southern part of Siberia to the north and east of Lake Baikal (Fig. 1). This region is characterized by extremely low population density and is represents predominantly natural areas of Siberian taiga. The remoteness and low accessibility of the territory is the reason for the poor study of landslides in the region. At the same time, North-Eastern Transbaikalia is located at the junction of two large lithospheric structures (Baikal rift system and Siberian craton), and is characterized by high tectonic activity and seismicity (with magnitudes up to 7.6–8.0), contrasting relief. This creates favorable conditions for the development of large-scale landslides. The presented article summarizes the results of the study of rock avalanches in North-Eastern Transbaikalia.

2 Natural Conditions

2.1 Climatic Conditions

The climate of the North-Eastern Transbaikalia is sharply continental with cold long winters and moderately warm summers (Fig. 2).

The orientation of the mountain ranges of the region contributes to the penetration of cold arctic air masses from the north. The duration of the frost-free period of the year in the region is up to 140–150 days. The complex character of the relief leads to great differences in microclimate.

The average annual temperature in the region is negative and is −6°C—−7°C. In winter, temperatures can fall below up to −40°C. In summer temperatures can exceed +30°C. The peculiarities of climatic conditions in Transbaikalia are caused by the decreasing influence of north-western atmospheric transport and the role of East Asian monsoons. In the

B. Abolmasov et al. (eds.), *Progress in Landslide Research and Technology, Volume 4 Issue 1, 2025*, Progress in Landslide Research and Technology, https://doi.org/10.1007/978-3-031-89836-5_7

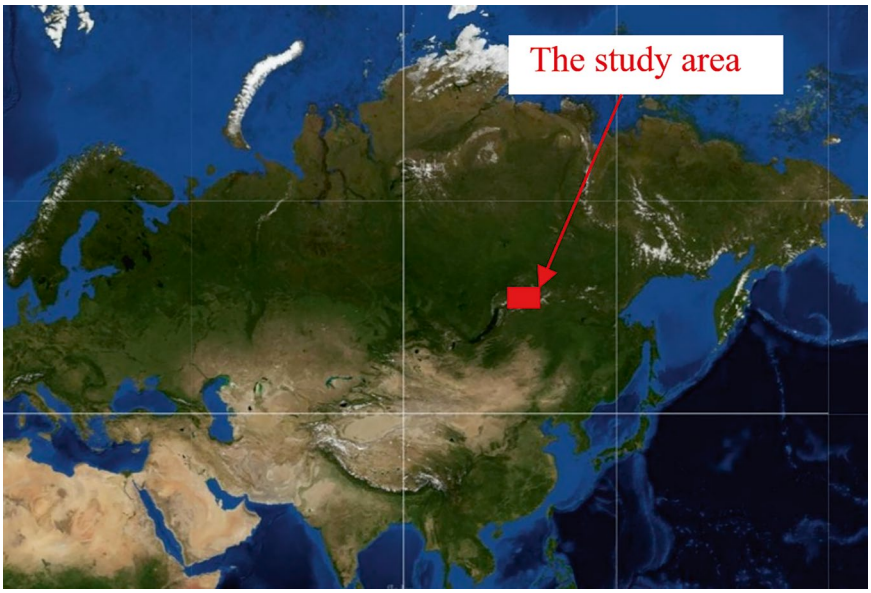

Fig. 1 Position of the study region

cold period, the Siberian anticyclone blocks their external influence (Ding 1990).

Negative annual temperatures predetermine permafrost development (Fig. 2).

Average annual precipitation in the area in question is 300–400 mm. However, in some years the precipitation may significantly exceed 600 mm. Intensive daily precipitation is typical for the region, reaching in some cases 80–90 mm/day.

2.2 Orographical Conditions

The orographic plan of the North-Eastern Transbaikalia is subject to a strict order. Mountain ranges (Southern Muysk Ridge, Northern Muysk Ridge, Kodar Ridge et other) and intermountain depressions (Muya-Kuanda Depression, Muyakan Depression, Chara Depression et other) are arranged in a regular pattern. They form a system of tectonically determined, subparallel morphostructures extending from southwest to northeast (Fig. 3). The orographic core of the region is a belt of intermountain troughs framed by mountain ranges with alpinotype relief and altitudes up to 3000 m. The bottoms of intermountain depressions are located at altitudes from 450–500 m a.s.l. (Muya-Kuanda Depression) to 650–750 m a.s.l. (Chara Depression).

The North-Eastern Transbaikalia is characterized by a well-defined altitudinal belt. The upper altitudinal level (>1800 m) is represented by the loaches (the zone of bald mountain—mountain tundra), where the main.

The numbers indicate: 1—Angarakan-Okuyakan landslide cluster, 2—Parama landslide cluster part of the territory is occupied by rocky placers ("rocky seas") and cliffs. These are highly deformed areas of the ancient (Cretaceous-Paleogene) leveling surface, strongly transformed by the processes of exaration, erosion, and denudation. The middle (mountain-taiga belt) altitude level is located at elevations from 1800 m to 1100–1000 m. These are areas partially affected by ancient glaciations, dissected by modern erosion and denudation. The lower altitudinal level (below 1100–1000 m) represents the bases of the slopes of intermountain depressions and their bottoms. Accumulation processes prevail in these areas, including as a result of repeated river backwatering in the middle and late Neopleistocene with the formation of very large paleolakes (Fig. 4).

The river system of the territory under consideration belongs to two basins—the Baikal basin (the Upper Angara River and its tributaries) and the Arctic basin. The Vitim River is one of the main tributaries of the Lena River, one of the largest rivers in Siberia, which flows into the Arctic Ocean. Unlike other major rivers in the region (Muya river, Muyakan river, Chara river, Kuanda river and others), which flow along the bottoms of intermountain depressions, the Vitim River flows from south to north, cutting through mountain ranges and crossing depressions.

2.3 Tectonic and Geological Background

North-Eastern Transbaikalia is located within the Baikal-Muisky belt, which is part of the Central Asian fold belt (Fedotova et al. 2014). The formation of the Baikal-Muisky belt structures took place in Mesoproterozoic time (PR_2^{2-3}). Subsequently, they were repeatedly (O-S-C_{2-3}) involved in tectonic activation zones. In the central part of the Baikal-Muisky belt, granite-gneisses of the Angara-Vitim areal-pluton are exposed. From the northeast, the granitoids are

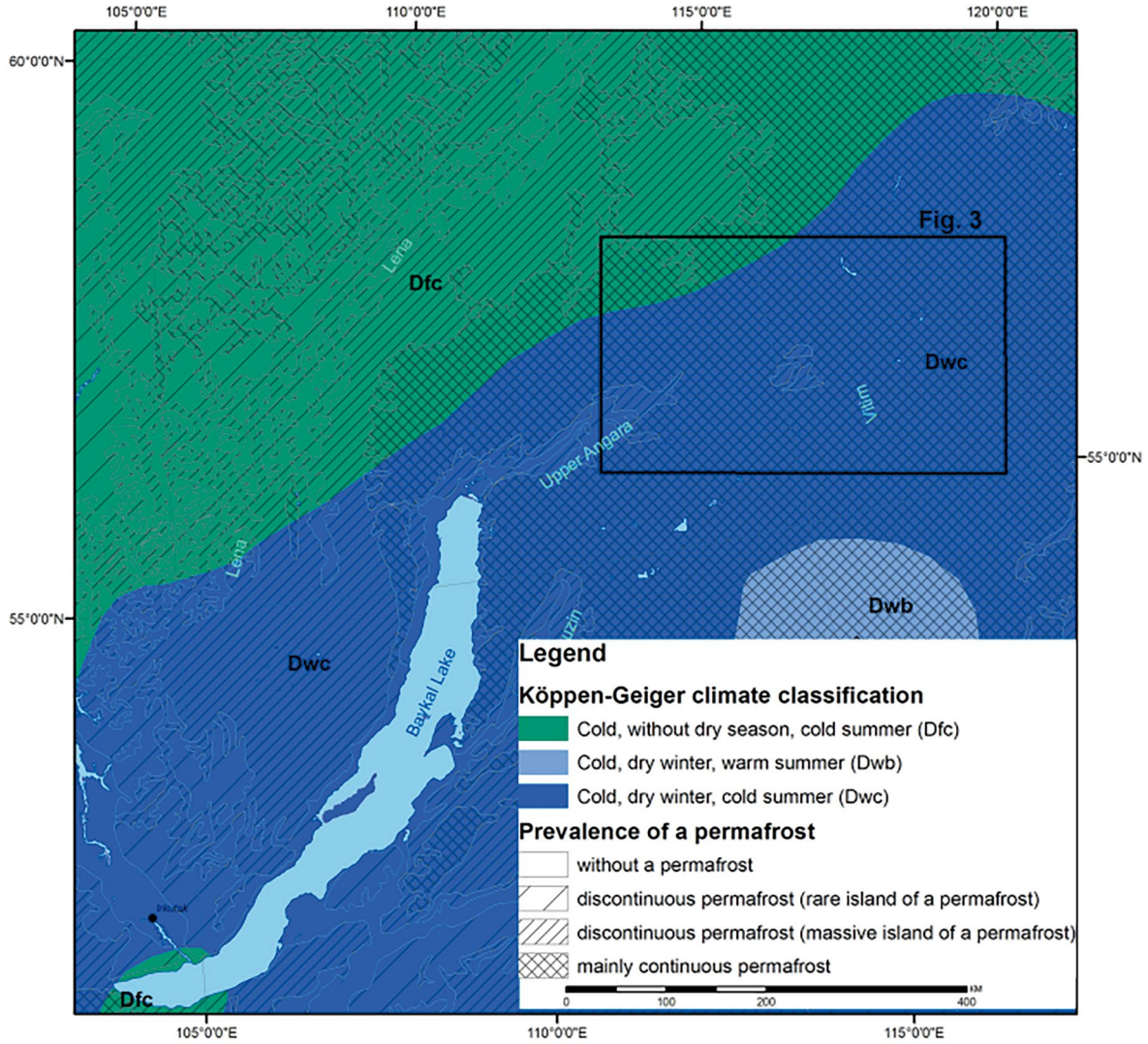

Fig. 2 Climate zoning of Transbaikalia (according to Köppen-Geiger climate classification) (after Peel et al. 2007)

flanked by Neoproterozoic-Cambrian carbonate-terrigenous and volcanogenic rocks.

In the Oligocene, the Baikal rift system was laid down. The area in question includes the north-eastern flank of the Baikal rift system. The main stage of rifting was confined to the Middle Pliocene. In the Quaternary, several phases of tectonic movement activation are also distinguished (Nyurgan (2.0 Ma), Littoral (1.0–0.8 Ma), Tyuy (0.15–0.12 Ma), and Post-Tyuy (60 thousand years)) (Mats and Yefimova 2011). The latter phases of tectonic movement activation correlate well with the deglaciation periods of the region.

During rifting, a chain of rift valleys and uplifts was formed. The blocks experiencing neotectonic uplift are expressed in the present-day relief as mountain ridges, and the blocks experiencing dip are expressed as intermountain troughs (Fig. 3). The tectonic boundaries of the blocks are strike-slip and upthrow-shift traced along the sides of the depressions and valleys. Sublatitudinally oriented faults are often characterized by left-lateral strike-slip displacements (Zelenin et al. 2022).

The total amplitude of neotectonic uplift during the Neopleistocene is estimated from 200 to 300 m (Budaev 2024). The maximum modern deformations rates detected by the persistent scatterers technique (using the multitemporal data of the Sentinel-1) is equal to 27 mm/year (for the Angarakan fault zone) (Chimitdorzhiev et al. 2021).

2.4 Seismicity

The consequence of active tectonic processes is high seismicity of the North-Eastern Transbaikalia territory. The strongest historical earthquake on the territory in question is

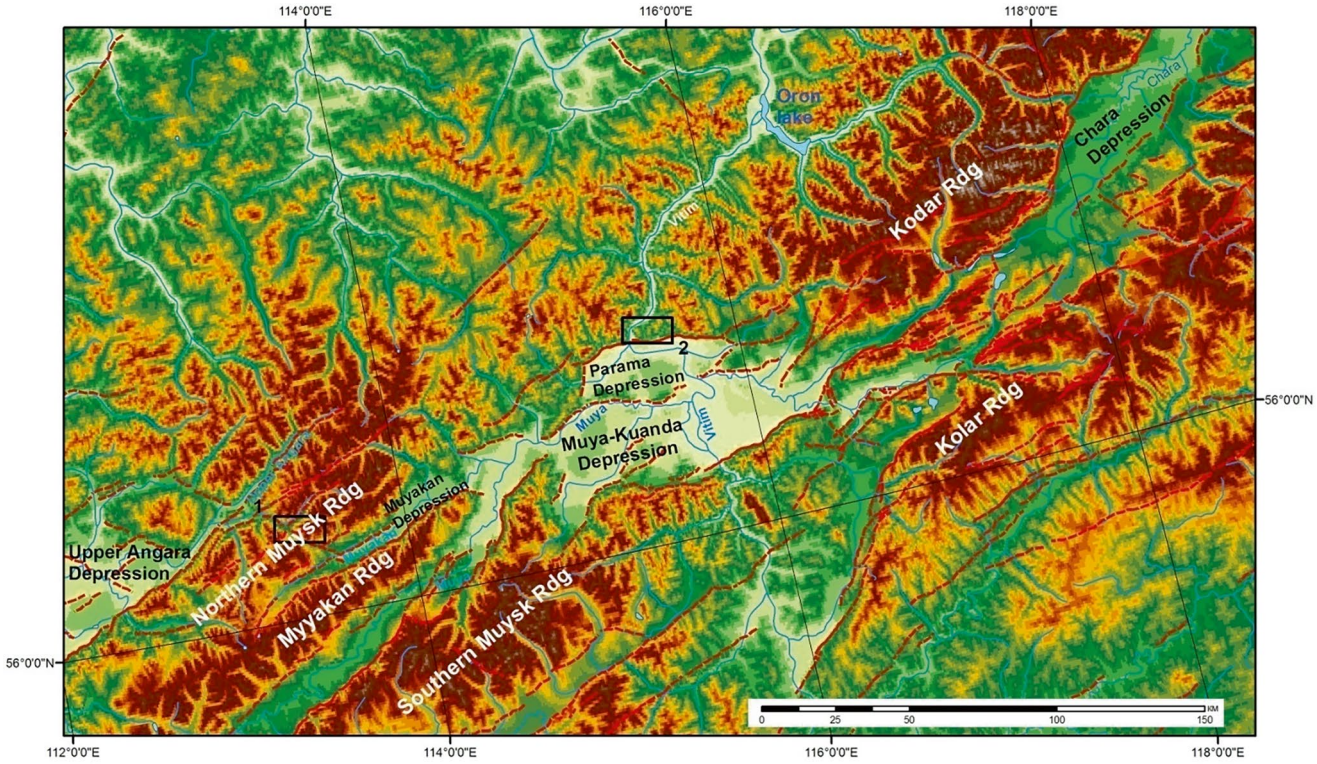

Fig. 3 Orographical conditions of North-Eastern Transbaikalia (DEM provided by the Shuttle Radar Topography Mission. The faults by E.A. Zelenin et al. (2022))

Fig. 4 View of the zone of bald mountains (mountain tundra), represented by rocky placers ("rocky seas") and cliffs

Great East earthquake (1725/02/01, M ≈ 8.2), intensity of which reached 11 MSK (Pisarenko et al. 2022).

The strongest earthquake in XX century (one of the strongest in USSR) in the region in question is Muya earthquake 1957/06/27 (Gileva et al. 2021). Its origin was located in the eastern part of Muya-Kuanda Depression. Magnitude of this earthquake was estimated at 7.6 ± 0.3 and intensity in the epicentral zone reached 10 MSK (Kondorskaya and Shebalin 1982).

Increased seismic activity in the region in question is noted mainly in the mountain spurs of the North-Muysk, Muyakan and Yuzhnomuysk ridges.

2.5 Geological History of Middle and Late Neopleistocene, Holocene. Glaciations and Paleolakes

One of the key stages in the geologic history of the region that influences the development of large-scale landslides is the time period starting from the second half of the Neopleistocene.

At the end of the Neogene—beginning of the Quaternary, the first epoch of cooling is noted in the South Siberian region. The maximum half-coated glaciation of the South Siberia mountains took place during the Tazov cooling (~180–125 thousand years ago), when the boundary of stable glacier existence descended to 900 ± 100 m (Levi et al. 2015). Traces of earlier glaciations were reworked by the Late Middle Pleistocene glacier and are not expressed in the modern relief. Degradation of the Tazovsky glacial cover during the Kazantsev thermochron (~125–110 thousand years ago) led to the formation of an extensive paleolake, the coastline of which is currently recorded at relative heights of 200–300 m above the bottoms of intermountain depressions.

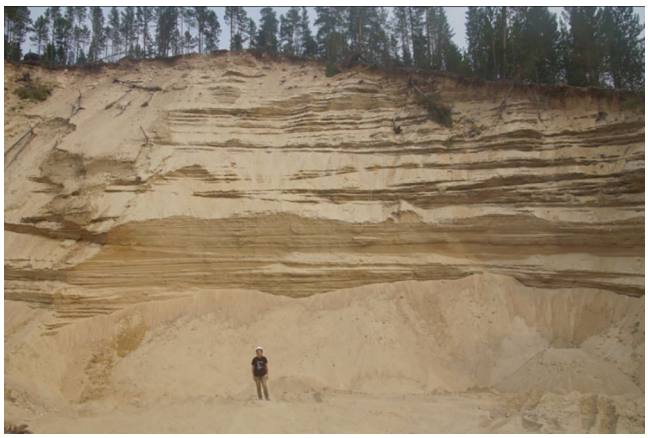

Fig. 5 Sandy lake sediments, left bank of the Muyakan River (Muyakan depression)

Thick sandy strata were accumulated within the paleolake (Fig. 5).

The Muruktin cooling that replaced the Kazantsev warming (~110–50 thousand years ago) was also accompanied by the formation of a half-coated glaciation, the area of which was much smaller than the Middle Pleistocene glacial cover. In the epoch of the subsequent Karginsky warming (~50–24 thousand years ago), the formation of an extensive paleolake (Muiskoye) is again noted (Levi et al. 2015) or Muisko-Vitimskoe (Margold and Jansson 2011; Margold et al. 2018) paleolake). The shoreline markings of the Late Neopleistocene paleolake are located ~100 m below the last Late Neopleistocene glaciations.

Traces of the last Late Neopleistocene Sartan glaciation (~24–10 thousand years) are most clearly expressed in the modern relief. They are spread over areas 2–3 times smaller than those of the preceding Murukta glacial cover.

One of the key issues in understanding the geologic history of the second half of the Neopleistocene are the ideas about the nature of dams of different-age Late Neopleistocene paleolakesas well as their breakthrough (cataclysmic outburst megafloods) with the formation of spillways. It is currently believed that the formation of all post-glacial lakes was due to the occurrence of ice dams (Levi et al. 2015; Margold and Jansson 2011; Margold et al. 2018). The possible formation of landslide dams as a result of large-scale rockslides and rock avalanches in the South Siberian region has not been considered.

3 Rockslides and Rock Avalanches

The study of the territory of the North-Eastern Transbaikalia has shown that several clusters of large-scale rockslides and rock avalanches (Angarakan-Okuyakan, Parama) are located in this region.

3.1 Rockslides and Rock Avalanches of Angarakan-Okuyakan Cluster

The Angarakan-Okuyakan landslide cluster includes eight large-scale rockslides and rock avalanches formed in the Itykit-Okusikan Pass area and near the Itykit River confluence with the Angarakan River. The Agarakhan-Okuyakan landslide cluster (Fig. 6) is located within the Severomuisky (North Muya) subregion of seismic activity formed as a result of segmentation of active faults in the Baikal Rift Zone (Pisarenko et al. 2022). The position of the Angarakan-Okuyakan cluster is confined to the zone of intersection of the Angarakan and Perevalny active faults.

The numbers indicate: 1—Angarakan-1 rock avalanche (RA); 1a—Angarakan-2 RA; 2—Itykit-1 RA; 3—Itykit-2 RA; 4—Perevalny complex slide (rock avalanche and rockslide (upper part)); 5—Okusikan-1 RA; 6—Okusikan-2 RA; 7—Angarakan-3 complex landslide.

The largest manifestation of landslide processes in the area in question is the "Perevalny" landslide (Fig. 6, number 4). The landslide has a complex (combined) mechanism of displacement. The upper part of the landslide massif is a detached granite block separated from the main ridge by an arc-shaped canyon-like graben (width up to 100–150 m, depth—up to 30–60 m). The landslide block is lowered by ~200 m relative to the undisturbed surface elevations of the North Muisky Ridge. The middle and lower part of the landslide massif is the frontally confined rock avalanche (by A.L. Strom (Strom et al. 2019)). The rock avalanche reached the opposite side (the lower part of the slope of the Muyakan ridge) and runup on it to a height of about 250 m. At present the landslide body formed by the displacement of the "Perevalny" landslide now forms the Itykit-Okusikan Pass in the relief.

The total runout of the landslide is about 3.2 km, 2.2 km of which is the length of the rock avalanche. The width of the landslide reaches about 1.3 km. The total height drop is estimated to be ~1.0 km. The coefficient of friction of the pathway H/L (by K. Hsü (Hsü 1978)) in this case is 0.31. The coefficient H/L for the rock avalanches is estimated to be 0.25 only.

The granites of the Angaro-Vitimsky areal-pluton, forming the southwestern slope of the North-Muisky ridge, were involved in landslide deformations. The total volume of rocks involved in the displacement is ~300 million m^3. During displacement granites were disintegrated to large angular blocks either without filler or with sandy multigrain filler (Figs. 7 and 8). The time of formation of the "Perevalny" landslide can be attributed to the beginning of late Neopleistocene (during the Kazantsev Warming).

On the opposite side of the valley (practically opposite "Perevalny" complex landslide) formed rock avalanche "Okusikan-1" (Fig. 6, number 5, Fig. 9). The total volume of

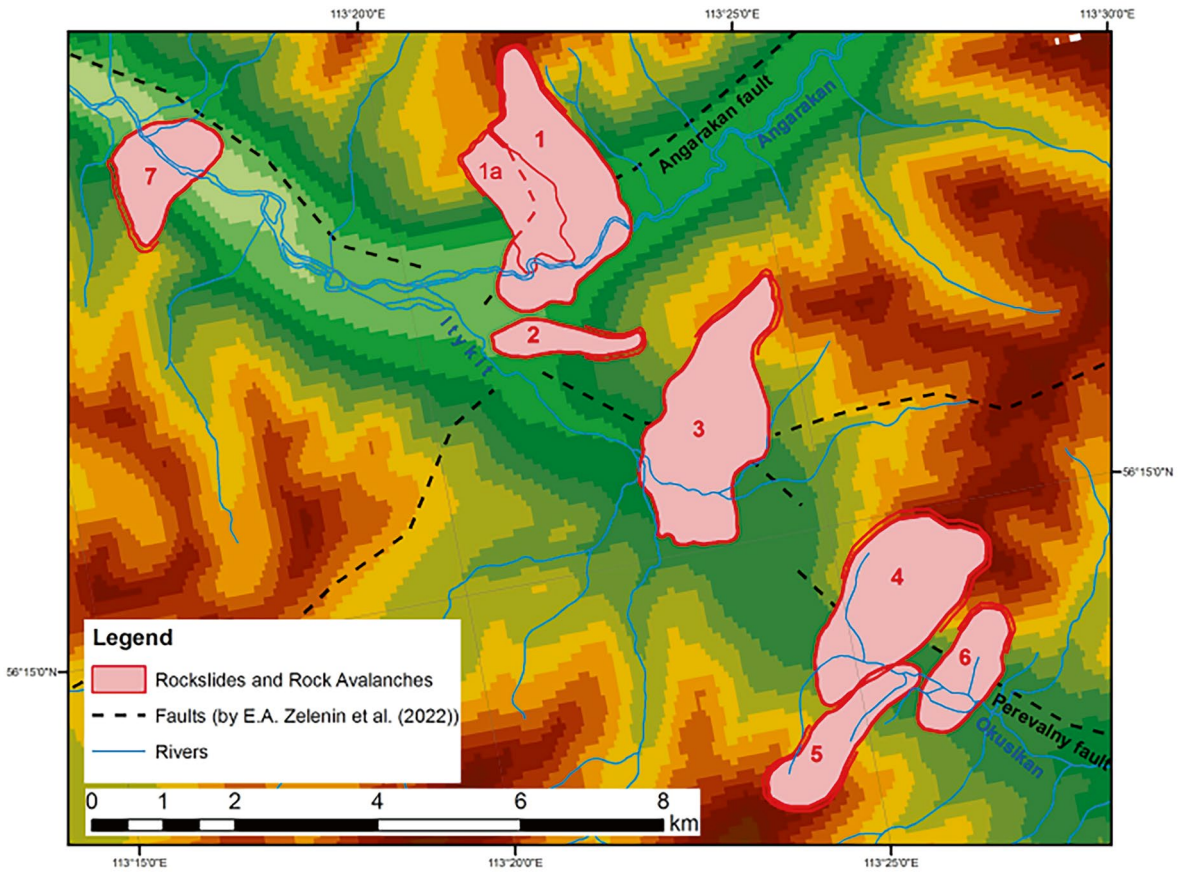

Fig. 6 Angarakan-Okuyakan landslide cluster (DEM provided by the Shuttle Radar Topography Mission)

Fig. 7 Field of chaotically located large boulders (up to 3.5–4 m in size) within the avalanche part of "Perevalny" complex landslide (mega-clast facie of rock avalanche deposit) and its width reaches about 1.4 km. The landslide deformations involved granites of the Angaro-Vitimsky areal-pluton forming the south-western slope of the North-Muisky Range. The total volume of soils involved in the displacement of the rock avalanche is about 60 million m^3. The coefficient H/L is 0.17. The time of formation of "Itykit-2" rock avalanche can be attributed to the Late Neopleistocene period.

Fig. 8 Granite blocks in dense sandy matrix (matrix-clast facie of rock avalanche deposit) within the avalanche part of "Perevalny" complex landslide

"Okusikan-2" rock avalanche is estimated at ~30 million m^3. Total runout is 2.7 km. The coefficient H/L is 0.30.

The "Okusikan-2" rock avalanche adjoins the "Perevalny" complex landslide from the southeast (Fig. 6, number 6). The total volume of "Okusikan-2" rock avalanche is estimated at 11 million m^3. Total runout is 1.9 km. The coefficient H/L is 0.29.

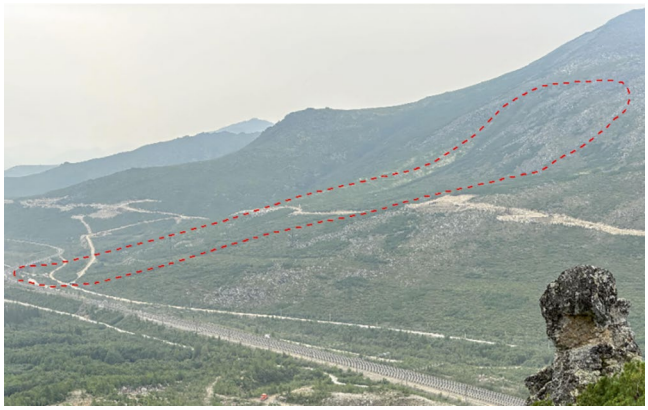

Fig. 9 General view of "Okusikan-1" rock avalanche

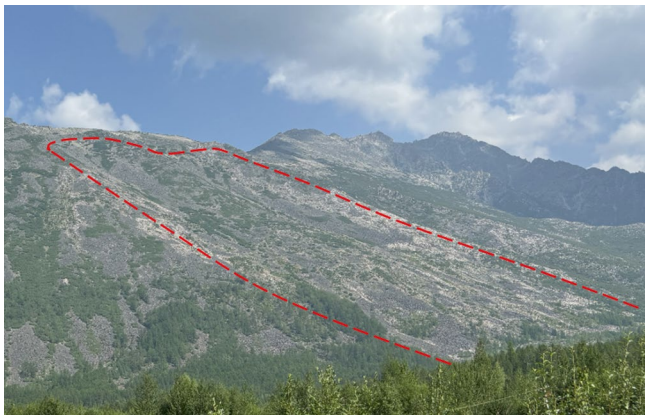

Fig. 10 General view of "Angarakan-2" rock avalanche

The "Okusikan-2" rock avalanche adjoins the "Perevalny" complex landslide from the southeast (Fig. 6, number 6). The total volume of "Okusikan-2" rock avalanche is estimated at 11 million m^3. Total runout distance is 1.9 km. The coefficient H/L is 0.29 of the Angaro-Vitimsky areal-pluton.

The formation of these rock avalanches probably occurred during the Karginsky thermochron. This is indicated by the presence of traces of glacial reworking of the upper parts of the escarpments, which apparently occurred as a result of the activity of small cirque glaciers during the last (Sartan) glaciation.

A smaller manifestation of slope processes in the area is "Itykit-2" rock avalanche located in the right side of the Itykit River valley, in the 1.4 km northwest of the "Perevalny" landslide (Fig. 6, number 3). The length of the massif along the direction of displacement is about 3.8 km,

The "Itykit-1"rock avalanche is located on the western slope of the North-Muisky Ridge (Fig. 6, number 2). The length of the massif along the direction of displacement is about 2.6 km, and its width reaches about 560 m. The slope deformations involved granites of the Angaro-Vitimsky areal-pluton. The total volume of rocks involved in the "Itykit-1" rock avalanche displacement is estimated to be about 16 million m^3. The coefficient H/L is 0.17.

The formation of the "Perevalny" complex landslide, "Itykit-1" and "Itykit-2"rock avalanches occurred in the sides of the through valley, which previously (until the Middle Neopleistocene) connected the Upper Angarakan and Muyakan—Muya-Kuanda depressions. The direction of this through valley coincides with the Pass Fault zone, which is active and seismogenic. Large-scale failures slopes, which are probably seismogenic, resulted in the formation of landslide dam, which now plays the role of Itykit-Okusikan pass cofferdam. The landslide dam probably did not collapse due to the fact that the paleo-lake breakthrough occurred in the northern direction, in the section of the modern Vitim River valley.

Another group of large-scale occurrences of landslide processes within the Angarakan-Okuyakan landslide cluster includes several rockslides and rock avalanches formed in the sides of the Angarakan River valley (Fig. 6, numbers 1, 1a, 7). The valley of the Angarakan River crosses the area of distribution of the granites of the Angaro-Vitimsky areal-pluton, which are involved in landslide deformations.

Among these failures slopes the largest is the "Angarakan-1"rock avalanche (Fig. 6, numbers 1). The "Angarakan-1"rock avalanche is located on the right side of the Angarakan river valley. At this site, the valley gravitates to the zone of the Angarakan active fault. The total runout distance of the "Angarakan-1"rock avalanche in the direction of displacement is about 4.0 km. The total drop height is estimated at ~1.1 km. The coefficient H/L is 0.28. The total volume of rocks involved in the displacement is more than 210 million m^3.

The "Angarakan-2" rock avalanche (Fig. 6, numbers 1a, Fig. 10) is located close to rock avalanche "Angarakan-1". The length of the massif along the direction of displacement is about 2.1 km, and its width reaches about 700 m. The total volume of rocks involved in the rock avalanche displacement is estimated to be about 11.0 million m^3. The coefficient H/L is 0.31. Currently, the tongue of the rock avalanche "Angarakan-2" is eroded by the Angarakan River. At the erosion site, the river has developed a narrow canyon-like channel up to 50 m wide with steep sides 25–30 m high.

The "Angarakan-3" complex landslide (Fig. 6, number 7) was formed in the left side of the Angarakan River valley, below the mouth of the Itykit River. In this section, the valley gravitates to the north-western continuation of the Perevalny active fault. The landslide "Angarakan-3" has a complex (combined) mechanism of displacement. The upper part of landslide massif is a block of granites. The lower part of landslide massif is the laterally confined rock avalanche (by A.L. Strom (Strom et al. 2019)).

Total volume of "Angarakan-3" complex landslide is estimated at ~30 million m^3. Total runout distance is 2.1 km. The coefficient H/L is 0.29.

3.2 Rockslides and Rock Avalanches of Parama Cluster

The Parama landslide cluster is located north of the Parama depression in the Vitim River valley, on the section from the mouth of the Parama River to the Parama rapids. In this area, the Vitim River channel narrows from 2 km to 100–200 m and the river flows for ~5 km in the narrow Parama gorge, the sides of which rise above the river by 700–800 m. The Parama landslide cluster is located to the north of the Parama depression. The Parama Gorge appears to be a through valley that submeridional cuts through the northern mountainous frame of the Parama depression. It should be noted that an active (displacements up to 2 mm/year) seismically generating (with M 6.8–7.4) Paramskiy fault (left strike-slip fault) is traced along the northern boundary of the Parama depression (Zelenin et al. 2022).

A.M. Lekhatinov suggested the presence of a pre-glacial cyclopean "tectonic landslide-cline" displaced in the Parama depression, the dam of which formed the Muiskoye paleo-lake (Lekhatinov et al. 1988). A.M. Lekhatinov suggested that the formation of a "tectonic" paleo-landslide resulted in the displacement of the Vitim River channel by 15–20 km. However, later studies did not confirm the existence of a cyclopean "tectonic landslide-cline" within the Parama depression.

At the same time, the study of the orographic and geological conditions of the northern mountainous frame of the Parama depression allows us to identify three narrow (about 1 km wide) linear submeridional paleo-valleys (in addition to the modern Parama gorge) at a distance of 15 km from the Vitim River bed. The bottom elevations of these valleys consistently decrease from east to west—from 950–955 m a.s.l. (eastern), 920 m a.s.l. (central), 700 m a.s.l. (western) and up to 450 m a.s.l. (Parama Gorge). A landslide dam is observed in each of the paleo-valleys (Fig. 11).

The numbers indicate: 1—Parama rock avalanche (RA); 2- Ugrum-1 rockslide (RS); 3—Ugrum-2 complex landslide (CS); 3a—Ugrum-2a CS; 3b—Ugrum-2b RA; 4- Ugrum-3 RA.

In the Parama Gorge there was a partial overlap of the Vitim River channel as a result of the formation of the Parama rock avalanche. The rock avalanche displacement occurred from the left side of the river valley. Total runout distance is 3.5 km. The total volume of the Parama rock avalanche is estimated at ~90 million m^3. The coefficient H/L is 0.26. Currently, deposits of the distal part of the rock ava-

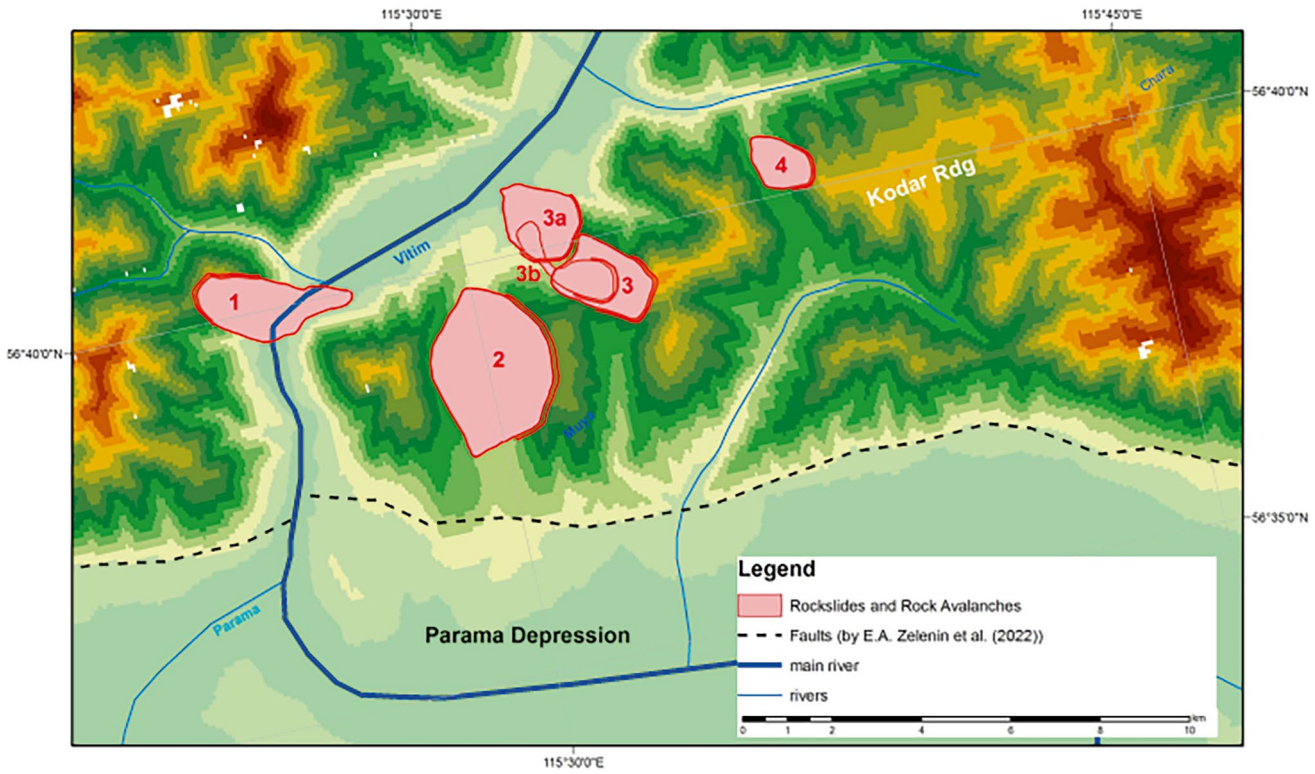

Fig. 11 Parama landslide cluster (DEM provided by the Shuttle Radar Topography Mission)

lanche are the cause of Parama rapids in the Vitim River channel.

The "Western" through meridional paleo-valley is located 3–3.5 km to the east of the modern channel of the Vitim River. The relative elevation of the bottom of this valley above the modern riverbed is up to 250 m. A landslide dam is located in the northern part of the Western paleo-valley. The dam was formed as a result of displacement of the giant rockslide "Ugrum-1", the total volume of which exceeds 1.5 km^3. The body of rockslide "Ugrum-1" is formed by a series of landslide blocks displaced from the right side of the Western paleo-valley. The length of the landslide body reaches 1.6 km, and the coefficient H/L is 0.57.

The displacement of rockslide "Ugrum-1", apparently, based on the paleo-valley bottom marks, refers to the middle of the Kargin thermochron (~50–24 thousand years ago). The resulting landslide dike was probably the cause of the extensive Muiskoye paleolake.

The "Central" through meridional paleo-valley is located 2–2.5 km east of the "Western" paleo-valley, 6–6.5 km from the modern bed of the Vitim River. The relative excess of the bottom of the "Central" valley over the modern bed of the Vitim River reaches 450–470 m, and the excess over the bottom of the "Western" paleo-valley is up to 200–220 m. In the northern part of the "Central" paleo-valley there is also a landslide dam, the formation of which occurred as a result of displacement of the "Ugrum-2" landslide. The length of the landslide formed in the right side of the valley is 1.5 km, and the total volume reaches 250 million m^3. The coefficient H/L is 0.33.

Subsequently, two more landslides were formed in the area of "Ugrum-2" landslide—"Ugrum-2a" complex landslide and "Ugrum-2b" rock avalanche with volumes of 50 million m^3 and ten million m^3, respectively.

The easternmost through meridional paleo-valley is located 11–12 km from the modern channel of the Vitim River. The marks of its bottom exceed the marks of the modern channel by more than 500 m. In the northern part of this paleo-valley there is also a landslide dame, which was formed as a result of displacement of the Ugrum-3 rock avalanche. Total runout distance is 1.6 km. The total volume of the "Ugrum-3" rock avalanche is estimated at 115 million m^3. The coefficient H/L is 0.34. The displacement of "Ugrum-3", apparently, based on the marks of the bottom of the paleo-valley, refers to the Kazantsev thermochron epoch (~125–110 thousand years). The relative antiquity of the rock avalanche is also indicated by the significant reworking of landslide morphostructures by later glacial processes.

Concluding the consideration of rockslides and rock avalanches of Parama landslide cluster it should be noted that all large-scale landslides described in this area are located in the vicinity of the active seismically generating Parama fault zone. The distance from the fault zone to the landslides is 3–6 km. This suggests that rockslides and rock avalanches of the Parama landslide cluster are seismogenic.

4 Regularities of Rockslides and Rock Avalanches of North-Eastern Transbaikalia

The investigation of rockslides and rock avalanches distributed in North-Eastern Transbaikalia has allowed to reveal common features and differences of large-scale landslides in the region (Table 1).

The common feature of practically all (except Parama rock avalanche) described large-scale landslides is their formation in Proterozoic granites having close strength characteristics in different areas. In this connection, it can be assumed that the existing differences in the parameters of landslides are due to a variety of conditions of their formation.

Consideration of the parameters of large-scale rock avalanches and complex landslides (distally transforming into rock avalanche), widespread in North-Eastern Transbaikalia, has shown that coefficient H/L from 0.28 to 0.34 (angle−16°−20°) is typical for them. Higher coefficient H/L (0.31–0.34) is typical for complex landslides transforming in the distal part into rock avalanche. Only for two rock avalanches (Itykit-1 and Itykit-2) the coefficient H/L was 0.16–0.17 (angle−9°−10°). The analysis showed that these rock avalanches (Itykit-1 and Itykit-2) belong to the laterally confined rock avalanche (by A.L. Strom), while all others are the frontally confined rock avalanche (by A.L. Strom) (Strom et al. 2019).

It should be noted that for rockslide "Ugrum-1" coefficient H/L is 0.57 (angle−~35°). Such a difference, apparently, is caused by significant differences in the mechanism of slopes failures.

Another important result is the fact of predominance of the frontally confined rock avalanches among the described rock avalanches distributed in North-Eastern Transbaikalia. The predominance of this type of rock avalanches in North-Eastern Transbaikalia is due to their formation in relatively narrow and deep valleys, which are widely represented in the Baikal rift zone.

For all the described large-scale rock avalanches and rockslides distributed in North-Eastern Transbaikalia, their proximity (not further than several kilometers) to the zones of active, seismogenic (up to M 7.9) faults is noted. This allows us to conclude that all described large-scale rock avalanches and rockslides are seismogenic.

The formation of large-scale rock avalanches and rockslides in North-Eastern Transbaikalia in relatively narrow and deep valleys resulted in the formation of landslide dams. These landslide dams in many cases overlapped through val-

Table 1 Overview and characteristics of large scale rockslides and rock avalanches

Name	Area (km^2)	Runout (km)	ΔH, total drop height [km](H_{max}- H_{min})	H/L	Volume (mln m^3)
Angarakan-Okuyakan landslide cluster					
Angarakan-1 rock avalanche (RA)	3.9	4.0	1.10	0.28	210
Angarakan-2 (RA)	1.4	2.1	0.65	0.34	11
Angarakan-3 (complex landslide)	1.5	2.1	0.76	0.29	30
Perevalny (complex landslide)	4.4	3.2	1.00	0.31	300
Part of the rock avalanche		2.2	0.55	0.25	
Itykit-1 (RA)	0.7	2.6	0.41	0.16	16
Itykit-2 (RA)	4.2	3.8	0.63	0.17	60
Okusikan-1 (RA)	1.5	2.7	0.80	0.30	30
Okusikan-2 (RA)	1.3	1.9	0.55	0.29	11
Parama landslide cluster					
Parama (RA)	3.3	3.5	0.91	0.26	90
Ugrum-1 (rockslide)	7.2	1.6	0.91	0.57	>1500
Ugrum-2 (complex landslide)	2.6	1.5	0.50	0.33	250
Ugrum-2a(complex landslide)	2.3	1.5	0.50	0.33	50
Ugrum-2b (RA)	1.3	2.6	0.79	0.30	10
Ugrum-3 (RA)	1.2	1.6	0.55	0.34	115

leys of river runoff, which caused formation of extensive Late Neopleistocene paleo-lakes in the hollows of intermountain depressions.

5 Conclusion

North-Eastern Transbaikalia is located at the junction of two large lithospheric structures (the Baikal rift system and the Siberian craton) and represents a region with contrasting mid-mountain relief. The orographic plan of this region is formed by the alternation of alpine-type mountain ranges and intermountain troughs connected by narrow through valleys. North-Eastern Transbaikalia is characterized by high tectonic activity with wide development of faults and seismicity (with magnitudes up to 8.0). This creates favorable conditions for the development of large-scale landslides. In the Quaternary period, the North-Eastern Transbaikalia was repeatedly covered by glaciations during the cooling epochs. During the warming epochs, extensive paleo-lakes also repeatedly appeared in the intermountain depressions.

The Angarakan-Okuyakan and Parama landslide clusters were described in the North-Eastern Transbaikalia, which are characterized by the development of large-scale rockslides and rock avalanches. Within the Angarakan-Okuyakan landslide cluster 8 large-scale rockslides and rock avalanches were identified, the largest of which are Perevalny complex landslide (300 mln m^3) and Angarakan-1 rock avalanche (210 mln m^3). The displacement of the Perevalny complex landslide is the result of the dam formation, which is currently a pass between the Upper Angara and Muya-Kuanda depressions.

Six large-scale rockslides and rock avalanches have been identified within the Parama landslide cluster, the largest of which is the Ugrum-1 rockslide (> 1.5 km^3). Three large scale failures slopes formed landslide dams that blocked the Vitim River flow along three multi-temporal paleo-valleys located at different altitudes.

Most of the large-scale rock avalanches distributed in North-Eastern Transbaikalia occurred in Proterozoic granites. This determines close values of the coefficient H/L parameters for them. At the same time, most of the described rock avalanches belong to the frontally confined rock avalanches.

Large-scale rockslides and rock avalanches formed several landslide dams that blocked the river flow. All the described large-scale rock avalanches and rockslides distributed in North-Eastern Transbaikalia are characterized by proximity (not more than a few kilometers) to active, seismic-generating fault zones. Thus, it can be reasonably assumed that all described large-scale rock avalanches and rockslides are seismogenic.

References

Budaev RT (2024) Middle Pleistocene Neotectonic activation of the mountain bordering the Muya-Kuanda Rift Valley (Baikal rift zone). Geodynamics Tectonophysics. 15(4):article 0773. https://doi.org/10.5800/GT-2024-15-4-0773

Chimitdorzhiev TN, Dmitriev AV, Dagurov PN (2021) Deformations of the Baikal-Amur Railway section at the Severomuisk tunnel: Results of persistent scatterer interferometry usingSentinel-1 data. Sovremennye problem distantsionnogo zondirovaniya Zemli iz kosmosa 18(3):320–324. (in Russian with English abstract). https://doi.org/10.21046/2070-7401-2021-18-3-320-324

Ding YH (1990) Buildup, air-mass transformation and propagation of Siberian high and its relations to cold surge in East Asia. Meteorol Atmospheric Phys 44(1–4):281–292

Fedotova AA, Razumovsky AA, Khain EV, Anosova MO, Orlova AV (2014) Late Neoproterozoic igneous complexes of the Western Baikal-Muya Belt: formation stages. Geotectonics 48(4):292–314. https://doi.org/10.1134/S0016852114040049

Gileva NA, Melnikova VI, Filippova AI, Radziminovich YB, Kobeleva EA (2021) Muyakan earthquake sequence in 2015 (Northern Baikal Region). Zemletriaseniya Severnoi Evrazii [Earthquakes in Northern Eurasia] 24(2015):245–257. (in Russian with English abstract). https://doi.org/10.35540/1818-6254.2021.24.24

Hsü K (1978) Albert Heim: observations on landslides and relevance to modern interpretations. Rockslides and avalanches. In: Voight B (ed) V. 1 natural phenomena. Elsevier, Amsterdam, pp 71–93

Kondorskaya NV, Shebalin NV (1982) New catalog of strong earthquakes in the U.S.S.R. In: From ancient times through 1977. NOAA, Boulder

Lekhatinov AM, Gravis GF, Poznanin VL, Trushina NA, Chustotiniv KV (1988) Exogenie geologicheskie protsessy [Exogenic geological processes]. Geology of the BAM zone. In: Kozlovsky EA, Sheko AI et al (eds) V. 2. Hydrogeology and engineering geology. Nedra Publ, Leningrad, pp 247–297. (in Russian)

Levi KG, Miroshnichenko AI, Kozyreva EA, Kadetova AV (2015) Models of the evolution of Lake basins in eastern Siberia in the late Pleistocene and Holocene. Bulletin of the Irkutsk state university. Geoarchaeology, Ethnology, and Anthropology Series 11:55–85. (in Russian with English abstract)

Margold M, Jansson KN (2011) Glacial geomorphology and glacial lakes of central Transbaikalia, Siberia. Russia J Maps 7(1):18–30. https://doi.org/10.4113/jom.2011.1132

Margold M, Jansen JD, Codilean AT, Preusser F, Gurinov AL, Fujioka T, Fink D (2018) Repeated megafloods from glacial Lake Vitim, Siberia, to the Arctic Ocean over the past 60,000 years. Quat Sci Rev 187:41–61. https://doi.org/10.1016/j.quascirev.2018.03.005

Mats VD, Yefimova IM (2011) Paleogeographic scenario of the late cretaceous—Cenozoic for the central part of the Baikal region. Geodynamics & Tectonophysics 2(2):175–193. (in Russian with English abstract). https://doi.org/10.5800/GT-2011-2-2-0040

Peel MC, Finlayson BL, McMahon TA (2007) Updated world map of the Köppen-Geiger climate classification. Hydrol Earth Syst Sci 11:1633–1644. https://doi.org/10.5194/hess-11-1633-2007

Pisarenko VF, Ruzhich VV, Skorkina AA, Levina EA (2022) The structure of the seismicity field in the Baikal rift zone. Izvestiya Physics of the Solid Earth 58(3):329–345. https://doi.org/10.1134/S1069351322030053

Strom A, Li L, Lan H (2019) Rock avalanche mobility: optimal characterization and the effects of confinement. Landslides 16(8):1437–1452. https://doi.org/10.1007/s10346-019-01181-z

Zelenin EA, Bachmanov DM, Garipova ST, Trifonov VG, Kozhurin AI (2022) The active faults of Eurasia database (AFEAD): the ontology and design behind the continental-scale dataset. Earth System Science Data 14:4489–4503. https://doi.org/10.5194/essd-14-4489-2022

Optical Flow: A Multifaceted Approach for Analyzing and Observing Mass Movements Through Optical and Radar Images

Mahmud Muhammad and Maqsad Suriev

Abstract

Landslides are triggered by various factors, including seismic activity, climate-related events, and gravitational forces. These events pose significant risks to life, property, and the environment, necessitating effective monitoring and quantification for mitigation and prevention. Traditional monitoring methods like in-situ sensors face limitations in cost, scalability, and real-time data processing.

In the realm of landslide and hazard mitigation, time is of the essence because the quicker data is processed, the sooner policymakers and emergency responders can act to protect lives and safeguard economic infrastructure. The urgency and the critical role of rapid, real-time data processing have inspired us to expand and further develop a novel open-source package called AkhDefo (Akh: Land in Kurdish language and Defo: Deformation in English Language) (https://pypi.org/project/akhdefo-functions/).

This study introduces new features to AkhDefo, transforming it from an open-source code into a standalone geospatial python library. These enhancements include optical flow algorithms for measuring displacement using satellite radar backscatter, optical images, and real-time live stream camera data from ground-based sources. The satellite radar and optical images were processed to derive volume estimates and study kinematic behavior in the May 2017 Mud Creek landslide in California, USA, and the Morenny rock-glacier in the Tien Shan Mountains, Kazakhstan between 2017 to 2023.

In addition, live-stream webcam data were used to investigate a rockfall event on the September 20, 2021, at Stawamus Chief in Squamish, British Columbia, Canada, and from this, developed a state-of-the-art rock-fall detection system.

Keywords

Landslides · AkhDefo · Rockfall · Rock glacier · Optical flow

1 Introduction

Landslides can occur due to multiple triggers, including seismic activity(Jibson 2013; Moro et al. 2017; Suriñach et al. 2005; Zimmer and Sitar 2015), climate-related processes (e.g., heavy rainfall, thawing permafrost) (Guthrie et al. 2012; Roberti et al. 2018; Warrick et al. 2019), and gravitational forces. Landslides can pose significant threats to life, property, and the environment and thus monitoring and quantifying the scale of the potential landslide beforehand is important to mitigate and/or prevent the landslide-related impacts.

Traditional monitoring methods such as in-situ sensors, while effective, often have limitations in terms of cost, scalability, and real-time data processing (Cosentino et al. 2024; Ferretti et al. 2007, 2011; Raspini et al. 2018). With advances in technology, satellite remote sensing (radar and optical) datasets have emerged as an important tool in landslide monitoring, offering new possibilities for early detection, risk assessment, and mitigation strategies (Bürgmann et al. 2006;

Supplementary Information The online version contains supplementary material available at https://doi.org/10.1007/978-3-031-89836-5_8.

M. Muhammad (✉)
Department of Physical Sciences (Geology), Thompson Rivers University, Kamloops, BC, Canada

Centre for Natural Hazards Research, Department of Earth Sciences, Simon Fraser University, Burnaby, BC, Canada
e-mail: mmuhammad@tru.ca

M. Suriev
Department of Physical Sciences (Geology), Thompson Rivers University, Kamloops, BC, Canada
e-mail: maqsad_suriev@sfu.ca

B. Abolmasov et al. (eds.), *Progress in Landslide Research and Technology, Volume 4 Issue 1, 2025*, Progress in Landslide Research and Technology, https://doi.org/10.1007/978-3-031-89836-5_8

Wei et al. 2010). Such tools are crucial for establishing a reliable and effective monitoring system that can support timely decision-making and improve overall disaster preparedness and response.

Radar images include two components—phase and amplitude. The phase represents the position of the radar wave in its cycle at a given time, while amplitude indicates the intensity or strength of the radar backscatter from the ground surface (Ferretti 2014; Ferretti et al. 2007; TRE ALTAMIRA 2018). Radar imagery is typically processed via various Interferometric Synthetic Aperture (InSAR) techniques which rely on the phase differences between successive radar pulses between multiple radar images and include Differential Interferometric Synthetic Aperture Radar (DInSAR) that processes pairs of radar images. Additionally, processing stacks of radar images using Permanent Scatterer (PS) and the Small Baseline Subset (SBAS) approaches enhances the capability of detecting sub-millimeter ground movement (Barnhart 2017; Ferretti 2014; Ferretti et al. 2015; Fobert et al. 2021; Ma et al. 2021; Moro et al. 2017; Sun et al. 2015; Wei et al. 2010; Zhang et al. 2020). The radar amplitude can be processed as complementary to the phase component which adds robustness to the analysis, especially in areas where the phase signal is compromised or in the presence of large displacements. The processing of the amplitude component of the radar images involves various techniques such as Speckle tracking (Liu et al. 2008; Scheiber et al. 2014) and digital image correlation (DIC) techniques (Louis et al. 2007; McCormick and Lord 2010; Pan and Li 2011). This often requires significant computing power and thus limits the real-time processing applications particularly when applied to large areas of interest.

Despite its strengths, InSAR is not without limitations as it is sensitive to movements only in the line of sight of the radar sensor, which can lead to underestimation of actual ground movement. In areas with heavy vegetation or rapid change, the radar signal may lose coherence over time, making it difficult to track long-term movements. Variations in atmospheric conditions can also introduce errors in the radar signal, affecting the accuracy of displacement measurements. Additionally, radar images use active remote sensing technology (Chen 1996) which requires a significant amount of energy to emit signals, which can be a limitation on the satellite's resources. This usually results in higher cost and lower spatial and temporal resolution. Alternatively, optical imagery uses passive remote sensing technology (Asner 1998) which involves detecting natural energy from sunlight that is emitted or reflected by the Earth's surface. Consequently, optical imagery has potentially superior spatial and temporal resolution and has been employed to complement some of the limitations of radar imagery (Amaki et al. 2019; Hermle et al. 2022; Kim and Gratchev 2021; Muhammad et al. 2022; Srokosz et al. 2021).

Several methods and techniques, including digital image correlation (DIC) and optical flow (Amaki et al. 2019; Hermle et al. 2022; Muhammad et al. 2022) have been applied to process and measure displacement from optical imagery. Currently, DIC stands out as the primary technique for assessing displacement via optical imagery. While DIC and related speckle tracking techniques are acknowledged for their proficiency in determining ground displacement from radar backscatter and optical images, their application in real-time is limited due to the considerable processing involved. Additionally, these techniques depend on a trial-and-error approach to select a suitable matching correlation window (Fig. 1a–d) influencing the precision of the measurements (McCormick and Lord 2010; Pan and Li 2011). If the window is too small, large displacements (Fig. 1a) may not be fully captured leading to inaccurate or incomplete measurements. The displacement could also move objects outside of the small window, causing the algorithm to lose track of the movement. With a large window, small displacements (Fig. 1d) may be diluted or lost amidst the larger area of analysis. Commonly employed methods for monitoring rockfalls encompass light detection and ranging (LiDAR), doppler laser scanning, and video image analysis (Casagli et al. 2023; Yan et al. 2019).

In terms of real-time monitoring doppler laser scanning is a reliable existing rockfall monitoring technique which depends on the use of costly and advanced radar systems based on the Doppler effect for real-time detection and alerting (Casagli et al. 2023). These radar systems emit microwave signals that are reflected and analyzed to identify fast-moving objects on slopes. If an object moves quickly enough, it alters the signal's frequency, triggering an alert through the observed Doppler effect (Casagli et al. 2023).

The optical flow algorithm is used extensively in a range of applied scientific disciplines, such as fluid mechanics, solar physics, navigation for autonomous vehicles, biomedical imaging, traffic management, virtual reality, face tracking and action recognition. However, its use in the fields of landslide study and Earth sciences has been relatively limited (Kim and Gratchev 2021; Muhammad et al. 2022; Srokosz et al. 2021) when compared to techniques like DIC. In this study, we expand upon the open-source optical flow Python code developed by (Muhammad et al. (2022) and show its proficiency in measuring and quantifying displacement from both satellite radar backscatter images and optical imagery (satellite and ground-based cameras). Furthermore, we demonstrate its effectiveness in measuring land deformation and analyzing landslide hazards by applying the new AkhDefo 2.0 Python package (Akh: Land in Kurdish language and Defo: Deformation in English Language) (developed here) to three extensively researched case studies: (1) the May 2017 Mud Creek landslide in California USA; (2) the September 2021 Stawamus Chief

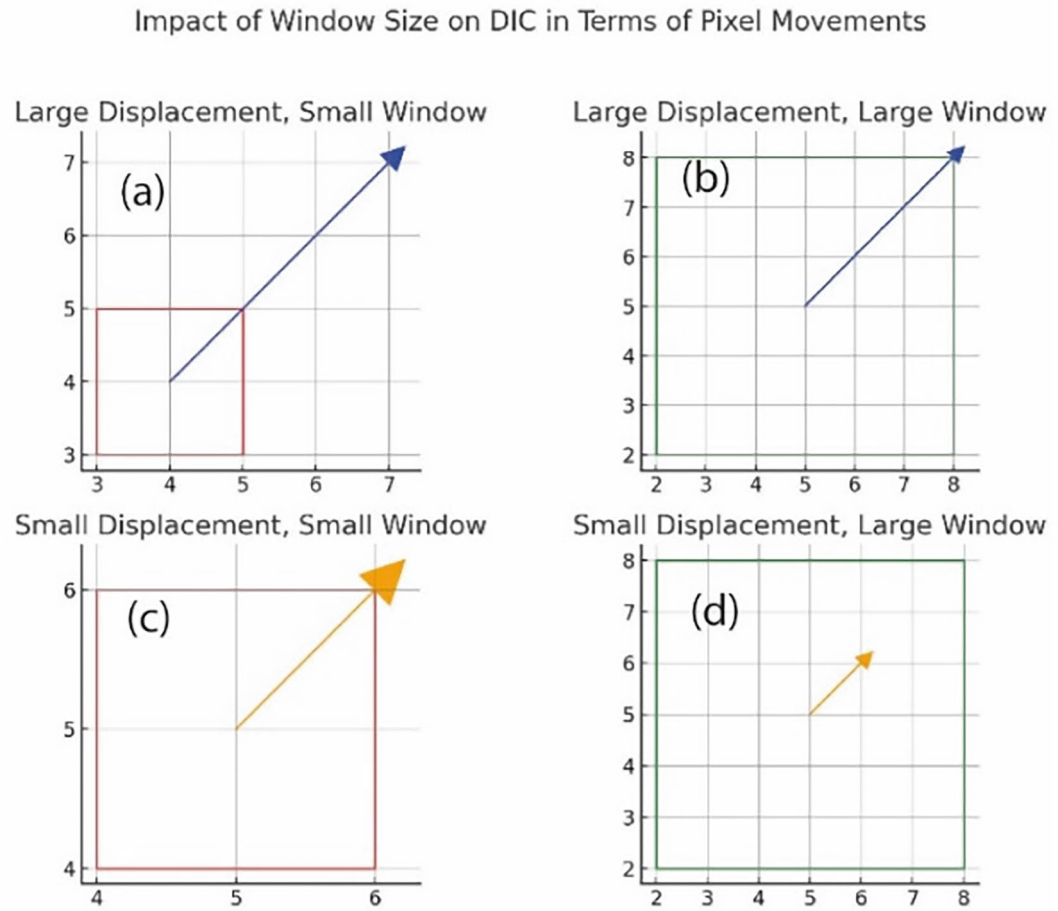

Fig. 1 Red square depicts matching window, and the arrow depicts movement. (**a**) Top Left—Large Displacement, Small Window. (**b**) Top Right—Large Displacement, Large Window. (**c**) Bottom Left—Small Displacement, Small Window. (**d**) Bottom Right—Small Displacement, Large Window

rockfall in BC, Canada, and (3) the Morenny rock-glacier in Tien Shan mountains of Kazakhstan.

1.1 AkhDefo- Package

The initial version of AkhDefo, developed by Muhammad et al. (2022), consisted of two Jupyter notebooks with approximately 1000 lines of Python code. This program was designed to measure displacement using optical satellite imagery and static hourly ground-based optical imagery. In contrast, the current study builds on that previous work by transforming it into a standalone Python library. This new version is capable of processing live video from webcams, satellite and ground-based optical imagery, in addition to satellite radar backscatter imagery.

The AkhDefo package, available on PyPI (https://pypi.org/project/akhdefo-functions/), is a collection of independent Python scripts that facilitate batch processing and manipulation of geospatial datasets, including both raster and vector data. It is especially useful for applications in geology, geotechnical engineering, and natural hazard studies, enabling the production and visualization of geospatial data. The package can download Sentinel-1 radar imagery via an Earthdata API account (https://search.asf.alaska.edu/) and daily PlanetScope imagery using a Planet Labs account (https://account.planet.com).

Alternatively, it can access and process data from static ground-based camera snapshots or live ground-based camera feeds. Additionally, AkhDefo can process both radar and optical imagery to generate temporal and time-series deformation maps.

2 Methodology

Optical flow refers to the perceived movement patterns of objects within a visual scene which occur due to the movement of either the object itself, the camera, or both. When a camera captures a scene over a period of time, the sequence

of images produced can be viewed as a function of the gray-scale values at specific pixel locations and the specific time. Movement within the scene, whether by the camera or an object, leads to a temporal shift in these gray scale values across the sequence of images. This creates a two-dimensional field of apparent motion within the image plane, known as the Optical Flow Field (Amaki et al. 2019; Kim and Gratchev 2021; Muhammad et al. 2022; Srokosz et al. 2021).

For ground-based imagery, one can establish a fixed camera position, however, for satellite-based imagery, it is necessary to apply corrections and orthorectification to ensure consistent ground pixel locations over time. Accurate computation of optical flow therefore represents a significant challenge in the field of computer vision (Barron et al. 1994; O'donovan 2005; Javier et al. 2013). Furthermore, since the primary assumption underpinning optical flow is that the patterns of light intensity in successive images exhibit temporal consistency, there has been only limited use in natural settings with highly variable environmental conditions.

In the current AkhDefo 2.0 workflow, we applied the coarse to fine dense optical flow implementation from OpenCV (Farnebäck 2003). By filtering and re-sampling, the original image at progressively lower resolutions, a pyramid structure of down-sampled images, ranging from coarse to fine, was generated. Initially, a rough match was established at the lower resolution level, which then guided the identification of a smaller region in the next higher resolution image. This process was iteratively refined, gradually moving towards the full resolution of the original image. The adoption of the coarse to fine optical flow algorithm significantly enhanced performance of optical flow calculation, yet these methods had inherent limitations. The main challenge of all methods of optical flow was to maintain stability of image illumination (O'donovan 2005; Javier et al. 2013; Amaki et al. 2019). Another inherent limitation was that objects smaller than their displacement magnitude can become obscured at coarser levels due to the smoothing process. There was a risk of error propagation since at coarser scales, overlapping motion layers could lead to errors that would be carried through to different scales (O'donovan 2005). To minimize the effect of illumination persistency error propagation, we implemented a number of approaches including the Structural Similarity Index Map (SSIM) (Palubinskas 2014), Scale Invariant Feature Transform (SIFT) (Lowe 2004) and statistical z-score outlier removal to mask invalid pixels.

A detailed methodological workflow addressing these issues is shown in the supplementary material along with a high-level summary of the application of AkhDefo Python package (https://pypi.org/project/akhdefo-functions/). The AkhDefo package also included a collection of independent Python codes to perform batch processing and manipulation of geospatial datasets such as raster and vector datasets. In the current study, we added scripts to the AkhDefo software to (1) download and process Sentinel 1 radar imagery via earth-data API account (https://search.asf.alaska.edu/) for Morenny rock-glacier in Kazakhstan, (2) download daily PlanetScope imagery using a Planetlab account (https://account.planet.com) for Mud Creek Landslide, USA and (3) process live-stream webcam video for the Stawamus Squamish Chief rockfall in Canada.

3 Case Study 1: The 2017 Mud Creek Landslide, California, USA

The 2017 Mud Creek landslide occurred in the Big Sur region along the California coast (Fig. 2), approximately halfway between Monterey and Morro Bay. This area, known for its rugged terrain is located on the western side of the Santa Lucia Mountains and boasts several peaks exceeding 1000 m in elevation. These mountains are linked to the Big Sur Bend of the San Gregorio-Hosgri Fault system, a region characterized by transpression along the transform plate boundary in this area (Warrick et al. 2019). The bedrock geology of the mountains includes Mesozoic granitic and pre-Cretaceous metamorphic rocks, as well as patches of Miocene marine sedimentary rocks and a diverse mix of Mesozoic rocks collectively known as the Franciscan Assemblage.

This variety of rock types leads to considerable spatial variability in the strength characteristics of the rock masses (Warrick et al. 2019), which in turn results in varying levels of susceptibility to landslides and differing spatial densities. Near Mud Creek, the primary bedrock geology consists of the Franciscan Assemblage, which is covered by loose colluvial deposits. This area is characterized by discrete planes of weakness within the mélange, which have been linked to landslides occurring within approximately 10 km of the Mud Creek area (Wills et al. 2001). The geological features that further influence stability and act as pathways for subsurface water movement include shear zones of various sizes and recent faults that intersect the region (Warrick et al. 2019). The area within 5 km of the Mud Creek site has been identified as having a high potential for landslides, and debris removal due to rockfalls is frequently required on Highway 1 crossing Mud Creek (Warrick et al. 2019). However, the likelihood of extensive, rapid changes in the landscape in the area remained unrecognized until 2017.

3.1 Landslide Kinematics

Another disastrous landslide like the one that occurred at Mud Creek on May 20, 2017, is likely given the highly altered and weathered bedrock geology, numerous shear

Fig. 2 Locations of the selected case studies at (**a**) Mud creek, California, USA, (**b**) Squamish Chief, British Columbia, Canda, and (c) Morenny rock glacier in Kazakhstan

zones in the Mud Creek site (Warrick et al. 2019) and the proximity to areas in California often affected by earthquakes, and the region's high rainfall.

The key aspect of landslide monitoring with remote sensing data is the ability to predict not only the timing of landslide failure but also recognize landslide behavior and deformation kinematics. Leveraging the capabilities of the AkhDefo Package, we collected, processed, and analyzed data to visualize and interpret both spatial and temporal displacement patterns. In Muhammad et al. (2022) we processed 1 month of daily cloud-free PlanetScope optical satellite imagery. The current analysis focused on daily satellite imagery from PlanetScope, covering the period from October 2, 2016, to May 16, 2017; 4 days before the landslide event. Specifically, we generated 7 months' worth of 2D horizontal displacement data (in east-west and north-south directions) for the Mud Creek site, utilizing imagery obtained from November 2016 through May 2017.

The following maps including aspect velocity map, plunge velocity map, height change map, bedrock volume change map (Fig. 3) and time-space inverse velocity map (Fig. 4) were constructed from both two-dimensional horizontal displacement datasets and a pre-failure digital elevation model. The maps were employed to assess the change in the slope, using the magnitude and direction of displacement on the digital elevation model, and in turn, the likely volume of the displaced bedrock material. Our estimate suggests a rock volume displacement of approximately $2.976 \times 106\ m^3$ which is in broad agreement with the volume of $3.5 \times 106\ m^3$ estimated by Warrick et al. (2019) from LiDAR point cloud change detection.

The inverse velocity, displacement aspect, and magnitude maps (Fig. 3) revealed two areas of downward movement (1) the lower area at the base of the failure plunging more than 50 degree south-southwest (Figs. 3a, b, and 4b) and (2) the upper area at the top of the landslide head-scarp (Figs. 3a, b and 4b). These maps also indicate that the onset of landslide failure began in early May 2017, with instability starting at the toe of the landslide, corresponding to the lower area, and then progressing to the formation of the landslide scar weeks before the catastrophic failure. The inverse velocity map and profile (Fig. 4b, c) indicates that the failure initiated around May 2, 2017, at least two weeks before the catastrophic landslide failure. Additionally, a previously identified upper swale earthflow, detected from the LiDAR digital elevation model study (Warrick et al. 2019) (Fig. 4a) and confirmed by the inverse velocity map (Fig. 4b), deformed around April 20, 2016, at least one month prior to the landslide event (Fig. 4b). This pattern aligns with the daily time-lapse PlanetScope imagery, the inverse velocity profile, and time-space inverse velocity map for the Mud Creek site (Figs. 4 and 5).

Our data identified creep-to-failure behavior at Mud Creek months before the major failure. We also pinpointed specific dates of increased landslide movement: November 30, 2016, March 2, 2017, April 10, 2017, and May 16, 2017 (Fig. 4c). In addition, the initial stages of the failure, starting in early May 2017, are clearly observable in the daily

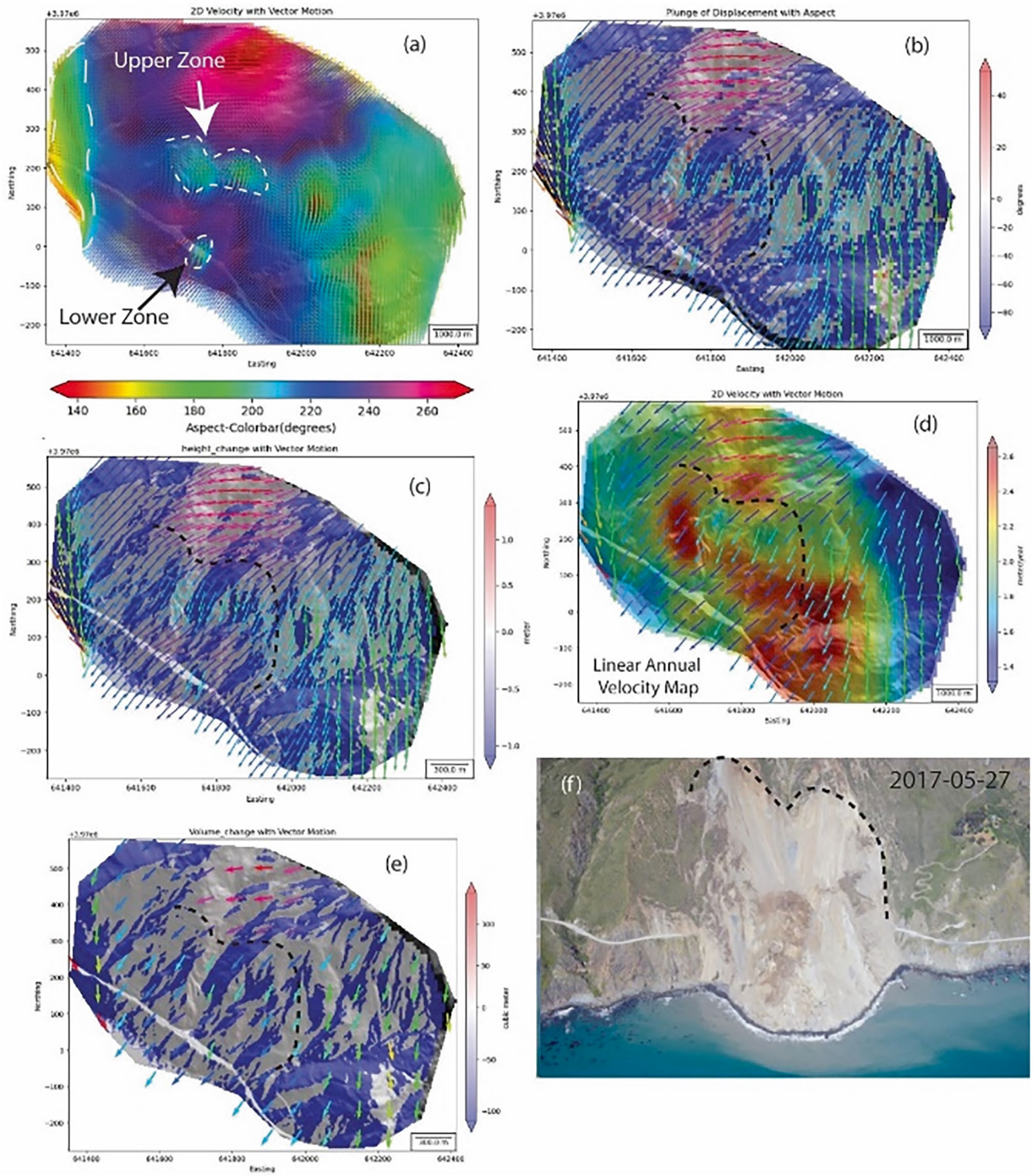

Fig. 3 Mud Creek deformation kinematics. (**a**) 2D Horizontal displacement aspect. (**b**) Plunge of displacement vector motion in degree; negative is downward movement, positive upward movement and zero is pure horizontal movement. (**c**) estimate elevation change map. (**d**) 2D linear annual displacement magnitude calculated between October 2, 2016, to May 16, 2017. (**e**) Estimated landslide volume map calculated from pre failure digital elevation model and linear annual velocity. (**f**) Oblique aerial photograph 1 week after the catastrophic failure (Warrick et al. 2019)

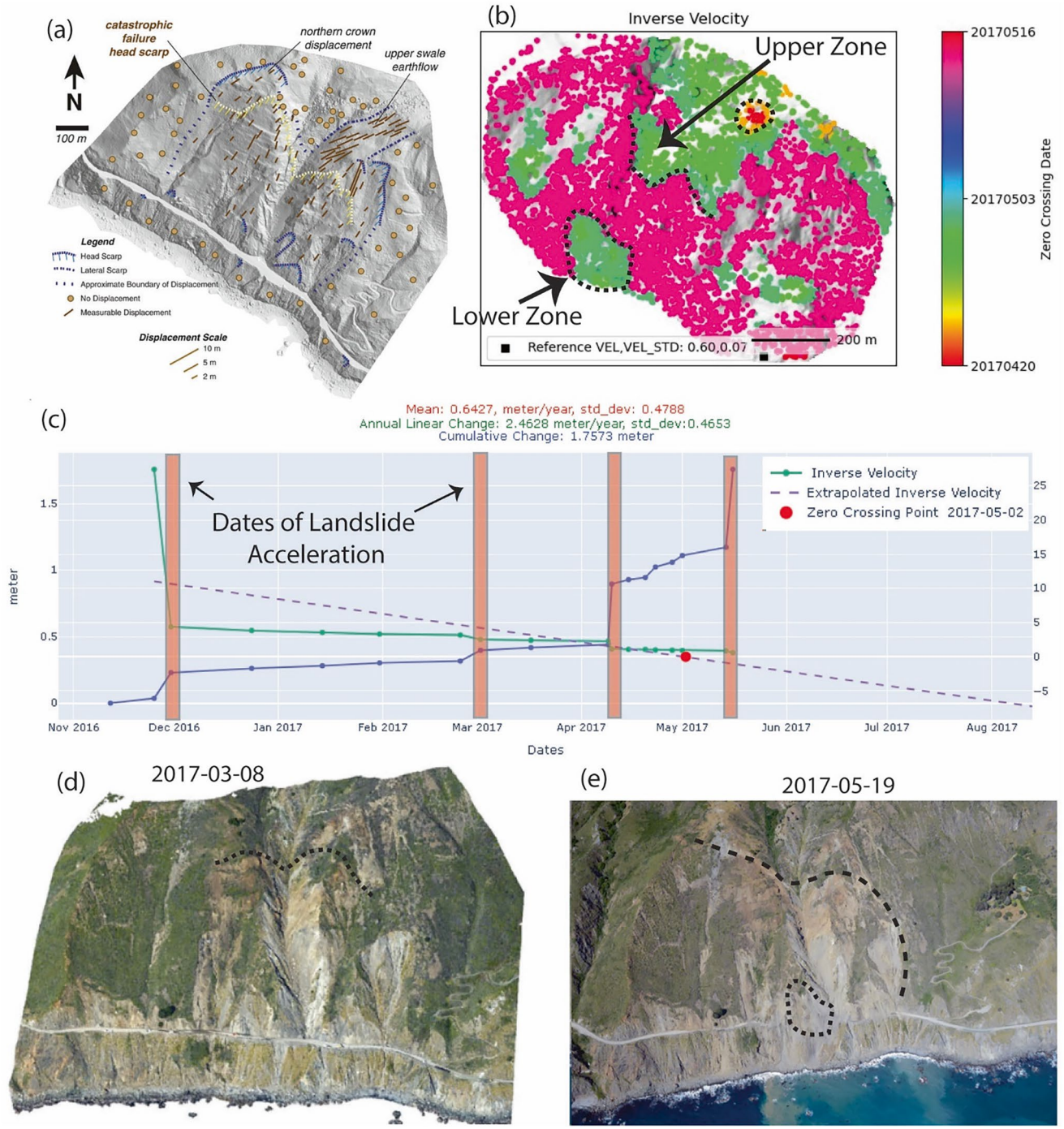

Fig. 4 (**a**) Horizontal displacement map shows active areas between 2010 and 2016 derived from LiDAR digital elevation model (after Warrick et al. 2019). (**b**) Inverse Velocity map shows spatial prediction date of deformation within the landslide body. (**c**) Time-series velocity and inverse velocity profile for the average pixels inside the lower zone denoted on plot b. (**d**) Oblique aerial ortho-photograph for Mud Creek slide on March 3, 2017 (after Warrick et al. 2019). (**e**) Oblique aerial orthophotograph for Mud Creek slide on May 19, 2017 (after Warrick et al. 2019)

PlanetScope time-lapse optical imagery (Fig. 5). Utilizing optical imagery that provides a daily acquisition interval, especially during April 2017 (Fig. 6), proves highly advantageous in the period preceding the landslide failure.

This frequent imaging enabled more precise and prompt tracking of the site's changing conditions, offering essential insights unattainable with less regular monitoring techniques like the 12-day data acquisition intervals of Sentinel 1 data-

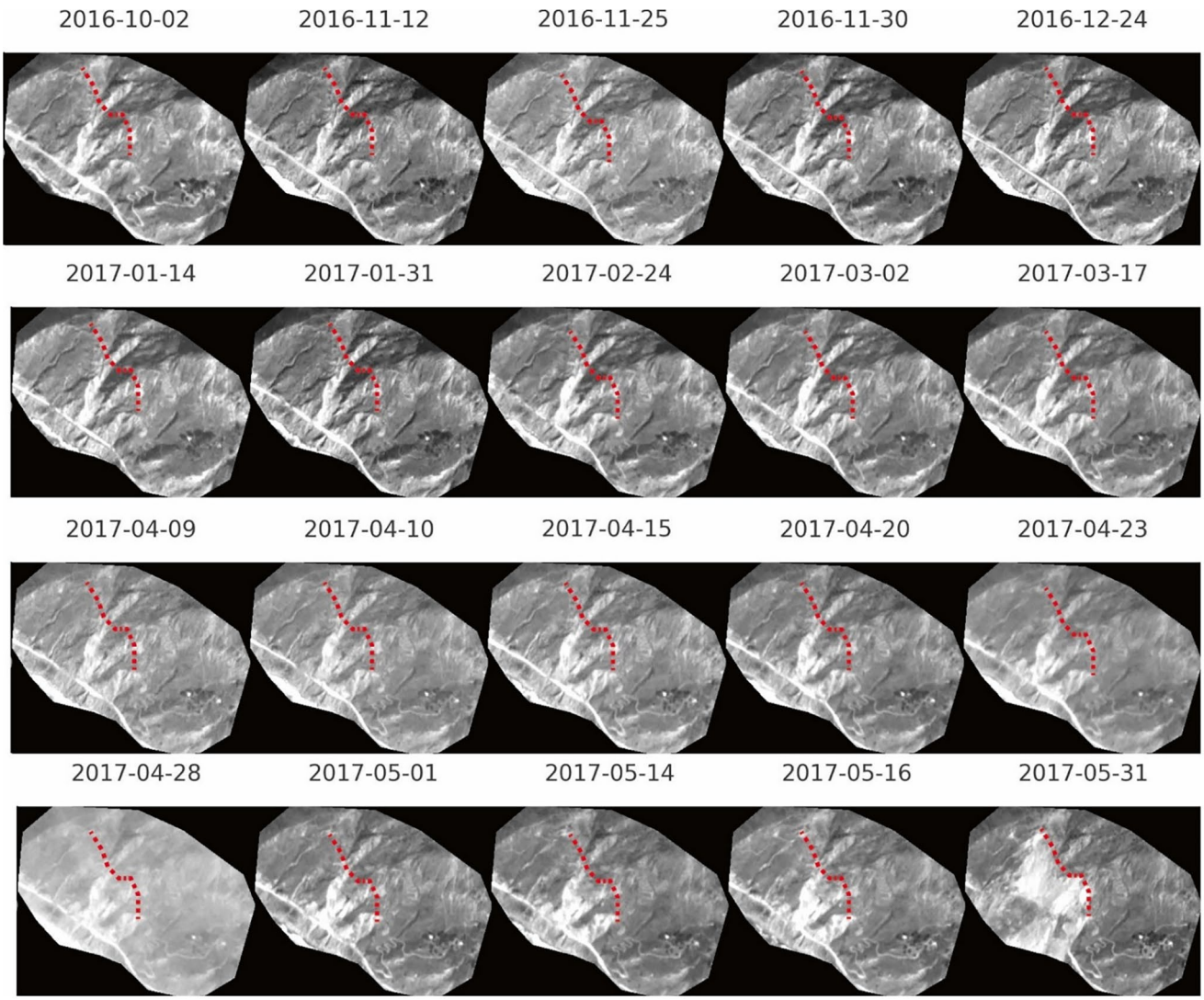

Fig. 5 Static Time-lapse for Mud Creek site before and after the catastrophic failure. Red dashed outline represents the location of the scar. A high resolution colour timestamp animation is available in the following link: https://raw.githubusercontent.com/mahmudsfu/AkhDefo/main/src_akhdefo/docs/notebooks/data/mudcreek/movie.gif

set. By contrast, previous work based on InSAR and LiDAR change detection (Handwerger et al. 2019; Warrick et al. 2019) were unable to identify the creep-to-failure behavior at Mud Creek due to limited temporal data acquisition and landslide movements greatly exceeding the measured InSAR deformation. Additionally, the 12-day interval of the Sentinel 1 InSAR dataset is too infrequent to closely monitor the daily-landslide deformation. Also, InSAR measures deformation along the line of sight, and is thus only capable of measuring deformation in one dimension. The annual displacement data showcased in this study, prior to the catastrophic event, not only had the potential to forecast such an incident but also to conduct a pre-event analysis of the landslide's movement. However, the accuracy of this assertion hinges on whether real-time or near-real-time monitoring was operational.

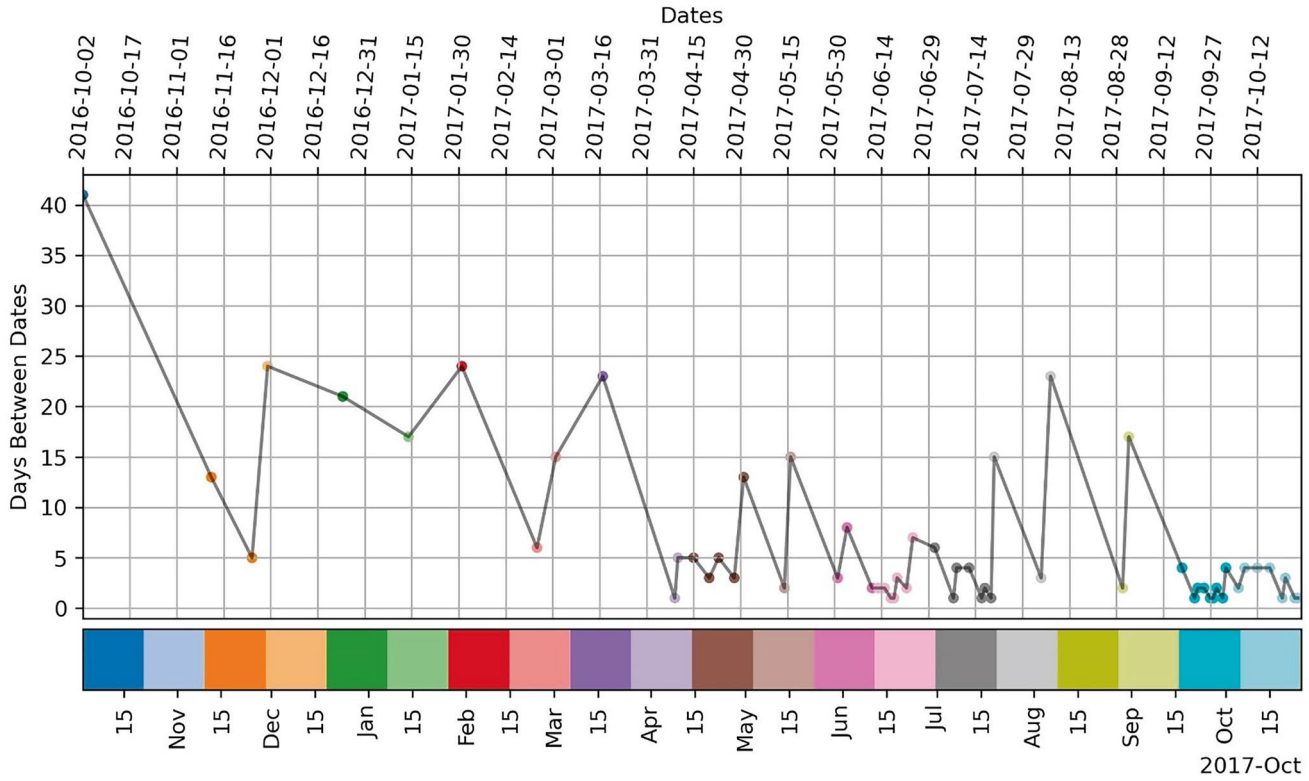

Fig. 6 Data frequency interval for cloud free PlanetLab optical imagery

4 Case Study 2: The Stawamus Chief Rockfall, British Columbia, Canada

The Stawamus Chief (also known as "The Chief"), is a significant granodiorite pluton situated next to Highway 99, near Squamish in British Columbia, Canada (Fig. 2). This geological formation, which originated around 100 million years ago during the early Cretaceous, became exposed through the tectonic activity that formed the Coast Mountain Range (Mathews and Monger 2005). In the most recent ice age, the region was blanketed by glaciers, reaching a depth of about 1300 m. The distinctive exfoliation joints seen on The Chief and similar granitic structures are the result of both tectonic forces and glacial pressure release (Coughlan et al. 2023; Sampaleanu 2017; Tuckey 2012). The area is a popular region for tourism particularly as a world-class rock-climbing site (Melanson 2015; Coughlan et al. 2023) and over the past decades has been subjected to increased rockfall activity (Coughlan et al. 2023; Sampaleanu 2017).

Currently, the only source of continuous visual surveillance for The Chief is from a live-stream webcam with the capacity of 30 frames per second, installed and operated by a citizen scientist residing in Squamish (Birkill 2024). The camera is affixed to a tree approximately 2.3 km away from The Chief. The Dahua IPC-HFW8232E-Z IP camera is equipped with a Sony Exmor sensor, capable of delivering clear images even during cloudy nights and with an estimated ground pixel resolution of 80 cm (Birkill 2024 pers. comm.). During September 20, 2021, the camera recorded a rockfall event at 1:34 am PST (Pacific Standard Time). The sound of tumbling rocks resonated across a large portion of Squamish, particularly in the Valleycliffe area, positioned near the base of The Chief's north side. The event led to vibrations in nearby homes (Birkill 2024), and the seismicity was recorded on the seismograph managed by the Canadian National Seismograph Network (Birkill 2024 pers. comm) at Watts Point, BC, approximately 10 km to the southeast of the Stawamus Chief.

4.1 Real-Time Rockfall Monitoring System

We processed the streaming webcam data with the AkhDefo real-time change detection module which uses an optical flow algorithm to measure the motion field between subsequent video frames. This module can process video frames directly from the server, facilitating instantaneous data analysis without the requirement to download video files.

Optical flow, like other techniques, has inherent limitations such as difficulty to maintain the stability of light exposure between subsequent video frames as well as proper installation of the webcam to avoid camera movement due to wind gusts. Those challenges were minimized using various techniques such as image frame alignment (Lowe 2004), masking of still objects as background (Muhammad et al. 2022; Verma et al. 2023) and use of a structural similarity index map (Kim et al. 2020; Muhammad et al. 2022) between subsequent frames. To assess the capacity of real-time monitoring and mitigating potential discrepancies caused by instrumental installation errors, such as webcam vibrations due to wind, a sensitivity analysis was conducted. On March 26, 2024, we executed a continuous four-hour live stream analysis from 3 pm to 7 pm, during which we also performed frame alignment procedures. The latency of video frame processing reaches a few minutes per hour (Fig. 7a, b) with a baseline displacement error of 1 cm (Fig. 7c). Additionally, our findings indicate a direct correlation between video frame shifts and wind speed. For example, in Squamish on March 26, between 3 pm and 4 pm, the wind speed increased to 21 km/h, coinciding with a 6-to-8-pixel shift in video frame alignment (Fig. 8c). Conversely, as the wind speed decreased to below 10 km/h between 4 pm and 5 pm, a concurrent decrease in video frame pixel shifts was observed, with shifts ranging between 2–6 pixels (Fig. 8d).

For more precise analysis, the September 20, 2021, video recording (approximately 2 min duration) was transferred to a local computer. As the video data was sourced from a local machine, the software examined each frame thoroughly, processing at a rate of 30 frames per second. This meticulous frame-by-frame analysis resulted in a prolonged processing period compared to live-stream webcam data ingestion, where the software selectively captures frames based on real-time occurrences.

The onset timing of rockfall occurrence was determined to be at 1:28:42 am and ended approximately around 1:28:55 am as it appears from the recorded video (https://akhdefo.readthedocs.io/en/latest/_images/frame_2024-03-26_0_image.gif). It is worth noting that although the area was covered with cloud and fog at the time of the rockfall, we were able to clearly differentiate between background noise and signal of the rockfall event (Fig. 9b).

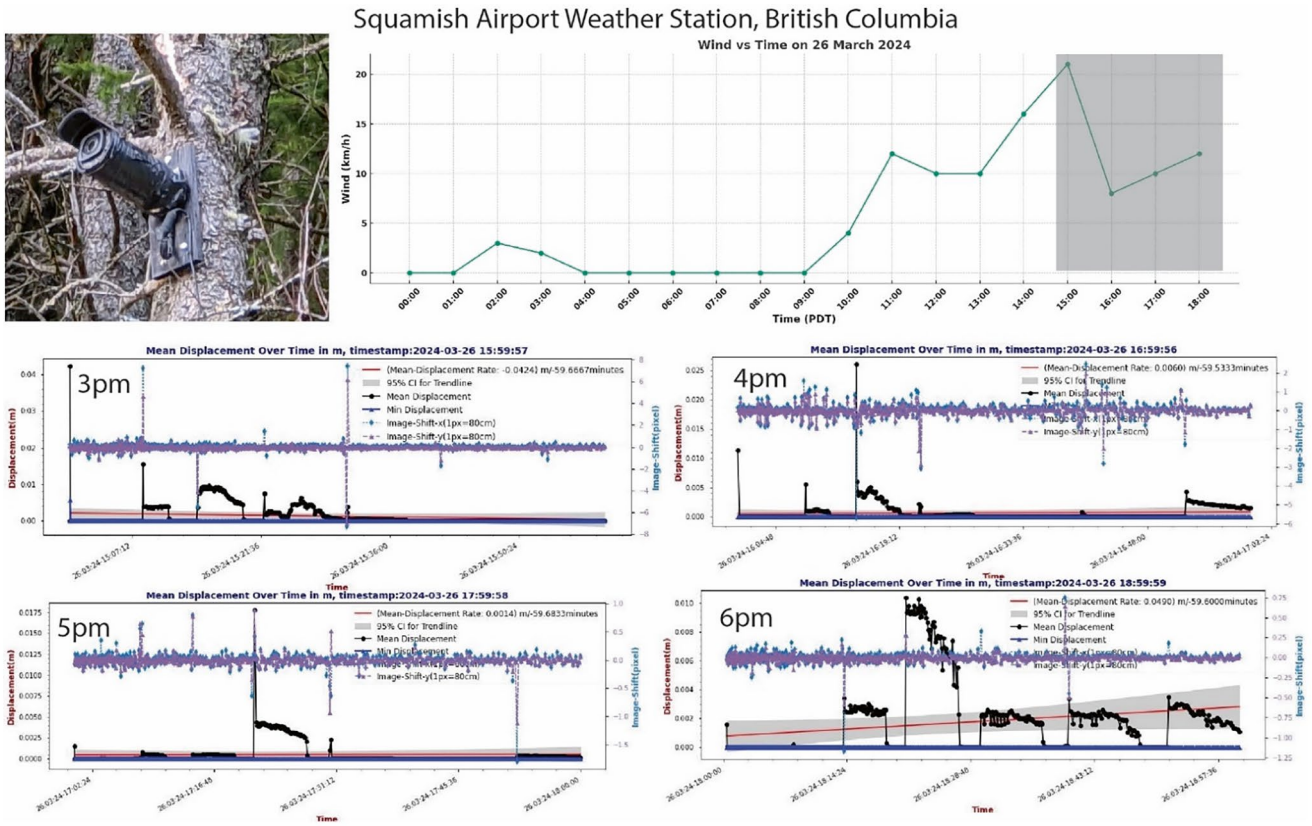

Fig. 7 (**a**) Photograph showing the installation of the webcam. (**b**) Hourly windspeed data at the Squamish airport weather station. (**c**) Mean displacement and image shift between subsequent video frames on March 26, 2024, between 3 pm and 4 pm. (**d**) Mean displacement and image shift between subsequent video frames, between 4 pm to 5 pm. (**e**) Mean displacement and image shift between subsequent video frames from 5 pm to 6 pm. (**f**) Mean displacement and image shift between subsequent video frames between 6 pm and 7 pm

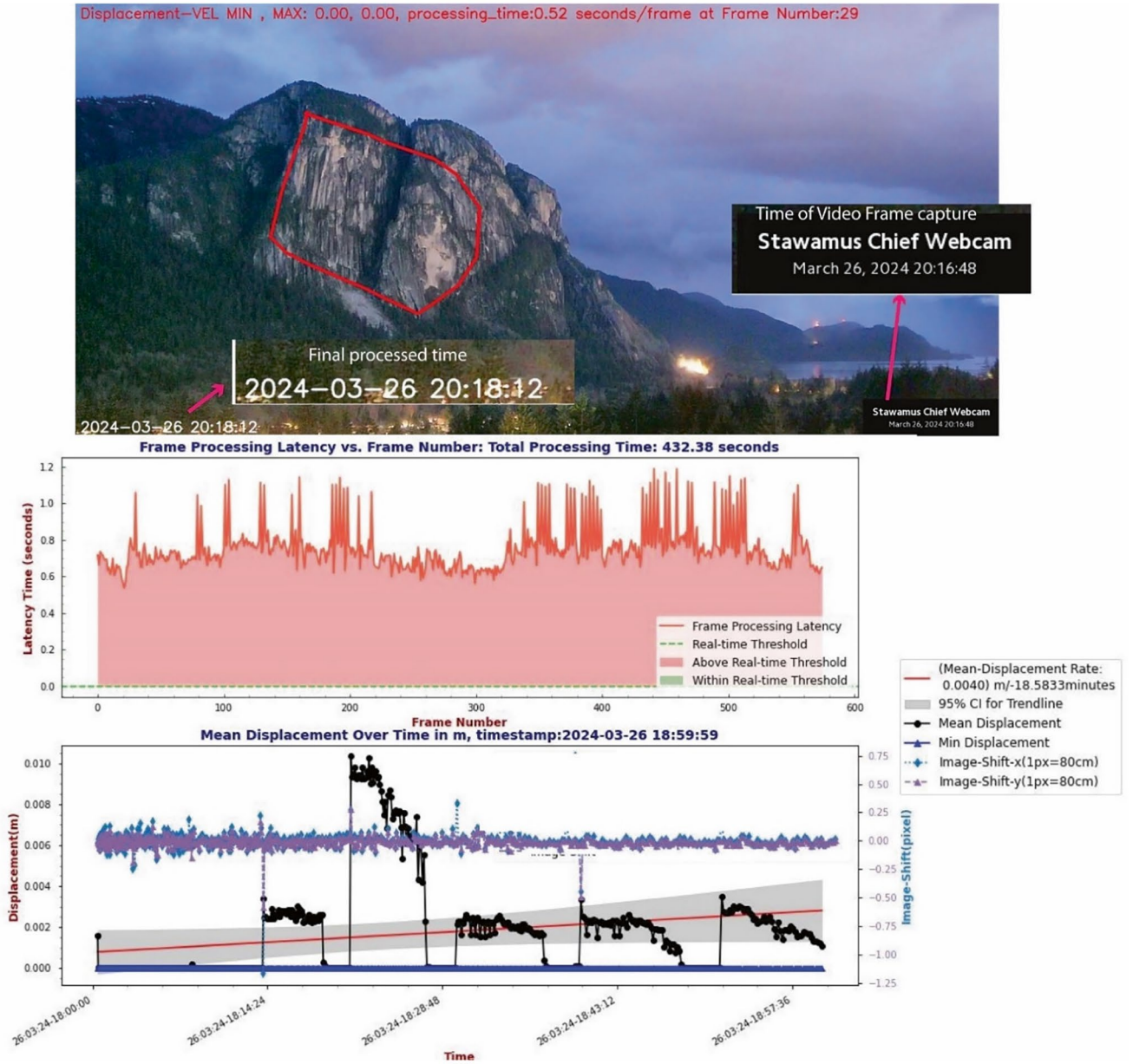

Fig. 8 Rockfall monitoring system latency time. (**a**) Video frame capture showing time of captured frame and time after frame being analyzed. (**b**) Plot of time required to process two consecutive frames and total latency time per two frames being processed over a period of one hour. (**c**) Mean displacement for the red polygon in a and sensitivity of the system to 1 cm (i.e., movements less than 1 cm is considered as noise)

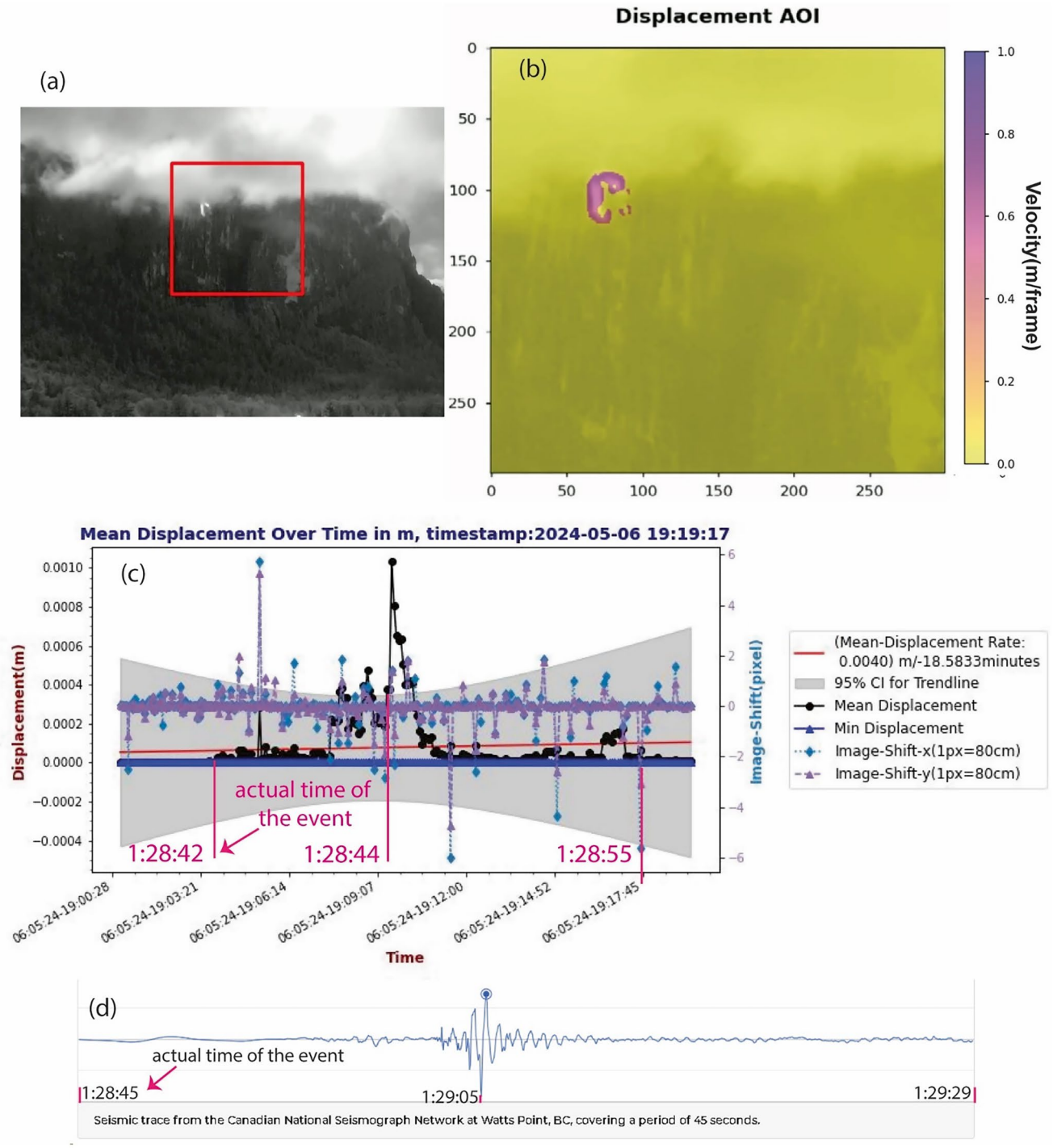

Fig. 9 Screen shot of processed video of the 20 September 2021 Stawamus Chief rockfall. (**a**) Screenshot of the rockfall site seen with night vision camera. (**b**) Processed displacement velocity for the red square area in a in meter per frame during the onset timing of rockfall event; note the background cloud and clarity of measured displacement velocity. (**c**) Time-series mean displacement in meters for the red square area in a and frame stability displacement shift in pixels. (**d**) Seismic trace from the Canadian National Seismograph Network at Watts Point, BC, covering a period of 45 seconds

5 Case Study 3: Morenny Rock-Glacier, Tien Shan Mountains, Kazakhstan

The Tian Shan is a vast system of mountain ranges in Central Asia that spans several countries, mainly located in Kyrgyzstan and the northwestern territory of China. Tectonic activity in the Tien Shan is a result of the northward-moving India plate colliding with the Eurasian plates that also uplifted other adjacent mountain ranges: Alai, Karakoram, Pamirs, and Hindu Kush (Avouac and Tapponnier 1993; Blayney et al. 2019; Komatsu 2016). The geological composition of the Tian Shan system varies across its expanse, with the geology in the northeast predominantly characterized granite formations, that have a role in shaping the landscape and influencing the hydrology of the area (Brunet et al. 2017). The northern Tien Shan mountains encompass a significant area of periglacial landscapes, representing extremely cold, non-glaciated terrain that is typically adjacent to alpine glaciers in mountainous regions (Bolch and Gorbunov 2014; Bolch and Marchenko 2009; Kääb et al. 2021; Liu et al. 2017). Common mass wasting types associated with cryogenic processes within the periglacial landscapes are creep, gelifluction, and sliding (Black 1976) which give rise to various distinctive landforms. As a response to warming of alpine permafrost in Tien Shan, rock glaciers have begun to creep faster, as has been observed in other alpine regions globally (Haberkorn et al. 2021; Haeberli et al. 2006).

The dynamics of rock glaciers is important to understand for assessing short- and long-term environmental changes that permafrost degradation can cause in alpine regions (Arenson and Jakob 2015; Harris 2005; Streletskiy et al. 2015). One of the fastest moving rock glaciers in the Bolshaya Almatinka valley in northern Tien Shan is the Morenny rock glacier, with displacement rates exceeding 1 m/year and classified as "active" according to the International Permafrost Association standardized guidelines for rock glaciers inventory (RGIK 2023).

The spatial and temporal changes in the movement of Morenny rock glacier were studied independently by analyzing image correlation techniques (Fig. 10a) via offset tracking of aerial, historical, and modern high-resolution optical images (Kääb et al. 2021) and differential SAR interferograms (Fig. 11a). The study has shown surface velocity on rock glaciers has increased 2–4 times within northern Tian Shan mountains compared to 1950 and 1960. Besides the overall rapid movement of Morenny rock glacier, exceeding displacement velocity by 1 m/year, a distinct fast-flowing branch with up to 2.5 m/year displacement diverts from the main body of the rock glacier towards the northwest (Figs.10 and 11).

We processed both PlanetScope optical imagery (Figs. 10 and 11) and Sentinel 1 (Ascending and Descending orbits) (Figs. 12 and 13) back-scatter radar imagery using AkhDefo software to produce temporal deformation maps for the summer periods between 2017 to 2023. Additionally, the land surface temperature over the northern Tien Shan region was estimated using Google Earth Engine from Landsat 8 dataset between 2017 to 2020 (Figs. 13 and 14) for summer months of July and August for each year.

5.1 Kinematics of the Rock Glacier Movement

The kinematic process of rock glaciers is characterized by gradual downslope movement, which results from the internal deformation of the permafrost ice within these landforms (Kummert et al. 2021; Müller et al. 2016; Strozzi et al. 2020). This movement is not just an internal phenomenon but is also apparent on the surface, showing displacement that varies across the landform exterior. This displacement is indicative of the underlying processes at work and is crucial for the study of rock glacier dynamics. In exploring the kinematics of rock glaciers, researchers (Kummert et al. 2021; Müller et al. 2016; Strozzi et al. 2020) focus on various parameters including the speed at which the surface moves, the patterns of flow observed, the displacement rates at which these movements occur, and how these movements change over time.

Understanding these kinematic attributes is essential for deciphering the complex behavior and dynamics of rock glaciers, especially considering the backdrop of evolving environmental conditions. Rock glaciers are complex systems influenced by a variety of factors including the amount of sediment and ice they receive, the state of the permafrost within them, and their geomorphological setting (Kummert et al. 2021). These factors collectively shape the physical properties and morphology of rock glaciers. Understanding the rock glacier movement patterns is essential for forecasting their reactions to climatic changes, which is becoming increasingly crucial as global temperatures rise.

During summer 2018 from August 24 to September 5, a previous study (Kääb et al. 2021) identified four zones of active deformation at Morenny rock glacier based on Sentinel 1 descending orbit interferogram (Fig. 11). However, due to the limitations of traditional InSAR, the study was unable to unwrap the interferogram hence, only an approximate deformation was provided. We reanalyzed the same Sentinel 1 descending orbit radar backscatter images (from August 24 to September 5) using an optical flow algorithm technique, which was incorporated into the

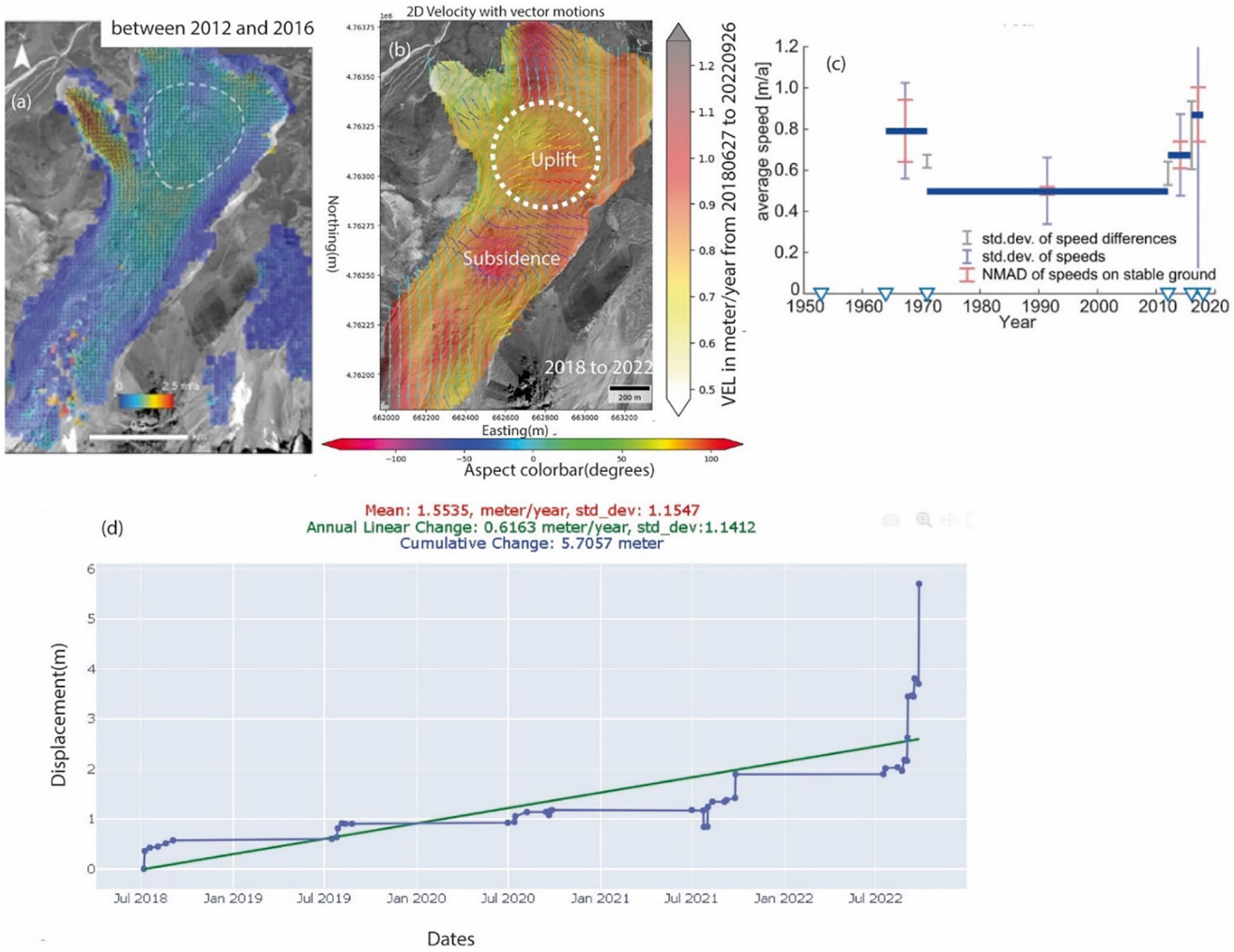

Fig. 10 Velocities and speed variations on the Morenny rock glaciers from optical imagery. (**a**) Colour-coded velocity fields with vectors superimposed from image matching between two images 2012 and 2016 high-resolution satellite images (after Kääb et al. 2021). (**b**) Mean annual velocity with vector motion from AkhDefo optical flow for 5 years during summers 2018 to 2022. (**c**) Average time series of speeds for clusters of points (white dashed outline in panel **a**). (**d**) Average time series profile shows cumulative deformation from 2018 to 2022 (white dashed outline in panel **b**)

AkhDefo software for this study. Zones 1 and 2 show displacement rates 30–40 cm per 12 days towards north northwest; hence, movement away from the satellite line of site. In contrast, zones 3 and 4 show slower displacement rate around 10 cm per 12 days towards north, northwest and north northeast, respectively. Our results are consistent with the aforementioned study and provide accurate deformation measurements along line of site for the four active zones with rock glacier body (Fig. 11a, c).

The analysis of Sentinel 1 radar backscatter images (Ascending and Descending) and PlanetScope optical imagery over seven summer seasons from 2017 to 2023, provides detailed deformation patterns of the Morenny rock glacier for documentation. The Morenny rock glacier exhibits a complex and varied movement pattern, with its slope oriented in a north-south direction (Fig. 12d).

Motion velocity vectors show significant subsidence exceeding 5–10 cm annually on the upper slope (Fig. 13), and an uplift exceeding 5–10 cm annually on the lower slope (Fig. 13) and overall north-northwest direction horizontal movement (Fig. 12). We conducted simulations of both subsidence and uplift patterns (Fig. 15) and used them for validation against the actual motion vectors observed on the rock glacier.

Specifically, subsidence is characterized by inward-moving vectors (Fig. 15), while uplift is indicated by outward-moving vectors (Fig. 15). These patterns are discernable in both radar (Ascending and Descending) and optical imagery datasets, with the motion vector patterns being more pronounced in optical imagery. This is attributed to the fact that optical satellites capture data from a nearly vertical perspective, whereas radar satellites acquire

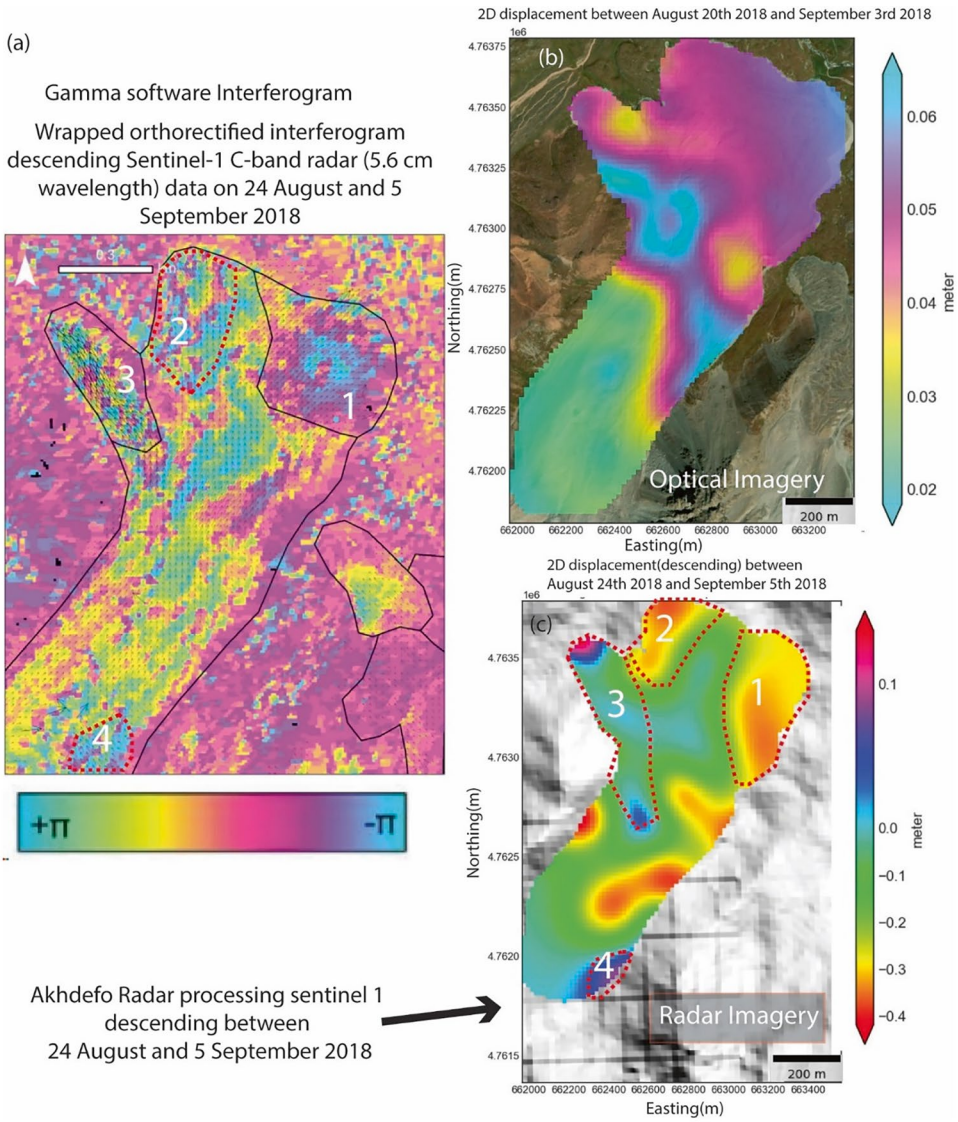

Fig. 11 Comparison between Gamma software interferogram with AkhDefo software processing results for both Radar and Optical imagery. (**a**) Wrapped orthorectified interferogram descending Sentinel-1 C-band radar (5.6 cm wavelength) data on 24 August and 5 September 2018. (**b**) Displacement product calculated from optical imagery between August 20 and September 3, 2018. (**c**) Displacement product calculated from Sentinel 1 Descending orbit radar back-scatter imagery between August 24 and September 5, 2018. Note, the decorrelation due to large movement appears in the interferogram which is beyond traditional InSAR capability to unwrap

data at an oblique angle, a difference that is clearly evident in our analysis of the velocity vector motions. This period also includes the analysis of processed land surface temperatures over four summers, from 2017 to 2020. The analysis points to a significant increase in the movement of the rock glacier by approximately 1 m annually since 2017, which aligns with findings from prior studies (Kääb et al. 2021). Additionally, a consistent annual increase in the summer land surface temperature of about 0.5 °C from 2017 to 2020 is observed, suggesting a correlation with the accelerating movement of the rock glacier (Kääb et al. 2021; Sorg et al. 2015).

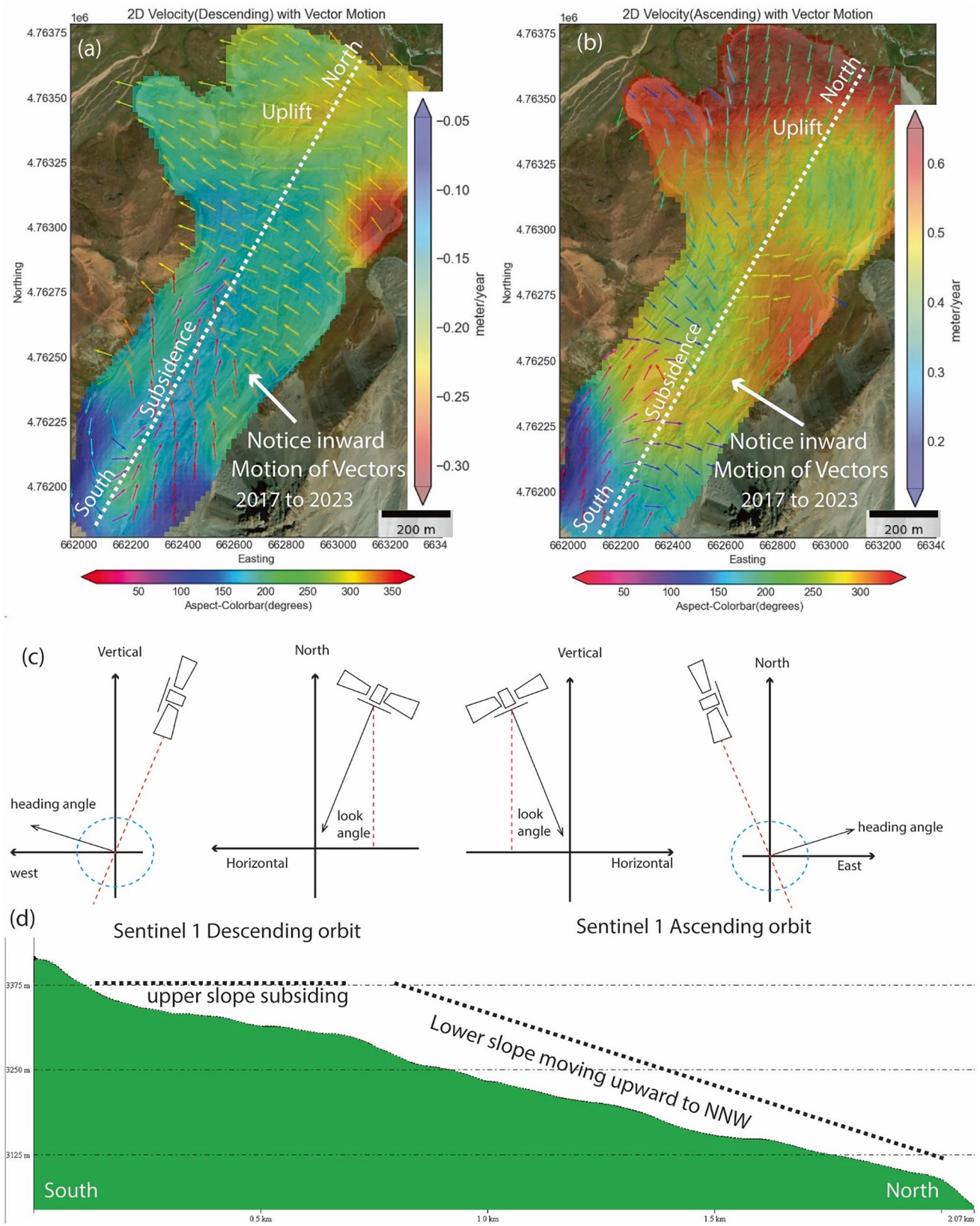

Fig. 12 2D linear annual displacement magnitude. (**a**) Mean annual velocity calculated based on Sentinel 1 Descending orbit Radar backscatter imagery between July 2017 and August 2023. (**b**) Mean annual velocity calculated based on Sentinel 1 Ascending orbit Radar backscatter imagery from July 2017 to September 2023. The arrows represent the displacement aspect; notice the displacement vectors in both Ascending and Descending indicate overall North and Northwest movement of the rock-glacier. (**c**) Diagram explaining the concept of radar satellite Line of Sight geometry. (**d**) Elevation profile from south to north show slope geometry along the white dotted line in **a** and **b**

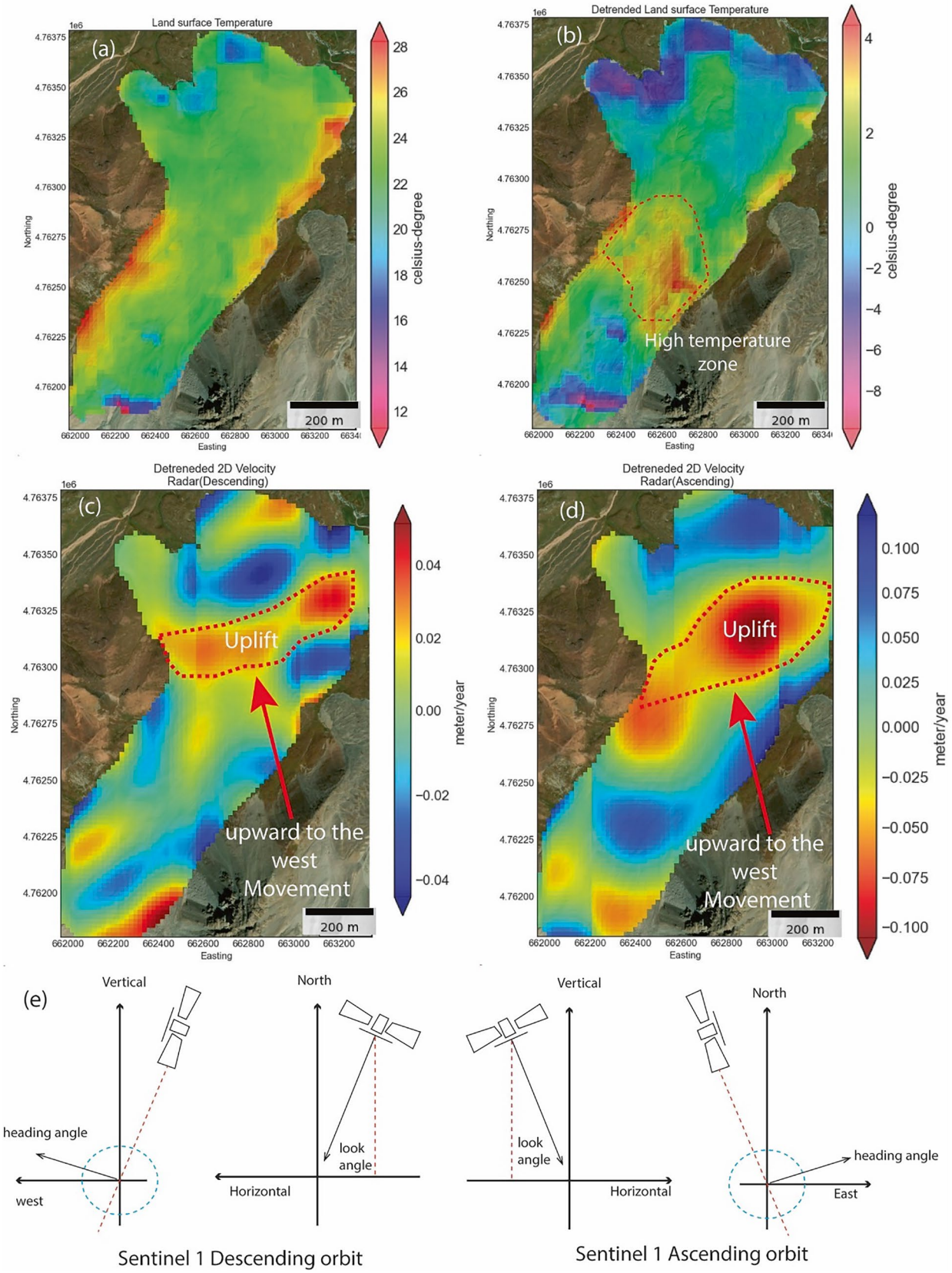

Fig. 13 Comparison between land surface temperature and detrended displacement velocity. (**a**) Mean land surface temperature for July and August between 2017 and 2020. (**b**) Detrended mean land surface temperature for July and August between 2017 and 2020. (**c**) Detrended linear annual velocity calculated based on Sentinel 1 Ascending orbit Radar back-scatter imagery from July 2017 to September 2023. (**d**) Detrended linear annual velocity calculated based on Sentinel 1 Descending orbit Radar back-scatter imagery from July 2017 to September 2023. Note, the dashed red polygon in both ascending and descending orbit moves upward to the west direction

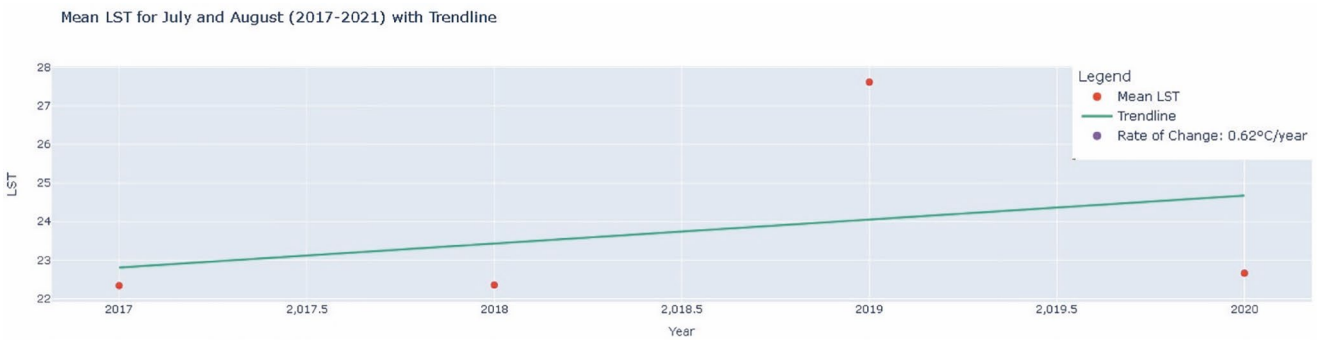

Fig. 14 Time-series for mean land surface temperature for combined months July and August between 2017 and 2020. Notice, increased land surface temperature rate by more than 0.5 °C per year particularly during the summer of 2019

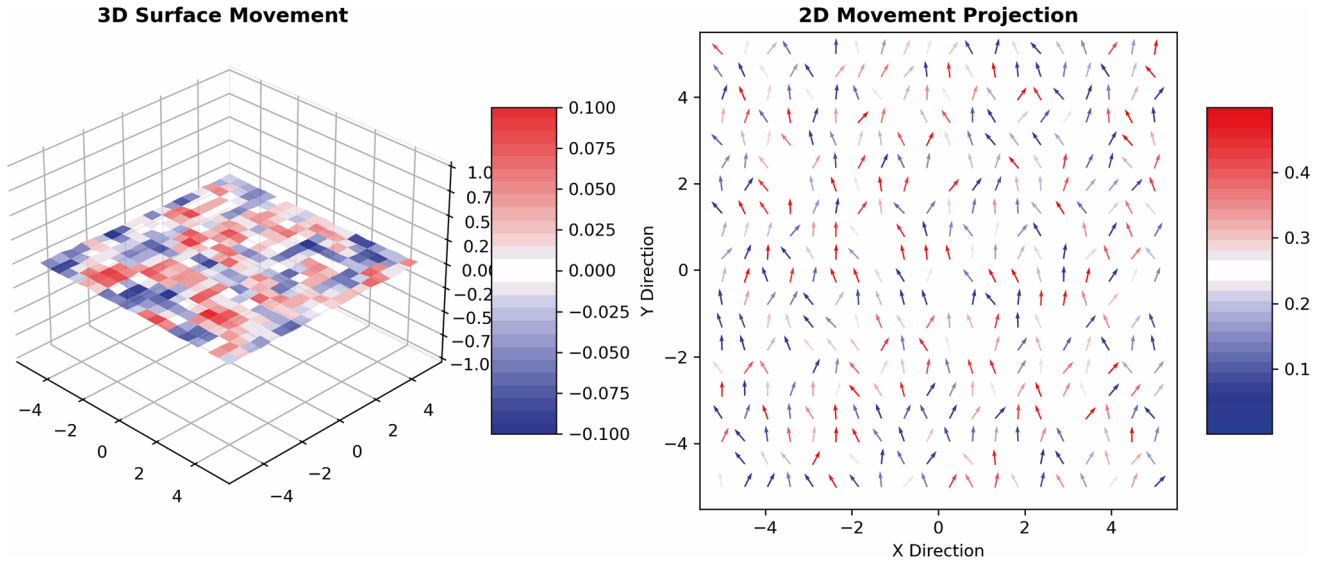

Fig. 15 (**a**) 3D synthetic simulation of motion pattern. (**b**) 2D projection of 3D motion pattern. Notice in case of upward motion (red arrows) the motion of arrows is outward and in case of subsidence (blue arrow) the motion of arrows is inward. See Figs. 5.12 and 5.13 and notice subsidence at the upper slope (south) and uplift at the lower slope (North). High resolution with animation can be viewed via https://github.com/mahmudsfu/AkhDefo/blob/main/src_akhdefo/docs/notebooks/animation.gif

6 Discussion

Remote sensing datasets, particularly those derived from satellite imagery such as radar and optical, have become invaluable tools in landslide monitoring. They offer new avenues for early warning, risk assessment, the formulation of mitigation strategies and also climate adaptation strategies (Bürgmann et al. 2006; Wei et al. 2010). Furthermore, there is a wide range of both commercial and open-source software options for analyzing these remote sensing datasets. However, in the realm of landslide and hazard mitigation, time is of the essence. The quicker the data is processed; the sooner policymakers and emergency responders can act to protect lives and safeguard economic infrastructure. The importance and the critical role of rapid, real-time data processing have inspired us to further develop a novel open-source package called AkhDefo (Muhammad et al. 2022). This study's contribution to the AkhDefo software package allows for the processing of both radar satellite imagery and optical imagery (from satellite and ground sources), using innovative techniques different from those found in existing software solutions (Cosentino et al. 2024; Kääb et al. 2021).

The core processing mechanism is anchored in the utilization of the hierarchical optical flow algorithm which operates on a principle of multi-resolution computation, initiating the process at a coarse lower resolution before progressively refining the analysis at higher resolutions. Such a multi-scale approach dramatically lessens the computational burden and accelerates the overall process. This efficiency enables quicker motion estimation compared to traditional exhaustive image correlation methods that analyze images at their

full resolution. Despite the advantages, optical flow techniques face certain challenges, including the assumption of consistent brightness across sequences of images and the handling of scenes with both minor and significant motion changes. Nevertheless, the AkhDefo implementation and workflow effectively mitigate these drawbacks. The strategies employed to overcome these challenges are described in the supplementary materials and the methodology section.

In this research, we applied optical flow techniques to analyze real-time ground-based webcam footage, optical satellite images, and radar imagery. These datasets were applied to study different types of landslides, including the Mud Creek rockslide in California, USA; a rockfall event at Squamish Chief in British Columbia, Canada; and rock glacier deformation at the Morenny rock-glacier in Kazakhstan. The well-studied May 2017 Mud Creek landslide was an ideal case study to perform back analysis, and to test various remote sensing datasets and hypotheses.

We processed daily satellite optical imagery and estimated the landslide volume solely based on pre-failure datasets. Our study provided reasonable estimates of 2,976,000 m3 which agreed with volume estimation from LiDAR point cloud change detection of 3,500,000 m^3 (Warrick et al. 2019). Additionally, we provided higher temporal resolution time-series deformation for the Mud Creek Landslide (up to one-day intervals), months before the landslide event, which had data been processed beforehand, we could have predicted the landslide occurrence based on the satellite optical imagery alone.

To scale the reliability of the landslide and rockfall monitoring system, it is important to assess its strength and limitations in terms of efficiency such as speed of data processing and measurement quality such as identifying uncertainty and reliability of the measurements. The system's capability to analyze 600 frames per hour (Fig. 7b, c) from a high-definition live video stream via an online server, which translates to roughly 0.167 frames per second, indicates the processing power.

Although, in real-time processing terms, the system seems slow for video processing to initiate instant warning, its application can nevertheless be seen as an important tool for natural hazard monitoring. For instance, this system can be used to monitor the frequency of rockfalls, and hence, to understand the mechanisms and patterns of occurrence. Additionally, unlike rockfalls which often occur without knowing precursor instability or warning if applied to other natural hazards such as rapid moving landslides and debris flows, the system allows the generation of timely warning and alerts to communities living in close proximity within a fraction of minutes.

The fast-moving Morenny rock glacier is a profound example of the recent permafrost warming problem in the high alpine regions of Central Asia. Developing countries in this region have significant areas of periglacial landscapes yet lack sufficient resources and infrastructure to study the alpine permafrost. This is also the case in many other alpine regions in the world. Thus, in developing countries, publicly available remote sensing data and accessible computational software, such as AkhDefo are often the only resources for scientists and practitioners to conduct research on the most recent environmental changes related to alpine permafrost.

Deformation data, such as displacement rates derived from Sentinel 1 radar imagery and PlanetLab satellite optical imagery, alongside land surface temperature measurements can be used as a foundation for forming preliminary assumptions about the driving forces behind the increased movement observed in Morenny rock glacier and for shedding light on the morphological characteristics of these movements.

7 Conclusions

In this research, we utilized optical flow techniques to analyze real-time ground-based webcam footage, optical satellite images, and radar images. These datasets were applied to study different types of landslides, including the Mud Creek rockslide in California, USA; rockfall at Squamish Chief in British Columbia, Canada; and deformation at the Morenny rock-glacier in Kazakhstan. Our findings include:

We achieved a higher temporal resolution, providing daily time-series deformation data for the Mud Creek Landslide, and calculated the volume of the landslide using a pre-failure dataset.

We created a near real-time system for detecting rockfalls using live-streamed webcam footage, with video processes latency time of a few minutes per hour. Therefore, we propose a low cost, near real-time rockfall detection workflow system as an additional toolbox to the existing rockfall monitoring methods.

We analyzed the temporal displacement rates of an active rock-glacier utilizing both satellite optical and radar imagery. The AkhDefo software is applied to rock glaciers as a relatively cost-effective and user-friendly method in contrast to more time-consuming and heavy data processing methods, including the DIC, and offset tracking techniques.

We introduced cutting-edge optical flow algorithm workflows, that have been incorporated into the open-source Python package AkhDefo, enabling the processing of various datasets, including live-streamed webcam footage, satellite optical, and radar backscatter imagery.

Our use of the AkhDefo software's workflow has shown that optical flow techniques can outperform traditional computer vision methods like DIC, particularly in handling large datasets for long-term, real-time analysis.

We have made the datasets, tutorials, and the open-source Python package publicly available, facilitating the replication of our research and methodologies worldwide.

Data Availability Statement The data supporting the findings of this study are available in the supplementary materials associated with this article. Additionally, all datasets, code, and relevant resources are publicly accessible on our GitHub repository at [https://github.com/mahmudsfu/AkhDefo]. Researchers and interested parties are encouraged to refer to these materials for full details on data collection, processing, and analysis methods.

Acknowledgments The corresponding author would like to express his deepest gratitude to his former PhD supervisors, Dr. Glyn Williams-Jones and Dr. Doug Stead, for their invaluable guidance, insightful comments, and constructive criticism throughout the development of this work. Additionally, the author extends his sincere appreciation to the members of his PhD examination committee: Dr. Sergio Sepúlveda (Simon Fraser University), Dr. Scott McDougall (University of British Columbia), and Dr. Giacomo Falorni (TRE-ALTAMIRA), for their thorough review and thoughtful feedback on the manuscript.

References

Amaki K, Yamaguchi T, Harada H (2019) Landslide occurrence prediction using optical flow. In: 2019 19th international conference on control, automation and systems (ICCAS), 2019-Octob(ICCAS), pp 1311–1315. https://doi.org/10.23919/ICCAS47443.2019.8971698

Arenson LU, Jakob M (2015) Periglacial Geohazard risks and ground temperature increases. In: Engineering geology for society and territory—volume 1. Springer, Cham, pp 233–237. https://doi.org/10.1007/978-3-319-09300-0_44

Asner GP (1998) Biophysical and biochemical sources of variability in canopy reflectance. Remote Sens Environ 64(3):234–253. https://doi.org/10.1016/S0034-4257(98)00014-5

Avouac J, Tapponnier P (1993) Kinematic model of active deformation in Central Asia. Geophys Res Lett 20(10):895–898. https://doi.org/10.1029/93GL00128

Barnhart WD (2017) Fault creep rates of the Chaman fault (Afghanistan and Pakistan) inferred from InSAR. J Geophys Res Solid Earth 122(1):372–386. https://doi.org/10.1002/2016JB013656

Barron JL, Fleet DJ, Beauchemin SS (1994) Systems and experiment performance of optical flow techniques. Int J Comput Vis 12(1):43–77

Birkill A (2024) Stawamus chief webcam. https://chiefcam.com

Black RF (1976) Periglacial features indicative of permafrost: ice and soil wedges. Quat Res 6(1):3–26. https://doi.org/10.1016/0033-5894(76)90037-5

Blayney T, Dupont-Nivet G, Najman Y, Proust J, Meijer N, Roperch P, Sobel ER, Millar I, Guo Z (2019) Tectonic evolution of the Pamir recorded in the Western Tarim Basin (China): Sedimentologic and magnetostratigraphic analyses of the Aertashi section. Tectonics 38(2):492–515. https://doi.org/10.1029/2018TC005146

Bolch T, Gorbunov AP (2014) Characteristics and origin of rock glaciers in northern Tien Shan (Kazakhstan/Kyrgyzstan). Permafr Periglac Process 25(4):320–332. https://doi.org/10.1002/ppp.1825

Bolch T, Marchenko S (2009) Significance of glaciers, rockglaciers and ice-rich permafrost in the northern Tien Shan as water towers under climate change conditions. IHP UNESCO. https://doi.org/10.5167/uzh-137250

Brunet M-F, Sobel ER, McCann T (2017) Geological evolution of central Asian basins and the western Tien Shan range. Geol Soc Lond, Spec Publ 427(1):1–17. https://doi.org/10.1144/SP427.17

Bürgmann R, Hilley G, Ferretti A, Novali F (2006) Resolving vertical tectonics in the San Francisco Bay Area from permanent scatterer InSAR and GPS analysis. Geology 34(3):221. https://doi.org/10.1130/G22064.1

Casagli N, Intrieri E, Tofani V, Raspini F (2023) Landslide detection, monitoring and prediction with remote-sensing techniques. Nat Rev Earth Environ 4:51–64. https://doi.org/10.1038/s43017-022-00373-x

Chen JM (1996) Evaluation of vegetation indices and a modified simple ratio for boreal applications. Can J Remote Sens 22(3):229–242. https://doi.org/10.1080/07038992.1996.10855178

Cosentino A, Brunetti A, Mazzanti P (2024) Photomonitoring as a tool for monitoring landslides: a technology within everyone's reach. Transp Res Rec 2024:03611981241270173. https://doi.org/10.1177/03611981241270173

Coughlan B, Sampaleanu C, Williams-Jones G, Stead D (2023) Rockfall instability on high granitic domes: Stawamus chief, B.C., Canada. In: 15th ISRM congress 2023 & 72nd geomechanics colloquium. Schubert & Kluckner

Farnebäck G (2003) Two-frame motion estimation based on polynomial expansion. In: Lecture notes in computer science (including subseries lecture notes in artificial intelligence and lecture notes in bioinformatics), vol 2749. Springer, Berlin, pp 363–370. https://doi.org/10.1007/3-540-45103-X_50/COVER

Ferretti A (2014) Satellite InSAR data: reservoir monitoring from space (EET 9). EAGE Publications bv. https://bookshop.eage.org/product/satellite-insar-data-reservoir-monitoring-from-space-eet-9/

Ferretti A, Colombo D, Fumagalli A, Novali F, Rucci A (2015) InSAR data for monitoring land subsidence: time to think big. Proc Int Assoc Hydrol Sci 372:331–334. https://doi.org/10.5194/piahs-372-331-2015

Ferretti A, Fumagalli A, Novali F, Prati C, Rocca F, Rucci A (2011) A new algorithm for processing interferometric data-stacks: SqueeSAR. IEEE Trans Geosci Remote Sens 49(9):3460–3470. https://doi.org/10.1109/TGRS.2011.2124465

Ferretti A, Monti-Guarnieri A, Prati C, Rocca F, Massonnet D (2007) InSAR principles: guidelines for SAR interferometry processing and interpretation. ESA Publications, pp 1–48. TM-19. ISBN 92-9092-233-8

Fobert M-A, Singhroy V, Spray JG (2021) InSAR monitoring of landslide activity in dominica. Remote Sensing 13:815. https://doi.org/10.3390/rs13040815

Guthrie RH, Friele P, Allstadt K, Roberts N, Evans SG, Delaney KB, Roche D, Clague JJ, Jakob M (2012) The 6 august 2010 mount meager rock slide-debris flow, Coast Mountains, British Columbia: characteristics, dynamics, and implications for hazard and risk assessment. Nat Hazards Earth Syst Sci 12(5):1277–1294. https://doi.org/10.5194/nhess-12-1277-2012

Haberkorn A, Kenner R, Noetzli J, Phillips M (2021) Changes in ground temperature and dynamics in mountain permafrost in the Swiss Alps. Front Earth Sci 9:1. https://doi.org/10.3389/feart.2021.626686

Haeberli W, Hallet B, Arenson L, Elconin R, Humlum O, Kääb A, Kaufmann V, Ladanyi B, Matsuoka N, Springman S, Mühll DV (2006) Permafrost creep and rock glacier dynamics. Permafr Periglac Process 17(3):189–214. https://doi.org/10.1002/ppp.561

Handwerger AL, Huang M-H, Fielding EJ, Booth AM, Bürgmann R (2019) A shift from drought to extreme rainfall drives a stable landslide to catastrophic failure. Sci Rep 9(1):1569. https://doi.org/10.1038/s41598-018-38300-0

Harris C (2005) Climate change, mountain permafrost degradation and geotechnical hazard. Springer, Dordrecht, pp 215–224. https://doi.org/10.1007/1-4020-3508-X_22

Hermle D, Gaeta M, Krautblatter M, Mazzanti P, Keuschnig M (2022) Performance testing of optical flow time series analyses based on a fast. High-Alpine Landslide Remote Sensing 14(3):455. https://doi.org/10.3390/rs14030455

Javier S, Meinhardt-Llopis E, Facciolo G, Sánchez Pérez J, Meinhardt-Llopis E, Facciolo G (2013) TV-L1 optical flow estimation. Image Processing On Line 3(2):137–150. https://doi.org/10.5201/ipol.2013.26

Jibson RW (2013) Models of the triggering of landslides during earthquakes. In: Landslides. Cambridge University Press, Cambridge, pp 196–206. https://doi.org/10.1017/cbo9780511740367.018

Kääb A, Strozzi T, Bolch T, Caduff R, Trefall H, Stoffel M, Kokarev A (2021) Inventory and changes of rock glacier creep speeds in Ile Alatau and Kungöy ala-too, northern Tien Shan, since the 1950s. Cryosphere 15(2):927–949. https://doi.org/10.5194/tc-15-927-2021

Kim D, Balasubramaniam AS, Gratchev I, Kim SR, Chang SH (2020) Application of image quality assessment for rockfall investigation. In: 16th Asian Regional Conference on Soil Mechanics and Geotechnical Engineering, ARC 2019. http://seags.ait.asia/16arc-proceedings/16arc-proceedings/

Kim DH, Gratchev I (2021) Application of optical flow technique and photogrammetry for rockfall dynamics: a case study on a field test. Remote Sens 13(20):1–17. https://doi.org/10.3390/rs13204124

Komatsu T (2016) Cenozoic tectonic evolution of the Pamir: a review. J Geography (Chigaku Zasshi) 125(5):661–698. https://doi.org/10.5026/jgeography.125.661

Kummert M, Bodin X, Braillard L, Delaloye R (2021) Pluri-decadal evolution of rock glaciers surface velocity and its impact on sediment export rates towards high alpine torrents. Earth Surf Process Landf 46(15):3213–3227. https://doi.org/10.1002/esp.5231

Liu G, Zhao L, Li R, Wu T, Jiao K, Ping C (2017) Permafrost warming in the context of step-wise climate change in the Tien Shan Mountains. China Permafrost Periglacial Processes 28(1):130–139. https://doi.org/10.1002/ppp.1885

Liu Q, Liu Q, Liu Y, Gao S, Yang T, Luo Y, Jin Z (2008) Magnetic study of mafic granulite xenoliths from the Hannuoba basalt, North China. Geochem Geophys Geosyst 9(6):n/a-n/a. https://doi.org/10.1029/2008GC001952

Louis L, Wong TF, Baud P (2007) Imaging strain localization by X-ray radiography and digital image correlation: deformation bands in Rothbach sandstone. J Struct Geol 29(1):129–140. https://doi.org/10.1016/j.jsg.2006.07.015

Lowe DG (2004) Distinctive image features from scale-invariant Keypoints. Int J Comput Vis 60(2):91–110. https://doi.org/10.1023/B:VISI.0000029664.99615.94

Ma P, Cui Y, Wang W, Lin H, Zhang Y (2021) Coupling InSAR and numerical modeling for characterizing landslide movements under complex loads in urbanized hillslopes. Landslides 18:1611–1623. https://doi.org/10.1007/s10346-020-01604-2

Mathews WH, Monger JWH (2005) Roadside geology of southern British Columbia. Mountain Press, p 403

McCormick N, Lord J (2010) Digital image correlation. Mater Today 13(12):52–54. https://doi.org/10.1016/S1369-7021(10)70235-2

Moro M, Saroli M, Stramondo S, Bignami C, Albano M, Falcucci E, Gori S, Doglioni C, Polcari M, Tallini M, Macerola L, Novali F, Costantini M, Malvarosa F, Wegmüller U (2017) New insights into earthquake precursors from InSAR. Sci Rep 7(1):1–11. https://doi.org/10.1038/s41598-017-12058-3

Muhammad M, Williams-Jones G, Stead D, Tortini R, Falorni G, Donati D (2022) Applications of image-based computer vision for remote surveillance of slope instability. Front Earth Sci 10(June):1–22. https://doi.org/10.3389/feart.2022.909078

Müller J, Vieli A, Gärtner-Roer I (2016) Rock glaciers on the run—understanding rock glacier landform evolution and recent changes from numerical flow modeling. Cryosphere 10(6):2865–2886. https://doi.org/10.5194/tc-10-2865-2016

O'donovan P (2005) Optical flow: techniques and applications. Int J Comput Vis 2005:1–26

Palubinskas G (2014) Mystery behind similarity measures mse and SSIM. 2014. In: IEEE International Conference on Image Processing (ICIP). IEEE, pp 575–579. https://doi.org/10.1109/ICIP.2014.7025115

Pan B, Li K (2011) A fast digital image correlation method for deformation measurement. Opt Lasers Eng 49(7):841–847. https://doi.org/10.1016/J.OPTLASENG.2011.02.023

Raspini F, Bianchini S, Ciampalini A, Del Soldato M, Solari L, Novali F, Del Conte S, Rucci A, Ferretti A, Casagli N (2018) Continuous, semi-automatic monitoring of ground deformation using Sentinel-1 satellites. Sci Rep 8(1):7253–7253. https://doi.org/10.1038/s41598-018-25369-w

RGIK (2023) Guidelines for inventorying rock glaciers. RGIK. https://doi.org/10.51363/unifr.Srr.2023.002

Roberti G, Ward B, van Wyk de Vries B, Friele P, Perotti L, Clague JJ, Giardino M (2018) Precursory slope distress prior to the 2010 mount meager landslide. British Columbia Landslides 15(4):637–647. https://doi.org/10.1007/s10346-017-0901-0

Sampaleanu CIA (2017) The role of intact rock fracture in Rockfall initiation by. https://summit.sfu.ca/item/17771

Scheiber R, Jager M, Prats-Iraola P, De Zan F, Geudtner D (2014) Speckle tracking and interferometric processing of TerraSAR-X TOPS sata for mapping nonstationary scenarios. IEEE J Selected Top Appl Earth Observ Remote Sensing 8(4):1709–1720. https://doi.org/10.1109/JSTARS.2014.2360237

Sorg A, Kääb A, Roesch A, Bigler C, Stoffel M (2015) Contrasting responses of central Asian rock glaciers to global warming. Sci Rep 5(1):1–6. https://doi.org/10.1038/srep08228

Srokosz PE, Bujko M, Bocheńska M, Ossowski R (2021) Optical flow method for measuring deformation of soil specimen subjected to torsional shearing. Measurement 174:1–27. https://doi.org/10.1016/j.measurement.2021.109064

Streletskiy D, Anisimov O, Vasiliev A (2015) Permafrost degradation. In: Snow and ice-related hazards, risks, and disasters. Elsevier, pp 303–344. https://doi.org/10.1016/B978-0-12-394849-6.00010-X

Strozzi T, Caduff R, Jones N, Barboux C, Delaloye R, Bodin X, Kääb A, Mätzler E, Schrott L (2020) Monitoring rock glacier kinematics with satellite synthetic aperture radar. Remote Sens 12(3):559. https://doi.org/10.3390/rs12030559

Sun Q, Zhang L, Ding XL, Hu J, Li ZW, Zhu JJ (2015) Slope deformation prior to Zhouqu, China landslide from InSAR time series analysis. Remote Sens Environ 156(December):45–57. https://doi.org/10.1016/j.rse.2014.09.029

Suriñach E, Vilajosana I, Khazaradze G, Biescas B, Furdada G, Vilaplana JM (2005) Seismic detection and characterization of landslides and other mass movements. Nat Hazards Earth Syst Sci 5(6):791–798. https://doi.org/10.5194/nhess-5-791-2005

TRE Altamira (2018) TRE ALTAMIRA InSAR products—handbook. TRE-ALTAMIRA

Tuckey ZS (2012) An integrated field mapping-numerical modelling approach to Characterising discontinuity persistence and intact rock bridges in large open pit slopes. Simon Fraser University. https://summit.sfu.ca/item/12708

Verma, P., Verma, K., Singh, A., Sundaram, A. K., & Bramhe, V. S. (2023). Real-time vehicle detection and tracking system using Cascade classifier and background subtractor. Springer, Cham 431–441. https://doi.org/10.1007/978-981-19-7892-0_34

Warrick JA, Ritchie AC, Schmidt KM, Reid ME, Logan J (2019) Characterizing the catastrophic 2017 Mud Creek landslide,

California, using repeat structure-from-motion (SfM) photogrammetry. Landslides 16(6):1201–1219. https://doi.org/10.1007/s10346-019-01160-4

Wei M, Sandwell D, Smith-Konter B (2010) Optimal combination of InSAR and GPS for measuring interseismic crustal deformation. Adv Space Res 46(2):236–249. https://doi.org/10.1016/j.asr.2010.03.013

Yan Y, Li T, Liu J, Wang W, Su Q (2019) Monitoring and early warning method for a rockfall along railways based on vibration signal characteristics. Sci Rep 9(1):6606. https://doi.org/10.1038/s41598-019-43146-1

Zhang Y, Meng XM, Dijkstra TA, Jordan CJ, Chen G, Zeng RQ, Novellino A (2020) Forecasting the magnitude of potential landslides based on InSAR techniques. Remote Sens Environ 241(March):111738. https://doi.org/10.1016/j.rse.2020.111738

Zimmer VL, Sitar N (2015) Detection and location of rock falls using seismic and infrasound sensors. Eng Geol 193:49–60. https://doi.org/10.1016/j.enggeo.2015.04.007

Monitoring and Characterization of Surface Movements in Rock Slopes

Tommaso Carlà, Tommaso Beni, Luca Lombardi, Massimiliano Nocentini, and Giovanni Gigli

Abstract

Surface movements in rock slopes may evolve at widely different rates (from millimeters per year to meters per second) and be the expression of widely different instability mechanisms (from detachment and fall of individual rock blocks to deep-seated gravitational slope deformations). The past two decades have seen a significant push in the development of remote sensing, close-range, and conventional geotechnical techniques to better deal with this variability and enhance the assessment of related slope hazards. As a result, comprehensive monitoring and characterization of rock slope movements may now be achieved even in complex scenarios and at fine scales, provided that the appropriate techniques are used. Building on the experience acquired by the engineering geology research group at the University of Florence (Italy), this paper briefly highlights a series of case studies—including kinematic analysis of potential rock slope movements as well as detection of ongoing "slow" and "very rapid" rock slope movements—which illustrate how important insights may be gained with different techniques according with the site-specific characteristics of the investigated hazard. It is shown that a more holistic view can generally be obtained using a combined approach, overcoming the limitations inherent to each single technique. Future developments should primarily concern optimizing the interoperability and compatibility between the large sets of output data, which would ultimately facilitate their manipulation from end-users and the derivation of informed decision-making.

Keywords

Rock slopes · Rock slope failure · Rockfall · Landslide monitoring · Remote sensing · Radar interferometry

1 Introduction

Rock slope movements exhibit considerable variability in terms of scale, evolutionary behavior, and velocity, making them a significant challenge in landslide hazard assessment and management. They include a broad spectrum of failure mechanisms, such as rockfalls, toppling, planar and wedge failures, translational and rotational sliding, and deep-seated gravitational slope deformations. Each of these landslide types can be influenced by structural and tectonic setting, lithological properties, internal shearing, tendency to disaggregation, and sensitivity to external triggers such as seismic activity, weathering, and hydrological forcing.

This heterogeneity highlights the need for deploying a range of remote sensing, close-range, and conventional geotechnical techniques tailored to the characteristics of each rock slope. Remote sensing techniques generally refer to tools that do not require physical contact with the investigated area and can be deployed via satellite or ground-based platforms, both of which are widely used in landslide studies. For instance, satellite-based remote sensing has been increasingly applied in landslide studies, with advancements in technology since the 2000s improving the quality of data through enhanced algorithms and the deployment of satellites with higher resolution and more frequent data acquisition (Mondini et al. 2021; Novellino et al. 2024); terrestrial laser scanning has become a standard tool for detecting and mapping slope instabilities (Jaboyedoff et al. 2012; Abellán et al. 2014; Francioni et al. 2018), with new sensors having recently been developed also to perform ground-based and

Award Memorial Article: Oldrich Hungr Award 2023

T. Carlà (✉) · T. Beni · L. Lombardi · G. Gigli
Department of Earth Sciences, Università degli Studi di Firenze, Florence, Italy
e-mail: tommaso.carla@unifi.it

M. Nocentini
Center for Civil Protection, Università degli Studi di Firenze, Florence, Italy

B. Abolmasov et al. (eds.), *Progress in Landslide Research and Technology, Volume 4 Issue 1, 2025*, Progress in Landslide Research and Technology, https://doi.org/10.1007/978-3-031-89836-5_9

drone-based dynamic acquisitions; other techniques, such as interferometric synthetic aperture radar, can be based on both satellite and ground-based platforms, allowing for highly precise measurements of slope surface displacements (Casagli et al. 2010, 2023; Wasowski and Bovenga 2022). Since the introduction of remote sensing techniques, the ability to map landslides over large areas, gain insights into their mechanisms and kinematics, and generate big data for early-warning systems has improved dramatically (Casagli et al. 2023). Among the various types of landslides, rockfalls and rock slope movements at a relatively small scale may also be monitored and characterized effectively by close-range topographic surveying and contact measurement instrumentation such as wire extensometers, crackmeters, and tiltmeters. In contrast, large-scale phenomena, ranging from rockslides/rock topples to deep-seated, more complex landslides, often are also suited to the use of satellite-based interferometric synthetic aperture radar, ground-based interferometric synthetic aperture radar, and geodetic monitoring (e.g., permanent or manually surveyed GNSS stations and robotic total stations), which may in turn be combined with subsurface methods such as inclinometers and piezometers to capture deformation and groundwater patterns at depth.

This paper briefly reviews a series of case studies to illustrate how different techniques (or different combinations of techniques) may be suitable to observe different types of rock slope movements and failure mechanisms. The presented case studies are derived from over a decade of experience acquired by the engineering geology research group at the University of Florence (Italy). This team provides scientific support to the Italian Department of Civil Protection and the UNESCO Chair on Prevention and Sustainable Management of Geo-Hydrological Hazards for the assessment, management, and mitigation of landslide hazards. Activities have often been carried out in scenarios where rock slope movements posed significant threats to local communities and infrastructure. The selected case studies demonstrate how different approaches may be effective across a variety of scenarios; they also underline the importance of a site-specific, multi-disciplinary assessment of rock slope hazards, depending on aspects such as failure mechanism, magnitude, and rate of movement.

The paper is structured as follows: the first section addresses the characterization of potential rock slope movements through kinematic analysis based on point-cloud data, which provides probabilistic insights into the spatial distribution of areas subject to block detachment leading to rockfall. Then, a section examining monitoring and characterization of "slow" rock slope movements is divided into three further subsections:

- the first subsection focuses on ground-based radar interferometry, which may be applied to a variety of contexts, from rockfall hazards at a relatively small scale to large-scale rock slope movements;
- the second subsection addresses satellite interferometry, which is mostly suitable to large-scale movements on steep (not sub-vertical) rock slopes and is particularly effective when integrated with its ground-based counterpart;
- the third subsection discusses how conventional geotechnical sensors and repeat topographic surveying, used in combination with interferometric data, may provide additional insights especially into complex, vegetated terrains where differential block movements occur.

In the third section, the focus shifts finally to monitoring and characterization of "very rapid" rock slope movements using ground-based Doppler radar.

The terms "slow" and "very rapid", with reference to the renowned landslide velocity classification system (Cruden and Varnes 1996; Hungr et al. 2014), are herein used in an extended manner to generally include the range of velocities from extremely slow to moderate velocities and from very rapid to extremely rapid velocities, respectively (Table 1).

Table 1 Landslide velocity classification system proposed by Cruden and Varnes (1996)

Classes	Description	Velocity (m/s)
7	Extremely rapid	5
6	Very rapid	$5{\cdot}10^{-2}$
5	Rapid	$5{\cdot}10^{-4}$
4	Moderate	$5{\cdot}10^{-6}$
3	Slow	$5{\cdot}10^{-8}$
2	Very slow	$5{\cdot}10^{-10}$
1	Extremely slow	$<5{\cdot}10^{-10}$

2 Characterization of Potential Rock Slope Movements

The geometrical characterization, or kinematic analysis, of rock slopes is aimed at assessing the predisposition to structurally controlled block instability. This goal can be achieved efficiently by using a high-resolution three-dimensional model of the investigated rock slope composed of millions of points with (x, y, z) coordinates. Over the last decade, kinematic analysis has become one of the most commonly used approaches for identifying structurally controlled instabilities, such as wedge and plane failures, block toppling, and flexural toppling (Gigli and Casagli 2011; Menegoni et al. 2019; Battulwar et al. 2021). This can be exploited to pinpoint the areas of a slope prone to block detachment, but does not provide temporal predictions; rather, a probabilistic assessment of where these phenomena are comparatively more likely to occur due to the slope orientation and rock mass structure.

Block detachment leading to rockfall poses significant hazards in mountainous regions, rock-carved cultural heritage sites and surface mining operations, with scales ranging from small rock fragments to localized rock mass failures. Managing these hazards relies on understanding both the whereabouts and timing of rockfall triggering, though predicting the latter is extremely challenging. Many studies thus focus on the concept of "rockfall susceptibility" to identify the source location of possible events.

The geometric arrangement of rock discontinuities primarily dictates failure mechanisms, with susceptibility often expressed in terms either of factors of safety or the kinematic feasibility of block movement. Topographic surveying tools like terrestrial and dynamic laser scanning (TLS and DLS, respectively) are nowadays commonly used to create high-resolution three-dimensional models of rock slopes, capturing both terrain morphology and key discontinuity properties at a local scale (Abellán et al. 2014; Carlà et al. 2024a). These technologies, often combined with digital photogrammetry derived from unmanned aerial vehicles (UAV-DP), have proven invaluable in large, dangerous, or otherwise inaccessible scenarios where traditional scanline surveys are not possible (Sturzenegger and Stead 2009; Mao et al. 2021; Beni et al. 2022). Discontinuities can be mapped either on polygonal meshes or directly on point cloud data. In this sense, several algorithms have been developed to semi-automatically extract discontinuity planes and key discontinuity properties (Gigli and Casagli 2011; Vöge et al. 2013; Riquelme et al. 2015, 2018; Matasci et al. 2018). One of these routines is called DiAna-K, which also incorporates a full-three dimensional derivation of kinematic analysis principles—i.e., with explicit consideration of overhanging geometries of the rock face—based on the outputted orientation and roughness of the detected discontinuity planes (Gigli et al. 2022). Probabilistic context is provided by coupling iteratively each mesh element of the rock slope model with the orientation of each mapped discontinuity, intersection of discontinuities, or possible combination thereof. It is therefore assumed that any mapped discontinuity and intersection of discontinuities may daylight at a given point of the rock face. Local susceptibility to plane failure, wedge failure, block toppling, and flexural toppling is consequently expressed by the relative amount of features theoretically able to satisfy the associated kinematic requirements. A global kinematic index (GKI) is also calculated to express the overall susceptibility to rockfalls, regardless of failure mechanism (Gigli et al. 2022). Practical use of DiAna-K has been well illustrated by two case studies, one to assess instabilities on a rock slope equipped for sport climbing in Italy and the other at a rock-carved cultural heritage site in the Kingdom of Saudi Arabia. Both cases relied on the acquisition of high-resolution point clouds from TLS and UAV-DP surveys (Figs. 1 and 2).

The first case study involves a steep rock wall located 5 km N of Florence which, as often occurs in Italy, has been equipped for rock climbing in a decommissioned quarry (Beni et al. 2022; Gigli et al. 2022). The quarry face, historically used to extract ornamental stones, exposes a sequence of foredeep turbidites belonging to the Macigno Formation, a feldspathic graywacke. This formation consists of alternating coarse-grained arenaceous layers and thin, sporadic layers of finer grained pelitic deposits, typical of the Tuscan Succession in the Northern Apennines. The lithological heterogeneity of the site is further increased by slumping and syn-sedimentary tectonics. In 2014, a ~120 m^3 rockfall affected several climbing routes, making it ideal for creating a rockfall susceptibility map with DiAna-K. Results highlighted the importance of properly addressing the subvertical nature of rock walls; in fact, while the kinematic feasibility of wedge and flexural toppling failure was found to be comparatively dominant over most portions of the surveyed face, in absolute terms the highest hazard was attributed to plane mechanisms potentially originating from highly steep areas of limited extent. This kind of distinction, often related to the presence of small-scale overhangs, may not be obtained from traditional methods of rockfall hazard assessment that employ airborne-based digital elevation models. In general, visual inspection of the rock face revealed that multiple feasible mechanisms of failure, conspicuous rock mass damage, and freshly exposed rockfall scars could be discerned in areas of high GKI.

Another illustrative example is provided by the Hegra Archaeological Site (al-Hijr/Madāʾin Ṣāliḥ), the first UNESCO World Heritage area inscribed in the Kingdom of Saudi Arabia in 2008. The site features over 110 monumental tombs carved into sandstone, attracting hundreds of tourists daily. Due to its composition and mineralogical assemblage, the Quweira Sandstone, in which the tombs were carved, is susceptible to weathering processes like cavernous weathering, also known as cavernous rock decay. Cavernous weathering encompasses a variety of alteration features and erosion patterns (e.g., tafoni, alveoli, honeycombs) that vary in scale from millimeters to several meters and pose significant challenges for the conservation of the site as well as public safety, as they increase rockfall hazard and contribute to the deterioration of the ancient tomb facades through material loss, exfoliation, and fissures (Whabi 2014; Gallego et al. 2022; Beni et al. 2023). Kinematic analysis was thus performed to assess the location of potential instabilities. Results were then integrated with explainable artificial intelligence to semi-automatically detect cavernous weathering features using three-dimensional data obtained from UAV-DP surveys (Beni et al. 2023). The results indicated a good spatial correlation between GKI and areas impacted by cavernous weathering; this suggested that, in similar lithologies and settings, the

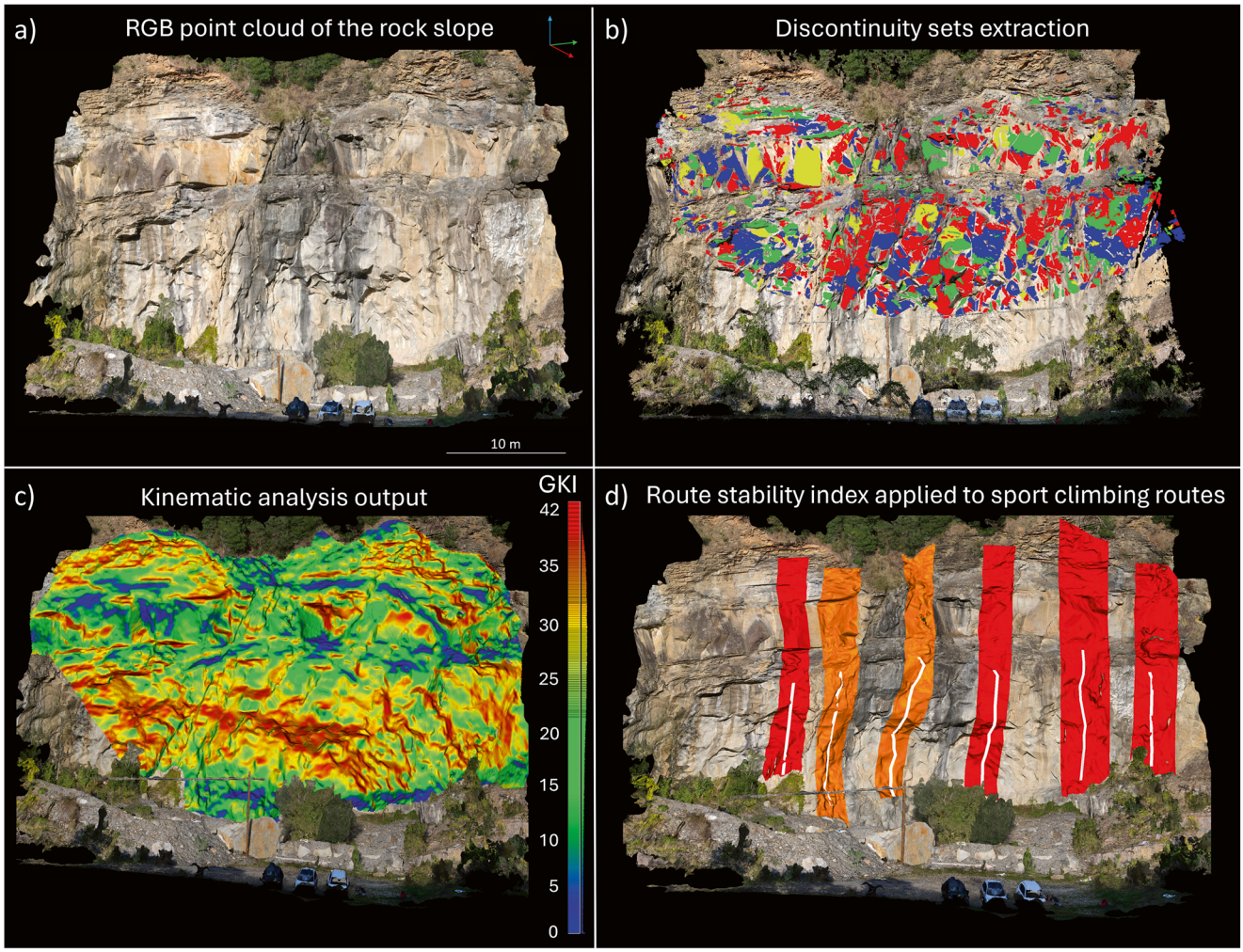

Fig. 1 Geometric characterization of the rock slope at a decommissioned quarry near Florence (Italy) by combined TLS and UAV-DP: (**a**) RGB-textured point cloud; (**b**) extraction of discontinuity sets by means of the DiAna-K routine (Gigli et al. 2022); (**c**) results of kinematic analysis expressed in terms of GKI; (**d**) practical application of the results to compute the Route Stability Index (RSI), used to assess the stability of each analysed sport climbing route. (After Beni et al. 2022)

output of kinematic analysis may also be a proxy for the weathering state of the rock slope. In particular, instability was found to primarily affect overhanging sectors with high GKI values and cavernous weathering activity (Figs. 2e–f), with potential block sizes determined by hollow dimensions—larger cavities corresponding to higher potential rockfall volumes and often involving vaults, ribs or thin walls between alveoli.

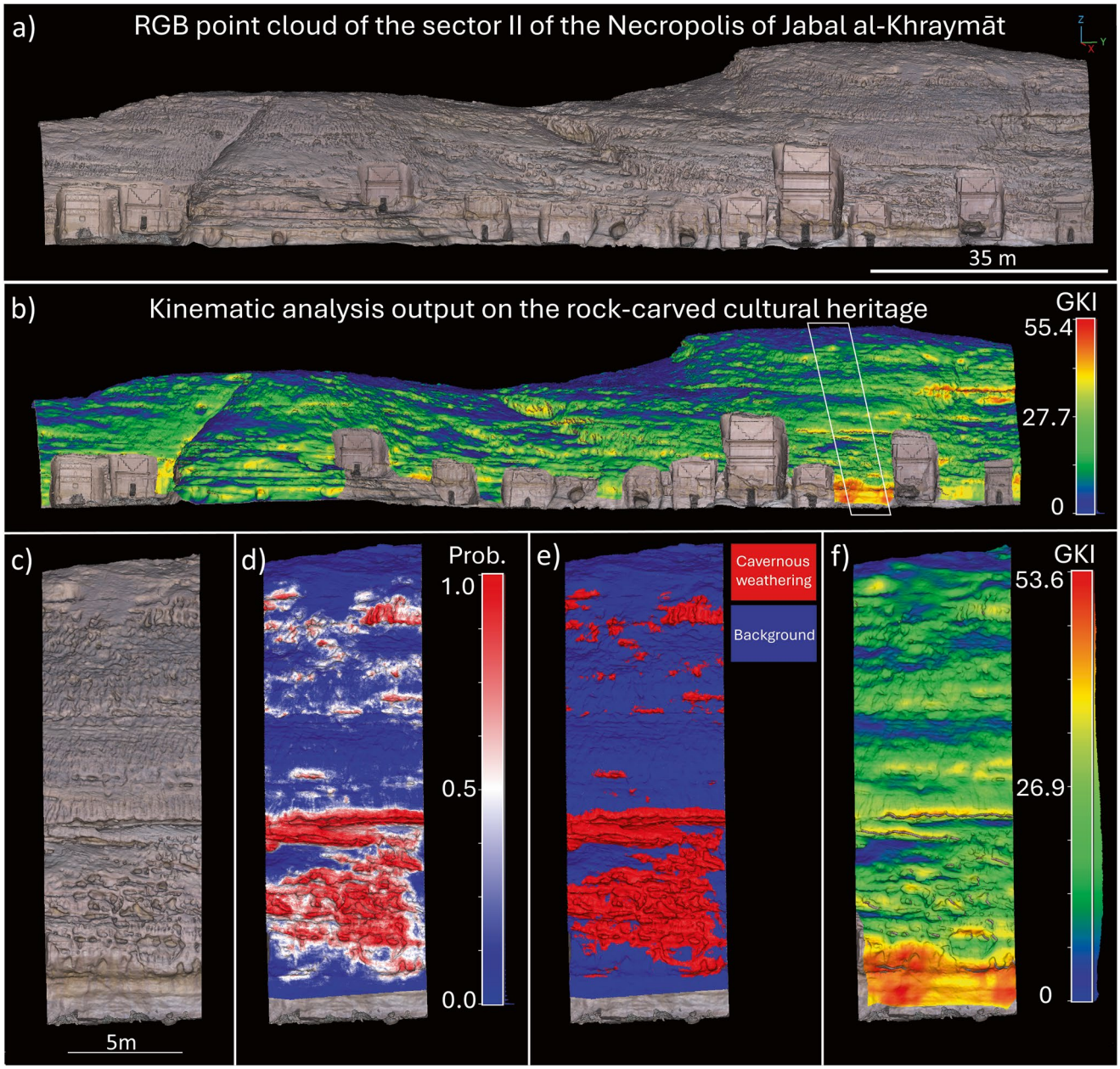

Fig. 2 Characterization of the rock-carved archaeological site of Hegra (Saudi Arabia) by combined UAV-DP (after Beni et al. 2023): (**a**) RGB-textured point cloud of Sector II of the Necropolis of Jabal al-Khraymāt; (**b**) results of kinematic analysis expressed in terms of GKI; (**c**–**f**) detail of the RGB-textured polygonal mesh of the rock slope, probability map derived from Random Forest modelling to predict the occurrence of cavernous weathering, classification of Random Forest modelling results based on a 0.5 probability threshold, and estimated GKI

3 Monitoring and Characterization of "Slow" Rock Slope Movements

Slow movements in rock slopes may represent a precursor to sudden movement, disaggregation, and associated large landslide displacements, thus posing significant risks to exposed infrastructure and public safety.

The development of Synthetic Aperture Radar (SAR) has revolutionized our ability to detect and analyse these subtle displacements. SAR systems, as active remote sensing instruments, provide their own illumination, enabling data acquisition independently of daylight and weather conditions. This ability is crucial for continuous monitoring applications in regions susceptible to landslides. SAR images are composed of pixels defined by amplitude and phase values: the phase component is particularly significant, as it may reflect changes in sensor-to-target distance caused by movement of the ground. Among the spaceborne applications, approaches based on multi-temporal interferometry

(MTInSAR) enhance the robustness of displacement measurements by analysing extensive stacks of co-registered SAR images (Wasowski and Bovenga 2014, 2022; Solari et al. 2020). These methods allow the identification of measurement points that exhibit stable radar signatures over time, facilitating the assessment of surface displacements with high temporal and spatial resolution. However, spaceborne applications are not rarely constrained by fixed acquisition parameters and topography-induced shadowing, which may limit signal reflection from potentially unstable areas. Ground-based interferometric synthetic aperture radar (GBInSAR) has emerged as a cutting-edge complementary tool, providing near-real-time monitoring capabilities for localized areas. These systems can achieve sub-millimetric precision and are comparatively less affected by atmospheric disturbance, making them particularly effective for monitoring slow movements.

In addition to these remote sensing techniques, the integration with conventional geotechnical sensors and repeat topographic surveying can further enhance our ability to assess slow movements. Conventional sensors, such as wire extensometers, crackmeters, tiltmeters, and GNSS stations offer high-resolution measurements of displacement or rotation over time. These tools can provide detailed insights into the mechanisms of slow and complex surface movements, complementing the broader spatial coverage offered by MTInSAR and GBInSAR technologies. Repeat topographic surveying by TLS or DLS may also allow detailed mapping and analysis of three-dimensional deformation at a high resolution; these techniques can in fact capture intricate topographical changes as well as rigid differential block deformation. By combining conventional geotechnical sensors and repeat topographic surveying with MTInSAR and GBInSAR, a comprehensive understanding of slow complex movements may eventually be achieved.

The presented case studies demonstrate the practical application of these advanced technologies in monitoring and characterization of slow movements across diverse landslide types; each case briefly summarizes the methodologies employed, the specific challenges addressed, and the implications for hazard assessment and management.

3.1 GBInSAR

GBInSAR systems typically operate in Ku-band (central frequency ~17 GHz) and move along a mechanical linear rail to create a synthetic aperture. Distance (range) and direction (azimuth) of the targets (i.e., pixels) are attained through transmission and reception of the electromagnetic wave. In principle, line-of-sight (LOS) displacements are calculated with sub-millimetric accuracy by exploiting the phase difference of the back-scattered signal between two or more coherent acquisitions, and by assessing the contribution that actually stems from the ground movement (Leva et al. 2003; Luzi et al. 2006; Casagli et al. 2010; Atzeni et al. 2015). A displacement time series can then be extracted from each pixel. No artificial reflectors on the slope are required, assuming that some parts of the area of interest are stable and exploitable for minimizing atmospheric contributions. As the availability of large sets of images enables the application of averaging and ad hoc statistical tools, the technique is scarcely affected by atmospheric noise and has proved to be suitable for analyzing the evolution of rock slope movements even in high alpine terrain (Noferini et al. 2007; Del Ventisette et al. 2012; Kieffer et al. 2016; Barla et al. 2017). Since a certain degree of customization is typically available for selecting critical parameters such as the angle of view, the bandwidth of the transmitted signal, the length of the mechanical linear rail, and the frequency of measurement acquisition, GBInSAR systems may achieve spatial resolutions in the order of a few m^2 or less, allowing detection of rock slope movements at fine scales.

Illustrative examples of this capability are the rockfall precursors detected over the steep anorthositic slopes of an undisclosed open-pit mine (Carlà et al. 2017) and at the top of the granitic cliff above the sanctuary of Gallivaggio in the Central Italian Alps (Carlà et al. 2019a). These cases are significant because inappropriate sampling rates may return seemingly instantaneous displacements that are not meaningful to perform reliable failure-time predictions. Given its characteristics, the GBInSAR technique provides a very efficient way of dealing with this problem.

The open-pit cases are highly representative of such "brittle" slope failures: with volumes ranging between ~500 m^3 and ~1500 m^3, it was demonstrated that tertiary creep may affect also rock slopes in very hard rock masses, though, importantly, it was observed to evolve on a scale of just minutes to hours (Fig. 3). This has obvious repercussions in terms of the frequency of measurement acquisition and reference interval of the data processing that are needed in order to successfully predict such failures and provide appropriate notice for the implementation of the necessary response actions and evacuation procedures. Adding to this topic, another interesting finding was the ability to separately characterize the observed failures from another set of events that, although showing accelerating displacements, ultimately did not evolve into failure ("non-failures"). By comparing detected peak velocities and accelerations, it was determined that the observed failures were anticipated by significantly larger values of these two parameters, in the order of several cm/h and cm/h^2, respectively.

At Gallivaggio, GBInSAR monitoring was used as an operational early-warning tool to manage the risks posed by rockfalls on a road and the buildings of a sanctuary located at the base of a ~500 m high granitic cliff. In particular, traffic

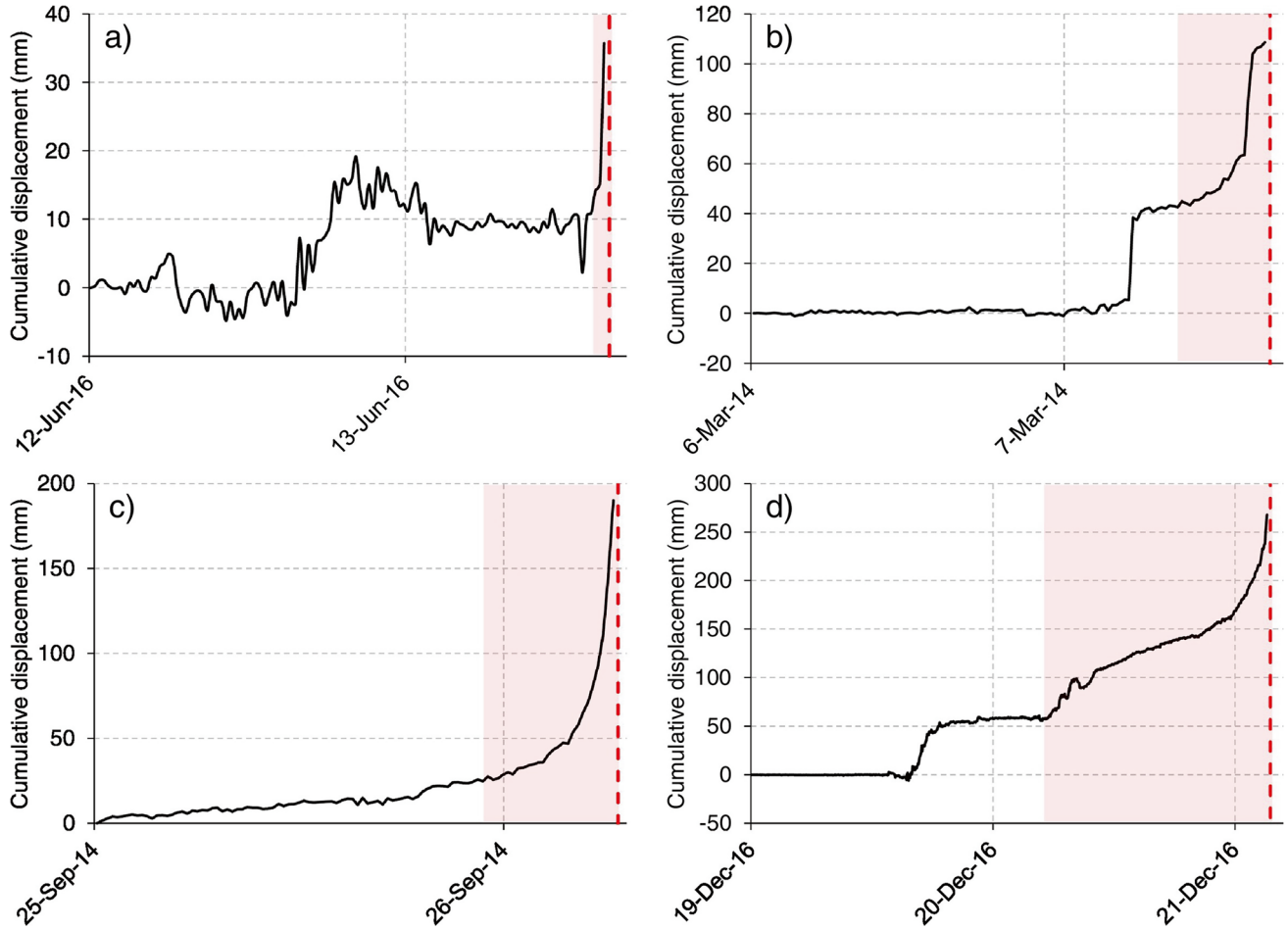

Fig. 3 Raw displacement time series of failures (**a**) #1, (**b**) #2, (**c**) #3, and (**d**) #4 reported in Carlà et al. (2017). The red dashed lines mark the failure-time of each event, while the red shaded areas highlight the final increment of displacement leading to failure. (From Carlà et al. 2017)

was regulated by a sequence of alert thresholds representative of increasing risk scenarios, with special attention devoted to a ~5000 m^3 highly fractured portion of rock mass at the top of the cliff. Since the beginning of the monitoring campaign in 2017, the GBInSAR data highlighted a 30 × 35 m deforming sector corresponding to the cited portion of rock mass (Fig. 4). Displacements finally started to escalate on the morning of 29 May 2018, with velocities gradually climbing up to about 7 cm/h at 4 pm; afterwards, the appearance of interferometric fringes related to phase wrapping testified the persistence of the acceleration and the imminence of the failure (Fig. 5). In light of the prompt identification of this final tertiary creep stage, a precise failure-time prediction was obtained by means of the inverse velocity method and the area was evacuated with appropriate notice (Carlà et al. 2019a).

GBInSAR monitoring is more widespread and more easily implemented in the case of large and complex rock slope movements, which, as opposed to rockfalls, may evolve to failure following an extended period (weeks to years) of well-detectable displacements. In this sense, while conventional geotechnical instruments may also capture variations of activity, they cannot provide the same type of spatially distributed information; moreover, they are subject to damage and/or exceedance of the maximum measurement range in highly active landslides. A remarkable illustrative example is the Ruinon landslide, a "translational rock-debris slide" (as per the definition of Glastonbury and Fell 2008) where the marked tendency for disaggregation of the phyllitic bedrock gives rise to the simultaneous, more or less interdependent deformation and sliding of different layers of rock and debris (Carlà et al. 2021). Between the late spring and the early summer of 2019, the landslide experienced a significant change of behavior and attained exceptional rates of surface displacement (often exceeding 1 m/day), which lasted for several months despite ultimately not developing into sudden movement and large-scale collapse (Fig. 6). Proper hazard assessment was hindered by the large extent of the slide area and by the fact that borehole logging and installation

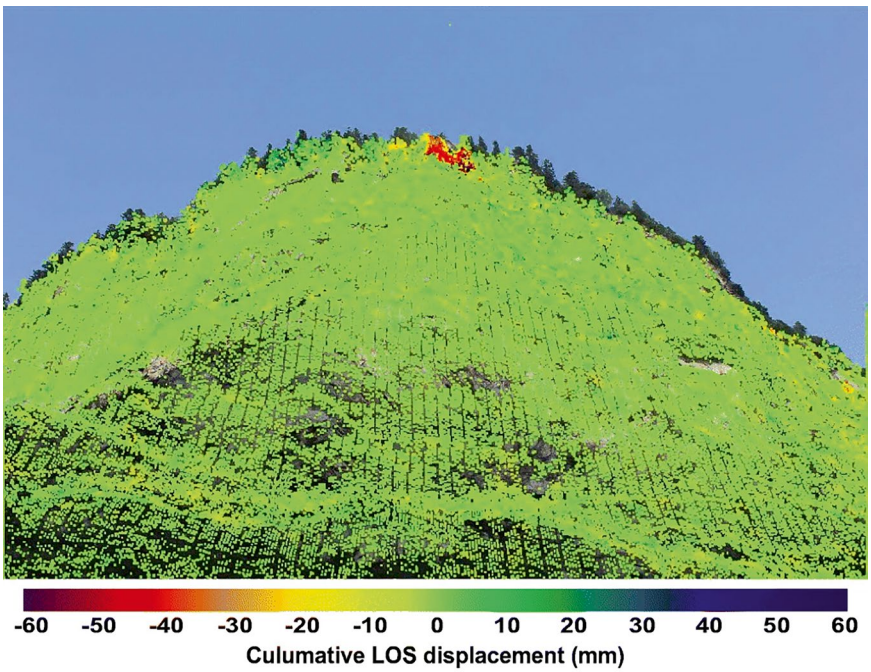

Fig. 4 Map of cumulative LOS displacements measured by the GBInSAR system at Gallivaggio in the period 13–26 April 2018, superimposed on an optical image taken from the look perspective of the instrument. Gray areas over the slope correspond to the parts of the optical image (i.e., rock surface) with no return signal. (From Carlà et al. 2019a)

of inclinometer casings had long been prevented by the continuing large displacements.

The availability of a unique 11-year long GBInSAR dataset allowed to reconstruct the remarkable evolution of the slope both in space and time, yielding additional insights into its deformation behavior. In particular, displacement measurements served as the basis to infer the thickness of the more active layer of upper chaotic debris through balanced cross-sections (Aryal et al. 2015). Importantly, activity across the entire slide area was confirmed to be closely and similarly correlated with seasonal peaks in piezometric levels (Fig. 7). The measured displacement field also served as a basis to constrain a finite-element analysis of the slope, which suggested the existence of a strikingly non-linear vertical velocity profile from slide base up to the surface modulated by groundwater recharge. In spite of the high variability of material composition, morphology, and activity, each sector in which the slide was divided appeared to share comparable relative trends of surface displacement—and thus the same underlying driving mechanism. The experience gained at Ruinon highlights that the implementation of long-term GBInSAR monitoring is especially essential in the case of highly disaggregated rock slopes that, being subject to recurrent reactivations and associated large displacements, would otherwise be difficult to investigate because of the inaccessibility of the site.

3.2 MTInSAR

MTInSAR usually exploits L-, C-, or X-band frequencies, whereby radar signals are transmitted and received by satellites along ascending or descending orbits to create a synthetic aperture. Range and azimuth coordinates of electromagnetically coherent targets (generally referred to as "persistent scatterers") are obtained by using radar pulse timing and phase data. LOS displacements are calculated down to a sub-millimetric accuracy by analysing the phase difference between different satellite passes over the same area and, similarly to GBInSAR, by isolating the contribution stemming from movement of the ground (Ferretti et al. 2001; Hanssen 2005; Wasowski and Bovenga 2014; Crosetto et al. 2016). A critical feature of MTInSAR is its ability to generate displacement time series for each "natural" measuring point without the need for artificial reflectors. This assumption holds true as long as certain areas within the scene are stable, which allows for reducing atmospheric noise effects (Colesanti and Wasowski 2006). Among the several types of processes that can be investigated with MTInSAR, large, slow-moving, and E-W facing landslides in high alpine environments are particularly well-suited to use of the technique. While significant challenges still remain for operational early-warning and time-to-failure predictions (Carlà et al. 2019b), MTInSAR has in fact proved decisive in the

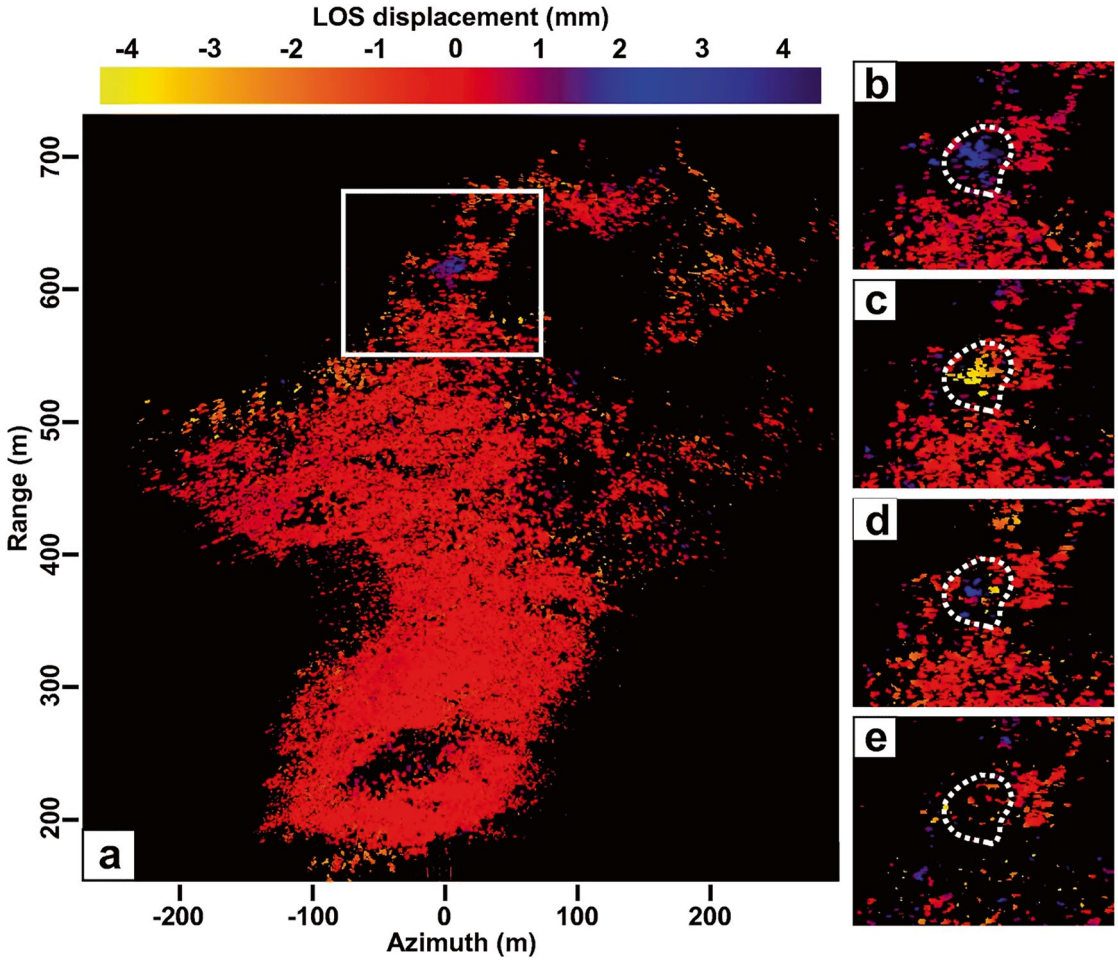

Fig. 5 Two-minute interferograms of the Gallivaggio cliff between 4:08 p.m. and 4:34 p.m. (local time) on 29 May 2018. The white rectangle in (**a**) delimits the area magnified in (**b**–**e**); the dotted polygons in (**b**–**e**) delimit the area affected by failure. In detail: (**a**) 4:08–4:10 p.m.: no wrapped phase; (**b**) 4:10–4:12 p.m.: increase of displacement, no wrapped phase; (**c**) 4:18–4:20 p.m.: wrapped phase (one fringe); (**d**) 4:25–4:27 p.m.: wrapped phase (two fringes); (**e**) 4:32–4:34 p.m.: failure, with general loss of coherence due to detachment of material and formation of a cloud of dust overshadowing the slope. Range and azimuth are the sensor-to-target distance and the direction parallel to the synthetic aperture, respectively. (From Carlà et al. 2019a)

characterization of such phenomena, helping to overcome issues related to the difficult accessibility of mountainous terrains.

One classical example is represented by the Bosmatto landslide, a highly disaggregated rockslide in metamorphic rock in the Western Italian Alps (Carlà et al. 2019c). Here, the availability of a large number of measuring points over the slide area in both ascending and descending orbit (Fig. 8) allowed decomposition of the recorded displacement into its E-W and vertical components. This information was then compared with displacement measurements from a group of seven GNSS stations, which made it possible to infer a gradual rotation of the dip angles of movement from slide head to toe in accordance with a broadly roto-translational mechanism, involving a volume of approximately 2.5–3.5 × 10^6 m^3. The reconstructed geometry of the slide was also found to be compatible with the location of a heavily brecciated layer at depths between ~30 and 40 m in the only borehole that was drilled on the slide area, which therefore may be interpreted as the active basal zone of shear.

Two other highly illustrative case studies are represented by the Quincinetto landslide (Carlà et al. 2024a) and another undisclosed open-pit mine (Carlà et al. 2018). The former is located on the steep eastern flank of the lower Aosta Valley (Northwest Italy), approximately 600 m above the valley floor (Fig. 9a). The slope presumably collapsed during a retreat phase of the former Dora Baltea Glacier, which dates back to the boundary between Early–Middle Pleistocene. The event (together with subsequent secondary rockfalls) produced a large talus cone extending down to the valley floor. The slide source area was left covered by a chaotic and highly disaggregated mass of large angular metamorphic blocks, some of which stopped precariously close to the abrupt increase in slope steepness that marks the transition

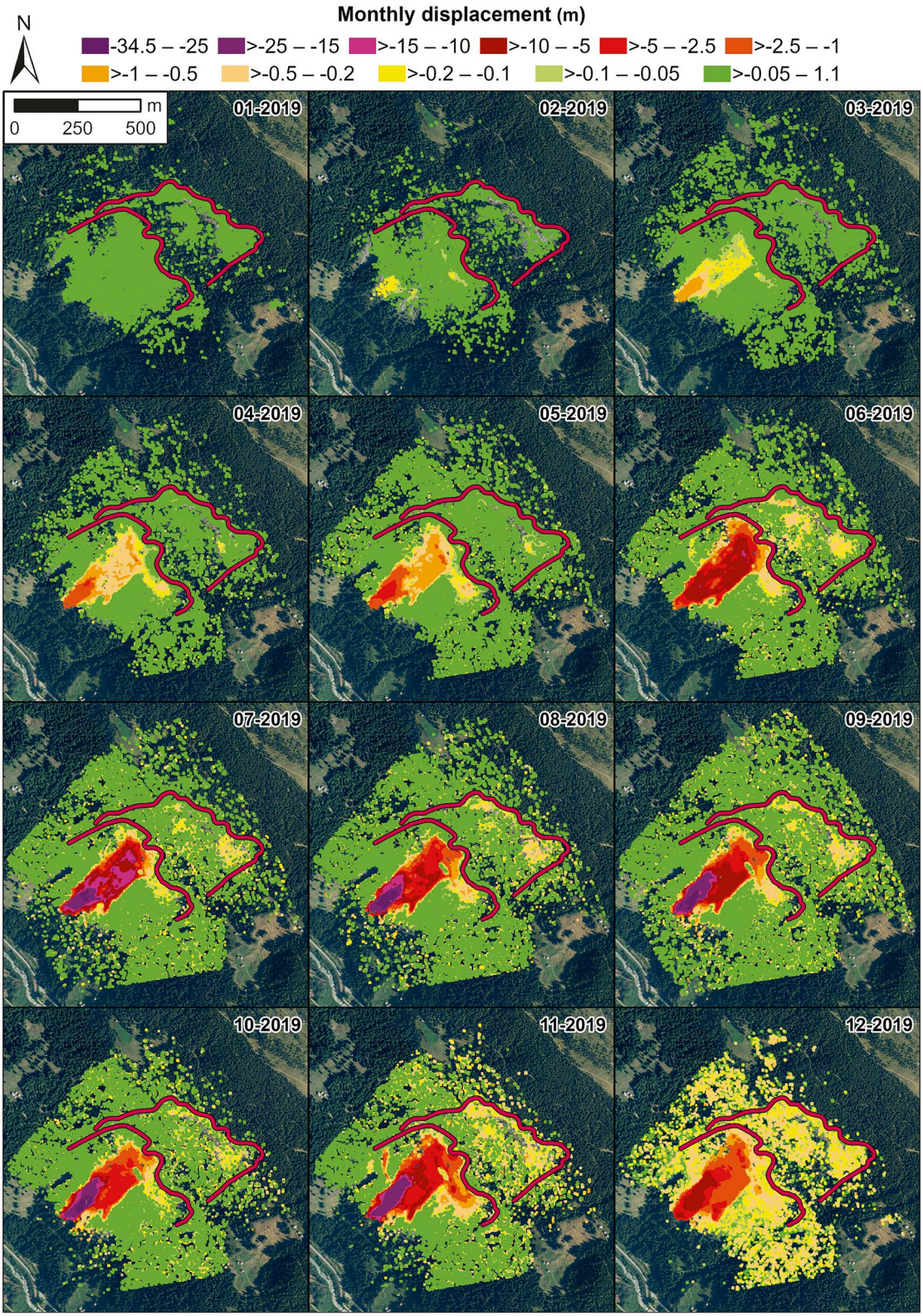

Fig. 6 Monthly cumulative displacements measured by the GBInSAR system at the Ruinon landslide from January to December 2019. (From Carlà et al. 2021)

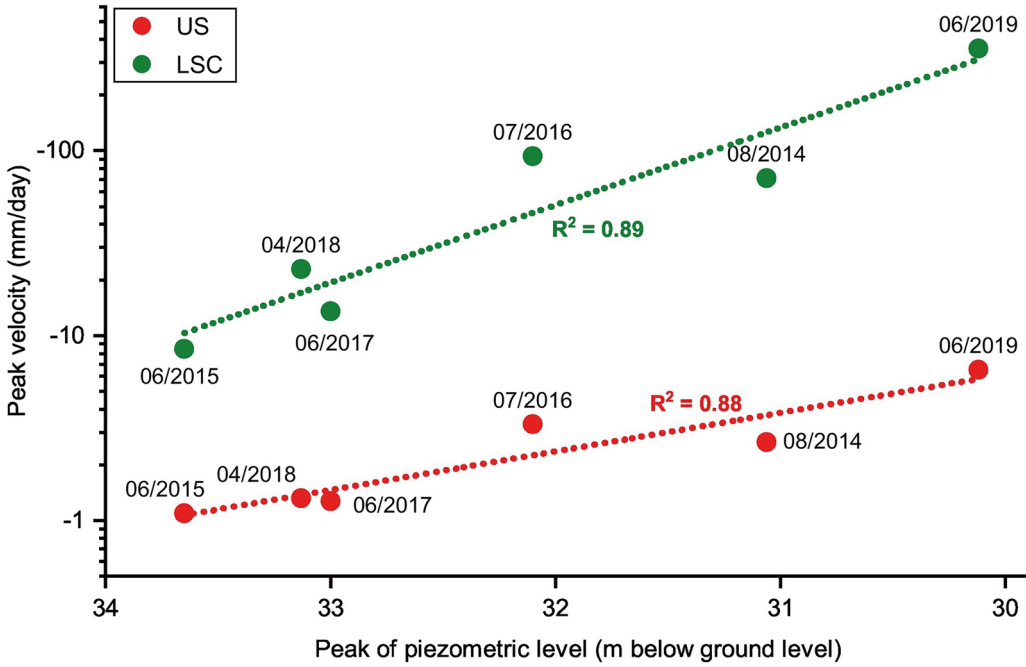

Fig. 7 Correlation between peak surface velocities of the Ruinon landslide (*US* upper scarp, *LSC* lower scarp) and peaks of piezometric level recorded each year during the spring/summer reactivation period. (From Carlà et al. 2021)

between the toe of the slide and the apex of the talus cone (Fig. 9b). Continued movements of the slope have been prompting further destabilization of these frontal blocks, which may slide/topple out of their position and fall at extremely rapid velocity along the talus cone. In the 1960s, construction of the northern branch of the Turin-Aosta A5 highway was commenced to create a high-capacity connection with the Mont Blanc and Great St. Bernard tunnels at the Italy–France and Italy–Switzerland borders. The highway route was unknowingly located tangentially to the distal edge of the talus cone formed by the Quincinetto landslide. In May 2012, a ~45 m^3 rockfall travelled within a few meters from the road, making it necessary to implement detailed monitoring and investigations. In particular, coupling MTInSAR and GBInSAR data was instrumental into unraveling the twofold deformation behavior of the slide. As a GBInSAR system was in fact installed in the valley floor, marked variations of displacement activity of two large rock blocks at the slide toe—each with volume in excess of a thousand cubic meters— were captured over a 3-year period, resulting in a maximum total displacement of roughly 0.5 m (Carlà et al. 2024a); however, no visibility could be obtained of the upper slopes due to the rugged topography. On the other hand, even though MTInSAR data yielded no information over the slide toe due to excessively large displacements and associated loss of temporal coherence, they allowed highly detailed measurement of the slower movements spreading over the rest of the slide area and delimitation of the corresponding slide boundaries, with estimated velocities around roughly constant values in the order of a few centimeters per year (Fig. 9c).

The significance of the second open-pit mine case stems from the fact that MTInSAR and GBInSAR datasets were jointly exploited for a retrospective analysis of an unexpected large slope failure (Carlà et al. 2018). Several casualties were counted in consequence of the incident, the main reason being the impossibility to perceive its actual proportions from the poor spatial coverage that could be obtained over the unstable area by GBInSAR monitoring. In fact, most of the slide source area was located above the upper limit of the open-pit mine, outside the extent of radar images; moreover, data were disturbed by the noise induced by mining operations. On the other hand, MTInSAR monitoring was not affected by such limitations, as the overview looking geometry meant that there were no shadow areas above the pit crest (Fig. 10); moreover, they provided the first clear example of slope tertiary creep leading to failure captured with the technique in an open-pit mine. Thanks to the large number of measuring points identified on the ground, tertiary creep was observed comprehensively across the entire slope sector that was eventually affected by the failure, and considerations on volume, development of the basal rupture surface, driving factor, and predictability of the failure were derived. The results indicated that the onset of instability likely began weeks earlier than GBInSAR alone could reveal, though this would have still offered clear advantages for

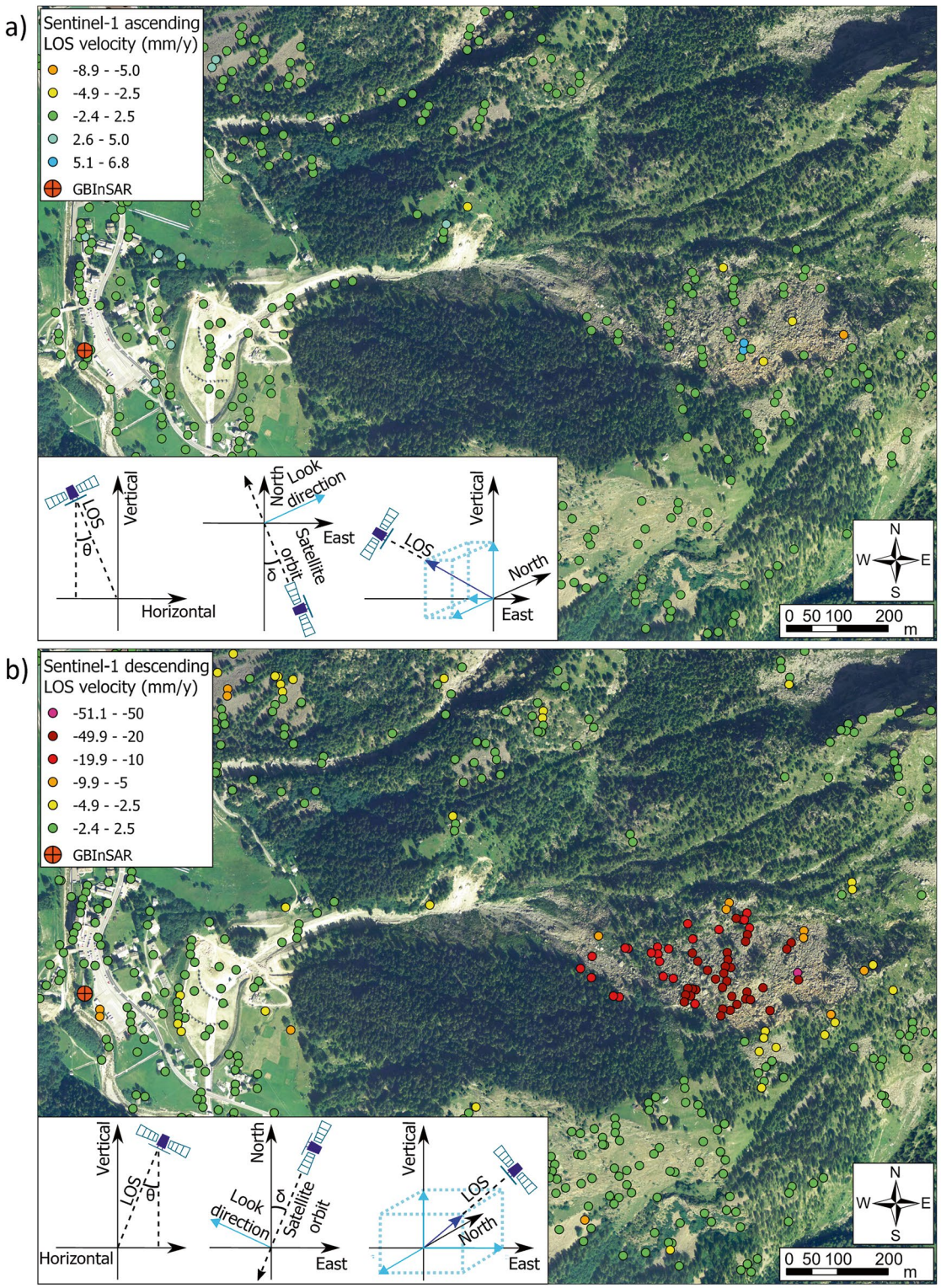

Fig. 8 MTInSAR data acquired in ascending (**a**) and descending (**b**) orbit over the Bosmatto landslide. (After Carlà et al. 2019c)

extrapolating accurate short-term predictions in a context of near real-time early-warning. Overall, the reported case studies highlight the importance that MTInSAR is combined with ground-based techniques to overcome limitations inherent to the frequency of measurement acquisition and the required temporal coherence of targets on the ground, thus enhancing characterization and monitoring of rock slope movements.

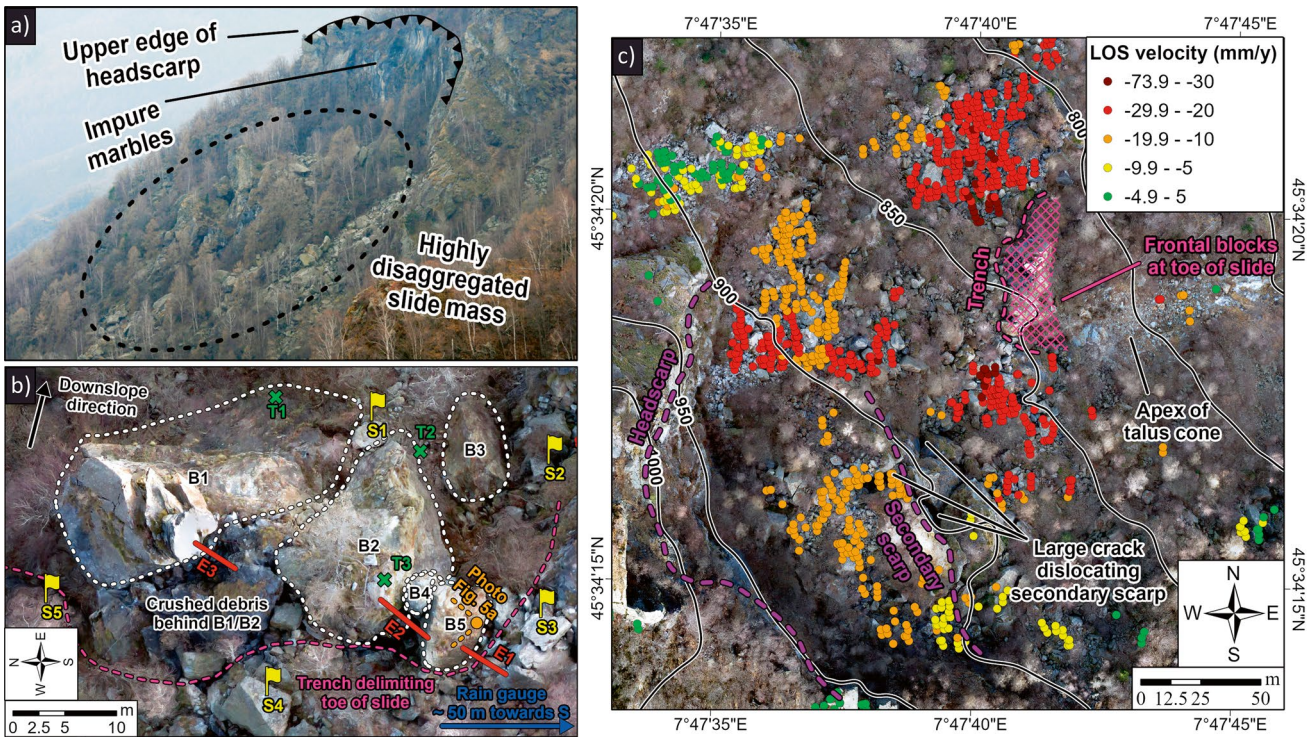

Fig. 9 (**a**) Oblique photograph of the Quincinetto landslide, outlining the ~50 m high sub-vertical headscarp and the highly disaggregated slide mass below; (**b**) detailed aerial view of the large rock blocks at the toe of the slide; and (**c**) aerial view of the slide source area. The background orthophoto in (**c**) is the product of a drone-based photogrammetric survey performed in March 2022 concurrently with a DLS survey (see next subsection). MTInSAR data acquired in ascending orbit by the Cosmo-SkyMed constellation were courtesy of TRE ALTAMIRA, with negative values denoting movement away from the satellite. (Modified from Carlà et al. 2024a)

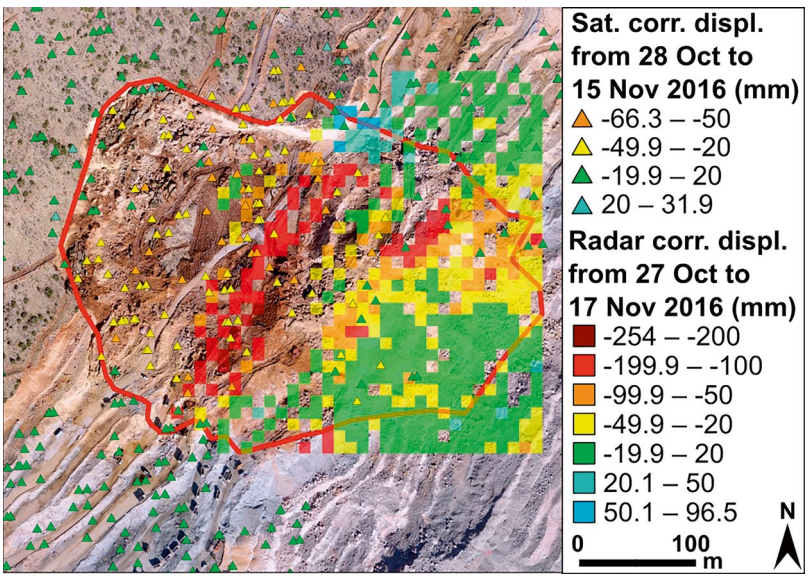

Fig. 10 Comparison between the spatial distribution of MTInSAR and resampled GBInSAR measurements acquired prior to an unexpected slope failure in an undisclosed open-pit mine, corrected according to the respective LOS sensitivity. (From Carlà et al. 2018)

3.3 Conventional Geotechnical Sensors and Repeat Topographic Surveying

While applicable to a variety of contexts, conventional geotechnical sensors and repeat topographic surveying may be especially useful to enhance monitoring and characterization of discrete rock blocks affected by rigid differential deformation on remote and densely vegetated slopes. In this regard, the Quincinetto landslide serves again as a remarkable example (Carlà et al. 2024a): in addition to the previously described interferometric campaigns, monitoring by a wireless network of conventional geotechnical sensors (e.g., wire extensometers and tiltmeters) and repeat topographic surveying by TLS and drone-based DLS were performed to enhance understanding of the kinematics and response to rainfall of the large rock blocks at the slide toe. Wire extensometers allowed detection of a distinct sequence of acceleration and deceleration phases (Fig. 11), with the intensity of the former being strictly promoted by rainfall and controlled by the background activity of the blocks (i.e., their instantaneous velocity at the onset of rainfall). This rate-weakening behavior was deemed evidence of basal slip along a through-going sub-planar joint, where available shear strength is controlled by water pressures and the age of frictional contacts; meaning that, as the latter decreases with renewed displacements, the predisposition to instability in response to additional rainfall inputs temporarily increases. Differential movements between the blocks were also assessed since lengthening and shortening of the cable were measured at different wire extensometers. Characterization of these differential movements was further improved by repeat close-range topographic surveying of the blocks; in

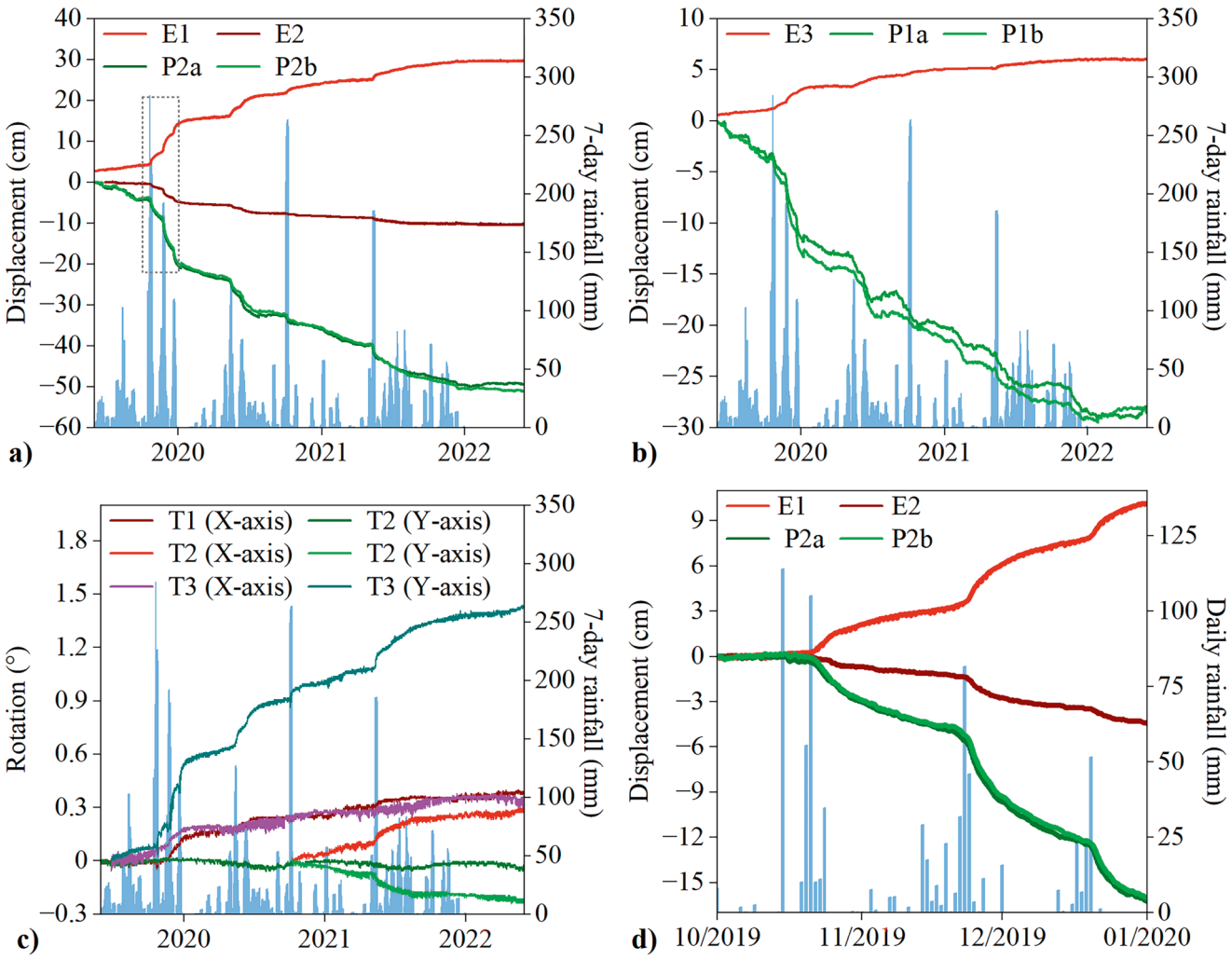

Fig. 11 (**a**, **b**) Measurements of displacement acquired by wire extensometers (E1, E2, and E3) and GBInSAR (P1a-b and P2a-b) at the toe of the Quincinetto landslide, along with measurements of rotation acquired by tiltmeters (**c**). The dashed black rectangle in (**a**) delimits the period of acceleration in late 2019 detailed in (d). In (**a**–**c**), rainfall measurements are cumulated on a weekly basis, whereas in (**d**) on a daily basis. (From Carlà et al. 2024a)

particular, two surveys were conducted, the first one (Fig. 12a) in September 2019 by use of a TLS sensor (model RIEGL VZ1000) from multiple viewpoints, and the second one (Fig. 12b) in March 2022 by use of a DLS sensor (model RIEGL VUX-1UAV) mounted on an ad hoc drone prototype (Rossi et al. 2018). The two point clouds were then co-registered by exploiting a group of stable tie points, and best-fitting planes were extracted from clusters of points belonging to coherent block faces. By observing how dip and dip direction of fitted planes changed between the two surveys, translational and rotational movements of individual blocks could be determined (Fig. 12c, d). Overall, the results made it possible to infer that ongoing block instability is promoted by a complex interplay of slow slope-scale deformation, local topography, and transient degradation of friction on a through-going basal rupture surface of varying roughness, likely associated with an outcropping sub-planar structure inclined ~35° on the apex of the adjacent talus cone. The two larger blocks at the slide toe were also interpreted to translate as mostly individual entities with negligible influence of brittle fracture damage, while a smaller adjacent block was found to be affected by significant clockwise rotation as seen in planimetric view. These types of investigation, more so when combined with interferometric monitoring, can be essential to reduce uncertainties related to the characterization of block instability in "highly data-limited" alpine rock slopes, providing a foundation for the development of hazard mitigation and control strategies.

4 Monitoring and Characterization of "Very Rapid" Rock Slope Movements

Certain types of landslides, such as rockfalls and debris flows, are characterized by a distinct lack of precursors. They initiate without significant accumulation of damage and deformation; moreover, many of their governing factors are of intrinsic stochastic nature. With specific reference to rockfalls, risk mitigation and control strategies are usually

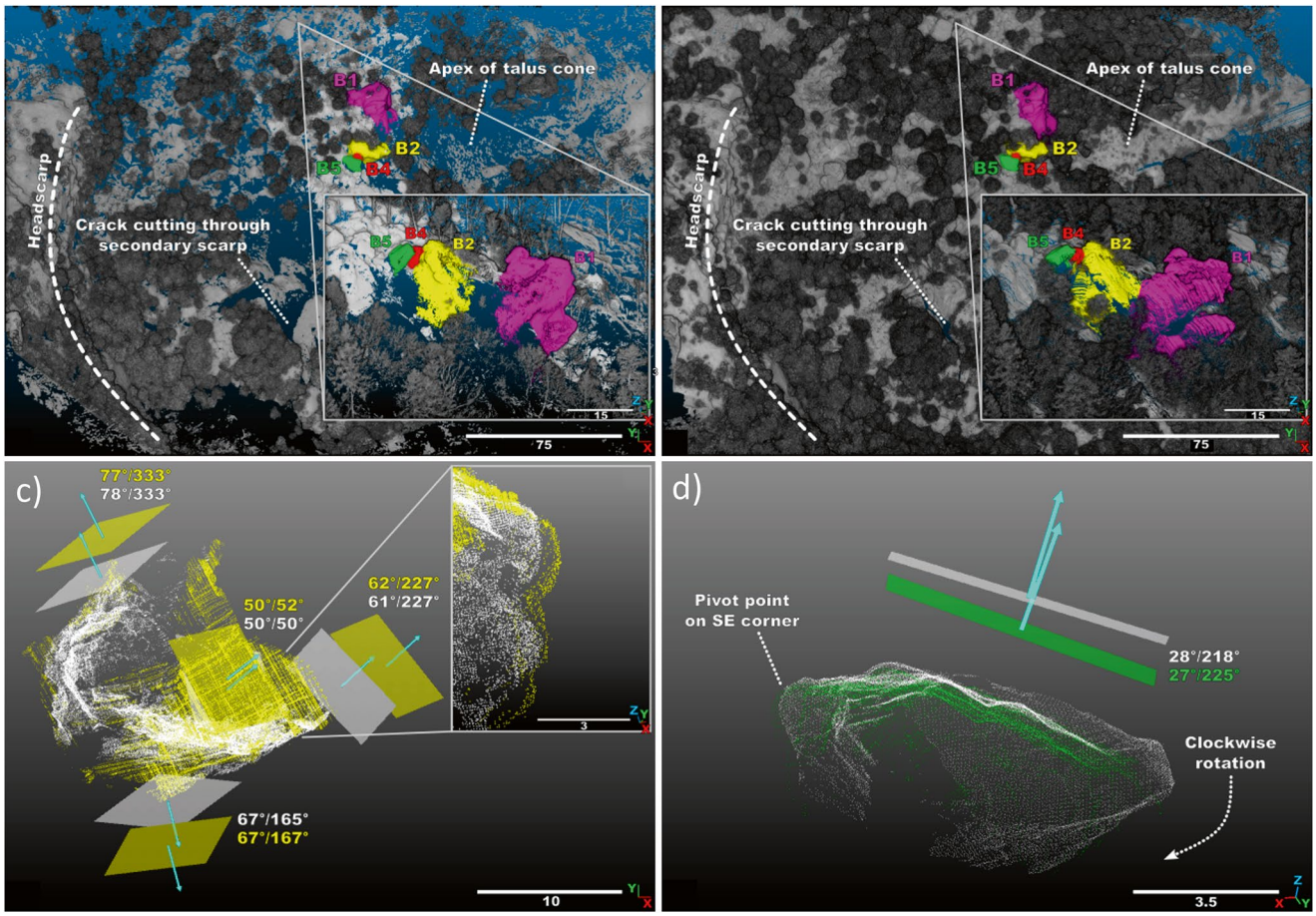

Fig. 12 (**a**) TLS-based and (**b**) DLS-based point cloud of the Quincinetto landslide, prior to removal of vegetation and co-registration. Four large blocks at the slide toe (B1, B2, B4, and B5) are depicted with distinct colors (B3 is hidden by vegetation at the base of B2). (**c**, **d**) Best-fitting planes derived from homologous clusters of points on the lateral and top sides of blocks B2 and B5. White points/planes/labels refer to the TLS survey and yellow ones to the DLS survey. (From Carlà et al. 2024a)

centred on the design of appropriate structural defences, either active or passive; when these are still not adequate to provide sufficient protection against every possible event size, they may be combined with ground-based Doppler radar monitoring of the slope to attain real-time detection and management of rockfall hazards. Justification for use of the technique derives from the discrete character of rockfall hazards affecting mountainous roads—either no rockfall is occurring and vehicles may safely travel along the segment of road at risk, or a rockfall is occurring and an exclusion zone should be enforced locally. In the latter case, provided that the expected travel time of rockfalls before impacting the road is sufficiently long, evacuation may effectively be achieved by stopping vehicles outside the boundaries of the potential runout area as soon as a rockfall initiates.

The main module of the system consists of an FMCW (Frequency-Modulated Continuous-Wave) Doppler radar operating in the X-band at a base frequency of 10 GHz and a bandwidth of 40 MHz (Carlà et al. 2024b). It is equipped with a transmitting antenna and two receivers to retrieve the angular position of the targets (i.e., pixels) through direction-of-arrival estimation. The transmitted and reflected signals have different frequencies because of the initial frequency modulation, which can be exploited to determine the distance (i.e., range) of a moving target with respect to the Doppler radar. An additional Doppler processing yields spectra of all moving targets within the field of view. Algorithms for classification of these spectra, developed on the basis of large training datasets from several rockfall sites (Meier et al. 2016), are iteratively run to distinguish movement from actual events while filtering the contribution of irrelevant sources (e.g., atmospheric effects, oscillation of tree crowns). Further refinement can be obtained by feeding data from events at the investigated site. The extent of the Doppler shift generated by a moving target is a complex function of the line-of-sight velocity, particle size distribution, and relative position of the rockfall. In broad terms, the instrument is normally run at a sensitivity that is suitable for spotting an object of ~1 m^3 moving at a distance of ~1 km at line-of-sight velocities of several meters per second. Detection occurs within seconds from the onset of the event. Final heat maps of Doppler shift "intensity" are georeferenced during post-processing by means of a GNSS unit to outline the area hit by the rockfall. This dimensionless parameter is proportional to the amplitude of the echo power from every moving target at every range and azimuth bin, integrated over the whole rockfall event. The central processing unit also communicates the real-time activation/deactivation of alarms (e.g., traffic lights, sirens, etc.) through dedicated output ports. The components must be mounted on a pole with a precast concrete base or similar fixed support. In principle, the technique may be extended to any extremely rapid landslide of the avalanche or flow type; however, calibration of the event detection threshold for hazard management of landslides other than rockfall (e.g., debris flows) would have to be adjusted on hitherto uncollected training datasets (Meier et al. 2016).

Due to its relatively recent development, high entailed costs, and narrower applicability with respect to other monitoring systems, case studies of long-term monitoring campaigns by ground-based Doppler radar are still rarely documented. Two significant examples of operational use of the technique with automatic activation of traffic lights are provided again by the Ruinon landslide (Carlà et al. 2024b) and the Brienz landslide (Schneider et al. 2023).

At Ruinon, another strong reactivation phase began in the summer of 2020, with similar intensity to that of 2019 described previously. Large displacements of the upper debris strongly promote the occurrence of rockfalls, as individual boulders ranging up to hundreds of cubic meters in volume can be rapidly dug out from below the ground surface; they may also create locally unstable slope geometries, leading to shallow slumps and more fragmental falls. This heavily impacts a road that runs down in the valley floor and enables vehicles to access the popular tourist town of Santa Caterina. Even though a 5 m high embankment bordered the segment of road at risk for rockfalls, large rolling boulders could build up sufficient kinetic energy to render any protective structure ineffective. A precedent was in this sense established in August 2019, when a ~65 m^3 block of rock landed on the road. On the other hand, the majority of rockfalls would be confined to higher slopes and stop before entering the catch ditch at the slope toe. Doppler radar monitoring of the highly active slide sector was thus implemented, and the system connected to two traffic lights via fiber-optic cabling. The field of view of the instrument was divided into a "region of interest" (ROI), corresponding to the debris-covered slopes from which rockfalls were most likely to originate, and a "danger zone" (DZ) at the slope toe. Since it could not be known a priori if a spotted falling object would eventually reach the road, the radar was programmed to switch the traffic lights to red at the instant the event detection threshold is first surpassed. A heat map of Doppler shift intensity is then produced once movement has ceased (Fig. 13), from which it is determined whether only the ROI or also the DZ has been affected by the rockfall. In the former case, the radar automatically switched the traffic lights back to green, minimizing traffic interruption; otherwise, a user-controlled reset was required pending appraisal of the integrity of the road and embankment. Authorities responsible for managing the road were informed of changes of status information via automated e-mail and short message service (SMS). A total of 60 rockfalls triggered an alarm between July and December 2020, and for each of them the system outputted an estimation of the timing, relative distance to the source area, duration, runout length, and average

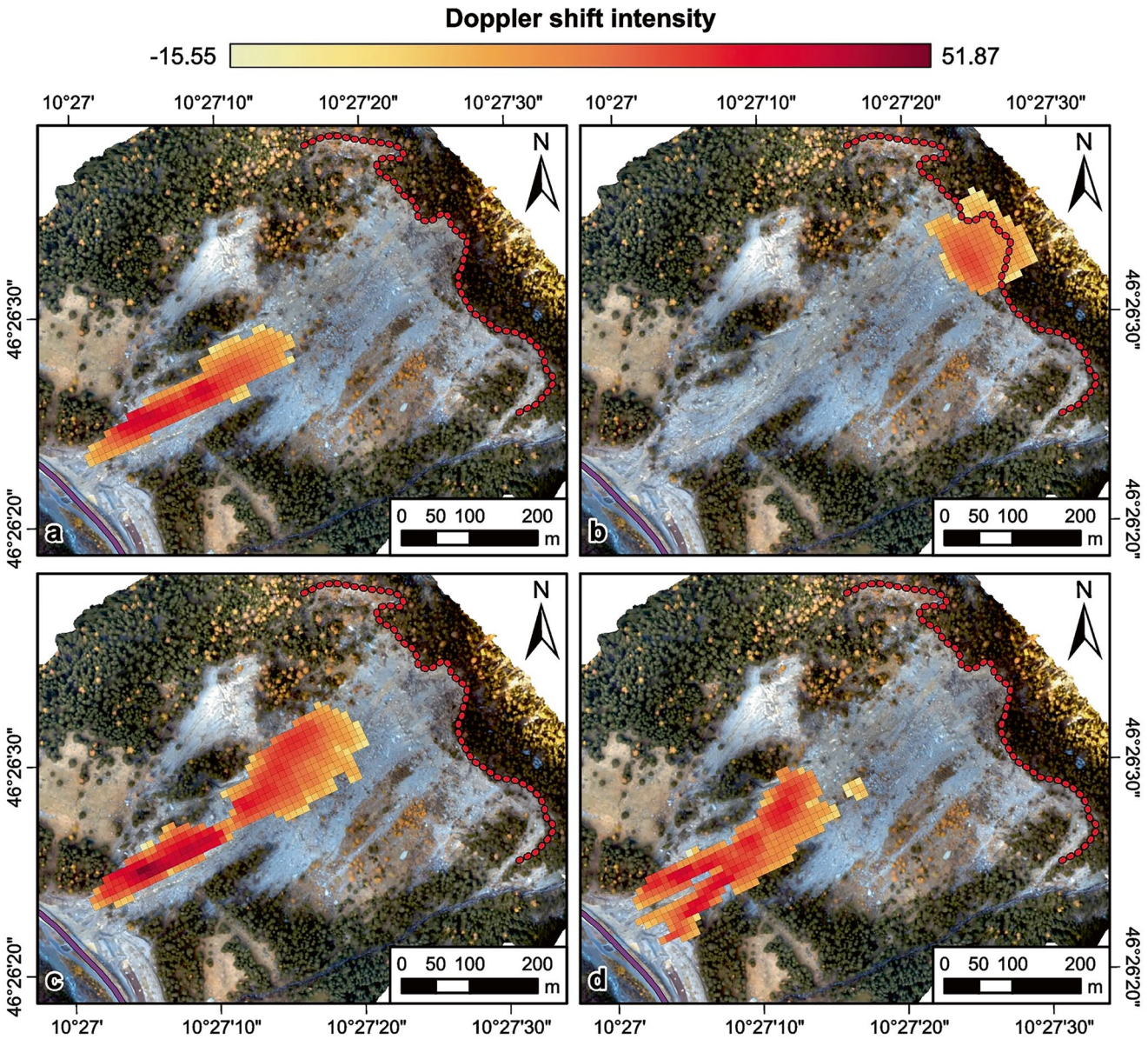

Fig. 13 Heat maps of Doppler shift intensity resulting from selected significant rockfalls occurred during the monitoring campaign at the Ruinon landslide (after Carlà et al. 2024b): (**a**) 27 July 2020; (**b**) 4 August 2020; (**c**) 12 September 2020; (**d**) 1 October 2020. The red dashed line and purple solid line define the lower scarp and the road to Santa Caterina, respectively. Note how the bifurcated trajectory of the 1 October 2020 rockfall is correctly captured by the heat map in (**d**)

velocity (Carlà et al. 2024b). Importantly, such information can also be instrumental into enhancing the calibration of rockfall runout models for hazard assessment and design purposes, as well as the quantitative evaluation of fluctuations in rockfall activity (Schneider et al. 2023).

5 Conclusions

The presented case studies highlight that current monitoring and characterization techniques—for a thorough description of which the reader is referred to other papers—allows for a comprehensive assessment of basically the full spectrum of rock slope movement mechanisms, from single-block to large instabilities; highly accurate spatial and temporal predictions of rock slope failures can also be attained if trends of precursory deformation are reasonably significant.

With specific reference to ground-based radar techniques (i.e., GBInSAR and Doppler radar), Casagli et al. (2023) underscored how these are already capable of covering much of the entire range of possible landslide velocities, with the only exception being the interval of velocities between approximately 10^{-4}–10^{0} m/s (corresponding to values between approximately 10 m/day and 1 m/s). Landslides

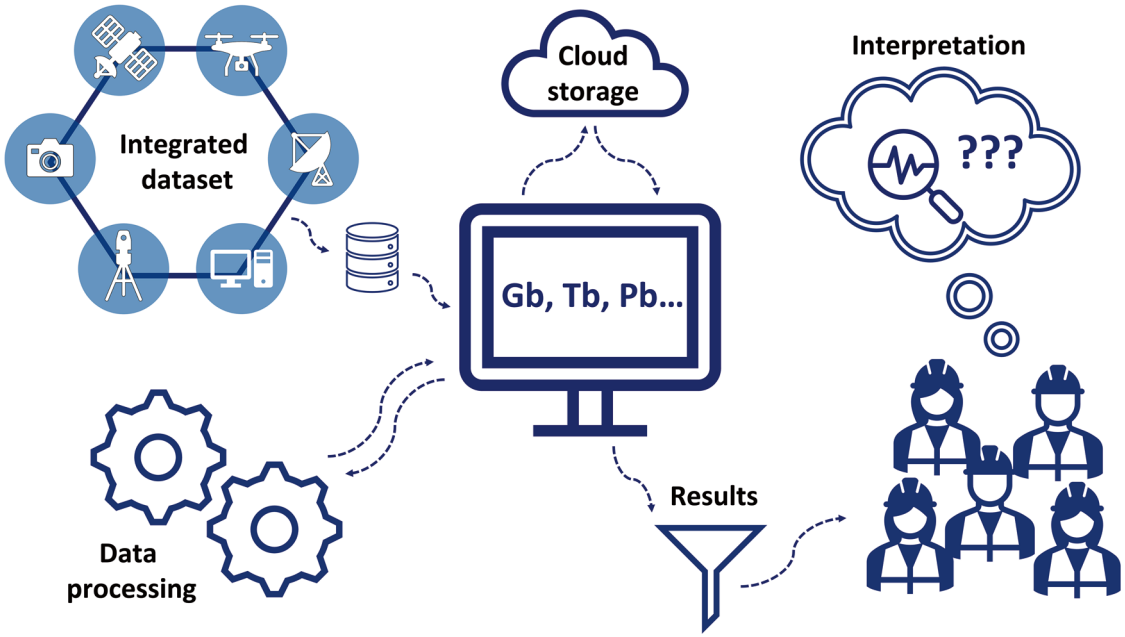

Fig. 14 The advancement of current techniques for monitoring and characterization of rock slope movements calls for streamlined processing, visualization, and integration of the large sets of outputted data

moving in the rapid velocity class, at the upper end of the moderate class, or at the lower end of the very rapid class (Table 1), are in fact the most elusive to monitor as they either move too quickly or too slowly for the sensitivity of radar-based techniques. Conventional techniques may still be applicable under those circumstances but for a limited time, since, contrarily to remote sensing instrumentation, they are constrained to a maximum measurement range after which maintenance or re-calibration is required (e.g., the cable of wire extensometers has a finite length of usually some meters, while most tiltmeters record rotations within a threshold of ±10°); likewise, repeat topographic surveying may be hindered, other than by the lower frequency of measurement acquisition, by the inherent processing times required to georeferencing, co-register, and compare different point clouds and so accurately characterize slope surface variations. Nonetheless, this "problematic" range of velocities is not typical of rock slopes, rather of landslides of the earthflow type during phases of fluidization that lead to temporary earthflow surges (Berti et al. 2022).

In the authors' opinion and experience, major emphasis to further enhance our ability to characterize and monitor rock slope movements should not be strictly placed on the development of more sophisticated instrumentation, but in the introduction of increasingly advanced, user-friendly software and/or cloud computing tools aimed at streamlined processing, visualization, and integration of the large sets of data outputted by modern remote sensing techniques (Fig. 14). For instance, GBInSAR easily accumulates tens to hundreds of giga-bytes of data due to the high frequency with which radar images are produced, and so may TLS/DLS with a single acquisition (depending on the extent of the investigated scenario and required resolution); in this regard, interpretation of radar images in range-azimuth coordinates may not be straightforward, hence an in-built workflow for their quick projection over updated three-dimensional models of the slope is advised. Finally, it should be stressed that the instrumentation used in the presented case studies, though often still expensive, has now a widespread commercial distribution and is well established beyond a prototypical stage of development. Facilitating procedures for the manipulation of outputs will be crucial to enhance the effectiveness of existing techniques, ensuring timely and actionable insights into ongoing rock slope movements.

References

Abellán A, Oppikofer T, Jaboyedoff M et al (2014) Terrestrial laser scanning of rock slope instabilities. Earth Surf Process Landf 39:80–97. https://doi.org/10.1002/esp.3493

Aryal A, Brooks BA, Reid ME (2015) Landslide subsurface slip geometry inferred from 3-D surface displacement fields. Geophys Res Lett 42:1411–1417. https://doi.org/10.1002/2014GL062688

Atzeni C, Barla M, Pieraccini M, Antolini F (2015) Early warning monitoring of natural and engineered slopes with ground-based synthetic-aperture radar. Rock Mech Rock Eng 48:235–246. https://doi.org/10.1007/s00603-014-0554-4

Barla M, Antolini F, Bertolo D et al (2017) Remote monitoring of the Comba Citrin landslide using discontinuous GBInSAR campaigns. Eng Geol 222:111–123. https://doi.org/10.1016/j.enggeo.2017.03.019

Battulwar R, Zare-Naghadehi M, Emami E, Sattarvand J (2021) A state-of-the-art review of automated extraction of rock mass discontinuity characteristics using three-dimensional surface models. J Rock Mech Geotech Eng 13:920–936. https://doi.org/10.1016/j.jrmge.2021.01.008

Beni T, Gigli G, Lombardi L et al (2022) Route Stability Index (RSI): an index for the assessment of rockfall-related hazards in rock slopes equipped for sport climbing. Geoheritage 14:80. https://doi.org/10.1007/s12371-022-00715-7

Beni T, Nava L, Gigli G et al (2023) Classification of rock slope cavernous weathering on UAV photogrammetric point clouds: the example of Hegra (UNESCO World Heritage Site, Kingdom of Saudi Arabia). Eng Geol 325:107286. https://doi.org/10.1016/j.enggeo.2023.107286

Berti M, Castellaro S, Zuccarini A (2022) Field measurements, laboratory tests and empirical relations for investigating the solid-to-fluid transition of a rapid earthflow. Eng Geol 296:106486. https://doi.org/10.1016/j.enggeo.2021.106486

Carlà T, Farina P, Intrieri E et al (2017) On the monitoring and early-warning of brittle slope failures in hard rock masses: examples from an open-pit mine. Eng Geol 228:71–81. https://doi.org/10.1016/j.enggeo.2017.08.007

Carlà T, Farina P, Intrieri E et al (2018) Integration of ground-based radar and satellite InSAR data for the analysis of an unexpected slope failure in an open-pit mine. Eng Geol 235:39–52. https://doi.org/10.1016/j.enggeo.2018.01.021

Carlà T, Nolesini T, Solari L et al (2019a) Rockfall forecasting and risk management along a major transportation corridor in the Alps through ground-based radar interferometry. Landslides 16:1425–1435. https://doi.org/10.1007/s10346-019-01190-y

Carlà T, Intrieri E, Raspini F et al (2019b) Perspectives on the prediction of catastrophic slope failures from satellite InSAR. Sci Rep 9:14137. https://doi.org/10.1038/s41598-019-50792-y

Carlà T, Tofani V, Lombardi L et al (2019c) Combination of GNSS, satellite InSAR, and GBInSAR remote sensing monitoring to improve the understanding of a large landslide in high alpine environment. Geomorphology 335:62–75. https://doi.org/10.1016/j.geomorph.2019.03.014

Carlà T, Gigli G, Lombardi L et al (2021) Monitoring and analysis of the exceptional displacements affecting debris at the top of a highly disaggregated rockslide. Eng Geol 294:106345. https://doi.org/10.1016/j.enggeo.2021.106345

Carlà T, Gigli G, Lombardi L et al (2024a) Mechanisms of block instability at the toe of a slowly deforming rock slope. Rock Mech Rock Eng 57:1543–1563. https://doi.org/10.1007/s00603-023-03674-9

Carlà T, Gigli G, Lombardi L et al (2024b) Real-time detection and management of rockfall hazards by ground-based Doppler radar. Landslides 21:155–163. https://doi.org/10.1007/s10346-023-02144-1

Casagli N, Catani F, Del Ventisette C, Luzi G (2010) Monitoring, prediction, and early warning using ground-based radar interferometry. Landslides 7:291–301. https://doi.org/10.1007/s10346-010-0215-y

Casagli N, Intrieri E, Tofani V et al (2023) Landslide detection, monitoring and prediction with remote-sensing techniques. Nat Rev Earth Environ 4:51–64. https://doi.org/10.1038/s43017-022-00373-x

Colesanti C, Wasowski J (2006) Investigating landslides with space-borne Synthetic Aperture Radar (SAR) interferometry. Eng Geol 88:173–199. https://doi.org/10.1016/j.enggeo.2006.09.013

Crosetto M, Monserrat O, Cuevas-González M et al (2016) Persistent scatterer interferometry: a review. ISPRS J Photogramm Remote Sens 115:78–89. https://doi.org/10.1016/j.isprsjprs.2015.10.011

Cruden DM, Varnes DJ (1996) Landslide types and processes. Special Report - National Research Council, Transportation Research Board 247, pp 36–75

Del Ventisette C, Casagli N, Fortuny-Guasch J, Tarchi D (2012) Ruinon landslide (Valfurva, Italy) activity in relation to rainfall by means of GBInSAR monitoring. Landslides 9:497–509. https://doi.org/10.1007/s10346-011-0307-3

Ferretti A, Prati C, Rocca F (2001) Permanent scatterers in SAR interferometry. IEEE Trans Geosci Remote Sensing 39:8–20. https://doi.org/10.1109/36.898661

Francioni M, Salvini R, Stead D, Coggan J (2018) Improvements in the integration of remote sensing and rock slope modelling. Nat Hazards 90:975–1004. https://doi.org/10.1007/s11069-017-3116-8

Gallego JI, Margottini C, Spizzichino D et al (2022) Geomorphological processes and rock slope instabilities affecting the AlUla archaeological region. In: Geotechnical engineering for the preservation of monuments and historic sites III, 1st edn. CRC Press, London, pp 456–466

Gigli G, Casagli N (2011) Semi-automatic extraction of rock mass structural data from high resolution LIDAR point clouds. Int J Rock Mech Min Sci 48:187–198. https://doi.org/10.1016/j.ijrmms.2010.11.009

Gigli G, Lombardi L, Carlà T et al (2022) A method for full three-dimensional kinematic analysis of steep rock walls based on high-resolution point cloud data. Int J Rock Mech Min Sci 157:105178. https://doi.org/10.1016/j.ijrmms.2022.105178

Glastonbury J, Fell R (2008) Geotechnical characteristics of large slow, very slow, and extremely slow landslides. Can Geotech J 45:984–1005. https://doi.org/10.1139/T08-021

Hanssen RF (2005) Satellite radar interferometry for deformation monitoring: a priori assessment of feasibility and accuracy. Int J Appl Earth Obs Geoinf 6:253–260. https://doi.org/10.1016/j.jag.2004.10.004

Hungr O, Leroueil S, Picarelli L (2014) The Varnes classification of landslide types, an update. Landslides 11:167–194. https://doi.org/10.1007/s10346-013-0436-y

Jaboyedoff M, Oppikofer T, Abellán A et al (2012) Use of LIDAR in landslide investigations: a review. Nat Hazards 61:5–28. https://doi.org/10.1007/s11069-010-9634-2

Kieffer DS, Valentin G, Unterberger K (2016) Continuous real-time slope monitoring of the Ingelsberg in Bad Hofgastein, Austria. Geomech Tunnel 9:37–44. https://doi.org/10.1002/geot.201500047

Leva D, Nico G, Tarchi D et al (2003) Temporal analysis of a landslide by means of a ground-based SAR interferometer. IEEE Trans Geosci Remote Sensing 41:745–752. https://doi.org/10.1109/TGRS.2003.808902

Luzi G, Pieraccini M, Mecatti D et al (2006) Advances in ground-based microwave interferometry for landslide survey: a case study. Int J Remote Sens 27:2331–2350. https://doi.org/10.1080/01431160600554975

Mao Z, Hu S, Wang N, Long Y (2021) Precision evaluation and fusion of topographic data based on UAVs and TLS surveys of a loess landslide. Front Earth Sci 9:801293. https://doi.org/10.3389/feart.2021.801293

Matasci B, Stock GM, Jaboyedoff M et al (2018) Assessing rockfall susceptibility in steep and overhanging slopes using three-dimensional analysis of failure mechanisms. Landslides 15:859–878. https://doi.org/10.1007/s10346-017-0911-y

Meier L, Jacquemart M, Blattmann B, Arnold B (2016) Real-time avalanche detection with long-range, wide-angle radars for road safety in Zermatt, Switzerland

Menegoni N, Giordan D, Perotti C, Tannant DD (2019) Detection and geometric characterization of rock mass discontinuities using a 3D high-resolution digital outcrop model generated from RPAS imagery—Ormea rock slope, Italy. Eng Geol 252:145–163. https://doi.org/10.1016/j.enggeo.2019.02.028

Mondini AC, Guzzetti F, Chang K-T et al (2021) Landslide failures detection and mapping using Synthetic Aperture Radar: past, present and future. Earth Sci Rev 216:103574. https://doi.org/10.1016/j.earscirev.2021.103574

Noferini L, Pieraccini M, Mecatti D et al (2007) Using GB-SAR technique to monitor slow moving landslide. Eng Geol 95:88–98. https://doi.org/10.1016/j.enggeo.2007.09.002

Novellino A, Pennington C, Leeming K et al (2024) Mapping landslides from space: a review. Landslides 21:1041–1052. https://doi.org/10.1007/s10346-024-02215-x

Riquelme AJ, Abellán A, Tomás R (2015) Discontinuity spacing analysis in rock masses using 3D point clouds. Eng Geol 195:185–195. https://doi.org/10.1016/j.enggeo.2015.06.009

Riquelme A, Tomás R, Cano M et al (2018) Automatic mapping of discontinuity persistence on rock masses using 3D point clouds. Rock Mech Rock Eng 51:3005–3028. https://doi.org/10.1007/s00603-018-1519-9

Rossi G, Tanteri L, Tofani V et al (2018) Multitemporal UAV surveys for landslide mapping and characterization. Landslides 15:1045–1052. https://doi.org/10.1007/s10346-018-0978-0

Schneider M, Oestreicher N, Ehrat T, Loew S (2023) Rockfall monitoring with a Doppler radar on an active rockslide complex in Brienz/Brinzauls (Switzerland). Nat Hazards Earth Syst Sci 23:3337–3354. https://doi.org/10.5194/nhess-23-3337-2023

Solari L, Del Soldato M, Raspini F et al (2020) Review of satellite interferometry for landslide detection in Italy. Remote Sens 12:1351. https://doi.org/10.3390/rs12081351

Sturzenegger M, Stead D (2009) Close-range terrestrial digital photogrammetry and terrestrial laser scanning for discontinuity characterization on rock cuts. Eng Geol 106:163–182. https://doi.org/10.1016/j.enggeo.2009.03.004

Vöge M, Lato MJ, Diederichs MS (2013) Automated rockmass discontinuity mapping from 3-dimensional surface data. Eng Geol 164:155–162. https://doi.org/10.1016/j.enggeo.2013.07.008

Wasowski J, Bovenga F (2014) Investigating landslides and unstable slopes with satellite Multi Temporal Interferometry: current issues and future perspectives. Eng Geol 174:103–138. https://doi.org/10.1016/j.enggeo.2014.03.003

Wasowski J, Bovenga F (2022) Remote sensing of landslide motion with emphasis on satellite multi-temporal interferometry applications. In: Landslide hazards, risks, and disasters. Elsevier, pp 365–438

Whabi AM (2014) Sedimentological and stratigraphic studies of the Cambro-Ordovician succession in Northwest Saudi Arabia. Master thesis, King Fahd University of Petroleum & Minerals, Dhahran, Saudi Arabia

Global Promotion of Understanding and Reducing Landslide Disaster Risk: Three Years on P-LRT

Shinji Sassa

Abstract

This article presents an overview and a concise review of a global promotion of understanding and reducing landslide disaster risk, based on 3 years of publication of Progress in Landslide Research and Technology (P-LRT). The Vol. 1 Issue 1, Vol. 1 Issue 2, Vol. 2 Issue1, Vol. 2 Issue 2, Vol. 3 Issue 1 and Vol. 3 Issue 2 of P-LRT were comprised of a total of 150 articles from 39 countries/regions from Africa, Asia, Europe, North America, Oceania, and South America. The three volumes and six issues embody recent Progress in Landslide Research and Technology for practical applications and the benefit for the society contributing to the Kyoto Landslide Commitment 2020.

Keywords

Early warning and real-time prediction · Climate change · Experimental/numerical analysis · Standards and patents · Landslide-induced tsunami · Hazard mapping · Resilience and sustainability · Advanced monitoring technology · Earthquake-induced landslide · Rainfall-induced landslide · Giant landslides on volcanic islands and mountains · Rockslide · Reservoir landslide and landslide dam · Cultural heritage · Landslide-structure interaction · Risk communication · Education and network · Design and countermeasures · Socio-economic significance

S. Sassa (✉)
National Institute of Maritime, Port and Aviation Technology, Port and Airport Research Institute, Yokosuka, Japan
e-mail: sassa@p.mpat.go.jp

1 Introduction

The Volumes 1–3 of P-LRT: Progress in Landslide Research and Technology were composed of the contributions of 150 relevant articles from 39 countries/regions worldwide, as shown in Fig. 1. The articles represented a total of 72 original articles, 16 review articles, 5 landslide lessons, a total of 28 articles on the projects of the International Programme on Landslides (IPL) and the World Centres of Excellence on Landslide Risk Reduction (WCoEs), and Kyoto Landslide Commitment 2020, eight teaching tools, 13 technical notes and case studies, and eight world landslide reports from a total of 622 researchers/practitioners. The themes were diverse and ranged from early warning and real-time prediction to climate change, experimental and numerical analysis, standards and patents, landslide-induced tsunami, hazard mapping, resilience and sustainability, advanced monitoring technology, earthquake-induced landslide, rainfall-induced landslide, giant landslides on volcanic islands and mountains, rockslide, reservoir landslide and landslide dam, cultural heritage, landslide-structure interaction, risk communication, education and network, design and countermeasures, and socio-economic significance. An overview and a concise review of each theme above can be described as below.

2 Global Promotion of Understanding and Reducing Landslide Disaster Risk

2.1 Early Warning and Real-Time Prediction

In light of the integrated disaster risk reduction (DRR) strategies perspective in line with the Sendai Framework for Disaster Risk Reduction (SFDRR) 2015–2030, Alcántara-Ayala and Garnica-Peña (2023a, b, c) reviewed the development and implementation of Landslide Early Warning Systems (LEWSs) in low-, lower-middle-, upper-middle-,

B. Abolmasov et al. (eds.), *Progress in Landslide Research and Technology, Volume 4 Issue 1, 2025*, Progress in Landslide Research and Technology, https://doi.org/10.1007/978-3-031-89836-5_10

Fig. 1 Global promotion of understanding and reducing landslide disaster risk: Countries/regions with contributions to P-LRT highlighted in red

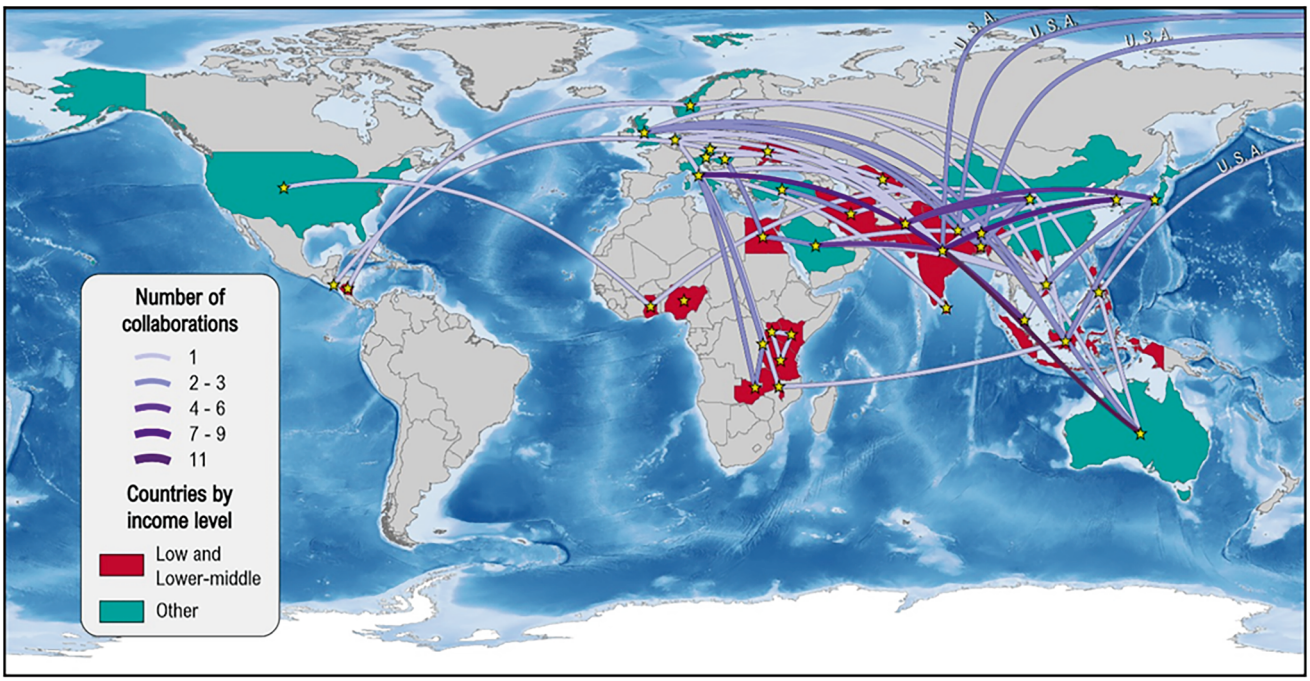

Fig. 2 Regional and international collaborations among LICs and MICs and other countries. (Fig. 10 in Alcántara-Ayala and Garnica-Peña 2023a)

and high-income countries (LICs, MICs, UMIs, and HICs, e.g. Fig. 2). Onishi et al. (2023, 2024) and Bandara and Onishi (2023) presented a recent development of real-time high-resolution predictions of orographic precipitation for facilitating early warning of rapid and long-travelling landsides due to orographic rainfall. Gariano et al. (2023) presented an implementation of frequentist rainfall thresholds for a landslide early warning system in two pilot areas in India (Fig. 3). Ha et al. (2023) proposed a landslide early warning system using a spatial multi-criteria evaluation (SMCE) method and an empirical rainfall threshold in a case study in Vietnam. Ramesh et al. (2023a) proposed an Internet

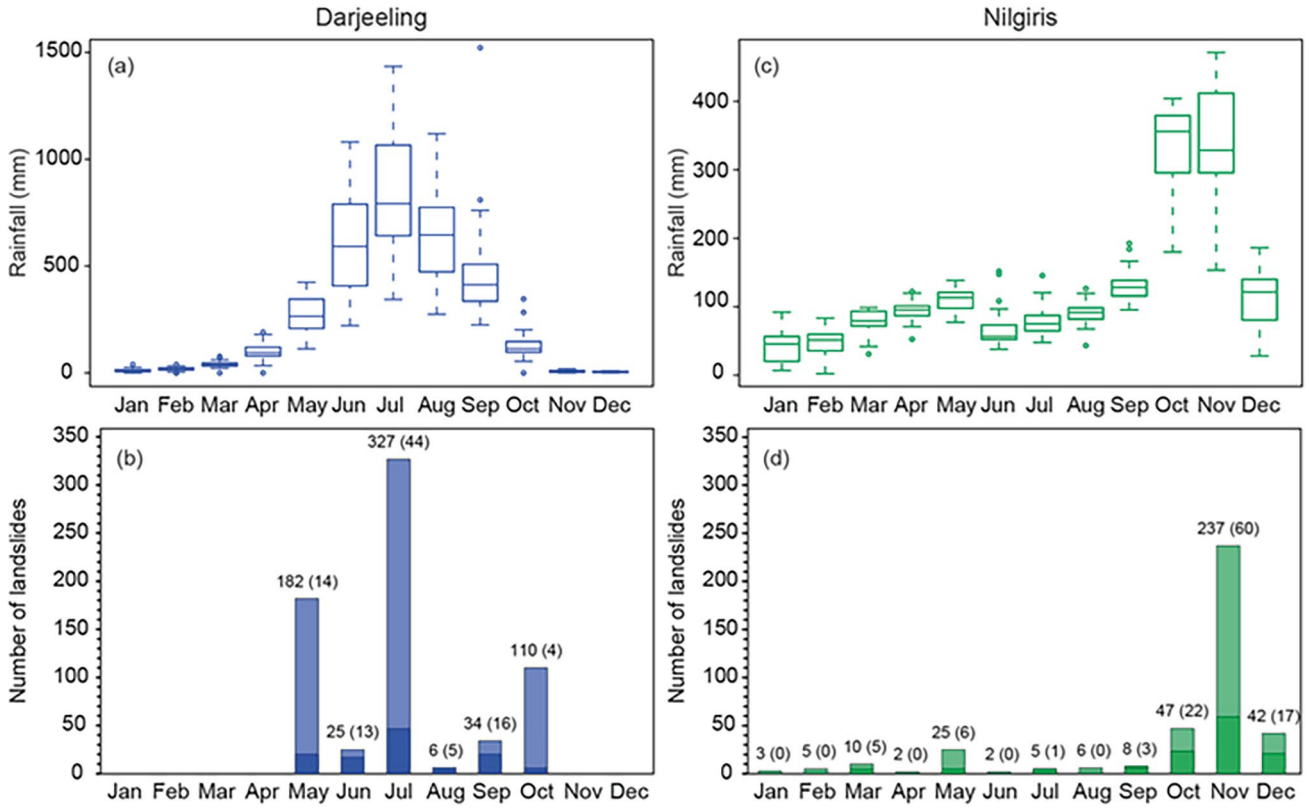

Fig. 3 Top: annual distribution of monthly rainfall in (**a**) Darjeeling (1959–2017) and (**c**) Nilgiris (1987–2017). Bottom: monthly distribution of landslides in (**b**) Darjeeling and (**d**) Nilgiris; lighter bars indicate the total numbers of catalogued landslides in each pilot area; darker bars indicate the landslides used to calculate the thresholds (values in brackets). (Fig. 3 in Gariano et al. 2023)

of things (IoT) solution for building the real-time landslide monitoring and early warning system to provide community-scale disaster resilience by gathering spatiotemporal triggers for multiple types of landslides (Fig. 4). Based on the fact that early warning and evacuation using a hazard map is a major system for landslide disaster risk reduction both in Japan and Sri Lanka, Fujita (2024) showed some essential conditions to be improved for the successful warning and evacuation with a need for better risk communication. Araki et al. (2024) reported on an early warning information delivery system using the Augmented Reality (AR) technology, targeting large-scale landslides induced by heavy rain in Aranayaka, Sri Lanka (Fig. 5).

2.2 Climate Change

Wijaya et al. (2023) presented a climate change-induced regional landslide hazard and exposure assessment in mountainous regions under extreme rainfalls in Nepal, to aid climate resilient road infrastructure planning. Under changing climate by the mid-twenty-first century, Beroya-Eitner et al. (2023) presented the projected decrease in rainfall and landslide susceptibility in a study area in Philippines, whereas other hazards such as drought and water shortage might increase, which underscores the need for a multi-hazard assessment (Fig. 6). Abolmasov et al. (2023a) presented the framework of a project titled "Mainstreaming Climate Resilience in the Road Transportation Management in Serbia (CliRtheRoads)", comprised of: a web portal for data entry and management for authorized users; a publicly available web-GIS application; a mobile GIS application; and a back-end database for climate change adaptation planning and management. Kitazato (2024) discussed a global warming-induced possible acceleration of landslides in the oceans, owing to the climate change-driven gas hydrate dissociation on continental slopes, providing possible disaster chain reactions (Fig. 7).

2.3 Experimental/Numerical Analysis

Bhandary (2023) experimentally simulated large-scale creeping landslides, using a modified ring shear machine on clayey materials for predicting landslide creep displacement and failure. Tan and Tang (2023) presented an in-situ triaxial

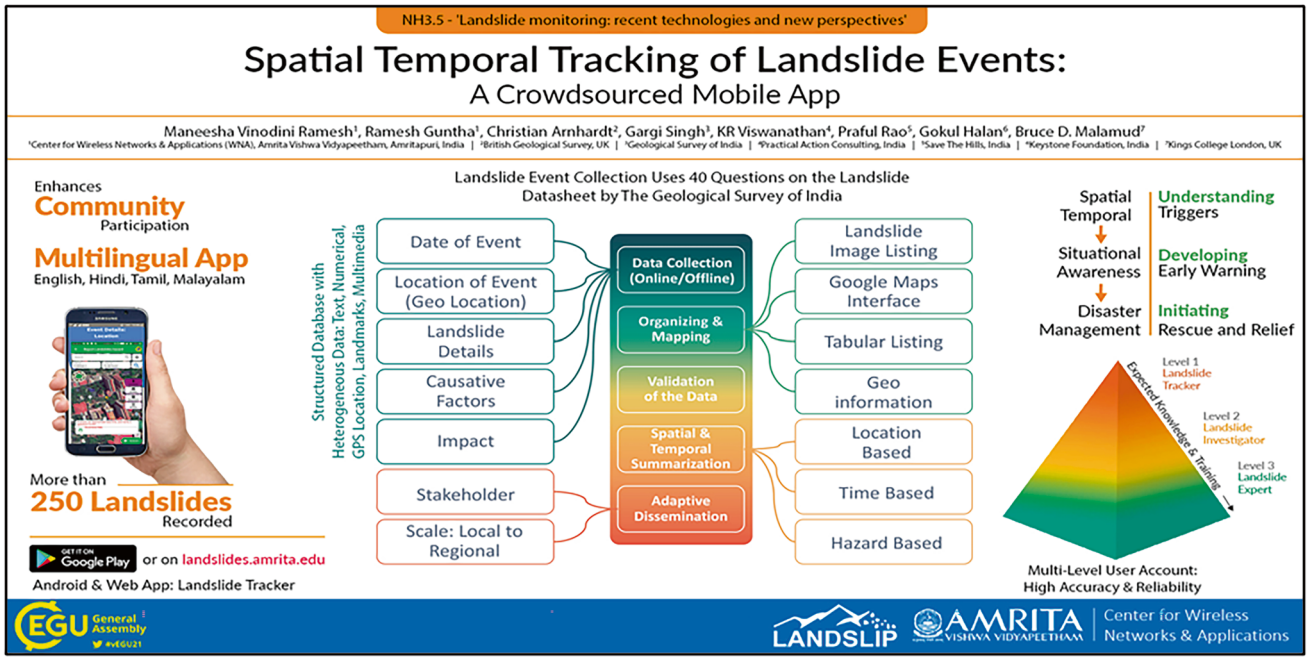

Fig. 4 Landslide tracker: a crowdsourced mobile application. (Fig. 19 in Ramesh et al. 2023a)

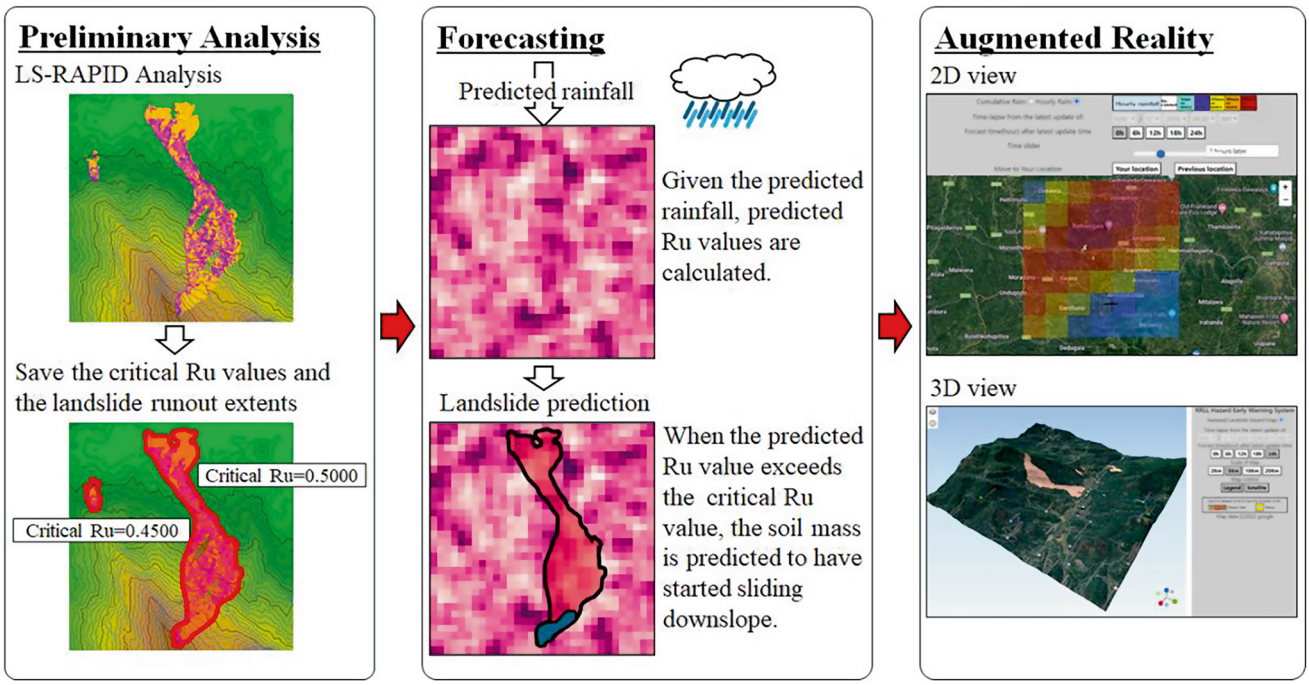

Fig. 5 Overview of the AR presentation for early warning. (Fig. 1 in Araki et al. 2024)

creep test on gravelly slip zone soil of a giant landslide in the Three Gorges area of China. Loi et al. (2023) presented the teaching tool for the undrained dynamic-loading ring-shear testing with video to experimentally study landslide dynamics from the initial stage of stresses to the formation of a sliding surface and the steady-state shear resistance.

Tiwari and Bhandary (2023) presented the application of spectral element method (SEM) in slope instability analysis with some benefits over the existing FEM procedures. Tiwari and Tran (2023) presented the use of experimental models to calibrate numerical models for slope stability and deformation analysis. Ajmera et al. (2023) presented the teaching

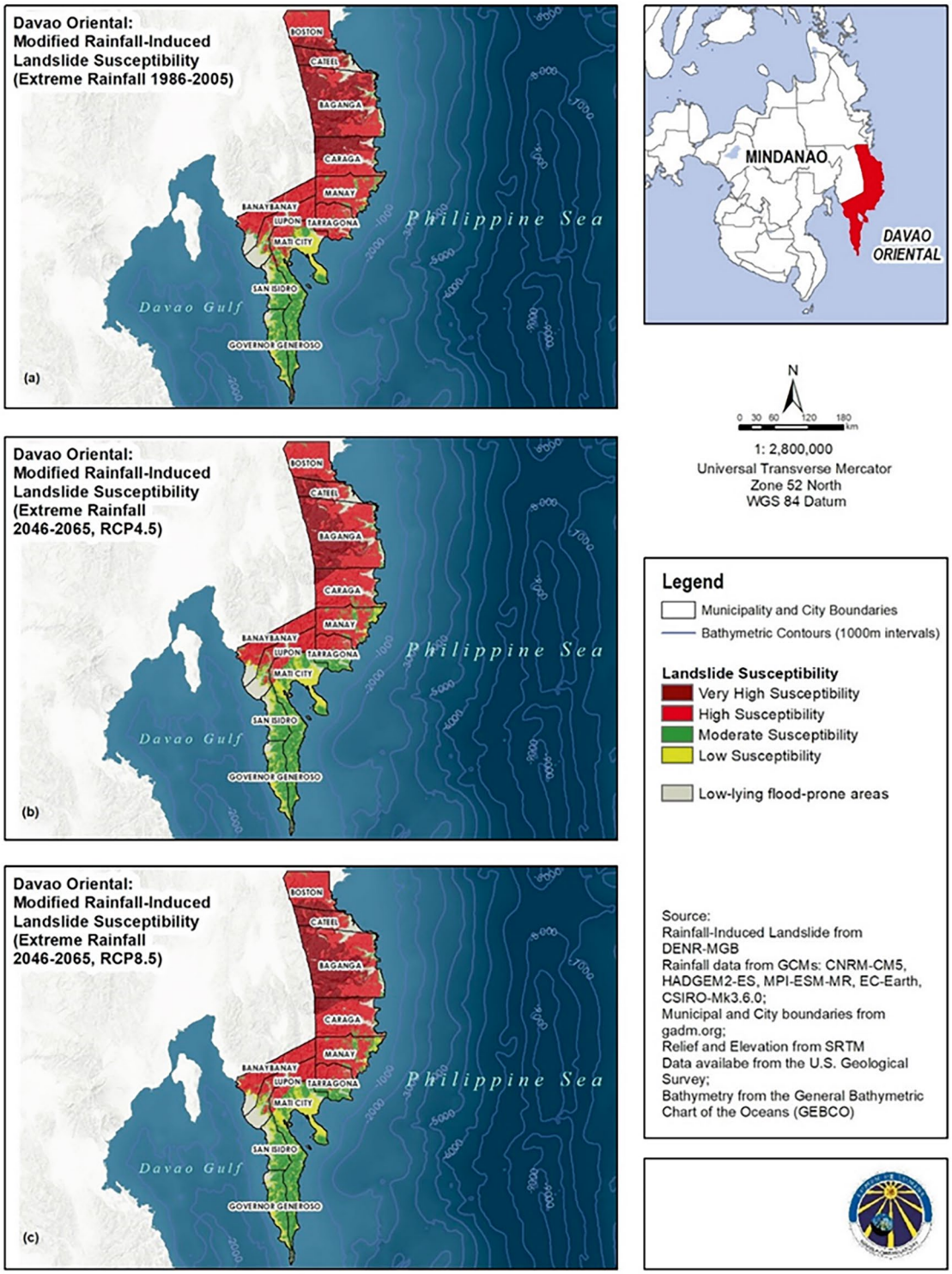

Fig. 6 Modified rainfall-induced landslide susceptibility maps of Davao Oriental (**a**) Historical (1986–2005), (**b**) Projected under RCP4.5 (2046–2065), and (**c**) Projected under RCP8.5 (2046–2065). A decrease in landslide susceptibility is expected by the mid-twenty-first century, mainly in Baganga, Cateel and Caraga, following a decrease in extreme rainfall in the area. (Fig. 8 in Beroya-Eitner et al. 2023)

tool and manual of LS-RAPID, an integrated simulation model capable of capturing the entire landslide process with the applications to (1) a rainfall-induced failure, (2) an earthquake-induced failure, and (3) the case study of the Atami debris flow, supplemented by the video tutorials.

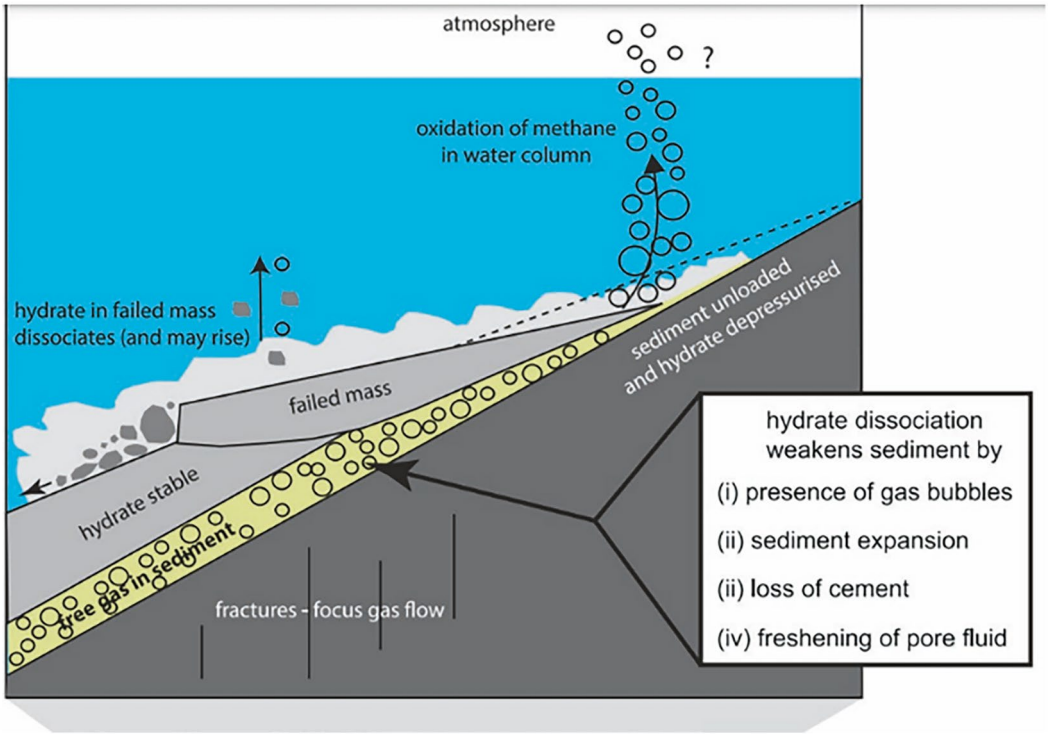

Fig. 7 Gas hydrate melting processes that may cause submarine landslides or cause methane emissions: from Talling, P.J.; Clare, M.; Urlaub, M.; Pope, E.; Hunt, J.E.; Watt, S. Large Submarine Landslides on Continental Slopes Geohazards, Methane Release, and Climate Change. *Oceanography* **2014**, *27*, 32–45. (Appendix in Kitazato 2024)

Sassa et al. (2023a) presented the sliding-surface liquefaction (SSL) concept (Fig. 8) and the undrained steady-state shear-strength to understand and reduce rapid landslide disaster risk. SSL occurs even in dense sandy layers and is caused by a series of phenomena, (1) grain-crushing due to shearing, (2) volume reduction in the shear zone, (3) generation of high pore-water pressure, and (4) liquefaction of the shear zone material. After SSL, a mass of soil layer above the liquified sliding surface moves at high speed, and the generated pore pressure reaches a certain constant value which is the undrained steady-state shear-strength (USS). The resultant feature of rapid and long- travelling landslides poses a high risk to people living in/near slopes. Tiwari and Ajmera (2023) presented recent advancements in shear strength interpretation, testing, and use for landslide analysis, based on various soil testing involving direct shear tests, triaxial tests, ring shear tests, and cyclic simple shear tests. They summarized correlations developed in the literature to estimate various shear strengths, including the fully softened and residual shear strengths of soil (Fig. 9).

Arbanas et al. (2023) presented and discussed the behaviour of small-scale slope models supported by various remedial measures under artificial rain in 1g conditions, showing the impact of the appropriate mitigation measures on retaining the stability of the slopes. Ariyarathna and Sasahara (2023) presented a procedure of data processing for the improvement of failure time prediction of a landslide based on the velocity and acceleration of the displacement in a small-scale model and a natural slope. Jayathilake et al. (2024) conducted a series of direct shear tests and single particle fragmentation tests on pumice pyroclastic fall deposits to investigate the effect of soaking time on the strength reduction of Tarumae d (Ta-d) pumice, showing a significant influence of intra-particle saturation ratio on strength degradation of pumice soil.

In the context of the machine learning (ML) and deep learning (DL) methods, Li et al. (2024) targeted the hydrodynamic pressure-driven landslides in China Three Gorges Reservoir (CTGR) area and presented the improved ensemble learning models called the multi-feature fusing transfer learning (MFTL) method for landslide displacement prediction by transferring the knowledge learned from a landslide with enough data to the other landslides with insufficient data (Fig. 10).

Amali et al. (2024) conducted a series of undrained monotonic shear-stress control ring shear tests to determine the residual shear strength of the soil samples taken from the Athwelthota landslide area, showing that the peak and steady-state shear strengths decreased when the fine content increased, resulting a higher brittleness index. Sakai et al.

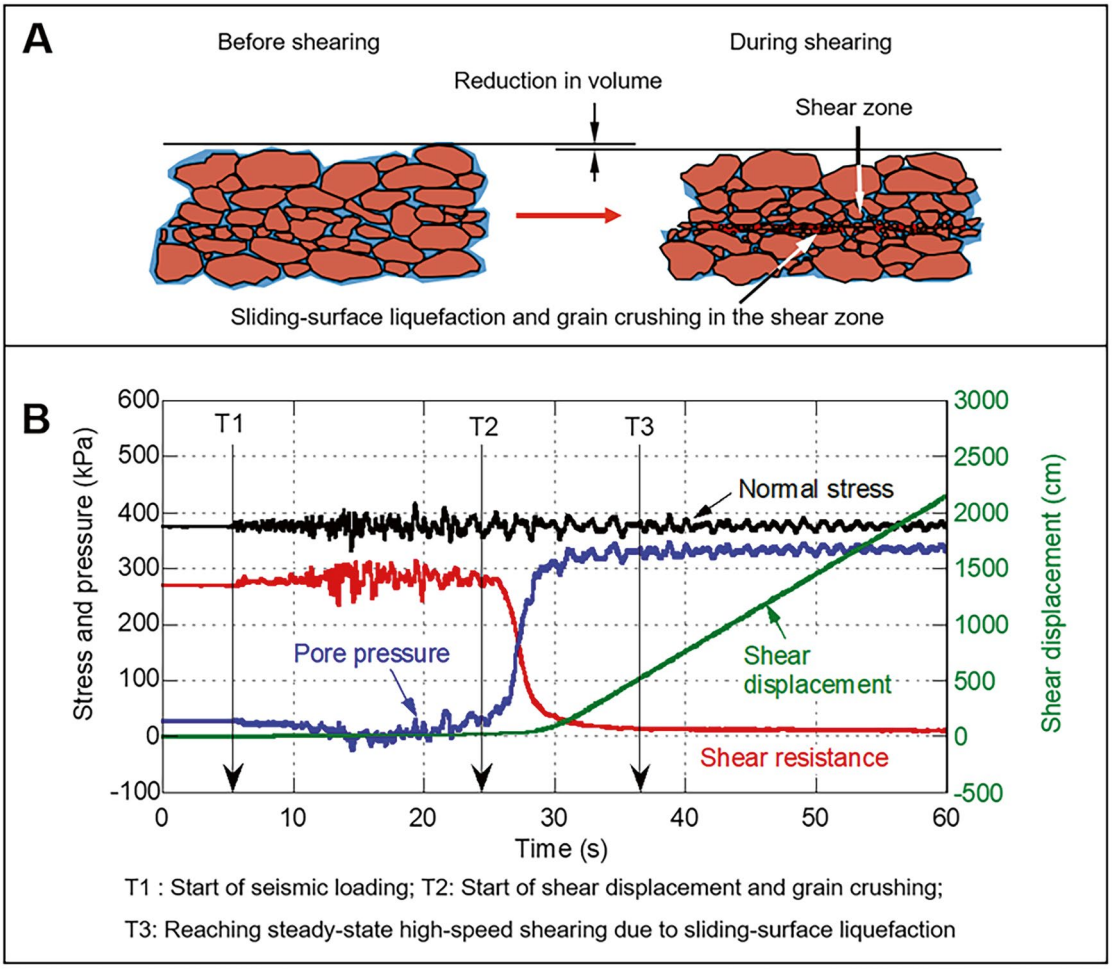

Fig. 8 Illustration and experimental data for the sliding-surface liquefaction. (Fig. 3 in Sassa et al. 2023a)

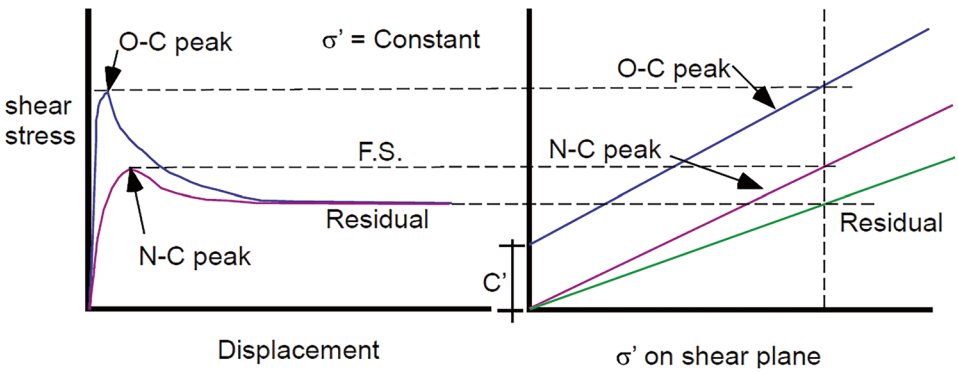

Fig. 9 Shear stress—shear displacement (left) and shear-stress-normal stress (right) relationship for over-consolidated and normally consolidated soils. (Fig. 7 in Tiwari and Ajmera 2023)

(2024) presented an experimental study on rain-induced landslide mechanisms using a large-scale rainfall experimental facility that realizes rainfall intensities between 15 and 300 mm/h, showing the intimate relationship between the rain-induced changes in groundwater levels and landslide deformation (Fig. 11).

2.4 Standards and Patents

Mikoš (2023a) extracted landslide-related patent documents from open-access databases to find more application in real word solutions when planning and executing landslide disaster risk reduction. Mikoš (2023b) also presented a list of 22

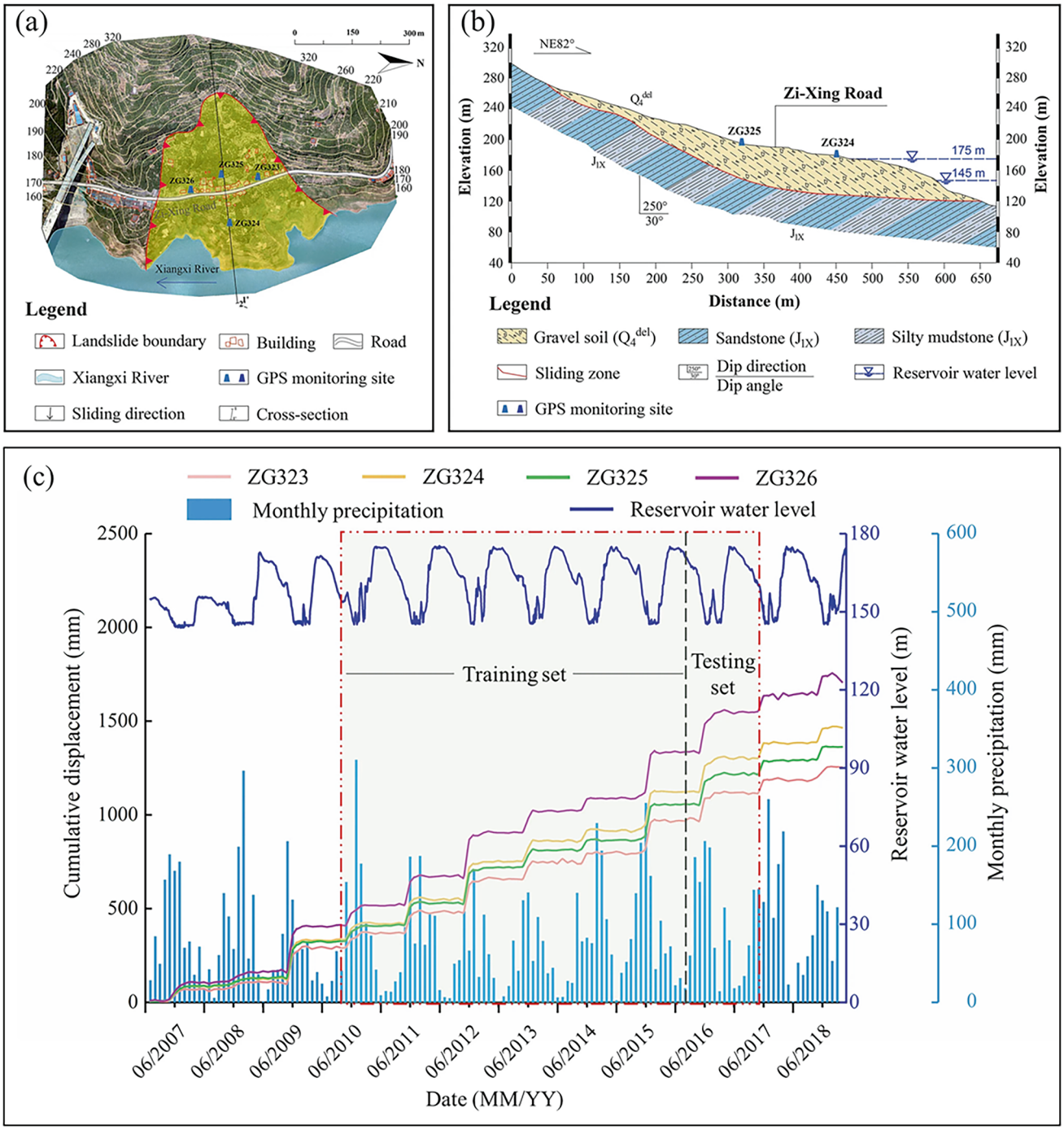

Fig. 10 (**a**) The plan map; (**b**) the profile map and (**c**) the monthly cumulative displacement, the monthly precipitation and reservoir water level of Baijiabao landslide. (After Long et al. 2022) (Fig. 2 in Li et al. 2024)

international standards containing landslide-related terms (landslide, debris flow, rock fall) using the Online Browsing Platform by the International Organization for Standardization (ISO). Fathani et al. (2023) reviewed a new standard published as ISO 22327:2018 to empower individuals and communities vulnerable to landslides for strengthening the communities' resilience to landslide disasters.

2.5 Landslide-Induced Tsunamis

Based on the outcome of a global panel discussion (Fig. 12) organized across America, Europe, and Asia and the review of the World Tsunami Awareness Day Special Event of the Fifth World Landslide Forum, Sassa (2023a, b; 2024) and Sassa et al. (2022, 2023b) presented some recent advances,

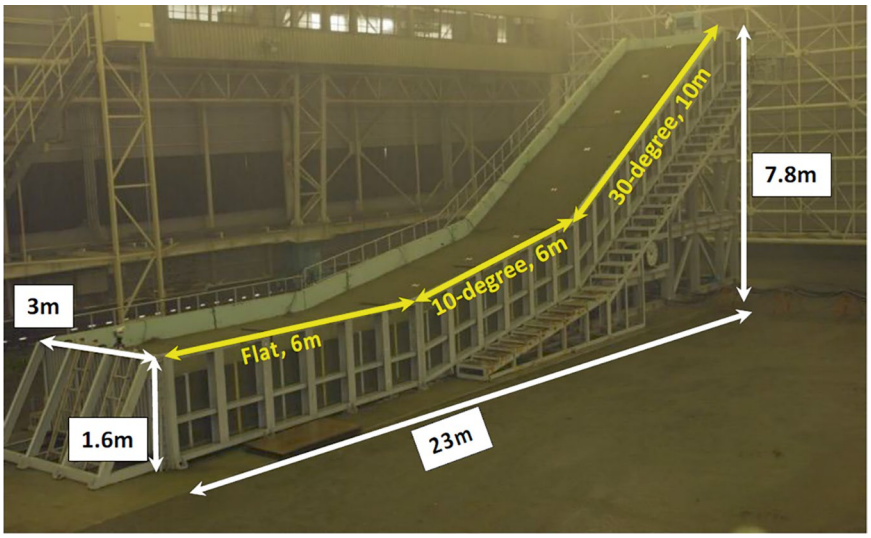

Fig. 11 Composite steel soil bin. (Fig. 5 in Sakai et al. 2024)

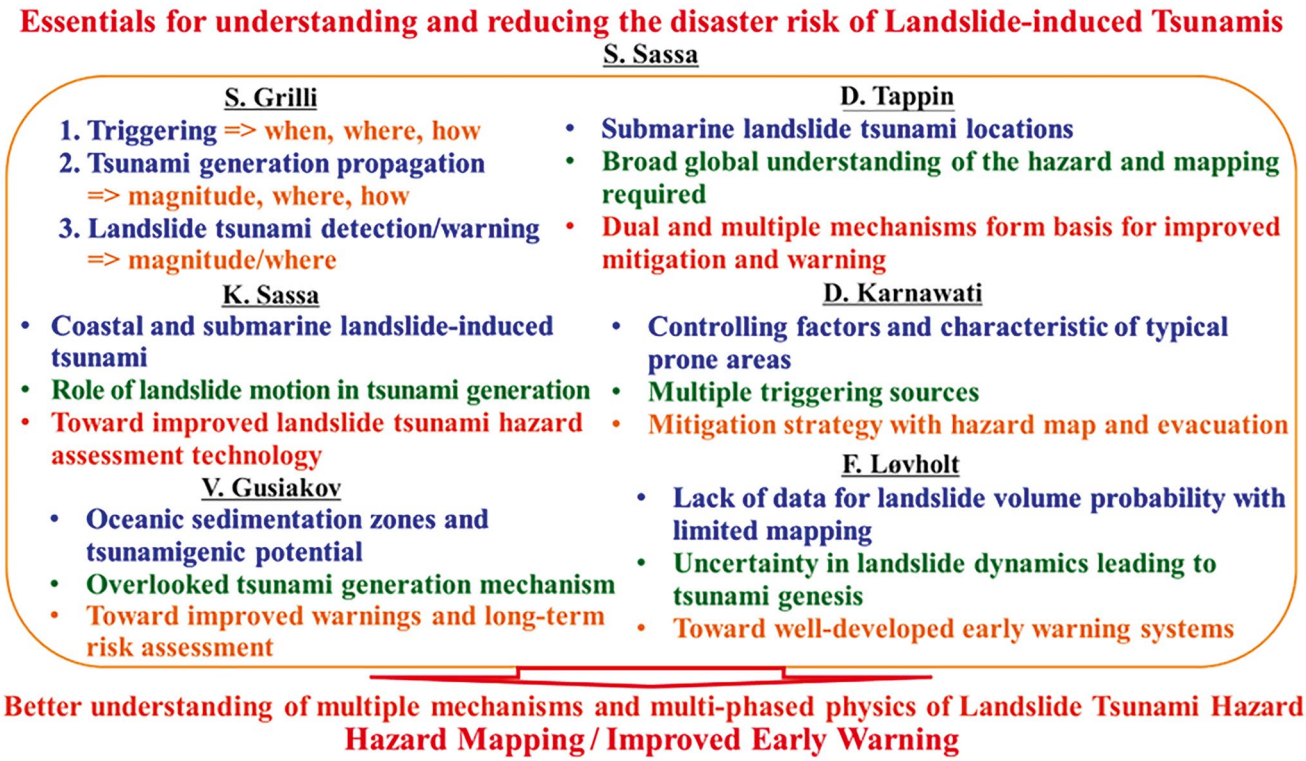

Fig. 12 The framework, essential content and a short summary of the panel discussion in the World Tsunami Awareness Day Special Event of the Fifth World Landslide Forum (Sassa et al. 2022). (Fig. 22 in Sassa et al. 2023b)

the current state and challenges in understanding and reducing the disaster risk of landslide-induced tsunamis (e.g. Figs. 13 and 14). Kawamura et al. (2023) reported ongoing persistent slope failures at the toe of a giant submarine slide in the Ryukyu trench that generated the AD 1771 Meiwa tsunami. Dang et al. (2023) presented the development and application of the LS-Tsunami simulation code as a teaching tool, which utilizes landslide motion data from LS-RAPID to model landslide-induced tsunamis.

2.6 Hazard Mapping

By analysing the database of 123 landslides from the Andean region of Colombia, Moncayo and Ávila (2023) presented the empirical-statistical modeling incorporating landslide travel distances associated with landslide volume, slope angle, maximum landslide height, and geomorphological environment (Fig. 15), resulting in a hazard map to identify possible zones affected by landslide processes in this area.

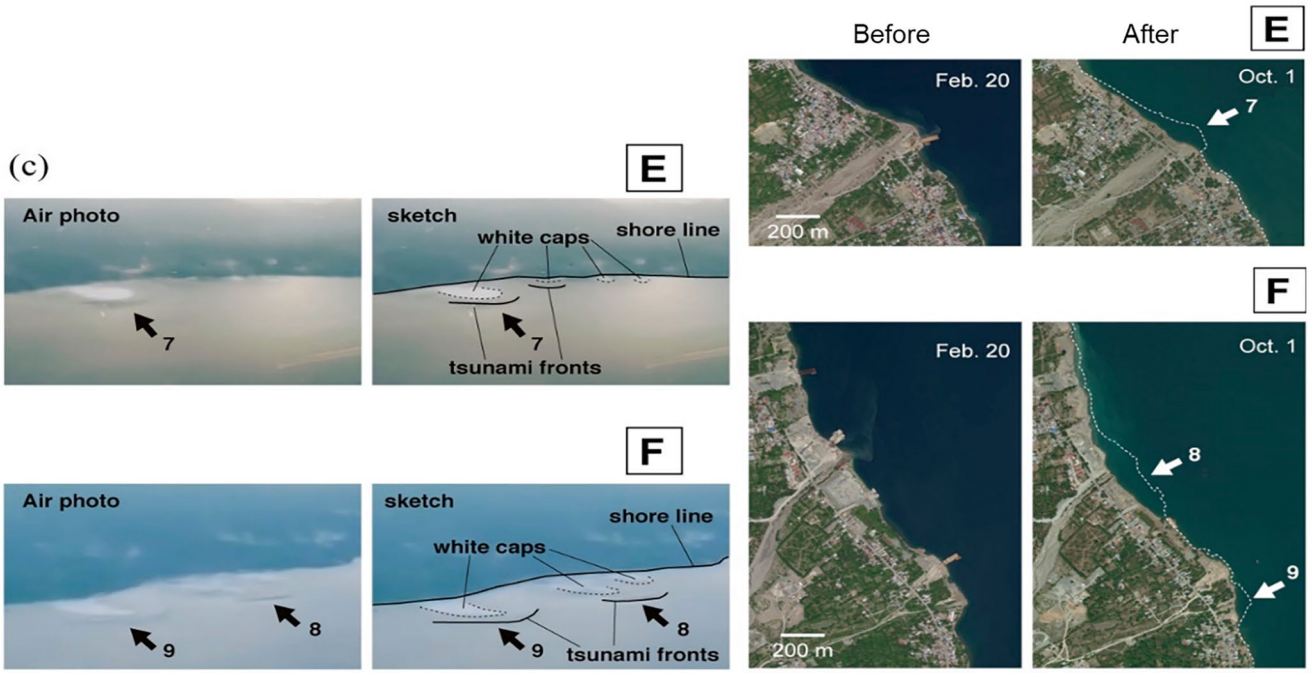

Fig. 13 Comparing the locations of multiple tsunami generations, alongshore distributions and directions with the locations, distributions and directions where the coastal lands collapsed and flowed due to the occurrence of liquefaction in the 2018 Indonesia Sulawesi earthquake. (Fig. 4(c) in Sassa and Takagawa 2019) (Fig. 8 in Sassa et al. 2023b)

Bornaetxea et al. (2023a) presented a landslide inventory mapping for the rocky mountains in British Columbia, Canada, based on the 1286 landslides. Nguyen et al. (2023a) presented the application of an Analytical Hierarchy Process (AHP) for landslide susceptibility mapping in a mountainous region of central Vietnam. Abolmasov et al. (2023b) and Tien et al. (2023) used the AHP method to construct the landslide susceptibility maps in the Republic of Serbia and in the tropical zone of Vietnam, respectively.

Paulín et al. (2023a, b) presented the landslide susceptibility assessment based on the digital terrain models (DTMs) derived from UAV and the multiple logistic regression (MLR) model in more than 600 landslides mapped into GIS and grouped into landform units in Mexico. Mihalić Arbanas et al. (2023) adopted the landslide inventory and landslide susceptibility maps based on LIDAR (Light Detection and Ranging) and DTM (Digital Terrain Model) for spatial and urban land-use planning in Croatia. Krkač et al. (2023) discussed the quality of a large-scale landslide susceptibility mapping, showing the impact of the spatial accuracy of the input data on the landslide susceptibility assessment in Croatia. Bornaetxea et al. (2023b) and Bernat Gazibara et al. (2023b) presented a statistically-based landslide susceptibility zonation tool, LAND-SUITE, with its applications to the Gipuzkoa province in Spain and the Hrvatsko Zagorje area in Croatia. Thirugnanam (2023) presented a review of deep learning for landslide detection and landslide susceptibility mapping, highlighting the need for further development.

Bernat Gazibara et al. (2023a) presented the landslide and soil erosion inventory mapping (Fig. 16) using the visual interpretation of high-resolution remote sensing data in a case study from Istria, Croatia. Vacha et al. (2023) presented the post-wildfire monthly erosion rates at the catchment scale on GIS in the north-western Italian Alps. Erzagian et al. (2023) developed a landslide susceptibility map using the frequency ratio (FR) approach with 744 landslide data through GIS in the Kulon Progo Mountains Area, Indonesia. Duong et al. (2023a) presented the frequency ratio (FR) approach combined with the fractal analysis to produce a landslide susceptibility map in Cao Bang province, Vietnam. Michel (2023) presented a consequence—frequency matrix approach to assess landslide susceptibility with its application to Swiss Prealps, Switzerland. Frodella et al. (2023a) presented a rainfall-induced shallow landslide susceptibility map for land-use planning in the High City of Antananarivo, Madagascar.

Miyagi et al. (2024) presented a three-dimensional mapping of landform features to visualize the areas at risk of landslide-induced disasters and showed a manual for landslide recognition by aerial photographs, AW3D-based wide-area maps, and specific landslide microtopography maps, which can be freely used to identify landslide landforms (Fig. 17). Wang et al. (2024) evaluated three assessment models such as the information value model, the frequency ratio model and the random forest model for landslide susceptibility mapping in permafrost areas, showing that thaw-

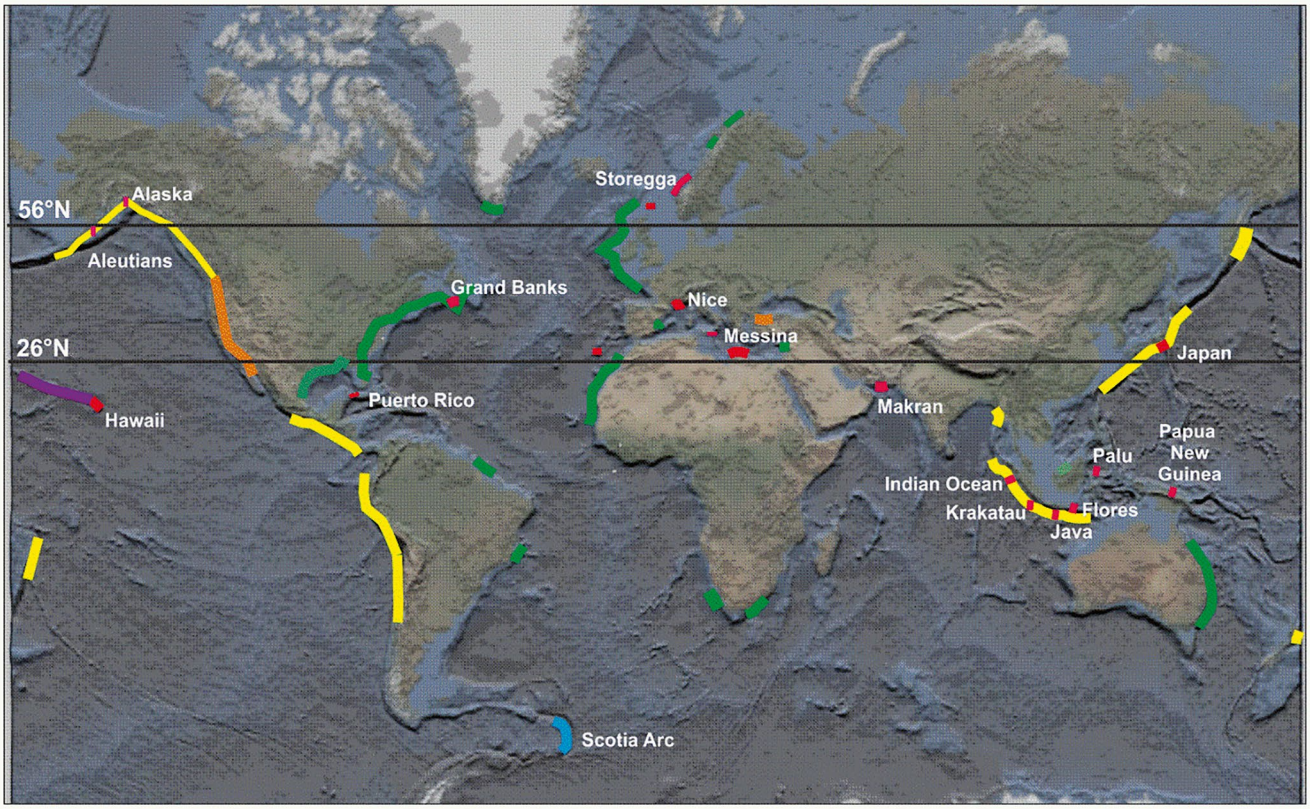

Fig. 14 Global distribution of mapped submarine landslides (SLs): Green, SLs on passive margins; Yellow, SLs located along convergent margins; Orange, SLs on strike slip margins; purple, volcanoes; Red, tsunamis associated with SLs (Tappin and Grilli 2020). Submarine landslide tsunamis (in red) are mainly located along convergent margins, but also along passive and strike slip margins and on flanks of volcanoes (Fig. 17 in Sassa et al. 2023b)

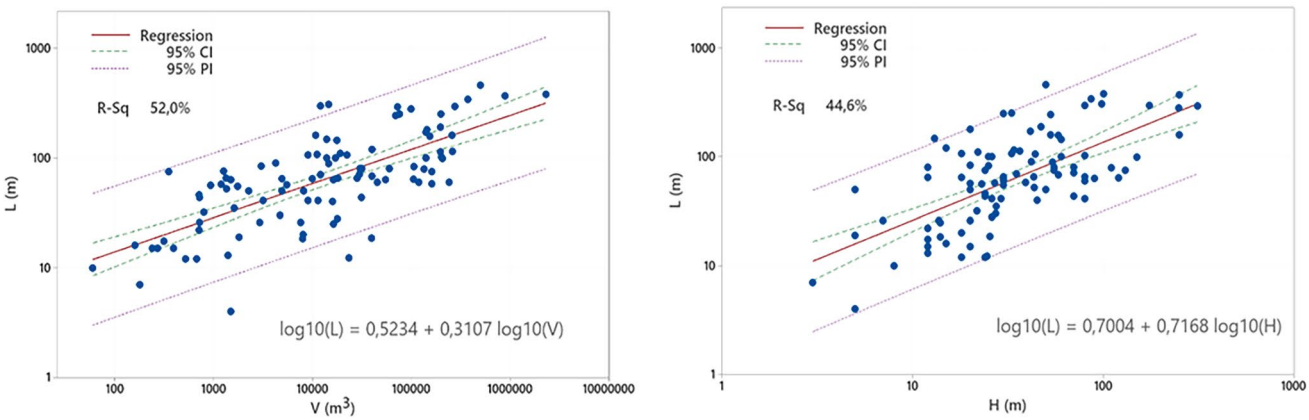

Fig. 15 Relationship between travel distance L and landslide volume V (Left) and maximum landslide height H (Right). (Figs. 3 and 4 in Moncayo and Ávila 2023)

ing and degradation of permafrost under climate warming need to be better predicted and will play a non-negligible role in influencing the occurrence of landslides in permafrost regions.

Marjanović et al. (2024) demonstrated a regional scale debris flow hazard assessment in a case study in Southern Serbia, covering about 37 km^2 of hilly-mountainous landscape, with a relatively simple geological setting, but intensively tectonized and weathered rock. Paulín et al. (2024) presented a landslide inventory map created from multi-temporal aerial photographs and field investigations

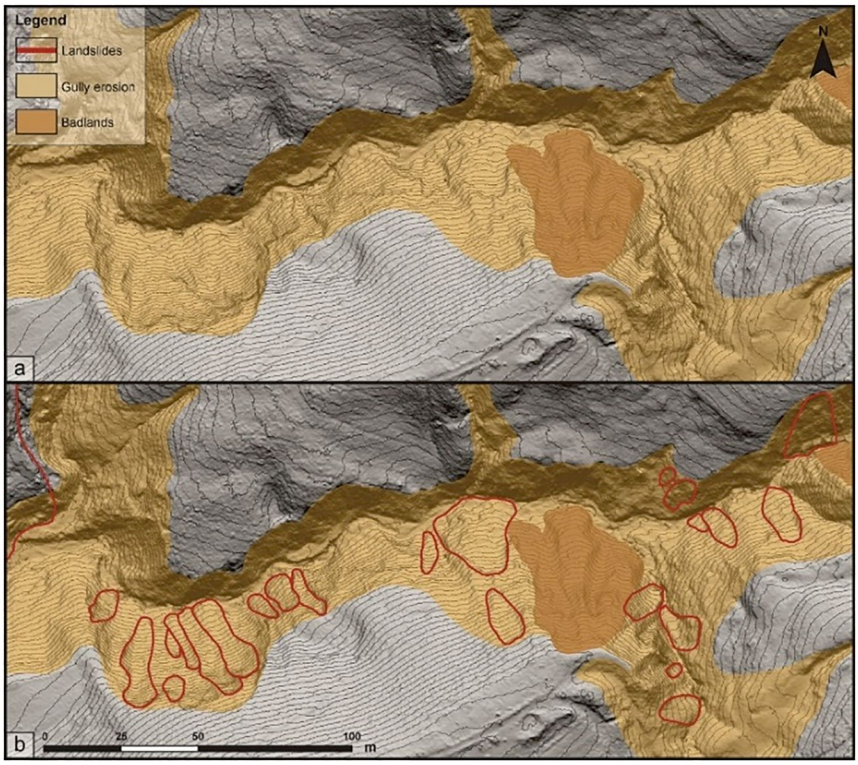

Fig. 16 Example of landslide mapping in areas affected by gully and combined erosion on LiDAR DTM derivatives. (Fig. 9 in Bernat Gazibara et al. 2023a)

using a GIS-based technology to assess the landslide distribution on the Western Flank of Iztaccihuatl Volcano, Mexico.

Karunarathna et al. (2024) presented geomorphological analyses and mapping using a raster slope shading of LiDAR, identifying potential natural slope failure zones in a case study from Kegalle, Sri Lanka. Duong et al. (2024) used the statistical index method (SI) and the integration of the fractal method and the statistical index method (FSI) to produce landslide susceptibility zonation maps in a Son La province, Vietnam. Dias and Gunathilake (2024) employed the Analytical Hierarchical Process (AHP) to prioritize factors responsible for landslide susceptibility analysis showing that the AHP methodology may be utilized to analyze and rank the relative importance of various factors influencing landslides. Patera and Fabbri (2024) used high-resolution digital elevation models to assess the spatial distribution of historical landslide forms and landslide susceptibility in Lake Albano, Italy, whose multi-hazard context may pose serious risks to urbanization, recreational activities and heritage sites.

Cordero et al. (2024) conducted community landslide risk assessment (CLRA) including hazard assessment, participatory community workshops, focus group discussions, and surveys to produce household-level risk maps for assessing and contextualizing the site-specific landslide risk in the Philippines (Fig. 18). Małka et al. (2024) analysed the accuracy of the geographical information system- and statistically-based susceptibility maps in a case study of Young Glacial River Valleys, Poland, showing that the inclusion of a quasi-3-D geological model such as a typical lithologic sequence strata (TLS) is important in the susceptibility mapping of the river valley region. Miyagi and Loi (2024) compared the landslide topography distribution map and the 2011 landslide disasters in the Kii Peninsula, Japan to determine the overlap of new landslides in 2011 and past landslides, and showed that over 60% of large-scale landslides took place in areas where previous landslides had been identified in the landslide topography distribution map, which may help in determining the location of potential future large-scale landslides. Hirota et al. (2024) presented a simple method of risk assessment (Fig. 19) for landslides based on a matrix diagram to classify risks by focusing on the relationship between the degree of landslide hazard and the number of houses free from landslides, creating a landslide risk map in Tegucigalpa, Honduras.

2.7 Resilience and Sustainability

Ramesh et al. (2023b) presented a framework to build and strengthen community-scale landslide resilience (Fig. 20) using a citizen-science approach involving a landslide tracker mobile app, social media data analysis, and community involvement, with its application to two case study areas Munnar and Chandmari in India. Damians et al. (2023) considered the sustainability of geosynthetics-based solutions to

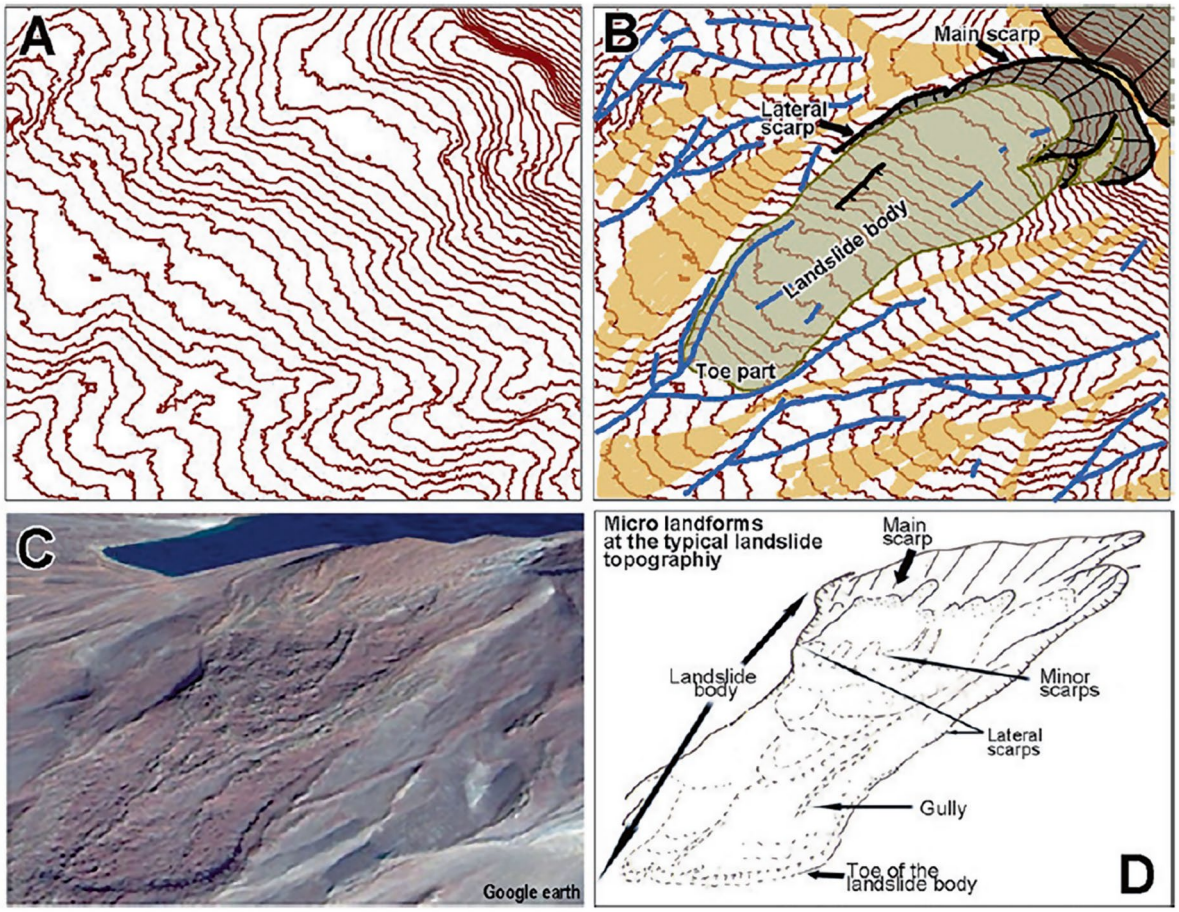

Fig. 17 Contour map generated from AW3D 2.5mDEM data, topographic readability status, etc. (**a**): 10 m contour map, (**b**): Landslide topography deciphered from contour lines, ridge lines, valley lines, (**c**): Google Earth image of almost the same location, (**d**): c topographic situation sketch. (Fig. 25 in Miyagi et al. 2024)

mitigate landslide disaster risk by using a value integrated model for sustainability evaluations (MIVES) methodology. Mikoš et al. (2023) discussed the use of natural-hazard-related-web-observatory to support the implementation of sustainable development by using geolocators for different regions and/or countries susceptible to landslides. UNESCO's new disaster risk reduction unit aims to contribute to global resilience against multi-hazards involving landslides (Delgado et al. 2023).

Matsuoka (2024) presented a statistical analysis of the Sendai Framework Voluntary Commitments (SFVC), looking into their deliverables, budgets, participating organizations, Sendai Framework targets and Sustainable Development Goals and showed that 64 percent of the voluntary commitments addressed the disaster risk reduction activities to build resilience against landslides (Fig. 21). As a strategy for increasing climate resilience on local roads infrastructure in the Republic of Serbia, Abolmasov et al. (2024a, b) presented a methodological approach utilizing the field and spatial data-based scores of exposure to main types of hazard (landslides, rockfalls, floods and flash floods) as well as related mobile and web GIS applications, labelled MaPLoRDs, which offers a sustainable solution for resolving road hazard events involving landslides encountered in road management at the local and municipality level (Fig. 22). Mikoš et al. (2024) summarized the activities of the University of Ljubljana, Faculty of Civil and Geodetic Engineering (UL FGG) as a Full Member of the International Consortium on Landslides, and an Official Promoter of the 2020 Kyoto Commitment for Landslide Risk Reduction, contributing to the UNESCO Intergovernmental Hydrological Program and its IX phase (2022–2029), the Sendai Framework on Disaster Risk Reduction (2015–2030), and the United Nations Sustainable Development Goals.

Parkash et al. (2024) highlighted some recent landslide disaster events as induced by geo-tectonics, heavy rainfall, Glacial Lake Outburst Floods (GLOFs), and anthropogenic activities, with the need of the advancement of innovative technology and tools such as Deep Learning (DL), data mining, Artificial Intelligence (AI), Machine Learning (ML),

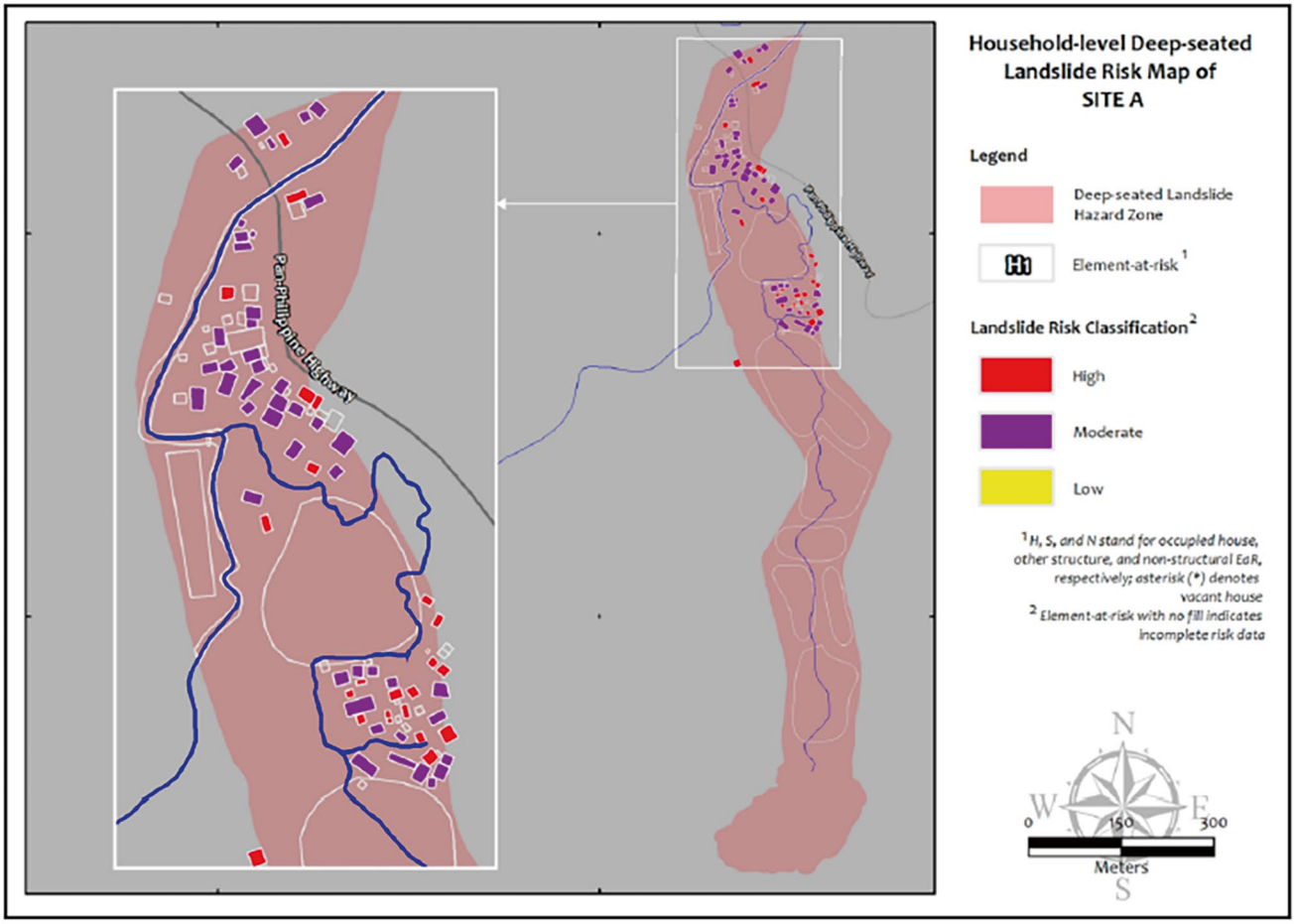

Fig. 18 Household-level landslide risk map of Site A. (Fig. 5a in Cordero et al. 2024)

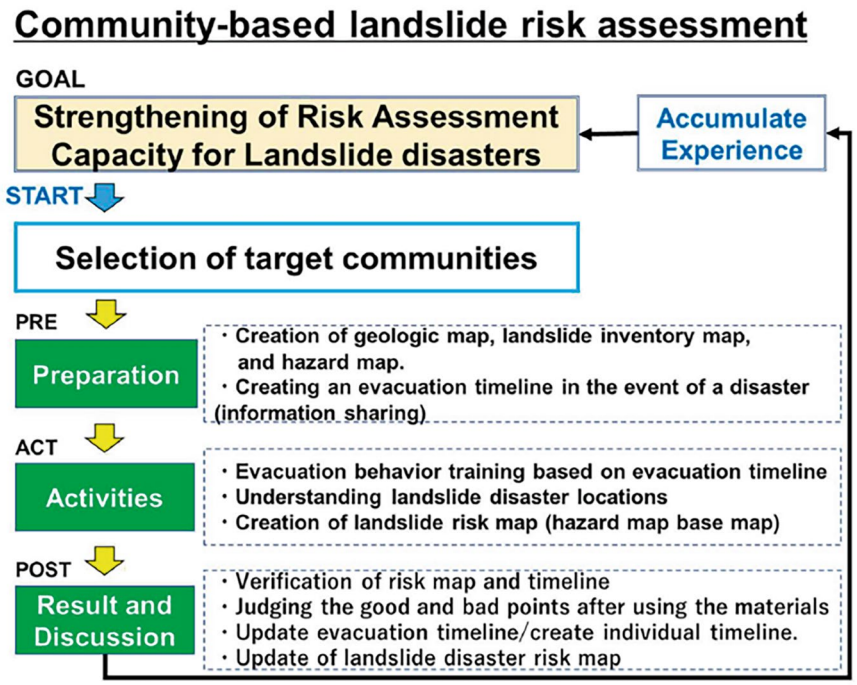

Fig. 19 Risk assessment cycle. (Fig. 15 in Hirota et al. 2024)

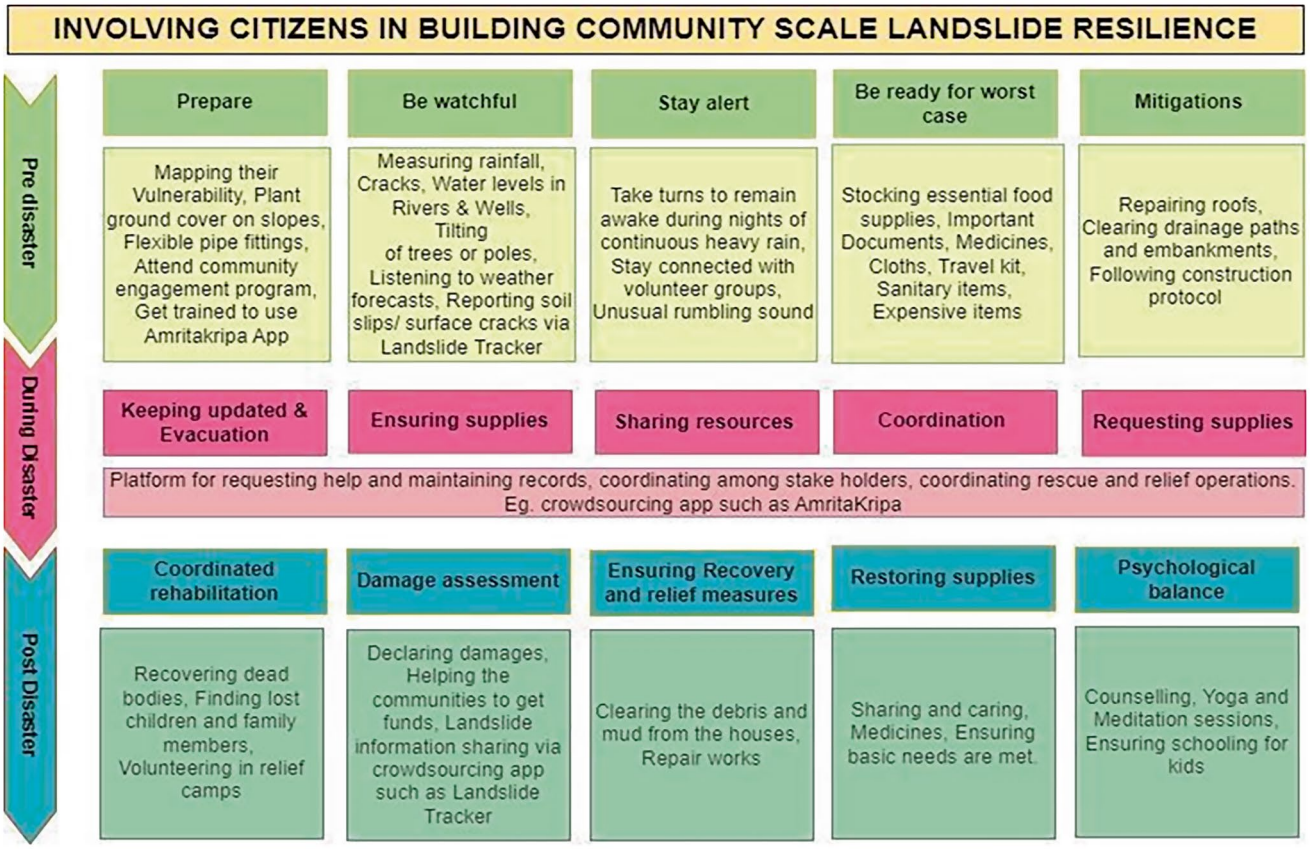

Fig. 20 Proposed framework for involving citizens in building community-scale landslide resilience. (Fig. 1 in Ramesh et al. 2023b)

Internet of Things (IOT) to generate reliable, field validated models of multi-hazards based early warning, risk assessment, mitigation for the landslide disaster risk reduction and resilience.

2.8 Advanced Monitoring Technology

For describing the form and function of a wide range of rapid and slow-moving landslides, Huntley et al. (2023a, b, c, d) reported an effective monitoring technology and practices involving the InSAR interferograms, UAV time-series photograms and the remotely piloted aircraft system (RPAS), and the RTK-GNSS surveys, combined with the field-based geological observations, terrain classification and boreholes, for the railway transportation corridors in southwestern British Columbia, Canada (e.g. Fig. 23). Casagli et al. (2023) reported advanced monitoring techniques to estimate the temporospatial deformational evolution of landslides by using GB-InSAR, LIDAR, PS-InSAR, UAVs equipped with different sensors, GPS antennas and infrared thermography, providing satellite-based services at regional scale in Italy (Fig. 24). Trofymchuk et al. (2023) reported the application of landslide monitoring with PS-InSAR, GIS database and DEM to the stability assessment of St. Andrew's Church in Ukraine. Poggi et al. (2023) applied an advanced PS-InSAR, SqueeSAR algorithm to the Humarri slide in the Hunza-Nagar River valley in northern Pakistan.

Hoang et al. (2023) applied an automatic real-time landslide monitoring system with multiple GPS antennas to a highway with steep sloping land in Chiayi County, Taiwan. Fukuhara et al. (2023) applied multi-point Micro Electro Mechanical Systems (MEMS) tilt sensors to detect the spatiotemporal variation of vulnerable slopes. Thanh et al. (2023) applied a community-level monitoring network with UAVs, AW3D Data, and Google Earth images to mountainous areas in northern Vietnam.

Lozano and Ávila (2024) presented a landslide hazard evaluation of a large waste landfill in Bogotá City, Columbia, based on the monitoring of pore pressures generated by leachate, and showed the probability of failure for static and pseudo-static conditions. Matsunami et al. (2024a) reported simultaneous observations of surface ground motion, pore-water pressure and groundwater level

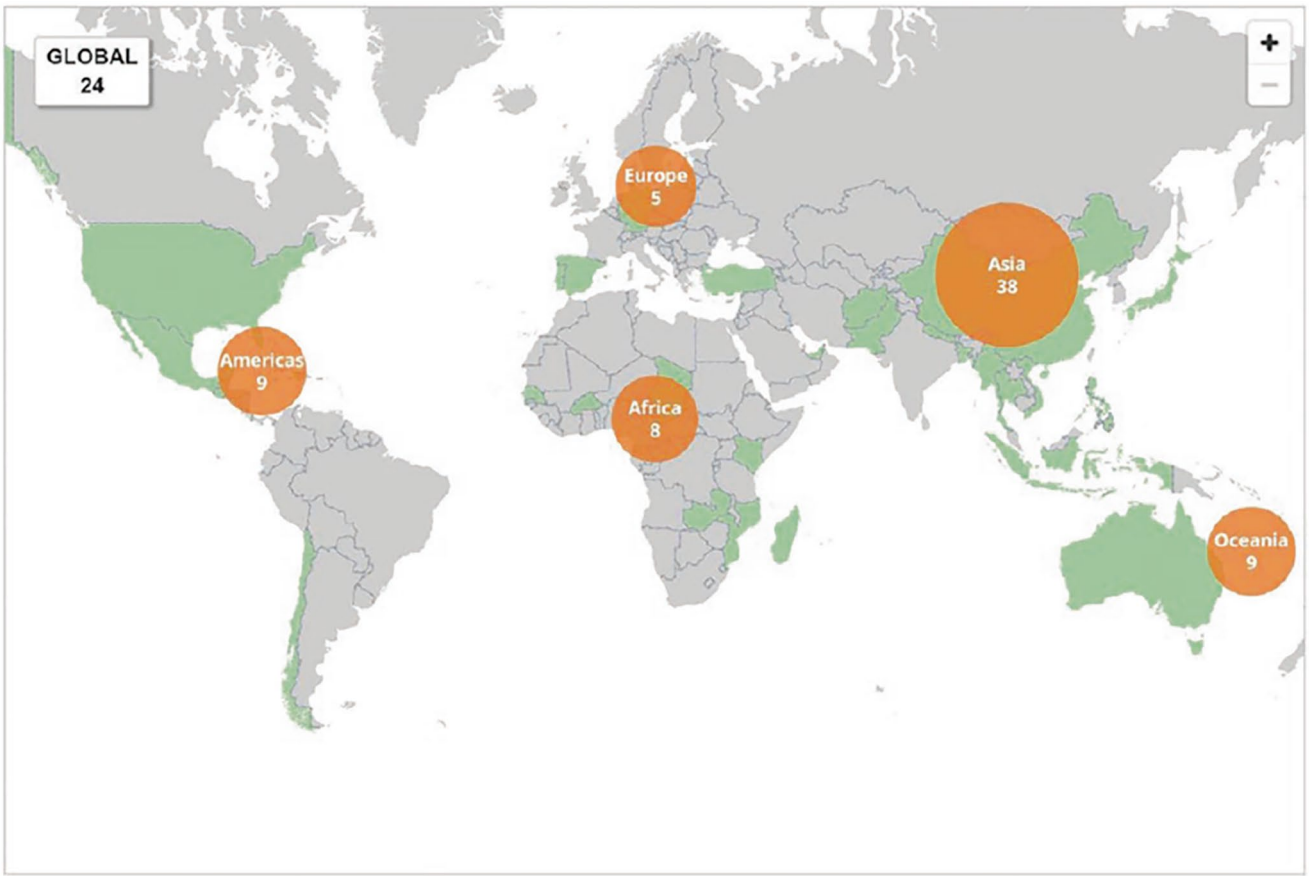

Fig. 21 Regions with countries and territories having VCs that cover landslide hazards around the world. (*Source:* UNDRR Voluntary Commitments) (Fig. 9 in Matsuoka 2024)

from several small- to medium-sized earthquakes in lineated valley fill of Wakayama, Japan, showing that the permanent tilt is of an order of 10^{-6} degree down nearly toward the direction of the valley line. Chung et al. (2024) presented a new slope monitoring method using an embedded system with optical-thermal image fusion and machine learning, based on on-site cameras that employ both optical and thermal imaging, building a three-dimensional point cloud, investigating image displacements, and tracking unstable areas of slopes.

Capparelli et al. (2024) presented an intelligent system for the integrated monitoring of the main landslide bodies of Gimigliano (CZ), southern Italy, whose station includes clusters for monitoring deep movements and piezometric levels and a network of sensors for topographic surface monitoring, indicating displacement rates of 2.5–5 cm/year. Matsunami et al. (2024b) analysed the site amplification effects of Aranayake landslide area in Sri Lanka using a wide dynamic-range earthquake motion array with soil- and rock-site stations, demonstrating that the landslide slope is frequently attacked by the microearthquakes with $Ts\text{-}p < 1.0$ sec and the velocity magnitude $2 < M < 3$.

2.9 Earthquake-Induced Landslide

Higaki et al. (2023) reviewed the mega slide of Unzen-Mayuyama of Quaternary volcanic rock due to the 1792 earthquake, and the numerous shallow landslides that disrupted highway and rail traffic due to the 2016 Kumamoto earthquake, Japan (Fig. 25), together with the subsequent unmanned slope stabilization works with earth retaining walls, embankments and re-vegetation (Fig. 26). Wang and Nam (2023) reported the characteristics of landslide disasters caused by the 2018 Eastern Iburi Earthquake in Hokkaido Japan, together with the implementation of a countermeasure by removing the surficial volcanic ashes over the slopes. Konagai et al. (2023b) reported long-lasting post-quake deformations following the occurrence of liquefaction and lateral spread after the 2018 Sulawesi Earthquake, Indonesia and the 2015 Gorkha earthquake, Nepal. Konagai (2023) also presented the characteristics of landslides in the 2004 Mid-Niigata Prefecture Earthquake, Japan.

Dias et al. (2024) investigated the emerging seismicity trends on the interpretation of major landslides and understanding catastrophic landslides settings in hill country, Sri

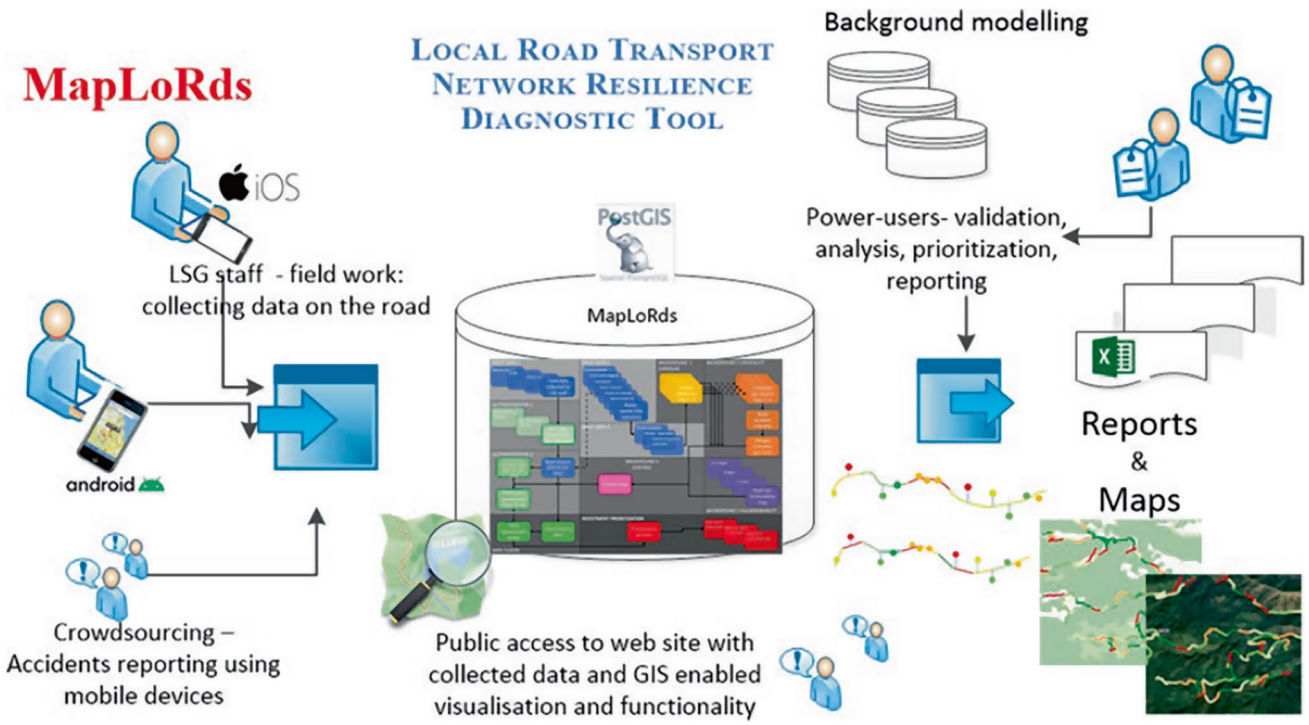

Fig. 22 MapLoRds system data collection and analysis workflow (Abolmasov et al. 2024b)

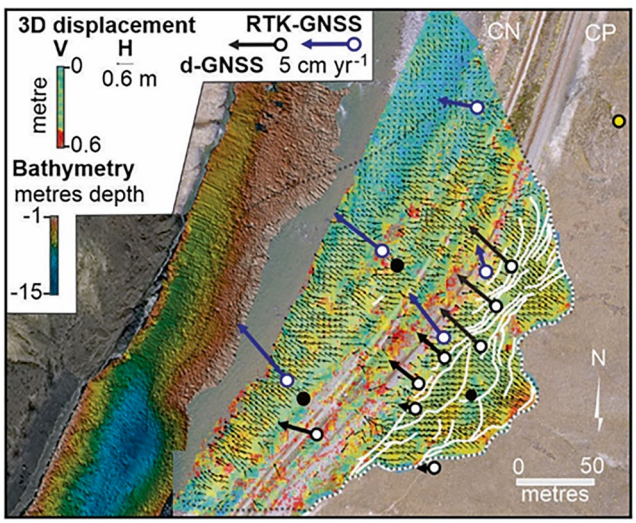

Fig. 23 Ripley Landslide surface displacement data derived from UAV overflights in 2016 and 2018 and multi-beam bathymetry data collected in 2018; plotted with RTK-GNSS (average annual rate for 2017, 2018 and 2019) and d-GNSS displacement data (November 2018 to June 2019, expressed as cm year^{-1}). Stable d-GNSS unit—yellow dot; active d-GNSS unit—black and white dot; inactive d-GNSS—black dot. Active GCP - blue dot. (Modified from Huntley et al. 2021) (Fig. 4 in Huntley et al. 2023b)

Lanka, highlighting the importance of considering evolving seismic factors in geological assessments and hazard mitigation efforts. Nakata et al. (2024) presented the dual impacts of rains and earthquakes on the multiple landslides that took place at the 2018 Hokkaido Eastern Iburi earthquake in an area draped in volcanic matters, revealing that as the peak ground acceleration (PGA) increased, the required threshold of rainfall for triggering landslides decreased. Nomura et al. (2024) presented a review of the 2008 Iwate-Miyagi Nairiku earthquake-induced landslides, which involved a debris flow that buried the Komano-Yu hot spring inn and a landslide mass of about 70 million m^3 that induced a tsunami in the reservoir of Aratozawa dam, highlighting the dynamics of these mass-wasting events.

Häusler et al. (2024) investigated the Brienz/Brinzauls landslide that took place in June 2023 Switzerland (Fig. 27) and highlighted the evolving seismic response of the active rock slopes before, during and after collapse events, potentially contributing to the development of new ways of seismic early-warning systems. Sassa et al. (2024) highlighted the importance of post-rainfall earthquakes in large-scale landslides based on the emergent seismicity trends in Sri Lanka, with special reference to the 2006 Leyte Landslide that destroyed the whole village and killed around 1000 people as triggered by the Ms = 2.6 earthquake after 1-week rainfall (Fig. 28). Fiorucci et al. (2024) presented a web-based GIS (web-GIS) database for the analysis of scientific literature on earthquake-triggered landslides, which may facilitate the preparation of interactive and visually appealing maps and charts.

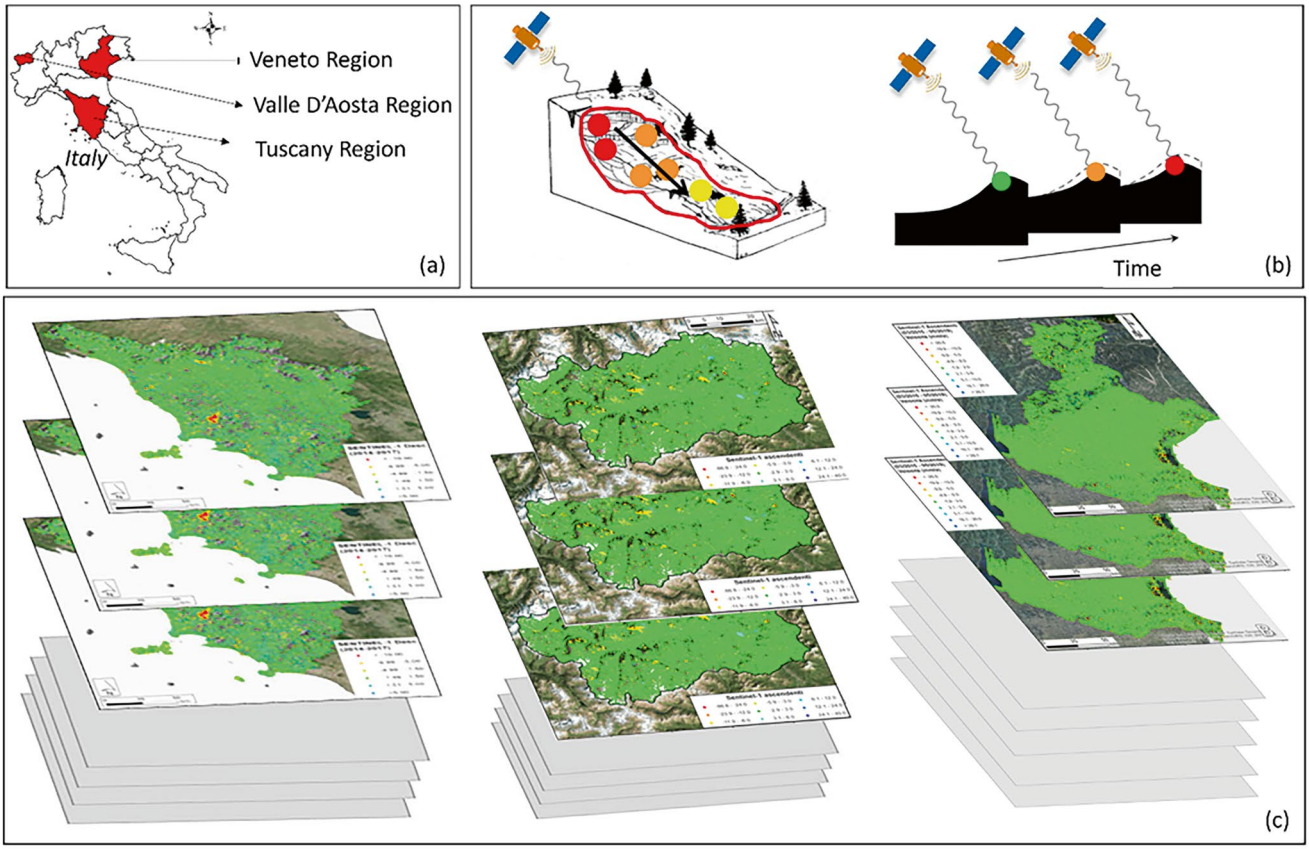

Fig. 24 Satellite-based services at regional scale in Italy: (**a**) Location of Tuscany, Valle d'Aosta, Veneto Region in Italy; (**b**) Example of "PS mapping" activity to highlight highest ground motion rates and of "PS monitoring" activity to periodically scan the territory across time; (**c**) Sketch of systematically updated ground deformation maps based on Sentinel-1 PSI data of Tuscany, Valle d'Aosta, Veneto Region. (Fig. 2 in Casagli et al. 2023)

Fig. 25 A slope failure induced by the mainshock near the Aso-Ohashi Bridge (Modified from the Kyushu Regional Development Bureau, MLIT 2021). (Fig. 10 in Higaki et al. 2023)

2.10 Rainfall-Induced Landslide

Nguyen et al. (2023a, b) investigated the effect of rainfall frequency on the susceptibility of rainfall-induced landslides by using the Regional Frequency Analysis (RFA) in a case study for a mountainous region in Central Vietnam. Zerkal and Barykina (2023) presented the characteristics of suffusion landslides associated with groundwater level rise due to rainfall in the European part of Russia. Yasufuku and Alowiasy (2023) and Higaki et al. (2023) presented the characteristics of heavy rainfall-induced landslides that took place in Kyusyu Island and Hiroshima, Japan, with the mitigation measures adopted in those areas. Konagai et al. (2023a) reviewed the rapid and long-travelling landslides that took place at Aranayake 2016 and Athwelthota 2017 in Sri Lanka and the joint research framework between Japan and Sri Lanka for developing essential technologies for an effective early warning system against rainfall-induced landslides (Fig. 29). Weerasinghe et al. (2024) and Loi et al. (2024) presented the numerical simulations of the

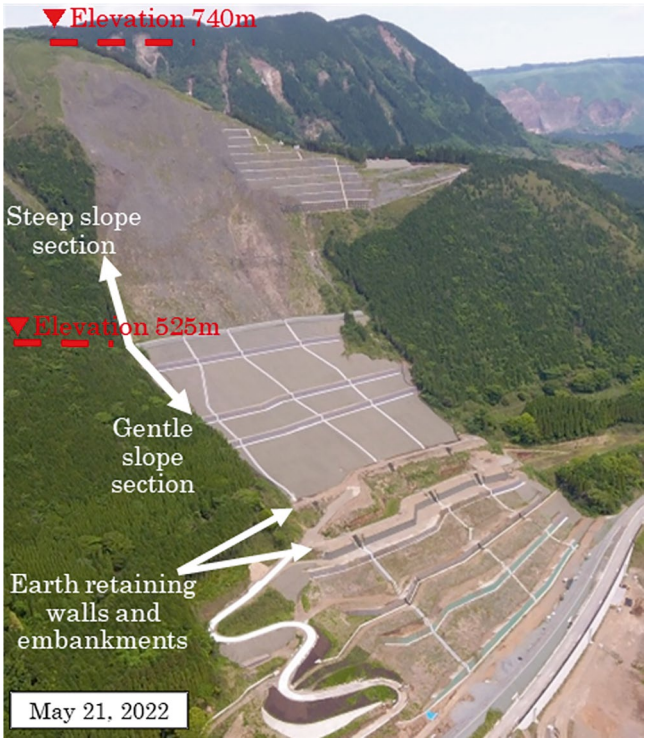

Fig. 26 Countermeasures adopted for the stabilization of each block (Embarkment and steel-reinforced soil at the lower slope and earth removal and soil shaping at the head slope) (Kyushu Regional Development Bureau, MLIT 2021). (Fig. 15 in Higaki et al. 2023)

Athwelthota landslide and the Aranayake landslide by using a LS-RAPID model and the physical properties of the soil samples onsite based on an undrained ring-shear apparatus, showing that the rainfalls, groundwater table fluctuations and pore water pressures played a pivotal role in causing those large-scale landslides (Fig. 30).

Zerkal and Barykina (2024) presented a high landslide activity in the regions of loesses that are widespread in Europe and Asia, and North America, where they form covers with thickness from several meters to the first tens of meters subject to rainfalls. Velásquez-Espinoza and Alcántara-Ayala (2024) presented an overview of the spatio-temporal distribution of rainfall-induced landslides in Nicaragua (2000–2022) that is highly susceptible to tropical cyclones, highlighting the need for creating strategies to communicate landslide disaster risks. Jayakody et al. (2024a) presented a centrifuge modeling of slopes subjected to groundwater flow and rainfall infiltration, showing that under the integrated effects of rain and groundwater flow, landslide initiation was accelerated. Dissanayaka et al. (2024) investigated the relationship between structural geology, hydrogeology, and geomorphology in the Athwelthota landslide area in Sri Lanka, showing that groundwater flow through geological discontinuities in weathered bedrock and intense rainfall during the Southwest Monsoon contributed to increased pore water pressure and reduced shear strength, triggering landslides.

Tofani et al. (2023) presented a high-resolution slope stability simulator (HIRESSS) model for analyzing the occurrence of shallow landslides during a rainfall event with its application to the Aosta Valley region in the northwest of the Alpine chain (Fig. 31). Duong et al. (2023b) presented the deterministic and probabilistic slope stability analysis using finite element (FEM) and limit equilibrium (LEM) methods for the heavy rainfall-induced landslides in the Sapa district, Vietnam. Gratchev et al. (2023) presented the mechanisms of rainfall-induced shallow landslides in Australia, involving the wetting front, water content increase, and excess pore water pressure in jointed, bedded, and weathered sandstone deposits.

Ávila and Guzmán (2024) presented the lessons learned from the great Gramalote landslide that took place in 2010 in Columbia, which destroyed a town of 3000 people located in the northeast of the country and made it necessary to evacuate all the population with the construction of a new village and relocation, which was caused by the strong rainfalls affected by the El Niño Southern Oscillation (ENSO) cycle.

2.11 Giant Landslides on Volcanic Islands and Mountains

With a total of 75 landslide events from the Atlantic Ocean and Mediterranean Sea, 67 landslide events from the Pacific Ocean, and 40 landslide events from the Indian Ocean, Rowberry et al. (2023) presented a comprehensive online database of giant landslides on volcanic islands (Fig. 32). Ríos and Ávila (2023) presented the landslide risk assessment on volcanic soils with reference to the landslide events that took place in 2019 and 2020 in the Central Cordillera of the Colombian Andes mountainous region.

2.12 Rockslide

Based on the field surveys in Japan, Taiwan, Switzerland, and Nepal, Abe et al. (2023) presented the role of translational rockslides in the evolution of cuesta topography. Strom (2023) presented large-scale rockslides, rock avalanches and manifestations of active tectonics leading to the Central Asia Rockslides Inventory from Afghanistan, China, Kazakhstan, Kyrgyzstan, Tajikistan, and Uzbekistan (e.g. Fig. 33). Dias et al. (2023) presented the characteristics of rock failures along mountainous road side slopes in Sri Lanka, involving wedge failure, translational slides and falling rocks. Nguyen et al. (2023a, b) presented the characteristics and remedial

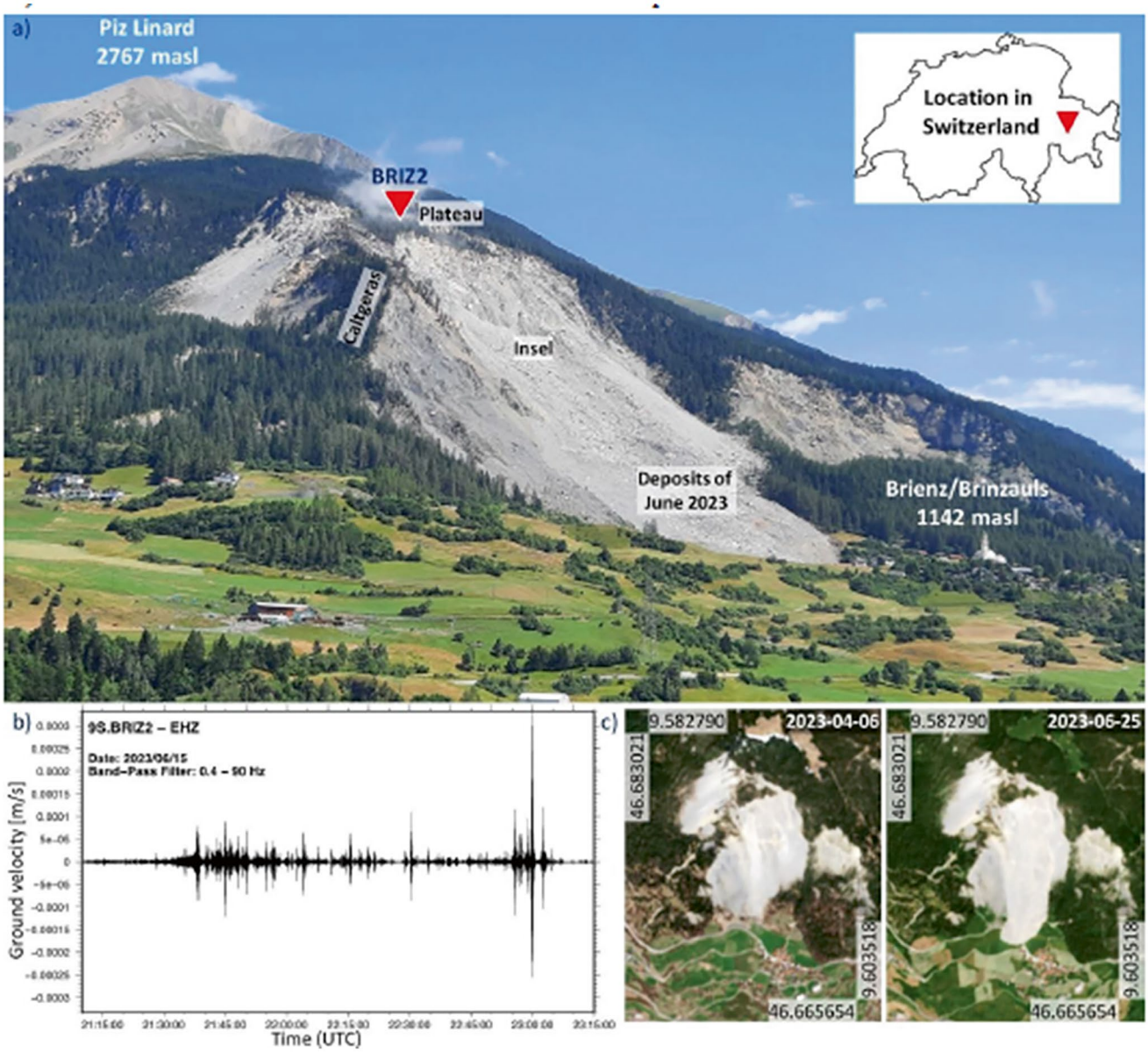

Fig. 27 Overview of the slope instability at Brienz/Brinzauls; (**a**) Photograph of the Brienz/Brinzauls rock slope instability looking in direction NE (Photo by Andrea Manconi, SLF, July 12, 2023) with location of seismometer BRIZ2; the inset shows the location in Switzerland; (**b**) Seismogram of the station BRIZ2 between 21:15 and 23:15 UTC on June 15 2023, showing the collapse of the "Insel" compartment; c) Sentinel-2 images from April 6, 2023 (left) and June 25, 2023 (right), coordinates in WGS84, EO Browser (2023). (Fig. 1 in Häusler et al. 2024)

measures of a deep-seated weathered rockslide that occurred in 2020 on a natural slope near a highway in the northwestern Vietnam. Wang et al. (2023) presented the spatial distribution, emplacement processes and mechanisms of rock avalanches in the Tibetan Plateau of China.

Peresan et al. (2024) presented an analysis of the spatial distribution pattern of rockfalls triggered by the 1976 Friuli earthquake seismic sequence, by considering various earthquake scenarios and incorporating both point and extended source models for the main shock as well as the strongest aftershocks, showing the impact of the strongest aftershocks on the final spatial distribution pattern of these rockfalls.

2.13 Reservoir Landslide and Landslide Dam

Barjasteh (2023) presented the stability analysis of Ambal Salt Ridge in the Gotvand dam reservoir, Southern Iran, based on a 4-year field observation and monitoring. Tang (2023) summarized the characteristics and the stability evaluation methods for the reservoir landslides in the Three

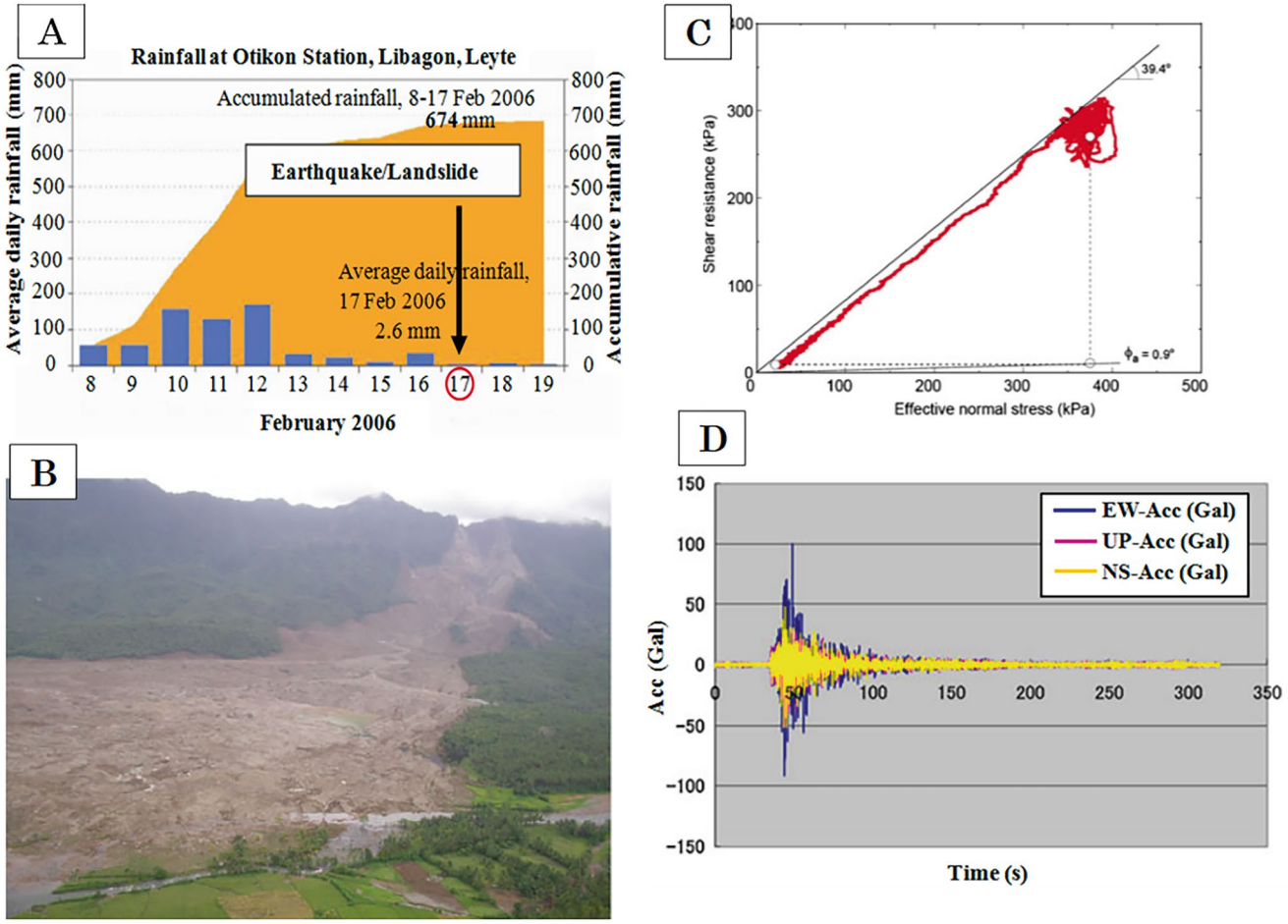

Fig. 28 Leyte landslide triggered by Ms = 2.6 earthquake after one weak rainfall, adopted from Landslides (Vol. 7–3, 2010) and P-LRT (Vol. 2–1, 2023) (**a**): Rainfall. (**b**): Photo of the Landslides (by K. Sassa), (**c**): Stress pass obtained by the undrained ring shear test, (**d**): seismic record (monitored at Maasin, Leyte). (Fig. 21 in Sassa et al. 2024)

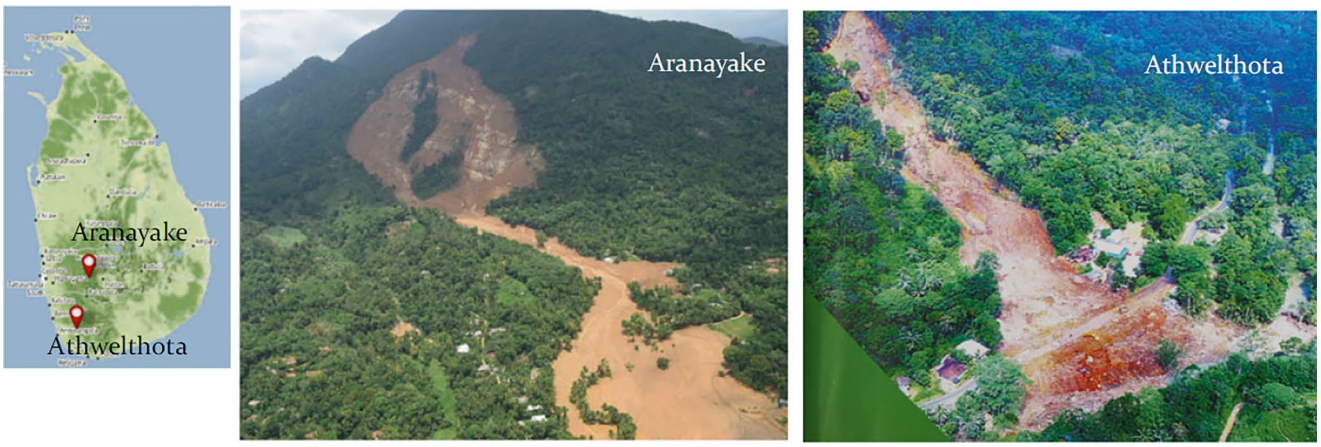

Fig. 29 Pilot study sites: (Left) Alanayake landslide in 2016, and (Right) Athwelthota landslide in 2017 (credit NBRO). (Fig. 10 in Konagai et al. 2023a)

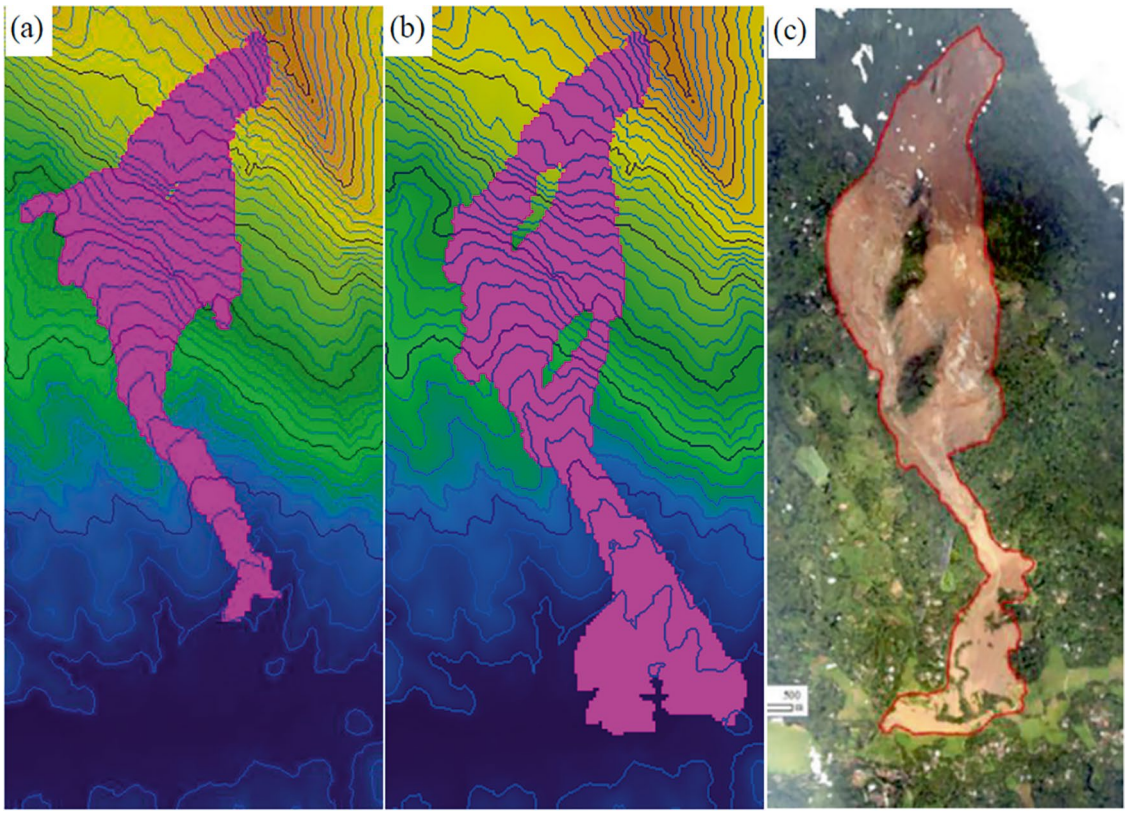

Fig. 30 LS-RAPID simulation results for 2016 Aranayake landslide and UAV photo (NBRO). (Fig. 24 in Loi et al. 2024)

Gorges Reservoir area (TGRA), China. Zerkal et al. (2023) reported the recent activity and analysis of the Buzulgan landslide that resulted in the formation of a landslide dam and its influence on the future debris flow hazard for the Tyrnyauz town in Northern Caucasus, Russia. Sattar and Konagai (2023) reported the post-formation behaviour of the Hattain Bala landslide dam formed by the 2005 Kashmir earthquake and the post-breaching situation of the landslide dam in Kashmir, Pakistan.

Tien et al. (2024) presented the physical mechanism of landslide dams and their entire formation process through three typical cases, namely the large-scale Kuridaira and Akatani landslide dams in Japan and the massive Jure landslide dam (Fig. 34) in Nepal, by using ring shear tests and an integrated simulation with LS-RAPID model, showing that the high mobility behavior that governs the rapid motion of the landslides is a primary contributing factor to the dam formation. Joshi and Subramanian (2024) presented a comprehensive review of the historical and contemporary landslide dams in Uttarakhand, India, categorizing existing research methodologies into past, present, and future studies, revealing debris slides as the most common landslide type and highlighted the impact of Landslide Lake Outburst Floods (LLOF) such as the 1970 mega-flood of Alaknanda, posing significant risks to infrastructure and livelihood.

2.14 Cultural Heritage

For the conservation of Georgian rupestrian cultural heritage sites, Frodella et al. (2023b) integrated field surveys and close-range remote sensing that led to the implementation of deep anchoring and retaining walls to protect the cultural heritage sites against slope instability (Fig. 35). Elshayeb (2023) presented the development of landslide risk assessment and associated preservation during the last 30 years of the various Egyptian cultural heritage sites. Gallego et al. (2023) reported the weathering and erosion-induced rock degradation processes and the potential slope instabilities affecting the AIUla archaeological sites shaped for thousand years in Kingdom of Saudi Arabia.

2.15 Landslide-Structure Interaction

Perna et al. (2023) presented the Material Point Method (MPM) based modelling of landslide-structure interaction, showing that landslide pore water pressures undergo significant tempo-spatial evolution during a dynamic impact on the structure. Ng et al. (2023) presented the impact mechanisms of water, dry granular and two-phase debris flows on barriers of varying stiffness, openings and numbers, showing that debris flow composition governs the impact dynamics on barriers (Fig. 36).

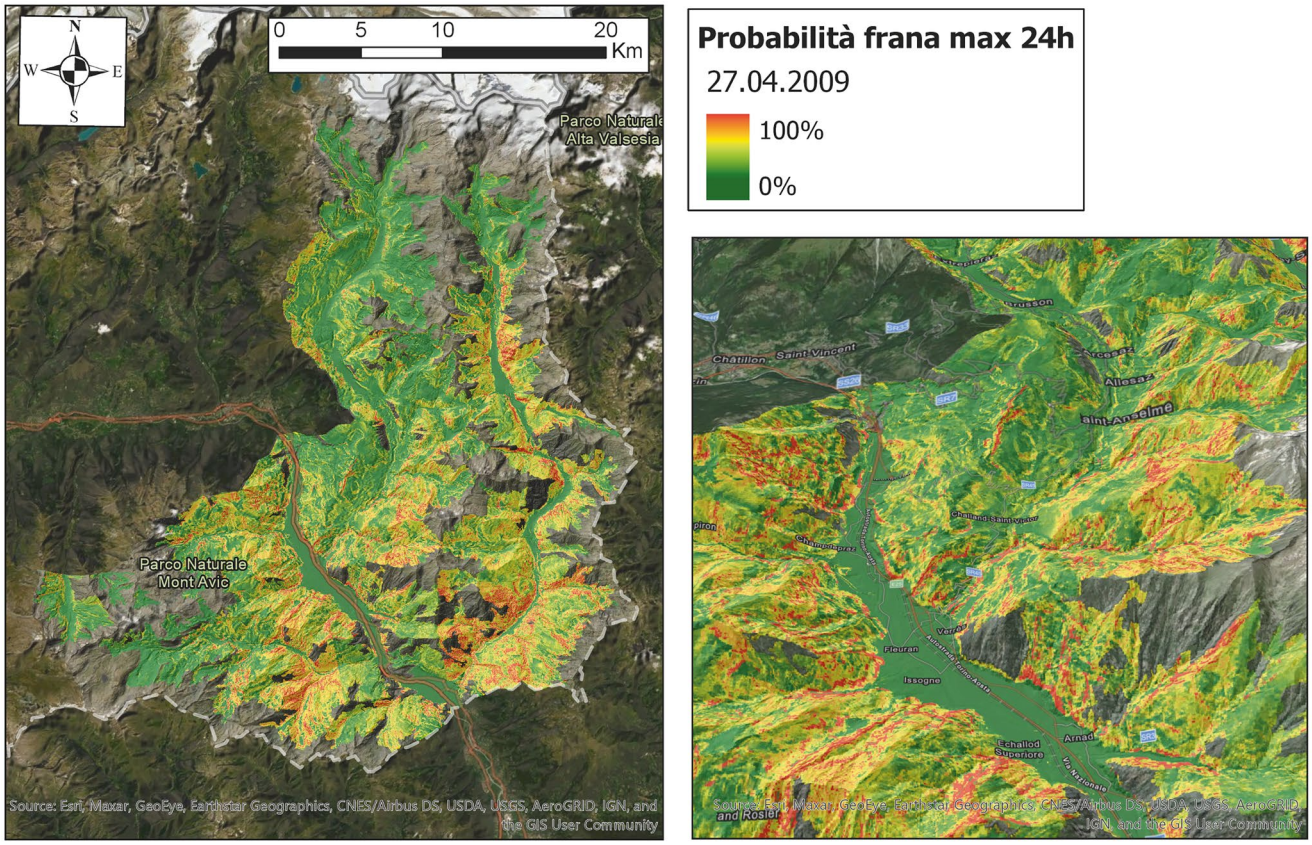

Fig. 31 HIRESSS 24-hr map of failure probabilities for the day of April 27. (Fig. 4 in Tofani et al. 2023)

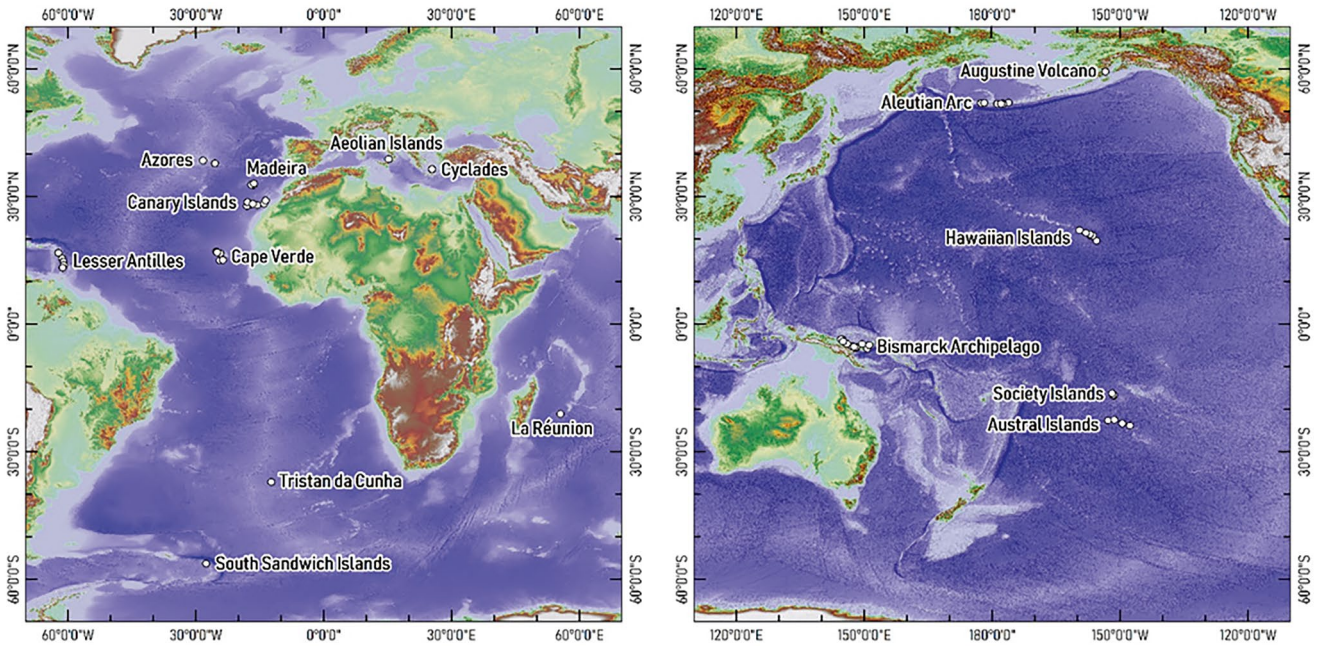

Fig. 32 Distribution of giant landslides on volcanic islands from the Atlantic and Indian Oceans (Left) and the Pacific Ocean (Right). (Source: Global relief model derived from Global Bathymetry and Topography at 15 Arc Sec: SRTM15+ V2.1 (Tozer et al. 2019)) (Figs. 4 and 5 in Rowberry et al. 2023)

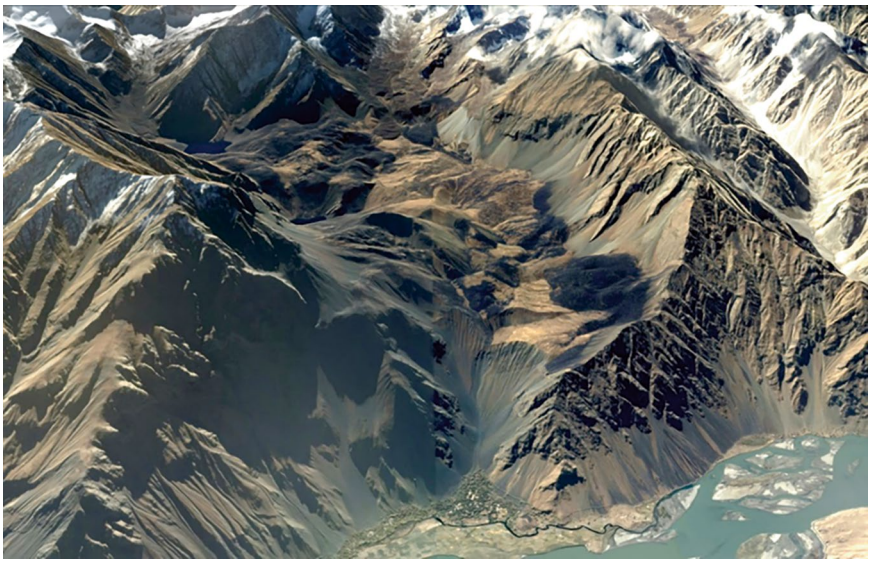

Fig. 33 Oblique view of the giant Padjvar rockslide in Afghan Badakhshan ca. 6 km^3 in volume. The entire ridge about 6 km long collapsed in the adjacent valley of the left tributary of the Pianj River and filled it almost completely with the deposits up to 650–700 m thick that cover 19.72 km^2, while the total affected area is about 27 km^2. (Fig. 12 in Strom 2023)

2.16 Risk Communication, Education and Network

Ahmed et al. (2023) reported the use of qualitative social science tools and techniques via key informant interviews to investigate the anthropogenic-induced landslide disasters in Chittagong hill districts, Bangladesh. Thanh et al. (2023) presented a communication-based evacuation mapping (CBEM) and the engagement of residents in slope disaster risk reduction in a mountainous area of northern Vietnam. Based on diverse web tools and databases, Mikoš (2023c) presented an assessment of worldwide efforts in teaching/education on landslides and their disaster risk reduction at higher education levels and beyond. Munasinghe et al. (2023) presented an outcome of a literature survey to consolidate a common set of risk assessment perspectives and approaches for measuring landslide disaster risk by using the PICO (Population, Intervention, Compression Intervention, and Outcome) method. Kamal et al. (2023) presented the refugees' perception of landslide disasters based on a structured questionnaire and survey of 400 people from the Rohingya camps in Cox's Bazar, Bangladesh.

Arbanas and Mihalić Arbanas (2023) reported the 10th Anniversary of the ICL Adriatic-Balkan Network by showing its establishment, objectives and activities during the last 10 years organizing biannual Regional Symposiums on Landslides in Croatia, Serbia, Slovenia, and Bosnia and Herzegovina. Garnica-Peña and Alcántara-Ayala (2023) reported a key recommendation to implement a landslide disaster risk awareness program associated with the expansion of an urban area in a mountain zone susceptible to landslides in México. Nishikawa (2023) presented the need to effectively raise public awareness about landslides with the application of an Ichi-Nichi-Mae (The Day Before the Disaster) Project for landslide awareness and risk communications.

Hernández-Cadena et al. (2024) assessed higher education students' perceptions of landslide risk, knowledge of hazards and exposure, previous experience with landslides, information and media, landslide preparedness, and communication (Fig. 37), which can be used to improve disaster awareness, reduce disaster risk and mitigate the impact of landslide disasters in the municipality of Teziutlán, Mexico and similar mountain regions.

2.17 Design and Countermeasures

Cuomo et al. (2023) presented different tools and options to design a protection barrier against flow-like landslides based on the analysis of landslide-structure interaction (Fig. 38). Higaki et al. (2023) presented an overview of the emergent and permanent countermeasures adopted following the 2018 heavy rainfall-induced landslide disaster in Hiroshima, Japan, involving channel stabilization works and construction of 20 Sabo dams to mitigate landslide and debris flow impacts. Hirota et al. (2023) presented the application of vegetation works to protect unstable cutting slopes along highway in Gangthangkha, Wangdue, Bhutan. Arbanas et al. (2023) presented a series of model slope experiments with various countermeasures such as a gabion wall, buttressing embankment and a pile wall, showing their effectiveness in retaining the stability of the slope, which otherwise collapsed. Tang et al. (2023) presented an optimal design and arrangement of stabilizing piles for the prevention and control of reservoir landslides with their applications to Hongshibao landslide (Fig. 39) and Majiagou landslide in the Three Gorges Reservoir area (TGRA), China.

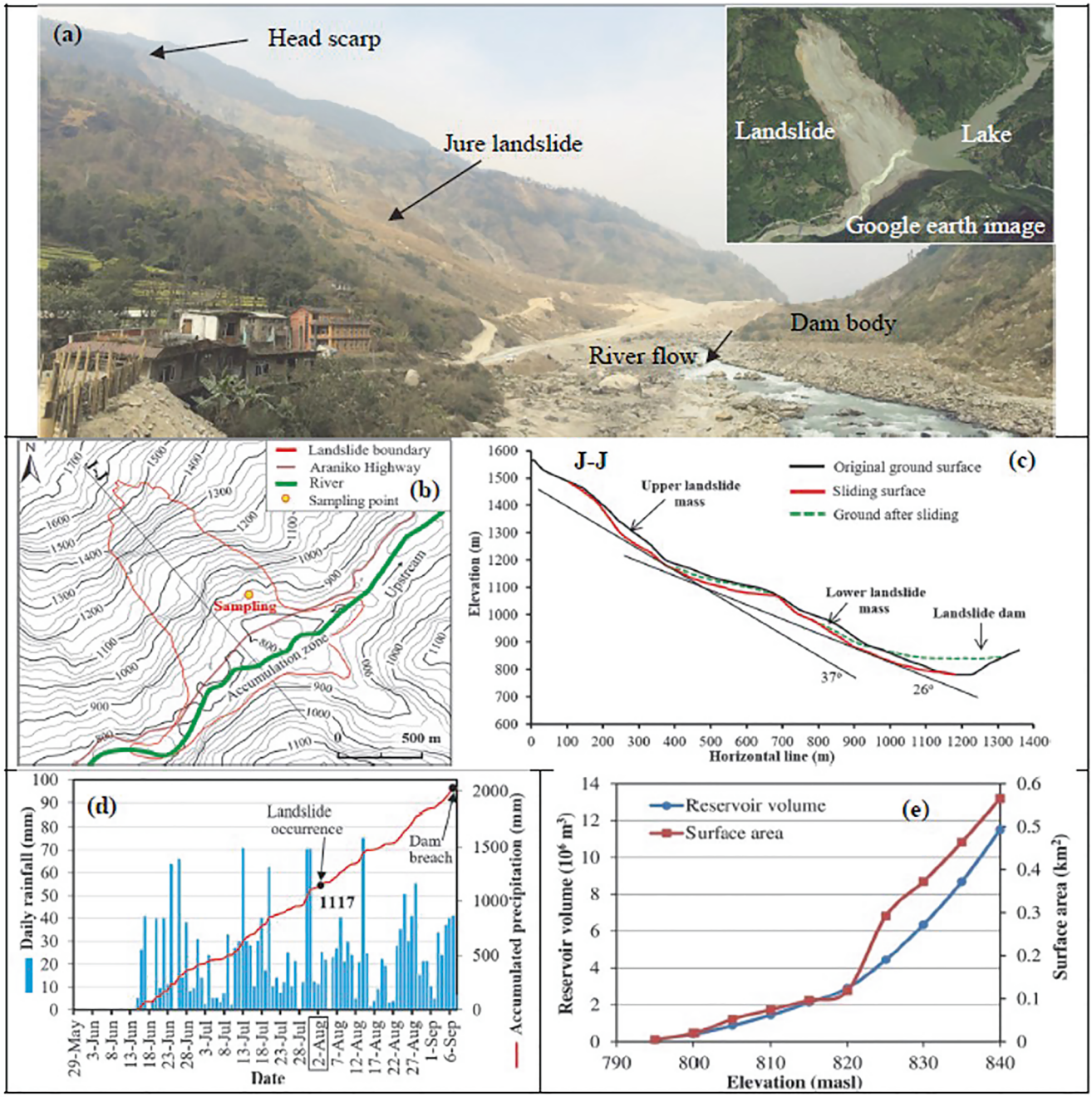

Fig. 34 (**a**) Photograph of the Jure landslide dam taken in December 2016 and a google image of the natural lake after damming in August 2014, (**b**, **c**) topographic map and longitudinal profile (J-J) of the landslide, (**d**) rainfall data at the Barhabise station and (**e**) elevation-volume and elevation-surface area curves of the dam reservoir (Fig. 2 in Tien et al. 2024)

Choi et al. (2024) presented a new analytical model to predict the peak pullout resistance for anchors subjected to dynamic loading in saturated sand, which can be used towards an optimization of foundation anchors of landslide-resisting flexible barriers. Jayakody et al. (2024b) discussed the use of subsurface drainage to stabilize a backslope of a retaining wall located at an arterial highway in Sri Lanka that had undergone failure due to excess water pressure, which improved the slope's stability and significantly avoided forming a perched water table, being a cost-effective solution for stabilizing the highly saturated unstable slopes. Woldearegay (2024) presented the characteristics of landslides that have been affecting road networks in Ethiopia over 25 years period (1997–2022), involving: (i) field inventory and characterization of 158 landslide-affected road sections, (ii) investigations of the geological, geohydrological

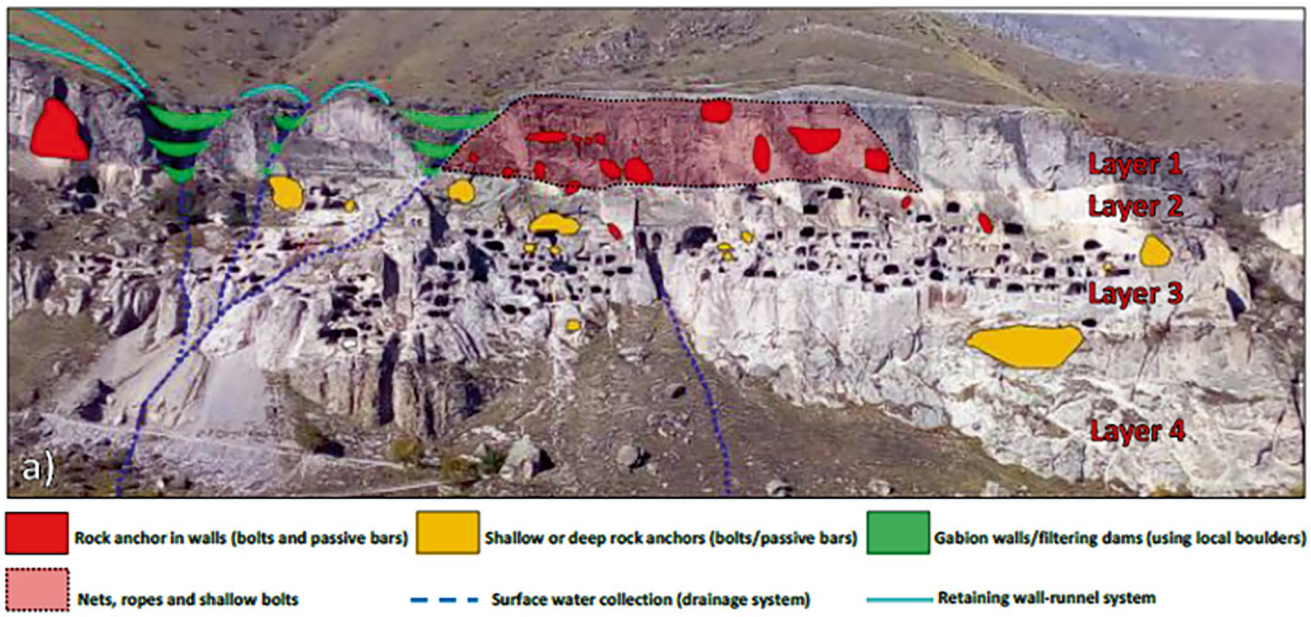

Fig. 35 General master plan for the proposed mitigation measures for the whole Vardzia Monastery. (Fig. 11 in Frodella et al. 2023b)

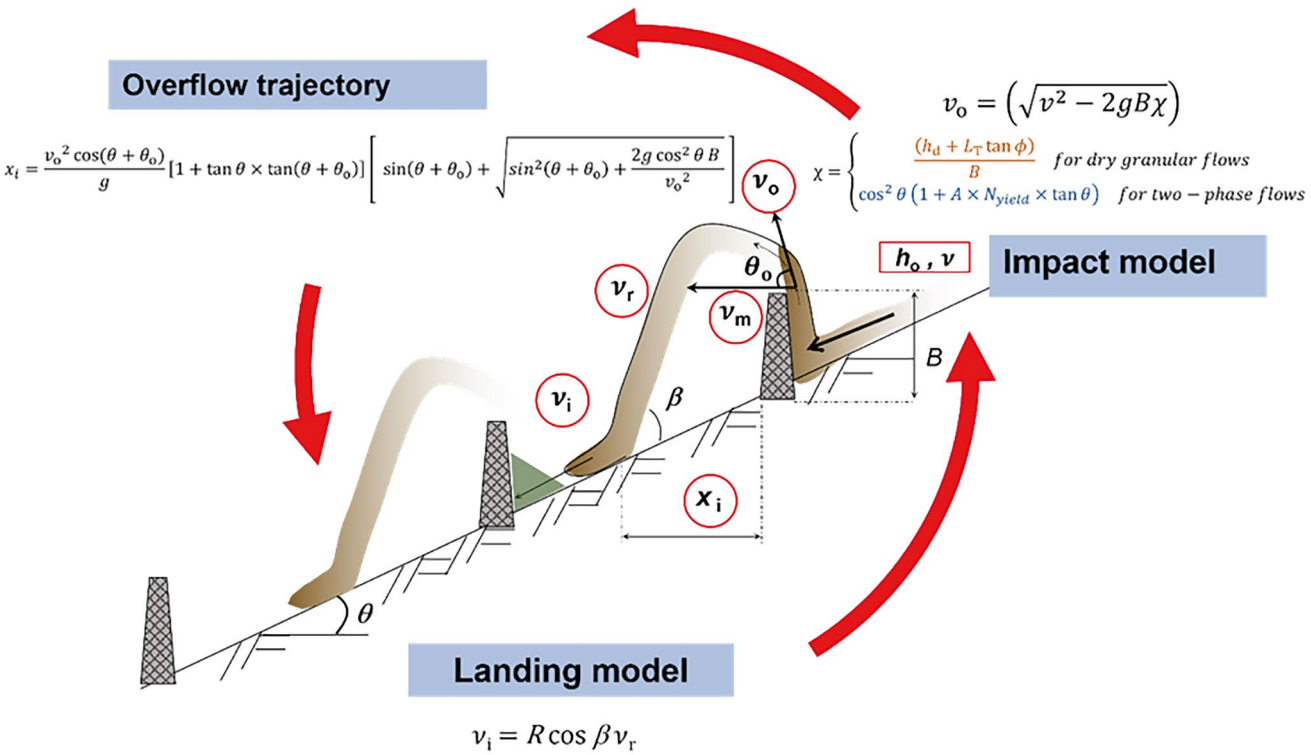

Fig. 36 A schematic diagram of the multiple barrier framework for both dry granular and two-phase flows. The framework includes (1) impact model, (2) overflow and landing kinematics, and (3) subsequent barrier impact. (Fig. 7 in Ng et al. 2023)

and geotechnical conditions, (iii) monitoring groundwater levels and spring discharges, (iv) measurement of flood levels of rivers/streams close to landslides, (v) in-situ and laboratory tests of the engineering properties of soils and rocks, (vi) assessments on the association of the landslides with gully erosion, construction, and other factors (Fig. 40), and (vii) assessments on the performances of mitigation measures implemented.

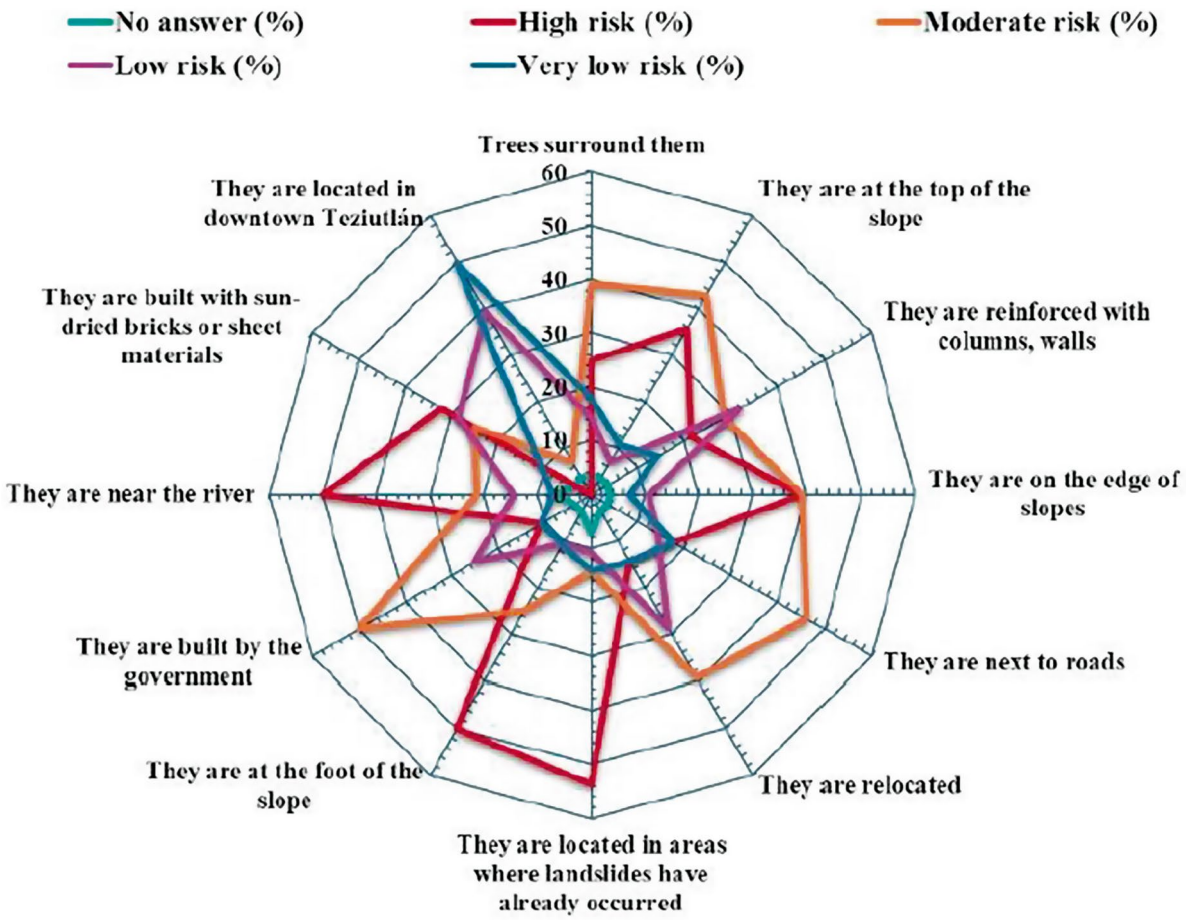

Fig. 37 Perception of the degree of risk homes have of being affected by landslides. (Fig. 5 in Hernández-Cadena et al. 2024)

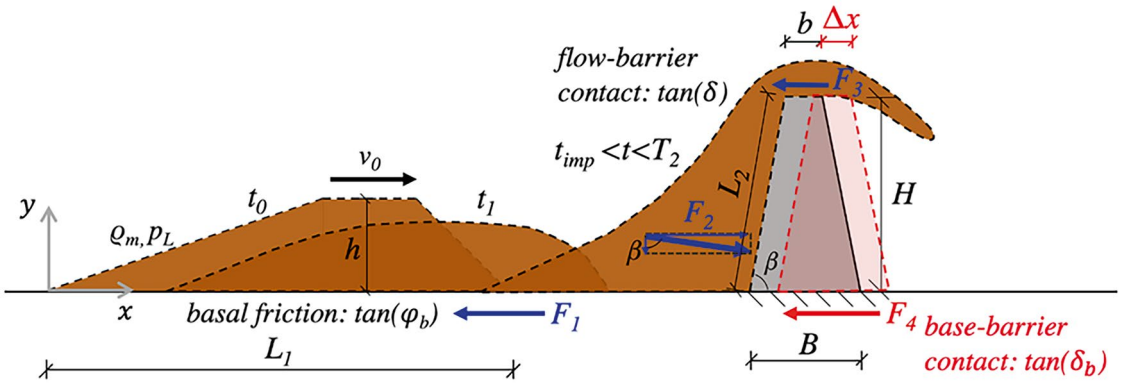

Fig. 38 General conceptual scheme for Landslide Structure Interaction (LSI). (Fig. 1 in Cuomo et al. 2023)

2.18 Socio-Economic Significance

By classifying a total of 412 landslides in India as low, moderate and high socio-economic significance, Parkash (2023) presented the archival records of socio-economically and environmentally significant landslides, differentiating the degree of damages and losses, together with the key lessons learned.

3 Conclusion

This article has presented an overview and a concise review of 3 years of publication of P-LRT: Progress in Landslide Research and Technology. The themes for the Volumes 1–3 of P-LRT were indeed diverse as described above, with a total of 622 researchers/practitioners from 39 countries/regions from Africa, Asia, Europe, North America, Oceania,

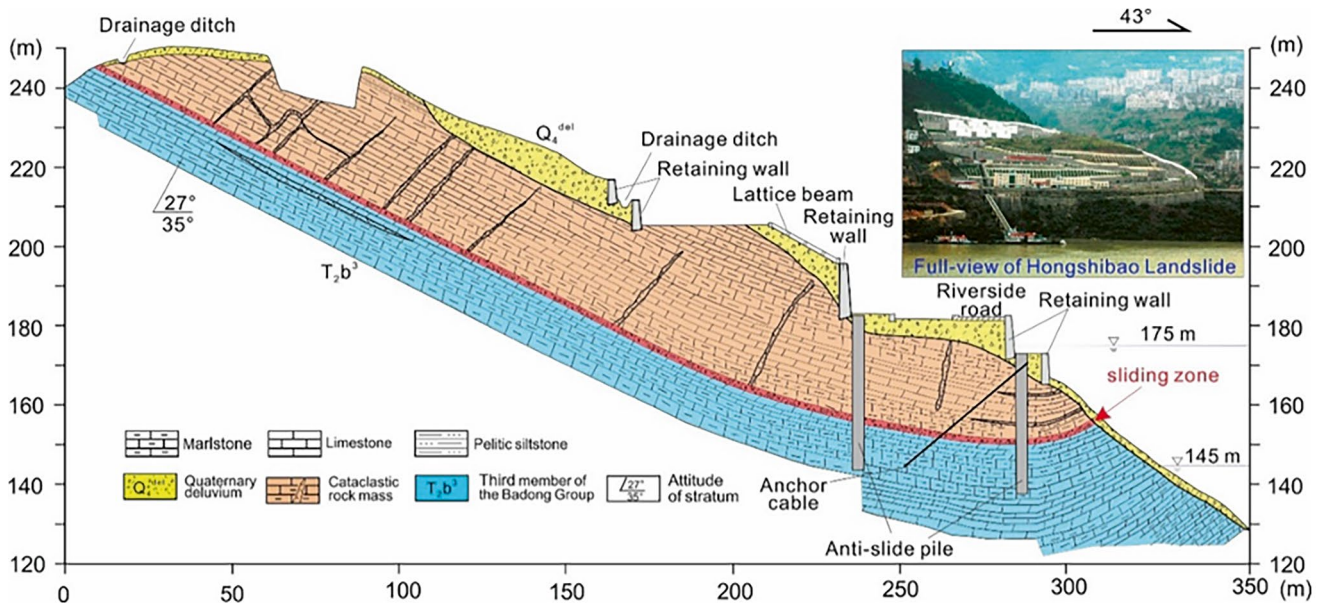

Fig. 39 Cross section of the Hongshibao landslide, whose toe is affected by fluctuations of the TGR level. Drainage ditches, retaining walls, lattice beams and stabilizing piles were constructed to stabilize this actively creeping landslide (Tang et al. 2019). (Fig. 2 in Tang et al. 2023)

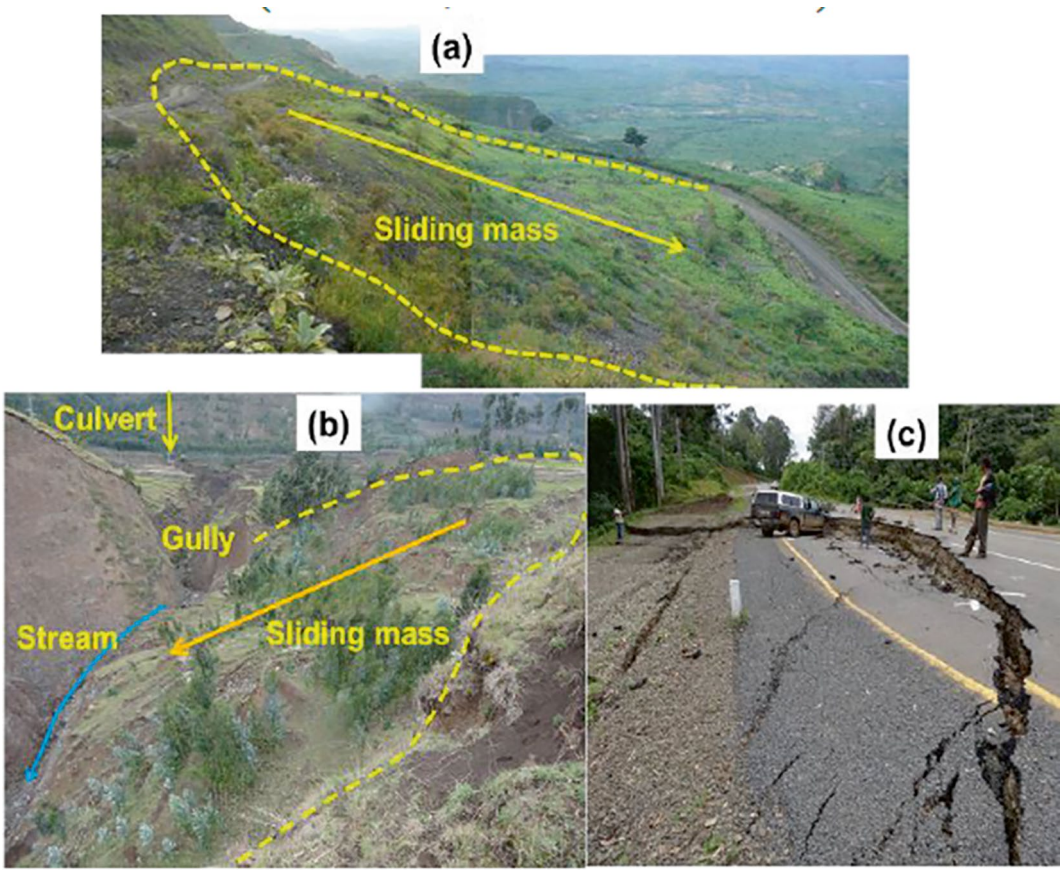

Fig. 40 Examples on the effects and interactions between landslides and roads: (**a**) panoramic view of landslide initiated by road construction which affected farm lands and roads along Lemi-Alemketema route, (**b**) unmanaged water from culvert which caused downstream gully erosion and associated landslides along Woldia Gashena road, and (**c**) car accident due to landslides. (Fig. 9 in Woldearegay 2024)

and South America, contributing to the Vols 1–3 of the ICL Open Access Book Series. In fact, the three volumes of P-LRT had a total of 150 articles from across the world.

It is hoped that P-LRT will continue to serve as a common platform for the publication of recent Progress in Landslide Research and Technology for practical applications and the benefit for the society contributing to the Kyoto Landslide Commitment 2020 for the global promotion of understanding and reducing landslide disaster risk.

References

Abe S, Higaki D, Hayashi K (2023) The role of translational landslides in the evolution of cuesta topography. In: Progress in Landslide Research and Technology, Vol 1, Issue 1. Springer, Cham, pp 149–161

Abolmasov B, Stanković R, Marjanović M, Vulović N, Đurić U (2023a) CliRtheRoads-an integrated approach to landslide risk management on roads in Serbia. In: Progress in Landslide Research and Technology, Vol 2, Issue 2. Springer, Cham, pp 403–409

Abolmasov B, Marjanović M, Đurić U, Krušić J (2023b) An integrated approach to landslides risk management for local and national authorities. In: Progress in Landslide Research and Technology, Vol 2, Issue 2. Springer, Cham, pp 355–360

Abolmasov B, Marjanović M, Stanković R, Đurić U, Vulović N (2024a) Increasing the local road network resilience from natural hazards in municipalities in Serbia. In: Progress in Landslide Research and Technology, Vol 3, Issue 1. Springer, Cham, pp 329–339

Abolmasov B, Stanković R, Vulović N, Marjanović M, Đurić U (2024b) MaPLoRds—mobile application for local road network risk assessment. In: Progress in Landslide Research and Technology, Vol 3, Issue 2. Springer, Cham

Ahmed B, Alam SMRA, Ahmed I, Sammonds P (2023) The anthropogenic aggravation of landslide disasters in Bangladesh: key informants' perspectives. In: Progress in Landslide Research and Technology, Vol 1, Issue 2. Springer, Cham, pp 385–401

Ajmera B, Ahari HE, Loi DH, Setiawan H, Dang K, Sassa K (2023) LS-RAPID manual with video tutorials. In: Progress in Landslide Research and Technology, Vol 1, Issue 1. Springer, Cham, pp 343–406

Alcántara-Ayala I, Garnica-Peña RJ (2023a) Landslide warning systems in low- and lower-middle-income countries: future challenges and societal impact. In: Progress in Landslide Research and Technology, Vol 1, Issue 1. Springer, Cham, pp 137–147

Alcántara-Ayala I, Garnica-Peña RJ (2023b) Landslide warning systems in upper middle-income countries: current insights and new perspectives. In: Progress in Landslide Research and Technology, Vol 1, Issue 2. Springer, Cham, pp 159–168

Alcántara-Ayala I, Garnica-Peña RJ (2023c) Landslide warning systems in high-income countries: past accomplishments and expected endeavours. In: Progress in Landslide Research and Technology, Vol 2, Issue 1. Springer, Cham, pp 147–157

Amali NPG, Maduranga HR, Weerasinghe ARP (2024) Experimental study on residual shear strength of soil using undrained ring shear apparatus. In: Progress in Landslide Research and Technology, Vol 3, Issue 1. Springer, Cham, pp 387–395

Araki K, Takimoto K, Yamazaki Y, Loi DH, Konagai K, Sassa K (2024) Time and site prediction of a potential large-scale landslides and the AR (Augmented Reality). Presentation for early warning. In: Progress in Landslide Research and Technology, Vol 3, Issue 2. Springer, Cham

Arbanas Ž, Mihalić Arbanas S (2023) 10th anniversary of ICL Adriatic-Balkan Network and 5th Regional symposium on landslides. In: Progress in Landslide Research and Technology, Vol 1, Issue 2. Springer, Cham, pp 223–234

Arbanas Ž, Peranić J, Jagodnik V, Prodan MV, Čeh N (2023) Remedial measures impact on slope stability and landslide occurrence in small-scale slope physical model in 1g conditions. In: Progress in Landslide Research and Technology, Vol 2, Issue 2. Springer, Cham, pp 197–220

Ariyarathna I, Sasahara K (2023) Procedure of data processing for the improvement of failure time prediction of a landslide based on the velocity and acceleration of the displacement. In: Progress in Landslide Research and Technology, Vol 2, Issue 2. Springer, Cham, pp 269–283

Ávila G, Guzmán MPA (2024) Lessons from the great Gramalote - Colombia landslide (2010) and its relocation process. In: Progress in Landslide Research and Technology, Vol 3, Issue 2. Springer, Cham

Bandara HAAIS, Onishi R (2023) High resolution numerical weather simulation for orographic precipitation as an accurate early warning tool for landslide vulnerable terrains. In: Progress in Landslide Research and Technology, Vol 2, Issue 2. Springer, Cham, pp 239–246

Barjasteh A (2023) March 2019 flood impact on the stability of Ambal Salt Ridge in the Gotvand Dam Reservoir, Southern Iran. In: Progress in Landslide Research and Technology, Vol 1, Issue 2. Springer, Cham, pp 415–423

Bernat Gazibara S, Jagodnik P, Lukačić H, Sinčić M, Krkač M, Šarić G, Arbanas Ž, Mihalić Arbanas S (2023a) Landslide and soil erosion inventory mapping based on high-resolution remote sensing data: a case study from Istria (Croatia). In: Progress in Landslide Research and Technology, Vol 2, Issue 1. Springer, Cham, pp 363–375

Bernat Gazibara S, Sinčić M, Rossi M, Reichenbach P, Krkač M, Lukačić H, Jagodnik P, Šarić G, Mihalić Arbanas S (2023b) Application of LAND-SUITE for landslide susceptibility modelling using difference mapping units. A case study in Croatia. In: Progress in Landslide Research and Technology, Vol 2, Issue 2. Springer, Cham, pp 343–354

Beroya-Eitner MAA, Vicente MCTM, Dado JMB, Dimain MRS, Maquiling JT, Cruz FAT (2023) Climate change as modifier of landslide susceptibility: case study in Davao Oriental, Philippines. In: Progress in Landslide Research and Technology, Vol 2, Issue 2. Springer, Cham, pp 247–257

Bhandary NP (2023) Experimental simulation of landslide creep in ring shear machine. In: Progress in Landslide Research and Technology, Vol 1, Issue 2. Springer, Cham, pp 75–85

Bornaetxea T, Blais-Stevens A, Miller B (2023a) Landslide inventory map of the Valemount Area, British Columbia, Canada. A detailed methodological description. In: Progress in Landslide Research and Technology, Vol 1, Issue 2. Springer, Cham, pp 373–381

Bornaetxea T, Rossi M, Reichenbach P (2023b) Zonation of landslide susceptibility in the Gipuzkoa province (Spain): an application of LAND-SUITE. In: Progress in Landslide Research and Technology, Vol 2, Issue 1. Springer, Cham, pp 349–362

Capparelli G, Artese S, Carri A, Lombardo M, Segalini A, Valletta A, Muto F (2024) The integrated landslides monitoring system of Gimigliano Municipality, Southern Italy. In: Progress in Landslide Research and Technology, Vol 3, Issue 1. Springer, Cham, pp 341–352

Casagli N, Tofani V, Moretti S, Fanti R, Gigli G, Bianchini S, Segoni S, Frodella W, Carlà T (2023) Advanced technologies for landslides—ATLaS (WCoE 2020–2023). In: Progress in Landslide Research and Technology, Vol 1, Issue 1. Springer, Cham, pp 267–275

Choi CE, Zhang J, Xiong D (2024) Towards an optimization of foundation anchors of landslide-resisting flexible barriers: dynamic pull-

out resistance of anchors. In: Progress in Landslide Research and Technology, Vol 3, Issue 1. Springer, Cham, pp 233–244
Chung CC, Chen BC, Tseng TW, Lee YT (2024) The slope monitoring using embedded system with optical-thermal image fusion and machine learning. In: Progress in Landslide Research and Technology, Vol 3, Issue 1. Springer, Cham, pp 175–187
Cordero CJ, Gesmundo K, Daag A (2024) Assessing and contextualizing site-specific landslide risk in The Philippines. In: Progress in Landslide Research and Technology, Vol 3, Issue 2. Springer, Cham
Cuomo S, Perna AD, Martinelli M (2023) Design protection barriers against flow-like landslides. In: Progress in Landslide Research and Technology, Vol 1, Issue 1. Springer, Cham, pp 123–136
Damians IP, Miyata Y, Rimoldi P, Touze N, Kraus J (2023) Sustainability of geosynthetics-based landslide stabilization solutions. In: Progress in Landslide Research and Technology, Vol 1, Issue 1. Springer, Cham, pp 197–205
Dang K, Sassa K, Loi DH (2023) Teaching tool for LS-Tsunami. In: Progress in Landslide Research and Technology, Vol 2, Issue 2. Springer, Cham, pp 375–400
Delgado LMB, Pavlova I, Yasukawa S, Esperancinha S (2023) Establishment of the disaster risk reduction unit in UNESCO and UNESCO's contribution to global resilience. In: Progress in Landslide Research and Technology, Vol 1, Issue 1. Springer, Cham, pp 209–213
Dias AAV, Gunathilake AAJ (2024) Analytical Hierarchical Process (AHP) prioritization of landslide-causing factors. In: Progress in Landslide Research and Technology, Vol 3, Issue 2. Springer, Cham
Dias AAV, Herath HMJMK, Kulathilake LKNS (2023) Landform geometry for restoration of mountain roads and landslide hazard resilience. In: Progress in Landslide Research and Technology, Vol 1, Issue 1. Springer, Cham, pp 327–339
Dias AAV, Gunathilake AAJ, Sassa K (2024) Emerging seismicity trends linked to catastrophic landslides behavior in Sri Lanka. In: Progress in Landslide Research and Technology, Vol 3, Issue 1. Springer, Cham, pp 137–149
Dissanayaka DMDS, Weerasinghe ARP, Jayakody SHS, Asano S, Bandara KN (2024) Assessment of the structural geological, hydrogeological, and geomorphological relationships of the Athwelthota Landslide, Sri Lanka. In: Progress in Landslide Research and Technology, Vol 3, Issue 1. Springer, Cham, pp 307–315
Duong BV, Fomenko IK, Nguyen KT (2023a) Fractal-based evaluation of the spatial relationship between conditioning factors and the distribution of landslides (A case study in Tnih Tuc, Cao Bang province, Vietnam). In: Progress in Landslide Research and Technology, Vol 2, Issue 2. Springer, Cham, pp 259–268
Duong BV, Fomenko IK, Nguyen LC, Nguyen KT, Do TN, Gorobtsov DN, Zerkal OV, Dinh HT (2023b) Mathematical and numerical modeling of slope stability for the Mong Sen landslide event in the Trung Chai commune, Sapa, Vietnam. In: Progress in Landslide Research and Technology, Vol 2, Issue 1. Springer, Cham, pp 193–207
Duong BV, Fomenko IK, Gorobtsov DN, Nguyen KT, Vu DH, Shubina DD, Pham HNT (2024) An integration of the fractal method and the statistical index method for mapping landslide susceptibility. In: Progress in Landslide Research and Technology, Vol 3, Issue 1. Springer, Cham, pp 409–417
Elshayeb Y (2023) 30 Years of cultural heritage landslides and block movements risk assessment: case studies from Egypt. In: Progress in Landslide Research and Technology, Vol 1, Issue 2. Springer, Cham, pp 169–175
Erzagian E, Wilopo W, Fathani TF (2023) Landslide susceptibility zonation using GIS-based frequency ratio approach in the Kulon Progo Mountains Area, Indonesia. In: Progress in Landslide Research and Technology, Vol 2, Issue 2. Springer, Cham, pp 115–126
Fathani TK, Karnawati D, Wilopo W, Setiawan H (2023) Strengthening the resilience by implementing a standard for landslide early warning system. In: Progress in Landslide Research and Technology, Vol 1, Issue 1. Springer, Cham, pp 277–284
Fiorucci F, Schilirò L, Rossi M, Polpetta F, Fortunato C, Reichenbach P (2024) A web-GIS for the analysis of scientific literature on earthquake-triggered landslides. In: Progress in Landslide Research and Technology, Vol 3, Issue 2. Springer, Cham
Frodella W, Spizzichino D, Lazzeri G, Margottini C, Tofani V, Casagli N (2023a) Assessing landslide hazard in the High City of Antananarivo, Madagascar (UNESCO tentative site). In: Progress in Landslide Research and Technology, Vol 2, Issue 2. Springer, Cham, pp 361–371
Frodella W, Gigli G, Spizzichino D, Margottini C, Elashvili M, Casagli N (2023b) Protection and conservation of Georgian rupestrian cultural heritage sites: a review. In: Progress in Landslide Research and Technology, Vol 2, Issue 1. Springer, Cham, pp 307–320
Fujita K (2024) Introducing Japanese landslide warning and evacuation system to Sri Lanka: field survey of social aspect in the Arayanake Area. In: Progress in Landslide Research and Technology, Vol 3, Issue 1. Springer, Cham, pp 223–232
Fukuhara M, Wang L, Tao S, Tang Z, Tang W, Dong L, Fan Z (2023) A risk evaluation method of unstable slopes using multipoint tilting sensors. In: Progress in Landslide Research and Technology, Vol 2, Issue 1. Springer, Cham, pp 237–246
Gallego JI, Margottini C, Perisse I, Spizzichino D, Beni T, Boldini D, Bonometti F, Casagli N, Castellanza R, Crosta GB, Fratttini P, Gigli G, Lusini E, Rigamonti S, Rusconi G, Vitrano L (2023) Rock slope instabilities affecting the AIUla archaeological sites (KSA). In: Progress in Landslide Research and Technology, Vol 2, Issue 2. Springer, Cham, pp 413–429
Gariano SL, Melillo M, Brunetti MT, Kumar S, Mathiyalagan R, Peruccacci S (2023) Challenges in defining frequentist rainfall thresholds to be implemented in a landslide early warning system in India. In: Progress in Landslide Research and Technology, Vol 1, Issue 1. Springer, Cham, pp 409–416
Garnica-Peña RJ, Alcántara-Ayala I (2023) Do not let your guard down: landslide exposure and local awareness in Mexico. In: Progress in Landslide Research and Technology, Vol 2, Issue 2. Springer, Cham, pp 155–165
Gratchev I, Ravindran S, Kim DH, Cui C, Tang O (2023) Mechanisms of shallow rainfall-induced landslides from Australia: insights into field and laboratory investigations. In: Progress in Landslide Research and Technology, Vol 1, Issue 1. Springer, Cham, pp 113–122
Ha ND, Duong NH, Khanh NQ, Viet TT, Vung DV, Van NTH, Ninh NH (2023) Landslide early warning system based on the empirical approach-case study in Ha Long City (Vietnam). In: Progress in Landslide Research and Technology, Vol 2, Issue 1. Springer, Cham, pp 209–225
Häusler M, Glueer F, Fäh D (2024) The changing seismic site response of the Brienz/Brinzauls rock slope instability: insights from 5 years of monitoring before, during and after a partial collapse in June 2023. In: Progress in Landslide Research and Technology, Vol 3, Issue 2. Springer, Cham
Hernández-Cadena KM, Garnica-Peña RJ, Sánchez JG, Alcántara-Ayala I (2024) Understanding landslide awareness: exploring students' disaster risk perception in higher education institutions. In: Progress in Landslide Research and Technology, Vol 3, Issue 2. Springer, Cham
Higaki D, Hirota K, Dang K, Nakai S, Kaibori M, Matsumoto S, Yamada M, Tsuchiya S, Sassa K (2023) Landslides and countermeasures in Western Japan: historical largest landslide in Unzen and earthquake-induced landslides in Aso, and rain-induced landslides in Hiroshima. In: Progress in Landslide Research and Technology, Vol 1, Issue 2. Springer, Cham, pp 287–307
Hirota K, Suganuma Y, Iwasaki T, Kuwano T (2023) How to teach remotely the vegetation works to protect slope against mass wast-

ing: a case of using video materials in Bhutan. In: Progress in Landslide Research and Technology, Vol 1, Issue 2. Springer, Cham, pp 361–370

Hirota K, Uzawa K, Kuwano T (2024) Simple method of risk assessment for landslides: a case study of the JICA Project in Honduras. In: Progress in Landslide Research and Technology, Vol 3, Issue 2. Springer, Cham

Hoang TV, Chou TY, Fang YM, Wang CT, Tsai MC, Nguyen QD, Nguyen QH, Bui QT, Nguyen QT (2023) Application of global satellite positioning and automatic monitoring in slopeland disaster prevention. In: Progress in Landslide Research and Technology, Vol 1, Issue 2. Springer, Cham, pp 147–158

Huntley D, Bobrowsky P, MacLeod R, Cocking R, Joseph J, Rotheram-Clarke D (2021) Ensuring resilient socio-economic infrastructure: field testing innovative differential GNSS-InSAR-UAV monitoring technologies in mountainous terrain near Ashcroft, British Columbia, Canada. J Mt Sci 18(1):1–20

Huntley D, Bobrowsky P, MacLeod R, Rotheram-Clarke D, Cocking R, Joseph J, Holmes J, Sattler K, Chambers J, Meldrum P, Wilkinson P, Donohue S, Elwood D (2023a) IPL Project 202: landslide monitoring best practices for climate-resilient railway transportation corridors in southwestern British Columbia, Canada. In: Progress in Landslide Research and Technology, Vol 1, Issue 1. Springer, Cham, pp 249–265

Huntley D, Rotheram-Clarke D, MacLeod R, Cocking R, LeSueur P, Lakeland B, Wilson A (2023b) Scalable platform for UAV flight operations, data capture, cloud processing and image rendering of landslide hazards and surface change detection for disaster-risk reduction. In: Progress in Landslide Research and Technology, Vol 1, Issue 2. Springer, Cham, pp 49–61

Huntley D, Rotheram-Clarke D, MacLeod R, Cocking R, Joseph J, LeSueur P (2023c) Landslide monitoring with RADARSAT Constellation Mission InSAR, RPAS-derived point-clouds and RTK-GNSS time-series in the Thompson River Valley, British Columbia, Canada. In: Progress in Landslide Research and Technology, Vol 2, Issue 1. Springer, Cham, pp 379–388

Huntley D, Rotheram-Clarke D, Sattler K, Elwood D (2023d) Surficial geology and geomorphology of the North Slide, Thompson River valley, British Columbia, Canada: application of fundamental geoscience information to interpretations of geospatial monitoring results. In: Progress in Landslide Research and Technology, Vol 2, Issue 2. Springer, Cham, pp 221–238

Jayakody SHS, Uzuoka R, Ueda K, Saito K (2024a) Centrifuge modeling of slopes subjected to groundwater flow and rainfall infiltration. In: Progress in Landslide Research and Technology, Vol 3, Issue 1. Springer, Cham, pp 151–161

Jayakody SHS, Kumarage B, Karunawardena A (2024b) Application of subsurface drainage for cost-effective mitigation strategies: a case study of Hakgala landslide, Sri Lanka. In: Progress in Landslide Research and Technology, Vol 3, Issue 2. Springer, Cham

Jayathilake D, Kiyota T, Konagai K, Shiga M, Nihaaj M (2024) Influence of intra-particle saturation ratio on strength degradation of pumice soil. In: Progress in Landslide Research and Technology, Vol 3, Issue 1. Springer, Cham, pp 205–212

Joshi S, Subramanian SS (2024) Landslide dam studies in Uttarakhand, India: past, present and future. In: Progress in Landslide Research and Technology, Vol 3, Issue 2. Springer, Cham

Kamal ASMM, Samm AA, Ahmed B, Sammonds P (2023) Refugees' perception of landslide disasters: insights from the Rohingya camps in Cox's Bazar, Bangladesh. In: Progress in Landslide Research and Technology, Vol 2, Issue 2. Springer, Cham, pp 431–439

Karunarathna S, Bandara P, Goto S, Bandaranayake S (2024) Identification of potential natural slope failure zones by geomorphological analyses using raster slope shading of LiDAR; case study from Kegalle, Sri Lanka. In: Progress in Landslide Research and Technology, Vol 3, Issue 1. Springer, Cham, pp 363–377

Kawamura K, Oguri K, Inoue M, Hsiung KH, Kudaka T, Takai K (2023) Ongoing persistent slope failures at the toe of a Giant submarine slide in the Ryukyu Trench that generated the AD 1771 Meiwa Tsunami. In: Progress in Landslide Research and Technology, Vol 1, Issue 2. Springer, Cham, pp 63–74

Kitazato H (2024) Global warming may accelerate submarine landslides in the oceans -possible disaster chain reactions-. In: Progress in Landslide Research and Technology, Vol 3, Issue 1. Springer, Cham, pp 83–91

Konagai K (2023) Coseismic stress changes, landslides in the 2004 Mid-Niigata Prefecture Earthquake, and their impact on post-quake rehabilitations. In: Progress in Landslide Research and Technology, Vol 1, Issue 2. Springer, Cham, pp 235–246

Konagai K, Karunawardena A, Bandara KN, Sassa K, Onishi R, Uzuoka R, Asano R, Sasahara K, Jayakody S, Ariyarathna I (2023a) Early warning system against rainfall-induced landslide in Sri Lanka. In: Progress in Landslide Research and Technology, Vol 1, Issue 1. Springer, Cham, pp 217–235

Konagai K, Kiyota T, Furuta R, Shiga M, Pokhrel RM, Ikeda T (2023b) Long-lasting post-quake deformation buildups in the grounds that spread laterally in recent earthquakes. In: Progress in Landslide Research and Technology, Vol 1, Issue 2. Springer, Cham, pp 213–222

Krkač M, Gazibara SB, Sinčić M, Lukačić H, Šarić G, Mihalić Arbanas S (2023) Impact of input data on the quality of the landslide susceptibility large-scale maps: a case study from NW Croatia. In: Progress in Landslide Research and Technology, Vol 2, Issue 1. Springer, Cham, pp 135–146

Kyushu Regional Development Bureau, Ministry of Land, Infrastructure, Transport and Tourism, 2016–2020 (2021) Materials for technical study meetings on the restoration of slope failure in the Aso-Ohashi Bridge area (1st to 10th meetings). (ref. Aug 7 2021) (in Japanese)

Li C, Long J, Liu Y, Huang D (2024) Landslide prediction model based upon intelligent processing of multi-point monitoring information: a review. In: Progress in Landslide Research and Technology, Vol 3, Issue 1. Springer, Cham, pp 279–291

Loi DH, Jayakody SHS, Sassa K (2023) Teaching tool "undrained dynamic loading ring shear testing with video". In: Progress in Landslide Research and Technology, Vol 1, Issue 2. Springer, Cham, pp 325–359

Loi DH, Tien PV, Dang K, Sassa K (2024) LS-RAPID estimation of the critical pore pressure able to initiate (activate) landslides within the existing large-scale landslides. In: Progress in Landslide Research and Technology, Vol 3, Issue 2. Springer, Cham

Lozano J, Ávila G (2024) Landslide hazard evaluation of a large waste landfill in Bogotá City. In: Progress in Landslide Research and Technology, Vol 3, Issue 1. Springer, Cham, pp 93–103

Małka A, Laskowicz I, Grabowski D (2024) The accuracy of landslide susceptibility mapping in Young Glacial River Valleys. In: Progress in Landslide Research and Technology, Vol 3, Issue 2. Springer, Cham

Marjanović M, Abolmasov B, Krušić J, Đurić U (2024) Regional debris flow hazard assessment of the Grdelica Gorge (Serbia). In: Progress in Landslide Research and Technology, Vol 3, Issue 1. Springer, Cham, pp 213–221

Matsunami K, Sassa K, Doan L, Weerasinghe R, Munasinghe T (2024a) Observation of seismic ground motion and pore water pressure in Lineated Valley Fill of Wakayama, Southwest Japan. In: Progress in Landslide Research and Technology, Vol 3, Issue 1. Springer, Cham, pp 65–81

Matsunami K, Sassa K, Weerasinghe R, Munasinghe T, Doan L (2024b) Challenges of earthquake and micro-earthquake monitoring in Sri Lanka. In: Progress in Landslide Research and Technology, Vol 3, Issue 2. Springer, Cham

Matsuoka Y (2024) Sendai framework voluntary commitments: monitoring landslide stakeholders' contributions. In: Progress in

Landslide Research and Technology, Vol 3, Issue 1. Springer, Cham, pp 189–204
Michel J (2023) Consequence-frequency matrix as a tool to assess landslides risk. In: Progress in Landslide Research and Technology, Vol 2, Issue 2. Springer, Cham
Mihalić Arbanas S, Gazibara SB, Krkač M, Sinčić M, Lukačić H, Jagodnik P, Željko A (2023) Landslide detection and spatial prediction: application of data and information from landslide maps. In: Progress in Landslide Research and Technology, Vol 1, Issue 2. Springer, Cham, pp 195–212
Mikoš M (2023a) Landslide research and technology in patent documents. In: Progress in Landslide Research and Technology, Vol 1, Issue 2. Springer, Cham, pp 29–48
Mikoš M (2023b) Landslide research and technology in international standards. In: Progress in Landslide Research and Technology, Vol 2, Issue 1. Springer, Cham, pp 179–191
Mikoš M (2023c) Landslide in higher education curricula and beyond. In: Progress in Landslide Research and Technology, Vol 2, Issue 2. Springer, Cham, pp 167–181
Mikoš M, Bezak N, Costa JP, Massri MB, Novalija I, Jermol M, Grobelnik M (2023) Natural-hazard-related web observatory as a sustainable development tool. In: Progress in Landslide Research and Technology, Vol 1, Issue 1. Springer, Cham, pp 83–97
Mikoš M, Bezak N, Jurček T, Kuzmanić T, Maček M, Rusjan S, Sodnik J (2024) Recent UL FGG contributions to the 2020 Kyoto commitment. In: Progress in Landslide Research and Technology, Vol 3, Issue 1. Springer, Cham, pp 329–339
Miyagi T, Loi DH (2024) How to detect the previous large-scale landslide: source of future landslides by interpretation of ground topography from digital maps. In: Progress in Landslide Research and Technology, Vol 3, Issue 2. Springer, Cham
Miyagi T, Ikeda K, Ishikawa H, Doan L, Thanh NK, Tien PV, Li Y, Zhang F (2024) Interpretation and mapping for the prediction of sites at risk of landslide disasters: from aerial photography to detection by DTMs. In: Progress in Landslide Research and Technology, Vol 3, Issue 1. Springer, Cham, pp 15–61
Moncayo S, Ávila G (2023) Landslide travel distances in Colombia from national landslide database analysis. In: Progress in Landslide Research and Technology, Vol 1, Issue 1. Springer, Cham, pp 315–325
Munasinghe D, Fernando T, Keraminiyage K, Karunawardena A (2023) A review of the disaster risk assessment perspectives. In: Progress in Landslide Research and Technology, Vol 2, Issue 2. Springer, Cham, pp 323–340
Nakata AM, Konagai K, Onishi R (2024) Multiple landslides in an area draped in volcanic matters: the dual impacts of rains and earthquakes. In: Progress in Landslide Research and Technology, Vol 3, Issue 1. Springer, Cham, pp 105–114
Ng CWW, Poudyal S, Liu H, Bhatta A, De Silva WARK, Jia Z (2023) Investigation of debris flow impact mechanisms and designs. In: Progress in Landslide Research and Technology, Vol 2, Issue 2. Springer, Cham, pp 311–322
Nguyen CC, Vo P, Doan VL, Nguyen QB, Nguyen TC, Nguyen QD (2023a) Assessment of the effects of rainfall frequency on landslide susceptibility mapping using AHP method: a case study for a mountainous region in Central Vietnam. In: Progress in Landslide Research and Technology, Vol 1, Issue 2. Springer, Cham, pp 87–98
Nguyen LC, Do TN, Nguyen QD (2023b) Characteristics and remedy solutions for a New Mong Sen Deep-Seated Landslide, Sapa Town, Vietnam. In: Progress in Landslide Research and Technology, Vol 1, Issue 2. Springer, Cham, pp 403–413
Nishikawa S (2023) Application of Ichi-Nichi-Mae (the day before the disaster) project for landslide awareness and risk communication. In: Progress in Landslide Research and Technology, Vol 1, Issue 2. Springer, Cham, pp 317–321
Nomura F, Konagai K, Aftabur Rahman M, Tajima Y (2024) Mud-mark-based estimations of mass-wasting processes caused by the 2008 Iwate-Miyagi Nairiku Earthquake, Japan. In: Progress in Landslide Research and Technology, Vol 3, Issue 1. Springer, Cham, pp 293–306
Onishi R, Hirai J, Kolomenskiy D, Yasuda Y (2023) Real-time high-resolution prediction of orographic rainfall for early warning of landslides. In: Progress in Landslide Research and Technology, Vol 1, Issue 1. Springer, Cham, pp 237–248
Onishi R, Bandara HAAIS, Matsumoto K (2024) High-resolution rainfall simulations for early warning of rain-induced rapid long-traveling landslides in Sri Lanka. In: Progress in Landslide Research and Technology, Vol 3, Issue 2. Springer, Cham
Parkash S (2023) Lessons learned from landslides of socio-economic and environmental significance in India. In: Progress in Landslide Research and Technology, Vol 1, Issue 2. Springer, Cham, pp 309–315
Parkash S, Singh R, Badola S (2024) Assessing landslide disaster risk reduction and resilience—case studies and insights, India. In: Progress in Landslide Research and Technology, Vol 3, Issue 2. Springer, Cham
Patera A, Fabbri AG (2024) Experiments of modelling subaqueous landslide susceptibility in Lake Albano of Castel Gandolfo. In: Progress in Landslide Research and Technology, Vol 3, Issue 2. Springer, Cham
Paulín GL, Parrot JF, Castro-Miguel R, Miguel RC, Salinas LA, Quesada FA (2023a) Digital terrain models derived from unmanned aerial vehicles and landslide susceptibility. In: Progress in Landslide Research and Technology, Vol 2, Issue 1. Springer, Cham, pp 389–399
Paulín GL, Anaya RMA, Salinas LA, Parrot JF, Miguel RC (2023b) Use of GIS to assess susceptibility per landform unit to gravitational processes and their volume. In: Progress in Landslide Research and Technology, Vol 2, Issue 1. Springer, Cham, pp 401–411
Paulín GL, Bursik M, Salinas LA, Jaen MM (2024) Assessing landslide distribution for landform hazard zoning purposes: a case study on the Western Flank of Iztaccíhuatl Volcano, Puebla, México. In: Progress in Landslide Research and Technology, Vol 3, Issue 1. Springer, Cham, pp 355–361
Peresan A, Alvioli M, Zuccolo E, Vaccari F, Badreldin H (2024) An approach to rockfall hazard scenarios based on earthquake ground motion. In: Progress in Landslide Research and Technology, Vol 3, Issue 2. Springer, Cham
Perna AD, Cuomo S, Martinelli M (2023) Modelling of Landslide-Structure Interaction (LSI) through Material Point Method (MPM). In: Progress in Landslide Research and Technology, Vol 2, Issue 1. Springer, Cham, pp 159–178
Poggi F, Montalti R, Intrieri E, Ferretti A, Catani F, Raspini F (2023) Spatial and temporal characterization of landslide deformation pattern with Sentinel-1. In: Progress in Landslide Research and Technology, Vol 2, Issue 1. Springer, Cham, pp 321–329
Ramesh MV, Thirugnanam H, Singh B, Kumar MN, Pullarkatt D (2023a) Landslide early warning systems: requirements and solutions for disaster risk reduction-India. In: Progress in Landslide Research and Technology, Vol 1, Issue 2. Springer, Cham, pp 259–286
Ramesh MV, Thirugnanam H, Kumar MN, Singh B, Harichandana E, Guntha R (2023b) Community scale landslide resilience: a citizen-science approach. In: Progress in Landslide Research and Technology, Vol 2, Issue 2. Springer, Cham, pp 183–196
Ríos D, Ávila G (2023) Lessons from 2019–2020 landslide risk assessment in an urban area of volcanic soils in Pereira-Colombia. In: Progress in Landslide Research and Technology, Vol 2, Issue 1. Springer, Cham, pp 331–345
Rowberry M, Klimeš J, Blahůt J, Balek J, Kusák M (2023) A global database of giant landslides on volcanic islands. In: Progress in

Landslide Research and Technology, Vol 1, Issue 1. Springer, Cham, pp 295–304
Sakai N, Ishizawa T, Danjo T (2024) Experimental research on rain-induced landslide mechanism using large-scale rainfall experimental facility: findings and challenges. In: Progress in Landslide Research and Technology, Vol 3, Issue 2. Springer, Cham
Sassa S (2023a) Review of the founding issue of P-LRT: Progress in Landslide Research and Technology. In: Progress in Landslide Research and Technology, Vol 1, Issue 2. Springer, Cham, pp 179–193
Sassa S (2023b) Landslides and Tsunamis: Multi-Geohazards. Landslides 20(7):1335–1341
Sassa S (2024) Global promotion of understanding and reducing landslide disaster risk: two years on P-LRT. In: Progress in Landslide Research and Technology, Vol 3, Issue 1. Springer, Cham, pp 247–277
Sassa S, Takagawa T (2019) Liquefied gravity flow-induced tsunami: first evidence and comparison from the 2018 Indonesia Sulawesi earthquake and tsunami disasters. Landslides 16(1):195–200
Sassa S, Grilli ST, Tappin DR, Sassa K, Karnawati D, Gusiakov VK, Løvholt F (2022) Understanding and reducing the disaster risk of landslide-induced tsunamis: a short summary of the panel discussion in the World Tsunami Awareness Day Special Event of the Fifth World Landslide Forum. Landslides 19(2):533–535
Sassa K, Loi DH, Dang K, Tien P (2023a) Sliding-surface liquefaction and undrained steady-state shear-strength. In: Progress in Landslide Research and Technology, Vol 2, Issue 1. Springer, Cham, pp 11–95
Sassa S, Grilli ST, Tappin DR, Sassa K, Karnawati D, Gusiakov VK, Løvholt F (2023b) Understanding and reducing the disaster risk of landslide-induced tsunamis: outcome of the panel discussion and the World Tsunami Awareness Day Special Event of the Fifth World Landslide Forum. In: Progress in Landslide Research and Technology, Vol 1, Issue 1. Springer, Cham, pp 65–81
Sassa K, Loi DH, Matsunami K, Miyagi T, Weerasnghe R, Munasinghe T, Thaldena N, Karunawardena A, Konagai K (2024) Risk identification of large-scale landslides triggered by rainfalls and post-rainfall earthquakes in Sri Lanka. In: Progress in Landslide Research and Technology, Vol 3, Issue 2. Springer, Cham
Sattar A, Konagai K (2023) Post-formation behaviour of Hattian Landslide Dam and post-breaching situation. In: Progress in Landslide Research and Technology, Vol 2, Issue 2. Springer, Cham, pp 299–309
Strom A (2023) Central Asia rockslides inventory: compilation, analysis and training—progress of the IPL WCoE. In: Progress in Landslide Research and Technology, Vol 1, Issue 1. Springer, Cham, pp 285–294
Tan Q, Tang H (2023) In situ triaxial creep test on gravelly slip zone soil of a giant landslide: innovative attempts and findings. In: Progress in Landslide Research and Technology, Vol 1, Issue 2. Springer, Cham, pp 109–121
Tang H (2023) Identification and mitigation of reservoir landslides: cases studied in the three gorges reservoir area of China. In: Progress in Landslide Research and Technology, Vol 2, Issue 1. Springer, Cham, pp 97–131
Tang H, Wasowski J, Juang CH (2019) Geohazards in the three gorges reservoir area, China—lessons learned from decades of research. Eng Geol 105267
Tang H, Wang L, Li C, Zou Z (2023) Key techniques of prevention and control for reservoir landslides based on evolutionary process. In: Progress in Landslide Research and Technology, Vol 1, Issue 2. Springer, Cham, pp 11–28
Tappin DR, Grilli ST (2020) The continuing underestimated tsunami hazard from submarine landslides. In: Sassa K, Mikoš M, Sassa S, Bobrowsky PT, Takara K, Dang K (eds) Understanding and reducing landslide disaster risk: volume 1 Sendai Landslide Partnerships and Kyoto Landslide Commitment. Part III landslide-induced tsunamis, Springer Nature, pp 343–350
Thanh NK, Miyagi T, Huy TC, Hamasaki E, Tien DV, Kasuya Y (2023) Community level slope disaster risk reduction program through multi-scale mapping by mountain ethnic group in Northern Vietnam-Project Study by JICA/Lao Cai DARD/ITST. In: Progress in Landslide Research and Technology, Vol 2, Issue 1. Springer, Cham, pp 249–274
Thirugnanam H (2023) Deep learning in landslide studies: a review. In: Progress in Landslide Research and Technology, Vol 1, Issue 2. Springer, Cham, pp 247–255
Tien DV, Thanh NK, Quang LH, Ngoc DHA, Sassa K, Miyagi T, Abe S (2023) Landslide risk assessment in the tropical zone of Vietnam as a contribution to the mitigation of natural disaster vulnerability. In: Progress in Landslide Research and Technology, Vol 2, Issue 1. Springer, Cham, pp 275–305
Tien PV, Nhan TT, Luong LH, Cuong TQ (2024) Physical mechanism and numerical simulation of landslide dam formation. In: Progress in Landslide Research and Technology, Vol 3, Issue 1. Springer, Cham, pp 399–408
Tiwari B, Ajmera B (2023) Advancements in shear strength interpretation, testing, and use for landslide analysis. In: Progress in Landslide Research and Technology, Vol 2, Issue 2. Springer, Cham, pp 3–54
Tiwari RC, Bhandary NP (2023) Application of spectral element method (SEM) in slope instability analysis. In: Progress in Landslide Research and Technology, Vol 1, Issue 1. Springer, Cham, pp 163–174
Tiwari B, Tran D (2023) Using experimental models to calibrate numerical models for slope stability and deformation analysis. In: Progress in Landslide Research and Technology, Vol 1, Issue 1. Springer, Cham, pp 185–195
Tofani V, Masi EB, Rossi G (2023) Physically-based regional landslide forecasting modelling: model set-up and validation. In: Progress in Landslide Research and Technology, Vol 2, Issue 2. Springer, Cham, pp 127–135
Tozer B, Sandwell D, Smith W, Olson C, Beale J, Wessel P (2019) Global bathymetry and topography at 15 arc sec: SRTM15+. Earth Space Sci 6:1847–1864. https://doi.org/10.1029/2019EA000658
Trofymchuk O, Kaliukh I, Lebid O, Klymenko V, Vyshniakov V, Kreta D, Elshayeb Y (2023) Effect of landslide deformation on the stability of St. Andrew's Church (Kyiv, Ukraine): applications of remote sensing and mathematical modeling. In: Progress in Landslide Research and Technology, Vol 1, Issue 2. Springer, Cham, pp 133–145
Vacha D, Mandrone G, Morresi D, Garbarino M (2023) Mapping post-fire monthly erosion rates at the catchment scale using empirical models implemented in GIS. A case study in Northern Italy. In: Progress in Landslide Research and Technology, Vol 1, Issue 1. Springer, Cham, pp 99–112
Velásquez-Espinoza G, Alcántara-Ayala I (2024) Spatio-temporal distribution of rainfall-induced landslides in Nicaragua (2000–2022): preliminary insights to communicate landslide disaster risk. In: Progress in Landslide Research and Technology, Vol 3, Issue 1. Springer, Cham, pp 125–136
Wang F, Nam K (2023) Landslide disasters caused by the 2018 Eastern Iburi Earthquake in Hokkaido Japan and the countermeasures to completely prevent the similar disasters in the future. In: Progress in Landslide Research and Technology, Vol 1, Issue 1. Springer, Cham, pp 305–313
Wang Y, Cheng Q, Lin Q, Shi A, Ming J, Feng Z, Song Z (2023) Rock avalanches in the Tibetan Plateau of China. In: Progress in Landslide Research and Technology, Vol 2, Issue 2. Springer, Cham, pp 55–111
Wang Y, Shan W, Guo Y, Zhang C, Liu S (2024) Evaluation of assessment models for landslide susceptibility mapping in permafrost

areas. In: Progress in Landslide Research and Technology, Vol 3, Issue 1. Springer, Cham, pp 163–173
Weerasinghe ARP, Jayakody SHS, Amali NPG, Maduranga HR, Loi DH (2024) Assessing the potential rapid and long travelling landslides in Sri Lanka: a case study of Athwelthota Landslide. In: Progress in Landslide Research and Technology, Vol 3, Issue 1. Springer, Cham, pp 379–385
Wijaya IPK, Towashiraporn P, Joshi A, Jayasinghe S, Dewi A, Alam MN (2023) Climate change-induced regional landslide hazard and exposure assessment for aiding climate resilient road infrastructure planning: a case study in Bagmati and Madhesh Provinces, Nepal. In: Progress in Landslide Research and Technology, Vol 1, Issue 1. Springer, Cham, pp 175–184
Woldearegay K (2024) Characteristics of landslides affecting road networks in Ethiopia: evidence from 25 years research, practice and documentation. In: Progress in Landslide Research and Technology, Vol 3, Issue 2. Springer, Cham
Yasufuku N, Alowiasy A (2023) Challenges and lessons learned from heavy rainfall-induced geo-disasters over the last decade in Kyushu Island, Japan. In: Progress in Landslide Research and Technology, Vol 1, Issue 2. Springer, Cham, pp 123–132
Zerkal OV, Barykina OS (2023) Suffosion landslides as a specific type of slope deformations in the European part of Russia. In: Progress in Landslide Research and Technology, Vol 1, Issue 2. Springer, Cham, pp 99–108
Zerkal OV, Barykina OS (2024) Loess landslides–peculiarities of deformation mechanism. In: Progress in Landslide Research and Technology, Vol 3, Issue 1. Springer, Cham, pp 115–123
Zerkal OV, Chernomorets SS, Iudina VA, Dokukin MD, Krylenko IN, Savernyuk EA, Vinogradova TA, Zaporozhchenko EV (2023) The modern activity of the Buzulgan landslide and its influence on the debris flow hazard for the Tyrnyauz town (Northern Caucasus, Russia). In: Progress in Landslide Research and Technology, Vol 2, Issue 1. Springer, Cham, pp 227–235

Landslides Risk Reduction with Focus on Mitigation in India

Surya Parkash, Ravinder Singh, and Shubham Badola

Abstract

India is vulnerable to landslides, with around 0.42 million km^2 (approx. 12.6%) of its land area at risk. The most affected regions include the northwestern Himalayas (Jammu & Kashmir, Himachal Pradesh, Uttarakhand), the northeastern sub-Himalayan states (Sikkim, West Bengal, Assam, etc.), and both the Western and Eastern Ghats (Maharashtra, Karnataka, Kerala, Andhra Pradesh, Tamil Nadu). These natural disasters can result in considerable loss of life and property and also disrupting economic activities, especially in mountainous areas. Landslides are more frequent during the monsoon season due to heavy rainfall, and their occurrence often coincides with earthquake-prone zones, heightening the risks. In many developing countries, landslides can lead to economic losses of 1–2% of the Gross National Product, with 80% of landslide-related fatalities occurring in these nations.

In response to these challenges, the National Disaster Management Authority (NDMA) has launched various initiatives, including the Landslide Risk Mitigation Scheme (LRMS) in July 2019. This scheme aims to provide financial and technical assistance for targeted mitigation projects and has fostered partnerships with states such as Sikkim, Mizoram, Nagaland, and Uttarakhand. Additionally, NDMA is emphasizing capacity building through training programs focused on landslide mitigation and disaster risk management. A pilot project has been initiated to develop low-cost landslide monitoring solutions, resulting in a predictive system that uses artificial intelligence. This system not only detects soil movement but also issues early warnings via SMS alerts and activates roadside safety measures. NDMA also released a comprehensive National Landslide Risk Management Strategy (A publication of the National Disaster Management Authority, Government of India, 2019) as per fifth target of Sendai Framework for Disaster Risk Reduction (SFDRR) i.e., "Substantially increase the number of countries with national and local disaster risk reduction strategies by 2020". Through these comprehensive strategies, NDMA is working to improve awareness and preparedness for landslides, promote community engagement, and drive technological advancements to effectively mitigate risks.

1 Introduction

India faces a substantial risk of landslides, which have the potential to cause severe destruction, including loss of life and property. According to the Geological Survey of India (GSI), approximately 0.42 million square kilometers, or nearly 12.6% of India's total land area, are vulnerable to landslides. Regions particularly prone to landslide disaster (Fig. 1) include the north-western Himalayas (Jammu & Kashmir, Himachal Pradesh, Uttarakhand), the sub-Himalayan region in the northeast (Sikkim, West Bengal-Darjeeling, Assam, Arunachal Pradesh, Manipur, Meghalaya, Mizoram, Nagaland, Tripura), the Western Ghats (Maharashtra, Goa, Karnataka, Kerala), and parts of the Eastern Ghats (Andhra Pradesh's Araku area and Tamil Nadu).

Landslides pose a serious risk to both life and property, greatly affecting livelihoods by disrupting routine economic

S. Parkash (✉) · R. Singh · S. Badola
National Institute of Disaster Management (NIDM), Delhi, India
e-mail: surya.nidm@nic.in

B. Abolmasov et al. (eds.), *Progress in Landslide Research and Technology, Volume 4 Issue 1, 2025*, Progress in Landslide Research and Technology, https://doi.org/10.1007/978-3-031-89836-5_11

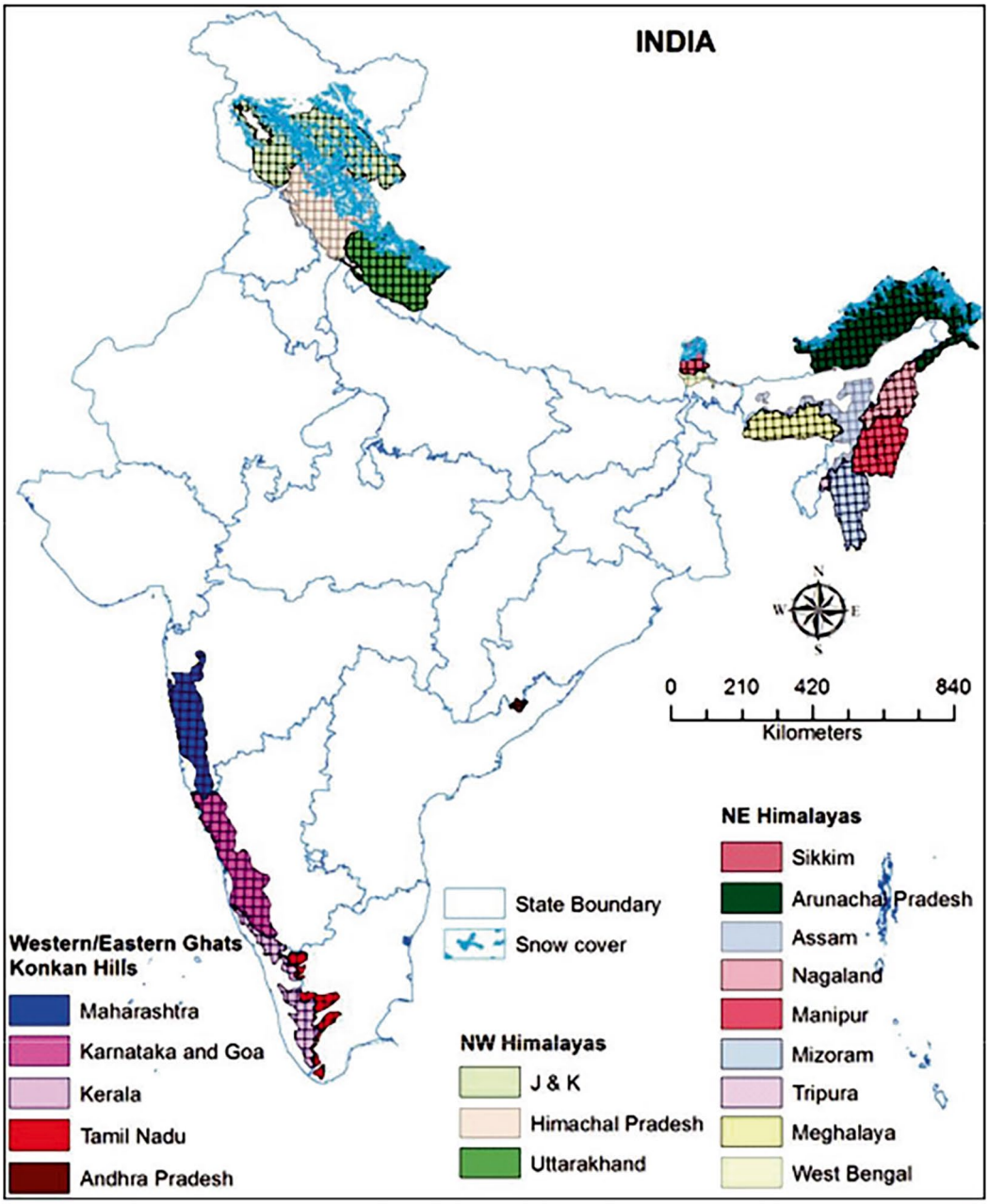

Fig. 1 Landslide-affected regions in India. (***Source:*** *NLRMS, NDMA* 2019)

activities in India's hill regions. Such disasters are common not only in the mountainous states like Himachal Pradesh, Uttarakhand, Jammu & Kashmir, and the northeastern states but also in hilly areas of Maharashtra, Karnataka, and Kerala. Landslides are common in these regions, particularly during the monsoon season, when intense rainfall often triggers large-scale landslides and debris flows. For instance, during the early morning hours of July 30, 2024, a massive landslide accompanied by debris flow struck Mundakki, Chooralmala, and Vellarimala Village in Wayanad District, Kerala, causing substantial loss of life and property. Similar rainfall-induced landslide events were reported in Kerala in August 2018 (Kanungo et al. 2020). Many landslide-prone areas are also located in seismically active zones, making them susceptible to earthquake-induced landslides as witnessed during events like the Sikkim (2011), Kashmir (2005), Chamoli (1999), and Uttarkashi (1991) earthquakes. Landslide-related economic losses in developing nations may reach 1–2% of Gross National Product, with developing countries accounting for 80% of landslide fatalities. This highlights the need for hazard assessment and mitigation as a priority for technocrats and policymakers in these regions.

In recent times, landslides have become more frequent due to extreme weather events, environmental degradation, and human activities, causing increased losses of life, livestock, and property. Addressing these losses is a growing challenge for technologists who also see this as an opportunity to develop AI-based solutions for mitigating landslide impacts in the future. Since local communities are often the first to respond to disasters, technological interventions must be designed with their needs in mind.

2 Background

The National Disaster Management Authority (NDMA) introduced the Guidelines on Management of Landslides and Snow Avalanches, establishing national policies for landslide management (NDMA 2009). Developed with input from the Ministry of Mines, GSI, and other central, state, and academic bodies, these guidelines set a framework for managing landslide-related activities. Despite their release, progress in implementing these guidelines has been slow in landslide-prone states and union territories (Fig. 2).

3 Discussion and Conclusion: Initiatives and Outcomes

3.1 Landslide Risk Mitigation Scheme (LRMS)

A critical element in landslide mitigation has been the active involvement of state governments and relevant agencies. On December 19, 2014, NDMA organized a state-level meeting with landslide-prone states, union territories, and key departments to address issues surrounding the **Landslide Risk Mitigation Scheme (LRMS)**. Representatives from 14 states and 9 departments participated, acknowledging the need for proactive measures. Prior to 2014, NDMA had engaged with these states to identify vulnerable locations and plan future mitigation projects. During the meeting, the states pledged to support NDMA's LRMS project by preparing and submitting detailed project reports (DPRs).

Following this consultation, NDMA issued a DPR preparation template for site-specific landslide risk mitigation in June 2015 (Fig. 3), which was circulated to all affected states

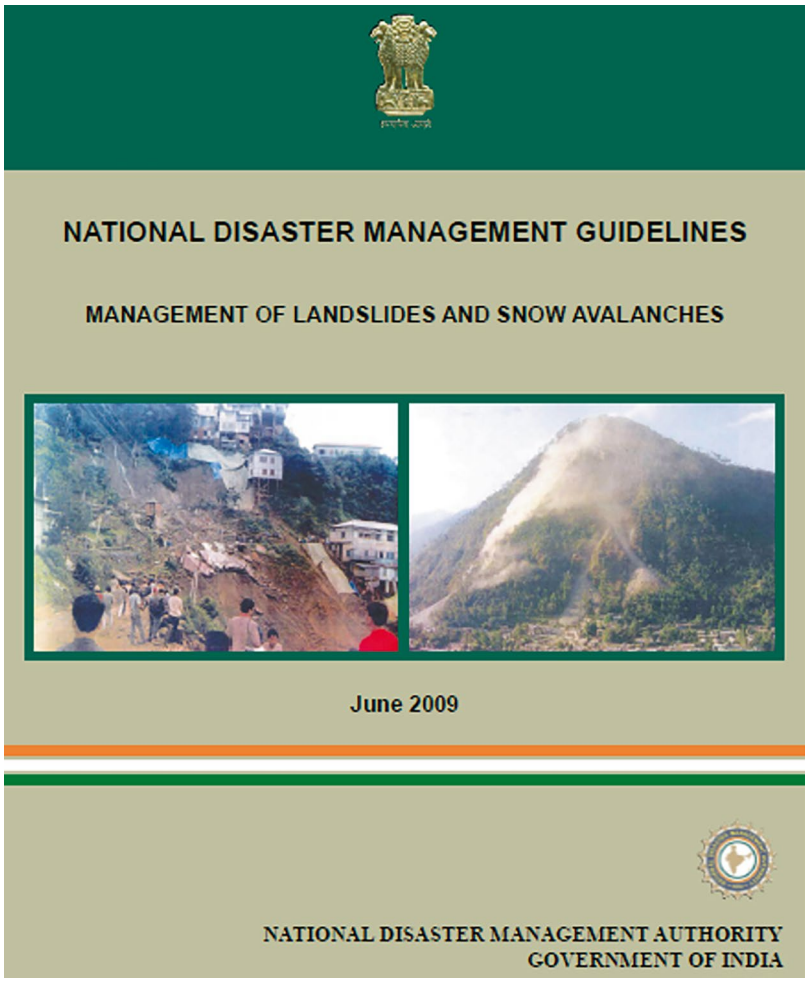

Fig. 2 NDMA guidelines on management of landslides and snow avalanches

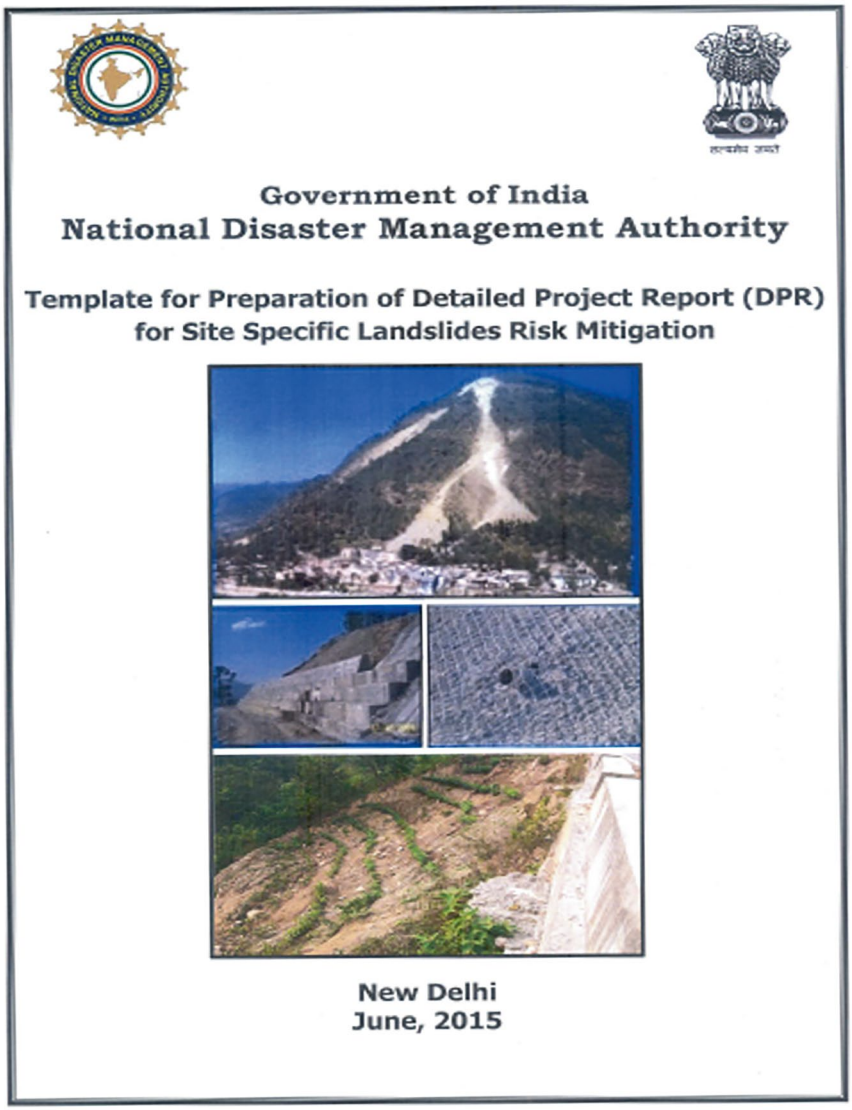

Fig. 3 NDMA template for preparation of DPR on landslide-risk mitigation

and union territories (NDMA 2015). The importance of individual, comprehensive disaster management plans was emphasized to state and UT governments through the National Disaster Management Plan of 2016, later updated in 2019.

In July 2019, NDMA launched the LRMS, a pilot program offering financial and technical support to landslide-prone states for site-specific landslide mitigation. LRMS serves to demonstrate the effectiveness of different slope stabilization methods alongside efforts in landslide monitoring, public awareness, and training. Under LRMS, DPRs were prepared based on NDMA template and Memorandums of understanding (MoUs) were signed with Sikkim, Mizoram, Nagaland, and Uttarakhand for projects at five sites such as Mangan (Sikkim), Hunthar Veng (Mizoram), the Kohima-Thizama road (Nagaland), and Kempty-Chadogi and Hardiyanala roads in Uttarakhand. The site photographs of the implementation of the DPR's under LRMS are shown in Fig. 4.

3.1.1 Outcomes

The LRMS scheme phase-I is in the final stage of completion and this project aims to assist landslide-prone states and union territories by enabling them to take proactive measures to mitigate future landslides. The lessons learnt and leveraging insights through the scheme will be implemented in the forthcoming National Landslide Risk Mitigation Project (NLRMP) as approved by the Government of India as per recommendations of 15th Finance Commission under National Disaster Mitigation Fund (NDMF).

Kohima-Thizama Road (Nagaland)

Hunthar Veng (Mizoram)

Mangan (Sikkim)

Kempty-Chadogi (Uttarakhand)

Hardiyanala (Uttarakhand)

Community Awareness Programme (Sikkim)

Fig. 4 Slope stabilization works and awareness programme carried out under LRMS

3.2 Training Programmes on Landslide Mitigation and DPR Preparation

During LRMS development, state and central government bodies faced challenges in preparing DPRs, stabilizing slopes, and conducting landslide studies. In response, NDMA launched a capacity-building project in June 2018, which included 5-day and 2-day professional training sessions on 'Landslide Mitigation and DPR Preparation' in collaboration with IITs, IISc, NEHU, CBRI, CRRI, and NIT-Mizoram. Training sessions were conducted at various institutions, including CRRI-New Delhi, CBRI-Roorkee, and IIT-Roorkee, and later shifted online due to the COVID-19 pandemic (Fig. 5). The National Institute of Disaster Management published a training module on Comprehensive Landslide Risk Management (Parkash 2020).

Fig. 5 Photographs from training programmes

3.2.1 Outcomes

The programme has been greatly beneficial to the landslide-affected states/UTs, with the master trainers turned out by the programme assisting them in the preparation of DPRs for landslide treatment and in building the capacities of other stakeholders in their respective states/UTs.

3.3 Development of Low-Cost Landslide Monitoring and EWS

The difficulties in preventing landslides are further compounded by the fact that existing landslide monitoring and early warning technologies cost crores of rupees, and that these technologies may not be capable of generating warnings for weather and slope movements ahead of time. The Himalayas and other mountain regions of India are vast and varying in nature, and the need for a low-cost landslide early warning system (EWS) has been long recognized.

In December 2017, NDMA launched a pilot project, **'Development & Evaluation of Low-Cost Landslide Monitoring Solutions'**, in collaboration with IIT Mandi and Defence Terrain Research Laboratory (DTRL)-DRDO. The project aimed to develop low-cost sensors and other instruments for landslide monitoring, using micro electro mechanical systems (MEMS)-based sensor technology and artificial intelligence. After detailed studies and experimentation, the project successfully developed a low-cost landslide monitoring, warning and prediction system.

3.3.1 Innovations and Artificial Intelligence

The system developed under this project addresses some of the issues of the existing technologies, such as their high cost and their lack of predictive capacity (Figs. 6 and 7). The new system detects whether there is significant soil movement and activates roadside blinkers and hooters wirelessly so that vehicular road traffic can be alerted. The blinkers and hooters come on for 10–15 s with lights and sound each time soil movement is recorded at the deployment site.

In addition, the system also sends SMS messages about soil movements to disaster managers and to the local people on their mobile phones. Recently, the system has been able to generate predictive messages about impending soil movements one day ahead of time as well as issue severe-weather advisories 2 h ahead of severe weather events. Predictions of soil movements and extreme weather events are generated using advanced artificial intelligence (AI) algorithms hosted on a cloud-based server. These algorithms analyze large datasets, including geological, meteorological, and environmental parameters, to identify patterns and anomalies that signal potential landslide risks. The cloud infrastructure enables real-time data processing and scalability, ensuring

Fig. 6 Low-cost landslide-monitoring and early warning system (EWS)

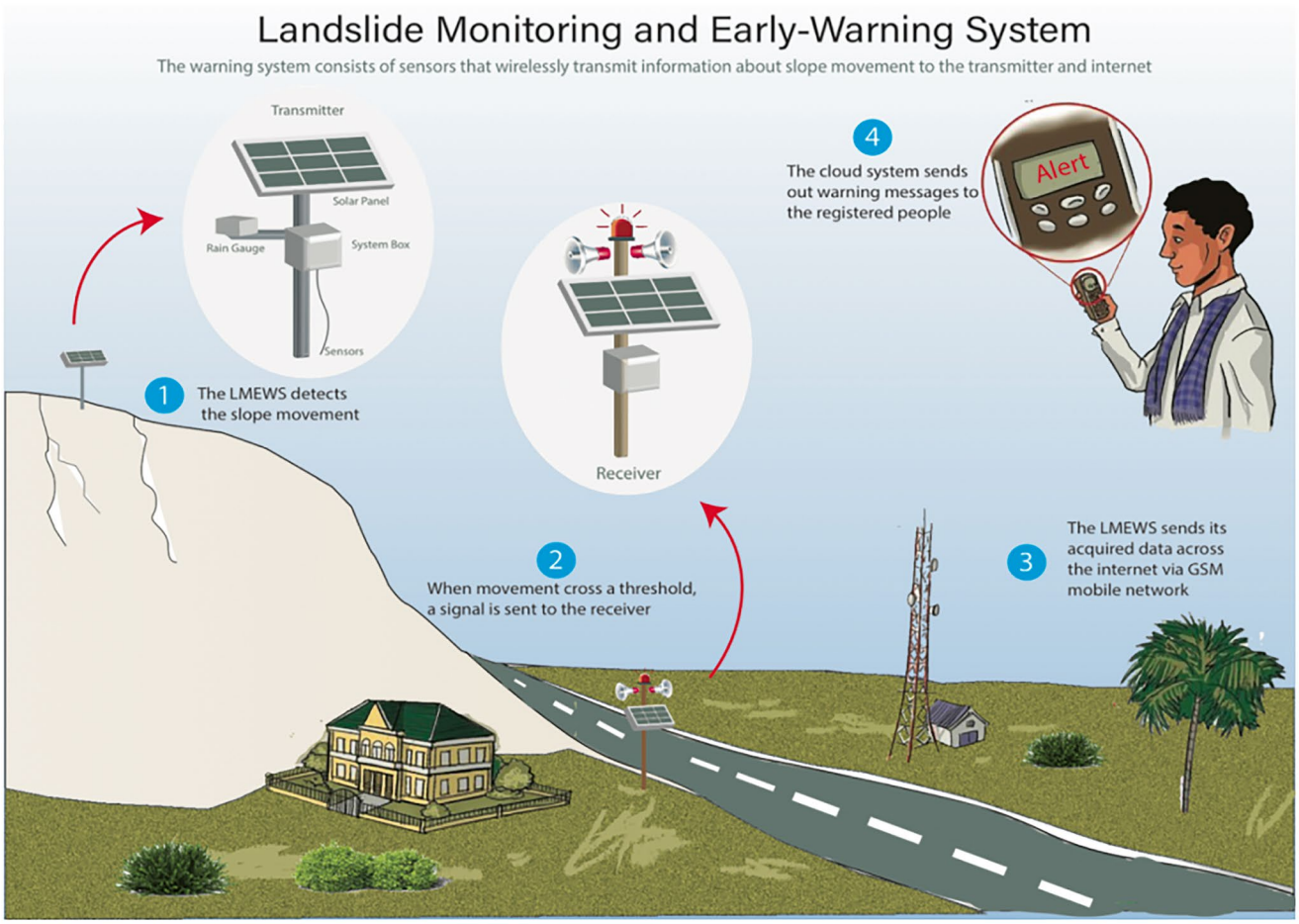

Fig. 7 Diagram showing how the low-cost landslide-monitoring, warning and prediction system operates

seamless integration of diverse data sources, such as satellite imagery, sensor networks, and weather forecasts. This approach enhances the accuracy and timeliness of predictions, providing early warnings that can support decision-making for disaster risk reduction and community preparedness.

The developed system predicts the amount and magnitude of soil movement. Although data on the number of landslides

is valuable for research purposes, information about their magnitude is crucial for issuing timely alerts to various stakeholders before an event occurs. The predictive algorithms are currently being refined, and the team from IIT Mandi is testing the system (Fig. 8). Due to its low cost and predictive abilities, the system provides immense possibilities for deployment at a number of landslide sites in India.

Earlier systems were designed primarily to monitor surface-level movements, but recent advancements have refined the technology to detect sub-surface movements as well. This involves drilling boreholes at landslide-prone sites and inserting a chain of sensor nodes to capture data on sub-surface activity. Each sensor node is equipped with an accelerometer to measure accelerations and displacements, a capacitive soil moisture sensor to monitor soil moisture, and a piezoelectric pressure sensor to assess soil stress. The collected data is transmitted to a cloud server via GSM mobile technology. Additionally, the patented system operates autonomously using solar power, eliminating reliance on grid electricity. The electronics are highly energy-efficient, allowing the system to function for several days on battery power alone during periods of low sunlight.

3.3.2 Collaboration with Local Administrations

With the support of NDMA, DTRL-DRDO and the Mandi district administration, more than ten systems have been installed by IIT Mandi in Mandi district at different landslide sites along the Mandi-Jogindarnagar and Mandi-Kullu highways. Each system can monitor soil movement and weather parameters at the deployed locations. These parameters can be monitored online on a dedicated website. In addition, the system has the capability of alerting the populations in the area about significant rainfall and slope-movement events in their vicinity via SMS service.

3.3.3 Outcomes and Beneficiaries

Calibration and validation of data obtained at different landslides sites are in progress to generate a reliable early warning model to save precious lives. This low-cost landslide monitoring technology will be beneficial in saving lives and property in the future by providing early warning alerts to the community members and local administration. The outcomes of this project will be shared with all landslide-affected states for replication of the low-cost landslide monitoring system and generation of early warnings in a cost-effective manner in collaboration with their own local communities and authorities. Now, the institute such as AMRITA University and CSIR-Central Building Research Institute (CBRI) have also started working on MEMS based technology of low cost landslide early warning system and IIT Mandi has also started calibration of this technology at ground level at multiple site. The efficacies of this technol-

Fig. 8 Sub-surface landslide monitoring system installed at Gharpa hill, Himachal Pradesh. (**a**) Installing the sensor. (**b**) Borehole. (**c**) Sensor installed at Gharpa hill

ogy are purely depend upon the data calibration and validation on algorithms and prediction of true and false early warning alerts by these sensor technology. Still these institutions are experimenting this technology to give accurate alerts of landslide early warnings with field validations.

3.4 Landslide Strategy and Public Awareness Generation

The National Landslide Risk Management Strategy was released on 27 September, 2019 at the 15th Formation Day of NDMA. NDMA released this comprehensive National Landslide Risk Management Strategy (2019) (Fig. 9) as per fifth target of SFDRR i.e., **"Substantially increase the number of countries with national and local disaster risk reduction strategies by 2020"** (NDMA 2019). This strategy document addresses all the components of landslide disaster risk reduction and management, such as hazard mapping, monitoring and early warning systems, awareness programmes, capacity building and training, regulations and policies, stabilization and mitigation of landslides, etc. The document envisages specific recommendations for the concerned nodal agencies, ministries, departments, states, civil society organizations (CSOs) and other stakeholders, to avert or reduce the impact of future landslide calamities.

NDMA is building awareness about landslides through print and electronic media, through a weekly panel discussion (*'Aapda Ka Saamna'*) and telecast of a programme on **'Landslide Hazard and its Prevention'** on Doordarshan channel. Additionally, a webinar on **'Landslide Risk Reduction through Community Participation'** was conducted on 29 October 2020.

In today's world the traditional knowledge of the people is very negligible due to the modernization and lavishing lifestyle. But this is the need of time that we have to live in

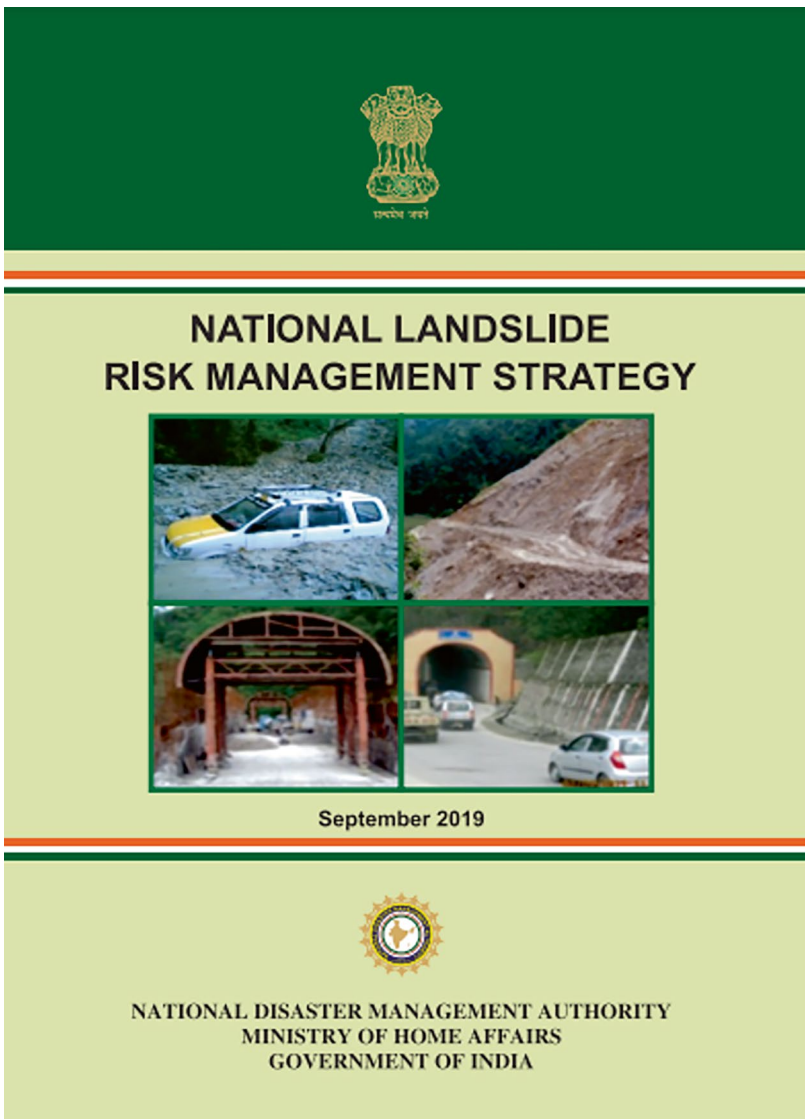

Fig. 9 National Landslide Risk Management Strategy (2019)

harmony with the nature like tradition knowledge as an old wine in new bottle. There must be an awareness and capacity building programmes for the local community by the local government/administration or disaster management authorities to disseminate the knowledge on the landslide triggering factors and creation of early warning signals before the occurrence of any mishap (Singh and Pande 2011). To promote landslide awareness, NDMA utilizes print and electronic media, holding weekly panel discussions, and broadcasting programs on Doordarshan. A webinar titled 'Landslide Risk Reduction through Community Participation' was held on October 29, 2020, furthering public education on landslide hazards and prevention.

Acknowledgments The authors express their gratitude to ICL for giving them the chance to write this chapter on the landslides difficulties and the risks they pose. The current study has no financial source, and the authors' work during the implementation of projects and field study.

References

Geological Survey of India (GSI). https://www.gsi.gov.in/

Kanungo DP, Singh R, Dash RK (2020) Field observations and lessons learnt from the 2018 landslide disasters in Idukki District, Kerala. Curr Sci 119(11):1797–1806

National Landslide Risk Management Strategy (2019) A publication of the National Disaster Management Authority. Government of India, New Delhi

NDMA (2009) Guidelines on management of landslides and snow avalanches

NDMA (2015) Template for preparation of detailed project report for site specific landslide risk mitigation

NDMA (2019) National landslide risk management strategy

Parkash S (2020) Training module on comprehensive landslide risk management. National Institute of Disaster Management (NIDM), New Delhi, pp 1–301. ISBN No.: 978-93-82571-34-6

Singh R, Pande RK (2011) Morphometry of landslides in Garhwal Himalaya, India. J Disaster Prev Manag 20(4):355–362

Sixth Regional Symposium on Landslides in the Adriatic-Balkan Region: ReSyLAB 2024

Biljana Abolmasov, Miloš Marjanović, and Uroš Đurić

Abstract

The Sixth Regional Symposium on Landslides in the Adriatic-Balkan Region was held in Belgrade, Serbia, from 15 to 18 May 2024. The Symposium was organised by the University of Belgrade, Faculty of Mining and Geology, as a member of the Adriatic-Balkan Network. The Adriatic-Balkan Network is one of eight regional and thematic networks of the International Consortium on Landslides (ICL). The Symposium started with workshops on May 15, 2024, followed by the Opening ceremony on the same day in the afternoon. The opening ceremony was started with welcome notes from ICL President Prof. Željko Arbanas from the University of Rijeka (Croatia) and ICL Vice President for Europe and a Dean of the Faculty of Mining and Geology Prof. Biljana Abolmasov (Serbia). Parallel scientific sessions continued from May 16 to May 17, 2024. The closing plenary session occurred on May 17, 2024, in the afternoon hours after the round tables' discussion. The field trip excursion was held on May 18, 2024. A total number of 84 participants from 15 countries attended the Sixth ReSyLAB.

Keywords

The Adriatic-Balkan Network, ReSyLAB, Belgrade

B. Abolmasov (✉) · M. Marjanović
Faculty of Mining and Geology, University of Belgrade, Belgrade, Serbia
e-mail: biljana.abolmasov@rgf.bg.ac.rs; milos.marjanovic@rgf.bg.ac.rs

U. Đurić
Faculty of Civil Engineering, University of Belgrade, Belgrade, Serbia
e-mail: udjuric@grf.bg.ac.rs

1 Introduction

The Adriatic-Balkan Network (ABN) was established in January 2012 as one of eight regional and thematic networks of the International Consortium on Landslides (ICL). The general objectives of the ICL ABN are to promote activities of the ICL and the International Programme on Landslides (IPL), as well as to advance landslide science and its practical application in the region for the benefit of society and the environment (Mihalić Arbanas et al. 2012). The objectives and planned activities were defined based on analyses of basic information about landslides in the Region and evaluation and mitigation of landslide hazards in the Adriatic-Balkan Region (Mihalić Arbanas et al. 2013). The most important ICL ABN outcome is to organize biannual landslide Symposiums, named Regional Symposium on Landslides in the Adriatic-Balkan Region (ReSyLAB) (Arbanas and Mihalić Arbanas 2023). The 1st ReSyLAB was held in Zagreb, Croatia in March 2013, and it was followed by the next five Symposiums held in Belgrade, Serbia, 2015; Ljubljana, Slovenia, 2017; Sarajevo, Bosnia and Herzegovina, 2019; Rijeka, Croatia 2022 and Belgrade, Serbia, 2024 (Fig. 1).

2 General Information

The Sixth Regional Symposium on Landslides in the Adriatic-Balkan Region (ReSyLAB) was held in Belgrade, Serbia, from 15 to 18 May 2024. The Symposium was organized by the University of Belgrade, Faculty of Mining and Geology, as a member of ICL ABN. The official website of the Symposium is available at https://resylab.rgf.bg.ac.rs. The Symposium started with workshops on May 15, 2024, and was followed by the official Opening plenary session on the same day in the afternoon. The opening ceremony was started with welcome notes from ICL President Prof. Željko Arbanas from the University of Rijeka (Croatia) and ICL

B. Abolmasov et al. (eds.), *Progress in Landslide Research and Technology, Volume 4 Issue 1, 2025*, Progress in Landslide Research and Technology, https://doi.org/10.1007/978-3-031-89836-5_12

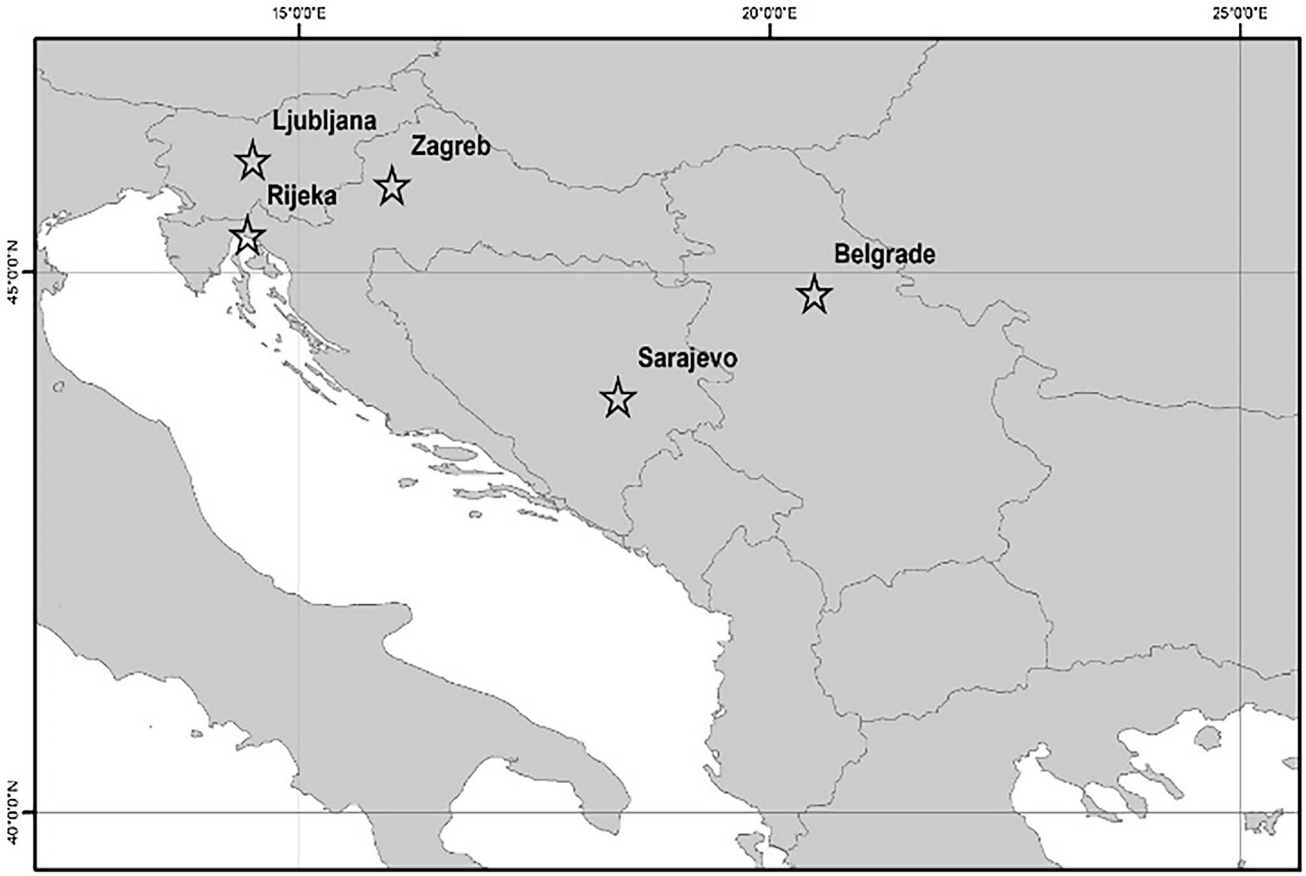

Fig. 1 The geographical position of ReSyLAB Symposium places

Vice President for Europe and a Dean of the Faculty of Mining and Geology Prof. Biljana Abolmasov (Serbia). The ice break party was organized in the Botanical Garden "Jevremovac" on May 15, 2024, in the evening hours (University of Belgrade, Faculty for Biology). Parallel scientific sessions continued from May 16 to May 17, 2024. The closing plenary session took place on May 17, 2024, in the afternoon. The field trip was held on May 18, 2024.

A total number of 84 participants from 15 countries attended the Symposium (Fig. 2, Table 1). In total 49 reviewed papers were published in Symposium Proceedings (Marjanović and Đurić 2024). Open access digital copy of Symposium Proceedings in PDF format is available at https://resylab.rgf.bg.ac.rs, as well as the Book of 64 abstracts (Fig. 3).

2.1 Scientific and Organizing Committee Members

The International Scientific Committee was composed of 31 members including ICL members and internationally recognized scientists in the field of landslide research and landslide risk reduction. The Local Organizing Committee was composed of 15 members and staff from the University of Belgrade, Faculty of Mining and Geology (https://resylab.rgf.bg.ac.rs).

2.2 Symposium Topics

The Symposium topics were concentrated on the five themes:

1. **Landslide monitoring and early warning** Attendees of this session presented the latest advancements in remote sensing techniques, monitoring strategies, and explored the development of early warning systems. This symposium topic offered a valuable opportunity to stay abreast of the evolving landscape of landslide science.
2. **Landslide susceptibility, hazard and risk assessment**; Attendees of this session presented the forefront of methodologies for assessing susceptibility, understanding hazards, and quantifying risks associated with landslides. The session was tailored for those keen on contributing to the discourse around landslide dynamics, offering a plat-

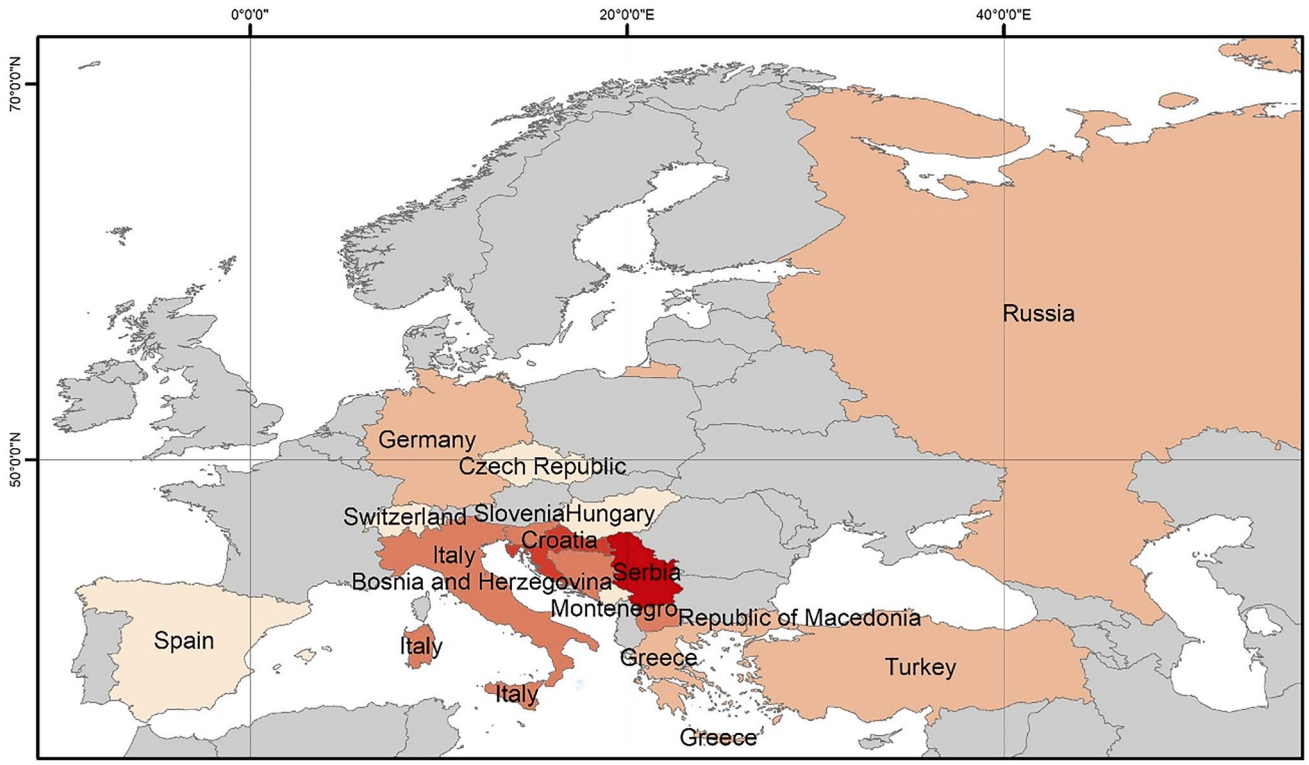

Fig. 2 Country classified by number of participants

Table 1 The number of participants by country

Country	Number
Bosnia and Herzegovina	4
Croatia	12
Czech Republic	1
Germany	2
Greece	2
Hungary	1
Italy	6
Montenegro	1
North Macedonia	6
Russia	2
Serbia	39
Slovenia	4
Spain	1
Switzerland	1
Turkey	2
Total	84

form to discuss innovative approaches, share insights, and collectively advance the field of the topic.

3. **Climate change and landslides**; This specialized session explored the complex relationship between climate dynamics and the occurrence of landslides, offering a platform for experts, researchers, and professionals to discuss the subtle interplay of environmental factors. Attendees were engaging in insightful conversations about the latest research, innovative methodologies, and practical strategies addressing the specific challenges posed by climate change-induced landslides.
4. **Testing, modeling and mitigation of landslides**; Participants in this session explored and presented advanced testing methodologies and cutting-edge modeling techniques, fostering in-depth discussions on effective landslide mitigation strategies.

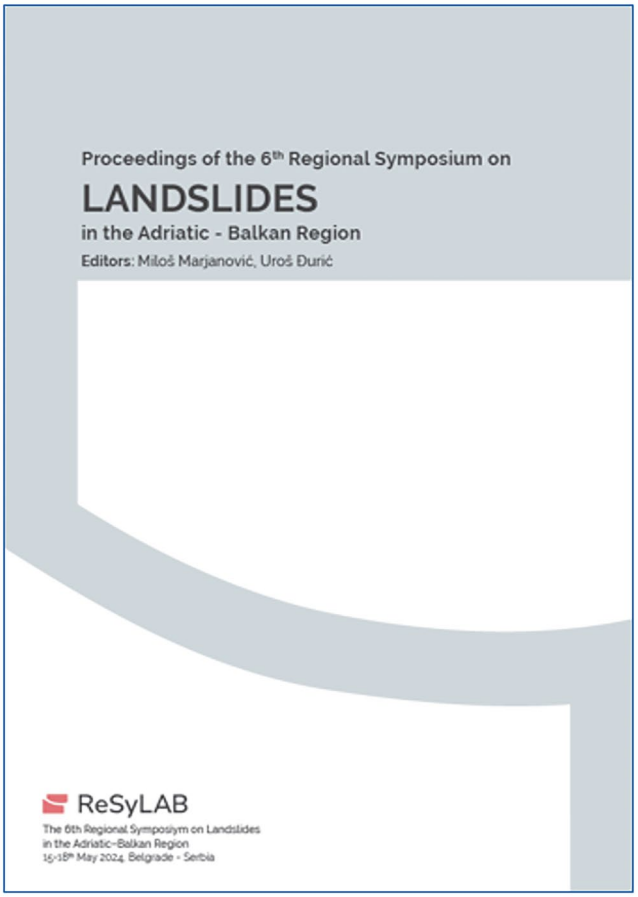

Fig. 3 Cover page of Sixth ReSyLAB Proceedings

5. **Landslides in practice—mining and infrastructure**; This session provided a focused platform for professionals, researchers, and practitioners to address the specific challenges posed by landslides in the context of mining activities and infrastructure development. Attendees examined real-world applications, shared practical experiences, and explored effective strategies for both prevention and response.

2.3 Keynote and Invited Lectures

We had arranged distinguished experts who shared invaluable insights, offering a glimpse into the latest state-of-the-art methodologies and prospects within the conference sessions. Each conference session was opened by the keynote lecturer. Also, specialized topics within the conference were presented by invited lecturers. These accomplished individuals bring focused insights, sharing specific research findings, methodologies, and applications in their respective fields. Each conference session was covered by the invited lecturer. The list of keynotes and invited speakers is shown in Table 2.

2.4 Workshops

Two Workshops were organized during the Sixth ReSyLAB in Belgrade on May 15, 2024, before the official opening. Both workshops were held in-house at the Faculty of Mining and Geology (room 267 and room 151).

The Title of Workshop 1 was "Slope Stability Assessment in Soils and Rock Masses—Beyond the Basics". The workshop was led by Anil Yunatci, PhD, GeoDestek Ltd., Rocscience Representative. The workshop was open to contributions from all participants of experience and interest in geomechanics with backgrounds in geology, mining and civil engineering. The event was designed to flow in a thought-provoking style and was designed to address undergraduate and graduate students, practitioners, and researchers. The following Software Tools were introduced: Rocscience Slide2 (2D Limit Equilibrium), Slide3 (3D Limit Equilibrium), RS2 (2D Finite Element), RS3 (3D Finite Element), RocSlope (3D Block Based Stability Assessment of Rock Masses). Workshop outlines were divided into three parts: (1) Present State of Practice and Challenges in Numerical Analysis of Natural and Man-Made Slopes, (2) Practical Cases and Hands-on Exercises Using Rocscience Software Tools and (3) Closure Remarks. Duration of the Workshop 1 was from 9:00 AM to 01:00 PM on May 15 (https://resylab.rgf.bg.ac.rs/inner-page.php?p=workshops).

The Title of Workshop 2 was "New trends in geotechnical monitoring for slow-moving landslide risk analysis (InSAR in GIS)".

The workshop was led by Prof. Dario Peduto, Ph.D. and Dr. Gianfranco Nicodemo, Ph.D. from the Department of Civil Engineering, University of Salerno (Italy). The workshop was open to contributions from all participants interested in earth observation and landslides risk analysis and management, subsidence monitoring, structural and infrastructural monitoring, and vulnerability assessment, with a background in civil engineering, engineering geology, mining, geodesy, and geomatics. The event was designed to be interactive addressing undergraduate and graduate students, practitioners, and researchers. The following Software Tools were introduced: Web GIS (Online Platform), Desktop GIS (ArcGIS, QGIS), and Excel. Workshop outlines were divided into three parts: (1) Multi-temporal multi-platform satellite DInSAR data for geotechnical applications, (2) The use of satellite DInSAR data for landslide characterization and consequence analysis to the built environment and (3) Closure Remarks. Duration of the Workshop 1 was from 9:00 to 13:00 on May 15 (https://resylab.rgf.bg.ac.rs/inner-page.php?p=workshops).

Table 2 The list of keynote and invited speakers with titles of lectures

Symposium topics	Keynote speakers	Title of keynote lectures
Landslide remote sensing monitoring and early warning	Assoc. Prof. Dario Peduto, Ph.D.—University of Salerno (ITA)	"Multi-source data analysis in the slow-moving landslide-affected built-up environment: a case study in Calabria Region (southern Italy)"
Landslide susceptibility hazard and risk assessment	Prof. Jaboyedoff Michel, Ph.D.—University of Lausanne, (CHE)	"Landslide susceptibility assessment: Chicken or the egg for the risk analysis?"
Climate change and landslides	Dr. Stefano Luigi Gariano, Ph.D.—CNR IRPI (ITA)	"Prediction of rainfall-induced landslides in a changing climate: issues and perspectives for regional-scale approaches"
Testing modelling and mitigation of landslides	Assoc. Prof. Svetlana Melentijević, Ph.D.—Universidad Complutense de Madrid (ESP) Prof. K. Önder Çetin, Ph.D.—Middle East Technical University—(TUR)	"Rock slope stability analysis of highly fractured rock mass under different flow rules" "Seismic Performance Assessment of Embankments"
Landslides in practice—mining and infrastructure	Prof. Jovanovski Milorad, Ph.D.—"Ss. Cyril and Methodius" University, Skopje (NMK)	"Integral approach in stability analyses for weak anisotropic rocks"
Symposium topics	**Invited speakers**	**Title of invited lectures**
Landslide remote sensing monitoring and early warning	Assoc. Prof. Marko Pejić, Ph.D.—University of Belgrade (SRB)	"High-Precision Landslide Monitoring Using Laser Scanning Technology"
Landslide susceptibility hazard and risk assessment	Assoc. Prof. Peshevski Igor, Ph.D.—"Ss. Cyril and Methodius" University (NMK) Neil Bar, Geotechnical Engineer—Gecko Geotechnic (VCT)	"Landslide mapping and zonation at national, regional and local scale—Recent experiences from Republic of North Macedonia" "Mapping, Modelling and Monitoring for the Safe and Economic Design and Management of Rock Slopes"
Climate change and landslides	Assoc. Prof. Mirjam Vujadinović Mandić, Ph.D.—University of Belgrade (SRB)	"PENDING Landslide risks in the Western Balkans under the climate change"
Testing modelling and mitigation of landslides	Assist. Prof. Josip Peranić, Ph.D.—University of Rijeka (CRO)	"Determination of the soil-water characteristic curve of the soil by physical modelling tests"
Landslides in practice—mining and infrastructure	Assist. Prof. Veljko Lapčević, Ph.D.—University of Belgrade (SRB)	"Tailing Dam Stability Evaluation using 3D Numerical Modeling"

2.5 Field Trip

The field trip was organized on 18 May 2024 to introduce Symposium participants to the Podunavlje Region and Frontiers of the Roman Empire—The Danube Limes in Serbia. The Roman Empire's frontier in Serbia, specifically in the Podunavlje region, offers a rich tapestry of historical significance, exemplified by three key field stops. The field trip was moderated by Prof. Miloš Marjanović (Faculty of Mining and Geology) and Prof. Uroš Đurić (Faculty of Civil Engineering).

The first stop was at the Golubac fortress, strategically positioned at the entrance of the Iron Gates Gorge (Danube River). This fortress played a crucial role in safeguarding the Roman Empire's Danubian frontier, and its well-preserved architecture stands as a testament to the military prowess and strategic foresight of the Roman, Bulgarian, Serbian, and Ottoman Empire in the defense of their territorial boundaries. Together, these field stops promised conference attendees an immersive experience, weaving the industrial, urban, and military facets of the Roman presence in the Podunavlje region. In recent years numerous geotechnical works on new road construction and slope protection were performed within the framework of the preservation of Golubac fortress as a targeted tourist area.

Fig. 4 Symposium participants during LiDAR demonstration on the Joc Rockfall site

The next stop was at Joc Rockfall where a short presentation about recent monitoring activities was presented (Fig. 4).

Fig. 5 Symposium participants in the coal mine "Drmno"

Joc Rockfall stands as a significant geological natural heritage site, offering a captivating showcase of rock formations and the forces that have shaped the landscape over millennia. The site provides a unique opportunity to appreciate the interplay between geological processes and the historical narrative of the region. This stop not only enriched the conference field trip with diverse perspectives but also underscored the intricate relationship between human history and the geological forces that have left an indelible mark on the landscape of the Podunavlje region.

The final stop was at the coal mine "Drmno", interesting not only for contemporary mining activity but also for unveiling layers of history, as the region is well known for the Roman mining operations. Numerous slope stability problems in the active coal open pit mine were presented (Fig. 5). The journey then led to Viminacium (a Roman city and a legionary Fort), a prominent archaeological site that was once a bustling Roman provincial capital, complete with impressive remnants of infrastructure, such as amphitheaters, temples, and necropolises. Besides archeological artifacts, the Viminacium site is a place where in 2009 a mammoth skeleton was found, preserved almost entirely. Furthermore, during the 2012 routine archaeological fieldwork more mammoth bones were found that indicate the unique "mammoth graveyard". Mammoths soon became the biggest attraction of Viminacium, immediately protected and preserved for visitors.

2.6 Sponsors

The Symposium was supported by 12 sponsors including the Ministry for Science, Technological Development and Innovation from The Republic of Serbia (Fig. 6).

3 Conclusions

In this paper activities of the Sixth Regional Symposium on Landslides in the Adriatic-Balkan Region are presented. The Adriatic-Balkan Network was established as one of eight thematic and regional networks of the International Consortium on Landslides. The Adriatic-Balkan Network was formally established in September 2012. Six Regional Symposiums were held in Zagreb, Croatia (2013); Belgrade, Serbia, 2015; Ljubljana, Slovenia, 2017; Sarajevo, Bosnia and Herzegovina, 2019; Rijeka, Croatia 2022 and Belgrade, Serbia, 2024. The next ReSyLAB is announced for 2027 in Skopje, North Macedonia.

Fig. 6 Symposium sponsors

References

Arbanas Ž, Mihalić Arbanas S (2023) 10th Anniversary of ICL Adriatic-Balkan Network and 5th Regional Symposium on Landslides. In: Alcántara-Ayala I et al (eds) Progress in landslide research and technology, vol 1(2), 2022. Progress in landslide research and technology. Springer, Cham. https://doi.org/10.1007/978-3-031-18471-0_18

Marjanović M, Đurić U (2024) Proceedings of the 6th regional symposium on landslides in the Adriatic-Balkan Region, ReSyLAB2024, Belgrade, Serbia 15-18 May 2024. University of Belgrade, Faculty of Mining and Geology, p 328. https://doi.org/10.18485/resylab.2024. ISBN 978-86-7352-402-3

Mihalić Arbanas S, Arbanas Ž, Abolmasov B, Mikoš M, Komac M (2012) Regional cooperation in the frame of the ICL Adriatic-Balkan Network. In: Sunarić D, Jevremović D (eds) Proceedings of 14th symposium on engineering geology and geotechnics, 27–28 Sept 2012, Belgrade, Serbia. Društvo geoloških inženjera i tehničara Srbije, Belgrade, pp 43–56

Mihalić Arbanas S, Arbanas Ž, Abolmasov B et al (2013) The ICL Adriatic-Balkan Network: analysis of current state and planned activities. Landslides 10:103–109. https://doi.org/10.1007/s10346-012-0364-2

Landslide Susceptibility Assessment and Modeling Landslide Volumes Using Geographic Information System (GIS) and Unmanned Aerial Vehicle (UAV): A Case Study in the Xopanac-Apitzato Basin on the Eastern Flank of Iztaccíhuatl Volcano, Puebla, Mexico

Gabriel Legorreta-Paulín, Marcus Bursik, Lilia Arana-Salinas, and Fernando Aceves-Quesada

Abstract

In volcanic mountain terrains, landslides are common and form a major natural hazard, posing risks to human settlements and economic activity. In Mexico, despite the importance of assessing such processes, there are few landslide inventory maps or landslide geo-datasets. Therefore, no practical and standardized methodology has developed to model landslide susceptibility and volume under a Geographic Information System (GIS), and by taking the advantage of Unmanned Aerial Vehicles (UAVs) and their products (aerial photos, orthophotos, dispersed or dense point clouds, and Digital Elevation Models (DEM)). The present text provides an overview of an on-going research project at the Institute of Geography in the National Autonomous University of Mexico (UNAM) presented as an International Programme on Landslides (IPL) project proposal. The aim of this research is to conduct a landslide inventory, produce a landslide susceptibility map, and estimate volume production and distribution within the stream system of the Xopanac-Apitzato watershed. The landslide inventory will be conducted by following the landslide hazard zonation protocol of Washington State DNR. Landslide susceptibility will be conducted by using landforms units and Multiple Logistic Regression. To estimate landslide volume and distribution we will implement the development and adequation of two models by using python.

The watershed is located on the eastern flank of Iztaccíhuatl volcano, the third highest mountain in Mexico. Anthropogenic factors such as land use changes and physiographic factors such as step hillslopes, volcano-tectonic earthquakes, high seasonal precipitation, and disaggregated material predispose the study area to experience episodic evacuation of material through landslide activity. Landslides are common along the stream system, and these slope failures create a potentially hazardous situation for people and property down the valley. In spite of this, there are no landslide inventory maps, and this precludes the mapping of landslide susceptibility and volume. The methodology of the present research encompasses three main levels of analysis. The technique and its implementation in a GIS-based technology is herein presented and discussed. The implementation of the technique yields information essential for policy makers here and in other areas of Mexico.

G. Legorreta-Paulín (✉)
Instituto de Geografía, Universidad Nacional Autónoma de México, Circuito Exterior, Ciudad Universitaria, Ciudad de México, Mexico

M. Bursik
Department of Geology, University at Buffalo, SUNY Buffalo, Buffalo, NY, USA
e-mail: mib@buffalo.edu

L. Arana-Salinas
Universidad Autónoma de la Ciudad de México, Colegio de Ciencias y Humanidades, Academia de la Licenciatura Protección Civil y Gestión de Riesgos, Ciudad de México, Mexico

F. Aceves-Quesada
Facultad de Ciencias, Universidad Nacional Autónoma de México, Circuito Exterior, Ciudad Universitaria, Ciudad de México, Mexico

Keywords

GIS · UAVs · Landslide inventory map · Landslide susceptibility map · Landslide volume · Iztaccíhuatl volcano

B. Abolmasov et al. (eds.), *Progress in Landslide Research and Technology, Volume 4 Issue 1, 2025*, Progress in Landslide Research and Technology, https://doi.org/10.1007/978-3-031-89836-5_13

1 Introduction

In volcanic environments, during the volcanic repose period, small but hazardous landslides and debris flows occur continually. This type of landslide can deliver volumes of some 10–100 m^3 (Montgomery and Dietrich 1994; Pack et al. 2001) and create a potentially hazardous situation for people and property down the valleys, due to the coalescence of upstream landslides that increases the destructive power of debris flows.

Worldwide, landslide cartography has been carried out by using GIS and remote sensing. This cartography is used as a tool to assess the type, distribution, frequency, size, density, geometry, and chronological sequences of landslides. All these attributes are recorded by using historical or multitemporal landslide inventory maps (Washington State Department of Natural Resources (DNR), Forest Practices Division 2006; Hervás and Bobrowsky 2009; Blahut et al. 2010; Guzzetti et al. 2012; Jasiewicz and Stepinski 2013; Slaughter et al. 2017; Du et al. 2020; Shao et al. 2022). To estimate landslide susceptibility, several inventory, heuristic, statistical, and deterministic approaches have been proposed for multiple scopes and spatial scales (Slaughter et al. 2017; Du et al. 2020; Shao et al. 2022). Among the statistical approaches, Multiple Logistic Regression (MLR) is popular for landslide susceptibility assessment because: (1) the evaluation of the model under natural conditions has proven that the model is successful at identifying landslide areas if an adequate set of predictor variables sampling strategy, and sample size are selected (Sujatha and Sridhar 2021; Cemiloglu et al. 2023) and (2) the model has no mechanical meaning, but it explores the relationship between landslide occurrence in the past and the terrain and environmental predictor variables to estimate the probability of landslide (Can et al. 2005; Cemiloglu et al. 2023). Techniques for calculating the volume of material displaced by a landslide in a watershed are based on the physical pre and post-landslide shape obtained by using detailed Digital Elevation Models (DEMs). DEMs could be obtained through the use of differential GPS, Light Detecting and Ranging (LiDAR) or unmanned aerial vehicles (UAVs) (UNEP 2013; Chen et al. 2014; Young 2015; Ray et al. 2020). Also, empirical relationships are established by use of a power-law function that links geometric measurements of landslide area to landslide volume (Peark et al. 2005; Kalderon-Asael et al. 2008; Guzzetti et al. 2009; Wenske et al. 2012). In addition, the distribution of landslide volumes has been determined through historical records, through field identification of the distribution of the materials and through semi-empirical equations that can predict the cross sections and planimetric areas of impact based on the field-estimated volumes (Muñoz-Salinas et al. 2009; Iverson et al. 2015; Andaru et al. 2022).

In Mexico, volcanic regions with stratovolcanoes and monogenetic fields are numerous. Among the three thousand volcanoes in Mexico, dormant stratovolcanoes are common (Centro Nacional de Prevención de Desastres 2001) and can trigger large landslides and debris flows through earthquakes, or in response to heavy rainfall. Despite the importance of assessing such processes, there are few landslide inventory maps derived from geo-datasets using GIS. Also, little work has been done on modelling landside susceptibility and landslide volumes (Capra et al. 2003; Capra and Lugo-Hubp 2006; Pérez-Gutiérrez 2007; Secretaría de Protección Civil 2010).

This is the case for Iztaccíhuatl volcano, the third highest mountain in Mexico (5215.128 m a.s.l.), which has great potential to produce landslides because of its large area of weakened deposits affected by steep slopes, high seasonal rainfall, and tectonic activity. The Río Xopanac-Apitzato on the eastern flank of Iztaccíhuatl volcano has been selected as a case study area. Landslides form major natural hazards in the hilly terrain and cause extensive damage to roads, human settlements, and agricultural land. Therefore, it is important to prepare a landslide inventory map, a susceptibility map, and calculate the volume contributed by landslides to the watershed.

In light of the above, the main goal of this project is to provide standardized methods for conducting landslide inventories, assessing landslide susceptibility, and landslide volumes; this will support governmental authorities in hazard mitigation and landscape planning in Mexico. The Xopanac-Apitzato watershed is selected as a case study area. It is prone to landsliding due to the combination of several factors: volcano-tectonic earthquakes, high precipitation, steep and hilly slopes, loose volcanic deposits, and land use changes.

The methodology encompasses three main levels with several steps of analysis to assess landslide distribution, landslide susceptibility, and volumes. Level 1 builds a historic landslide inventory; Level 2 calculates the landslide susceptibility per landform unit and by using multiple logistic regression (MLR) for the watershed; and Level 3 maps the landslide volume distribution and uses a power law function to estimate the potential total material delivered to the main stream drainage channel by all landslides in the catchment.

2 Method

The overall method followed in this study has 3 major levels with 11 steps (Fig. 1).

Step 1. Selection of a study area: The general procedure is exemplified by a case study on the eastern flank of Iztaccíhuatl

volcano, within Puebla State, Mexico. There, the Xopanac-Apitzato watershed has been selected for landslide mapping, modeling landslide susceptibility, and calculating volumes delivered to its stream system. The study area continually experiences hazardous landslides and debris flows. The study area covers 17.7 km^2 with elevations from 2278 to 3012 m a.s.l. The area is characterized by hilly and steep terrain with slopes between <5° (inner valleys of relatively flat plains) and 66° (mountainous terrain). The Xopanac-Apitzato river is a sub-basin of Río Atoyac, which flows into the Pacific Ocean (Fig. 2).

The stream system of the Xopanac-Apitzato watershed erodes through Tertiary and Quaternary volcanic avalanche deposits, pyroclastic flows, lahars, and fall deposits (García Tenorio 2008).

Along the Xopanac-Apitzato stream system, shallow landslides predominate on steep hills capped by ash and pyroclastic deposits. The steep hills typically experience episodic evacuation of debris by shallow-rapid mass movement followed by slow refilling with colluviums. The debris slides and debris flows are triggered by tecto-volcanic earthquakes, rain, and anthropogenic land use changes (Fig. 3). Active debris slides are abundant on the left hillslopes of the river bank where more anthropic activity takes place (Fig. 4).

Step 2. Background information will be collected to provide context and establish a generalized of landslide processes and to aid analysis, interpretation, and mapping of mass wasting potential within the watershed. Information includes topographic paper maps at scale 1:50,000, and paper maps of geology, land use, climate, and hydrology at

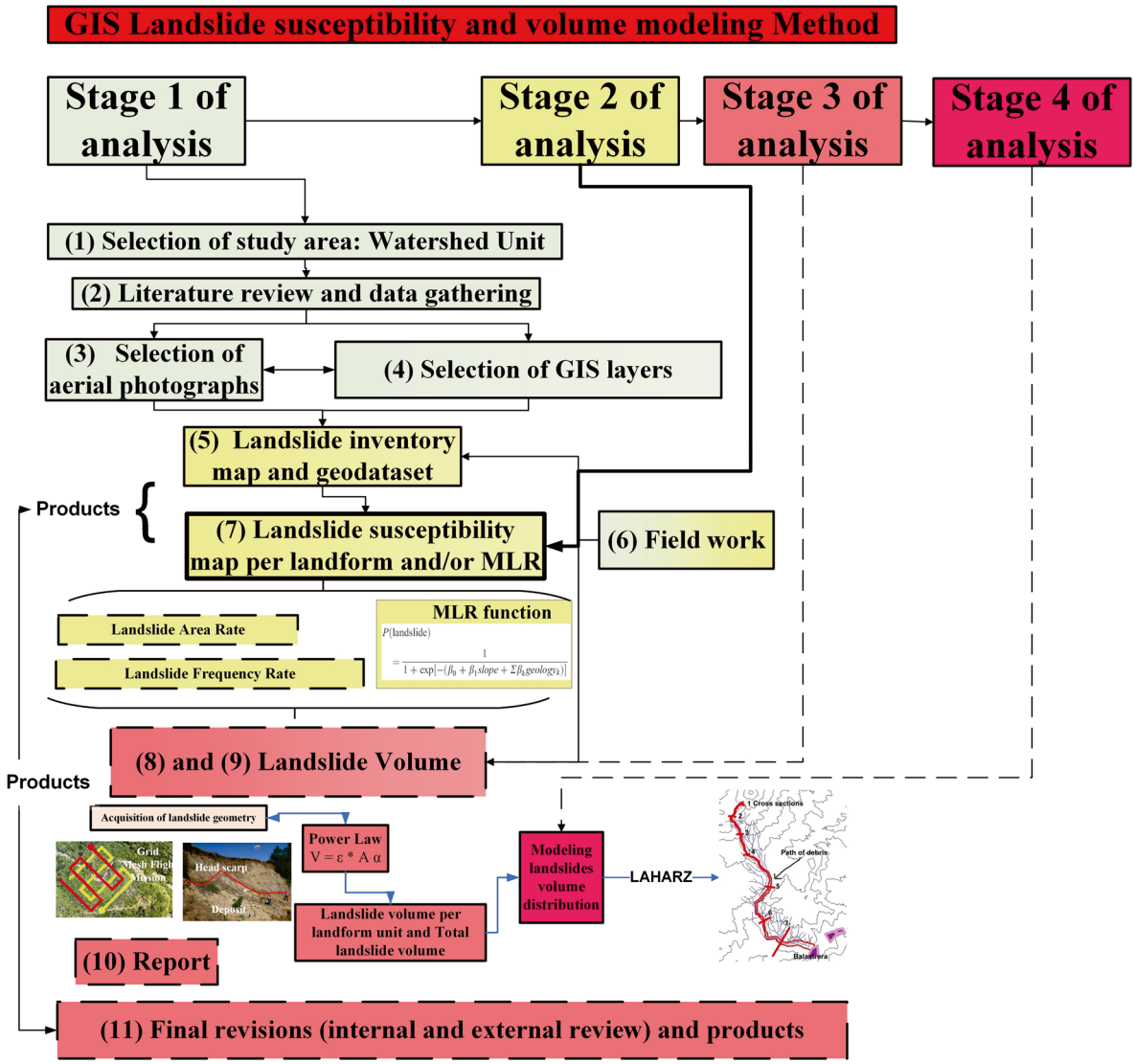

Fig. 1 General procedure for conducting landslide inventories, landslide susceptibility using landforms and MLR statistical method, and landslide volumes calculation

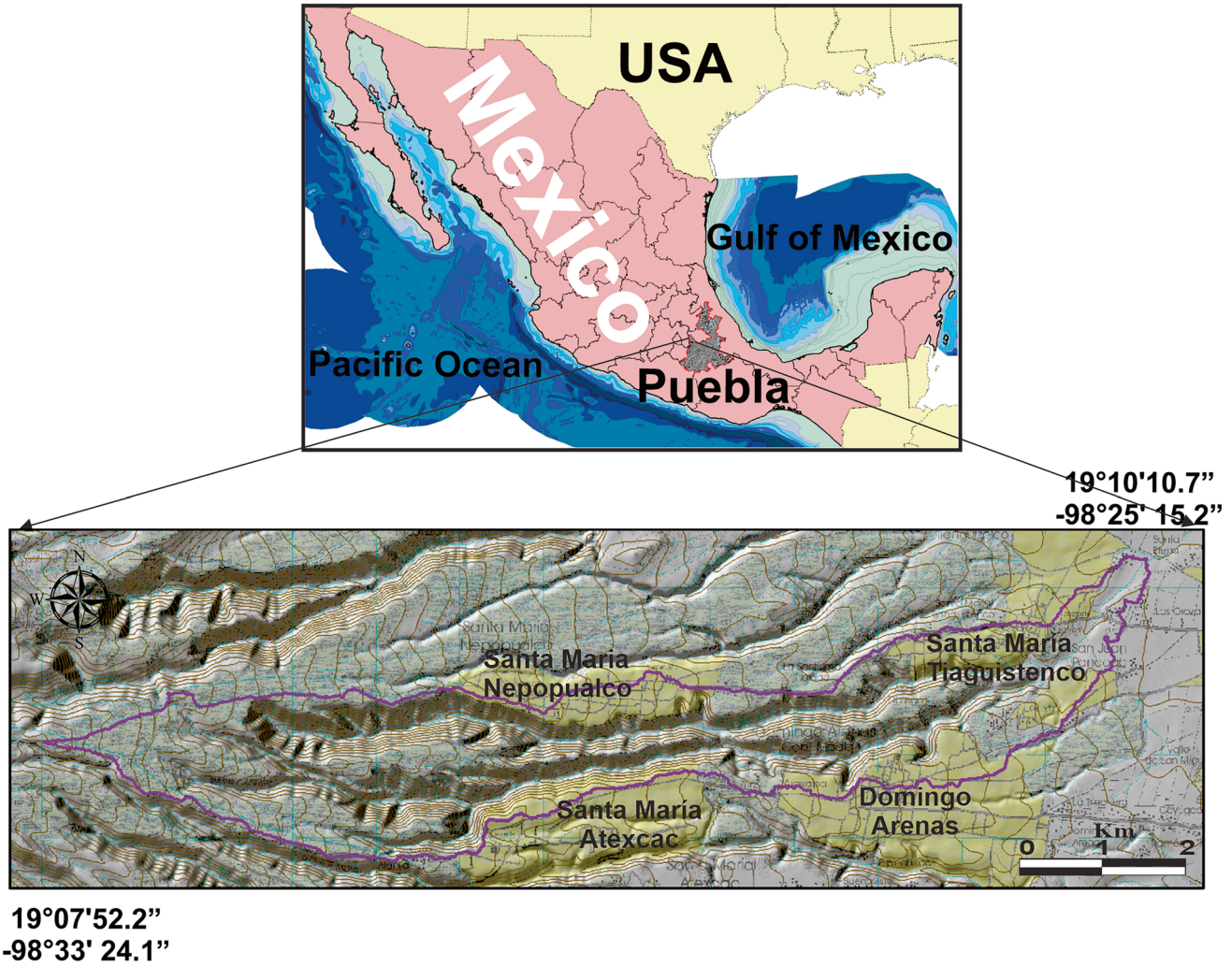

Fig. 2 Study area, Xopanac-Apitzato watershed, State of Puebla, Mexico

scale 1:250,000. All paper maps will be converted to a raster format, georeferenced, and incorporated as GIS layers. Background information also includes orthophotographs at 1:20,000 as well as a 5 m LiDAR digital elevation model (DEM), and its derived thematic maps of slope angle, aspect, curvature, drainage density, and vertical erosion. These topographic derived maps are considered as a good and important controlling predictor factor for landslides. They spatial variations could lead to differences in environmental disturbance and land use patterns that in turn affect the distribution, types, and sizes of landslides. The slope will be mapped in degrees with the ArcGIS slope module. The aspect will be mapped in nine classes to show slope direction terms of degrees from north in a clockwise direction. Terrain curvature is a factor that affects erosion and deposition processes along the hillslope. The curvature map will be calculated with the ArcGIS build-in curvature module and classified into straight and smooth surfaces, concave surfaces, and convex surfaces. The drainage density map will be calculated by splitting the study area into a 1 km^2 grid and obtaining the total length of stream in each. The vertical erosion will be calculated by splitting the study area into a grid of 1 km^2, and the maximum vertical distance between the talweg and the maximum height will be obtained in each cell of the grid.

Step 3. Selection of aerial photographs: In the study area, two sets of aerial photographs will be used: from 1993 and 1995 at a scale of 1:20,000, a Google Earth image from 2001 and an image of 2002 from Planet. The photographs will be analyzed using a mirror stereoscope with 3× magnification and they will be used as a layer during GIS analysis and mapping.

Step 4. Creation of base map using GIS layers: By retrieval and on-off switching of the layers in the GIS system, a base map will be created to assist in the digitizing of landslides and landform units. The digital layers include the watershed boundary, topography, shaded relief, hydrology, roads, geology, and orthophotograph.

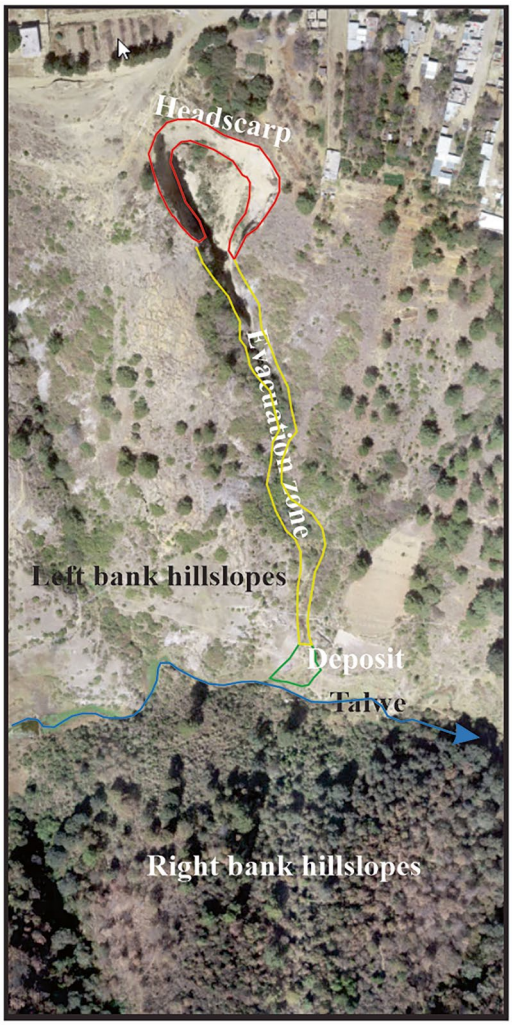

Fig. 3 Debris slide and debris flow in N section of the watershed

Catchment area, stream length, stream patterns, stream orders, drainage density and vertical erosion will be generated from GIS analysis and will be incorporated as background information.

Steps 5 and 6. Landslide map and field work: All landslides will be mapped by "heads-up" digitizing in ArcGIS. This involves mapping on photo-transparencies and digitizing directly onto the screen into GIS at the same scale as the photographs. Landslides will be mapped according to the landslide hazard zonation protocol (2006) of Washington State DNR Forest Practices Division. The protocol classifies landslides into shallow undifferentiated landslides, debris flows, debris slides, deep-seated landslides, earthflows, and rock falls. In the landslide inventory will be mapped for each landslide head scarp, evacuation zone, and deposit (these last two will be not always visible). Some attributes of mapped landslides will be recorded in the GIS database, namely (1) landslide type, (2) landslide size, (3) landslide activity, (4) landslide parts (head scarp, evacuation zone, and deposit), (5) landslide geometry (area, length, width, depth), (6) location of the landslide on the right or left river bank, and (7) certainty of the observation. The interpretation with aerial photographs for landslide mapping will be aided by field work. Two sessions of field work per year will be conducted during the dry and wet season along the main and secondary rivers, for data validation, landslide and landform mapping, verification, and landslide volume measurements.

Step 7. The landslide susceptibility will be modeled by use of landform units and Multiple Logistic Regression (MLR). Once landslides have been mapped, areas of similar landslide potential will be grouped into individual landform units. Landform units will be defined by rules adopted by the Washington Forest Practices Protocol to address landslide

Fig. 4 Debris slide triggered by 2017 earthquake and anthropic activity

hazards (Washington State Department of Natural Resources (DNR), Forest Practices Division 2006).

These landform units are called rule-identified landforms (inner gorges, bedrock hollows, convergent headwalls, outer edges of meanders, and active scarps of deep-seated landslides). Their differentiation is based on slope gradient and shape, lithology, landslide density and sensitivity to forest practices. The aerial photos, the landslide inventory, and GIS layers will be also used to identify other areas that do not meet the rule-identified landform definitions. These areas are called non-rule-identified landforms (such as non-rule-identified inner gorges, non-rule-identified bedrock hollow, steep-gradient hillslopes, moderate-gradient hillslopes, low-gradient hillslopes). Both rule- and non-rule-identified landforms will be entered into GIS as part of a landform polygon feature. For each landform unit, a semi-quantitative hazard rating will be derived from values that correspond to the landslide area rate and the landslide frequency rate; this will lead to an overall hazard rating for each landform and for the watershed.

For MLR analysis, random sampling from landslide areas and non-landslide areas for a training and a validation dataset will be conducted for each thematic independent variable. Assessment of multicollinearity by determination of the variance inflation factor (VIF) and Backward MLR will be conducted on the SPSS statistical package. The variables will be used in MLR to make the final susceptibility map.

To evaluate the models, the "predicted model vs. inventory matching" approach will be used. The percentage of overlay between landform units and MLR model susceptibility maps and the inventory map will be the gauge of how well the models predict the reality. A two-classification scheme (landslide and non-landslide) will be used for the inventory map and model susceptibility maps to facilitate the comparison. The models will be assessed and compared by use of a contingency table and the area under the ROC (receiver operating characteristic) curve (AUC) that shows the amount of overlap and relation between inventory and predicted maps. In the contingency table, the evaluation of the susceptibility model vs. the landslide inventory will be expressed in terms of producer's accuracy (ratio of the number of correctly classified pixels in each category to the total number of true pixels for that category), user's accuracy (ratio of the number of correctly classified pixels in each category to the total number of pixels that are classified by the model in that category), and model efficiency (ratio of correctly minus incorrectly indicated landslide pixels to the total number of true landslide pixels mapped in the inventory map).

In this stage of the project, landform units and MLR susceptibility models will be evaluated to select the one that meets stated criteria for scientific accuracy, technical accessibility, and applicability.

Steps 8 and 9. Landslide volume. Detailed geometric measurements of individual landslides visited during the field work and observed via UAV will indicate the landslide area and volume. The area and volume of the representative landslide head scarp in the watershed will be measured with a UAV. We will exclude the volume and area of the deposits and the slip evacuation area. Geometrical measurement of landslides will be conducted by using a Mavic 3E quadcopter with a camera with 20 megapixels resolution and a CMOS sensor of 1″. Flight planning will used the DJIFlightPlanner software. Aerial images will be acquired with an average flight height of 120 m and at a speed of 7 m/s. The front and side overlaps between aerial photographs will be 80%. We will use a DJI D-RTK 2 base station to obtain a precision of 3 cm during the aerial-photographs capture.

The post-processing of the images will use Agisoft PhotoScan photogrammetric software. We followed a standard post-processing workflow adapted after Ouédraogo et al. (2014). The workflow in PhotoScan will be as follows. (1) Selection and addition of all captured photos for each landslide. (2) Alignment of the loaded aerial photographs. (3) Construction of a cloud of dense point values. (4) Reclassification of the dense point cloud values into ground and the other elements (vegetation, buildings etc.). (5) Creation of a DEM, and 6) creation of an orthophotograph. DEMs at 3 cm per pixel will be obtained.

In ArcMap, the post-sliding topography and the reconstructed pre-sliding topography will be created. This pre-sliding topography will be set heuristically by field observation and reconstruction of the original topography from the post-sliding topography generated by the UAV. The nodes from polygons that represent the current landslide headscarp boundary will be used to create a point file which in turn will be used to extract the elevation data from the DEM for the topography of the landslide. The nodes will be interpolated to create the interpolated pre-sliding topography. The landslide volume will be calculated from the algebraic difference between the reconstructed pre-sliding topography and the actual topography, multiplied by the area of the pixel. To accomplish the above task, we use a model implemented as a tool in ArcGIS called VolumeByInterpolationUNAM-DNRv2.py which calculates the total landslide volume as well as the negative and positive values. Negative values represent accumulation of material in the landslide area while positive values represent loss of material. With the area and volume of the selected landslides an empirical relationship between area and volume will be expressed as a power law with a scaling exponent. This relationship of known landslides will then be used to estimate the potential total material delivered to the main stream drainage channel by all landslides in the watershed. Once the volume has been calculated, a selected landslide will be used to model landslide volume distribu-

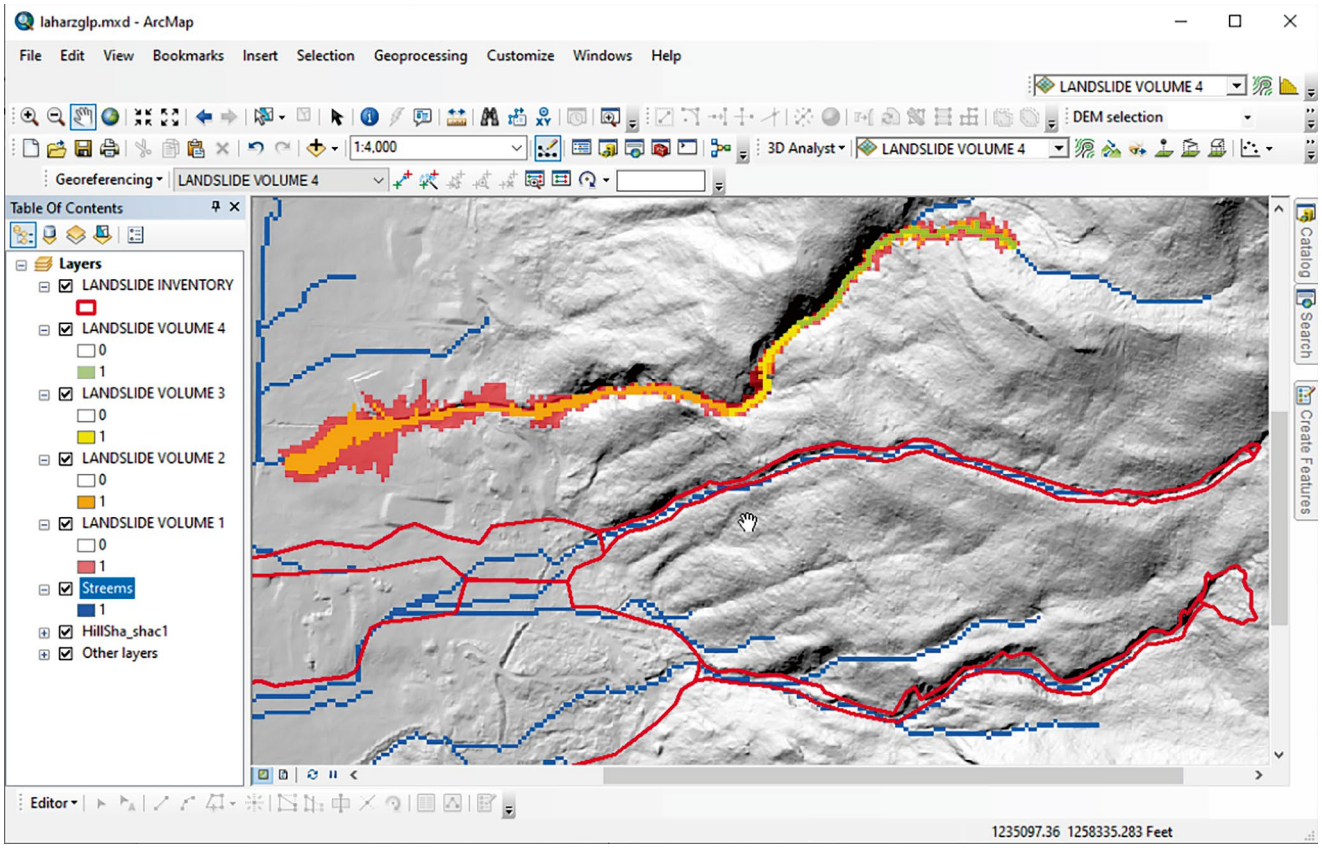

Fig. 5 Theoretical example of 4-volume distribution of a shallow landslide using the adequation of Laharz model

tion. Adequation using Laharz software will allow prediction of areas likely to be at risk (Fig. 5). The adequation is still under development in a program called VolumeDistributionUNAMv0.py.

Step 10. Report: A written report will describe the analysis and include an explanatory text, landform descriptions, landslide triggering mechanisms and the landslide susceptibility and volume findings in the watershed.

Step 11. Final revisions and products: Prior to public release of the report and the corresponding 1:20,000 landslide and landform or MLR susceptibility maps, a tri-level review will be conducted. The first two will be internal peer-reviews carried out by another analyst and a licensed Engineering Geologist. The third review will be external, voluntarily performed by reviewers such as geoscientists, foresters, and other interested parties. The comments received will be used to improve the products prior to final public release on the Institute of Geography website.

Acknowledgments The authors thank authorities from the International Consortium on Landslides (ICL) and the International Programme on Landslides (IPL) for their approval and help.

This research was supported by the Programa de Apoyo a Proyectos de Investigación e Innovación Tecnológica (PAPIIT), UNAM. # IN100223.

Declarations of Interest The authors declare no competing interests.

References

Andaru R, Rau JY, Prayoga AS (2022) Determination of potential secondary lahar hazard areas based on pre- and post-eruption UAV DEMs: automatic identification of initial lahar starting points and supplied lahar volume. Int J Appl Earth Obs Geoinf 115:103096

Blahut J, Van Westen CJ, Sterlacchini S (2010) Analysis of landslide inventories for accurate prediction of debris-flow source areas. Geomorphology 119(1–2):36–51

Can T, Nefeslioglu HA, Gokceoglu C, Sonmez H, Duman TY (2005) Susceptibility assessments of shallow earth flows triggered by heavy rainfall at three catchments by logistic regression analyses. Geomorphology 72:250–271

Capra L, Lugo-Hubp J (2006) Fenómenos de remoción en masa en el poblado de Zapotitlán de Méndez, Puebla: Relación entre litología y tipo de movimiento. Revista mexicana de ciencias geológicas 20(2):95–106

Capra L, Lugo-Hubp J, Borselli L (2003) Mass movements in tropical volcanic terrains: the case of Teziutlán (México). Eng Geol 69:359–379

Cemiloglu A, Zhu L, Mohammednour AB, Azarafza M, Nanehkaran YA (2023) Landslide susceptibility assessment for Maragheh County, Iran, using the logistic regression algorithm. Land 12(7):1397

Centro Nacional de Prevención de Desastres (CENAPRED) (2001) Las cenizas volcánicas del Popocatépetl y sus efectos para la aeronavegación e infraestructura aeroportuaria. Instituto de Geofísica, UNAM, Mexico City

Chen Z, Zhang B, Han Y, Zuo Z, Zhang X (2014) Modeling accumulated volume of landslides using remote sensing and DTM data. Rem Sens 6(2):1514–1537

Du J, Glade T, Woldai T, Chai B, Zeng B (2020) Landslide susceptibility assessment based on an incomplete landslide inventory in the Jilong Valley, Tibet, Chinese Himalayas. Eng Geol 270:105572

García Tenorio F (2008) Avalancha de escombros del pleistoceno tardío del cono Los Pies, complejo volcánico Iztaccíhuatl (Master thesis). Escuela Superior de Ingeniería, Sección de Estudios de Posgrado e Investigación, Unidad Ticomán, Instituto Politécnico Nacional, México, 147 pp

Guzzetti F, Ardizzone F, Cardinali M, Rossi M (2009) Landslide volumes and landslide mobilization rates in Umbria, central Italy. Earth Planet Sci Lett 279:22–229

Guzzetti F, Mondini AC, Cardinali M, Fiorucci F, Santangelo M, Chang KT (2012) Landslide inventory maps: newtools for an old problem. Earth Sci Rev 112:42–66

Hervás J, Bobrowsky P (2009) Mapping: inventories, susceptibility, hazard and risk. In: Sassa K, Canuti P (eds) Landslides—disaster risk reduction. Springer, Berlin, pp 321–349. ISBN 978-3-540-69966-8

Iverson RM, George DL, Allstadt K, Reid ME, Collins BD, Vallance JW, Bower JB (2015) Landslide mobility and hazards: implications of the 2014 Oso disaster. Earth Planet Sci Lett 412:197–208

Jasiewicz J, Stepinski T (2013) Geomorphons—a pattern recognition approach to classification and mapping landforms. Geomorphology 182:147–156

Kalderon-Asael B, Katz O, Aharonov E, Marco S (2008) Modeling the relationship between area and volume of landslides. Geological Survey of Israel. Report (GSI/06/2008), pp 1–16

Montgomery DR, Dietrich WE (1994) A physical based model for the topographic control on shallow landslides. Water Resour Res 30:1153–1171

Muñoz-Salinas E, Castillo-Rodríguez M, Manea V, Manea M, Palacios D (2009) Lahar flow simulations using LAHARZ program: application for the Popocatépetl volcano, Mexico. J Volcanol Geotherm Res 182(1–2):13–22

Ouédraogo MM, Degré A, Debouche C, Lisein J (2014) The evaluation of unmanned aerial system-based photogrammetry and terrestrial laser scanning to generate DEMs of agricultural watersheds. Geomorphology 214:339–355

Pack RT, Tarboton DG, Goodwin CN (2001) Assessing terrain stability in a GIS using SINMAP. In: Proceedings of the 15th annual GIS conference, Vancouver, British Columbia

Peark MR, Ng KY, Zhang DD (2005) Landslide and sediment delivery to a drainage system: some observations from Hong Kong. J Asian Earth Sci 25:821–836

Pérez-Gutiérrez R (2007) Análisis de la vulnerabilidad por los deslizamientos en masa, caso: Tlacuitlapa, Guerrero. Bol Soc Geol Mex 59(2):171–181

Ray RL, Lazzari M, Olutimehin T (2020) Remote sensing approaches and related techniques to map and study landslides. In: Landslides—investigation and monitoring, vol 2. IntechOpen, London, pp 1–25

Secretaría de Protección Civil (2010) Atlas de peligros geológicos e hidrometeorológicos del estado de Veracruz. Comp.: Ignacio Mora González; Wendy Morales Barrera, Sergio Rodríguez Elizarrarás. Xalapa: Secretaría de Protección Civil del estado de Veracruz: Universidad Veracruzana: UNAM. 1V

Shao X, Xu C, Wang P, Li L, He X, Chen Z, Huang Y, Xu X (2022) Two public inventories of landslides induced by the 10 June 2022 Maerkang Earthquake swarm, China and ancient landslides in the affected area. Nat Hazards Res 2(4):269–272

Slaughter SL, Burns WJ, Mickelson KA, Jacobacci KE, Biel A, Contreras TA (2017) Protocol for landslide inventory mapping from lidar data in Washington State: Washington Geological Survey Bulletin 82, 27 p. text, with 2 accompanying ESRI_le geodatabases and 1 Microsoft Excel_le.http://www.dnr.wa.gov/Publications/ger_b82_landslide_inventory_mapping_protocol.zip

Sujatha ER, Sridhar V (2021) Landslide susceptibility analysis: a logistic regression model case study in Coonoor, India. Hydrology 8(1):41

UNEP (2013) A new eye in the sky: eco-drones. UNEP Global Environmental Alert Service. 13 p. http://na.unep.net/geas/getUNEPPageWithArticleIDScript.php?article_id=100. Accesado 10 Feb 2021

Washington State Department of Natural Resources (DNR), Forest Practices Division (2006) Landslide Hazard Zonation (LHZ) mapping protocol, version 2.0. http://www.dnr.wa.gov/BusinessPermits/Topics/LandslideHazardZonation/Pages/fp_lhz_review.aspx

Wenske D, Jen CH, Böse M, Lin JC (2012) Assessment of sediment delivery from successive erosion on stream-coupled hillslopes via a time series of topographic surveys in the central high mountain range of Taiwan. Quat Int 263:14–25

Young AP (2015) Recent deep-seated coastal landsliding at San Onofre State Beach, California. Geomorphology 228:200–212

Implementation of the Early Warning Technology for Rain-Induced Rapid and Long-Traveling Landslides in Sri Lanka

Kazuo Konagai, Kumiko Fujita, Jayalath Edirisinghe, Imaya Ariyarathna, Tania Munasinghe, Dayan Munasinghe, Miwa Abe, Toyohiko Miyagi, Ryo Onishi, Anuththara Bandara, Keisuke Takimoto, Asiri Karunawardena, and Kyoji Sassa

Abstract

Landslides occur frequently in Sri Lanka, where there has been a marked increase in torrential rainfall with the onset of climate change. To predict a day in advance the occurrence and range of rain-induced rapid and long-traveling landslides (RRLLs), which are particularly severe, SATREPS Project RRLL has started since 2020. The project develops a system for early transmission of information predicting torrential rains and landslides and for supporting risk assessment, incorporating cutting-edge technology that predicts accumulated rainfall within a 500-m grid. As the project enters its final fiscal year in 2024, it has reached the stage at which community engagement will be promoted. The system developed in the project is subject to Internet connectivity. Therefore, mobile phones are often the only means of communication to the last mile, where Internet connection is unavailable in torrential rain in the mountains. To fully utilize the information on the predicted rains and RRLL occurrences under these circumstances, it is imperative for residents and the relevant officers who have jurisdiction over the area to know the environment in which they live. This last piece of the project's Jigsaw puzzle is the village-watching activities involving local people and relevant officers in the project's target study sites. This article reports the project's outcomes focusing on the village-watching activities.

Keywords

RRLLs · SATREPS project · Sri Lanka · Early warning technologies · Social implementation

1 Introduction

Sri Lanka, located at the southern tip of the Indian Subcontinent, is an isolated island experiencing two monsoon rain peaks. The first peak, from May to September, brings heavy rain, particularly in the central mountain region, which covers about 30% of the island's land area and is occupied by about 35% of the nation's population.

The geology of this mountainous area is Precambrian. Sri Lanka's hot and humid tropical climate has left these mountain slopes covered with thick, weathered gneissic rock, making them landslide-prone. Slopes composed of weathered gneissic rock and its colluvial soils with high permeability are suitable for cultivating the nation's critical agricultural products such as tea, coconut, cinnamon, and rubber. In addition to this, the region has many World Heritage sites. However, as

K. Konagai (✉) · K. Fujita · T. Miyagi · K. Sassa
International Consortium on Landslides, Kyoto, Japan
e-mail: Secretariat@landslides.org

J. Edirisinghe
University of Peradeniya, Peradeniya, Sri Lanka
e-mail: jayalath@eng.pdn.ac.lk

I. Ariyarathna · D. Munasinghe · A. Bandara · A. Karunawardena
National Building Research Organization, Colombo, Sri Lanka

T. Munasinghe
ICL/SATREPS Office, NBRO, Colombo, Sri Lanka

M. Abe
Tokai University, Kumamoto, Japan
e-mail: abe.miwa.k@tokai.ac.jp

R. Onishi
Institute of Science Tokyo, Tokyo, Japan
e-mail: onishi.ryo@gsic.titech.ac.jp

K. Takimoto
Godai Kaihatsu Co. Ltd., Kanazawa, Japan
e-mail: takimoto@godai.co.jp

B. Abolmasov et al. (eds.), *Progress in Landslide Research and Technology, Volume 4 Issue 1, 2025*, Progress in Landslide Research and Technology, https://doi.org/10.1007/978-3-031-89836-5_14

human activities extended into mountainous areas, the threat of rain-induced rapid and long-traveling sediment disasters increased in severity, underscoring the role of human actions in exacerbating the natural risk of landslides.

The Aranayake landslide, a catastrophic event that occurred on May 17, 2016, in the Aranayake area of Sri Lanka, resulted in the tragic loss of 127 lives. This event, triggered by relentless rainfall, is a stark reminder of the devastating potential of landslides, particularly when they turn into debris flows. The tragic consequences of the Aranayake landslide underscore the urgent and pressing need for effective risk reduction measures.

The National Building Research Organization (NBRO) is a crucial government agency established in 1984 in Sri Lanka. It has been playing a pivotal and reassuring role in various programs to assist a disaster-free built environment, focusing on landslide disaster reduction. Both NBRO and the Secretariat of the International Consortium on Landslides (ICL hereafter) have jointly compiled a research proposal within the framework of SATREPS (Japan Science and Technology Agency 2020); SATREPS, "Science and Technology Research Partnership for Sustainable Development," is a Japanese government program, with two funding organizations, namely, the Japan International Cooperation Agency (JICA hereafter) and the Japan Science and Technology Agency (JST hereafter), that promotes international joint researches. It passed the final round of selection on May 16, 2019. This 5-year SATREPS project for Sri Lanka about "Development of early warning technology of Rain-induced Rapid and Long-travelling Landslides (Project RRLL hereafter)" started in 2020 (Konagai et al. 2023).

The project has been divided into three groups. Group No. 1 (G1) oversees and coordinates all research activities and promotes the development of young human resources on the Sri Lankan side, inviting young scientists to Japan for both short- and long-term research and training. The mission of Group No. 2 (G2) is to develop specific techniques for day-ahead prediction of rainfall and landslides in mountainous areas. The mission of Group 3 (G3) is to establish a system to disseminate the predicted rainfall and landslide information to the last mile, which includes local people and the agencies in charge of disaster management in the area for better disaster preparedness actions.

As the project enters its final fiscal year, it has reached the stage at which Group 3 (G3) will lead in promoting the community engagement.

This article mainly summarizes G3 members' activities and achievements and outlines the remaining issues and policies for continued development after the project's completion.

2 Target Study Sites

The SATREPS Project RRLL targets two 10 × 10 square kilometer study areas, Aranayake and Athwelthota, as shown in Fig. 1a.

Aranayake area is in the Kegalle District of Sabaragamuwa Province in Sri Lanka. Its agricultural economy revolves around rubber, tea, banana, and mahogany plantations. The Aranayake landslide was one of the recent examples of a devasting rain-induced rapid and long-travelling landslide (RRLL, Fig. 1b). The landslide triggered on May 17, 2016, by prolonged rainfall associated with a slow-moving tropical cyclone is unique due to its size and runout distance. The fluidized landslide mass from the relative elevation of about 600 m ran over an approximately 2 km distance, claiming the lives of 127 people. This landslide is unique because it is much more prominent in size and runout distance than the other. Though this type of landslide rarely occurs, a large RRLL can cause a big disaster. This landslide mass ran across two local communities, Elagipitiya and Debathgama Pallebage, with about 1500 and 1100 inhabitants.

The Athwelthota landslide on May 26, 2017, in the Palindanuwara Divisional Secretariat of the Kalutara District (Fig. 1c) is another example of RRLLs in Sri Lanka. The landslide claimed nine lives, the destruction of nine houses, and the landslide mass stopped traffic on Thiruwanaketiya-Agalawatta Road (B421). Each landslide of the Athwelthota type will not cause a surprisingly large disaster, but the number of landslides of this type can be huge, causing extensive losses of human lives and properties. During the heavy rain of 2017, 37 RRLLs reportedly took place all at once, claiming the lives of 262 people. There remain unstable soil masses in the above two pilot

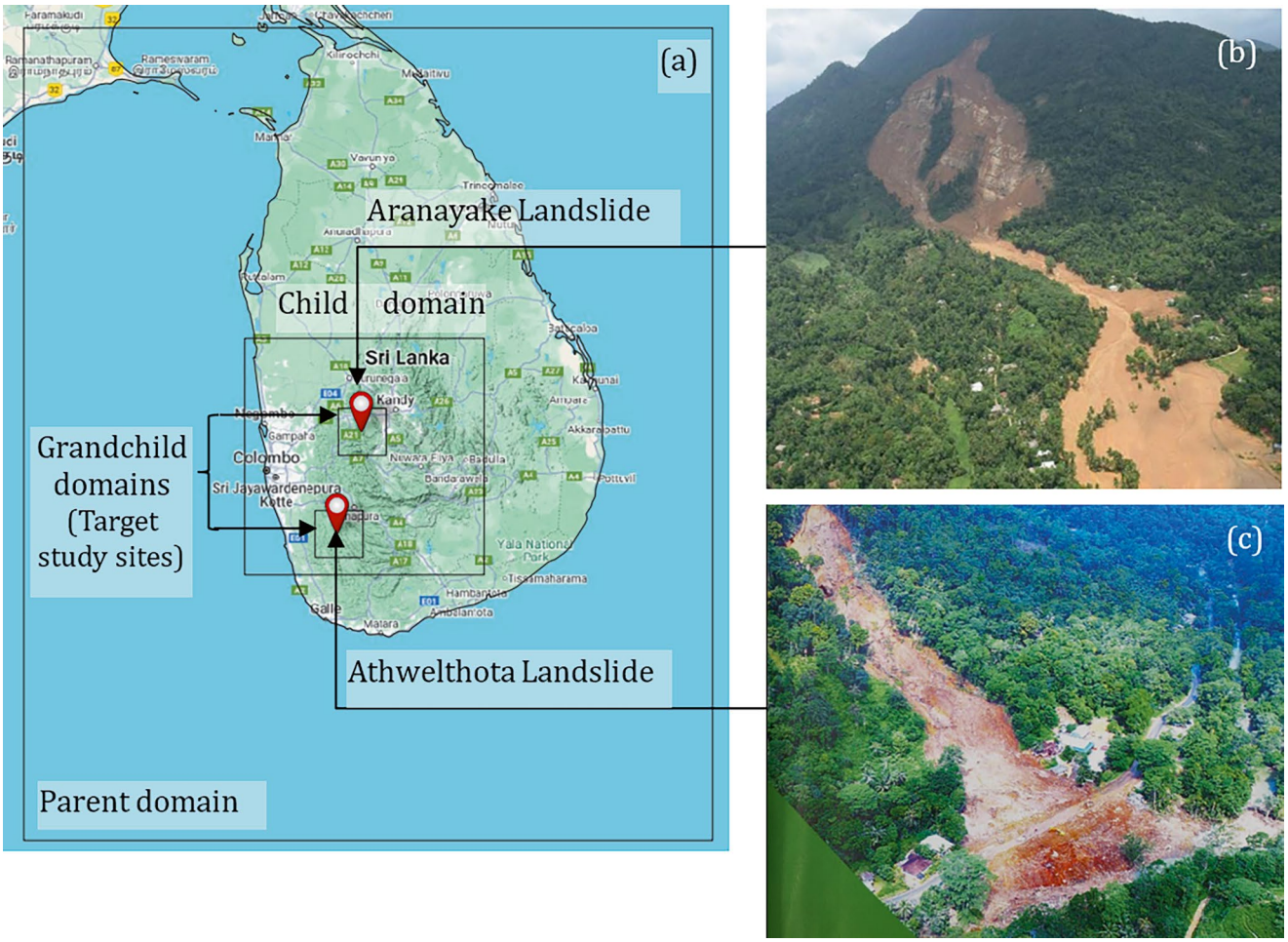

Fig. 1 Two devastating Rain-induced Rapid and long-traveling Landslides (RRLLs) that occurred in the project's target study sites, Aranayake and Athwelthota: (**a**) Google Terrain Map of Sri Lanka showing nested computational domains for weather simulation, (**b**) 2016 Aranayake Landslide (credit: NBRO), and (**c**) 2017 Athwelthota Landslide (credit: NBRO)

study sites perching in and around the tops of the exposed bare-earth slopes, highlighting the urgent need for action to prevent further loss.

3 Technologies for the Predicted Information Transfer to the Last Mile

The core of the technology to transfer in the SATREPS Project RRLL is a system that visualizes rainfall and RRLL occurrences predicted one day in advance in virtual reality space on computer and smartphone screens. This Augmented Reality (AR) Viewing System requires two fundamental technologies for (1) mountain rainfall prediction and (2) prediction of RRLL occurrences given the predicted rains.

3.1 Prediction of Mountain Rains

Multi-Scale Simulator for the Geo-environment (MSSG) is a coupled non-hydrostatic atmosphere-ocean-land model developed in the Earth Simulator Center of the Japan Agency for Marine-Earth Science and Technology (Takahashi et al. 2008). In the SATREPS Project RRLL, MSSG is the platform for one-day-ahead forecasts of rainfalls in mountainous areas. MSSG can consider the precise topographic effect and the boundary-layer turbulence that affects the cumulonimbus cloud development, particularly over slopes against the wind. Thus, it suits better one-day-ahead predictions of heavy mountain rainfalls (Onishi et al. 2023).

A straightforward weather simulation using MSSG with a high 500 m spatial resolution (High Resolution, HR) cover-

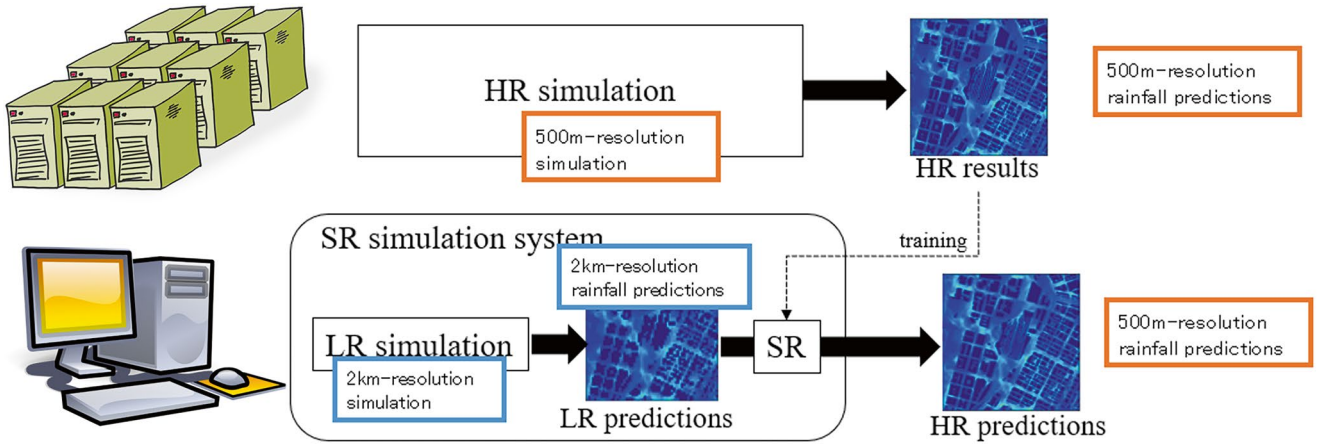

Fig. 2 Super-resolution (SR) simulation system (Bandara and Onishi 2023): by conducting an LR simulation on an affordable workstation and then using an SR method to map the resulting LR prediction images to HR predictions, this system can provide predictions comparable to those obtained from HR simulations on a super-computer while significantly reducing the computational cost

ing the two 10 ×10 square kilometer study areas while offering superior predictive capabilities to low-resolution (LR) simulations requires enormous computer capacities. The straightforward, high-resolution weather forecast for the day ahead was updated on an affordable Dual-socket Workstation with two Intel Xeon Processors (Intel Xeon 6226 2.72933 MHz) every 6 h.

Downscaling techniques, including machine learning models such as artificial neural networks and support vector machines, are employed to enhance the spatial resolution of low-resolution models. The super-resolution (SR) simulation system effectively addresses this challenge with its innovative two-step approach. By conducting an LR simulation and then using an SR method to map the resulting LR prediction images to HR predictions, this system can provide predictions comparable to those obtained from HR simulations while significantly reducing the computational cost (Fig. 2, Bandara and Onishi 2023). The implemented SR simulation system has reduced the update time to 3 h.

Case history analyses were conducted to confirm that this technology using MSSG could adequately predict rainfalls. Figure 3a shows the chronological changes in rains in Aranayake (Onishi et al. 2024); the rain finally caused the killer 2016 Aranayake landslide. Although the predicted values of individual rainfall peaks deviate in time and space from the measured values, MSSG could reproduce the overall rainfall pattern; namely, it could reproduce the temporal increase of the cumulative rain, which must have triggered the 2016 Aranayake Landslide.

Figure 3b shows the rains in Athwelthota, where an unstable soil mass perched on top of the slope of the past landslide in 2017 retrogressively slid on June 2, 2024 (Fig. 3c). Regrettably, this AR Viewing System was not released to the public until after this landslide. In the MSSG simulation, the computational domains are triply nested. The outermost domain (Parent domain), which covers the whole Sri Lankan land area as well as the southern tip of the Indian subcontinent, requires its boundary ambient parameters from a Global Spectrum Model (GSM) provided by the Japan Meteorological Agency (JMA) or the United States National Centers for Environmental Prediction (NCEP), both dedicated to the scientific observation and research of natural phenomena with a particular focus on weather. Overall, the NCEP model produces more rainfall than the JMA model for Athwelthota, near the island's western coast. The current system uses the JMA Global Spectrum Model. However, we may have to consider switching to the NCEP model to be safe in prediction.

3.2 Prediction of RRLL Occurrences and Runouts

In predicting RRLL occurrences and their runouts, we utilize two numerical tools, LS-Rapid and the SLIDE model, which have been developed and used for many years.

LS-Rapid is an integrated simulation model that captures the entire landslide process, from stability to initiation and movement to mass deposition (Sassa et al. 2010). The LS-RAPID model concept was established by considering that the unstable slope consists of the landslide mass and stable ground as a vertical imaginary column, using the two-dimensional depth-integrated shallow water equations for the incompressible fluid with the Coulomb-type friction term.

The LS-RAPID model is a significant tool in predicting landslides. It offers the unique advantage of simulated rainfall-induced and earthquake-induced landslides, providing a comprehensive understanding of potential landslide scenarios. The model can be configured to simulate rainfall-

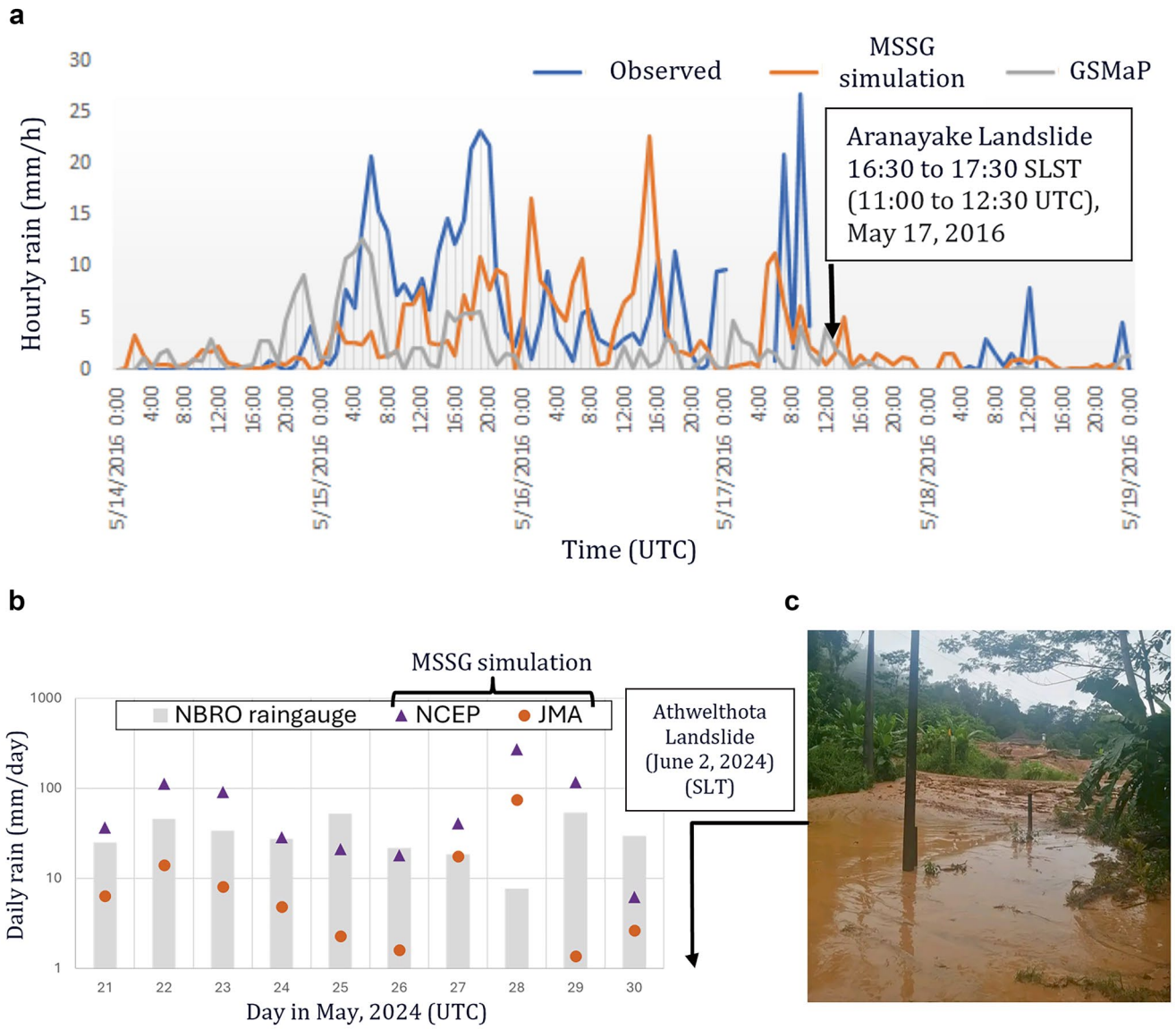

Fig. 3 (**a**) Chronological changes of the observed and predicted hourly rains (in mm) at Aranayake in May 2016 (Onishi et al. 2024): The blue line shows the monsoon rain from May 14 to 19 observed at the rain gauge (7.159N, 80.459E), while the orange line shows the estimated rain with MSSG. The gray line shows the satellite observation of the rain retrieved from the Global Satellite Mapping of Precipitation (GSMaP), which provides a global hourly rain rate with a 0.1 × 0.1° resolution. The 2016 Aranayake Landslide occurred from 16:30 to 17:30 SLST (11:00–12:30 UTC), May 17, 2016. (**b**) Temporal variation of daily rains in May 2024 at the Athwelthota Landslide site: The outermost domain (Parent domain in Fig. 1a), which covers the whole Sri Lankan land area as well as the southern tip of the Indian sub-continent, requires its boundary ambient parameters from a Global Spectrum Model (GSM) provided by the Japan Meteorological Agency (JMA) or the United States National Centers for Environmental Prediction (NCEP). (**c**) Athwelthota Landslide on June 2, 2024: An unstable soil mass perched on top of the slope of the past landslide in 2017 retrogressively slid on June 2, 2024. (Credit: NBRO)

induced landslides based on either the pore water pressure ratio or hourly rainfall data time series.

The SLIDE Model (Liao et al. 2010) considers simplified hypotheses on the vertical water downflow and defines a direct correlation between the slope's pore-water pressure increase and rainfall.

The combined use of LS-Rapid and SLIDE models has been verified using the case history of the 2016 Aranayake landslide by Dang et al. (2019); the LS-RAPID Manual with Video Tutorials (Ajmera et al. 2023). is also available online in the ICL's open-access book series "Progress in landslide Research and technology," Volume 1, Issue 1.

4 AR Viewing Software

Mountain slopes in the project's target study site are meticulously terrain-interpreted to extract unstable soil masses perching on them. Then, some scenario rains are given to each identified unstable slope to identify the critical pore-pressure ratio for initiating the landslide movement. A data set of critical pore pressure ratios for these slopes is prepared by performing this calculation for all extracted unstable slopes. Then, the pilot study site is subject to the possible rains that MSSG predicted one day in advance. Suppose the pore water pressure ratio within a slope exceeds the pre-calculated critical pore water pressure ratio for the slope. In that case, the slope is assumed to slide, and a polygon representing the unstable soil mass and its potential runout extent is displayed on the AR Viewing System map canvas (Fig. 4).

The software allows stakeholders to interact with it in a way that combines the real world (geographic information of pilot study sites) and computer-generated content (predicted rains and RRLLs).

4.1 Specifications

The real world is provided by Google Earth, rendering a 3D representation of the terrain profile based primarily on satellite imagery.

1. The predicted rainfall pattern for the next 24 h is updated every 3-h interval.
2. Predicted RRLL occurrences for the next 24 h.
3. The software features an interactive time slider, which empowers stakeholders with greater control over viewing predicted information's timestamps, enhancing their understanding of the data.

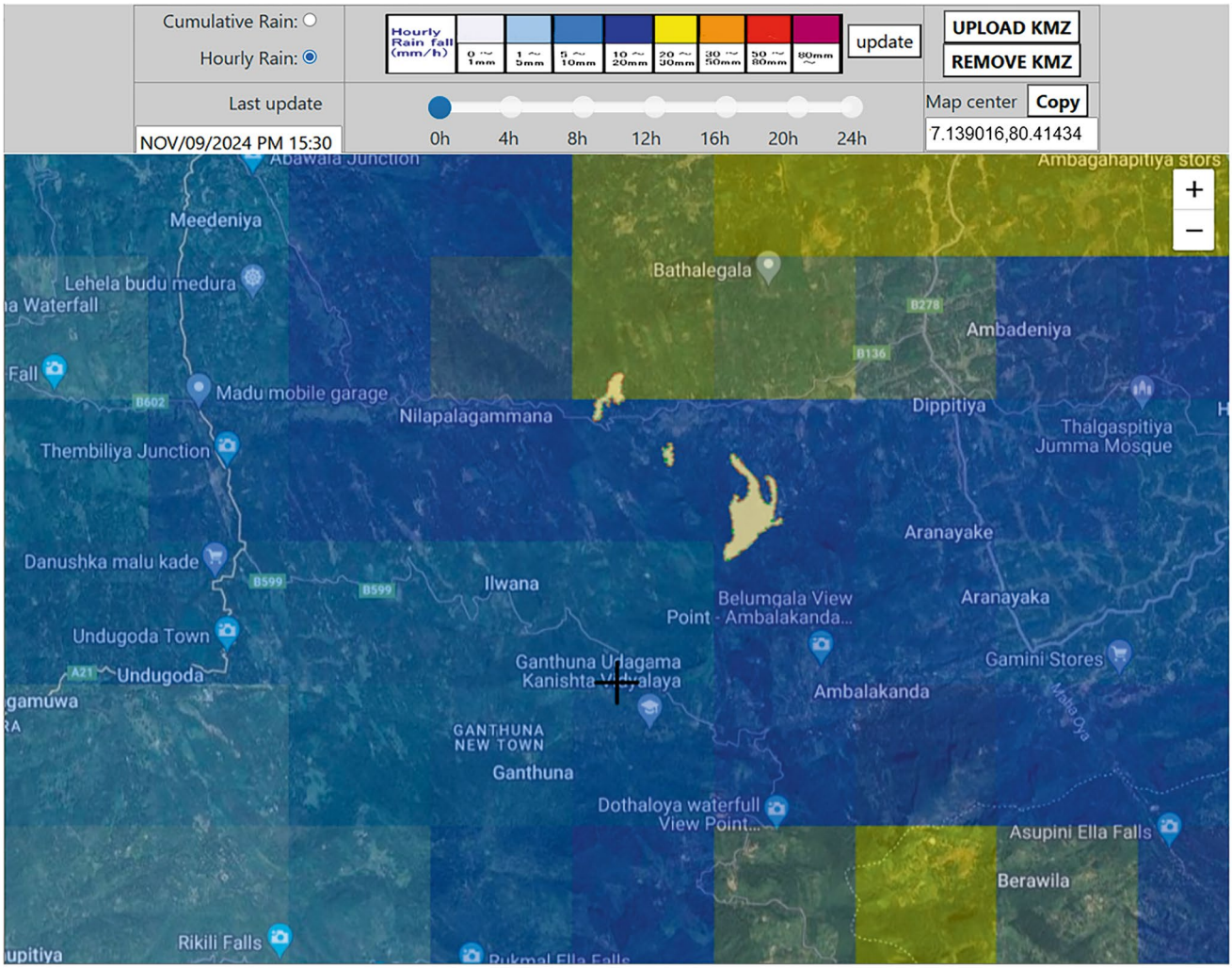

Fig. 4 Predicted RRLLs displayed on the Augmented Reality (AR) Viewing Canvas: To check the performance of the AR Viewing System, a hypothetical torrential rainfall was given in the simulation

4. Arbitrary layers can be laid over the terrain image (Fig. 5a).
5. The center coordinates of the background map are displayed, and a button is provided to copy these coordinates (Fig. 5a).

The last item (5) in the specification was prepared to compare the predicted rainfall and RRLL occurrences displayed in the virtual reality space with the map layers held by the beneficiary and overlaid on the separate map canvas of GIS software, such as Google Earth (Fig. 5b). The beneficiary's map layers can contain a wide range of information about local people, their living environment, and their lives, represented with points, lines, shapes (polygons), or surfaces. Of course, such map layers can be

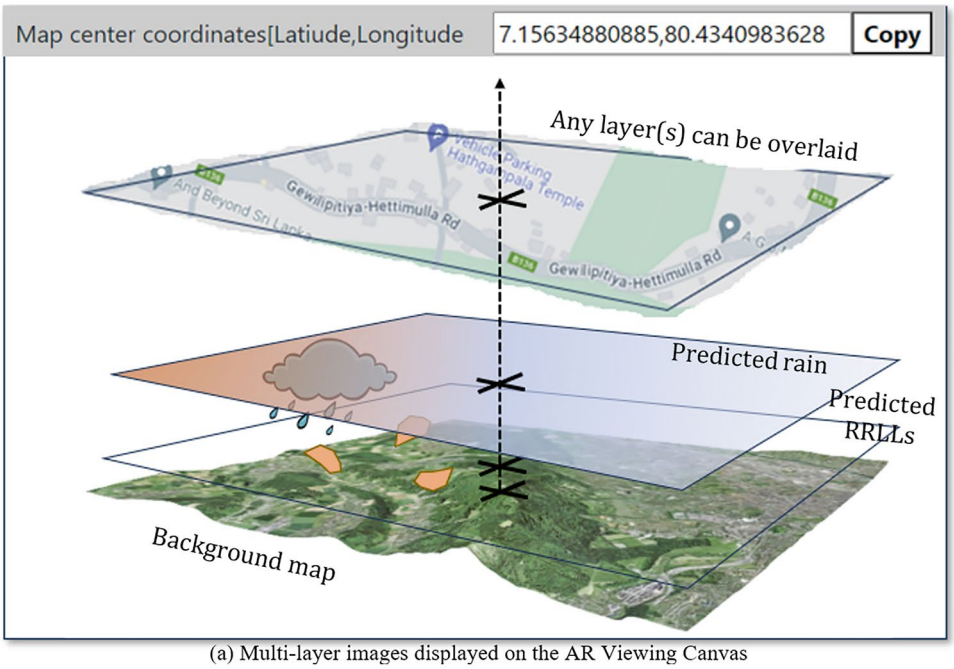

(a) Multi-layer images displayed on the AR Viewing Canvas

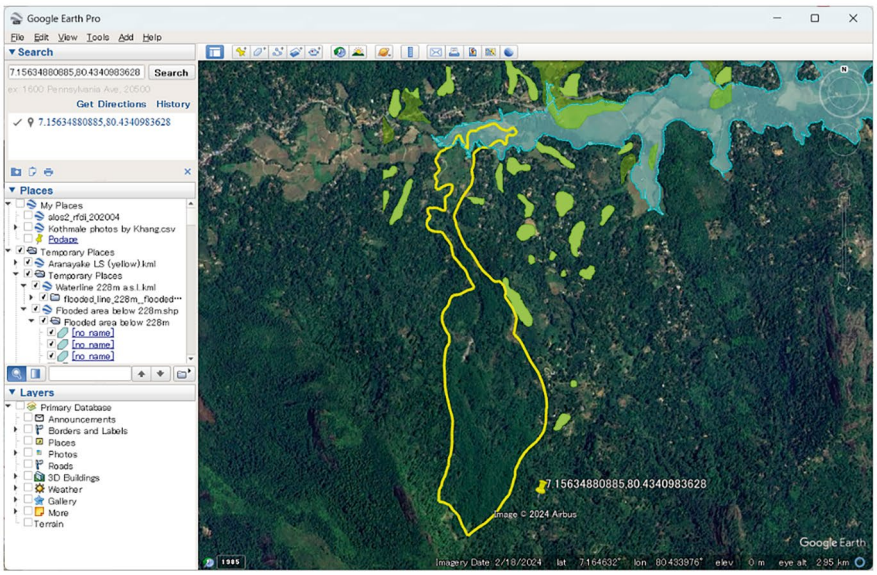

(b) A separately opened window (Google Earth map canvas) with its map center aligned to the AR Viewing Canvas center shown above in Fig. 5(a)

Fig. 5 Multi-layer structure of the AR Viewing Canvas: The center coordinates of the AR background map are displayed on its control panel (**a**), and a button is provided to copy these coordinates. (**a**) Multi-layer images displayed on the AR Viewing Canvas. (**b**) A separately opened window (Google Earth map canvas) with its map center aligned to the AR Viewing Canvas center shown above in (**a**)

directly overlaid on the virtual reality space. However, the system administrator is the only one who can operate overlaying layers, and too many layers can also hinder smooth screen operation.

The AR views of the project's target areas operating as of October 2024 can be viewed at the websites shown in Fig. 6. These sites may be subject to change.

5 Social Implementation of the AR Viewing System

Given the poor mobile Internet connection at local communities in Aranayake, a relevant officer must decipher the information necessary to respond to the residents from the forecasted rainfall and RRLL occurrence information dis-

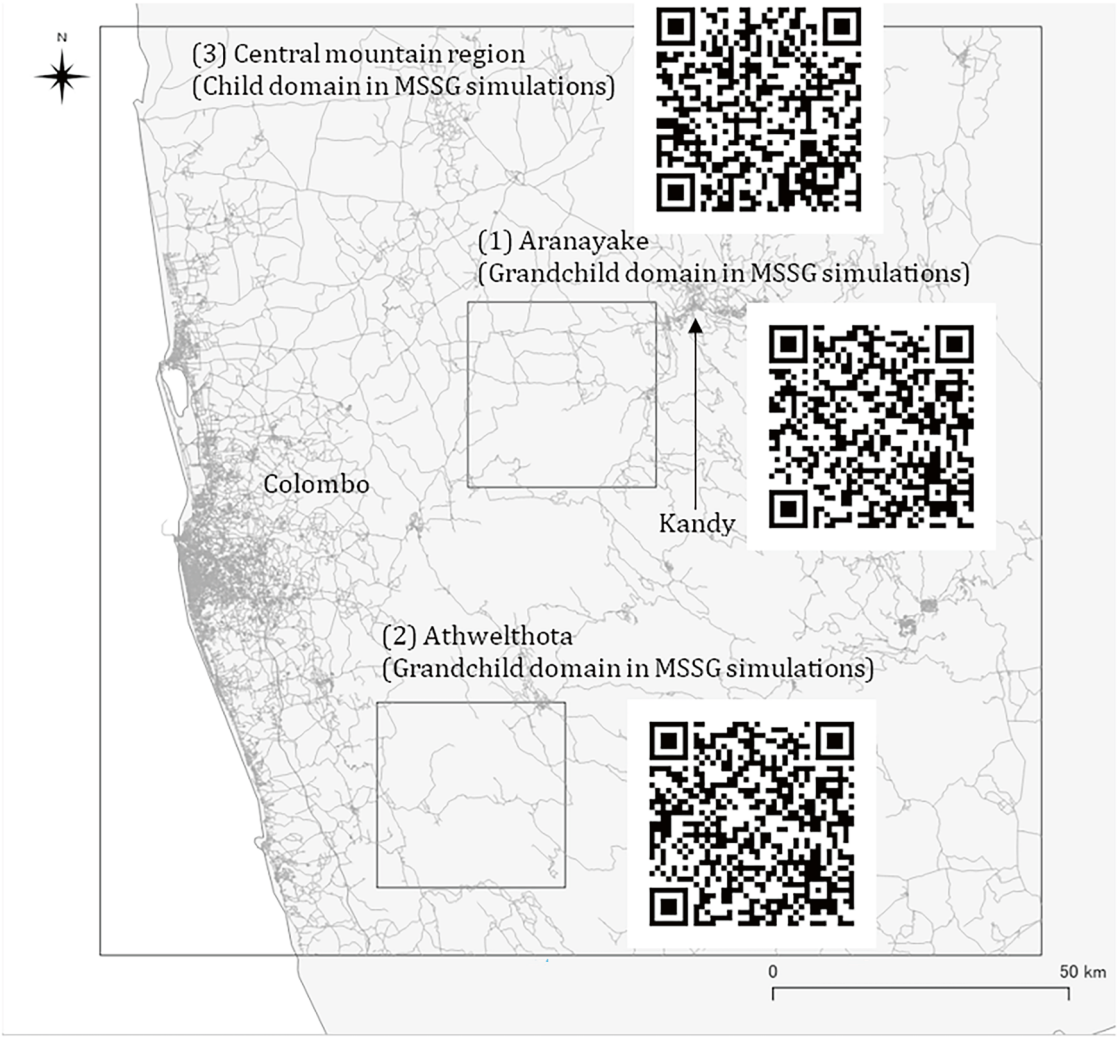

(1) For Aranayake with a 500 m resolution
http://210.150.201.76/maptest/index810.php?AREA_NAME=Area1&MESH_SIZE=500&MODE=1
(2) For Athwelthota with a 500 m resolution
http://210.150.201.76/maptest/index810.php?AREA_NAME=Area2&MESH_SIZE=500&MODE=1
(3) For the mountain region (MSSG child domain) covering both Aranayake and Athwelthota with a 2 km resolution
http://210.150.201.76/maptest/index810.php?AREA_NAME=Area1&MESH_SIZE=2000&MODE=1

Fig. 6 QR codes and links to the AR Viewing Windows for (1) Aranayake, (2) Athwelthota, and (3) the Central Mountain region of the island. The links may be subject to change. (1) For Aranayake with a 500 m resolution http://210.150.201.76/maptest/index810.php?AREA_NAME=Area1&MESH_SIZE=500&MODE=1. (2) For Athwelthota with a 500 m resolution http://210.150.201.76/maptest/index810.php?AREA_NAME=Area2&MESH_SIZE=500&MODE=1. (3) For the mountain region (MSSG child domain) covering both Aranayake and Athwelthota with a 2 km resolution http://210.150.201.76/maptest/index810.php?AREA_NAME=Area1&MESH_SIZE=2000&MODE=1

Table 1 Workshops and village-watching activities

Date	Workshops/village watching	Venue	Participants
2024/02/16	Explanatory session of the SATREPS Project RRLL	DS Aranayake	Officers: 12 Project members: 10
2024/02/17	Explanatory session of seismic/rain Monitoring System	Rathnajothia temple	Villagers: 20 Officers: 2 Project members: 5
2024/03/26	Explanatory session of the AR Viewing System	DS Aranayake	Village leaders: 7 Officers 25 Project members: 7
2024/03/27	Village watching in Hathgampala	Hathgampala primary school	Pupils: 21 Teachers: 10 Trainers: 8
2024/03/28	Village watching in Hathgampala	Hathgampala secondary school	Pupils: 17 Teachers: 10 Trainers: 8
2024/08/09	Explanatory session about layers on the AR Viewing Canvas	DS Aranayake	Officers: 22 Project members: 8
2024/08/10	Village watching in Elangapitiya	Elangapitiya community center	Villagers: 34 Project members: 7
2024/08/11	Village watching in Podape	Podape community center	Villagers: 27 Project members: 6
2024/08/11	Explanatory session of the AR Viewing System	DS Palin-danuwara	5

played on the AR Viewing system and call the representatives of each village, etc. Meanwhile, the villagers cannot go to a distant evacuation shelter through bad and narrow roads in the dark of night in a downpour. The villagers should know where and when to evacuate. Therefore, G3 group members have conducted workshops at the Divisional Secretariat Office of Aranayake and town-watching activities at some villages in Aranayake, Hathgampala Primary and Secondary Schools (Table 1).

"Town watching," which may be better rephrased as "Village watching" in our target study areas, is a tool used by local people, local schools, students, teachers, parents, and local government members to reduce risks in their residential areas by monitoring both the vulnerable and invulnerable aspects of their living environments (Rajib and Takeuchi 2009).

A village watching in our project comprises four steps (Fig. 7):

Step 1: The first step is mainly for schools and is the Training of Trainers (ToT) program, which engages master trainers (NBRO scientists) in coaching new trainers (school teachers) who are less experienced with a particular topic of landslide disaster preparedness.

Step 2: Participants (school pupils, local people, etc.) learn basic ideas about rain-induced landslide disasters and what a village-watching activity is.

Step 3: The participants are split into several groups. Each group walks through the local area to identify the positive and negative aspects of their area regarding disaster risk management.

Step 4: Each group discusses an appropriate action plan in an emergency and creates a community-based hazard map (a layer laid over the AR Viewing Canvas). Each group then presents its hazard map and ideas to the other groups for better disaster management.

If an RRLL occurrence is predicted in advance, we must assume that flooding can co-occur and make some paths for evacuation impassable. For this reason, it is essential to record past flood history. During these activities in the Hathgampala area, residents and school pupils testified that they witnessed flooding during the torrential monsoon rains in 2016; the rain triggered the 2016 Aranayake landslide. Figure 8 shows the locations where they witnessed the flood. High water marks remain on the wall of a house near these locations (House #1 in Fig. 9); the watermark represents the maximum rise of water over land. A Digital Elevation Model of this area with a 2-m spatial resolution tells that the ground level around the house is 225.7 m above Mean Sea Level (MSL). Therefore, the watermark, about 30 cm above the ground level, indicates the maximum water rise at this location was 226 m MSL. Figure 10 shows a cross-section of the terrain 50 m west of the house (BB' in Fig. 9) with the main-

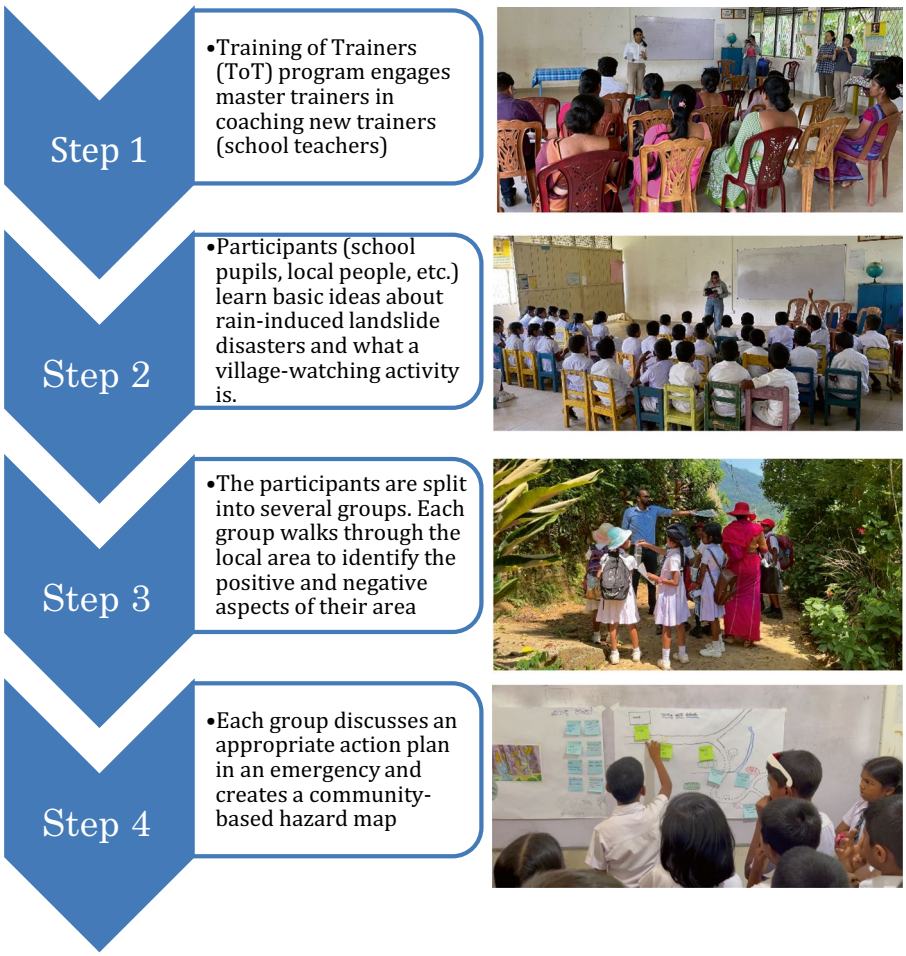

Fig. 7 Learning scheme associated with village watching. (Photos taken at Hathgampala Primary School on March 27, 2024)

stream of the Hathgampala valley in its middle. Given the maximum water rise of 226 m MSL at this location and that the average hydraulic gradient along the stream and the Gauckler–Manning roughness coefficient for a natural stream are about 0.0045 and 0.03 (s/m1/3), respectively, the Manning formula (Manning 1891), estimating the average velocity of a liquid in an open channel flow, yields the maximum discharge of the flood reached 2.66 m^3/s. The stream's catchment area above this location was about 5.0 km^2, as shown in Fig. 8. Given the peak hourly rain of about 25 mm/h, the peak discharge of 2.66 m3/s at this location is about 21% of the total amount of the rain falling in 1 s in this catchment.

The cross-section shown in Fig. 10 shows several river terraces. While it is not easy to predict how much flooding will occur in the future, the actual flooding in 2016 tells us that the low-lying terrace adjacent to the stream can be subject to flooding. This information, which is vital for emergency evacuation routes, and the result of terrain interpretation by Dr. T. Miyagi, one of the G3 group members, to identify safer locations in the village for evacuation, were marked on the terrain map of the area. The map and its 3D model were given to the Hathgampala Primary School. Its extended version (Fig. 11) was used for the following village-watching activity in Elangapitiya.

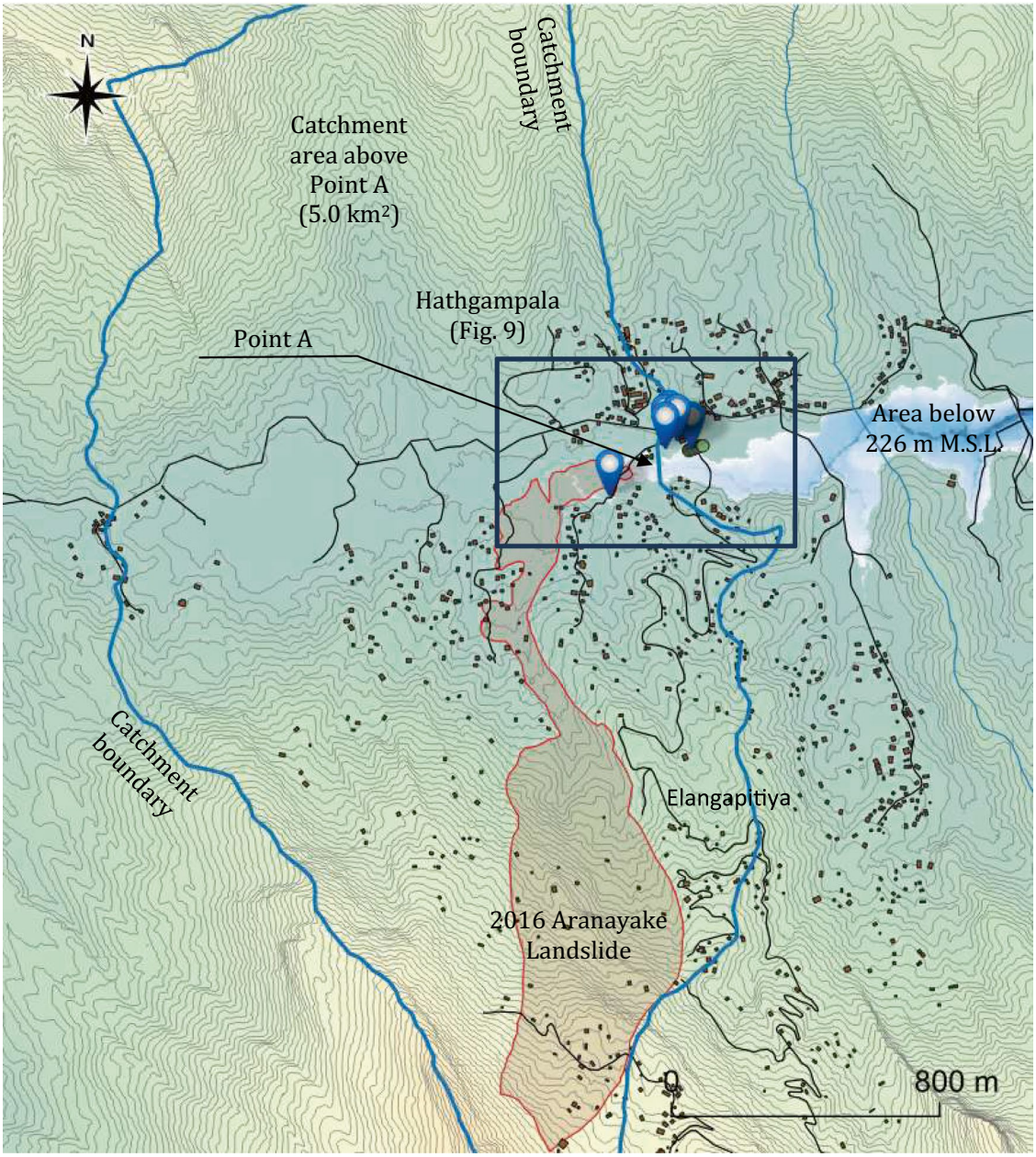

Fig. 8 The area of village watching activities, Hathgampala and Elangapitiya: residents and school pupils testified that they witnessed flooding during the torrential monsoon rains in 2016 at the placemarks near Point A. The blue closed curve shows the catchment area of about 5.0 km^2 above Point A

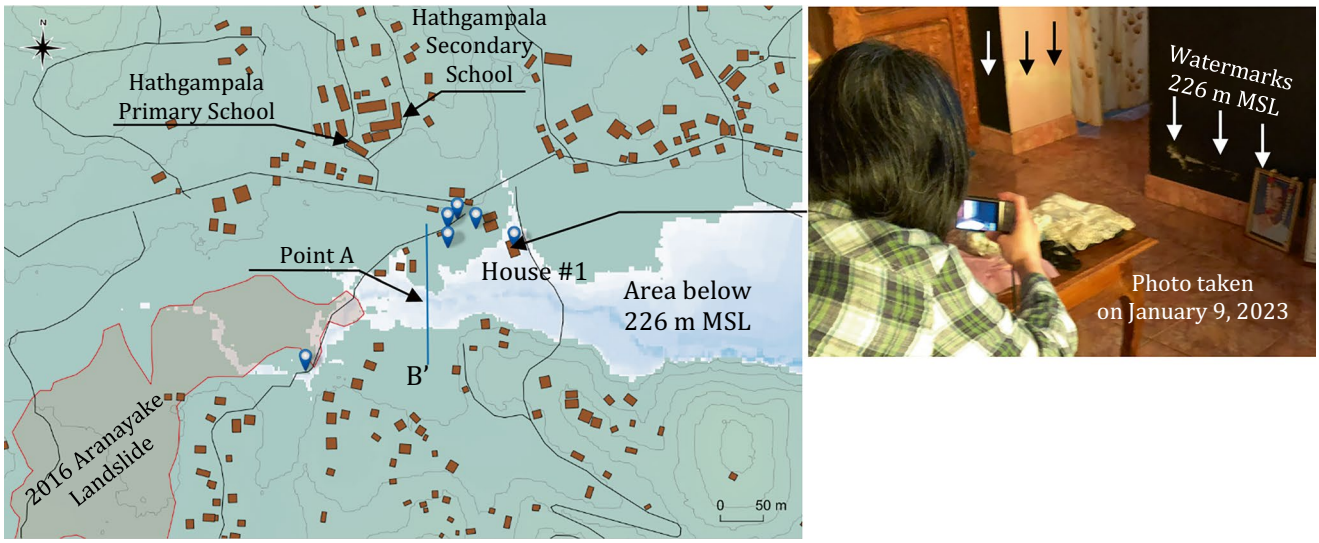

Fig. 9 The area of village watching activities, Hathgampala: residents and school pupils testified that they witnessed flooding at the placemarks near Point A during the torrential monsoon rains in 2016

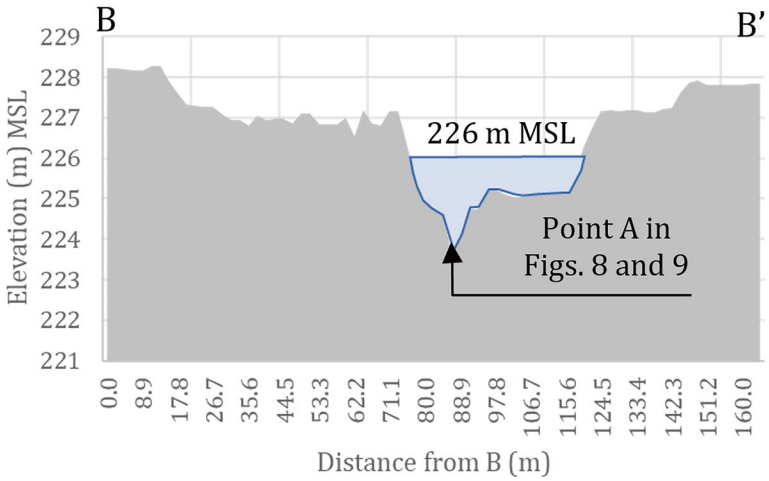

Fig. 10 Cross-section BB′ in Fig. 9 when flooded in 2016: Given this flooding flow cross-section and the average hydraulic gradient of the flow, 0.0045, and the Gauckler–Manning roughness coefficient for a natural stream (0.03 $s/m^{1/3}$), the Manning formula (Manning 1891) yields the maximum discharge of the flood in 2016 reached 2.66 m^3/s

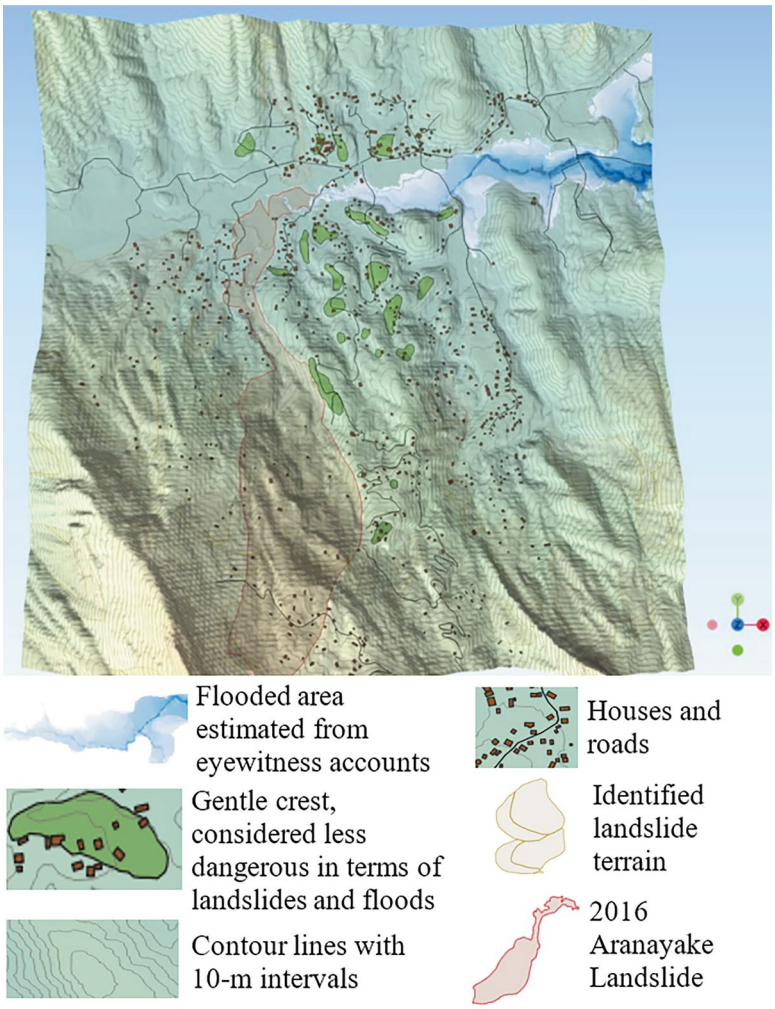

Fig. 11 The area of village-watching activity in Elangapitiya: The 2D and 3D versions of the map were prepared and distributed to participants. The maps helped residents identify nearest safe locations to evacuate in case of emergency

6 Ongoing Challenges and Challenges Being Planned

Participants of the workshops held at the Divisional Secretariat (DS) Office of Aranayake on March 26 and August 6, 2024, are village leaders (Grama Niladhari (GN) in Sinhala), officers from the DS office and the Kegalle Regional Office of the Disaster Management Center (DMC). The Divisional Secretariat (DS) of Aranayake is one of the third-level administrative divisions of Kegalle District, Sabaragamuwa Province, Sri Lanka, with jurisdiction including one of our project target study sites. DMC was established in the wake of the devastating 2004 Indian Ocean Tsunami in recognition of the need to create a cross-agency organization dedicated to disaster response in Sri Lanka. DMC is mandated to implement and coordinate national and sub-national level programs to reduce the risk of disasters with the participation of all relevant stakeholders. The 2016 Aranayake Landslide was the first and the last time that DMC set up a cross-agency disaster response headquarters.

The officers who attended the workshops commended the developed augmented reality (AR) forecast display for its capabilities based on their experiences. Simultaneously, the feedback from the officers highlighted the following point: in mountainous areas where mobile internet connection can be poor, particularly in torrential rains and smartphone penetration is not high, not residents but district administrative officers in charge of disaster management must look at the AR screen and decipher the information required for residents' disaster preparedness from the AR view to communicate with residents over the phone.

Fig. 12 Manual rain gauge with a scale on its side: The scale has the color-coded upper three levels (Yellow for 50–100 mm/day), (Orange for 100–150 mm/day), and (Red for 150 mm and beyond). The photo on the left was taken at 7.1620N, 80.436E, on January 9, 2023

Since 2016, NBRO has implemented a "Community-Based Landslide Early Warning (CBLEW) approach" for the country's identified landslide-vulnerable communities. The CBLEW approach aims to empower communities and establish systematic preparedness plans for timely self-evacuation in case of a landslide event. In this course, the communities are educated on preparedness and self-decision based on the rainfall data obtained by manual rain gauges in the village (Fig. 12). Each rain gauge is an acrylic transparent cylindrical bucket with a scale on its side. The scale has the upper three levels, (50–100 mm/day), (100–150 mm/day), and (150 mm and beyond). Yellow, orange, and red colors are assigned respectively to these upper three levels. These colors determine the actions to be taken by residents and concerned officers.

However, this protocol requires an instant decision based on the just-observed rain accumulation, and more time may be needed for the persons concerned to prepare adequately for possible cascading disasters. The developed AR Viewing System will solve this difficulty by providing the predicted information they need one day in advance. The current AR Viewing System has an option button (the uppermost radio button in Fig. 4) to switch the screen from hourly rains to cumulative rains or vice versa. Once the cumulative rain screen with the color-bar legend having yellow, orange, and red colors assigned to the abovementioned upper three levels appear, the officer in charge of a particular community can identify which color will appear in the concerned community one day in advance. So, the current system can be used as is.

NBRO has so far promoted two landslide response projects (before the SATREPS Project RRLL) with the support of JICA: the "Technical Cooperation for Landslide Mitigation Project (TCLMP)" and the "Technical Cooperation Project for Capacity Strengthening on Development of Non-Structural Measures for Landslide Risk Reduction (Project-SABO)." In the latter project (Project SABO), the NBRO has adopted a method of determining disaster response based on where we are in the SNAKE line space, with hourly rainfall on the horizontal axis and the soil water index on the vertical axis. The AR Viewing system may reflect this protocol for issuing EWs and evacuation orders.

Village-watching activities are expected to continue even after the project is over for the information receivers (villagers). The activity has the "Training of Trainers (ToT)" program, with the intention that it will automatically be inherited and spread over a wide area in Sri Lanka. However, the G3 group members must continue to be involved in any possible way.

7 Summary

The 5-year SATREPS Project RRLL started in 2020. It aims to develop and implement early warning technology for rain-induced rapid and long-traveling landslides in Sri Lanka. As the project enters its final fiscal year in 2024, it has reached the stage at which the integrated early warning technologies will be socially implemented. The core technology of the project is the Augmented Reality (AR) Viewing System, transferring spatial distribution of rains and possible occurrences of rain-induced rapid and long traveling landsides (RRLLs) predicted one day in advance, using the cutting-edge technologies for mountain weather forecast and numerical tools for simulating initiation and downslope movements of landslides.

Though the developed AR viewing system can transfer crucial information about rain and possible landslide disasters predicted one day in advance, it must be assumed that district administrative officers in charge of disaster management look at the AR screen, decipher the information required for residents' disaster preparedness, and tell it to the last mile where the Internet connection is bad in the torrential rain in the mountains.

Simultaneously, the information receivers (villagers) cannot go to a distant evacuation shelter through poor road condition in the dark of night in a downpour. The villagers should know where and when to evacuate.

The village-watching activities have been very effective in addressing the abovementioned issues practically. They have helped the stakeholders (villagers and the concerned officers) identify specific responses to these issues. For example, through a village watching in Hathgampala, residents and school pupils testified that they witnessed flooding during the torrential monsoon rains in 2016; the rain triggered the 2016 Aranayake landslide. This information is a reminder that a rain-induced landslide and flooding can occur in tandem, which is vital for the beneficiaries of the Early Warning System to develop rational and feasible disaster responses.

Village-watching activities are expected to continue even after the project to promote the steady social implementation of the developed early warning technologies further.

Acknowledgments The ICL launched the International Programme on Landslides (IPL) in 2002 to reduce landslide disaster risk worldwide. The IPL was then developed into a global cooperation program by international organizations supporting ICL activities (Mikoš et al. 2023). This SATREPS project (Project RRLL) has been approved as one of the IPL projects, IPL-249. This approval led to the authors getting all kinds of advice at every possible opportunity from high-performing professionals in the various disciplines of landslide disaster management. Of particular note is that we were given valuable advice at the sixth World Landslide Forum, Florence, Italy, by Dr. Irasema Alcántara-Ayala, Professor of Natural Hazards and Risk at the National Autonomous University of Mexico, about how we would promote the social implementation of the developed RRLL early warning technology. The authors are also grateful to Ms. Shamali Piyathissa, Head of the Divisional Secretariat of Aranayake (DS Aranayake), Mr. Saman Kumara Galapita, Disaster relief officer at DS Aranayake, Mr. H.M. Anushke Chamile Bandara, Assistant Director, Disaster Management Center (DMC) Kegalle Office, Ms. Nimali Weerasinghe, District Chief Scientist, NBRO Kegalle, and Mr. D.M.C.P. Bandara, NBRO Kegalle, for their assistance in organizing workshops and village-watching activities as well as their valuable feedbacks regarding how the developed system would be improved.

The authors acknowledge logistical support from Dr. Jagath K. Gunatilake, University of Peradeniya and ICL Advisor at the ICL/SATREPS Office, NBRO, and Dr. Gamini Jayathissa, Director of the Landslide Research and Risk Management Division, NBRO. Their support was crucial in all the project's activities in Aranayake and Athwelthota.

Last but not least, the authors are greatly indebted to Mr. Taichi Minamitani, Mr. Akira, Inaba, Disaster Risk Reduction Group, JICA, Mr. Takafumi Sakurazawa, JICA Sri Lanka Office, Dr. Takashi Asaeda, Research Supervisor, SATREPS, and Mr. Naoki Furukawa, Assistant Research Supervisor, SATREPS, Japan Science and Technology Agency (JST) for their ceaseless efforts to support the project.

References

Ajmera B, Ahari HE, Loi DH, Setiawan H, Dang K, Sassa K (2023) LS-RAPID manual with video tutorials. In: Sassa K, Konagai K, Tiwari B, Arbanas Ž, Sassa S (eds) Progress in landslide research and technology, vol 1(2). Springer, Cham. https://doi.org/10.1007/978-3-031-16898-7_26

Bandara HAAIS, Onishi R (2023) High-resolution numerical weather simulation for orographic precipitation as an accurate early warning tool for landslide vulnerable terrains. In: Alcántara-Ayala I et al (eds) Progress in landslide research and technology, vol 1(2). Springer, Cham. https://doi.org/10.1007/978-3-031-44296-4_11

Dang K, Sassa K, Konagai K et al (2019) Recent rainfall-induced rapid and long-traveling landslide on 17 May 2016 in Aranayaka, Kagelle District, Sri Lanka. Landslides 16:155–164. https://doi.org/10.1007/s10346-018-1089-7

Japan Science and Technology Agency (2020) SATREPS, Science and Technology Partnership for Sustainable Development, https://www.jst.go.jp/global/english/index.html

Konagai K et al (2023) Early warning system against rainfall-induced landslide in Sri Lanka. In: Sassa K, Konagai K, Tiwari B, Arbanas Ž, Sassa S (eds) Progress in landslide research and technology, vol 1(1). Springer, Cham. https://doi.org/10.1007/978-3-031-16898-7_16

Liao Z, Hong Y, Wang J et al (2010) Prototyping an experimental early warning system for rainfall-induced landslides in Indonesia using satellite remote sensing and geospatial datasets. Landslides 7:317–324. https://doi.org/10.1007/s10346-010-0219-7

Manning R (1891) On the flow of water in open channels and pipes. Trans Inst Civil Eng Ireland 20:161–207

Mikoš M, Sassa K, Han Q (2023) International programme on landslides—a short overview of its historical development. In: Sassa K, Konagai K, Tiwari B, Arbanas Ž, Sassa S (eds) Progress in landslide research and technology, vol 1(1). Springer, Cham. https://doi.org/10.1007/978-3-031-16898-7_3

Onishi R, Hirai J, Kolomenskiy D, Yasuda Y (2023) Real-time high-resolution prediction of orographic rainfall for early warning of landslides. In: Sassa K, Konagai K, Tiwari B, Arbanas Ž, Sassa S (eds) Progress in landslide research and technology, vol 1(1). Springer, Cham. https://doi.org/10.1007/978-3-031-16898-7_17

Onishi R, Bandara HAAIS, Matsumoto K (2024) High-resolution rainfall simulations for early warning of long-traveling landslides in Sri Lanka. In: Progress in landslide research and technology, vol 3(2). Springer, Cham

Rajib S, Takeuchi Y (2009). Town watching handbook for disaster education: enhancing experiential learning, European Union United Nations Office for Disaster Risk Reduction (UNDR) - Regional Office for Asia and Pacific. https://www.undrr.org/publication/town-watching-handbook-disaster-education-enhancing-experiential-learning

Sassa K, Nagai O, Solidum R et al (2010) An integrated model simulating the initiation and motion of earthquake and rain-induced rapid landslides and its application to the 2006 Leyte landslide. Landslides 7, 219–236. https://doi.org/10.1007/s10346-010-0230-z

Takahashi K et al (2008) Impact of coupled nonhydrostatic atmosphere-ocean-land model with high resolution. In: Hamilton K, Ohfuchi W (eds) High-resolution numerical modelling of the atmosphere and ocean. Springer, New York. https://doi.org/10.1007/978-0-387-49791-4_15

JICA's Policy on Disaster Risk Reduction and Future Outlook

Taichi Minamitani, Go Sato, and Satoru Nishikawa

Abstract

Landslide disaster risk is likely to be created at the nexus with human activities. Many developing countries are experiencing rapid urbanization and therefore tend to be vulnerable to and exposed to landslide disaster risk. Disaster risk reduction is critical to overcoming poverty alleviation, and sustainable development. Because developing countries, however, have many social issues, a sufficient budget is unlikely to be allocated to DRR. The international framework, including the Sendai Framework for Disaster Risk Reduction (2015–2030), emphasizes the importance for developed countries to help developing countries through international cooperation, such as the Official Development Assistance (ODA). This article overviews Japan's ODA for landslide disaster risk reduction and attempts to outline the characteristics of Japan's ODA.

Keywords

Official Development Assistance (ODA) · Sendai Framework for Disaster Risk Reduction (SFDRR) · Japan International Cooperation Agency (JICA) · Disaster risk reduction (DRR) · Program-based approach

T. Minamitani (✉)
Disaster Risk Reduction Team 1, Disaster Risk Reduction Group, Global Environment Department, Japan International Cooperation Agency (JICA), Tokyo, Japan
e-mail: Minamitani.Taichi@jica.go.jp

G. Sato
Faculty of Environmental Studies, Tokyo City University, Yokohama, Kanagawa, Japan
e-mail: satogo@tcu.ac.jp

S. Nishikawa
Disaster Risk Reduction Group, Global Environment Department, Japan International Cooperation Agency (JICA), Tokyo, Japan
e-mail: Nishikawa.Satoru@jica.go.jp

1 Introduction: Importance of landslide disaster risk reduction in developing countries

Landslides have resulted in a significant number of fatalities and economic losses, remarkably increased long-term displacement and migration of affected people, and then worsened economic and mental health outcomes for a long time afterward (Baseler and Henning 2023). Landslide disaster risks are created in a complex nexus of natural, social, and environmental contexts and therefore have a significant socio-economic impact on the societies in which we live. It is often the case that many impoverished people tend to live on risky slopes (Lan et al. 2022). Moreover, in mountainous countries like Nepal or Bhutan, essential infrastructure facilities, including roads, are located on slopes with a high risk of landslide disaster. Hence, once a landslide occurs, it not only causes many deaths and victims but often has a serious impact on economic activities and livelihoods (Assilzadeh et al. 2010).

It can be assumed that the risk of landslide disasters is further increasing in developing countries. According to the Emergency Events Database (EM-DAT), landslides killed 20,604 people and caused economic losses of USD 6.99 billion globally between 2000 and 2024 (EM-DAT 2024). Also, the frequency of landslides has increased compared to 50 years ago (Besl 2022). This is due to an increase in rainfall intensity and amount (Khan et al. 2020), which may be attributed to climate change. At the same time, it is worth considering that deteriorating land use patterns have also contributed to increased landslide disaster risk, particularly in developing countries where rapid urbanization is poorly managed. (Alam 2020; Dille et al. 2022). Landslides are a hazard that adversely affects economic growth and poverty reduction in developing countries. Figure 1 shows some cases where human activities have created landslide hazards in developing countries.

Under such a circumstance, disaster risk reduction (DRR), in general, is a global challenge. The international community adopted the frameworks in 2015, including the Sendai

B. Abolmasov et al. (eds.), *Progress in Landslide Research and Technology, Volume 4 Issue 1, 2025*, Progress in Landslide Research and Technology, https://doi.org/10.1007/978-3-031-89836-5_15

Fig. 1 Landslide disaster risks are created at the nexus of human livelihood activities. (**A**) is the case of a risky slope in Tegucigalpa, Honduras, where many houses have been erected; (B) is the gully erosion, which has been active due to uncontrolled house constructions in Nacala city, Mozambique. (Photos were taken by the author)

Framework for Disaster Risk Reduction (SFDRR) (2015–2030), the Sustainable Development Goals (SDGs), and the Paris Agreement. These frameworks are intertwined within the context of climate-related hazards, which include landslides.

These frameworks claim that DRR is an agenda that links with development issues, and each government needs to address DRR on its own. However, most developing countries have many social issues to address, such as ones to meet basic human needs (e.g., health and education) and failed to allocate sufficient resources to DRR. Therefore, the international society has called for enhanced international cooperation, including the Official Development Assistance (ODA). Japan is one of the most active donor countries that has contributed to addressing DRR by focusing on ex-ante investment in proactive actions (Kellett and Caravani 2013).

2 Japan's Official Development Assistance (ODA)

ODA is a part of development cooperation and is operated under the rules set by the Development Assistance Committee of the Organisation for Economic Cooperation Development (DAC/OECD). OECD defines ODA as:

- Development cooperation provided by official agencies, including state and local governments or their executive agencies to eligible countries;
- Development cooperation to promote the economic development and welfare of developing countries; and
- Development cooperation that is concessional

As illustrated by Fig. 2, Japan's ODA can be bifurcated into bilateral and multilateral assistance. The former is provided through JICA although the latter is given by international organizations such as the United Nations and the multilateral development banks (e.g., the World Bank and the Asian Development Bank). Following its merger with the then-Japan Bank for International Cooperation (JBIC) in 2008, the Japan International Cooperation Agency (JICA) is the sole ODA executing agency on behalf of the Japanese government, dealing with several ODA schemes: technical cooperation, finance and investment cooperation, and grant aid. These are implemented based on the official request from recipient governments, which are characterized as Japan's bilateral assistance.

Technical cooperation is a scheme that supports the recipient government from a technical point of view, including the capacity development of government officials and the support to formulate a development plan or master plan. This scheme is performed by dispatching experts, providing equipment, and offering training programs. As the core of technical cooperation, the technical cooperation project is implemented by combining the various inputs mentioned above. Also, there is another sub-scheme called technical cooperation for development study, which helps recipient governments elaborate relevant policies or plans. In addition, there is also a science-based technical cooperation called the Science and Technology Research Partnership for Sustainable Development (SATREPS).

On the other hand, another is financial support, divided into two groups: financial and investment cooperation and grant aid. First, financial and investment cooperation involves low-interest, long-term concessional loans. One of them is ODA loans. Second, grant aid is a different assistance scheme with no repayment obligation, unlike ODA loans. In the schemes, funds are used to procure equipment, materials, and services, as well as civil works, which are required for the project goal. For each scheme, JICA agrees with the implementing agency of the recipient government about the maximum amount for a project based on the loan agreement (L/A) and the grant agreement (G/A), respectively.

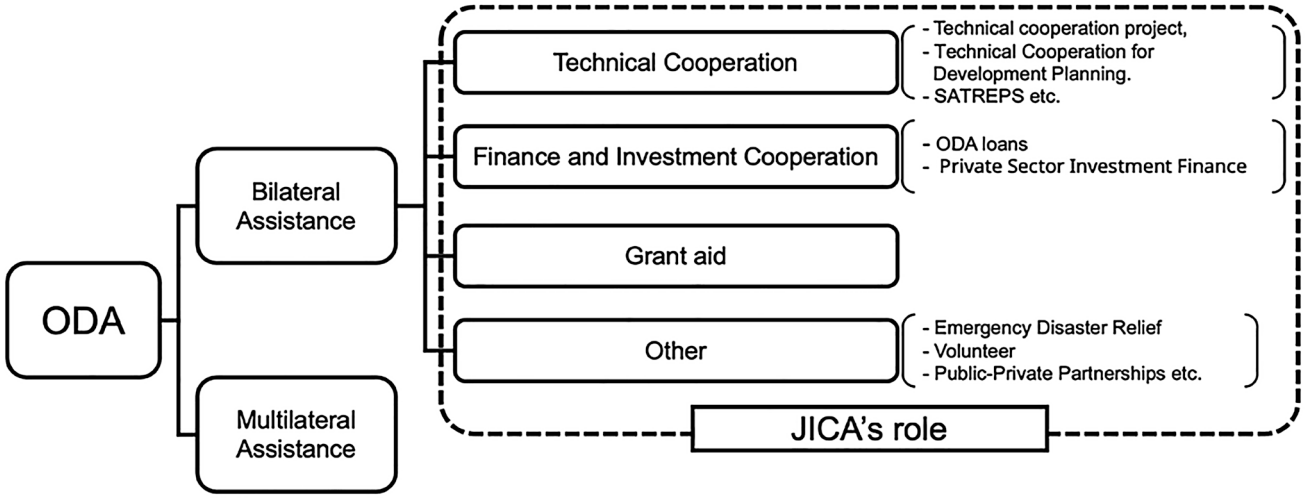

Fig. 2 Japan's ODA schemes can be divided into two: bilateral and multilateral assistance. Bilateral assistance is implemented by the Japan International Cooperation Agency (JICA). JICA provides bilateral ODA through technical cooperation, ODA loans, or grant aid based on requests from recipient governments (JICA 2022a)

Besides these types, JICA has other schemes implemented based on the proposals submitted by NGOs and private companies. These are called grass-roots technical cooperation and public-private partnership programs. Moreover, JICA plays a role as an office for disaster relief. Experts are sent to an affected area, and emergency equipment is supplied.

The Japanese government and JICA, respectively, examine the official request from a recipient government from the perspective of consistency with their respective policies. The Japanese government elaborates on the Country-based Development Cooperation Policy for the respective country. JICA also formulates the JICA Country Analysis Paper (JCAP) for each country and the JICA Global Agenda (JGA) for the twenty (20) disciplines, of which DRR is one.

3 JICA's Policy Regarding Disaster Risk Reduction

JICA's policy for DRR is called the JICA Global Agenda for "Disaster Risk Reduction through Pre-disaster Investment and Build Back Better" (hereinafter referred to as "GA-DRR") (JICA 2024). Before overviewing the GA-DRR, this section begins by reviewing the two important terms: DRR and disaster risk management (DRM).

UNDRR defines the two terms as shown in Table 1. As seen from this definition, UNDRR considers that DRR can be achieved by avoiding the creation of new risks, reducing existing risks, and managing residual risks. On the other hand, another term DRM is seen as a means to practice something. In essence, DRM can be thought of as meaning meticulous actions to achieve DRR.

Table 1 Definitions of DRR and DRM

Term	Definition by UNDRR
DRR	"*[aiming] to strengthen resilience and contribute to the achievement of sustainable development by preventing new disaster risks, reducing existing disaster risks and managing remaining risks*"
DRM	*"the application of disaster risk reduction policies and strategies to prevent new disaster risk, reduce existing disaster risk and manage residual risk, contributing to the strengthening of resilience and reduction of disaster losses"*

UNDRR (2023)

Despite some differences between scholars, Fig. 3 shows the categorization of DRM, which can be divided into risk control and risk finance. First, risk control includes both a proactive and a responsive approach. Risk avoidance is an approach to prevent creating new disaster risks, while loss prevention and separation and dispersal are approaches to reduce existing disaster risks. Separation and dispersal is a way to diversify risk, and a business continuity plan, called BCP, is the case. Besides, loss mitigation is an attempt to minimize the spread of damage after a disaster has occurred. In other words, it includes the preparedness for and implementation of emergency responses. In addition, it is thought that managing residual risks through early warning for appropriate evacuation behaviors is a part of it.

Second, on the other hand, risk finance refers to an area that focuses on addressing the financial consequences of natural hazards for the purpose of risk transfer. Risk transfer is a method of pricing disaster risk on financial instruments, such as disaster insurance. The last one is risk retention, which means that although disaster risks are recognized to some extent, no action is taken. That is, when a disaster hits, the economic burden should be accepted.

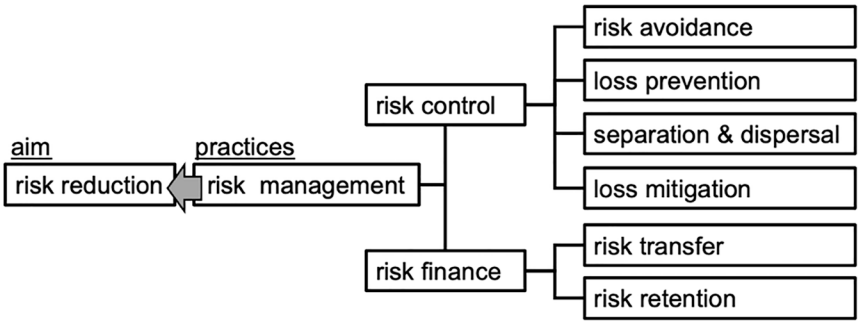

Fig. 3 This is a categorization of the DRM approach. DRM can be divided into two: risk control and risk finance. Although there are a variety of management approaches, proactive actions—risk avoidance and loss prevention—are considered important by the SFDRR. (Prepared by the author)

Table 2 Examples of various countermeasures for landslide disaster risk reduction

Management approach	Example of countermeasures	Example of JICA's project
Avoiding the creation of new disaster risk	Land use restriction, urbanization control by law	Project for capacity strengthening regarding non-structural measures for landslide risk reduction (Sri Lanka)
Reducing existing disaster risk	Structural measures (control works against landslides, prevention works)	Port-Louis City Landslide Protection Project (Mauritius)
Managing residual disaster risk	Early warning, evacuation, preparedness to responsive action	Strengthening the capacity to cope with and minimize damages caused by flash floods and landslides for the northern mountainous region of Vietnam (Vietnam)

Prepared by the author

In the context of landslide disaster risk, risk avoidance (preventing new disaster risk) can be achieved by enforcing land use control regulations, and loss prevention (reducing existing disaster risk) can be realized by relocating people or assets exposed to landslide potential and implementing structural measures (e.g., slope control works). However, even if we attempt to prevent and reduce landslide disaster risk as much as possible, not all risks can be eliminated. Hence, there is a residual landslide disaster risk. For this, appropriate evacuation behavior using early warning systems and preparedness for responsive action are also necessary. Table 2 summarizes the examples of countermeasures for landslide disaster risk reduction and indicates the example of JICA's projects. Indeed, it is worth noting that there is a project case where an ODA project covers more than two management approaches, and Japan's ODA project addresses DRR from multiple management approaches.

Here, the GA-DRR is reviewed in detail. As described in the Introduction, DRR is an issue that is closely related to economic development and poverty reduction. Therefore, the GA-DRR aims to build a resilient society by avoiding the loss of economic assets and human lives. To achieve this, proactive DRR is indispensable, and the GA-DRR sets three pillars (JICA 2024).

First, under circumstances where many developing countries have been reluctant to increase ex-ante investment in proactive DRR (Paton 2019), however, JICA believes that advocating for developing countries to advance proactive DRR is critical. Although proactive DRR encompasses risk avoidance by, for example, land use restriction, existing disaster risk needs to be reduced proactively through structural measures. Being relatively costly, structural measures are not expedited by the governments of developing countries (UNISDR 2015). Then, the GA-DRR sets the first pillar, where investment in structural measures needs to be enlarged. Otherwise, existing disaster risks would not be reduced, and very large residual disaster risk will remain, and there is a risk that early warning and evacuation actions will not work. Many structural measures are likely to be taken mainly by government to protect the people of a country, and this is considered a key responsibility of the government.

Indeed, each government has primary responsibility for DRR, according to the SFDRR (UNISDR 2015). Structural measures promise to reduce disaster risks if designed and constructed properly, but do not eliminate all disaster risks from a society. Therefore, because balancing structural and non-structural measures is important, it is essential to have a sound governance system. Government needs to understand the difference in management approaches, described in Table 2. Otherwise, disaster risks cannot be managed properly. Then, as the second pillar, the GA-DRR looks at enhancing the entire governance of a recipient government.

DRR requires a long time. Because it is impossible to control natural hazards, including landslides, a disaster may take place despite structural and non-structural measures being taken. Then, the reconstruction process becomes an important turning point to make a society more robust and resilient. As stated in the SFDRR, the concept of 'Build Back Better' (BBB) becomes critical. Hence, the GA-DRR promotes the BBB when a disaster hits, as the third pillar.

4 JICA's Contribution to Landslide Disaster Risk Reduction

For decades, JICA has implemented projects in many parts of the world for landslide disaster risk reduction. Table 3 lists representative Japan's ODA projects regarding landslide disaster risk reduction since 1990, containing projects that indirectly contributed to landslide disaster risk reduction. An example is a road construction project that required slope management.

Depending on the project schemes, the project contents vary. First, the ODA loan has been used for relatively large-scale prevention works, for example, as a part of the road construction and river improvement project. Besides, forestation was also a case for ODA loans to prevent soil erosion.

Table 3 JICA projects list regarding disaster risk reduction after 1990 (ODA loan (A); Grant aid (B); Technical cooperation (C))

Country	Project title	Signing date of L/A (month/year)	Maximum amount (L/A base) (mil. JPY)
A: ODA Loan			
Nepal	Kulekhani Disaster Prevention Project	10/1990	2710
Indonesia	Mount Kelud Volcanic Urgent Mitigation Project (*)	9/1991	3235
Mauritius	Port-Louis City Landslide Protection Project	8/1994	2922
Indonesia	Mt. Merapi and Mt. Semeru Volcanic Disaster Countermeasures Project (2)	12/1995	4405
Philippines	Pinatubo Hazard Urgent Mitigation Project	3/1996	6911
Nepal	Kulekhani Disaster Prevention Project (2)	5/1996	3484
India	Tamil Nadu Afforestation Project	2/1997	13,324
Philippines	Pinatubo Hazard Urgent Mitigation Project (Phase 2)	12/1999	9013
Philippines	The Laoag River Basin Flood Control and Sabo Project	5/2001	6309
China	Gansu Afforestation and Vegetation Cover Project	3/2003	12,400
China	Inner Mongolia Afforestation and Vegetation Cover Project	3/2003	15,000
India	Tamil Nadu Afforestation Project (II)	3/2005	9818
India	Karnataka Forest Management and Biodiversity Conservation Project	3/2005	15,209
Indonesia	Urgent Disaster Reduction Project for Mount Merapi and Lower Progo River Area	3/2005	16,436
Morocco	Watershed Management Project	3/2007	3165
Philippines	Pinatubo Hazard Urgent Mitigation Project (Phase 3)	12/2007	7604
Indonesia	Countermeasure for Sediment in Wonogiri Multipurpose Dam	5/2009	6060
Sri Lanka	Landslide Disaster Protection Project of the National Road	3/2013	7619
Indonesia	Countermeasure for Sediment in Wonogiri Multipurpose (II)	2/2014	4954
Indonesia	Urgent Disaster Reduction Project for Mount Merapi 2	2/2014	5111
Kyrgyzstan	International Main Roads Improvement Project	10/2015	11,915
India	North East Road Network Connectivity Improvement Project (Phase 1)	3/2017	67,170
India	North East Road Network Connectivity Improvement Project (Phase 2)	3/2018	38,666
India	North East Road Network Connectivity Improvement Project (Phase 3) (1)	10/2018	79,059
India	North East Road Network Connectivity Improvement Project (Phase 4)	3/2020	14,926
India	North East Road Network Connectivity Improvement Project (Phase 5)	3/2021	15,285
India	North East Road Network Connectivity Improvement Project (Phase 6)	3/2022	23,129
India	North East Road Network Connectivity Improvement Project (Phase 3) (2)	2/2024	34,537
Indonesia	Volcanic Disaster Risk Reduction Sector Loan	12/2024	28,500
Country	**Project title**	**Signing date of G/A (month/year)**	**Maximum amount (G/A base) (mil JPY)**
B: Grant Aid			
Nepal	The Project for Construction of Institutional Facilities of Water-induced Disaster Prevention Technical Centre	Unrecorded	842
Nepal	The Project for Construction on Sindhuli Road (Section 4 Nepalthok-Dhukikhel)	6/1997	2651
Honduras	The project for control of inundation and sedimentation in the Choloma River	6/1999	1812
Philippines	The Project for Flood Disaster Mitigation in Camiguin Island	6/2009	1013
Philippines	The Project for Evacuation Shelter Construction in Disaster Vulnerable Areas in Province of Albay	8/2011	739
Honduras	The Project for Landslide Prevention in Tegucigalpa Metropolitan Area	6/2011	1053
Nepal	The Project for Countermeasure Construction against the Landslides on Sindhuli Road Section 2	7/2012	901

(continued)

Table 3 (continued)

Nepal	The Project for Construction of Sindhuli Road(Section 2: Sindhuli Bazar-Khurkot)	7/2012	2439
Kyrgyzstan	The Project for Avalanche Protection on Bishkek-Osh Road	3/2017	4288
Honduras	The Project for Landslide Prevention in National Road No. 6	9/2017	958
Saint Lucia	The Project for Reconstruction of Bridges in Cul-De-Sac Basin	8/2017	1530
Bolivia	The Project for Road Disaster Prevention of National Road No. 7	7/2018	1698
Fiji	The Project for the Reconstruction of Tamavua-i-wai Bridge (Detailed Design)	10/2020	60
Nepal	The Project for the Rehabilitation of Sindhuli Road affected by Earthquake	8/2021	35
Kyrgyzstan	The Project for the Improvement of Equipment for Road Maintenance and Pavement in Batken	3/2023	700
Honduras	The Project for Construction of Bridge in National Road No. 6	1/2024	2863
Country	**Project title**	**Sub-scheme type**	
C: Technical Cooperation			
Indonesia	Volcanic Sabo Technical Centre	TCP	
Nepal	The Water Induced Disaster Prevention Technical Center in Nepal	TCP	
Mauritius	The Study on landslide protection project in Port Louis (*)	Development planning	
China	Landslide Disaster Prevention Research Equipment (*)	Equipment	
Honduras	Study for Planning for the control of Flood and Sediment Disaster in the Chamerecon River Basin Flood Control (*)	Development planning	
Nepal	The Study on Construction of the Water-induced Disaster Prevention Technical Center (*)	TCP	
Indonesia	Sabo Technology (Third country training program) (*)	Training Program	
Venezuela	Equipment for debris flow forecasting and warning (*)	Equipment	
Honduras	Equipment for river erosion control testing (small scale) (*)	Equipment	
Philippines	Study on Sabo and Flood Control in the Laoag River Basin (*)	Development planning	
Iran	The study on watershed management plan for Karoon River (*)	Development planning	
Indonesia	Sabo Technology (Third country training program) (*)	Training Program	
Iran	Sabo (Country-focused training program) (*)	Training Program	
Indonesia	Sabo technology and water hazard measures (Third country training program) (*)	Training Program	
Nicaragua	The Study on Vulnerability assessment of major road networks to natural disasters and road disaster prevention planning in Nicaragua (*)	Development planning	
Armenia	Study on Landslide Disaster Risk Prevention and Management Plan (*)	Development planning	
China	The Study for Prevention of Landslide Disaster at Xioajing	Development planning	
Philippines	Study on Risk Management for Sediment-Related Disaster on Selected National Highways	Development planning	
Armenia	Development of Communities affected by Landslides	TCP	
Indonesia	Sabo Engineering (Third country training program)	Training Program	
Indonesia	Sabo Policy	Expert	
Uzbekistan	The Project on Capacity Development for Landslide Monitoring	TCP	
Nepal	The Study on Disaster Management for Narayangharh-Mugling Highway	Development planning	
Philippines	Road Disaster Inspection and Assessment (Country-focused training program)	Training Program	
Venezuela	Sabo Training/Training of Disaster Administration	TCP	
Iran	Study on flood and debris flow in the Caspian Coastal Area focusing on the flood-hit region in Golestan Province	Development planning	
Jordan	Arid Land Sabo Technology and Water Management Technology	TCP	
Guatemala	Landslide Mitigation	Expert	
Colombia	The Study on Monitoring and Early Warning System for Landslides and Floods	Development planning	
Peru	Technology Transfer and Capacity Building Project Strengthening Landslide Risk Reduction	Grass-root TC	
Ethiopia	Project for Developing Countermeasures against Landslide in the Abay River Gorge	Development planning	
Croatia	Project on Risk Identification and Land-use planning for Disaster Mitigation of Landslides and Floods	SATREPS	
Honduras	Project for Landslide Prevention in Tegucigalpa Metropolitan Area	Expert	
Nepal	Participatory Watershed Management and Local Governance Project	TCP	
Malaysia	Research and Development for Reducing Geo-Hazard Damage in Malaysia caused by Landslide and Flood	SATREPS	
Ethiopia	Experts for Landslide Countermeasure works and Horizontal Drainage Drilling	Expert	
Indonesia	Promoting Project for Geotechnical Disaster Prevention Technology in hilly and Mountainous Areas in Indonesia	Grass-root TC	

(continued)

Table 3 (continued)

Honduras	The study on flood control and landslide prevention in Tegucigalpa metropolitan area	Development planning
Nepal	Development and utilization of mitigative technologies for slope-induced disasters in developing countries (Master's or Doctor's Degree in Engineering)	Training Program
Vietnam	Development of Landslide Risk Assessment Technology along Transport Arteries	TCP
Mauritius	The Project for Landslide Management	TCP
Honduras	Hazard geology focusing on the landslides in Tegucigalpa	JSPS
Ethiopia	Advisor to DG on Landslide related Disasters Mitigation Management	Expert
Armenia	Landslide Disaster Management Project	TCP
Sri Lanka	Technical Cooperation for Landslide Mitigation Project	TCP
Bolivia	Advisor for the Identification of Critical Points for Preventive Measures in Disasters in the Principal and Departmental Routes	Expert
Honduras	Assistance for Strengthening and Capacity Building of Professional techniques for the Control and Mitigation of Landslide in Tegucigalpa Metropolitan Area	Expert
Kyrgyzstan	The Project for Capacity Development for Road Disaster Prevention Management	TCP
Sri Lanka	Capacity Development Project for Creating Digital Elevation Model Enabling Disaster Resilience	Development planning
Vietnam	Feasibility Survey for Ground Anchor Construction Method for Disaster Prevention of Road Slope	PPP
Mauritius	Landslide Adviser	Expert
India	The Project for Natural Disaster Management in Forest Areas in Uttarakhand	TCP
Sri Lanka	Feasibility Survey for Disseminating of Landslide Remote Monitoring System	PPP
Nepal	Project for Penetration in Nepal of Local Adaptation-Based Gabion Techniques for Both Disaster Management and Environmental Protection	Grass-root TC
Paraguay	Project for Strengthening Integrated Management of Yguazu Lake Watershed	TCP
Honduras	Project for strengthening of sustainable watershed management with community participation in the forest protected area of El Cajon dam	TCP
Indonesia	Building a Disaster-Resistant Community through the Utilization of Local Universities as a Base for Responding to Low-Frequency, Large-Scale Disasters	Grass-root TC
Kyrgyzstan	Feasibility Survey for Road Disaster Prevention Management	PPP
Georgia	Road Maintenance and Sediment disaster prevention training program (Country-focused training program)	Training Program
Georgia	Collaboration Program with the Private Sector for Disseminating Japanese Technology for Road Safety against falling rocks	PPP
Sri Lanka	Feasibility Survey for Environmental Protective Slope Protection Technology Using GEOFIBER Method (Continuous Fiber Reinforced Soil Method)	PPP
Sri Lanka	Verification Survey with the Private Sector for Disseminating Japanese Technologies for Slope Disaster Mitigation Technology with Shotcrete Cribwork using Unit Type Wire Net Formwork	PPP
Vietnam	Verification Survey with the Private Sector for Disseminating Japanese Technologies for Ground Anchor Construction Method for Disaster Prevention of Road Slope	PPP
Honduras	Project for Control and Mitigation of Landslide in Tegucigalpa Metropolitan Area	TCP
Sri Lanka	Verification Survey with the Private Sector for Disseminating Japanese Technologies for Disseminating of Landslide Remote Monitoring System	PPP
Sri Lanka	Project for capacity strengthening regarding non-structural measures for landslide risk reduction	TCP
Nepal	Collaboration Program with the Private Sector for Disseminating Japanese Technology for Environment-friendly Slope Restoration with Soil Algae	PPP
Bhutan	Feasibility Survey for Countermeasure Technologies and Methods for Road-Side Slope Disasters	PPP
Timor-Leste	Feasibility Survey for Road Slope Disaster Prevention	PPP
Brazil	Collaboration Program with the Private Sector for Disseminating Japanese Technology for Steel Slit Dam and Sabo Soil-Cement Gravity Dam	PPP
Brazil	Project for Strengthening National Strategy of Integrated Natural Disaster Risk Management	TCP
Sri Lanka	Development of early warning technology of rain induced rapid and long traveling landslides	TCP
Vietnam	SDGs Business Model Formulation Survey with the Private Sector for the Solutions to Prevent Landslide Disaster	PPP

(continued)

Table 3 (continued)

Samoa	Verification Survey with the Private Sector for Disseminating Japanese Technologies for Environmental Improvement and Disaster Risk Reduction Using the Biolog Filter	PPP
Brazil	Capacity Development Project for Structural Measures against Sediment related Disaster for Resilient Cities	TCP
Honduras	Small and Medium-Size Enterprise (SME) Partnership Promotion Survey for Monitoring Device of Slope Disasters	PPP
Bhutan	SDGs Business Verification Survey with the Private Sector for Road-Slide Slope Disasters Countermeasure Technologies and Methods	PPP
Bhutan	Project for Capacity Development on Countermeasures of Slope Disaster on Roads	TCP
Vietnam	Strengthening the capacity to cope with and minimize damages caused by flash floods and landslides for the northern mountainous region of Vietnam	TCP
Vietnam	Capacity Building of Local Community for Slope Disaster Risk Reduction	Grass-root TC
Ethiopia	Landslide countermeasure works for trunk roads (Country-focused training program)	Training Program
Ethiopia	The Project for Development and Operation Model of Plant-derived Soil Additives for Road Disaster Reduction on Problematic Soil	TCP
Iran	The Project on capacity development for participatory forest and rangeland management in upper Karoon Basin	TCP
Ecuador	Project on Capacity Building for Risk Reduction of Slope Disasters at Technical and Territorial Level	TCP
Indonesia	Landslide Disaster Risk Reduction (Sector-focused training program)	Training program
Thailand	The Project for Technology Development on Life Time Management of Road and Bridge for Strengthening Resilience in Thailand	SATREPS
Tajikistan	SDGs Business Model Formulation Survey with the Private Sector for Road Slope Protection Facilities	PPP
Honduras	SDGs Business Verification Survey with the Private Sector for Monitoring Device of Slope Disasters in Honduras	PPP
Indonesia	Invitation on Project for Upgrading Sutami Dam under Operation in Brantas River Basin	TCP
Cambodia	SDGs Business Model Formulation Survey with the Private Sector for Drainage sheet with a function to eliminate rainfall infiltration water causing existing road collapse in Cambodia road network	PPP
Sri Lanka	SDGs Business Model Formulation Survey with the Private Sector for Strengthening Landslide Warning using Low Visibility Rainfall Detection System	PPP
Philippines	Project for Road Disaster Preventions and Other Countermeasures on Mountainous Roads	TCP
Vietnam	SDGs Business Model Formulation Survey with the Private Sector for the Solutions to Prevent Landslide Disaster	PPP
Timor-Leste	SDGs Business Verification Survey with the Private Sector for Road Slope Disaster Prevention	PPP
Chile	Integrated rehabilitation of degraded soils and watersheds with emphasis on disaster risk reduction and recovery of climate resilience (Third country training program)	Training program
Brazil	SDGs Business Model Formulation Survey with the Private Sector for Early warning monitoring system for landslides disasters	PPP
Indonesia	Expert in Dam Construction	Expert
Tajikistan	Development and Maintenance of Resilient Roads in Mountainous Regions with Disaster Risk (Group-focused training program)	Training program
Philippines	SDGs Business Model Formulation Survey with the Private Sector for introduction of technologies that enable both slope disaster prevention and forest conservation	PPP

(Note) **TCP:** Technical Cooperation Project; **Development planning:** Technical Cooperation for Development Planning; **Grass-roots TC**: Grass-roots Technical Cooperation; **PPP**: Public-Private Partnership
Although the Public-Private Partnership and Grass-root technical cooperation are not categorized as technical cooperation, the projects using those schemes are also included in this table. Also, (*) depicts the project name provisionally translated by authors because the project names (English) could not be found in any documents

Second, when it comes to grant aid, there is a similar tendency with the ODA loans, but it has been earmarked for smaller facilities in terms of project cost. The Japanese government constructed structural measures. Also, it includes a project to help the Nepali government establish the Disaster Prevention Technical Centre, where training programs are provided to enhance the capacity of officials in terms of landslides. Before 1990, Indonesia also had a project to construct the Sabo Technical Center in 1982 under the grant aid.

Third, regarding technical cooperation, the project contents are diverse. Of them, technical cooperation for development planning has been performed to elaborate on a master plan, including the facility layout plan. Moreover, technical cooperation projects have been implemented to enhance the capacity of the recipient government, for example, regarding monitoring and risk assessment. The capacity of the local community was also enhanced through the grass-root technical cooperation. Furthermore, research-focused technical cooperation (e.g., SATREPS) and the Public-Private Partnership activities also exist. The former often focused on enhancing the research capacity by developing a new method for risk assessment and forecast, and the latter has been carried out by private companies to test their products (e.g., monitoring equipment, prevention works etc.) or to survey the market for their business.

5 JICA's Case Studies in the Context of Landslide Disaster

The section overviews detailed cases in representative countries such as Honduras, Brazil, and Sri Lanka to discuss how the GA-DRR is practiced. These countries are cases where JICA has long provided several ODA projects in landslide disaster risk reduction.

5.1 Honduras

5.1.1 Context

The metropolitan area of Tegucigalpa, the capital of Honduras, is located in a basin and is surrounded by slopes, which makes it prone to landslides, especially when heavy rain falls. The urban population influx from rural areas has also led to many residents living in areas exposed to landslide disaster risks. In the wake of the landslides due to Hurricane Mitch, which resulted in the human loss and injuries of over 1000 people, the Honduran government began arguing about landslide disaster risk reduction.

In this country, the Permanent Contingency Commission (COPECO) is a national agency responsible for disaster-related issues, including emergency response and rehabilitation/reconstruction. Also, in the context of landslide disaster risk reduction in the metropolitan area, the Central District Municipal Government (AMDC) plays a pivotal role. In the AMDC, there are several departments that address landslide disaster risk reduction. Moreover, The National University Autonomous of Honduras (UNAH) is a national university, which provides insights from an academic point of view.

It seems that Honduras had never had a landslide-specific legal framework until the National System of Risk Management Law (SINAGER) was enforced in 2010, amended in 2014. This allows municipalities with a sufficient capacity to take necessary actions in cooperation with COPECO. Also, AMDC behaves per some ordinances, including permission for house construction on risky slopes. Moreover, in the proxy to landslide, relevant legal frameworks exist, including the Law of Territorial Planning and the Environmental Law. The former compels the municipalities to be liable for incorporating the risk identification process into land use, and the latter regulates that vegetation shall cover slopes where erosion is accelerated. In this country, JICA has performed several projects as illustrated in Table 4.

Table 4 Project list in Honduras regarding landslide disaster risk reduction

Project name	Project period	Type of project	Project outline	References
The study on flood control and landslide prevention in Tegucigalpa metropolitan area	2001–2002	Development study	Formulation of a master plan	JICA (2002)
The Project for Landslide Prevention in Tegucigalpa Metropolitan Area	2011–2013	Grant aid	Implementation of structural measures and installation of monitoring equipment	JICA (2016)
Geological Disaster Research Focused on Landslides in the Tegucigalpa Metropolitan Area	2011–2013	Dispatch of Science and Technology Researchers	Technical transfer on stereoscopic interpretation and topographic feature analysis of aerial photographs, satellite images, and field surveys	Moncada and Yamagishi (2018)
Dispatch of Senior Volunteer	2011–2013	Volunteers	Technical transfer by revising the UPI's teaching curriculum and improving the field survey	JICA (2018)
Assistance for Strengthening and Capacity Building of Professional Techniques for the Control and Mitigation of Landslide in Tegucigalpa Metropolitan Area	2015–2016	Technical Cooperation (Dispatch of Expert)	Capacity development to enhance the capacity of UNAH and AMDC in terms of measures against landslide disaster risks	JICA (2018)
The Project for Landslide Prevention in National Road No. 6	2016–2021	Grant Aid	Implementation of structural measures on National Road No. 6	JICA (2017)
Project for Control and Mitigation of Landslide in Tegucigalpa Metropolitan Area	2019-	Technical Cooperation Project	Capacity development for landslide observation, risk assessment, and layout planning	JICA (2018)

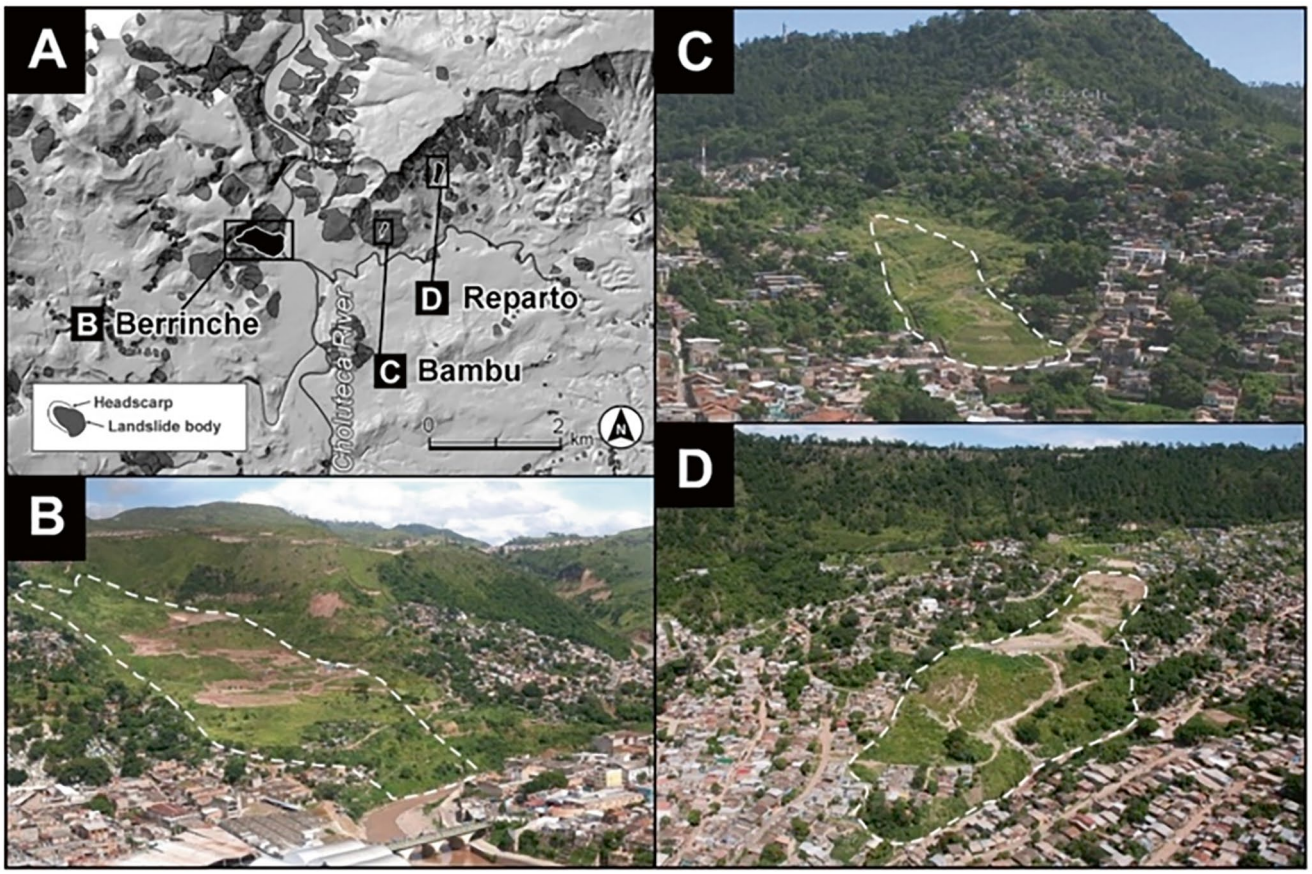

Fig. 4 Tegucigalpa metropolitan area has numerous landslide topography, and there is a risk of reactivation. Photo **a** shows the distribution of landslide topography in northern Tegucigalpa. During the heavy rains of Hurricane Mitch in 1998, large-scale landslides occurred in Photo **b**–**d**. Photo **b** is El Berrinche landslide site, Photo **c** is El Bambu landslide site, and Photo **d** is the El Reparto landslide site. These photos were taken in November 2012. The white dashed lines shown in these three photographs indicate the areas of the landslide bodies; no activity has been observed on these landslides since the end of JICA's countermeasure works. (Modified from Sato et al. 2015)

6 The Study on Flood Control and Landslide Prevention in Tegucigalpa Metropolitan Area (2001–2002)

Even after Hurricane Mitch, the rehabilitation work along the Choluteca River, which the landslide at Berrinche blocked, had not been advanced, and many people continued to live in the risky zones (See Fig. 4). Then, the Honduran government requested the Japanese government to formulate a master plan that identifies prioritized projects to protect landslides and floodings under the development study (current technical cooperation for development study).

Concerning landslides, this project developed a landslide distribution map and landslide hazard map through aerial photo interpretation, identified areas exposed to landslide hazard with the categorization of three levels, and then designated 17 high-risk areas that required countermeasures. Out of the designated high-risk areas, this project extracted three sites[1]—El Berrinche, El Bambu, and El Reparto—as very high-risk areas that necessitated urgent prevention works, including earth clearance works, surface water exclusion works, culvert works, and catchment well works, and

[1] In El Bambu, necessary prevention works were implemented under the other scheme.

Fig. 5 These are photos of the water catchment wells installed in El Berinche, under the grant aid project. Even now, the wells function appropriately while keeping the safety factor at a safe level. (Taken by Hirota, K.)

formulated the layout plans of countermeasures for the three sites (See Fig. 5).

7 The Project for Landslide Prevention in Tegucigalpa Metropolitan Area (2011–2013)

This is a grant aid project requested by the Honduran government based on the afore-mentioned development study, aiming at reducing landslide disaster risks by taking detailed countermeasures at very high-risk areas. Although the official request included the three designated areas, El Bambu was excluded because this project judged that it was not easy to take measures in El Bambu.

This project installed landslide monitoring equipment including rain gauges, extensometers, borehole tiltmeters, and groundwater level gauges in addition to the implementation of detailed preventive works, such as water catchment wells, collecting boring works, horizontal drainage boring works, draining boring works, soil removal works, and embankment works. Besides, this project included soft components to enhance the capacity for monitoring sliding mass and issuing and lifting an evacuation order.

8 Geological Disaster Research Focused on Landslides in the Tegucigalpa Metropolitan Area (2011–2013)

JICA, in cooperation with the Japan Society for the Promotion of Science (JSPS), dispatched Japanese professors as short-term experts to the Universidad Politécnica de la Innovación (UPI). The dispatched experts extracted over 1500 landslide topographies while teaching how to interpret aerial photos to produce a detailed landslide distribution map (Fig. 6). The landslide distribution map was used not only as a tool for furthering prevention works and urban planning but also to raise the awareness level of residents.

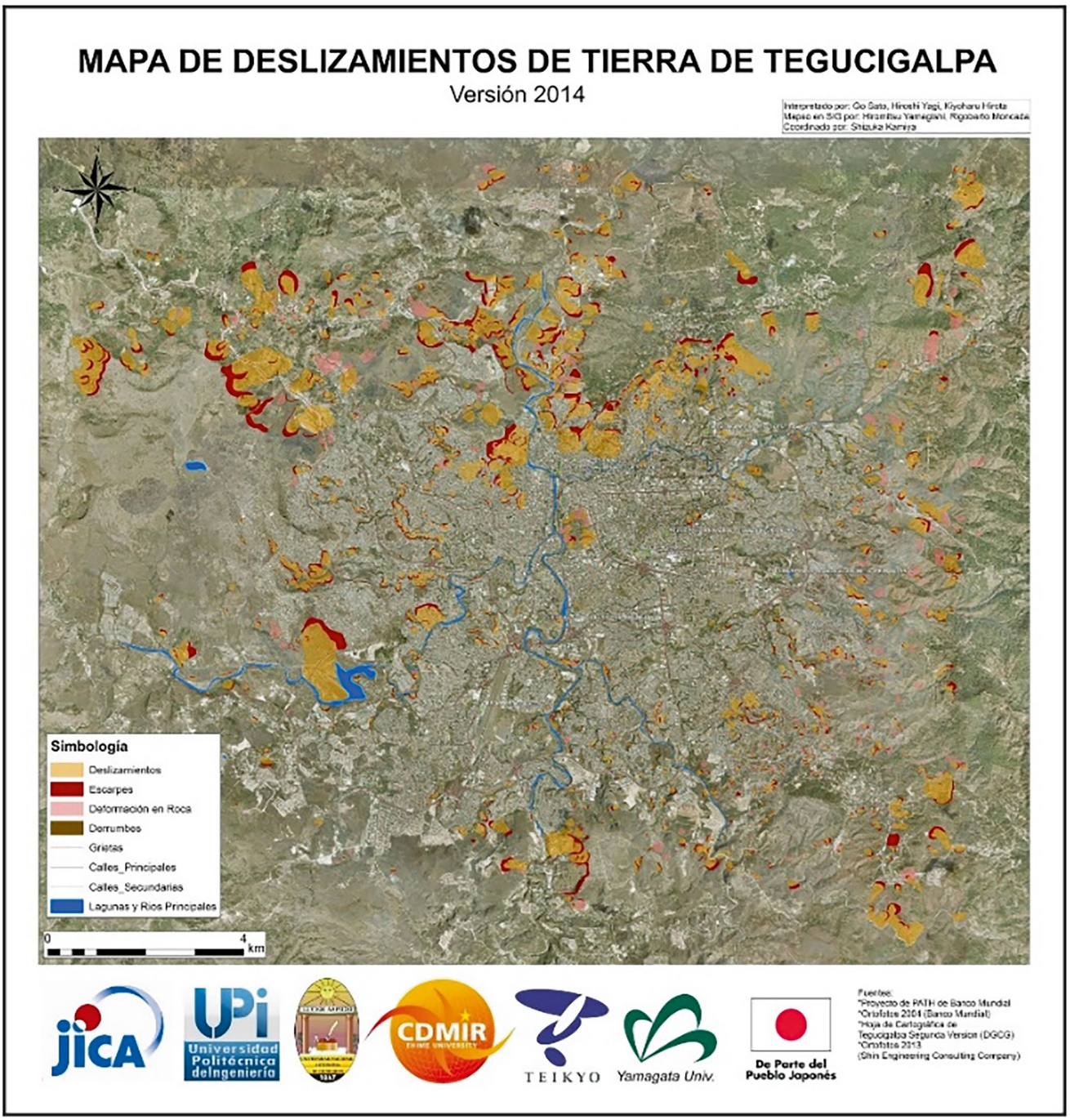

Fig. 6 Landslide distribution map of the Tegucigalpa metropolitan area. Through this project, the distribution of landslides across the entire metropolitan area has been clarified. This map continues to serve as a fundamental reference for considering landslide disaster prevention in the Tegucigalpa metropolitan area. In the legend, "Deslizarrientos" indicates landslide bodies, "Escapes" indicates scarps of landslides, "Defoemacion en Roca Defoemacion en Roca" indicates the area of rock creep slope, and 'Derrumbes' indicates a slope failure (Sato et al. 2015)

9 Dispatch of Senior Volunteer

A senior volunteer in the field of geotechnical engineering was dispatched to improve the research level of the geology department at UPI by reorganizing the curriculum and providing on-the-job training for landslide site surveys and the maintenance of landslide prevention works. These activities extended to the Zamorano University.

10 Assistance for Strengthening and Capacity Building of Professional Techniques for the Control and Mitigation of Landslide in Tegucigalpa Metropolitan Area (2015–2016)

The experts offered researchers at UNAH and technical staff at AMDC with advice on:

- UNAH's plan to institutionalize a new geological research organization;
- Establishment of a system for landslide countermeasures at AMDC;
- Establishment of a Collaboration system regarding landslide countermeasures between UNAH and AMDC;
- Development of landslide ledger of AMDC; and
- Operation and Maintenance of landslide monitoring equipment and landslide countermeasures while holding seminars for the counterparts at UNAH and AMDC to understand the sequence of landslide information collection, investigation, analysis, design, construction, and maintenance

As one of its recommendations, JICA report emphasized that experience and knowledge on landslide countermeasures cannot be acquired by intensive teaching at a desk for a short time but that it is important to see and experience many cases in the field. JICA also developed a report of recommendations and a manual for the operation and maintenance of landslide control works and monitoring equipment. It also added recommendations on how important it is for counterparts to continue these activities.

11 The Project for Landslide Prevention in National Road No. 6 (2016–2021)

National Road No. 6 is a vital connection between Nicaragua and Honduras, with over 8000 vehicles and trolleys using it daily. This route crosses mountainous areas that are prone to rock falls and landslides. In the event of rock falls or landslides, the national road may be closed for a long time, forcing significant detours of around 50 km. In light of this situation, the Honduran Government asked the Japanese Government to construct landslide preventive measures along the important road.

The grant aid project involved the outline design and implementation at three sections on National Road No. 6 by installing anchor works, spraying works, replacement works, groundwater drainage works, paving works, cross pipe replacement work, steel pipe pile work, reinforced earth method, slope prevention work, and earthwork excavation.

12 Project for Control and Mitigation of Landslide in Tegucigalpa Metropolitan Area (2019-Ongoing)

Despite the implementation of several projects by JICA, there were still rooms for improvement in structural measures and land use regulations. In this regard, challenges in implementing structural and non-structural measures were identified through workshops with counterparts conducted during the detailed planning survey for this technical cooperation project.

Therefore, this technical cooperation project focused on capacity building in the following areas.

- In-depth research and analysis to elucidate slope hazard phenomena;
- Design, construction, construction management, and maintenance for small and medium-scale slope disaster management;
- Preparation of hazard and risk maps for slope hazards; and
- Land use regulations on slope hazards

This follows a sequence of steps (investigation, analysis (diagnosis), planning, implementation of countermeasures, and operation and maintenance of the countermeasures) for slope disaster risk reduction. The project is conducting risk assessment and implementation of countermeasures under the guidance of experts. During the project period, a landslide disaster occurred in the vicinity of the pilot area. As a result, counterparts had to take emergency measures. New monitoring equipment, landslide surveys, and necessary analyses are being carried out to correct the situation.

12.1 Brazil

12.1.1 Context

It was reported that inappropriate land use has increased landslide disaster risk since the 1950s, and Brazil is therefore exposed to landslide disaster risk. In January 2011, a massive flash flood hit Rio de Janeiro, leaving 400 people missing and 800 dead. This disaster became a turning point for the Brazilian government to address landslide disaster risk reduction, and the government incorporated the DRR perspective into the multi-year plan, which is a part of the National Development Plan.

Table 5 ODA projects regarding landslide disaster risk reduction in Brazil

Project name	Period	Type of project	Project outline	References
Project for Strengthening National Strategy of Integrated Natural Disaster Risk Management	2013–2017	Technical Cooperation Project	Capacity development on landslide disaster risk assessment, land use control, and early warning system	Giustina (2019)
Collaboration Program with the private Sector for Disseminating Japanese Technology for Rader Rain Gauge in Parana State	2015–2019	Public-Private Partnership	Introduction of the wide-area rainfall observation sensor using the X-band dual polarization Rader for a more precise landslide prediction	JICA (2019a)
Collaboration Program with the private Sector for Disseminating Japanese Technology for Steel Slit Dam and Sabo Soil-Cement Gravity Dam	2018–2021	Public-Private Partnership	Introduction of Steel Slit Dam and Sabo Soil-Cement Gravity Dam for accelerating landslide disaster risk reduction using structural measures	JICA (2019b, 2021), Moncada and Yamagishi (2018)
Capacity Development Project for Structural Measures against Sediment related Disaster for Resilient Cities	2021-	Technical Cooperation Project	Capacity development on structural measures against landslide disaster	

After the 2011 disaster, the institutional arrangement was also improved under the federal governance system. For example, the National Center for Monitoring and Early Warning of Natural Disaster (CEMADEN), which is responsible for the observation and prediction of precipitation, is an example. On another stance, the National Center for Risk and Disaster Management (CENAD) was established to strengthen risk assessment and preparedness for and implementation of emergency responses post-disaster. The federal system commissions state governments and municipalities to take necessary measures against disasters. Such institutional arrangement applies to landslide disasters. In Brazil, JICA has implemented several projects, as shown in Table 5.

13 Project for Strengthening National Strategy of Integrated Natural Disaster Risk Management (GIDES) (2013–2017)

The new governance system and institutions established after the 2011 landslide disaster lacked many things. For example, CEMADEN did not have the accumulated data set of rainfall, and it was necessary to increase the capacity of forecasting the occurrence of landslide disasters. Also, CENAD did not have enough institutional capacity for landslide disaster risk assessment. Moreover, in Brazil, where uncontrolled development on risky slopes has been remarkable, land use regulations to control land misuse were established by law.

Because of this, the Brazilian government requested this GIDES project to establish a comprehensive approach, including observation, risk assessment, early warning, and urban planning. This project included the capacity development for (1) hazard identification, vulnerability, and risk assessment; (2) urban planning with a consideration of disaster risk; (3) the issuance of disaster risk information and early warning. These activities were implemented in Teresópolis City, Nova Friburgo City in Rio de Janeiro State, and Blumenau City in Santa Catarina State. The Ministry of Cities (now the Ministry of Regional Development) played a role as the project director, which coordinated with other stakeholders including the Ministry of National Integration, CEMADEN, CENAD, and the Ministry of Science, Technology, Innovation and Communication.

This project developed seven technical manuals, including:

1. Hazard and Risk Mapping
2. Landslide disaster risk mitigation for urban planning
3. Planning of countermeasures for steep slopes
4. Structural measures against debris flows
5. Contingency planning for landslides
6. Planning, issuance, and utilization of early warning for landslide disasters
7. Visualization of alert against landslide disasters

These technical manuals were prepared collaboratively by Japanese and Brazilian experts and were approved by the federal government. In the process, diverse stakeholders with different levels and in fragmented locations had opportunities to collaboratively engage in these activities. This enabled the stakeholders to enhance the interrelationship among them.

14 Collaboration Program with the Private Sector for Disseminating Japanese Technology for Rader Rain Gauge in Parana State (2015–2019)

In this project, an X-band dual-polarization radar was installed to monitor areas at high risk of landslides, and rainfall intensity was accurately observed within a radius of 80 km on a 150 m × 150 m mesh. The goal was to build a system that could make high-precision, real-time measurements, determine landslide risk, and provide evacuation guidance based on these measurements.

15 Collaboration Program with the Private Sector for Disseminating Japanese Technology for Steel Slit Dam and Sabo Soil-Cement Gravity Dam (2018–2021)

To expedite ex-ante investment in structural measures against landslide disaster risk, Japanese companies investigated the market of landslide control structures, particularly steel slit dams and Sabo soil-cement gravity dams under a JICA scheme. This project aimed to introduce the technologies the Japanese company owns and form technical committees in Blumenau City and Nova Friburgo City. These activities were expected to expand the market of the check dams.

16 Capacity Development Project for Structural Measures Against Sediment Related Disaster for Resilient Cities (SABO) (2021-Ongoing)

On the contrary to the GIDES project, previously implemented with a focus on non-structural measures, the Brazilian government had recognized the importance of prevention works against debris flows and requested the SABO project. Because it is essential to have technical manuals for the implementation, this project aimed to strengthen the capacity for designing, supervising, and maintaining the prevention works.

In the SABO project, the Brazilian government by itself, allocated the necessary budget for the pilot work in Teresópolis City, Nova Friburgo City in Rio de Janeiro State (See Fig. 7). In Teresópolis, where large rocks are predominant, the first-ever permeable Sabo dam is piloted. In Nova Friburgo, where a river bed is covered with finer sand, an impermeable Sabo dam is constructed. Because Brazil has never had a Sabo dam, these are benchmarking attempts. During the pilot countermeasures, the counterparts work hard to overcome problems, including a series of negotiations with private land owners.

16.1 Sri Lanka

16.1.1 Context

Landslides have brought the most serious impact in terms of the number of people killed or missing in Sri Lanka (JICA 2013a). Because of its geological and topographical conditions, as well as changes in rainfall patterns and intensity due to climate change, landslide disaster risks are increasing. The other factors are the uncontrolled development of land and infrastructure in mountainous and hilly areas due to population growth and economic development. In particular, damage to key roads has been severe.

In this country, the National Building Research Organization (NBRO) is positioned as a central agency for landslide disaster risk reduction, working a series of activities toward landslide disaster risk reduction such as ground observation, risk assessment, planning, and implementation

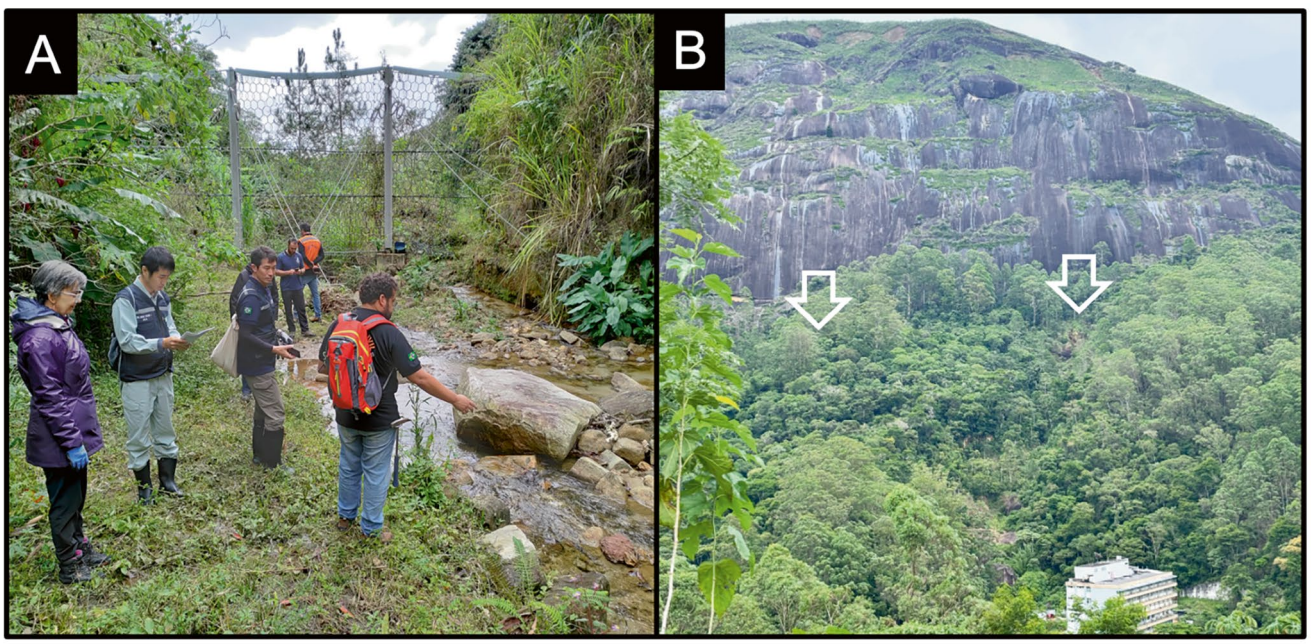

Fig. 7 Both photos are from the SABO project. (**a**) Japanese experts provided the Brazilian counterparts with on-site technical transfer opportunities at a place where a permeable SABO dam will be constructed, Telesopolis (Photo **a** and **b** provided by the Yachiyo Engineering Consultant Co.) (**b**) The entire site landscape where debris flow occurred and hit Sao Lucas. White arrows indicate the scarps

Table 6 ODA projects regarding landslide disaster risk reduction in Sri Lanka

Project name	Period	Type of project	Project Outline	References
The Disaster Management Capacity Enhancement Project Adaptable to Climate Change	2010–2013	Technical Cooperation Project	Capacity development of NBRO in terms of monitoring for landslide disaster risk reduction	JICA (2013b)
Landslide Disaster Protection Project of the National Road	2013–2017	ODA Loan	Implementation of landslide protection work along the National Road	JICA (2013c)
The Technical Cooperation for Landslide Mitigation Project	2014–2018	Technical Cooperation Project	Capacity Development of NBRO in terms of landslide disaster risk management through structural measure	JICA Sri Lanka Office (2023)
Project for Capacity Strengthening on Development of Non-structural Measures for Landslide Risk Reduction	2019–2022	Technical Cooperation Project	Capacity development of NBRO in terms of early warning and land use based on hazard and risk analyses	JICA (2022b)
The Project for early warning technology of rain induced rapid and long travelling landslide	2020–2025	SATREPS	Capacity development of early warning by understanding rain-induced rapid and long-travelling landslides	Konagai et al. (2021)

of countermeasures. Also, the NBRO offers capacity development and advocacy within the Sri Lankan government. Other than the NBRO, the Road Development Authority (RDA) is also an important agency responsible for implementing and maintaining slope management works along national roads. The RDA follows technical instructions from the NBRO. At the local level, divisional secretariats t and municipalities are also liable for reducing the risk of landslide disasters.

After the Indian Ocean Tsunami of 2004, the Sri Lankan government enacted the Disaster Management Law, which positions landslides as the most focused hazard and regulates taking necessary actions to mitigate the disaster risks. In this country, JICA has performed projects listed in Table 6.

17 The Disaster Management Capacity Enhancement Project Adaptable to Climate Change (2010–2013)

In the wake of the Indian Ocean Tsunami in December 2004, the Sri Lankan Government enacted the Disaster Management Act and restructured its disaster risk governance system. JICA has helped formulate relevant plans and provided equipment and materials for several projects since the tsunami event.

However, it became clear that Sri Lanka needed further capacity building to operate these plans and equipment. Sri Lanka faced a need to improve its capacity to adapt to climate change. In particular, although the NBRO had experiences to implement preventive measures against landslides, these measures were not based on adequate surveys, including monitoring, and could not be considered to be properly implemented with the correct procedures. Therefore, although landslide was a part of the project's inputs, the project developed 'The Manual for Landslide Monitoring, Analysis and Countermeasure' to solve the problem.

18 Landslide Disaster Protection Project of the National Road (2013–2017)

In Sri Lanka, frequent landslide disasters have resulted in extensive damage to the road network, which has disputed the economic activities. In particular, between 2007 and 2012, five provinces (Central Province, Uba Province, Sabaragamuwa Province, and West Province) had more than 700 landslides, which resulted in the victims of more than 34,000 people. These landslides were triggered not only by the original ground fragility but also by the increases in instability due to inadequate slope excavation and groundwater drainage systems associated with roads.

Under such circumstances, the NBRO enhanced the monitoring of planned national projects in areas exposed to landslide disaster risks. One of them is road construction projects led by the RDA. However, RDA also lacked the resources of finance, technique, and institutional capacity. Therefore, the Sri Lankan government requested the Japanese government to implement an ODA loan project for national road construction.

The ODA loan project included prevention works on national roads in the five risky provinces to reduce landslide disaster risks. The prevention works included anchor works. Also, procuring equipment for early warning systems was a part of the Project.

19 The Technical Cooperation for Landslide Mitigation Project (2014–2018)

This project aimed to improve the landslide management capacity of the NBRO in the four districts of Kandy, Matale, Nuwara Eliya, and Badulla in Sri Lanka and contribute to landslide mitigation in the target areas. The project aimed to contribute to landslide risk reduction in the target areas. The project focused on knowledge and expertise in (1) research

and assessment of landslide prevention measures; (2) design, supervision, and monitoring of landslides, slope failure, and rockfall; and (3) landslide mitigation measures, including non-structural measures.

The project was implemented as an associated project of the yen loan project and other related projects. Specifically, the Project aimed to improve the NBRO's capacity for landslide risk reduction, including appropriate landslide prevention measures using Japanese technologies in the pilot project sites to be developed under the ODA loan. Through this project, in addition to the dispatch of experts, extensometers, inclinometers, groundwater level gauges, and pipe strain gauges with piezometers were provided.

20 Project for Capacity Strengthening on Development of Non-structural Measures for Landslide Risk Reduction (2019–2022)

The Sri Lankan government recognized the importance of further enhancing the capacity for non-structural measures although previous JICA projects had focused on the designing and construction of prevention works for three types of landslides (rockfall, slide, and slope failure) by preparing relevant standards and technical manuals and the implementation of the prevention works. Therefore, the Sri Lankan government requested the Government of Japan to assist the NBRO.

Specifically, this project aimed to enhance the NBRO's capacity for (1) hazard and risk assessment; (2) issuance of an early warnings; and (3) land use regulation. Relevant project activities were performed in Matara province, Kegall province, and Badulla province.

In terms of (1) hazard and risk assessment, although NBRO had attempted to quantify the susceptibility of landslides since 1995, the approach did not guarantee the preciseness applicable to early warning and land use control. This project reevaluated the assessment approach to reflect the reality at the site, elaborated the manuals (See Fig. 8), and carried out the hazard assessment in the pilot sites. Base maps of the target pilot areas were collected to conduct hazard and risk assessments, and aerial topographic interpretations were also performed. The project guided the establishment of Yellow/Red zones.

Regarding (2) the issuance of early warnings, this project developed the remote monitoring system and set a warning

Fig. 8 Manuals formulated by the technical cooperation "Project for Capacity Strengthening on Development of Non-structural Measures for Landslide Risk Reduction". (L) manual for Site-specific landslide hazard zoning; (R) Manual on Risk Assessment for Landslide Yellow/Red Zone (JICA 2022b)

threshold using the soil rainfall index. Because early warnings must be delivered to evacuees in an appropriate and timely manner, the project developed the manual, including the method to determine the thresholds and the protocol for information dissemination. It is worth noting that ground surveys with extensometers and tiltmeters and rainfall amounts were monitored (See Fig. 9). This activity collaborated with the SDGs Business Model Formulation Survey with the Private Sector for Strengthening Landslide Warning using Low Visibility Rainfall Detection System, which attempted to have a common interface to lower the running cost of the monitoring system.

When it comes to (3) land use regulations, this project classified the land use into four: Development zone, Restricted zone, Controlled zone, and Warning zone, based on the Yellow/Red zoning, which was developed in the context of (1). The Red zone is consistent with the Restricted and Controlled zones, while the Yellow zone is the Warning zone. Although land use zoning and land use planning are handled by other public entities than the NBRO, the project concluded that the Yellow zone (Warning zone) is expected to be used as parks and the Red zone (Restricted and Controlled Zone) shall not be used for urbanization. In addition, posters were distributed to local authorities and residents to raise awareness of landslide hazard risks (See Fig. 10).

21 Development of Early Warning Technology of Rain-Induced Rapid and Long-Travelling Landslides in Sri Lanka (2020–2025)

The research-focused technical cooperation project, called SATREPS, attempted to develop technologies for the assessment of rain-induced rapid and long-travelling landslides

Fig. 9 Photos of the project site of the "Project for Capacity Strengthening on Development of Non-structural Measures for Landslide Risk Reduction". (**a**) is a photo of the installed extensometers, and (**b**, **c**) show on-site technical guidance between Japanese experts and Sri Lankan counterparts. (These photos were provided by the Earth System Science Co, Ltd.)

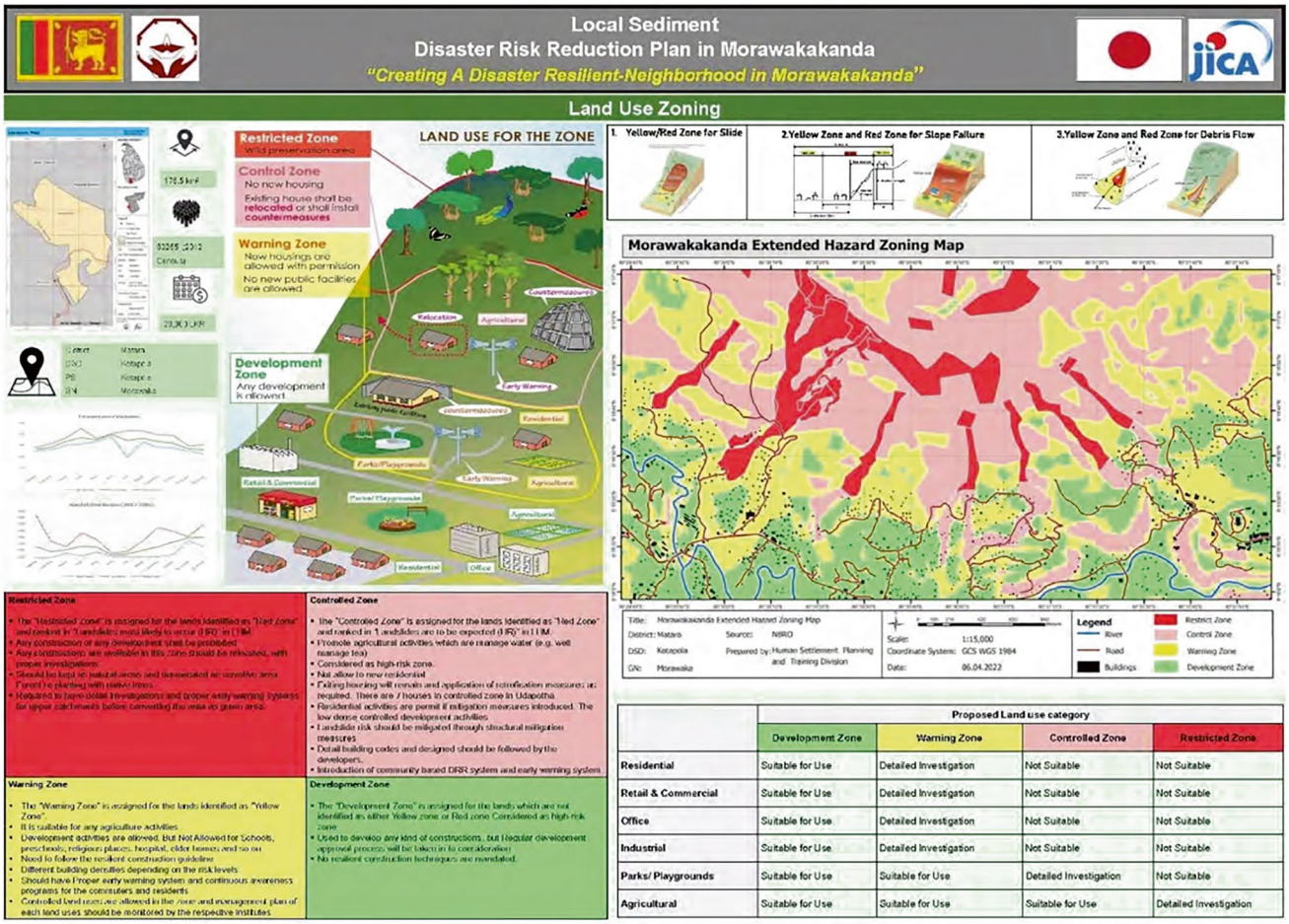

Fig. 10 Poster that helps local government and local people raise awareness of appropriate land use while considering landslide disaster risk (Morawakkanda) (JICA 2022b)

Table 7 Summary of JICA's approach to landslide disaster risk reduction

					Non structural measures	
	Observation	Risk analysis	Planning	Structure measures	Land use	Early warning
Honduras	☐	☐	☐	☐	☐	☐
Brazil	☐	☐	☐	☐	☐	☐
Sri Lanka	☐	☐	☐	☐	☐	☐

(RRLL), analyzed the landslide mechanism, and enhanced risk communication methods and procedures at pilot sites in Sri Lanka, thereby applying early warning technologies for RRLL that integrate these technologies. The project was expected to contribute to strengthening the early warning capacity of the RRLL in Sri Lanka.

In particular, the project installed monitoring equipment to observe landslide displacement in the Aranayaka and Athwelthota districts and developed a ring-shear apparatus that helps to understand the landslide mechanism at the laboratory level. Furthermore, based on these, the project tried to improve the quality of risk communication, including public education, while using Augmented Reality.

22 Remarks

This article reviewed Japan's ODA in the context of landslide disaster risk reduction, referring to the JICA's sectoral policy on DRR (GA-DRR), and then presented case studies of Japan's ODA practices in Honduras, Brazil, and Sri Lanka, implemented by JICA.

JICA's ODA practices are featured as below.

– Diverse countries are facing a need to address landslide disaster risk reduction. Because of the wide range of needs from recipient governments, JICA is using several

assistance schemes to fit the aim of each project. Particularly, recipient governments tend to gain momentum to challenge DRR in the wake of a disaster event.
- At the same time, JICA has attempted to maximize the intervention effect of ODA by combining multiple projects as a program as highlighted by case study[2] because it is not easy to substantially address DRR. For example, it covered both structural and non-structural measures in the presented cases.
- In addition to the dichotomy between structural and non-structural measures, JICA has attempted to address the reduction of disaster risk in a recipient government by practicing multiple ODA projects as a program. As indicated in Table 7, the cases presented included a series of steps necessary for DRR. Focusing on avoiding the creation of new risks and reducing existing risks, many projects considered the appropriation of land use and urban planning as non-structural measures and master planning and prevention works as structural measures.

In JICA's ODA program, many stakeholders, even in the government and public entities, need to be involved. All the cases presented reflected this. The sequence toward DRR can be fragmented when different agencies take charge of each work process because they behave to achieve their institutional mission (Minamitani et al. 2024). Where a project exists, collaborative works are likely to emerge because there is a common goal shared by the stakeholders. However, where no project exists, this can become critical.

Therefore, ODA programs should not only cover every sequence but also need to be managed in such a way that the sequence meshes well to achieve disaster risk reduction. ODA interventions will not last forever, and ODA should be designed to help partner governments ensure sustainable interagency collaboration. ODA should be designed to ensure that the government of the partner country can ensure sustainable interagency collaboration. It will be necessary to devise ways to do so.

In this context, there has recently been a growing interest in green infrastructure and nature-based solutions (NbS) in the international community. Studies also discussed the methodology and effectiveness of the approach (Kumar et al. 2020). For example, the Asian Development Bank, in collaboration with the French Development Bank (AFD) launched the Nature Financing Initiative for Asia and the Pacific in June 2024. This aims at accelerating investment in NbS to achieve both environmental prevention and economic growth (ADB 2024). Undoubtedly, the environmental perspective is also important but more importantly, the cases show that it is critical to interlink monitoring, risk assessment, and planning to select and implement appropriate and effective countermeasures.

That is, setting a relevant design force is essential. In that sense, it should also be noted that green infrastructure fundamentally differs from grey infrastructure in terms of the expected performance of their measures. According to the SFDRR, DRR must aim to save human lives and then reduce disaster risks that can lead to poverty and economic loss. For such a catastrophe that leads a country to serious crises, there may be a case where green infrastructure may not be effective in stopping landslides. Indeed, it is not expected that tree roots stop a deep-seated landslide.

Again, the environment is nonnegligible in considering DRR; but both grey and green infrastructure have a demand and role, and ensuring investment effect is more important. The international society also needs to pay attention to avoid distorted investment in either and needs to draw more attention to effective and meaningful ex-ante investment in DRR for the aim of realizing poverty alleviation and economic development. Such distortions may also be caused by excessive reliance on early warning. Early warning is an important measure for the protection of human life, but it may not contribute to sustainable economic growth, as the possibility of suffering the same disaster damage remains as long as the original society is formed after the disaster. Besides, without effective reduction of disaster risk, an early warning system may not offer sufficient lead-time for people to evacuate. In that sense, the authors believe that dispassionate discussions are necessary in the international society to achieve the goal of the SFDRR. DRR is under the responsibility of each government, and it is important to consider what a role donor agency, like JICA, needs to play based on experiences and lessons in Japan.

Acknowledgments The authors would like to sincerely thank the staff in JICA for the support in compiling the project list. The authors would also like to take this opportunity to congratulate the Yachiyo Engineering Co, Ltd. and the Earth System Science Co, Ltd. for providing photos in this article.

[2]According to the project and program management (P2M), which is a well-known body of knowledge for program management, "project" is defined as a value-creation activity to accomplish the project mission under specific time, resource, circumstance, and other constraints, "Program" is used for activities that combine multiple projects to achieve a specific program mission that an individual project cannot obtain (Yamamoto 2019).

References

ADB (2024) Nature-based solutions for Asia and the Pacific (Publications Brochures and Flyers). ADB, Manila

Alam E (2020) Landslide hazard knowledge, risk perception and preparedness in Southeast Bangladesh. Sustainability 12:6305. https://doi.org/10.3390/su12166305

Assilzadeh H, Levy JK, Wang X (2010) Landslide catastrophes and disaster risk reduction: a GIS framework for landslide prevention and management. Remote Sens 2:2259–2273. https://doi.org/10.3390/rs2092259

Baseler T, Henning J (2023) Disastrous displacement: the long-run impacts of landslides (no. policy research working paper 10535). World Bank, Washington, DC

Besl J (2022) Protecting poor neighborhoods from landslide risk [WWW Document]. https://www.preventionweb.net/news/protecting-poor-neighborhoods-landslide-risk. Accessed 17 Oct 2024

Dille A, Dewitte O, Handwerger AL, d'Oreye N, Derauw D, Ganza Bamulezi G, Ilombe Mawe G, Michellier C, Moeyersons J, Monsieurs E, Mugaruka Bibentyo T, Samsonov S, Smets B, Kervyn M, Kervyn F (2022) Acceleration of a large deep-seated tropical landslide due to urbanization feedbacks. Nat Geosci 15:1048–1055. https://doi.org/10.1038/s41561-022-01073-3

EM-DAT (2024) The International Disasters Database [WWW Document]. https://www.emdat.be/. Accessed 17 Mar 2024

Giustina YRD (2019) Project for strengthening national strategy of integrated natural disaster risk management, GIDES project, in Brazil. IJECE 11:51–53. https://doi.org/10.13101/ijece.11.51

JICA (2002) The study on flood control and landslide prevention in Tegucigalpa metropolitan area of the Republic of Honduras final report: supporting report. JICA, Tokyo

JICA (2013a) Data collection survey on disaster risk reduction in Sri Lanka (no. 4R(JR)13-016). JICA, Tokyo

JICA (2013b) The disaster management capacity enhancement project adaptable to climate change: final report (no. GE(JR)13-069). JICA, Tokyo

JICA (2013c) Ex-ante evaluation: landslide disaster protection project of the national road (in Japanese). JICA, Tokyo

JICA (2016) FY 2016 external ex-post evaluation of Japanese Grant Aid Project "The Project for Landslide Prevention in the Tegucigalpa Metropolitan Area". JICA, Tokyo

JICA (2017) Final report for the project for landslide prevention in national road no.6. JICA, Tokyo

JICA (2018) Project for control and mitigation of slope disaster in central district. JICA, Tokyo

JICA (2019a) Collaboration program with the private sector for disseminating Japanese technology for radar rain gauge in Parana State Final Report (no. OS(JR)19-138). JICA, Tokyo

JICA (2019b) Ex-post evaluation: capacity development project for structural measures against sediment related disaster for resilient cities. JICA, Tokyo

JICA (2021) Final report on collaboration program with the private sector for disseminating Japanese technology for Steel Slit Dam and Sabo Soil-Cement Gravity Dam. JICA, Tokyo

JICA (2022a) Japan International Cooperation Agency annual report 2022. JICA, Tokyo

JICA (2022b) Project for capacity strengthening on development of non-structural measures for landslide risk reduction: final report (no. GE(JR)22-116). Tokyo, JICA

JICA (2024) JICA global agenda for no. 20 disaster risk reduction through pre-disaster investment and build back better. JICA, Tokyo

JICA Sri Lanka Office (2023) Internal ex-post evaluation for technical assistance under finance and investment account: technical cooperation for landslide mitigation project. JICA Sri Lanka Office, Colombo

Kellett J, Caravani A (2013) Financing disaster risk reduction. Overseas Development Institute, London

Khan MJU, Islam AKMS, Bala SK, Islam GMT (2020) Changes in climate extremes over Bangladesh at 1.5 °C, 2 °C, and 4 °C of global warming with high-resolution regional climate modeling. Theor Appl Climatol 140:1451–1466. https://doi.org/10.1007/s00704-020-03164-w

Konagai K, Karunawardena A, Sassa K (2021) SATREPS project for Sri Lanka with regard to "Development of early warning technology of rain-induced rapid and long-travelling landslides". In: Sassa K, Mikoš M, Sassa S, Bobrowsky PT, Takara K, Dang K (eds) Understanding and reducing landslide disaster risk, ICL contribution to landslide disaster risk reduction. Springer International Publishing, Cham, pp 205–214. https://doi.org/10.1007/978-3-030-60196-6_12

Kumar P, Debele SE, Sahani J, Aragão L, Barisani F, Basu B, Bucchignani E, Charizopoulos N, Di Sabatino S, Domeneghetti A, Edo AS, Finér L, Gallotti G, Juch S, Leo LS, Loupis M, Mickovski SB, Panga D, Pavlova I, Pilla F, Prats AL, Renaud FG, Rutzinger M, Basu AS, Shah MAR, Soini K, Stefanopoulou M, Toth E, Ukonmaanaho L, Vranic S, Zieher T (2020) Towards an operationalisation of nature-based solutions for natural hazards. Sci Total Environ 731:138855. https://doi.org/10.1016/j.scitotenv.2020.138855

Lan H, Tian N, Li L, Liu H, Peng J, Cui P, Zhou C, Macciotta R, Clague JJ (2022) Poverty control policy may affect the transition of geological disaster risk in China. Human Soc Sci Commun 9:80. https://doi.org/10.1057/s41599-022-01096-6

Minamitani T, Isagawa T, Okiura F (2024) Structure of problems hindering inter-agency collaboration through ODA programmes for disaster risk reduction—a project and programme management perspective. https://doi.org/10.20702/iappmproc.2024.Spring.0_48

Moncada R, Yamagishi H (2018) TXT-tool 1.504-1.1: landslide inventory educational methodology derived from experiences in Latin America. In: Sassa K, Guzzetti F, Yamagishi H, Arbanas Ž, Casagli N, McSaveney M, Dang K (eds) Landslide dynamics: ISDR-ICL landslide interactive teaching tools. Springer International Publishing, Cham, pp 95–111. https://doi.org/10.1007/978-3-319-57774-6_6

Paton D (2019) Disaster risk reduction: psychological perspectives on preparedness. Aust J Psychol 71:327–341. https://doi.org/10.1111/ajpy.12237

Sato G, Kamiya S, Hirota K (2015) Investigation and mitigation of landslides in Republic of Honduras as Japan's International cooperation program. J Japan Landslide Soc 52:161–167. https://doi.org/10.3313/jls.52.161

UNDRR (2023) Sendai framework terminology on disaster risk reduction [WWW Document]. https://www.undrr.org/terminology. Accessed 19 Dec 2023

UNISDR (2015) Sendai framework for disaster risk reduction 2015–2030. UNISDR, Geneva

Yamamoto H (2019) Management of projects that involve people with different perceptions of what constitutes 'value.' https://doi.org/10.20702/iappmjour.14.1_456

Design Ways of Vegetation Work and Drainage System for Bioengineering on the Landslide Slope at Gopini in Bhutan

Kiyoharu Hirota, Gyeltshen Wangdi, Sonam Yezer, Hari-Maya Dahal, and Tomohiro Nishimura

Abstract

This article is a teaching tool focusing on the bioengineering efforts applied to the road slope in Gopini, southern Bhutan, where a previous landslide occurred.

Following the landslide event, gabions were constructed at the base of the slope. Still, some gabions protruded toward the roadway due to the earth pressure exerted from behind. Therefore, it was essential to ensure the slope's stability and mitigate erosion caused by heavy rainfall. A functional drainage system was implemented on the surface, accompanied by efforts to establish vegetation.

The drainage system includes French, Cascade, Berm, Toe drains, and energy dissipators. This teaching tool article utilized bioengineering techniques such as pot, spread, and sandbag planting. For spread planting, a laminate sheet was made by layering a plastic mesh net between two jute nets, resulting in a three-layer design. Pot planting involved tubes, each measuring 40 cm in diameter and 50 cm in length, placed next to the upper section of Berm drains Br. 2 and Br. 3, which also functioned to help alleviate earth pressure. Sandbag planting was conducted concurrently with pot planting in areas vulnerable to landslides.

K. Hirota (✉) · T. Nishimura
Kokusai Kogyo Co., Ltd., Tokyo, Japan
e-mail: Tomohiro_nishimura@kk-grp.jp

G. Wangdi
Department of Surface Transport, Ministry of Infrastructure and Transport, Punakha, Bhutan
e-mail: gwangdi@moit.gov.bt

S. Yezer
Norbu Yeabar Construction, Pelkhil Lam Near Lhaki Hotel Phuntsholing Thromde, Chukha Dzongkhag, Bhutan

H.-M. Dahal
Samtse Sub-division, Department of Surface Transport, Ministry of Infrastructure and Transport, Samtse, Bhutan

Keywords
Bioengineering · Landslide · Drainage System · Vegetation work

1 Introduction

This teaching tool article illustrates the bioengineering techniques implemented in the "Project for Capacity Development on Countermeasures of Slope Disaster on Roads in Bhutan," organized by the Japan International Cooperation Agency (JICA). The current bioengineering method used in Bhutan involves brush laying and live staking. This technique has successfully established vegetation coverage on gentle and stable slopes. However, in the case of steep cut slopes, particularly those maintaining a bare angle of 45° or greater, this combination of brush laying and live staking fails to fully cover the slope with vegetation, resulting in gully erosion and exposures of bare soils. Addressing slope stability along Bhutan's national highways post-cutting is an urgent concern, and the JICA initiative also emphasized the necessity of bioengineering to curb surface erosion on stable slopes. In the bioengineering plan for the Gopini slope, ensuring slope stability is essential, as it is adjacent to Prime National Highway 2 (PNH-2). Consequently, a drainage system was developed that fits the on-site ground conditions, facilitating proper surface drainage. The vegetation efforts were aimed at enhancing slope stability. The materials needed for the bioengineering initiatives can be easily sourced within Bhutan. Thus, the ground surface was contoured to maintain its current slope angle, and a spread planting strategy was integrated using laminated sheets to cover the ground. This combined approach will help avert slope failure due to surface erosion and sudden rainwater infiltration and reduce the surface layer's movement. Given the above background, this teaching tool article shows how to design vegetation that works with an effective drainage system for the Gopini slope, which has experienced previous landslides.

B. Abolmasov et al. (eds.), *Progress in Landslide Research and Technology, Volume 4 Issue 1, 2025*, Progress in Landslide Research and Technology, https://doi.org/10.1007/978-3-031-89836-5_16

The drainage system consists of various elements such as French drains, Berms, Cascades, Toe drains, Box drains (catch basins), and Check dams used as energy dissipators for surface runoff. The overall vegetation coverage aims to prevent erosion by spreading over a significant area. Pot planting, which involves strategically arranging groups of vegetation pots, is employed to help manage localized deformations in the surface layer. Three D20 rebars are installed inside these vegetation pots to form a structure that withstands earth pressure and facilitates drainage. In areas prone to landslides where minor collapses happen, sandbags filled with mixed seeds may be utilized for planting (sandbag planting).

The term "vegetation work" is more suitable for the project than "bioengineering," as it fully utilizes the drainage system, unlike "soil bioengineering," which is a term endorsed by the United States Department of Agriculture (NRCS). Lewis (2000) pointed out that the term bioengineering has led to misunderstandings and posed challenges for researchers in the United States, where it primarily relates to medical research. NRCS currently designates this kind of work as "soil bioengineering," highlighting the geotechnical aspect of the work.

2 Bioengineering in Bhutan

In Bhutan, bioengineering utilizes brush layering and live staking techniques to plant willows and various tree species. This approach has proven effective on slopes with minimal surface erosion (Fig. 1).

After 8 months of planting, the vegetation is thriving (Fig. 2).

Conversely, on slopes with a gradient of 1:1.0 or greater, erosion has progressed to such an extent that certain regions have transformed into badlands (Fig. 3).

Fig. 1 Bioengineering site in Bhutan on February 7, 2024 (photo by Nishimura, the arrow shows the same point in Fig. 2)

Fig. 2 Bioengineering site in Bhutan on October 11, 2024 (photo by Nishimura)

Fig. 3 Gully erosion developed on the slope after bioengineering work (Rabuna, Wangdue, photo by drone on January 11, 2024)

The upper layer of the Rabuna slope is made up of weathered gneiss soil that contains minimal clay, enabling rain to infiltrate readily. Weathering has resulted in the presence of quartz and muscovite of gneiss. The drone image in Fig. 4 illustrates the landform configuration following mass movement.

Three bioengineering testing locations have been chosen in Bhutan as part of the JICA initiative. The first site is Gangthangka (Hirota et al., 2023), which falls under the Lobesa Regional Office (abbreviated as R.O.) of the Department of Surface Transport (DoST). The second site is Yangkhil, under the jurisdiction of the Trongsa R.O. of DoST. At the same time, the third location, Gopini, is managed by the Phuentsholing R.O. of DoST and is situated midway between Samtse and Phuentsholing (see Figs. 5 and 6).

R.O. of DoST and is situated midway between Samtse and Phuentsholing (see Figs. 5 and 6). The initial two bioengineering testing sites included cut slope and gabion projects as the primary slope stabilization efforts. The Gopini site is a slope that faces the PNH-2, where existing gabions have been installed at the base of the slope as a countermeasure. Due to landslides on the site, the authors chose strategies that reshape the slope surface rather than cutting into it, forming the fundamental concept for ensuring slope stability.

Fig. 4 Bare soil exposed after bioengineering work (Rabuna, Wangdue on January 11, 2024)

3 Vegetation Work and Drainage System at Gopini

3.1 Gopini Site

The Gopini slope is located 75 km southeast of the capital, Thimphu, in a straight line, halfway between Samtse and Phuentsholing on the PNH-2 line (Fig. 6).

Although there is no documented report of the Gopini landslide, heavy rainfall in July 2016 triggered it, making the PNH-2 route between Samtse and Phuengtholing unusable (Barman and Choudhury 2023). Analyzing Google Earth images suggests the landslide probably occurred between December 19, 2014, and August 4, 2020 (Figs. 7 and 8). The significant rainfall on July 1, 2016, occurred within this period.

Fig. 5 Three Bioengineering sites in Bhutan

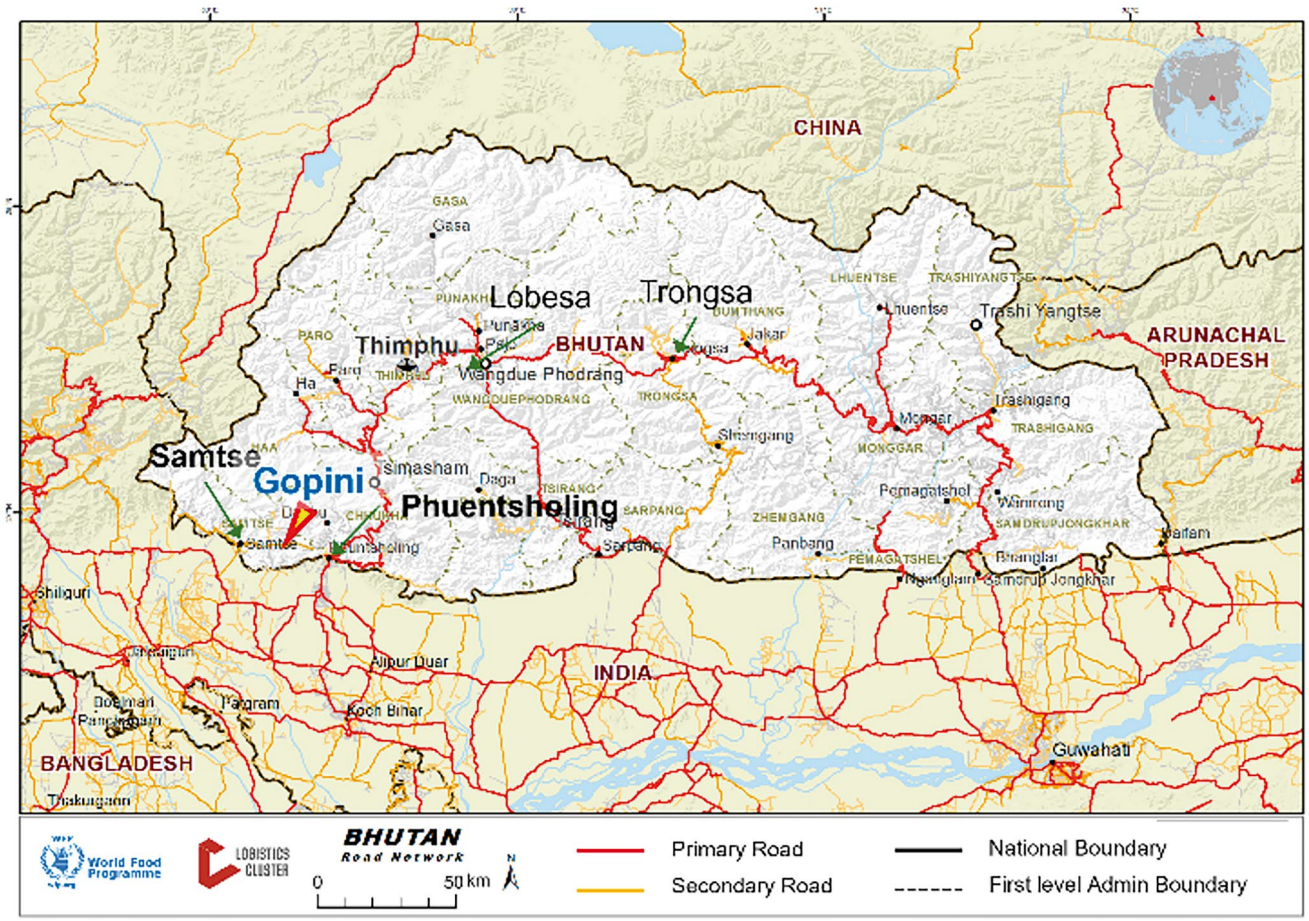

Fig. 6 Bioengineering site in Gopini, Bhutan (https://dlca.logcluster.org/23-bhutan-road-network#id-2.3BhutanRoadNetwork-Overviewoad viewed on May 29, 2023, and added)

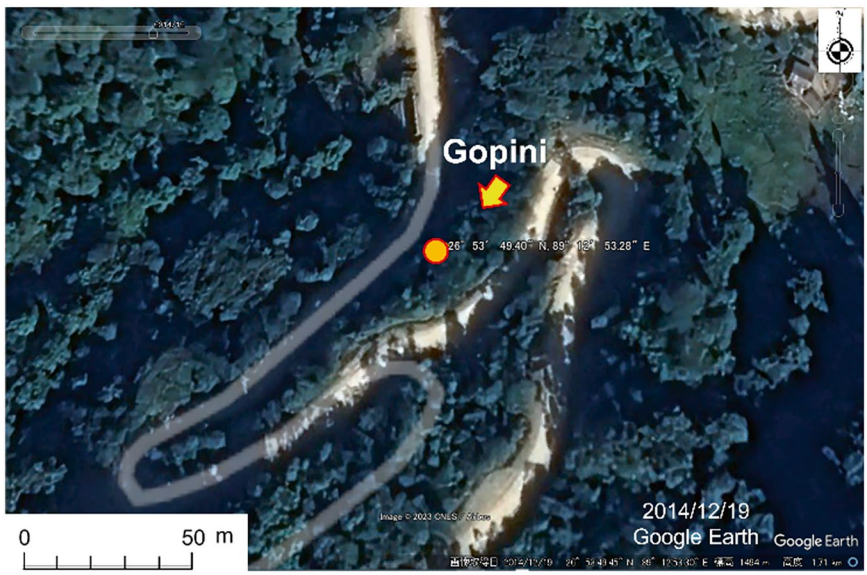

Fig. 7 Pre-landslide image, Gopini (Google Earth, on December 19, 2014, the circle and the arrow show the same points in Fig. 8)

Fig. 8 Post-landslide image, Gopini (Google Earth, on December 19, 2014)

3.2 Procedure

Figure 9 shows the bioengineering flow carried out at Gopini.

Preparation: The task includes trimming the grass to set up the environment for contouring the ground surface, assessing the area through drone images, and assembling materials for bioengineering: laminate sheets, plant pots, and sandbags (containing seeds).

Earthwork: Initially, the ground surface is contoured, and the drainage system is adjusted on-site using ribbon tape to align with the original design plan.

Drainage system: As part of the drainage system relocation, French drains, Berm drains, Toe drains, and Cascade drains are incorporated alongside Lateral drains, with box-like catch basins positioned at key junctions to control excessive water flow. Using cobblestones arranged horizontally in Cascade drains minimizes hydraulic energy, while additional mitigation of hydraulic energy is accomplished through step-shaped waterways and check dams.

Vegetation work: Three vegetation activities will be performed following the drainage system's installation. Laminate sheets will be utilized for spread planting, while vegetation pots with cut tubes will be employed for pot planting. Sandbag planting, which serves a restraining purpose, will be implemented in areas where earth sure is exerted.

3.3 Germination Test

Before starting the bioengineering steps shown in Fig. 9 at Gopini, the authors conducted a germination test on the same slope (Fig. 10).

The chosen seeds are from two species that exhibited strong germination at the initial test location, Gangthangka, as well as at the subsequent site, Yangkhil: *Paspalum atratum* and *Brachiaria ruziziensis* (commonly known as Ruzi grass). The conditions and results of the germination test are shown in Figs. 11 and 12. Observations indicated that nearly 100% of both species successfully germinated. Among the two species, *B. ruziziensis* (Ruzi grass), widely utilized in southern Bhutan, was selected.

Conditions

1. Seeds: *Paspalum atratum* (see Fig. 11a) and Ruzi grass (see Fig. 11b).
2. Fertilizer: NPK = 1:1:1 (trial: 5 g/t = 1 cm/m^2): the thickness of the added soil [cm]
3. Soils: Using soils near the germination test site. Soils are sieved by using a 5 mm meshed sieve.
4. Target coverage rate: 60% (at the time of the observed state after germinating)

3.3.1 Test Process

The germination test lasted from July 12, 2023, to September 4, 2023.

Two seeds, P. atratum and B. ruziziensis (Ruzi Grass), were germinated outdoors or covered with a jute net. In Fig. 12a, the B. ruziziensis seeds were planted behind the white line where two people are seen squatting, while P. atratum seeds were planted in front of the white line.

(a) The germination test commenced on July 12, 2023.
(b) Assessment of the germination test condition: on July 19, 2023, sections of the eroded germination zone were secured with a jute net.
(c) Continued monitoring of the germination test's state on July 27, 2023.

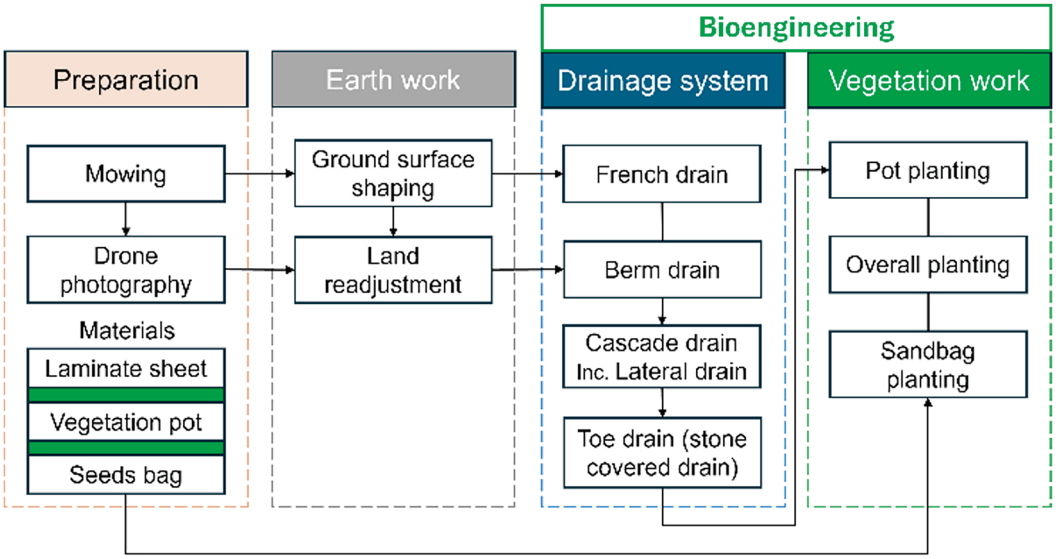

Fig. 9 Bioengineering work flow at Gopini site

Fig. 10 Germination test site (indicated by the arrow in the middle) at Gopini slope (September 4, 2023)

(d) Ongoing observation took place on August 4, 2023.
(e) Evaluation on September 4, 2023, revealed that the entire area had become vegetated with the germination of two seed varieties.

3.4 Drone Photography

3.4.1 Before Bioengineering

An officer from the DoST captured images using a drone to understand the general features of the slope where bioengineering would take place (Fig. 13). After checking the partial unevenness of the ground surface and the direction of surface runoff, a suitable plan for the types of work was developed. After the drainage system was completed, vegetation work was carried out.

While checking the terrain features with the drone photo images, the locations designated for installing the drainage system were measured on-site and displayed with ribbon tape (Fig. 14).

3.4.2 After Bioengineering

The basic drainage system was rearranged based on the drone photography results and the site conditions (Fig. 15, to the previous page).

4 Materials and Methods

4.1 Plants

Seeds were selected based on their germination test results and ease of acquisition. Flowers were chosen from those grown in southern Bhutan. The seeds and flowers below were selected for bioengineering (Fig. 16).

Seeds: Ruzi grass (*Brachiaria ruziziensis*).

Flowers: Madagascar periwinkle (*Catharanthus roseus*), Boat Lily (*Tradescantia spathacea*).

4.2 Drainage System

Table 1 illustrates the various kinds of drainage systems employed for surface drainage. The materials and

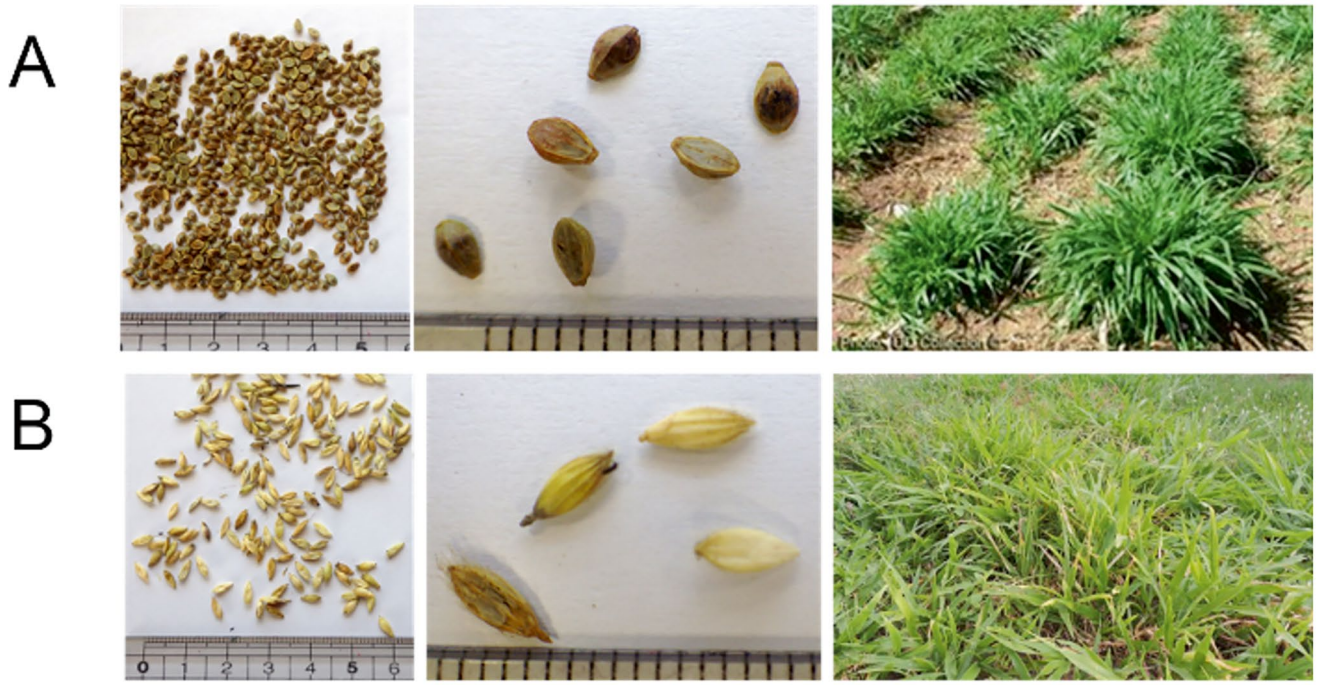

Fig. 11 Seeds chosen for germination test ((**a**) *Paspalum atratum*, (**b**) *Brachiaria ruziziensis* (Ruzi grass))

Fig. 12 Germination test at the Gopini slope. (**a**) July 12, 2023: Begin germination test, (**b**) July 19, 2023: Observe the state of the germination test, (**c**) July 27, 2023: Continue observing the germination test, (**d**) August 4, 2023: Continue observation, (**e**) September 4, 2023: Observation

Fig. 13 Gopini slope before shaping work (drone photography on December 14, 2023)

Fig. 14 Measuring at Gopini slope on January 3, 2024 ((**a**) upper part of the site, (**b**) measuring the cascade drain dimension, (**c**) measuring the ground height)

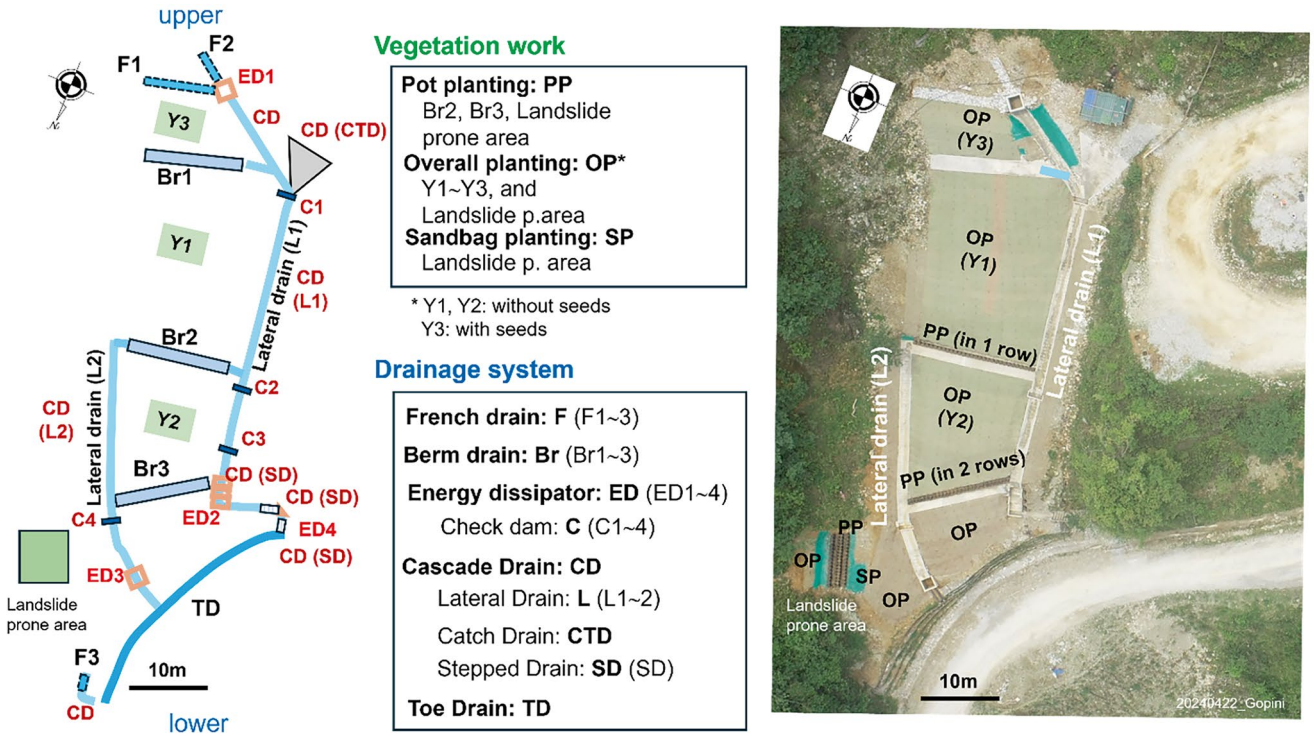

Fig. 15 Layout of drains (left), overhead view of the completed drainage system (right)

Fig. 16 Plants and seeds used in the bioengineering work ((**a**) *Brachiaria ruziziensis*, (**b**) *Catharanthus roseus*, (**c**) *Tradescantia spathacea*)

composition of these drainage systems include cement, sand, aggregate cobblestone, and a 12 mm reinforcement bar. The mixing ratio is 1:3:6 (M10), which consists of 1%, 3%, and 6%, with water constituting 1–2% of the mixture.

4.2.1 French Drain (F)

A French drain is a subsurface drainage system designed to drain shallow groundwater and prevent it from seeping from the shallow to deeper soil layers (Figs. 17 and 18).

The perforated pipe is 110 mm in diameter and is made of High-density polyethylene (HDPE) tube (Fig. 19).

4.2.2 Cascade Drain (CD)

A cascade drain is a longitudinal drainage system that allows water to flow downhill along slopes, featuring structures designed to reduce energy. When cascade drains extend over long distances on both sides of a slope, they are called lateral drains (L1, L2). In this teaching tool article, the cascade drain consists of a catch drain (CTD) and a stepped drain (SD) based on these designs (Fig. 20). Their purposes remain identical. The Cascade and Catch drains have horizontal ribs with cobblestones spaced nearly uniformly on the drainage surface, while the Stepped drain has concrete steps.

4.2.3 Berm Drain (Br)

Berm drains are systems designed to collect and redirect water from the ground. They are also referred to as curtain drains. Berm drains were installed at three locations on the Gopini slope (Figs. 21, 22, 23, 24, and 25). Berm drain Br.2 has a single row of pot planting (Fig. 22b), while Berm drain Br.3 has two rows of pot planting (Fig. 22c) on the mountainside.

4.2.4 Energy Dissipator (ED)

The energy dissipator includes boxes (catch basins), check dams (C), and Stepped drains (SD), which are cascade drains.

Check Dam (C)

Check dams are commonly built to mitigate the impact of debris flows; however, at the Gopini location, the authors designed small concrete check dams (C1–C4, Fig. 26) along cascade drains (lateral drains: L1, L2) to dissipate the energy of drained water flowing along the lateral drains. The Bhutanese "Soil Conservation Manual" presents the use of small stone and log check dams to prevent surface erosion (National Soil Service Centre 2019).

Box (Catch Basin)

There are two box-shaped energy dissipators: the first one (ED1, Fig. 27) is at the top of the slope where the water from the French drain converges (F1, F2), while the second one (ED3) is at the bottom of the lateral drain (Cascade Drain) L2.

The energy dissipator was installed at the end of the Lateral drain (L2). Water runs through two pipes (HDPE110) across the top gabion to the toe drain (Fig. 28). During the design phase, gravel was planned to be placed inside the box; however, for ease of post-construction maintenance, the decision was made not to use gravel.

Stepped Drain (SD)

Stepped drains fall under the category of Cascade drains. Nonetheless, this section will refer to them as "Energy dissipators (ED)" because they possess superior energy dissipation abilities and are recognized as energy dissipators at the Gopini site. Energy dissipator ED2 is linked to a stepped

Table 1 List of drainage systems

Drainage system	Type	Ingredient, etc.	Note
French drain	Culvert: French drain	Gravel (50–75, 75–100), geo-textile (non-woven fabric), perforated pipe as high-density polyethylene (hereafter HDPE) tube*2 with diameter 110 mm	Two above and one below *2 Length, 6000 mm/pcs
Cascade drain	Open ditch: Cascade drain, catch drain, stepped drain	Materials and composition of drainage system are used with cement, sand, aggregate cobble stone and reinforcing bar (deformed steel bar) of 12 dia. (D12). Ratio is 1:3:6 (M10*3) (1 cement 3 sand and 6 aggregate) 1–2% of water	*1: Names in parentheses are synonymous *3: Indian standard 1062 (2009), compressive strength 10 MPa (=N/mm^2), pebble cobble stones on the top of cascade drain
Berm drain	Open ditch: Berm drain (curtain drain)		
Energy dissipator (energy reducer, sump)*1	Check dam, box (catch basin), (stepped drain)		
Toe drain	Road gutter covered with flat stones	Flatten stone on the top, mortal, 5 mm sieving sand, deformed steel bar D12	

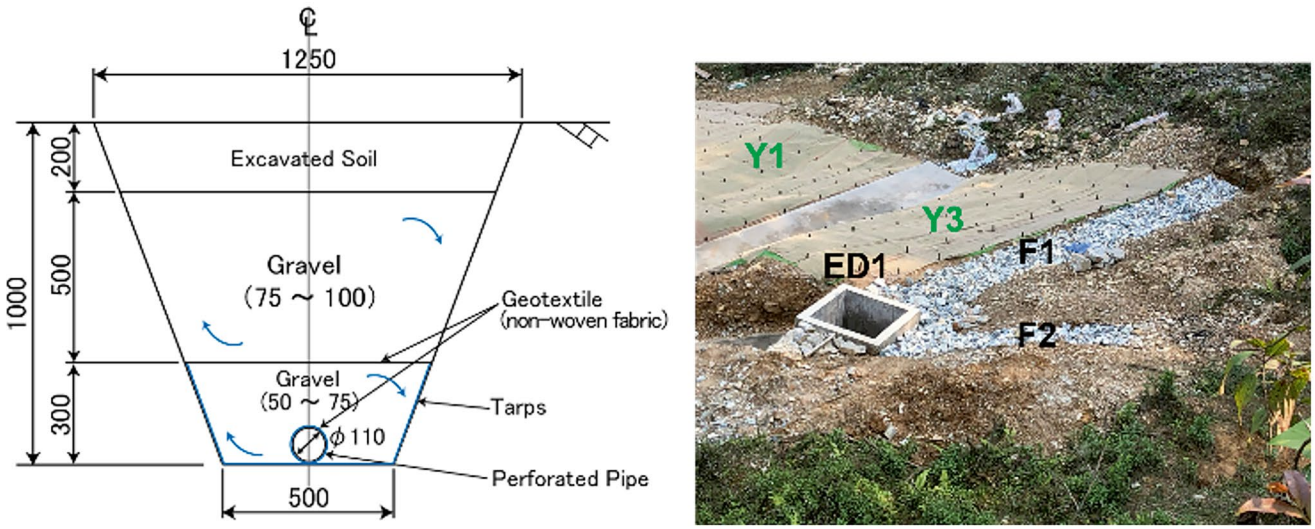

Fig. 17 A French drainage F1 (l = 9.1 m), F2 (l = 4.0 m) (left: cross-section: right: Bird's-Eye view of the French drains) drain)

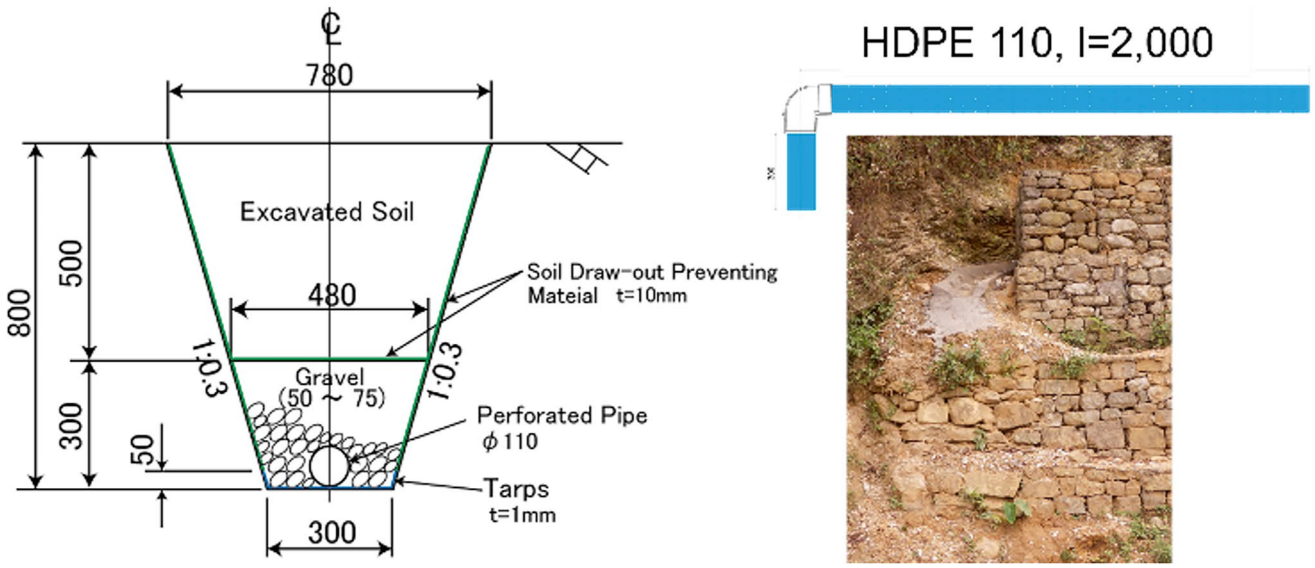

Fig. 18 French drain F3 (l = 2.0 m) (cross-section)

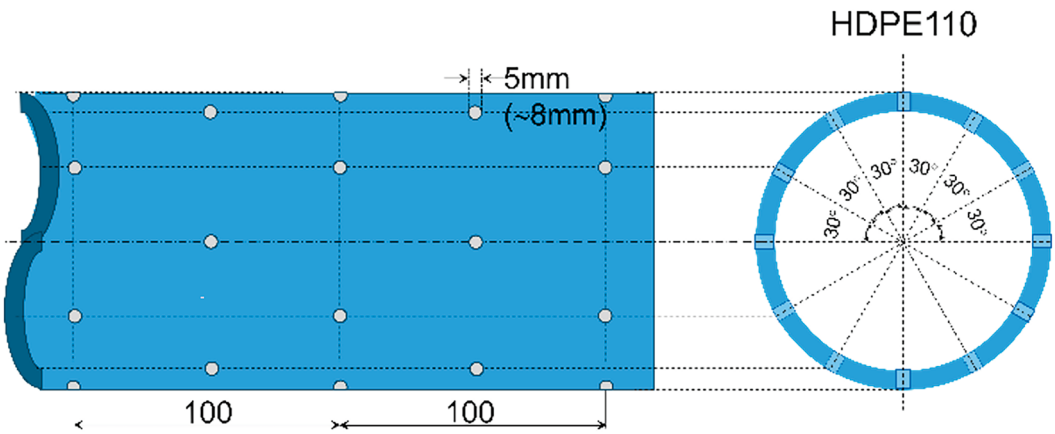

Fig. 19 Perforated pipe for the French drain (cross section)

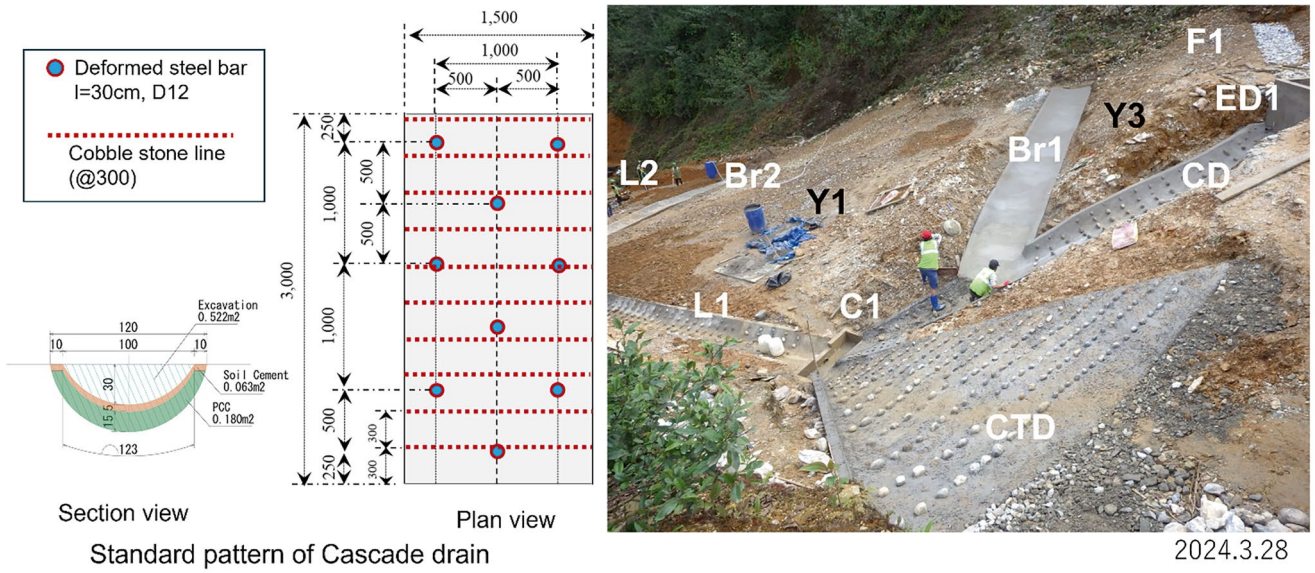

Fig. 20 Cascade drains. *CTD* catch drain, *CD* cascade drain, *ED* energy dissipator, *F* French drain, *Br* Berm drain

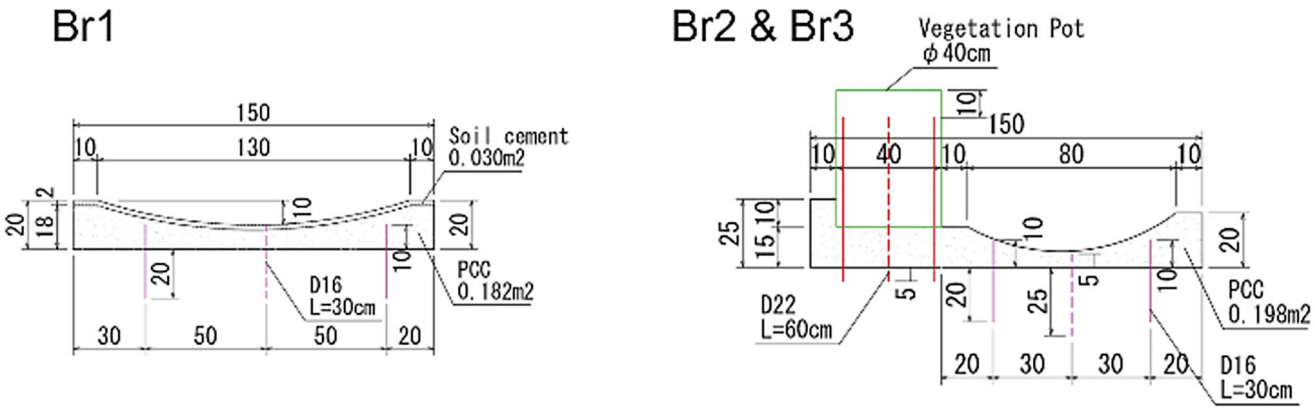

Fig. 21 Berm drains (cross-section)

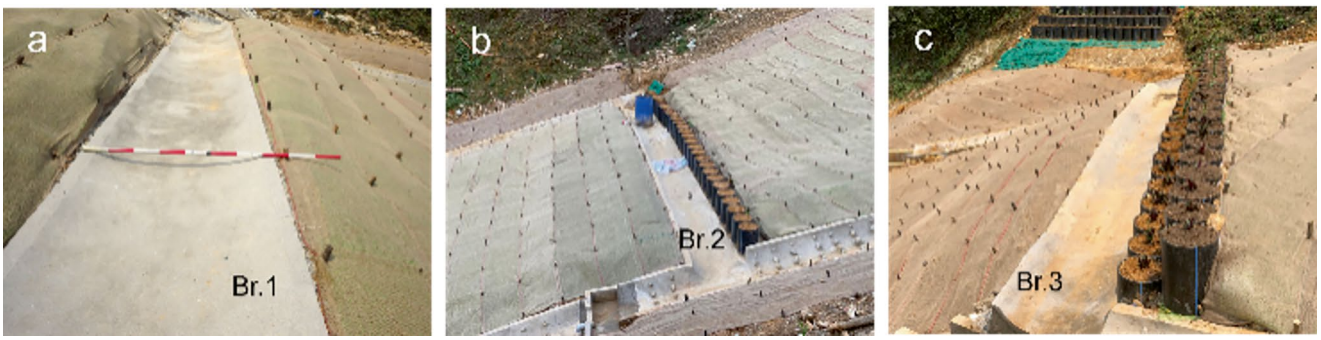

Fig. 22 Berm drains ((**a**) Br 1, (**b**) Br 2, (**c**) Br 3)

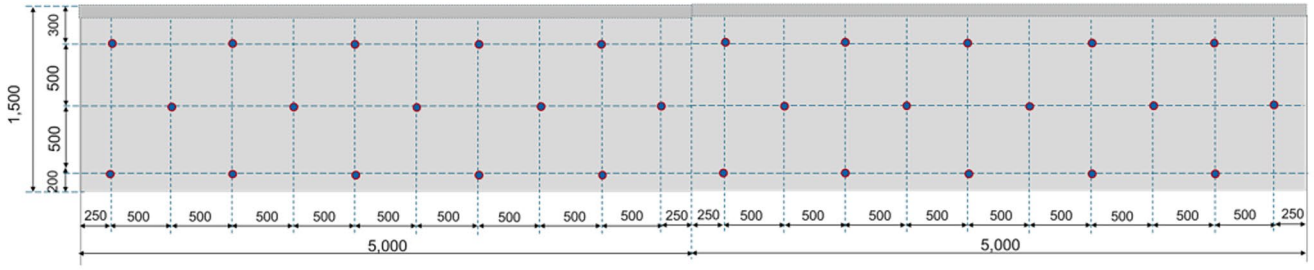

Fig. 23 Berm drain, Br 1 (dots show deformed steel bars, D16-L = 30 cm)

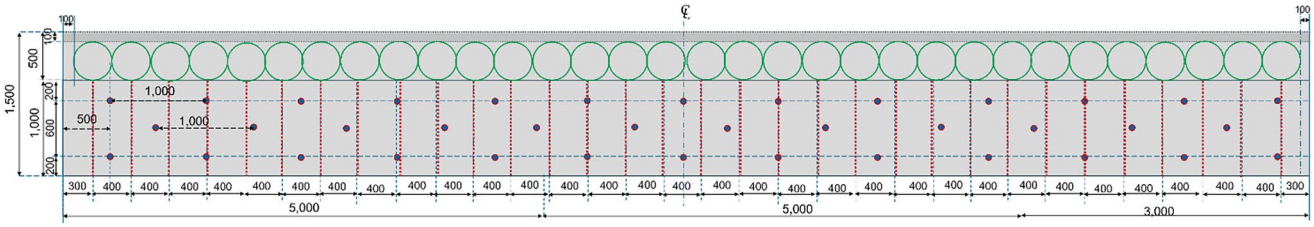

Fig. 24 Berm drain, Br 2 (dots show deformed steel bars, D16-L = 30 cm, green colored circle: vegetation

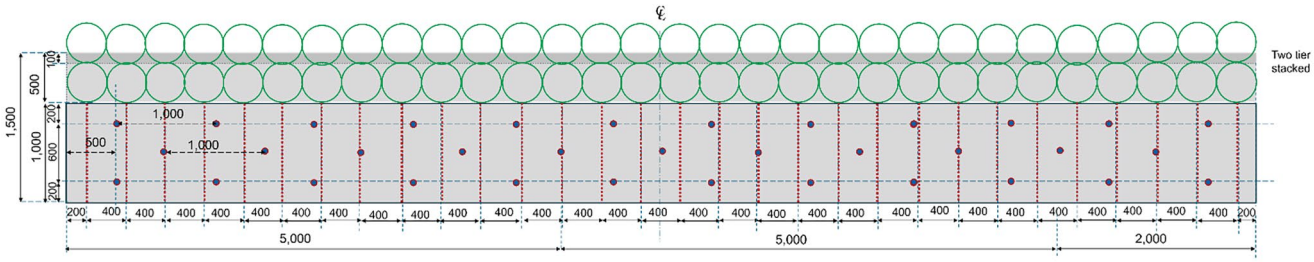

Fig. 25 Berm drain, Br 3 (dots show deformed steel bars, D16-L = 30 cm, green colored circle: vegetation pots)

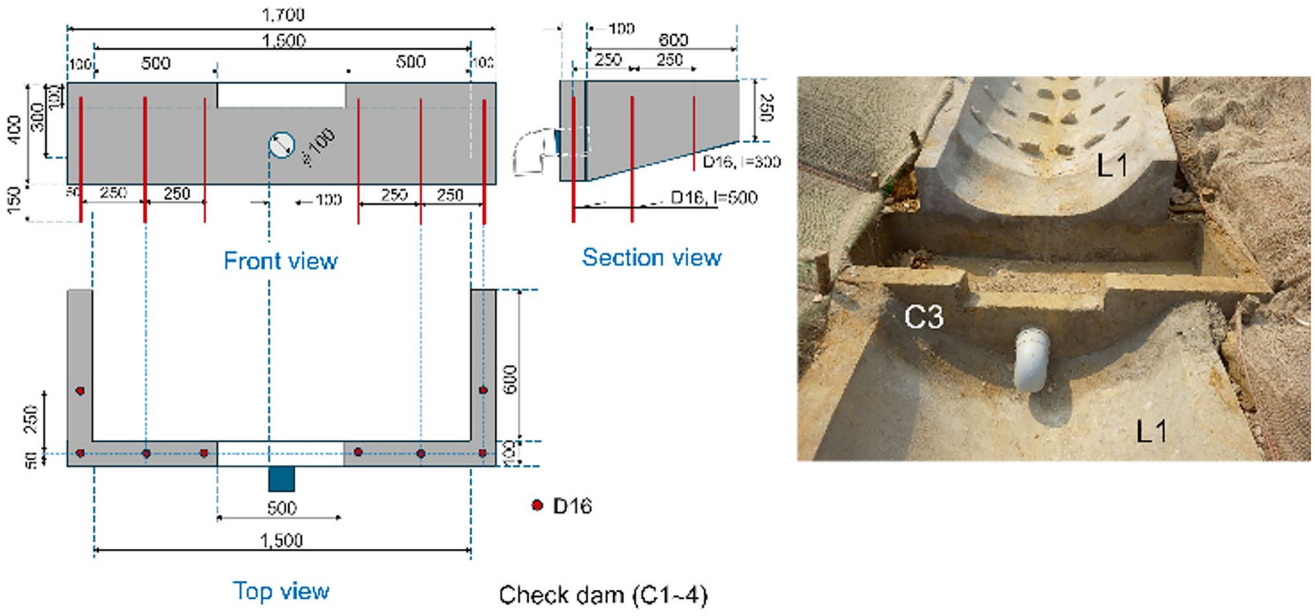

Fig. 26 Check dam (left: design, right: photo of check dam C3 on the lateral drain L1)

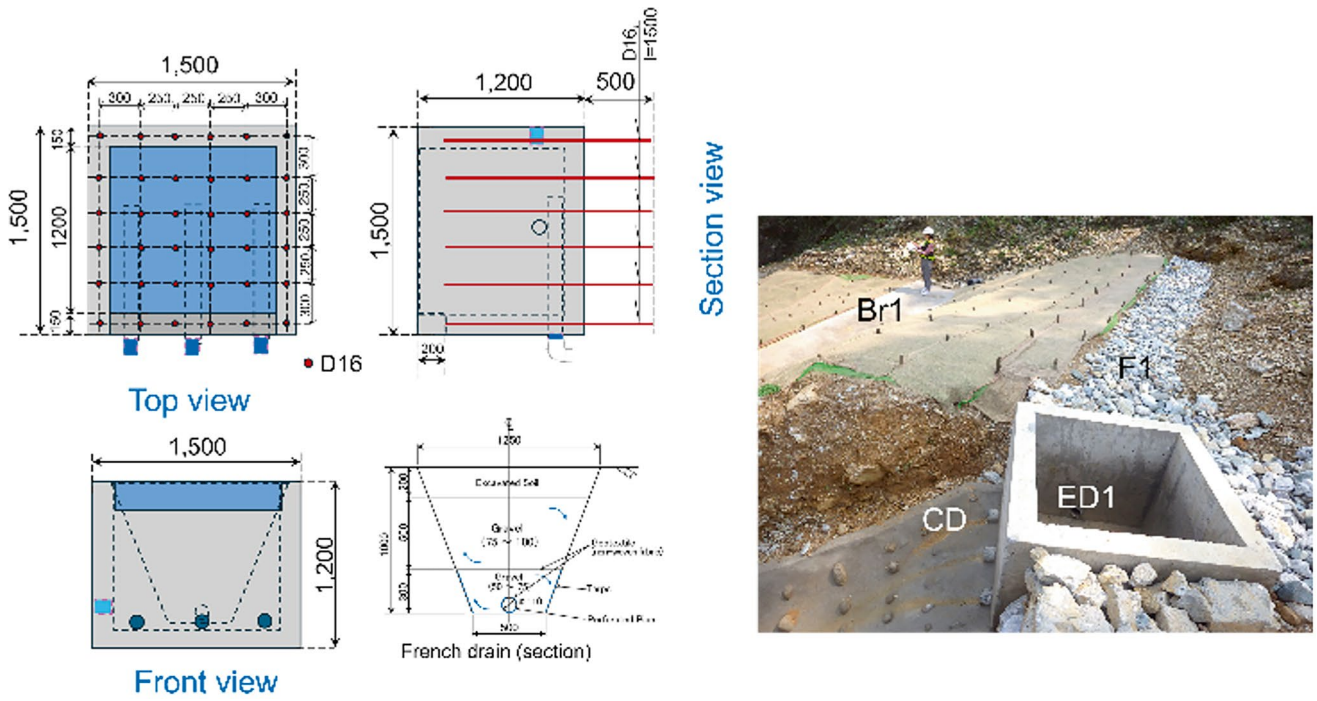

Fig. 27 Energy dissipator ED1 (1500 × 1500, Thickness: 15–16 cm)

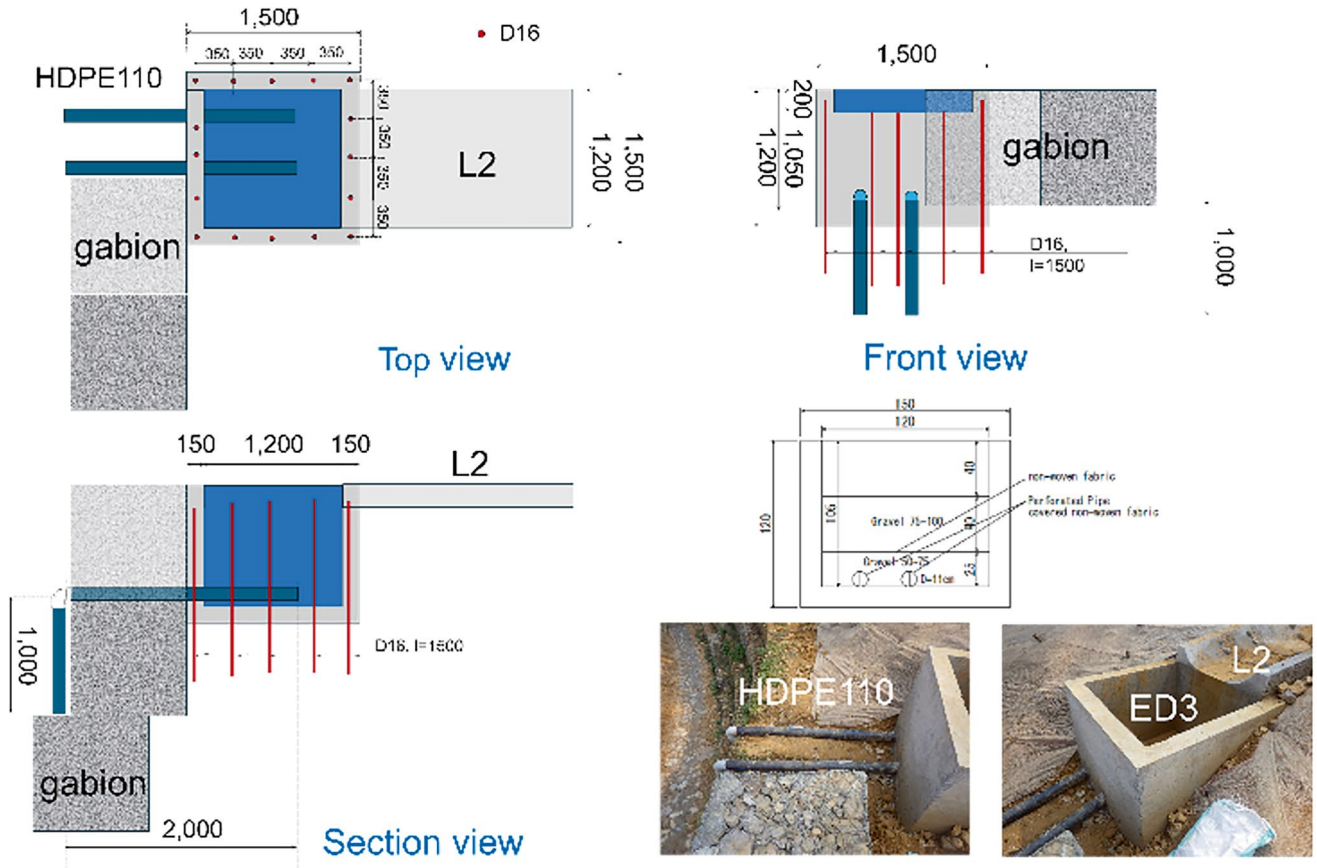

Fig. 28 Energy dissipator (ED3), box-type (1500 × 1500)

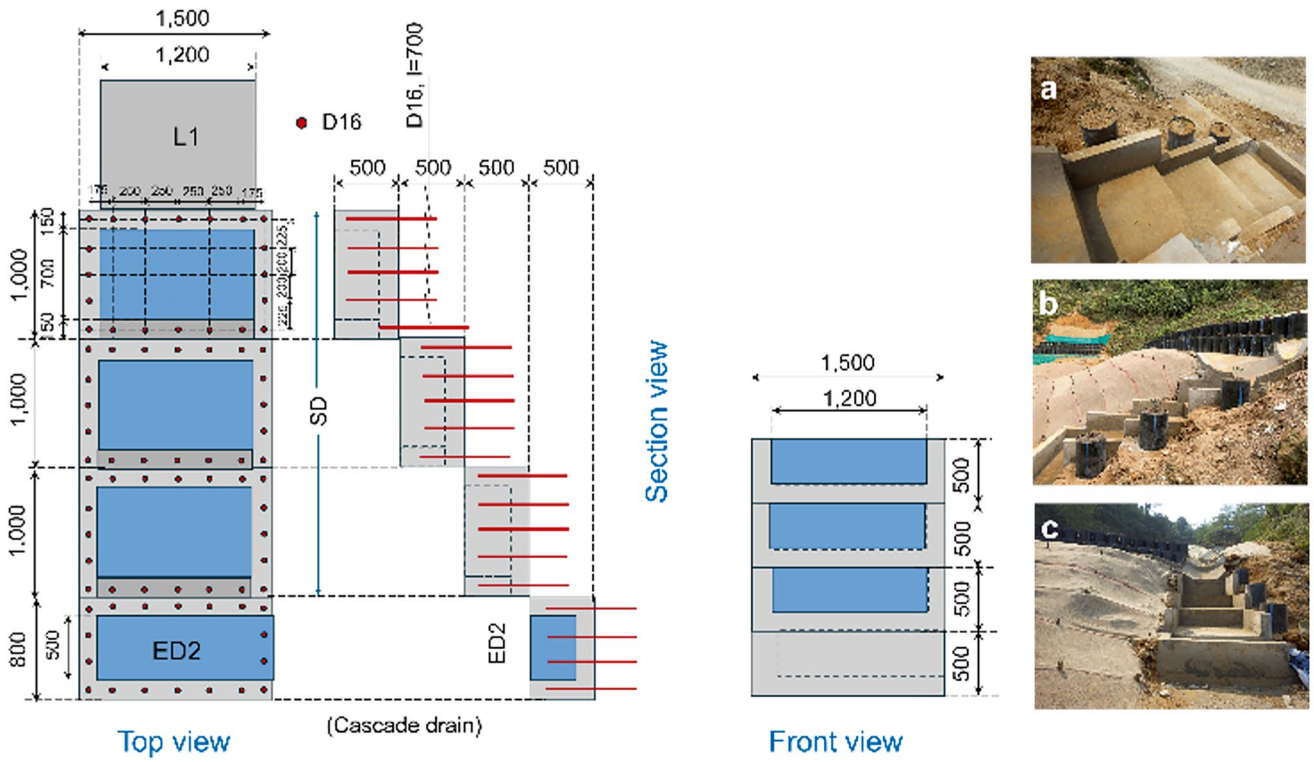

Fig. 29 Stepped drain at foot ((**a**) top view, (**b**) section view, (**c**) front view, *ED* energy dissipator, *SD* stepped drain)

drain (U-shaped type cascade drain), which alters the direction of flowing water (Fig. 29), allowing the water to flow through the lower stepped drain and arrive at the toe drain.

The Energy dissipator ED4 was initially designed as a square landing for the step drain but was altered to a triangular configuration to accommodate the site conditions (Figs. 30 and 31). Additionally, the number of stepped drains below the Energy dissipator was adjusted to align with the local conditions.

The drainage system extends from the upper Cascade drain and links to the toe drain, functioning as a roadside gutter. Surface water is redirected away (Fig. 32).

Toe Drain (TD)

The toe drain is a road gutter featuring a flat stone surface. It is built using a sequence of overlapping materials arranged from bottom top: non-woven fabric, crusher-run c40, nylon netting, mortar, and flat stones (Fig. 33). To construct the road gutter; excavation is performed near the slope's toe followed by the placement of non-woven fabric, which is then topped with crusher-run c40. Nylon netting is secured using D12 rebar, after which mortar is applied, and finally, flat stones are laid on top.

This road gutter was chosen for two reasons: (1) The drainage system is easy to maintain, and (2) It allows for the straightforward installation of new gabions over the current ones. If there are indications that the existing gabions are shifting, new gabions can be placed beside them to prevent shallow mass movement. During the construction of gabions on the toe drain, two rows of HDPE110 pipe can be laid longitudinally. After the new gabions are installed, the original road gutter retains its drainage capabilities.

4.3 Bioengineering as Vegetation Work

The types of vegetation work covered in Bioengineering are pot planting, spread planting, and sandbag planting (Table 2).

4.3.1 Pot Planting

Objective Flowers can be planted by installing pots, which help inhibit soil movement in the upper layer. The vegetation pots used for bioengineering are 40 mm-in-diameter HDPE pipes produced by Bhutan Polythene Company Ltd. in Phuentsholing, Bhutan. To implement this in areas where gabions are not feasible, we incorporated three deformed steel bars (D20) within the pot to resist earth pressure. Furthermore, the pot put on the berm drain (Br2, 3) prevents the displacement of shallow soil and sustains the vegetation.

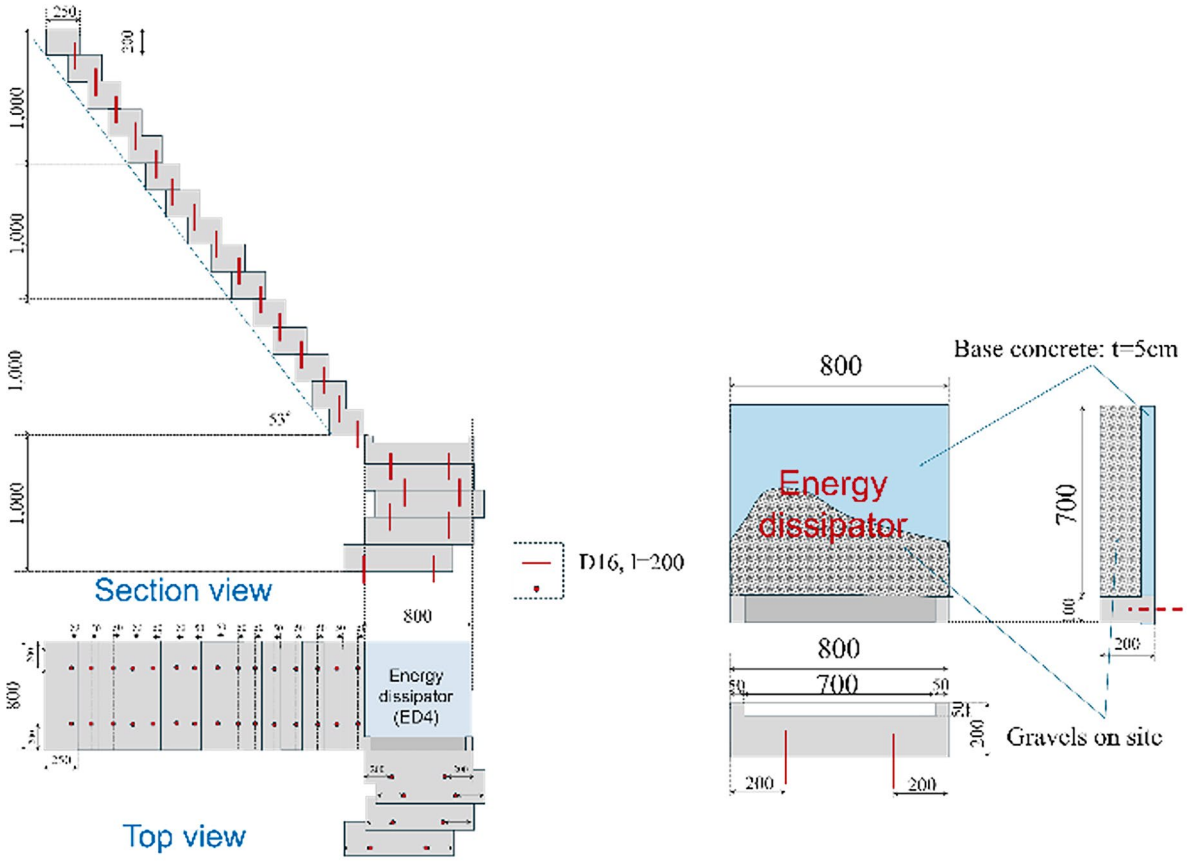

Fig. 30 Stepped drain with energy dissipator ED4

Fig. 31 Cascade drains under construction ((**a**) stepped drain, (**b**) cascade drain leading to the toe drain)

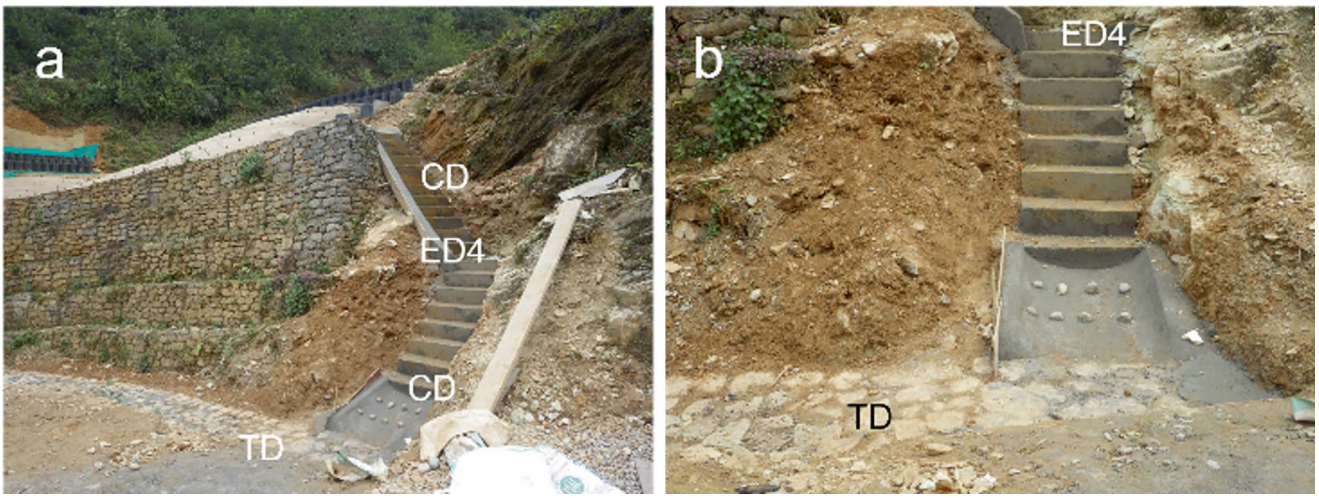

Fig. 32 Cascade drains under construction ((**a**) cascade drain leading to toe drain, (**b**) close-up view. *ED* energy)

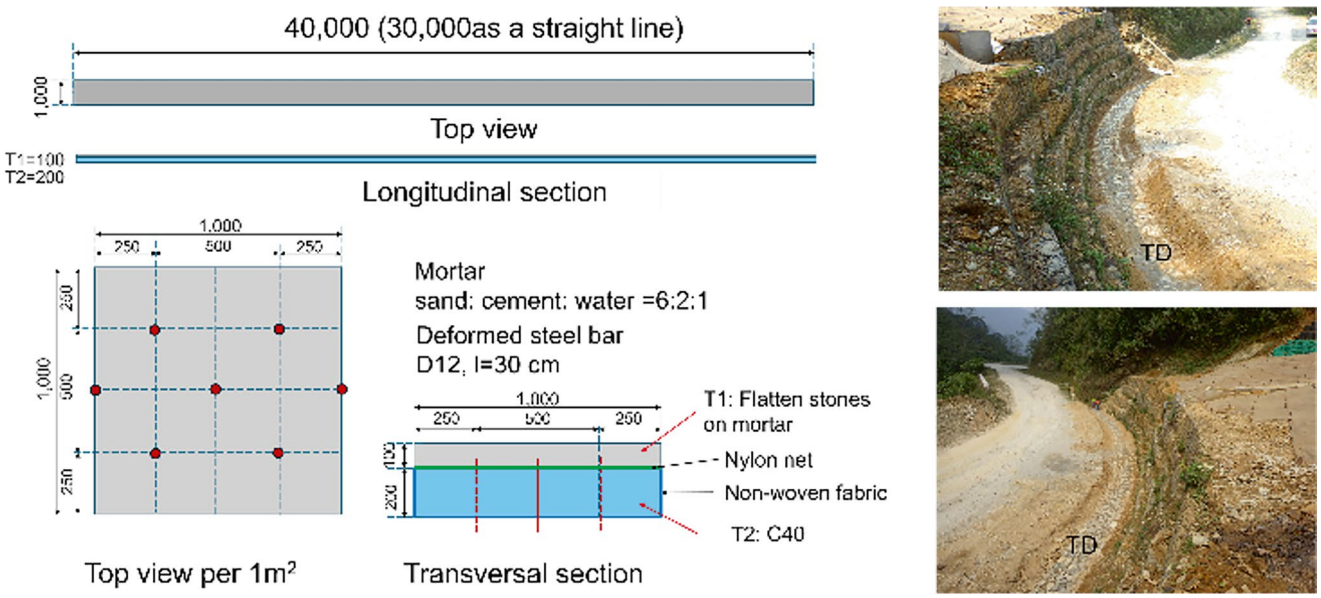

Fig. 33 Toe drain (left: design, right: photo, *TD* toe drain)

Table 2 List of bioengineering works (vegetation works)

Type	Materials used	Contents	Memo
Pot planting	Vegetation pot	Using HDPE tube (6000 mm-length, 400 mm dia., t = 5 mm) Pot: 400 mm dia., 500 mm height, deformed bar D20 (l = 600 mm): three pieces/pot	Plants: Madagascar periwinkle (*Catharanthus roseus* L.), Boat Lily (*Tradescantia spathacea*)
Spread planting	Laminated sheet	Plastic mesh net (opening 10 mm), Jute net (op. 5 mm)	Structure is which plastic mesh net sandwiched between jute nets (Fig. 41) Seeds: Ruzi grass (*Brachiaria ruziziensis*)
Sandbag planting	Seeds bag	Double bag: plastic mesh bag (outer) and jute sac (inner). Size: 30 × 50 × 10 cm	Seeds: Ruzi grass *(Brachiaria ruziziensis*)

The Vegetation Pot comprises a Tube/Pipe (40 cm diameter, l = 50 cm), deformed steel bars (D20, l = 60 cm, three pieces), non-woven fabric, gravel (40–100 mm), sand (5 mm), and soil (Fig. 34).

Pots Arrangement

The fundamental setup of pots is in a single line (Fig. 35). For a dual-row configuration, either standard (Fig. 36a) or half-diameter-staggered (Fig. 36b) spacing of parallel pot lines can be chosen.

To mitigate vertical earth pressure from thick soil, opt for a multi-tier arrangement, stacking parallel pot lines in tiers one atop the other in a standard (Fig. 37a) or half-diameter-staggered fashion (Fig. 37b). In both cases, the vegetative area will be reduced. A lengthy 6.0 m HDPE pipe is sliced into 50 cm sections (pots) at a processing factory.

Figure 38 shows the tube being cut for site preparation. The initial plan was to work with a 50 cm diameter pipe. Nevertheless, the largest HDPE tube available in Bhutan measured 40 cm in diameter and 6.0 m in length. As a result, it was sliced into 50 cm-long sections to serve as pots for vegetation.

Figure 39a, b show the layout of pots for planting flowers, while Fig. 39c demonstrates how to prepare each vegetation pot. The bottom of the pot is lined with non-woven fabric.

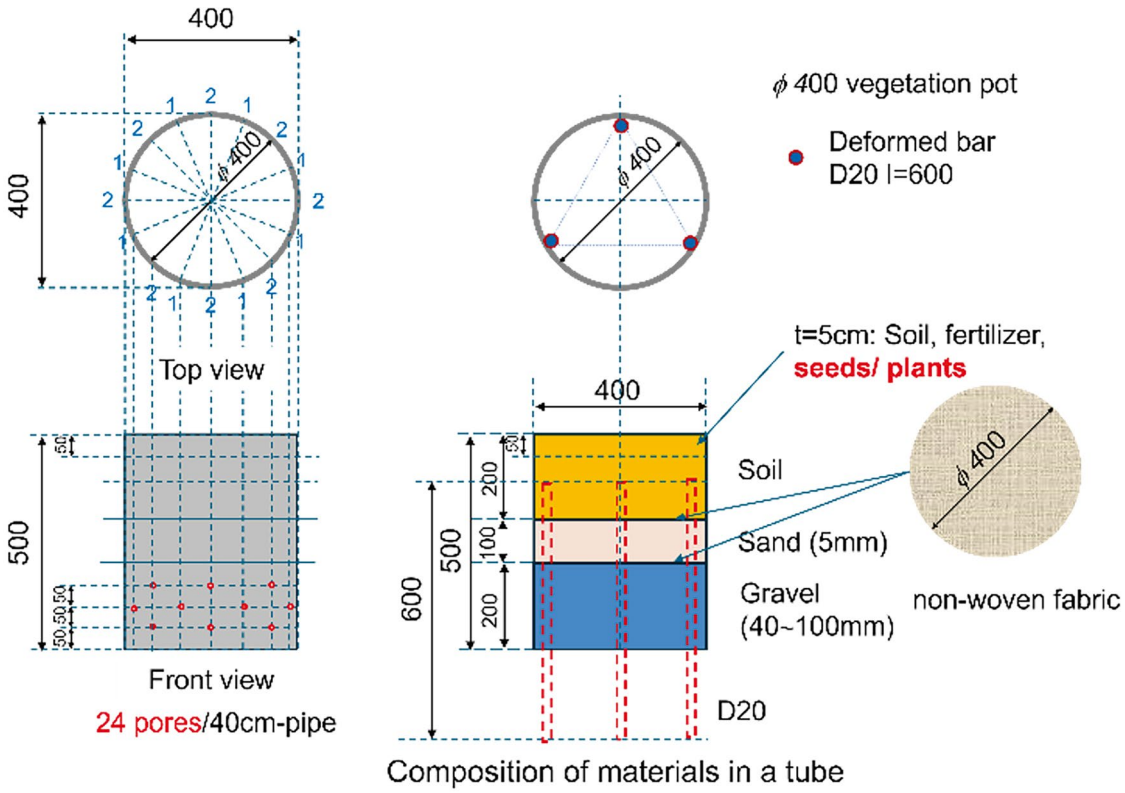

Fig. 34 Vegetation pot

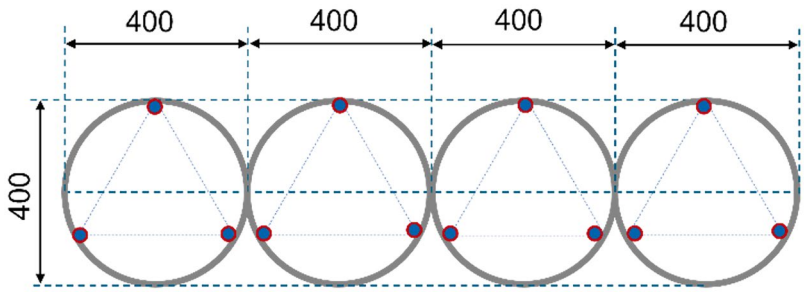

Fig. 35 Single-row arrangement of vegetation pots

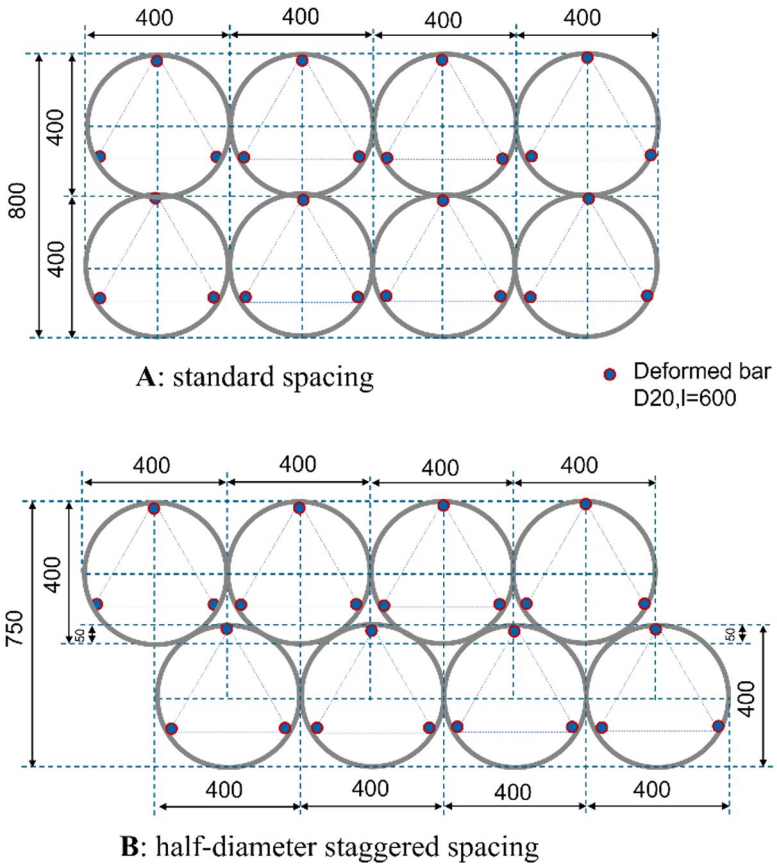

Fig. 36 Two rows arrangement of vegetation pots ((**a**) standard spacing, (**b**) half-diameter-staggered spacing)

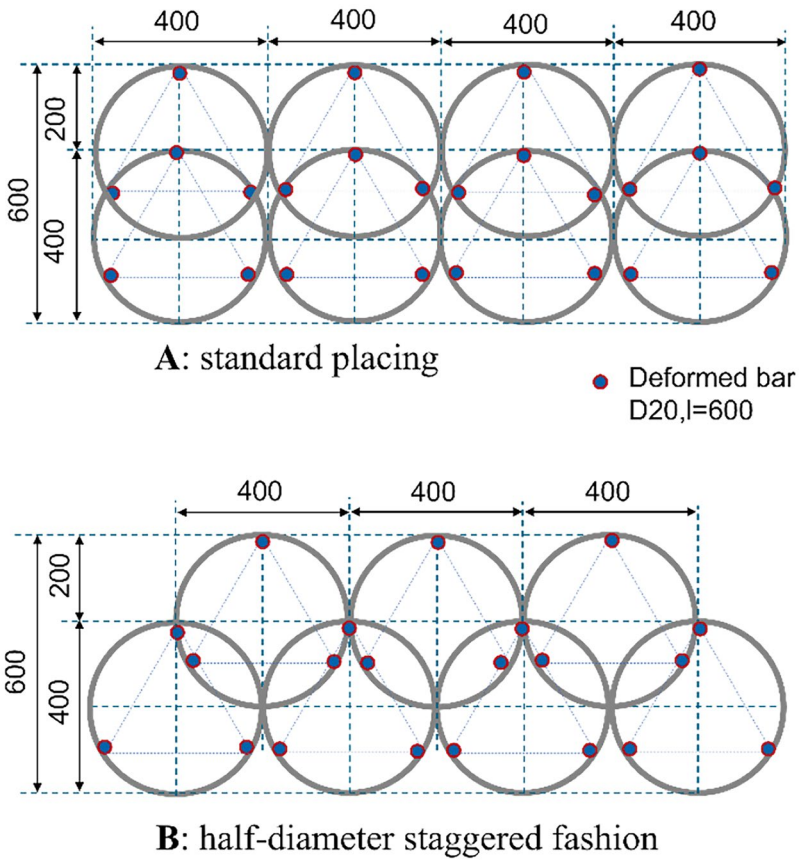

Fig. 37 Multilayer placing: pot lines stacked in tiers one atop the other in an (**a**) standard and (**b**) half-diameter-staggered fashion

Fig. 38 Preparation of vegetation pots ((**a**) Cutting machine, (**b**, **c**) vegetation pots, (**d**, **e**) HDPE tube)

Applied 'Pot Planting'

The third test location in Gopini did not use another pot planting. Yet, the authors optimized the material composition used in the pots (Fig. 40): The authors considered the following aspects: Pot planting would be incorporated into this teaching tool article, as it is deemed valid, for instance, in the fortification and restoration of road edges. Additionally, flowers can be cultivated. The pot structures were initially meant to be placed in the landslide-sensitive region of the Gopini slope and planted with grass instead of flowers. When installed on the shoulder of a road, the deformed steel bar inside the pot should be 80 cm long, and half of that, 40 cm, should be inserted into the ground. The arrangement and size of steel bars can change based on how they are piled on slopes. When pot lines are stacked up in tiers, one atop the other in a half-diameter-staggered fashion (Fig. 37b), the steel bars can be diagonally arranged to connect the stacked pot lines; thus, the bars function as reinforcement. This method is more economical and easier to handle than gabions. Each pot has 24 holes drilled in it, so there is no need to worry about drainage. In addition, the stacked structure of these pots is much lighter than gabions and can be placed directly on road shoulders.

4.3.2 Spread Planting

Spread planting consists of two categories: laminate sheets containing seeds and laminate sheets without seeds.

Objective Natural vegetation is anticipated to establish itself on the slope's shoulder to mitigate erosion and capture soil along with airborne seeds on the surface of the clastic rock slope.

Creating Laminate Sheet

Materials: Jute net, plastic mesh net, Fastener/ stopper (ex: wood stakes).

Procedure: Create a 3-layer laminate sheet with a plastic mesh net sandwiched between Jute nets. These are installed

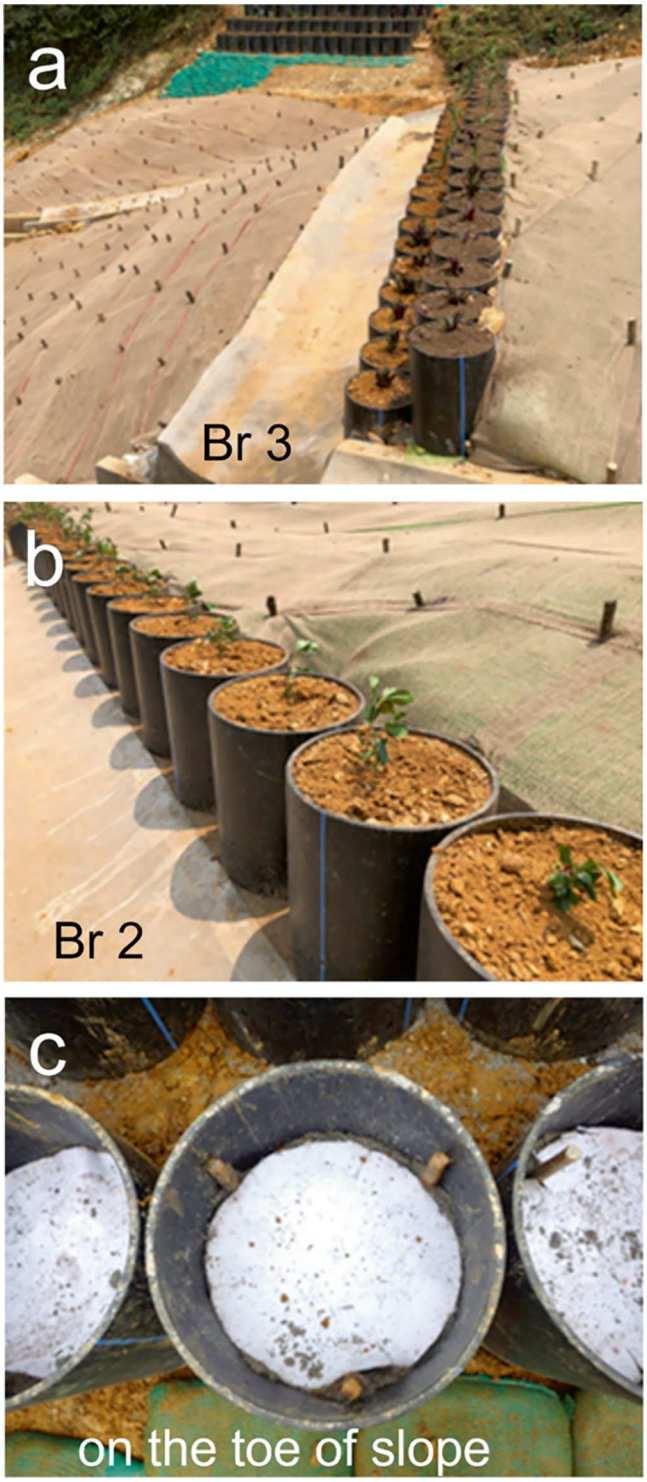

Fig. 39 Vegetation works with pots ((**a**) pots on Br 3, (**b**) pots on Br 2, (**c**) inside the pots on the toe of slope)

in areas prone to collapse, such as the shoulders of slopes, to prevent erosion and collapse.

Laminate sheet: The laminate sheet is composed of a plastic mesh net that measures 15 meters in length and 1 meter in width, with mesh openings of 12 × 12 mm, along with a jute net that is 15 m long and 1 m wide. To install the laminate sheet, start by placing the jute net, then the plastic net on top, and finally, cover it with another jute net (creating a sandwich). For added stability, a wooden pick should be inserted. This product was produced in India. The laminated sheet features a three-layer design, with a plastic mesh net between two jute nets (see Fig. 41).

In the Yard

The spread planting approach utilized laminate sheets in yards Y1 to Y3 and landslide-prone locations. In other regions, only plastic mesh nets (shown in Fig. 42a, greenish area) or jute nets (like the lower portion of the slope in Fig. 42b) were applied as protective covers. These coverings prevent erosion on the slope's surface, allowing plants to invade and gradually establish roots in the surrounding area.

4.3.3 Sandbag Planting

Objective Avert landslides and support soil retention to allow for vegetation growth.

The sandbag utilized for sandbag planting consists of a jute sack lined on the inside and a plastic mesh sack on the outside. Figure 43 illustrates sandbags containing seeds stacked in an area susceptible to landslides. Figure 43b shows some signs of germination.

Figure 44 shows a cross section of vegetation work in the landslide prone area. From the bottom, there is sandbag planting, pot planting, and overall planting.

5 Results and Discussion

The drainage system (Fig. 45) was constructed half a year ago and operates effectively with robust vegetation growth.

1. The drainage system's configuration ensures that the outlets from the cascade drain's lateral drains (L1 and L2) do not discharge into the gabions' bulging regions.

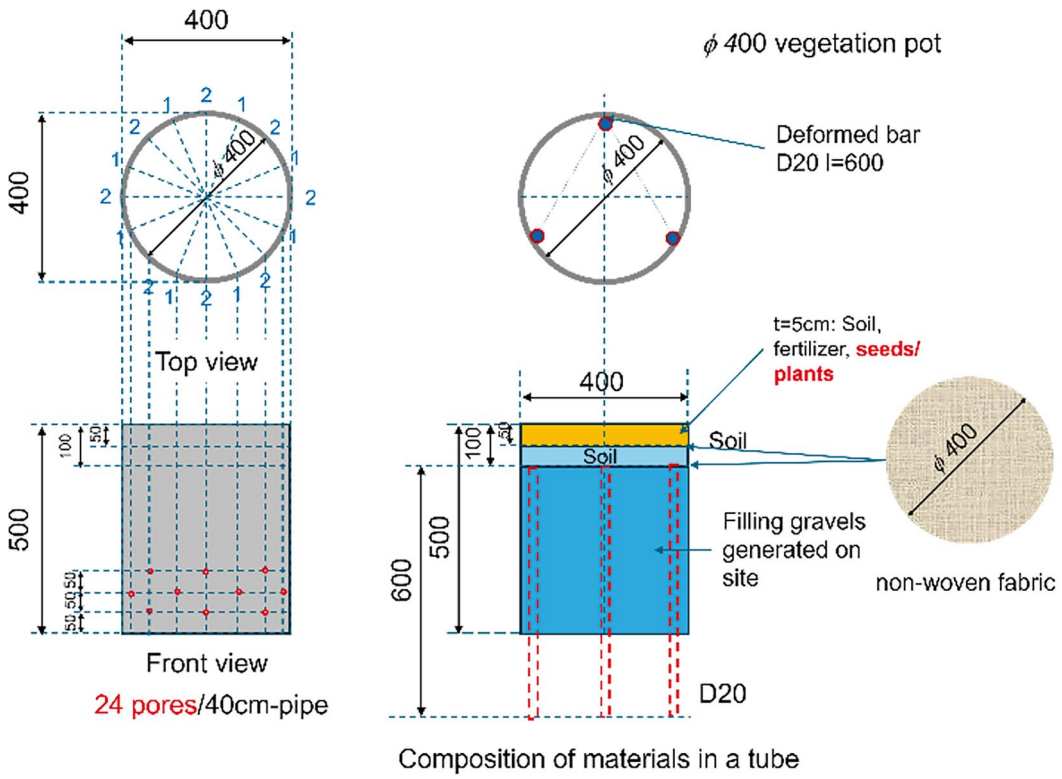

Fig. 40 Simplified pot structure

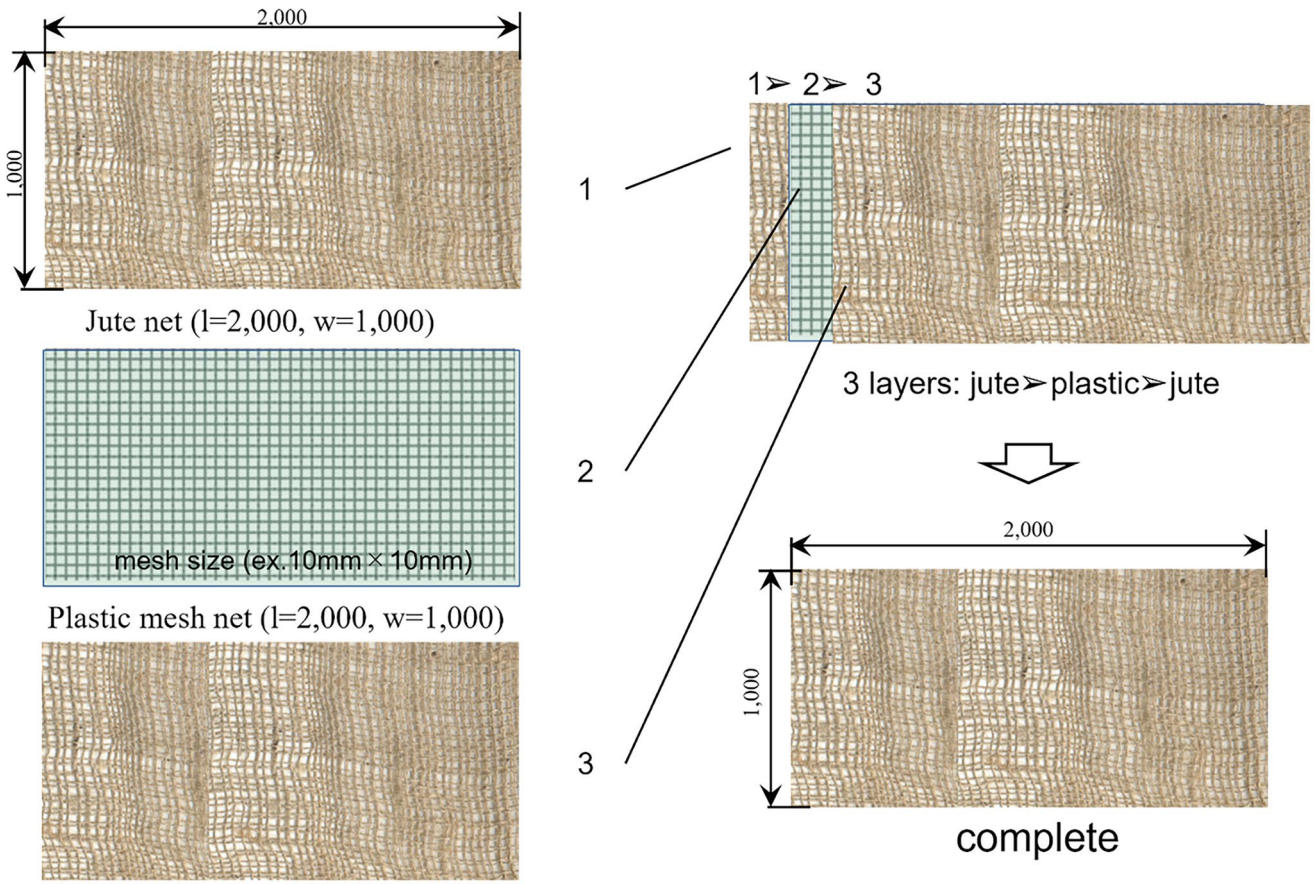

Fig. 41 Composition of the laminate sheet

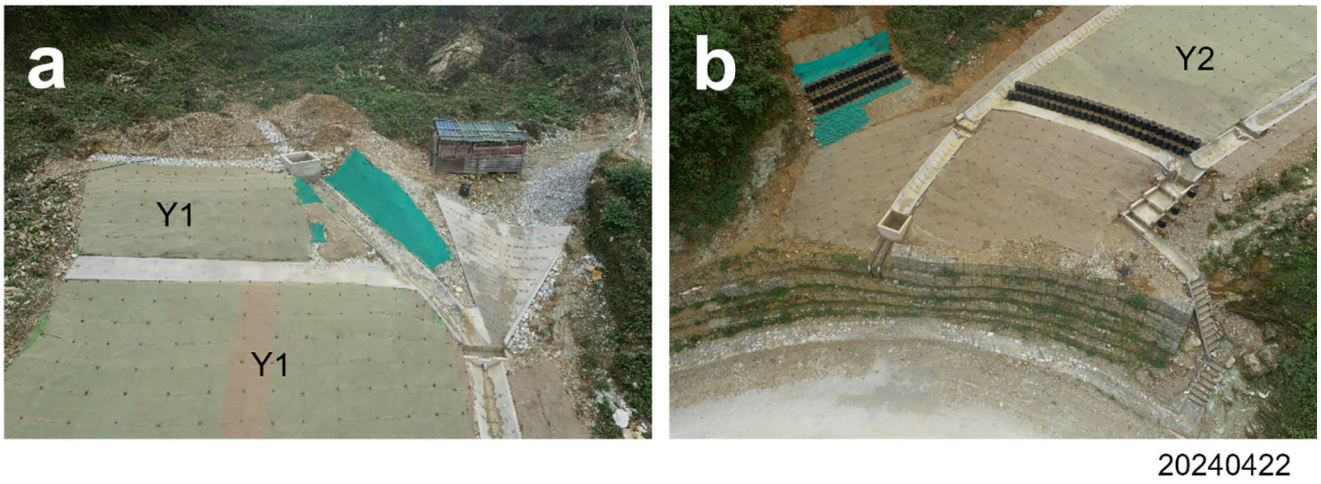

Fig. 42 Spread planting (Y: Yard, Y1–Y2 without seeds, Y3 with seeds; (**a**) Y1 to Y3, (**b**) Y2, landslide prone area

Fig. 43 Sandbag planting ((**a**) materials, (**b**) piled seeds bags, (**c**) sandbag layout)

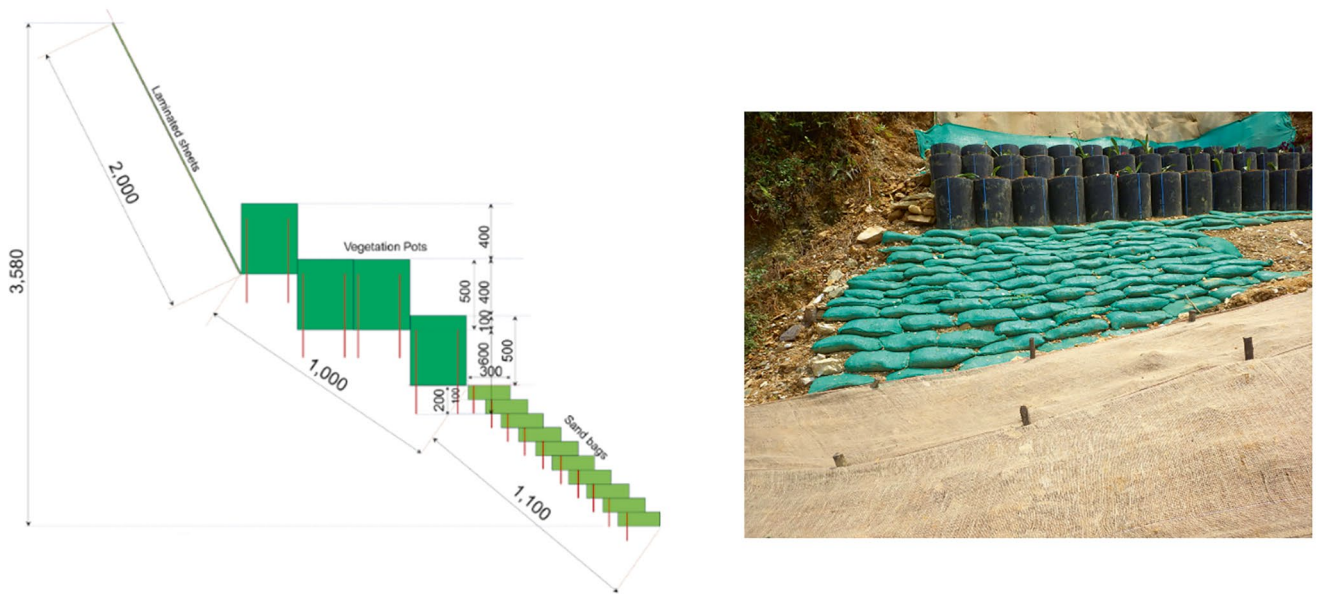

Fig. 44 Vegetation works at the landslide prone area (left: sandbag planting colored light green, right: spread planting, pot planting, sandbag planting from toe)

Fig. 45 Overhead view of the vegetation work

2. Utilizing flat stones for the road gutter enables the addition of gabions as measures against the preset gabions without the need to build a new road gutter. This feature facilitates the rapid installation of new gabions when signs of mass movement are observed on the preset gabions.
3. The Gopini site showcases accomplishments in bioengineering. The outcomes of the vegetation efforts were positive across all three methods: spread planting, pot planting, and sandbag planting.

The results and discussion are as follows.

Spread Planting Spread planting has been integrated into the layout for Yard 1 through Yard 3 (Fig. 46), while the leftover uncovered land from other shaping works has been secured with nets. The vegetation has been established, so no erosion occurs on the ground's surface.In areas such as Gopini, using vegetation-inducing laminate sheets to cover the slopes is likely an efficient strategy.Pot Planting The pot planting was carried out behind the two berm drains, Br.2 and Br.3, as well as in the area susceptible to landslides, ensuring that earth pressure above the berm drains was effectively managed. After the construction, the vegetation is thriving. Flowers bloomed on October 10, 2024 (Fig. 47c, Madagascar periwinkle).

Flower seedlings have taken root in each pot; however, weeds are also beginning to emerge. If the primary objective is to promote greening, the overgrowth of vegetation is not an issue. Nevertheless, maintenance tasks such as weeding and replanting will be necessary if the landscape holds significance. It is anticipated that similar maintenance will be conducted in other vegetation zones.

Sandbag Planting Planting with sandbags was implemented in an area at risk for landslides. Half a year following the completion on April 21, 2024, the vegetation flourishes as of October 10, 2024 (Fig. 48b).Sandbag planting at the base of a slope following a small landslide is an excellent construction method, as it not only promotes vegetation but also stabilizes the slope.

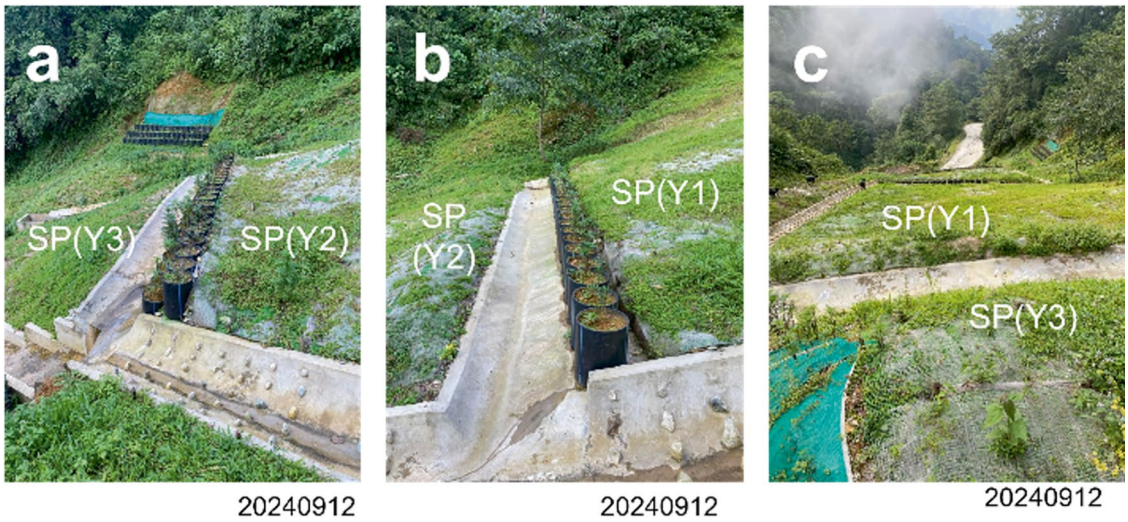

Fig. 46 Completed vegetation works (*SP* spread planting, *Y* yard)

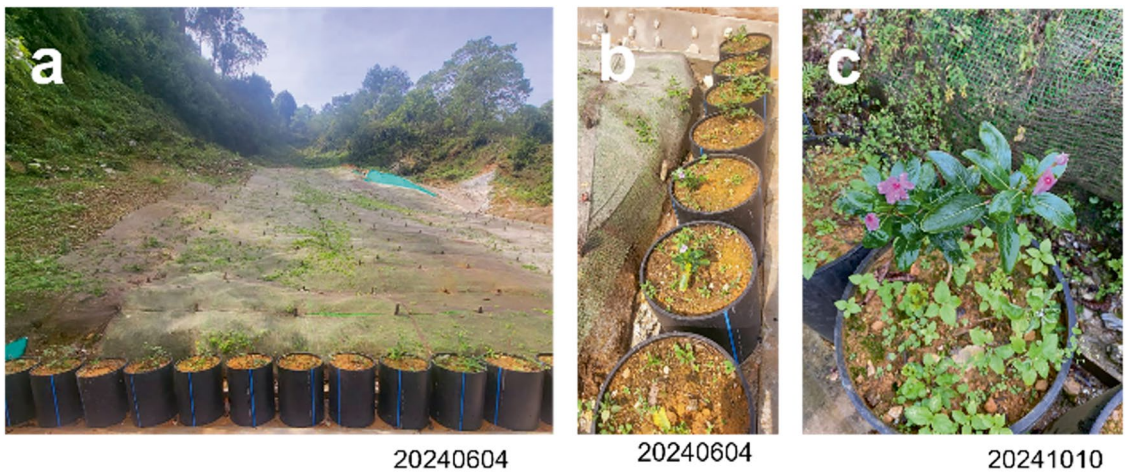

Fig. 47 Completed vegetation works. (**a**) Pot planting: View from the bottom of the slope, (**b**) Pot planting rows, (**c**) Madagascar periwinkle in bloom)

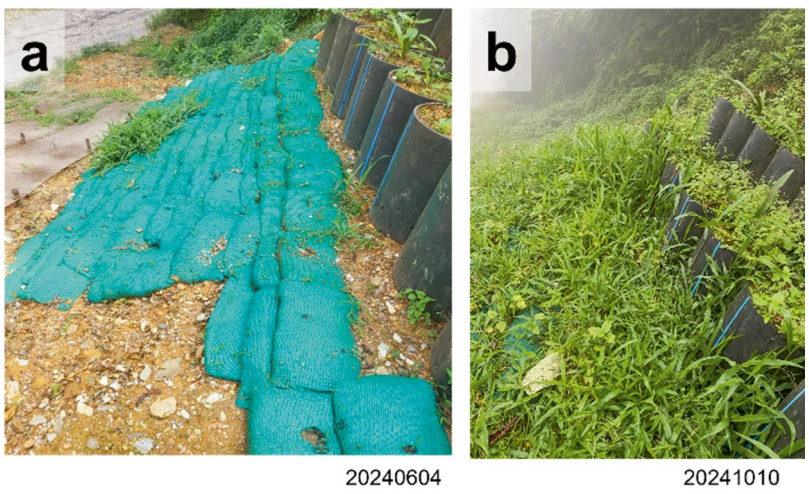

Fig. 48 Completed pot plantings. (**a**) Sandbag planting installation status, (**b**) Sandbag planting germination status

Acknowledgments At the Gopini vegetation work test site, the DoST Headquarters and the Phuentsholing R.O. of DoST cooperated with us from planning to implementation. We would like to thank the following engineers: Mr. Thinley Wangchuk, who operated the drone and took photos at the site; Mr. Lotay Tenzin of the Maintenance Division of DOST, who consulted with us at the planning stage; Mr. Tanka Bdr., Powdel of Samtse subdivision, who supported the germination test and site management; Mr. Pema Tshering of the JICA Expert Office, who supported us with on-site measurements; and Ms. Yamuna Kafley of the same office, who supported us with construction management. Thanks to these engineers, we could smoothly carry out the germination test, the placement of each work type on site, and construction management. We would also like to thank the staff at the JICA Bhutan Office and headquarters, who greatly supported the project.

References

Barman N, Choudhury M (2023) Landslides in the India Bhutan Border area historical evidences, causes and consequences. J Geogr Nat Disasters 13:281

Hirota K et al (2023) How to teach remotely the vegetation works to protect slopes against mass wasting: a case of using video materials in Bhutan. Prog Landslide Res Technol 1(2):361–363. https://doi.org/10.1007/978-3-031-18471-0_26

Lewis L (2000) Soil bioengineering—an alternative to roadside management—a practical guide. Technical Report 0077–1801-SDTDC. Department of Agriculture, Forest Service, San Dimas Technology and Development Center, Wangdue Phodrang, p 44

National Soil Service Centre (2019) Soil conservation manual. Department of Agriculture Ministry of Agriculture & Forests Royal Government of Bhutan, Wangdue Phodrang, p 57

Application of Nature-Based Solutions in Mitigation of Hillside Unstable Road Cuts in Sri Lanka

Madara Dissanayake, Sardhanee Dias, and Nishantha Peiris

Abstract

Environmental considerations are becoming an important factor in the choice of suitable remedial measures in addressing mitigation of landslides. This paper highlights the use of Nature-based Solutions (NbS) that are based on natural processes and ecosystems in the mitigation of eighteen unstable slopes along the Kandy-Mahiyangana Road in the Kandy district of Sri Lanka, which was implemented by the Road Development Authority and National Building Research Organisation. The sites were in the central fragile area of the country with high erosion susceptibility and reservoir siltation. The mitigation designs were hybrid-type with both structural engineering mitigations and NbS. NbS were chosen considering the critical habitat conditions, susceptibility to slope erosion, ecosystem functionality, adaptability to co-exist with the existing environment and other co-benefit functions of NbS. An array of on-site environmental management and bioengineering mitigation were used as NbS. This study portrays the application of NbS at every stage of the project cycle to ensure long-term disaster resilience and environmental sustainability.

Keywords

Mitigation of unstable slopes · Nature-based solutions · Hybrid · Environmental sustainability

1 Introduction

Sri Lanka is considered vulnerable to climate change impacts, ranked 110th of 181 countries in the 2022 ND-GAIN Index (https://gain-new.crc.nd.edu/country/sri-lanka). Unpredictable variability of rainfall patterns in the country could probably be due to global climate change with the increase in the frequency of extreme weather events. Landslides have become a frequently occurring natural disaster in Sri Lanka and rainfall is the triggering factor for this disaster and commonly occur during monsoon season. The records of landslides are high in the months of May and June and once again from November to January, showing a clear relationship with two monsoon seasons in Sri Lanka. In the past decade, the south-west monsoon has caused flooding and landslides throughout the monsoon season. According to Sri Lanka Rapid Post Disaster Needs Assessment-Floods and Landslides (2017), within the month of May 2017 alone, 35 major landslide events have occurred causing 176 deaths out of total number of 219 deaths caused due to floods and landslides. It is accounted, landslides cause an annual economic loss of 0.02% from the total GDP. That is 0.11% of total government expenditure, which is LKR 1.8 billion (World Bank Group 2016). Hence, there is an urgent need and essential requirement of managing the landslide risk in the country. (University of Notre Dame 2022)

As indicated in Fig. 1, there is a reduction in number of landslides and number of deaths in Sri Lanka afterwards 2018. This may be associated with national programs on landslide hazard risk management implemented by National Building Research Organisation (NBRO) being the focal point for landslide risk management in the country such as (1) issuance of landslide clearance for construction in landslide prone districts in the country (Kandy, Matale, Nuwara-Eliya, Badulla, Kegalle, Ratnapura, Kalutara, Galle, Matara, and Hambantota), (2) issuance of early warning alerts to vulnerable communities when rainfall intensities reach certain threshold levels and (3) mitigation measures aiming correc-

M. Dissanayake (✉) · S. Dias
National Building Research Organisation, Environmental Studies and Services Division, Colombo, Sri Lanka

N. Peiris
National Building Research Organisation, Landslide Studies and Risk Management Division, Colombo, Sri Lanka

B. Abolmasov et al. (eds.), *Progress in Landslide Research and Technology, Volume 4 Issue 1, 2025*, Progress in Landslide Research and Technology, https://doi.org/10.1007/978-3-031-89836-5_17

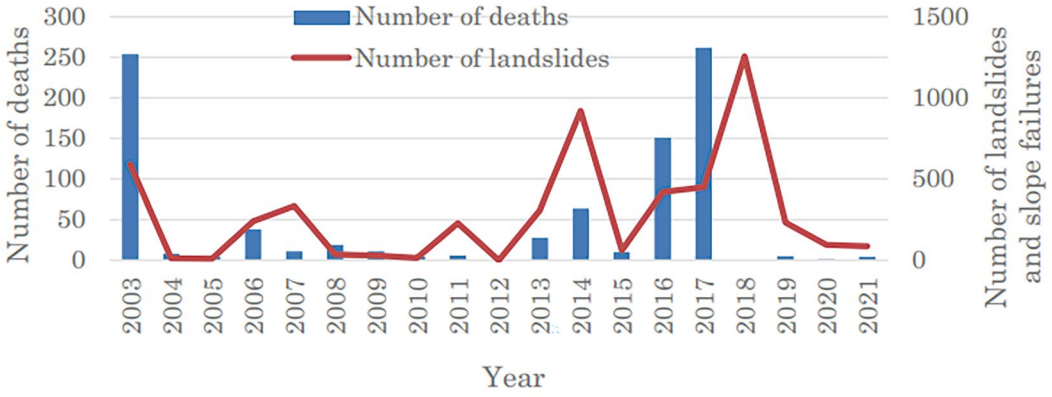

Fig. 1 Number of landslides and deaths from 2003 to 2021 in Sri Lanka (Credit: NBRO)

tion of existing landslides or prevention of pending landslides. Several landslide mitigation projects; such as Technical Cooperation for Landslide Mitigation Project (TCLMP), Climate Resilience Improvement Project were implemented by NBRO as the key agency for landslide hazard risk management aiming at mitigation of landslide hazard risk.

2 Environmental Management Planning in the Landslides Mitigation

Mitigation of landslides directly reduces the national expenditure on repair and reconstruction of damaged public buildings and infrastructure facilities, resettlement, and expenditure on disaster relief services and emergency operation services. Further, it creates disaster-resilient built environment by ensuring safety with overall positive significant impacts on boosting especially agriculture, cash crops, plantation sector and tourism sector economies in the country.

Direct use of structural engineering slope stabilization measures (the physical structure, the design, and the construction process) for mitigation can harm habitat integrity and functionality in many ways. The pollution sources arising from poor construction waste management, and construction site management can lead to water pollution, soil erosion, reservoir sedimentation, accumulation of construction debris, hazardous substances, damage to critical habitats, animal trails, and endangered and threatened fauna and flora.

However, landslide mitigation projects are not identified as prescribed projects in the National Environmental Act of Sri Lanka, which requires environmental impact assessment despite most landslide mitigation projects are implemented in the highly erosion-pronecentral fragile area of the country within or near protected areas (forests and wild life sanctuaries) or their buffer zones.

In this context, NbS can serve as a strategy to enhance the overall environmental sustainability and ecosystem integrity of the entire project cycle.

3 Nature Based Solutions

The concept of nature-based solutions (NbS) in environmental sciences and nature conservation was first developed by international organizations, such as the International Union for Conservation of Nature (IUCN) and the World Bank, as solutions to work with ecosystems as an alternative to relying on conventional engineering interventions to adapt to mitigate climate change effects for improving sustainable livelihoods and protecting natural ecosystems and biodiversity.

Defined by the IUCN; NbS as: “Actions to protect, sustainably manage and restore natural or modified ecosystems, which address societal challenges effectively and adaptively, while simultaneously providing human well-being and biodiversity benefits” (Cohen-Shacham et al. 2016).

NbS is best considered an umbrella concept that covers a range of different approaches. The common focus on ecosystem services aims to address societal challenges.

According to IUCN, NbS approaches can be classified into the following five categories, as shown in Fig. 2.

1. Ecosystem restoration approaches (e.g. ecological restoration, ecological engineering and forest landscape restoration)
2. Issue specific ecosystem-related approaches (e.g. ecosystem-based adaptation, ecosystem-based mitigation, and ecosystem-based disaster risk reduction)
3. Infrastructure-related approaches (e.g. natural infrastructure and green infrastructure approaches)
4. Ecosystem-based management approaches (e.g. integrated coastal zone management and integrated water resources management) and

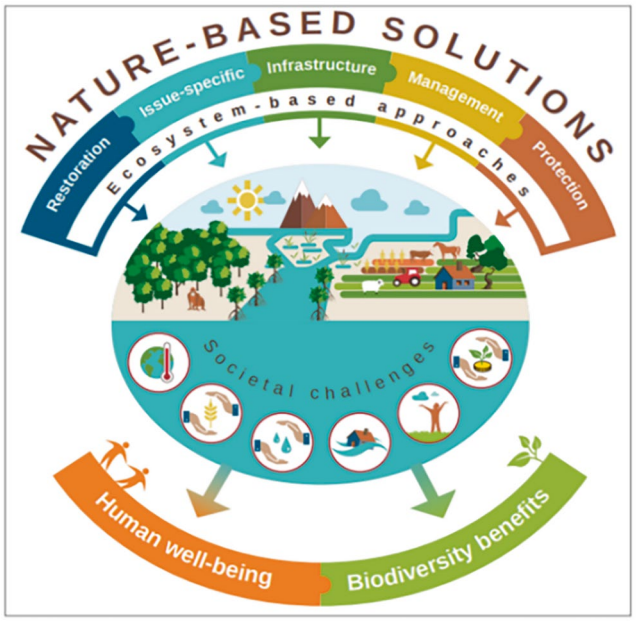

Fig. 2 NbS as an umbrella term for ecosystem-related approaches (Cohen-Shacham et al. 2016)

Fig. 3 Kandy–Mahiyangana 18-bend road (photo by Attractions Sri Lanka 2019)

Fig. 4 Rock falls in Kandy–Mahiyangana Road (Credit NBRO)

5. Ecosystem protection approaches (e.g. area-based conservation approaches including protected area management)

4 Study Background

NbS approaches (1) issue specific ecosystem—related approach with ecosystem-based adaptation and mitigation and (2) ecosystem-based restoration approaches were used in a landslide disaster mitigation project in Sri Lanka.

Kandy, Mahiynganaya Road–18 bend road is situated along the central highlands of Sri Lanka (Fig. 3). The road is popular as a very challenging drive even for the most experienced drivers. The road had to close due to frequent rockfalls during rains (example is shown in Fig. 4). Inadequate assessment of the landslide potential and not adhering to slope protection structures during road rehabilitation are the causes of this roadside rock instability.

Eighteen unstable slopes (Fig. 5) along the Kandy-Mahiyangana road were mitigated under Climate Resilience Improvement Project (CRIP) with financial assistance from the World Bank and was implemented by Road Development Authority (RDA) and NBRO. The NBRO involved in investigation, designing and supervising slope stabilization works in the project.

The sites were in Randenigala–Rantembe reservoir in a fragile area of the country with high erosion susceptibility and reservoir siltation.

The mitigation designs were hybrid-type with both structural mitigation and NbS. Structural mitigation involves modifications of the natural conditions of landslides, such as topography, geology, surface and subsurface drainage management, and other conditions that indirectly control portions or the entire landslide movement.

5 Nature-Based Solutions

The project included site-specific environmental and social assessments to understand specific ecosystem features, their processes, identification of site specific NbS requirements and rationalized selection of the most appropriate NbS.

6 Issue-Specific Ecosystem Related Approaches: Ecosystem-Based Adaptation and Mitigation

NbS were chosen considering the critical habitat conditions, with special reference to habitat connectivity, integrity, drainage management, erosion control, biodiversity, and

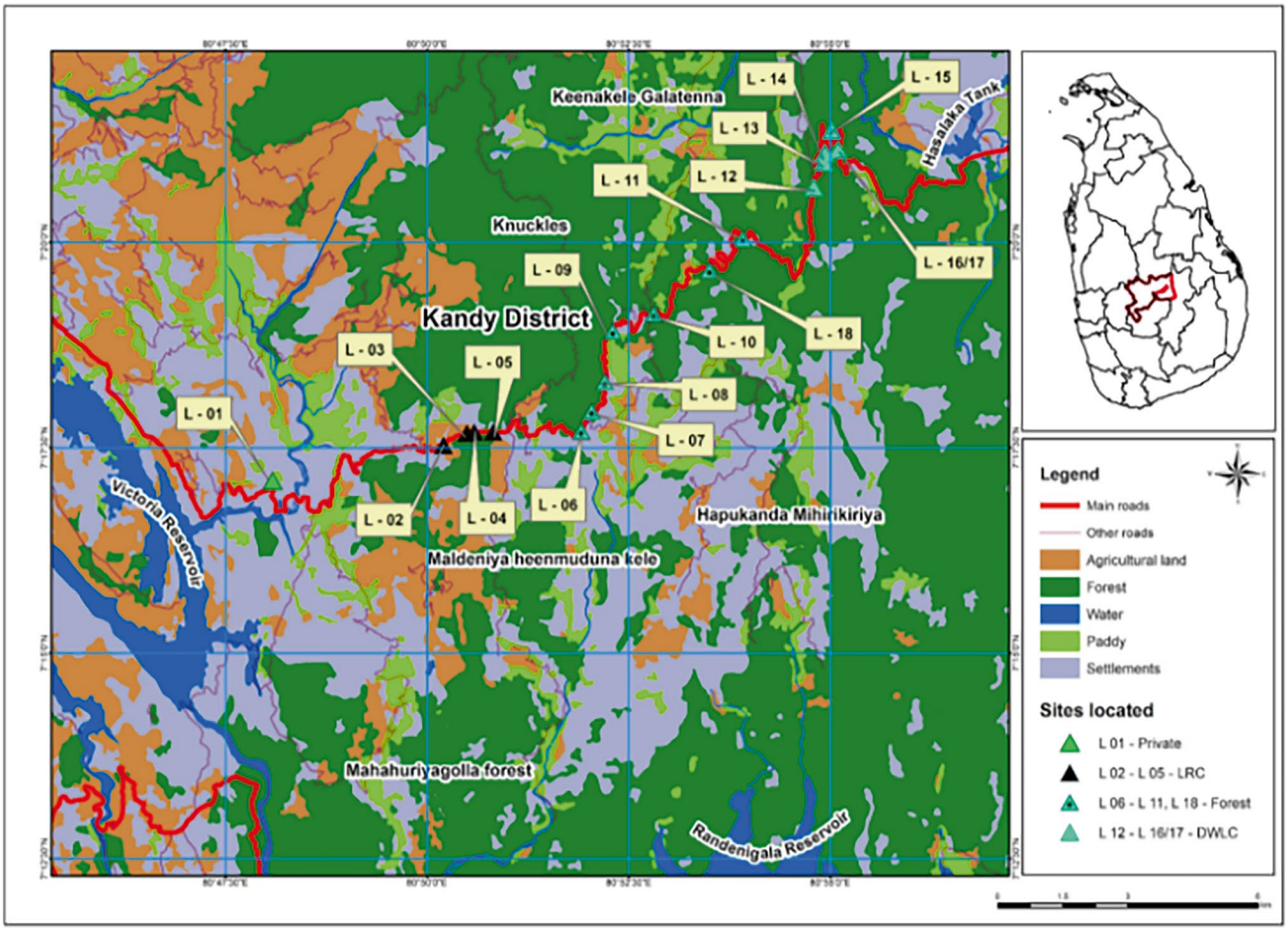

Fig. 5 Locations of the slopes mitigated along Kandy-Mahiyangana Road

adaptability to co-exist with the existing environment together with other co-benefit functions of NbS. An array of on-site environmental management and bioengineering mitigation were used as NbS.

To address the potential environmental impacts of the project, the environmental assessment and management framework (EAMF) was prepared during the project planning stage and according to EAMF, the project should comply with the regulations set by the Government of Sri Lanka and the funding agency–World Bank Environmental Safeguard Policies. According to the EAMF, during the mitigation the Environmental Management Plan (EMP) had to be followed. Accordingly, the project had to comply with several laws and regulations of Sri Lanka as mentioned below.

1. The National Environment Act (NEA) No. 471988 and subsequent amendments- legislative framework for overall Environmental Management
2. Fauna and Flora Protection Act No.2 of 2009 Forest Act No. 34 of 1951 (some of the sites are located close to forest and wildlife areas)
3. Felling of Trees Control Act No. 9 of 1953 (to cut/ uproot trees)
4. Soil Conservation Act No.9 of 1953 (for erosion control)

The Environmental Management Plan (EMP) of the project included a set of on-site mitigation and management measures to be taken during project implementation to avoid, reduce, mitigate, or compensate for adverse environmental impacts as mentioned below.

1. The extent of vegetation cleared was minimal by demarcating allowable areas to be cleared and limiting the contractor's movement of his employees and equipment within the project area.
2. The sensitive plants and critical habitats in forest reservations were protected by demarcating any sensitive environmental areas as "no-entry" zones.

3. By maintaining connection vegetation strips and animal trials, during the land clearing, habitat connectivity was not altered.
4. By practising on-site management of sediment and debris, and restricting disposal of all debris and any left earth to reservations/stream banks, contamination of run-off and siltation of reservoirs and streams were prevented.
5. After introducing plant species, if exotic plants were grown, they were removed.
6. Sensitive habitats were protected, and relocation of protected species was identified as a high priority.

7 Vegetative Slope Erosion Control and Run-off Control Measures

As a bioengineering measure, plant species were used for erosion control, slope protection, and beautification for the road users. The vegetation cover and the root system embedded into the soil matrix act as improved soil conditions for groundwater infiltration, control over land erosive water channelling during rainfall events and loss of excess water via evapotranspiration process.

Some cut slopes were 20–30 m in height, where normal sodding or grass establishment methods were not practical. Therefore, the focus was on species selection and the vegetation engineering properties, especially concerning their root architecture and ground cover.

Several seeds of annual or perennial legumes with woody tap-roots, endemic or native, were selected for slope protection.

Biodegradable geotextiles were used as another bioengineering measure for faster root-soil matrix formation and for better erosion control.

8 Ecosystem Restoration: Nature-Based Solutions (NbS)

To recover an ecosystem that has been degraded, damaged, or destroyed, restoration programmes were conducted.

9 Challenges Faced During the Implementation Period

Seeds were first introduced to the coir mesh laid over the soil-nailed area using hydroseeding (the application of a mixture of seed, wax, fertilizer, and mulch).

The seeds of 3 species *Arachis pintoi*, *Desmodium ovalifolium*, *Desmodium triflorum*, *Desmodium heterophyllum* were used for this and none of the species was success due to challenges faced during the seed germination period, such as wash off from irrigation water, rain, and poor seed germination due to animal activities (seeds were used as food for birds and ants) and germination of invasive species with the time. Then hormone-applied roots of the same species were planted manually on the holes of coir mesh, and slow growth of seed germination was observed. Then seeds were grown in nurseries and were allowed to develop into seedlings, and were then transplanted manually on the coir mesh laid on the soil nailed surface. The growth of *Desmodium heterophyllum* was successful over the other species (Fig. 6).

During the early stages of plant growth regular monitoring and maintenance were essential. Adequate watering, protection from excessive foot traffic, and weed management were other important factors in ensuring the successful establishment of the vegetation.

Over time, the plants grew, and their root systems became more established (Fig. 7). The root network further stabilized the soil, preventing erosion caused by wind and water. The vegetative cover helps retain soil particles and prevents sediment run-off into nearby water bodies.

It has been observed that biodegradable geotextiles worked as mesh and promoted the growth of new vegetation by absorbing water and preventing the topsoil from drying out.

10 Lessons Learned

1. In addition to engineering, ecological, and economic benefits, NbS contribute to sustainable development practices as they reduce the ecological impacts of construction, and enhance the aesthetics of the appearance of the overall slope.
2. Moreover, the NbS proved to be effective at every stage of the project cycle to ensure long-term disaster resilience and environmental and ecosystem sustainability without harming structural mitigation measures.

Fig. 6 *Desmodium heterophyllum*

Fig. 7 Growth of *Desmodium heterophyllum on* soil nailed area

3. However, integration of NbS in landslide mitigation is given less consideration in Sri Lanka and mitigation are mainly done on structural/engineered measures.
4. Even though the mitigation impacts are small and localized, measures must be taken to avoid and minimize the environmental impacts as the landslide-prone areas of the country fall in the central fragile area, susceptible to erosion.
5. Therefore, on-site environmental management is to be considered in the planning and design stage of mitigation, and Environmental professionals should be involved from the planning stage of the mitigation.
6. National and international organizations must consider NbS in landslide mitigation, and professional knowledge on NbS for landslide mitigation must be raised to make the mitigation sustainable.

Acknowledgments Authors of this paper would like to acknowledge Dr. Asiri Karunawardena—Director General/NBRO, Eng. D.C.S. Elakanda-Project Director/CRIP, Mr. RMS Bandara—Director LRRMD/NBRO, Ms. Kumari Weerasinghe, Former Deputy Project Director-CRIP, Mr. U.K.N.P. Dharamsena—Project Engineer (Construction)/CRIP, Ms. K.M.D.N.K. Kahahengoda-Project Engineer/CRIP and Mr. D.M.S. Dissanayake Environment Officer/RDA for their guidance and assistance in the process of monitoring EMP.

References

Attractions Sri Lanka (2019) 18 bend road. https://www.attractionsinsrilanka.com/travel-directory/18-bend-road/. Accessed 26 September 2024

Cohen-Shacham E, Walters G, Janzen C, Maginnis S (2016) Nature-based solutions to address global societal challenges. IUCN, Gland, pp 2–10

Sri Lanka Rapid Post Disaster Needs Assessment-Floods and Landslides (2017) Ministry of Disaster Management & Ministry of National Policy and Economic Affairs in collaboration with the United Nations, World Bank and European Union, Colombo

University of Notre Dame (2022) Country rankings. https://gain-new.crc.nd.edu/ranking-2022. Accessed 26 September 2024

World Bank Group (2016) Fiscal disaster risk assessment and risk financing options: Sri Lanka. http://hdl.handle.net/10986/24689. Accessed 26 September 2024

Slope Stability Analysis Using the Slope Mass Rating (SMR) Method on Provincial Road Section, Kebumen Regency, Central Java Province, Indonesia

Muhammad Hanif Syariefudin, Egy Erzagian, Nugroho Imam Setiawan, Hendy Setiawan, Teuku Faisal Fathani, and Wahyu Wilopo

Abstract

Road construction in mountainous areas has various challenges in the construction and maintenance stages. One of the hazards that is often found is landslides. Therefore, to ensure safety for users, it is necessary to study slope stability along the road. The research aims to evaluate the slope stability condition of the road section based on the slope mass rating (SMR) method. This research was conducted on a provincial road in Central Java, Indonesia. The SMR value is based on the rock mass quality values according to the rock mass rating (RMR) method and the weighting of adjustment factor values consisting of slope orientation, discontinuity orientation, and excavation method. The RMR values consist of uniaxial compressive strength (UCS), rock quality designation (RQD), discontinuity spacing, discontinuity condition, and groundwater condition. The results of rock mass quality according to the RMR method are divided into good (61–80), fair (41–60), and poor (21–40) qualities. In addition, slope stability analysis using the SMR method shows that the slope stability conditions on the road section are divided into stable (61–80), partially stable (41–60), and unstable (21–40) conditions. This paper describes the achievements and the current activities of the IPL-WCoE on Risk Management and Technological Innovation for Landslide Mitigation.

Keywords

Rock mass rating · Slope mass rating · Slope stability · Kebumen

1 Introduction

Safety and economic aspects are the most crucial in construction (Vallejo and Ferrer 2011). Road construction related to the morphology of mountains, valleys, or similar will face slope stability problems (Abramson et al. 2001). Slope failure can cause many negative impacts, ranging from damage to road construction and vehicles to injury to death for road users and economic disruption (Wyllie and Mah 2004). Natural slopes or engineered slopes for construction purposes can collapse suddenly, even if they have been relatively stable for some time. The slope stability is influenced by several factors, ranging from geometric, geological, and hydrogeological to geomechanical characteristics (Vallejo and Ferrer 2011). Many studies have been carried out regarding the quality of rock masses on slopes with different rock types, such as metamorphic rocks (Ramadhani et al. 2018), volcanic rocks (Juhari et al. 2021), igneous rocks (Irvani et al. 2013) and limestone (Wijaya et al. 2015).

As shown in Fig. 1, one of the provincial roads is built about 150 m above sea level and passes through a fairly steep hilly slope. The location of the road section, which is administratively located in Sempor District, Kebumen Regency, Central Java, Indonesia, is included in an area with medium to high susceptibility to landslides (PVMBG (Pusat

M. H. Syariefudin · E. Erzagian · N. I. Setiawan · H. Setiawan · W. Wilopo (✉)
Department Geological Engineering, Gadjah Mada University, Yogyakarta, Indonesia
e-mail: muhammadhanif@mail.ugm.ac.id; Nugroho.setiawan@ugm.ac.id; hendy.setiawan@ugm.ac.id; wilopo_w@ugm.ac.id

T. F. Fathani
Department of Civil and Environmental Engineering, Gadjah Mada University, Yogyakarta, Indonesia
e-mail: Tfathani@ugm.ac.id

B. Abolmasov et al. (eds.), *Progress in Landslide Research and Technology, Volume 4 Issue 1, 2025*, Progress in Landslide Research and Technology, https://doi.org/10.1007/978-3-031-89836-5_18

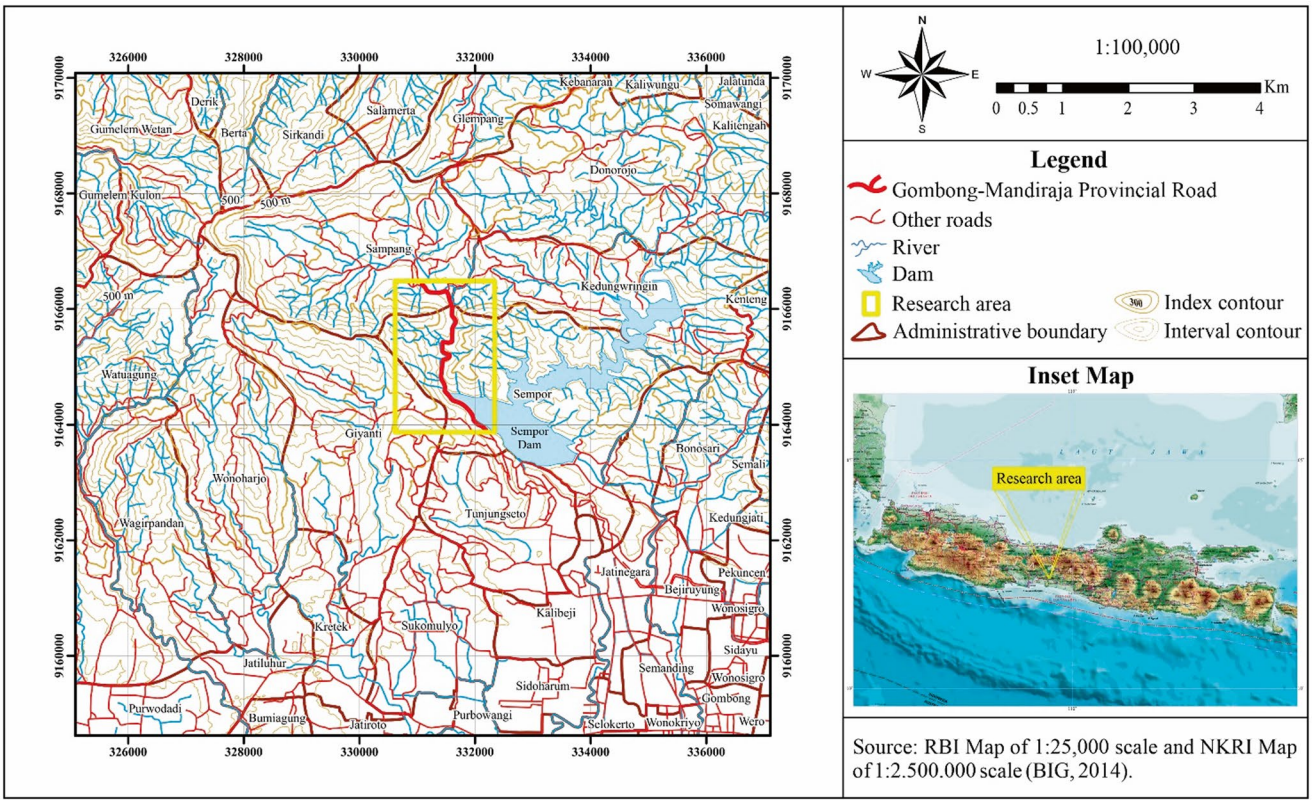

Fig. 1 Research location of the Provincial Road in Kebumen, Central Java, Indonesia (BIG 2014, 2021)

Vulkanologi dan Mitigasi Bencana Geologi) 2013). Several landslides and rock falls occurred along the road due to the fairly complex geological structure (Asikin et al. 1992). This area comprises three rock formations: the Tuff Member of the Waturanda Formation, the Waturanda Formation, and the Penosogan Formation (Asikin et al. 1992).

This research aims to evaluate the slope stability condition of the provincial road section based on the slope mass rating (SMR) analysis. Geological mapping was used as a reference to determine the influence of morphological, lithology, and geological structure conditions in the research area. The results of this study are expected to be used as inputs regarding the slope stability condition on the road section and its potential for failure so that appropriate slope-reinforcement efforts can be made based on the classification (Romana 1985). Moreover, the research is important for the local government to maintain and strengthen the slope of the road from landslides.

2 Research Method

The research area is located in the Provincial Road section, Sempor District, Kebumen Regency, Central Java, Indonesia, with a length of around ±3.8 km, as shown in Fig. 1. The research on the condition of slope stability on the Gombong-Mandiraja Provincial Road Section was carried out through a literature review, data collection, laboratory tests, data analysis, and reporting stages. The main methods in this research's data collection and analysis stages include geological mapping, RMR analysis, kinematics analysis, and SMR analysis. Geological mapping was conducted to determine the geological conditions along the road section, including morphology, lithology, and geological structure. The name and properties of the rock were identified based on petrography analysis for the thin section of rock. Furthermore, observations of rock discontinuity and slope conditions were carried out as the primary data in the rock mass quality analysis, referring to the RMR classification. Data on discontinuity orientation and slopes are used for kinematics analysis to determine the failure type and stability level. Furthermore, the slope stability level is evaluated using the SMR method based on rock mass quality data referring to the RMR classification and several adjustment factors based on the discontinuity orientation and slope.

The rock mass rating (RMR) is a geomechanical classification developed by Bieniawski in 1972–1973. The weighting of RMR values is done as part of the SMR analysis (Irvani et al. 2013), which includes the basic parameter in its calculation. The RMR_{basic} is an RMR value that does not

include the discontinuity orientation parameter in the analysis. The RMR_{basic} consists of 5 parameters, namely: uniaxial compressive strength (UCS), rock quality designation (RQD), discontinuity spacing, discontinuity condition, and groundwater condition (Bieniawski 1989).

Each parameter in the RMR has a different value weight according to the condition of the data obtained in the field or through laboratory tests. The UCS value in this study is obtained from the point load test results following the ASTM D 5731–95 standard (ASTM D 5731-95 1995), which is converted into the UCS value. The scanline method obtains the RQD value from the outcrop (Priest and Hudson 1976). The discontinuity spacing value is measured directly on the outcrop using a length-measuring instrument according to the existing joint set. Data on the discontinuity condition is obtained from direct observation of the outcrop related to the sub-parameters of persistence, aperture, roughness, infillings, and weathering. The groundwater condition is obtained from observing groundwater on the slope that can be observed from the surface. All parameters are weighted based on the classification of rock mass quality (Bieniawski 1989). The results are summed using Eq. (1) to obtain the total basic value of RMR for each observation point station, which can be classified into five classes: very poor (<20), poor (21–40), fair (41–60), good (61–80) and very good (81–100) (Bieniawski 1989).

$$RMR_{basic} = A_1 + A_2 + A_3 + A_4 + A_5 \quad (1)$$

where A_1 weighted value of uniaxial compressive strength (UCS), A_2 weighted value of rock quality designation (RQD), A_3 weighted value of discontinuity spacing, A_4 weighted value of discontinuity condition, A_5 weighted value of groundwater condition.

Kinematics analysis is a projection method used to project discontinuity and slope data in 3 dimensions into two dimensions. Kinematics analysis in this study was conducted only to determine the type of failure, while the level of slope stability was determined by the SMR classification (Romana 1993). The data used in this analysis are dip and strike data of the slope and discontinuity, such as fractures, faults, joints, and bedding. The data is then analyzed using a stereographic projection by Dip's software. There are four types of slope failure: plane, wedge, toppling, and circular failures (Hoek and Bray 1981; Goodman 1989).

Slope Mass Rating (SMR) is a slope stability classification method developed by Romana (1985) to evaluate the stability of rocky slopes. This method is suitable for application as an initial assessment of the stability condition of a slope because it uses simple parameter weighting related to the type of instability and the required support method. In addition, the SMR method provides adjustment factors, field guidelines, and recommendations on slope-strengthening methods that allow geomechanical classifications for systematic slope analysis (Romana 1993). The SMR values are based on the RMR_{basic} data, with additional adjustment factors related to slope orientation values, discontinuities (F_1, F_2, and F_3), and excavation methods (F_4) on the slope. The weighting of F_1, F_2, F_3, and F_4 values adjusts to the Romana classification (Romana 1993). To obtain the SMR value, Eq. (2) was used.

$$SMR = RMR_{basic} + \left(F_{1^*}F_{2^*}F_3\right) + F_4 \quad (2)$$

where RMRb is the basic RMR index from Bieniawski's rock mass classification, F1 depends on the parallelism between discontinuity dip direction and slope dip, F2 is related to the probability of discontinuity shear strength and depends on the discontinuity dip, F3 depends on the relationship between slope and discontinuity, dips, F4 is a correction factor that depends on the excavation method.

3 Results

3.1 Geological Conditions

Geological conditions are divided into three main aspects: morphological, lithology, and geological structures. Furthermore, from the results of geological mapping, the distribution of rocks and geological structures can be seen as shown in Fig. 2. The relationship between rock units and geological structure conditions can be seen in the geological profile presented in Fig. 3. The stratigraphy of the research area can be divided into four rock units. The rock units from the oldest are interbedded tuff, sandstone, and carbonate claystone units, andesite breccia with sandstone insertion units, carbonate sandstone units, and interbedded carbonate sandstone and siltstone units. Several types of geological structures, such as joints and faults, were identified.

3.2 Rock Mass Rating Analysis

Based on the weighting results that have been carried out on five basic RMR parameters, including the UCS value obtained from the point load test, the RQD value obtained from direct measurements at the outcrop with the scanline method (Priest and Hudson 1976), discontinuity spacing, groundwater conditions, and discontinuity conditions consisting of several sub-parameters such as persistence, roughness, aperture, infillings, weathering as shown in Table 1 obtained three rock mass quality classes consisting of good rock class with RMR value (61–80), fair rock class with RMR value (41–60), and poor rock class with RMR value

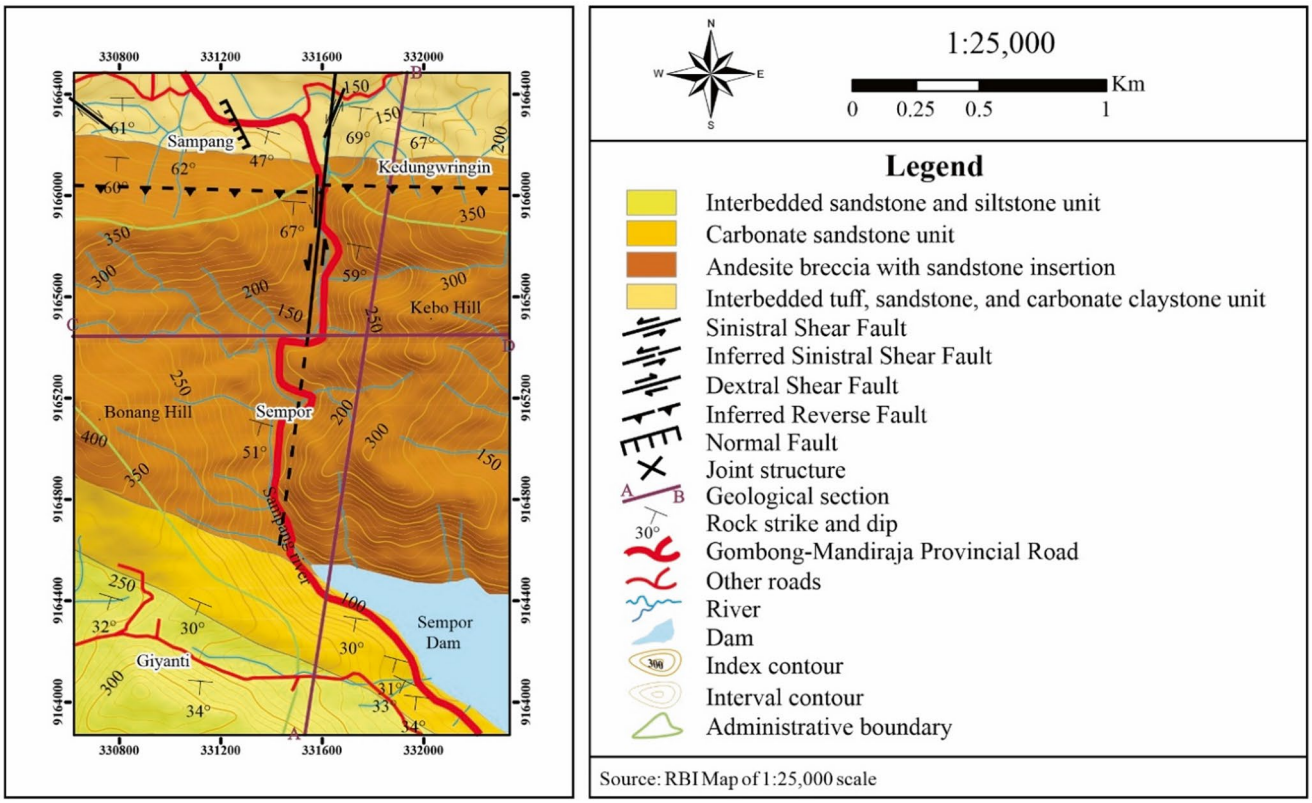

Fig. 2 Geological map of the research area

(21–40). The distribution of RMR values in the research area is shown in Fig. 4.

3.3 Kinematics Analysis

The kinematics analysis carried out on 21 stations along the Provincial Road Section shows that wedge failure is the dominant type of collapse. Twenty slopes have a wedge-type failure, and only one has a plane failure, as shown in Table 2. Figure 5 shows an example of slope appearance, including the results of the kinematic analysis. The results of this kinematics analysis can then be used to calculate the slope stability value on each slope according to the existing failure type, referring to Eq. (2).

3.4 Slope Mass Rating Analysis

Based on the results of the SMR calculation using Eq. (2), three classes of slope stability level, namely stable slope class with SMR value of 61–80, partially stable slope class with SMR value of 41–60, and unstable slope class with SMR value of 21–40. Table 2 shows examples of SMR calculation involving basic RMR values and weighting correction factors consisting of F_1, F_2, F_3, and F_4. The distribution of SMR values in the research area is shown in Fig. 6.

4 Discussions

4.1 Geological Condition

4.1.1 Lithology

The research area can be divided into four rock units. The oldest rock units consist of interbedded tuff, sandstone, and carbonate claystone units, andesite breccia with sandstone insertion units, carbonate sandstone units, and interbedded sandstone and carbonate siltstone units. However, the road section evaluated for slope stability conditions based on the SMR method only contains three rock units: interbedded tuff, sandstone, and carbonate claystone unit, andesite breccia with sandstone insertion unit, and carbonate sandstone unit. The type of rock itself will affect the value of the rock's mass quality and instability.

The various rock characteristics in the research area are reflected in the different UCS values obtained from the point load test results for each type of rock. When ranked from the strongest, andesite breccia has the highest value with a UCS

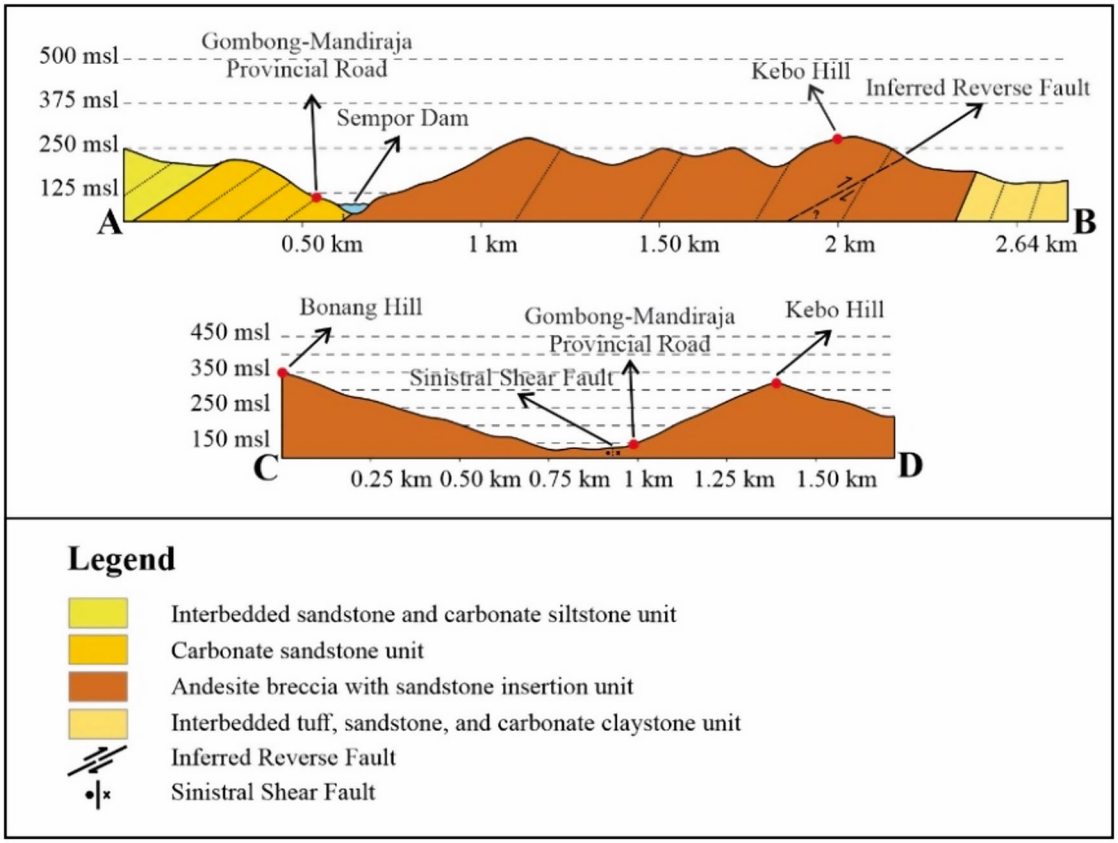

Fig. 3 Geological profile of the research area

value range of 66.69–185.25 MPa, then various kinds of sandstone consisting of micritic sandstone (part of the carbonate sandstone unit) with UCS values in the range of 17.61–36.54 MPa, lithic wacke (part of andesite breccia with sandstone insertion unit) with UCS values in the range of 11.4–19.63 MPa, arkose (part of interbedded tuff, sandstone, and carbonate claystone unit) with an average UCS value of 18.1 MPa. In comparison, the lowest value for rock compressive strength is found in tuff, which has an average UCS value of 9.4 MPa.

The results of the petrographic analysis are in line with the values obtained from the point load test. As shown in Tables 3 and 4, the influence of rock type characteristics in general on the compressive strength value of the rock is based on the percentage of pores obtained from the petrographic analysis. In addition, observations on the sandstone's packing characteristics and intergranular contacts were discussed because three different types of sandstone were found in the study area.

The andesite breccia rock (part of andesite breccia with sandstone insertion unit), represented by the compressive strength value of the fragments in it, is reviewed based on the results of petrographic analysis for andesite igneous rocks. In fresh conditions, andesite rock fragments have UCS values of 100–500 MPa (Vallejo and Ferrer 2011). Figure 7 shows the petrographic appearance of andesite fragments with a porphyry aphanitic texture with constituent minerals in plagioclase, quartz, pyroxene, opaque minerals, and a groundmass of volcanic glass. The constituent aggregates' characteristics influence the compressive strength value of andesite rock. The relationship between the minerals interlocks each other due to being formed simultaneously when the magma undergoes cooling and solidification. The dense mineral texture illustrates the low porosity value. Based on the petrographic analysis, andesite rock fragments have a pore abundance of 5%. In general, porosity values for andesite rock fragments vary from 10–15% to very low or less than 1% (Vallejo and Ferrer 2011), where the range of values is lower than the pores in sandstone and tuff. This follows the point load test results, where generally, the andesite rock fragments in the breccia have a higher range of compressive strength values than sandstones and tuff. Table 3 comparison of the petrographic characteristics of rocks and their strength value.

Tuff (part of interbedded tuff, sandstone, and carbonate claystone unit) has a petrographic appearance. Figure 8 shows good sorting and a composition dominated by fine-sized volcanic glass. In fresh condition, the tuff rock has a

Table 1 RMR calculation in some road points

Observation Point	COORDINATE		LITHOLOGY	UCS		RQD		DISCONTINUITY SPACING		DISCONTINUITY CONDITION										GROUNDWATER		RMR		
										Persistence		Roughness		Aperture		Infilling		Weathering						
	x	y		MPa	Rating	%	Rating	Meter	Rating	Meter	Rating	Description	Rating	Millimetre	Rating	Description	Rating	Description	Rating	Description	Rating	Total	Class	Description
1	332035	9164018	Carbonate sandstone	28.12	4	75-90	17	0.2-0.6	10	1-3 m	4	*Slightly rough*	3	1-5 mm	1	None	6	*Slightly weathered*	5	*Wet*	7	57	III	Fair
4	331940	9164187	Carbonate sandstone	33.44	4	50-75	13	0.06-0.2	8	3-10 m	2	*Slightly rough*	3	>5 mm	0	None	6	*Slightly weathered*	5	*Damp*	10	51	III	Fair
8	331482	9164645	Andesite breccia	166.8	12	75-90	17	0.2-0.6	10	1-3 m	4	*Slightly rough*	3	1-5 mm	1	None	6	*Moderately weathered*	3	*Wet*	7	63	II	Good
14	331429	9165064	Sandstone	11.4	2	75-90	17	0.2-0.6	10	1-3 m	4	*Slightly rough*	3	1-5 mm	1	None	6	*Moderately weathered*	3	*Wet*	7	53	III	Fair
15	331451	9165118	Andesite breccia	181.8	12	90-100	20	0.6-2	15	1-3 m	4	*Rough*	5	>5 mm	0	None	6	*Slightly weathered*	5	*Damp*	10	77	II	Good
17	331606	9165538	Andesite breccia	81.13	7	75-90	17	0.2-0.6	10	1-3 m	4	*Rough*	5	>5 mm	0	None	6	*Highly weathered*	1	*Damp*	10	60	III	Fair
18	331670	9165774	Sandstone	19.63	2	50-75	13	0.06-0.2	8	3-10 m	2	*Smooth*	1	1-5 mm	1	None	6	*Slightly weathered*	5	*Wet*	7	45	III	Fair
20	331602	9165978	Sandstone	17.99	2	50-75	13	0.06-0.2	8	1-3 m	4	*Smooth*	1	1-5 mm	1	None	6	*Moderately weathered*	3	*Wet*	7	45	III	Fair
21	331266	9166291	Interbedded tuff, sandstone, and carbonate claystone	13.8	2	<25	3	<0.06	5	<1 m	6	*Smooth*	1	0.1-1 mm	4	None	6	*Highly weathered*	1	*Damp*	10	38	IV	Poor

Note: blue = good, yellow = fair, pink = poor

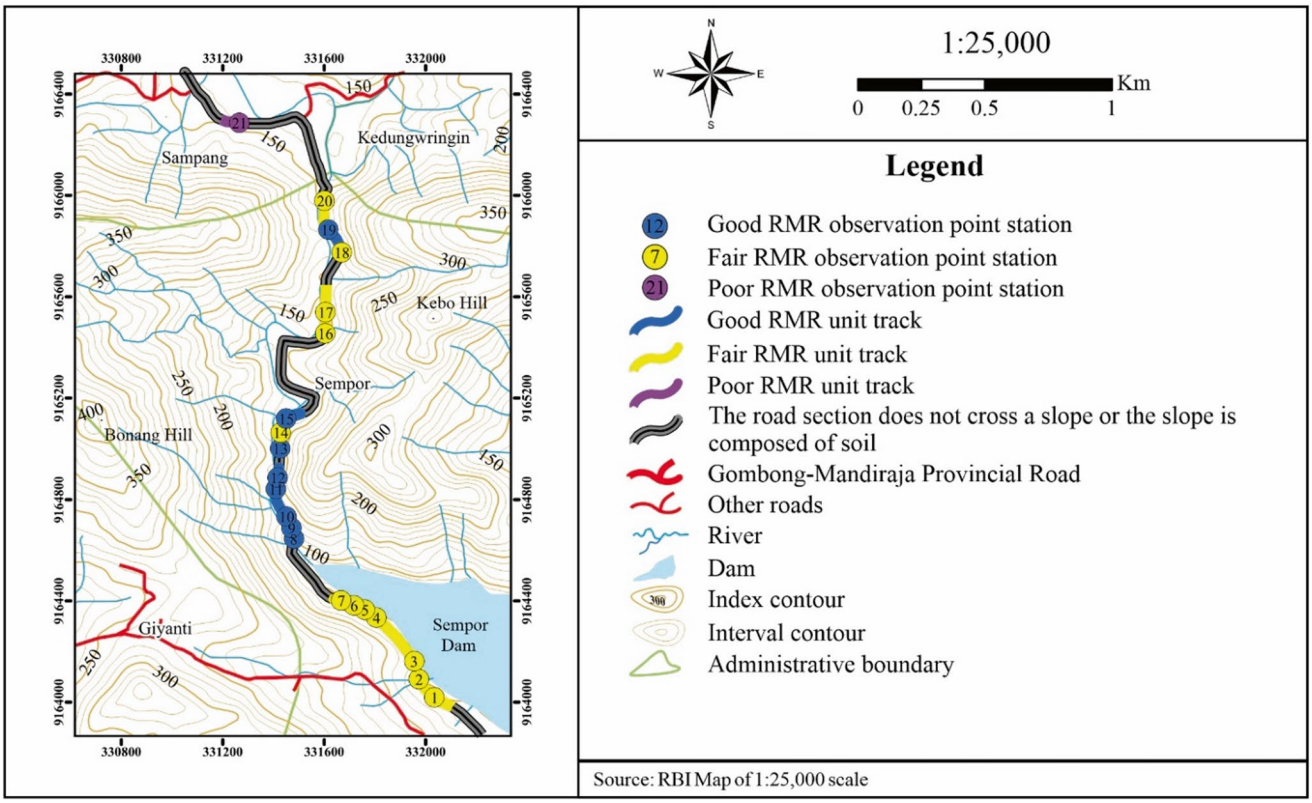

Fig. 4 Rock mass quality map of the Provincial Road Section, Kebumen, according to the RMR classification

UCS value of 10–46 MPa (Vallejo and Ferrer 2011). The strength of pyroclastic rocks is influenced by the level of solidification, where the characteristics of pyroclastic rocks composed of fine-sized volcanic glass tend to be weak. Based on the petrographic analysis, tuff has a pore abundance of 9% (Bell 2007). Generally, the porosity value for tuff rocks varies from 14–40%, with a higher value range than the pores in sandstone and andesites (Vallejo and Ferrer 2011). This follows the point load test results, where tuff generally has a lower compressive strength value range than sandstone and andesite rock fragments in breccia.

Sandstones that affect slope stability in the study area are divided into three types, namely micritic sandstone (part of carbonate sandstone units), lithic wacke (part of andesite breccia with sandstone insertion unit), and arkose (part of interbedded tuff, sandstone, and carbonate claystone unit). Table 4 shows the variety of characteristics in several types of sandstone in the study area in microscopic appearance, reflecting the different UCS values for each kind of sandstone present. In fresh conditions, sandstones have UCS values of 30–235 MPa (Vallejo and Ferrer 2011). In general, UCS values for sandstones found in the study area have a higher range of values when compared to tuff and lower when compared to andesite igneous rock fragments in breccias. Figures 9 and 10 show that sandstone (micritic sandstone) and sandstone (lithic wacke) in petrographic appearance in plane-polarized light (*PPL*) and cross-polarized light (*XPL*) show similarities in interparticle porosity. The difference lies in the number of pores present. From observations of several fields, the number of pores in lithic wacke, micritic sandstone, and arkose has a value of 23%, 16%, and 15%, respectively.

The sandstone's porosity varies from 5–25% (Vallejo and Ferrer 2011). The presence of pores in sedimentary rocks affects the compressive strength value of the stone, where the more significant the porosity value in the rock, the lower the compressive strength value of the stone (Jeng et al. 2004). When viewed from the pack, micritic sandstone, and arkose sandstone were grain-supported, while lithic wacke was matrix-supported. The weak sandstones are generally characterized by low packing (Dobereiner and de Freitas 1986). When viewed from the relationship between grains, lithic wacke has float and point contact characteristics, while micritic sandstone and arkose have floating, point contact, and prolonged contact characteristics. The relationship between sediment grains shows the compaction that occurs in a rock. The denser a rock is, the closer the contact of each sediment grain will be. This compaction is also related to porosity; the higher the rock compaction, the less porosity (Bell 2007). When viewed from the mineral composition, micritic sandstone, lithic wacke, and arkose have almost the same mineral composition, ranging from plagioclase, quartz,

Table 2 SMR calculation in some road points

Observation Point Station	COORDINATE		Failure type	RMR	Slope strike in-plane failure & dip direction in wedge failure	a_j (discontinuity strike)	ai (trend of the intersecting discontinuity)	b_s (slope dip)	b_j (discontinuity dip)	b_i (plunge of the intersecting discontinuity)	F_1	Rating	F_2	Rating	F_3	Rating	F_4	Rating	SMR Value	Class	Description
	x	y																		
1	332035	9164018	Wedge	57	30	-	61	70	-	66	31	0.15	66	1	-4	-50	Natural Slope	15	64.5	II	Stable
4	331940	9164187	Wedge	51	36	-	42	77	-	43	6	0.85	43	0.85	-34	-60	Natural Slope	15	22.65	IV	Unstable
8	331482	9164645	Wedge	63	251	-	244	52	-	39	7	0.85	39	0.85	-13	-60	Natural Slope	15	34.65	IV	Unstable
14	331429	9165064	Wedge	53	260	-	271	71	-	33	11	0.7	33	0.7	-38	-60	Natural Slope	15	38.6	IV	Unstable
15	331451	9165118	Wedge	77	8	-	20	69	-	44	12	0.7	44	0.85	-25	-60	Natural Slope	15	56.3	III	Partially stable
17	331606	9165538	Wedge	60	273	-	295	71	-	50	22	0.4	50	1	-21	-60	Natural Slope	15	51	III	Partially stable
18	331670	9165774	Plane	45	208	196	-	67	60	-	12	0.7	60	1	-7	-50	Natural Slope	15	25	IV	Unstable
20	331602	9165978	Wedge	45	277	-	243	75	-	46	34	0.15	46	1	-29	-60	Natural Slope	15	51	III	Partially stable
21	331266	9166291	Wedge	38	6	-	334	58	-	42	32	0.15	42	0.85	-16	-60	Natural Slope	15	45.35	IV	Partially stable

Note: blue = stable, yellow = partially stable, pink = unstable

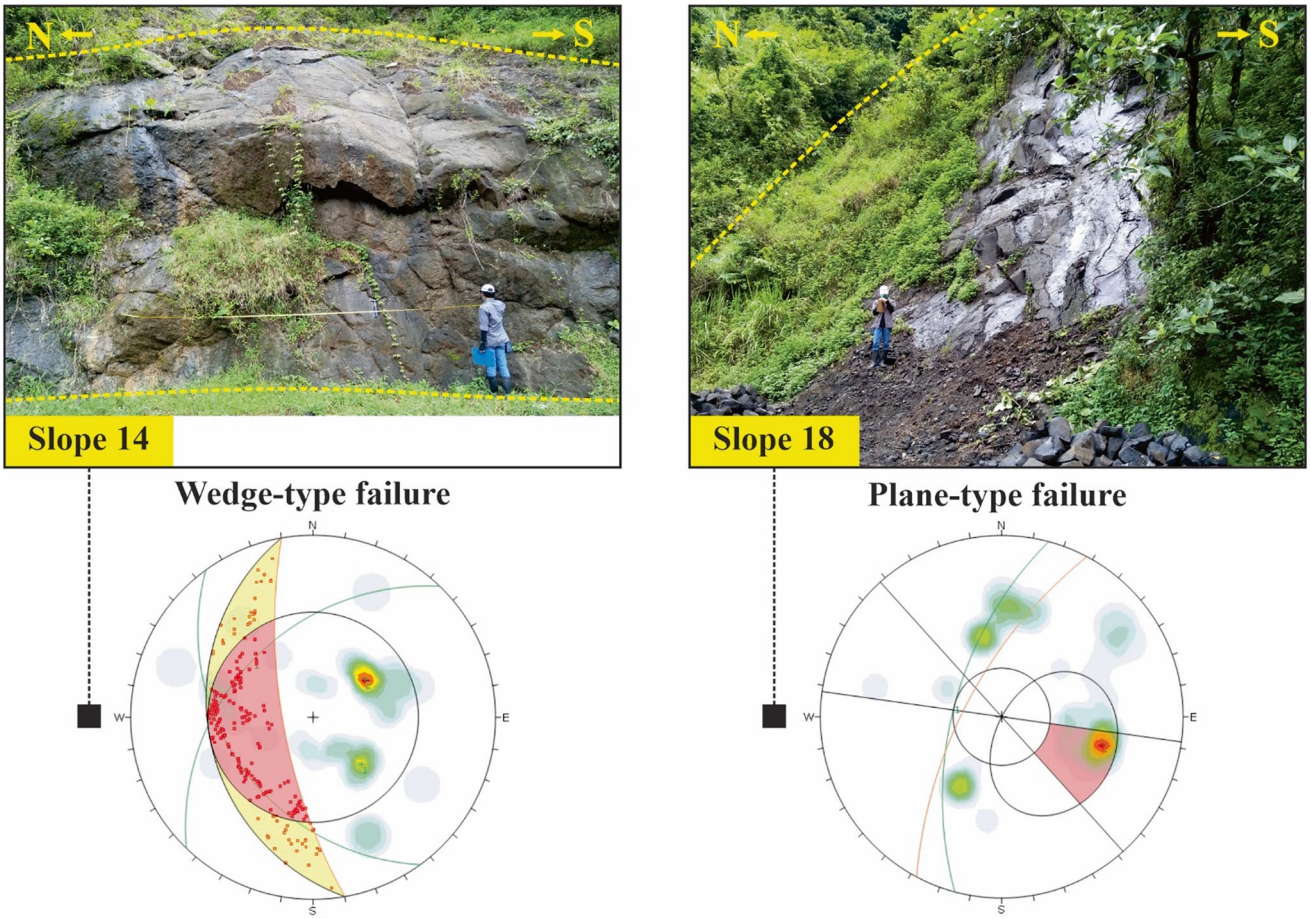

Fig. 5 Examples of kinematic analysis carried out at two observation point stations on Slope 14 shows the dominance of wedge-type failure, and Slope 18 presents the dominance of plane-type failure

and clay-sized materials. The difference in the design of these rocks lies in the percentage of minerals and carbonate material in micritic sandstone. The mineral composition is related to the resistance of sedimentary rocks to weathering. The higher the rate of resistant minerals or materials, such as quartz, in sedimentary rocks, the more resistant the rocks will be to weathering (Bell 2007).

The UCS values obtained from the point load test are generally lower than those of fresh rocks' standard UCS value range (Vallejo and Ferrer 2011). This condition is interpreted as a result of the influence of the weathering process. In addition, the effect of rock characteristics on slope stability in the study area can also be seen from the presence of sedimentary structures in the form of bedding that can be found in some observation points as discontinuity planes that can reduce the quality value of the rock mass.

4.1.2 Geological Structure

Geological structures in the research area consist of a shear joint, an extension joint, and several types of faults. Based on the analysis of the main force direction on the faults, it is found that the main force has a relative north-south direction. The study results of the shear joint and extension joint also confirm it. In addition, the direction of the main force is also shown from the distribution of rock orientation, which is indicated to be influenced by geological structures in the form of folds from the DEM image and Regional Geological Map (Asikin et al. 1992). The direction of the force itself can be determined perpendicular to the value of the alignment of the rock layers. In general, the research area has the alignment of the rock layers in the west-east direction; therefore, it is interpreted that the direction of the main force acting has a relative north-south direction, known as the Java direction. The minor faults encountered, such as sinistral thrust fault, sinistral shear fault, and dextral shear fault, are interpreted as third-order faults that accompany the development of first-order faults as the main product of the tectonic forces acting in the area (Moody and Hill 1956). The major structures in inferred reverse and sinistral shear faults were identified based on DEM images and field observation. This inferred

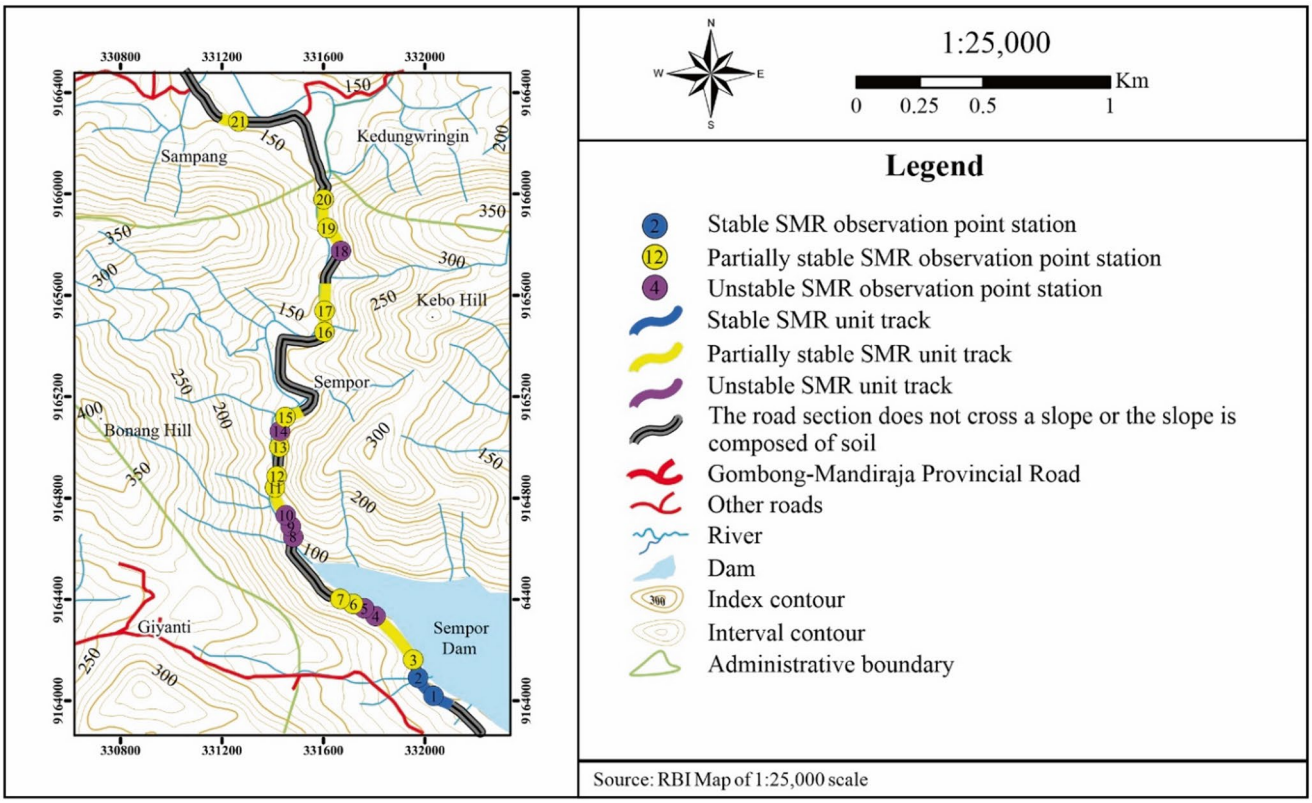

Fig. 6 Slope stability map of Provincial Road Section, Kebumen, according to SMR classification

reverse fault is located north of the research area and is relatively west-east oriented. The alignment, morphology, and appearance of fault scarps on the DEM images indicate the existence of the reverse fault.

4.2 Rock Mass Quality Based on the RMR Method

Based on the RMR analysis, there are three rock mass quality units: a good RMR unit (RMR value 61–80), a fair RMR unit (RMR value 41–60), and a poor RMR unit (RMR value 21–40). Table 5 summarizes the rock mass quality characteristics of each type of RMR unit.

Good RMR units are located on road segments at kilometres (KM) 1 + 127 to KM 1 + 428, KM 1 + 481 to KM 1 + 521, KM 1 + 624 to KM 1 + 686, and KM 2 + 611 to KM 2 + 671. These units have a range of RMR values from a low of 63 to a high of 77. UCS values based on point load tests range from 82.27 to 185.25 MPA. The RQD values obtained based on the scanline method were recorded in the value classes of 75–90% (good) and 90–100% (excellent). The discontinuity spacing consists of 2 classes: the moderate spacing class with values between 0.2 to 0.6 m and the wide spacing class with values between 0.6 and 2 m. Then, the results of observations of the discontinuity conditions in this unit include length, roughness, aperture, filler, and weathering at each observation point station, showing several classification classes. The discontinuity length is recorded to have two value classes, namely <1 m and 1–3 m value classes. The roughness of the discontinuities had values ranging from rough to slightly rough, and the aperture of the discontinuities had values of 1–5 mm and >5 mm. In general, the discontinuities in this unit do not have fillers. The degree of weathering consists of 2 values: slightly weathered and moderately weathered. The overall groundwater condition in this unit is damp and wet.

Fair RMR units are located on road segments at KM 0 + 160 to KM 0 + 829, KM 1 + 521 to KM 1 + 624, KM 2 + 240 to KM 2 + 459, and KM 2 + 531 to KM 2 + 611, and KM 2 + 671 to KM 2 + 848. These units range in value from a low of 45 to a high of 60. The UCS values obtained based on the point load test range from 11.44 to 81.13 MPa. The RQD values obtained based on the scanline method were recorded in the value classes of 75–90% (good) and 50–75 (fair). The discontinuity spacing consists of 2 classes: the moderate spacing class with values between 0.2 to 0.6 m and the close spacing class with values between 0.06 to 0.2 m. Then, the observation results of the discontinuity conditions in this unit, including

Table 3 Comparison of the petrographic characteristics of rocks found in the study area is related to the compressive strength values obtained based on the point load test results

Lithology	Porosity based on petrographic analysis (%)	General rock porosity values (Vallejo and Ferrer 2011) (%)	Characteristics	Rock compressive strength values based on point load test results (MPa)	Rock compressive strength values for rocks in fresh condition (Vallejo and Ferrer 2011) (MPa)
Fragments of andesite igneous rock in breccia rock	5	10–15	The composition consists of quartz minerals, plagioclase, pyroxene, opaque minerals, and volcanic glass, where the relationship between the mineral grain interlocks	66.69–185.25	100–500
Sandstone consisting of micritic sandstone, arkose, and lithic wacke	14–23	5–25	Three types of sandstone affect the stability of slopes in the study area. The composition generally consists of quartz, plagioclase, pyroxene, lithics, and opaque minerals and has a variety of textures such as packing, grain contact, and pore abundance, as shown in Table 6	11.4–36.54	30–235
Vitric tuff	9	14–40	The composition is dominated by fine-sized volcanic glass	9.4	10–46

Table 4 Comparison of petrographic characteristics of several types of sandstones in the study area is related to the compressive strength values obtained based on the point load test results

Type of sandstone	Porosity based on petrographic analysis	Packing	Grain contact	Rock compressive strength values based on point load test results (MPa)	Rock compressive strength values for rocks in fresh condition (Vallejo and Ferrer 2011) (MPa)
Micritic sandstone	16%	Grain supported	Floating, point contact, and prolonged contact	17.61–36.54	30–235
Arkose	15%	Grain supported	Floating, point contact, and prolonged contact	18.1	
Lithic wacke	23%	Matrix supported	Floating and point contact	11.4–19.63	

length, roughness, openings, fillers, and weathering at each observation point station, show several classification classes. The discontinuity length is recorded to have three value classes, namely <1 m, 1–3 m, and 3–10 m value classes, as shown in Table 1. The roughness of the discontinuity has values ranging from rough, slightly rough, to smooth. The discontinuity aperture ranges from 1–5 mm and > 5 mm. In general, the discontinuities in this unit have no filler. The degree of weathering consists of 3 values: slightly weathered, moderately weathered, and highly weathered. The overall groundwater condition in this unit is damp and wet. The poor RMR unit is on the road segment at KM 3 + 405 to KM 3 + 493. Based on the RMR classification (Bienawski 1989), the unit has an RMR value 38. The UCS value obtained based on the point load test was recorded at 13.8 MPA. The RQD value received based on the scanline method was recorded to be in the <25% value class (very poor). The discontinuity spacing is in the very close spacing value class with a value of <0.06 m. The discontinuity length in this unit has a value in the <1 m class. The roughness of the discontinuity is smooth. The discontinuity aperture has a value of 0.1–1 mm. In general, the discontinuities in this unit have no filler. The weathering level has a high weathering class value. The overall groundwater condition in this unit is damp.

Good, fair, and poor rock mass quality units can be found in 3 different rock units. Ideally, each rock unit has one type of rock mass quality due to the same rock characteristics. However, in the research area, more than one type of rock mass quality can be found in each rock unit. It can occur because each rock that forms the slope in the same rock unit has different conditions. The difference is assumed to come from the frequency of discontinuities on each slope, the condition of the discontinuities, the UCS value, groundwater conditions, and the level of rock weathering. The rock mass

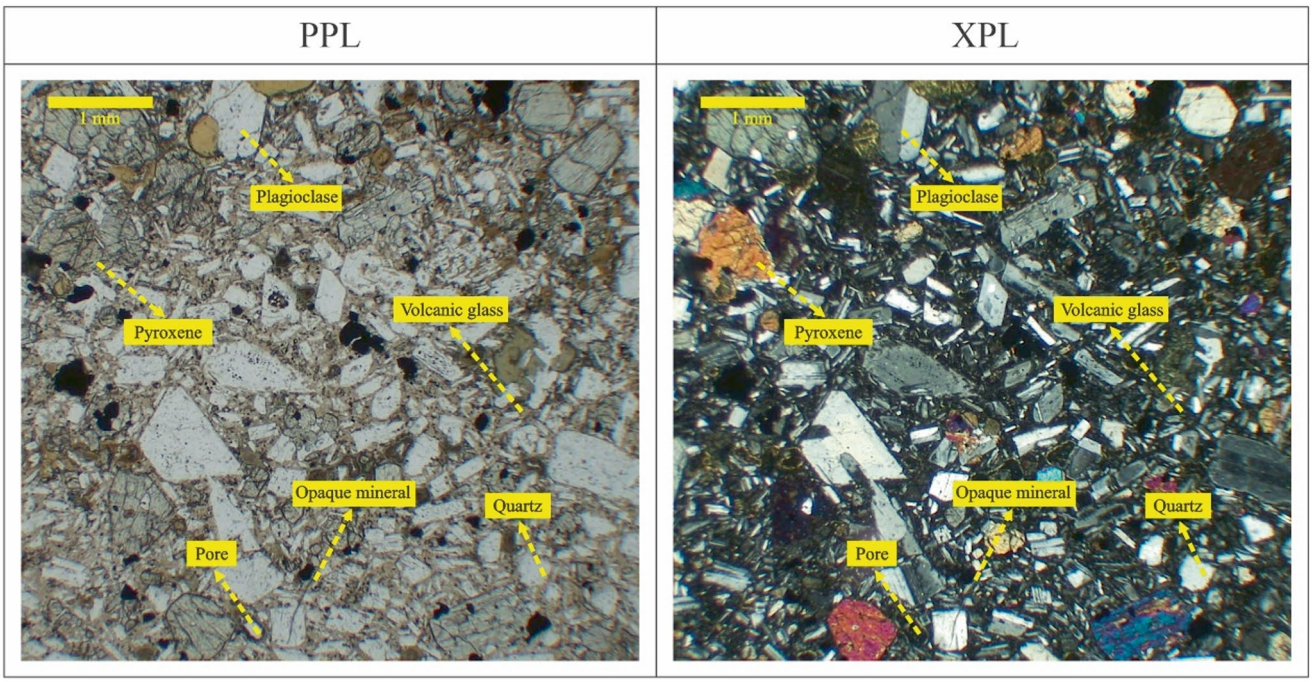

Fig. 7 Andesite (Streckeisen 1980) fragment in breccia rock (part of andesite breccia with sandstone insertion units) in thin section

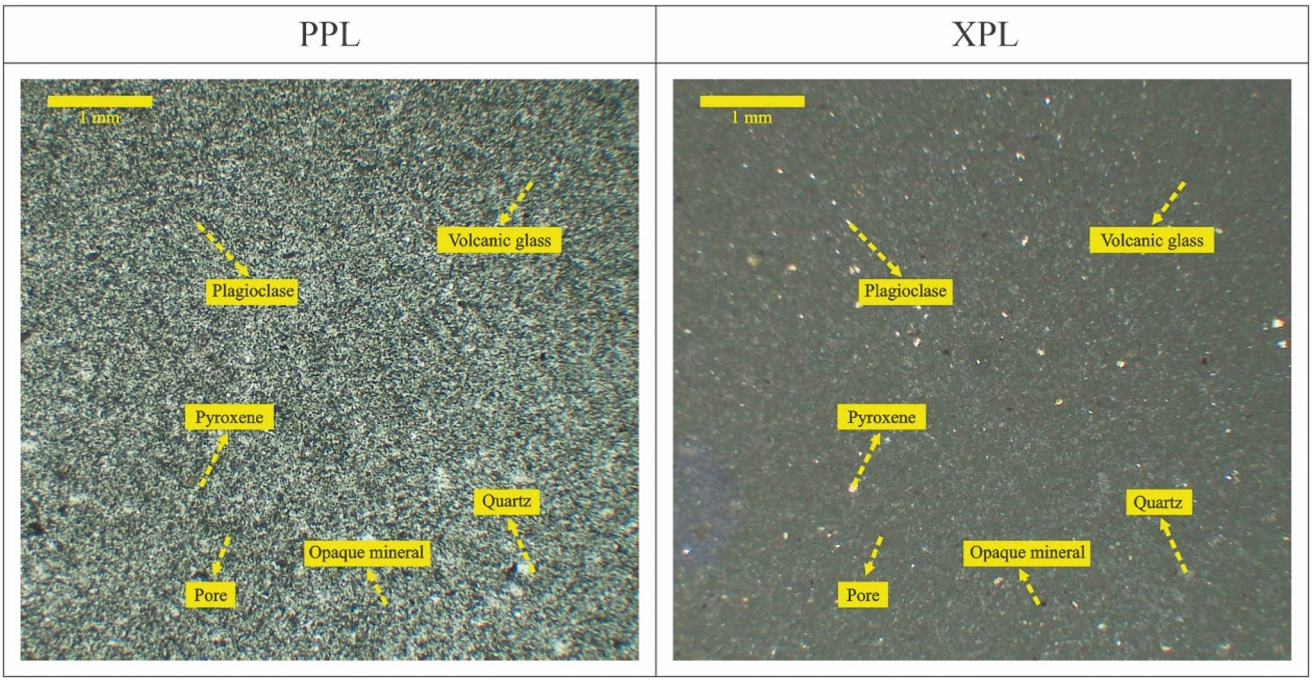

Fig. 8 Vitric tuff (Schmid 1981) (part of the interbedded tuff, sandstone, and carbonate claystone unit) in thin section

quality value will be lower or worse when more discontinuities are found in the rocks, such as weak planes or sliding planes, the low weighting of discontinuity conditions, low UCS values, high amounts of groundwater in the rock, and high rock weathering. The opposite situation will make the rock mass quality value better.

4.3 Slope Stability Condition Based on SMR Method

There are three slope stability units based on the SMR analysis. The SMR units consist of stable SMR units (SMR value 61–80), partially stable SMR units (SMR value 41–60), and

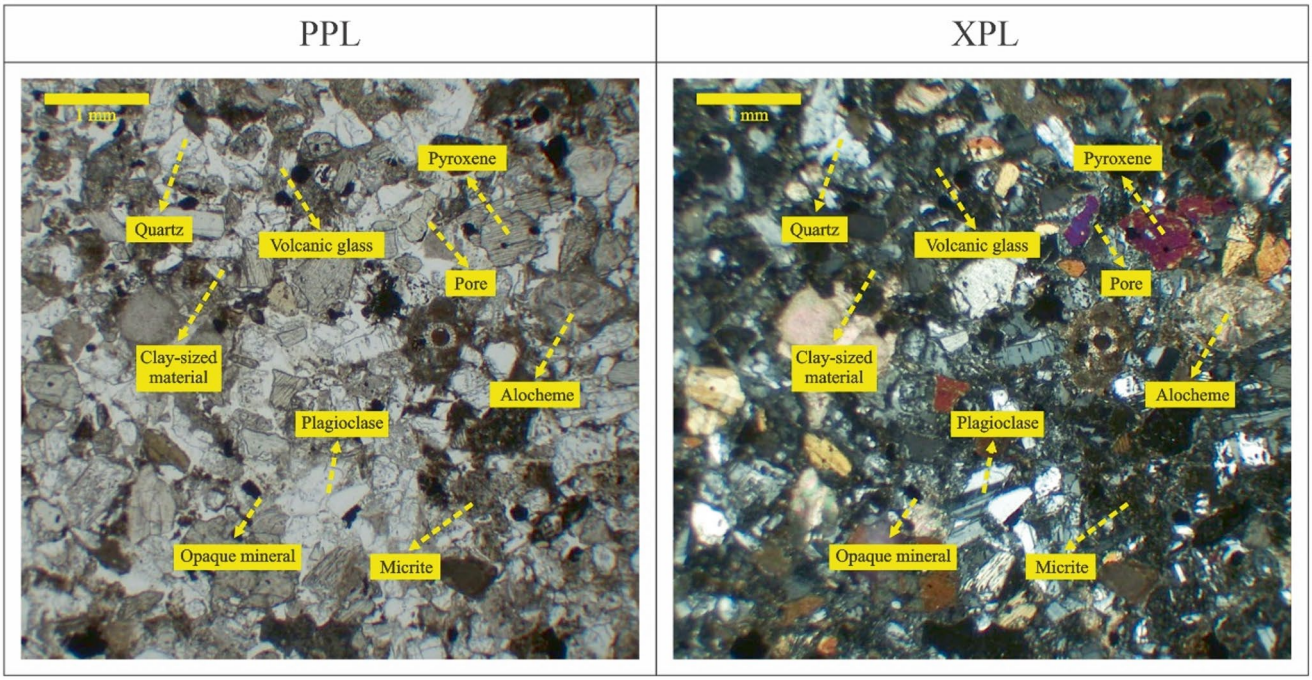

Fig. 9 Micritic sandstone (Mount 1985) (part of carbonate sandstone units) in thin section

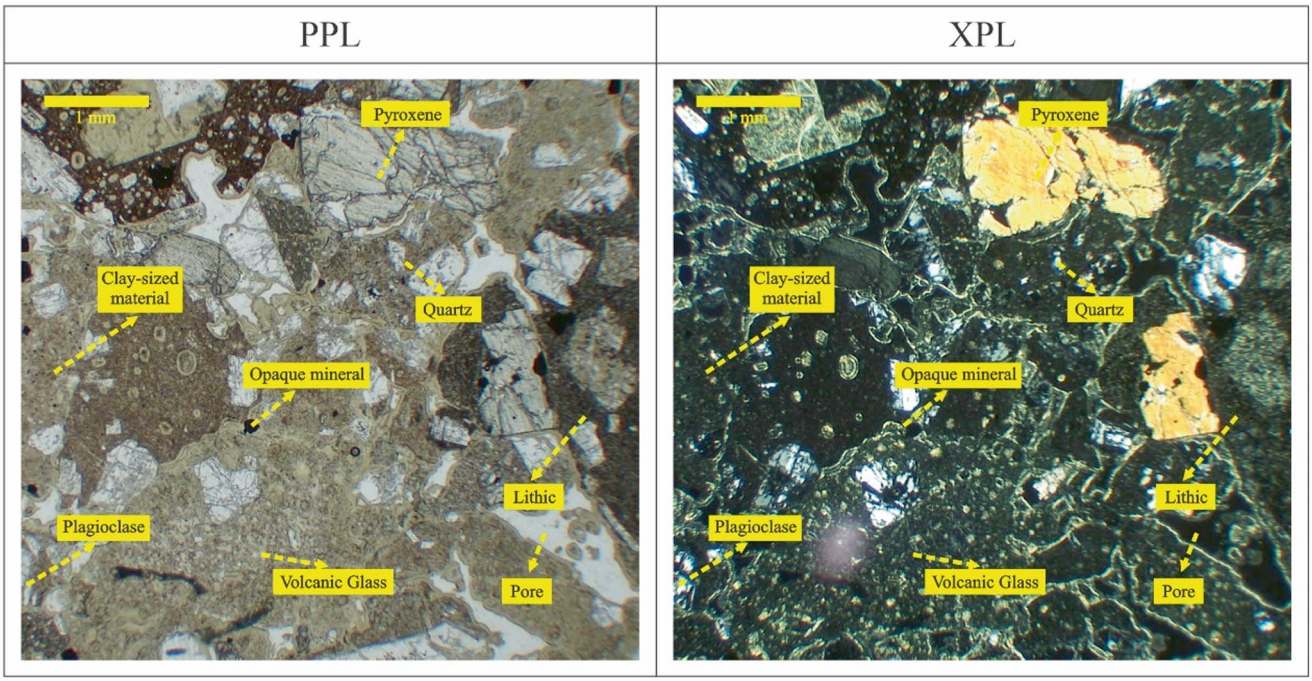

Fig. 10 Lithic wacke (Pettijohn et al. 1987) (part of andesite breccia with sandstone insertion units) in thin section

unstable SMR units (SMR value 21–40). The summary of slope stability condition characteristics in each SMR unit is presented in Table 6.

The stable SMR unit is located on the road segment at KM 0 + 160 to KM 0 + 383. The unit has a range of SMR values from the lowest, 63.5, to the highest, 64.5. Based on the kinematics analysis, this unit's type of slope failure is generally a wedge-type failure. This unit has an F_1 value of 33–31 with a weighting of 0.15 (very favorable), an F_2 value of 66–68 with a weighting of 1 (very unfavorable), and an F_3

Table 5 Rock mass quality conditions summary of the research area based on Rock Mass Rating classification

RMR class	Good	Fair	Poor
Slope position on the road	Observation points station 8, 9, 10, 11, 12, 13, 15, 19	Observation points station 1, 2, 3, 4, 5, 6, 7, 14, 16, 17, 18, 20	Observation points station 21
RMR value	63–77	49–60	38
UCS value	32.55–185.25 MPa	11.44–81.13 MPa	13.8 MPa
RQD	75–90% (good) and 90–100% (excellent)	50–75 (fair), 75–90% (good), and 90–100% (excellent)	<25% (very poor)
Discontinuity spacing	0.2–0.6 m (moderate) and 0.6–2 m (wide)	0.2–0.6 m (moderate) and 0.06–0.2 m (close)	<0.06 m (very close)
Discontinuity condition	Persistence: <1 m and 1–3 m	Persistence: 1–3 m and 3–10 m	Persistence: <1 m
	Roughness: *rough and slightly rough*	Roughness: rough, slightly rough, and smooth	Roughness: smooth
	Aperture: 1–5 mm and > 5 mm	Aperture: 1–5 mm and > 5 mm	Aperture: 0.1–1 mm
	No infilling	No infilling	No infilling
	Weathering: slightly weathered and moderately weathered	Weathering: slightly weathered, moderately weathered, and highly weathered	Weathering: highly weathered
Groundwater condition	General consists of wet and damp conditions	General consists of wet and damp conditions	General consists of damp conditions

Table 6 Slope stability conditions summary of the research area

SMR class	Stable	Partially stable	Unstable
Slope position on the road	Observation points station 1 and 2	Observation points station 3, 6, 7, 11, 12, 13, 15, 16, 17, 19, 20, 21	Observation points station 4, 5, 8, 9, 10, 14, and 18
SMR value	66.5–67.5	45.35–58	22.65–38.6
The dominant type of failure	Wedge failure	Wedge failure	Wedge failure, and there is one observation point station with plane failure
F_1	33–31 › weighting value 0.15 (very favorable)	34–16 › weighting values of 0.15 (very favorable), 0.4 (favorable) and 0.7 (fair)	12–6 › weighting values of 0.7 (fair) and 0.85 (unfavorable)
F_2	66–68 › weighting value 1 (very unfavorable)	39–58 › weighting value 0.7 (fair), 0.85 (unfavorable), and 1 (very unfavorable)	33–60 › weighting values 0.7 (fair), 0.85 (unfavorable), and 1 (very unfavorable)
F_3	−4 to −8 › weighting value −50 (unfavorable)	−16 to −42 › weighting values −50 (unfavorable) and − 60 (very unfavorable)	−7 to −38 › weighting values −50 (unfavorable) and −60 (very unfavorable)
F_4	Natural slope › weighting value 15	Natural slope › weighting value 15	Natural slope › weighting value 15
Stability	Stable	Partially stable	Unstable
Probability of failure	0.2	0.4	0.6
Slope support methods	• Spot bolting, systematic bolting	• Shotcrete, dental concrete	• Re-excavation
	• Toe ditch, toe or slope fences, nets	• Spot bolting, systematic bolting	• Walls
	• Scaling	• Toe walls	• Surface drainage, deep drainage
		• Toe ditch, toe or slope fences, nets	• Shotcrete, dental concrete
			• Spot bolting, systematic bolting

value of −4 to −8 with a weighting of −50 (unfavorable). Then, the F_4 value related to the slope excavation method used produces a weighting value of +15 because the slopes contained in the unit are assumed to be formed as natural slopes in consideration of limited information and the appearance of visible slopes influenced by the process of erosion, weathering, and the appearance of vegetation. The stable SMR class ideally has good rock mass quality values (Romana 1985). However, the study area has stable SMR units with fair rock mass quality values. It can happen because the SMR value is also influenced by calculating the correction factor value related to discontinuity orientation and slope. Slopes in the stable SMR class have a 20% probability of failure in the form of several block failures, ideally.

Methods used for slope reinforcement in this SMR class are spot bolting, systematic bolting, toe ditch, toe or slope fences, nets, and scaling (Romana 1985).

Partially stable SMR units are located on road segments at KM 0 + 383 to KM 0 + 610, KM 0 + 722 to KM 0 + 829, KM 1 + 244 to KM 1 + 428, KM 1 + 481 to KM 1 + 549, KM 1 + 623 to KM 1 + 686, KM 2 + 153 to KM 2 + 459, KM 2 + 531 to KM 2 + 582, KM 2 + 605 to KM 2 + 848, and KM 3 + 405 to KM 3 + 493. The unit has a range of SMR values from a low of 43.3 to a high of 58. Based on the kinematics analysis that has been done, the type of slope failure found in this unit is generally a wedge-type failure. This unit has an F_1 value in the range of 34–16 with a weighting of 0.15 (very favorable), 0.4 (favorable), and 0.7 (fair). It has an F_2 value in the range of 39–58 with a weighting of 0.7 (fair), 0.85 (unfavorable), and 1 (very unfavorable). This unit has an F_3 value in the range of −16 to −42 with a weighting of −50 (unfavorable) and −60 (very unfavorable). Then, the F_4 value related to the slope excavation method used produces a weighting value of +15 because the slopes contained in the unit are assumed to be formed as natural slopes in consideration of limited information and the appearance of visible slopes influenced by the process of erosion, weathering, and the appearance of vegetation. Ideally, the partially stable SMR class has fair rock mass quality values (Romana 1985).

However, the study area has partially stable SMR units with good to poor rock mass quality values. This can happen because the SMR value is also influenced by the calculation of correction factor values related to discontinuity orientation and slope. Slopes in the partially stable SMR class have a 40% probability of failure in the form of plane failure in some discontinuity planes and many wedge failures ideally. Methods used for slope reinforcement in this SMR class are shotcrete, dental concrete, spot bolting, systematic bolting, toe walls, toe ditches, toe or slope fences, and nets (Romana 1985).

Unstable SMR units are located on road segments at KM 0 + 610 to KM 0 + 722, KM 1 + 127 to KM 1 + 244, KM 1 + 549 to KM 1 + 623, and KM 2 + 582 to KM 2 + 605. These units have a range of SMR values from a low of 22.65 to a high of 38.6. Based on the kinematics analysis that has been done, the type of slope failure found in this unit is generally a wedge-type collapse, and there is one station with a dominance of plane failures. This unit has an F_1 value for wedge-type failure in the range of 11 to 6 with a weighting of 0.7 (fair) and 0.5 (unfavorable). This unit has an F_1 value for plane failure 12 with a 0.7 (fair) weighting. This unit has an F_2 value in the range of 33 to 60 with a weighting of 0.7 (fair), 0.85 (unfavorable), and 1 (very unfavorable). This unit has an F_3 value of −7 to −38 with a weighting of −50 (unfavorable) and −60 (very unfavorable). Then, the F_4 value related to the slope excavation method used produces a weighting value of +15 because the slopes contained in the unit are assumed to be formed as natural slopes in consideration of limited information and the appearance of visible slopes influenced by the process of erosion, weathering, and the appearance of vegetation. The unstable SMR class ideally has poor rock mass quality values (Romana 1985). However, the study area has unstable SMR units with fair rock mass quality values. It can happen because the SMR value is also influenced by the calculation of correction factor values related to discontinuity orientation and slope. Slopes in the unstable SMR class have a 60% probability of failure in plane failure and large-scale wedge failure. Methods used for slope reinforcement in this SMR class include re-excavation, walls, surface drainage, deep drainage, shotcrete, dental concrete, spot bolting, and systematic bolting (Romana 1985).

5 Conclusions

The slope stability of the research area is divided into three classes: stable SMR units, partially stable SMR units, and unstable SMR units with rock mass quality values based on the RMR classification divided into three classes, consisting of good, fair, and poor units. The rock units that compose the research area are comprised of 4 units. From the oldest, the rock unit consists of interbedded tuff, sandstone, and carbonate claystone unit, andesite breccia with sandstone insertion unit, carbonate sandstone unit, and interbedded sandstone and carbonate siltstone unit. Geological structures in the research area consist of sinistral shear faults, dextral shear faults, normal faults, inferred reverse faults, shear joints, and extension joints. Due to their properties, interbedded tuff, sandstone, and carbonate claystone units have the lowest rock mass rating. However, the rock unit with the lowest SMR value is not interbedded tuff, sandstone, and carbonate claystone unit but carbonate sandstone due to the more massive geological structure and joint orientation, which is more conducive to slope failure. The result of the study can be used as basic information to mitigate landslides along the road.

References

Abramson LW, Lee TS, Sharma S, Boyce GM (2001) Slope stability and stabilization method, 2nd edn. Wiley, Hoboken, p 736

Asikin S, Handoyo A, Prastistho B, Gafoer S (1992) Peta Geologi Lembar Banyumas, Jawa, Skala 1:100,000. Pusat Penelitian dan Pengembangan Geologi, Bandung

ASTM D 5731-95 (1995) Standard test method for determination of rock's point load strength index. ASTM International, West Conshohocken

Bieniawski ZT (1989) Engineering Rock Mass Classification. John Willey and Sons, New York, 251 p.

Bell FG (2007) Engineering geology, 2nd edn. Butterworth-Heinemann, Oxford, p 592

BIG (2014) Peta Negara Kesatuan Republik Indonesia Skala 1:2.500.000. https://indonesia.go.id/peta-indonesia/22
BIG (2021) Peta Rupa Bumi Indonesia Skala 1:25.000. https://tanahair.indonesia.go.id/
Dobereiner L, de Freitas MH (1986) Geotechnical properties of weak sandstones. Geotechnique 36:79–94
Goodman RE (1989) Introduction to Rock Mechanics. 2nd Edition, John Wiley & Sons Ltd, New York, p 562
Hoek E, Bray J (1981) Rock slope engineering, 3rd edn. CRC Press, London, p 368
Irvani, Wilopo W, Karnawati D (2013) Determination of nuclear power plant site in West Bangka based on rock mas rating and geological strength index. J Appl Geol 5(2):78–86
Jeng FS, Weng MC, Lin ML, Huang TH (2004) Influence of petrographic parameters on geotechnical properties of tertiary sandstones from Taiwan. Eng Geol 73:71–91
Juhari AS, Indrawan IGB, Wilopo W (2021) The engineering characteristics and classifications of rock masses along road section from Prambanan to Patuk, Yogyakarta, Indonesia. J Appl Geol 6(2):119–127
Moody JD, Hill MJ (1956) Wrench-fault tectonics. Bull Geol Soc Am 67(9):1207–1246
Mount J (1985) Mixed siliciclastic and carbonate sediments: a proposed first-order textural and compositional classification. Sedimentology 32:435–442
Pettijohn FJ, Potter PE, dan Siever R (1987) Sand and sandstone, 2nd edn. Springer, New York, p 553
Priest SD, Hudson JA (1976) Discontinuity spacings in rock. Int J Rock Mech Min Sci Geomech 13:135–148
PVMBG (Pusat Vulkanologi dan Mitigasi Bencana Geologi) (2013) Peta Zona Kerentanan Gerakan Tanah Jawa Bagian Tengah. Pusat Vulkanologi dan Mitigasi Bencana Geologi, Jawa Tengah
Ramadhani S, Rifa IA, Suryolelono KB, Wilopo W (2018) Slope stability of metamorphic rocks based on rock mass classification at Poboya gold mine, Central of Sulawesi Province. Int Rev Civil Eng 9(3):91–97
Romana M (1985) New adjustment ratings for application of bieniawski classification to slopes. In: Proceedings of the international symposium on the role of rock mechanics in excavations for mining and civil works. International Society of Rock Mechanics, Zacatecas, pp 49–53
Romana MR (1993) A geomechanical classification for slopes: slope mass rating. In: Hudson JA (ed) Comprehensive rock engineering, vol 3. Pergamon Press, Oxford, pp 575–600
Schmid R (1981) Descriptive nomenclature and classification of pyroclastic deposits and fragments: recommendations of the lugs subcommission on the systematics of igneous rocks. The Geological Society of America, Boulder
Streckeisen A (1980) Classification and nomenclature of volcanic rocks, lamprophyres, carbonatites and melilite rocks IUGS Subcommission on the Systematics of Igneous Rocks. Geol Rundsch 69:194–207
Vallejo LG, Ferrer M (2011) Geological engineering. CRC Press, London, p 700
Wijaya AE, Karnawati K, Srijono W, W. (2015) Quarry mine design of cavity limestone in Sawir Block Tuban East Java. Jurnal Promine 3(2):10–17
Wyllie DC, Mah CW (2004) Rock slope engineering-civil and mining, 4th edn. CRC Press, London, p 456

The Landslide Occurrence Under Extreme Rainfall Events: The Central Italy Case on September 15, 2022

Stefano Morelli, Giulio Fabrizio Pappafico, and Erica Guidi

Abstract

On September 15, 2022, a stationary V-shaped thunderstorm formed over the Apennines in central Italy, dumping up to 419 mm of rain in just 9 h near the town of Cantiano, causing widespread severe flooding and landslides over an area of 5000 km^2. This study highlighted the relationships between the landslides mapped after the event in the mountainous areas with the highest rainfall intensity (E-LIM inventory), the surrounding territory, and the rainfall event itself. Then, their comparison with those of a detailed mapping conducted before the event at the national level (IFFI inventory), based on a collection of data accumulated over the years, allowed for an initial examination of the variability in the territory's response to an event outside the typical climatic conditions upon which the spatial information regarding landslide risks is currently founded. The analyses were conducted over an area of 550 km^2, considering the findings deriving from field surveys and a detailed GIS analysis. These landslides were concentrated in areas with rainfall between 285 and 419 mm in 24 h, corresponding to carbonate lithologies. Relatively high values in the last class of precipitation (45–125 mm) are instead related to the predominant occurrence of Quaternary slope debris. The main landslide types are debris flow, debris slide and debris slide-flow, and almost ¾ of the overall dataset are new landslides. In cases of overlay with already mapped areas, eighty per cent of the E-LIM debris flows correspond to roto-translational slides and slow earth flows recorded in the IFFI inventory. The new landslides did not develop along slopes with aspects significantly different from the oldest landslides, and the occurrence of both pre-existing and post-extreme event landslides was determined by geology and morpho-structural settings.

Keywords

Extreme event · Slope instabilities · Landslide inventories · GIS analysis · Italy

1 Introduction

Landslides pose a serious threat to people worldwide, leading to fatalities, extensive damage, and substantial economic losses. Various factors influence slope stability and can trigger landslides, with rainfall being the primary cause. Rainfall patterns are heavily regulated and influenced by the climate and its fluctuations. As such, climate change is expected to impact slope stability on different temporal and geographical scales. In recent years, a rise in global average temperatures has been widely acknowledged (Kabir et al. 2023; Allen et al. 2018). Consequently, the frequency and severity of extreme weather events are also on the rise, such as in the Mediterranean area being affected by the new phenomenon of Medicanes (Diakakis et al. 2023; Kushabaha et al. 2024), although in some regions, the annual average rainfall shows no significant change. Assessing the impact of climate change on landslides (and other related geo-hydrological hazards) remains an open challenge for the scientific community. Currently, systematic and timely documentation of triggered landslides is fundamental to building extensive datasets worldwide that may help further analyses like trends in response to climate change. Based on a landslide inventory compiled by Santangelo et al. (2023a, b) concerning an extreme rainfall event that caused significant geo-hydrological impacts (floods and landslides, resulting in damage to urbanised areas) in the Marche region of Italy in 2022, this study aims to highlight relationships between landslides, the surrounding territory, and the rainfall event itself. A comparison with a detailed mapping conducted

S. Morelli (✉) · G. F. Pappafico · E. Guidi
Department of Pure and Applied Sciences, University of Urbino Carlo Bo, Urbino, Italy
e-mail: stefano.morelli@uniurb.it; giulio.pappafico@uniurb.it; e.guidi16@campus.uniurb.it

B. Abolmasov et al. (eds.), *Progress in Landslide Research and Technology, Volume 4 Issue 1, 2025*, Progress in Landslide Research and Technology, https://doi.org/10.1007/978-3-031-89836-5_19

before the event, based on a collection of data accumulated over the years, allows for an initial examination of the variability in the territory's response to an event outside the typical climatic conditions upon which the spatial information regarding landslide risks is currently based.

2 Study Area

2.1 The Severe Pluviometric Event

On September 15, 2022, a stationary, self-regenerating V-shaped thunderstorm formed over the Apennines mountain chain in central Italy due to a warm, humid air mass coming from North Africa and collecting additional moisture from the Tyrrhenian Sea. The real first storm cells formed on the Tyrrhenian side, meeting the first mountain peaks in the border areas between the Marche and Umbria regions, which helped the lifting of hot and humid air in the lower troposphere (Corti et al. 2024). As the system migrated eastwards, a "V"-shaped supercell started forming, locating its vertex near the Cantiano town, persisting here for some hours at very high rainfall intensities. The rain gauge of Cantiano recorded 384 mm in 6 hours and a peak of 419 mm in 9 h, about a third of the average annual rainfall. The storm weakened as it moved towards the Adriatic Sea, impacting an area of 5000 km^2. This led to widespread issues and sudden criticalities from mountain areas to coastal flooding plans at a later time (Morelli et al. 2023). For this reason, the Italian Council of Ministers deliberated the emergency state, activating the National Civil Protection Department to address the emergency through its reference operational structures.

Before the thunderstorm, the soil was dry due to a prolonged summer drought, with no significant rainfall in the 30 days prior. Only minimal precipitation occurred between August 15 and September 15 (Santangelo et al. 2023a). This dryness, combined with the heavy rainfall, caused rapid rises in river levels, leading to sudden, destructive flooding and numerous landslides, which increased downstream solid transport (Donnini et al. 2023).

2.2 The Geographical and Geological Framework

The study area consists of the mountainous zones with the highest rainfall intensity, extending for about 550 km^2 (Donnini et al. 2023). It also corresponds to the study area considered by Santangelo et al. (2023a) for the realisation of an event landslide inventory map (called E-LIM: Guzzetti et al. 2012) as a result of a field survey in the aftermath of the rainfall event (Fig. 1). This area includes contiguous slopes affected by widespread landslides throughout the landscape, including natural slopes, cultivated lands, and reprofiled lands by cuts and fills (e.g., road slopes).

The study area is part of the northeast-verging fold-and-thrust belt of the Northern Apennines. It is characterised by outcropping lithological units belonging to the Umbria-Marche succession and spanning a time interval from the Jurassic to the middle-upper part of the Neogene. These units can be more broadly subdivided into a Jurassic-to-Paleogene carbonate-marl succession and a Neogene predominantly siliciclastic-terrigenous succession (Fig. 1). The first sedimentary succession represents platform sedimentation during tectonic phases of continental breakup followed by a period of tectonic quiescence with pelagic sedimentation and then by pelagic and turbiditic sedimentation due to extensive tectonic reactivation. The second sedimentary succession represents the transition to compressional tectonics with pre- and syn-orogenic sedimentation (Calamita et al. 1986; Montanari et al. 2023; Pierantoni et al. 2013).

2.3 Data

The analyses were conducted considering the findings deriving from two different moments of activity:

- the field survey to support regional civil protection in managing emergencies under the supervision of the national civil protection department. The field survey focused on verifying the site conditions and post-event hazardous situations for the involved population, enabling a timely assessment of the residual risk.
- The GIS Analyses comparing the event landslide data from the new inventory realised by Santangelo et al. (2023a) with pre-existing landslide databases and each other geographic information helpful in understanding the landslide occurrence in the context of the study area.

The primary data are listed in Table 1.

The **E-LIM** landslides mapped by Santangelo et al. (2023a) in this area are 1687, of which 1243 were mapped as polygons and 444 were mapped as points due to their too-small area of only a few square meters (Donnini et al. 2023). The landslides were classified based on the type of material involved and the type of movement, following Hungr et al. (2014) (in Santangelo et al. 2023a; Donnini et al. 2023). The number and the total area of the landslide types are summarised in Table 2 by Donnini et al. (2023).

The **Italian Landslide Inventory** (**IFFI** Project) was realised by the Institute for Environmental Protection and Research (ISPRA)-Geological Survey of Italy and by the 21 Italian Regions and Self-Governing Provinces (Trigila et al. 2007, 2010; Trigila and Iadanza 2008). IFFI is Italy's most complete and detailed landslide database (Trigila and

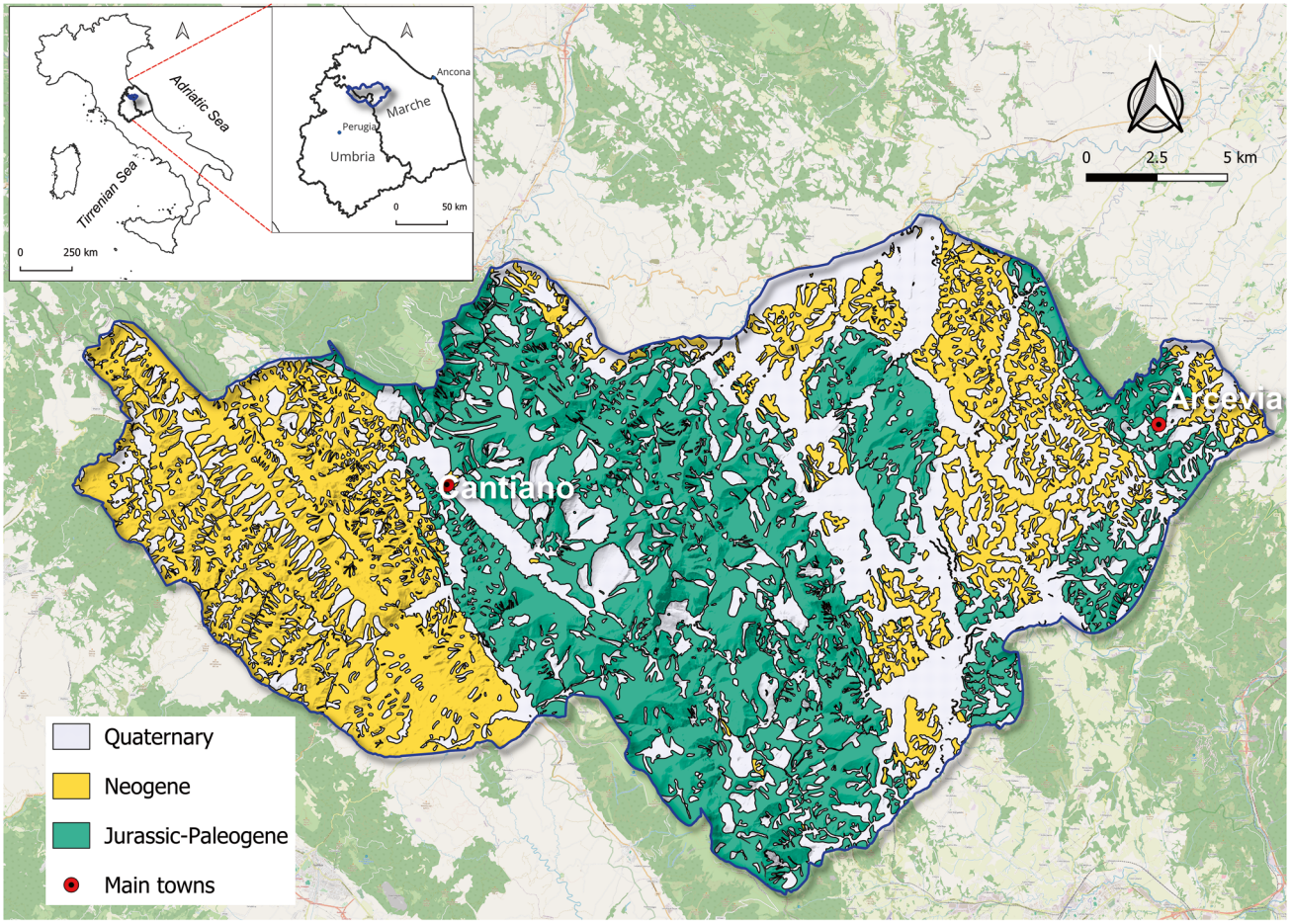

Fig. 1 Study area delimited by blue boundary corresponding to the Area of Interest (AOI) by Santangelo et al. (2023a) with the representation of the three lithological successions, different in overall composition

Table 1 Used primary data and their sources

Name	Characteristics	Year of publication	Sources
TINITALY DEM (digital elevation model of the bare ground with 10 m-resolution)	TINITALY/1.1 of the TINITALY DEM, released in 2023. It is the DEM of the whole Italian territory obtained from DEMs of single regions of Italy	*2007 and upgraded in January 2023*	*Istituto Nazionale di Geofisica e Vulcanologia—Sezione di Pisa* (Tarquini et al. 2007; Tarquini et al. 2023) link: https://tinitaly.pi.ingv.it/
IFFI project (the Italian Landslide Inventory)	A detailed landslide database of Italy for the number of recorded parameters and the 1:10,000 map scale (Trigila et al. 2010) The database also stores the type of movement and landslide activity. ISPRA,[a] Regions and Autonomous Provinces realised it	The database was updated to 2007 for the Marche Region and 2018 for the Umbria Region (Trigila et al. 2021)	ISPRA[a] IdroGeo—The Italian web platform on landslides and floods
E-LIM Event Landslide Inventory Map	Inventory of landslides triggered by the extreme rainfall occurred in the Marche and Umbria regions (Italy) on September 15, 2022	The database is publicly available from 2023: Santangelo et al. (2023a, b)	E-LIM database
CARG Project	The CARG (Geological CARtography) project provides a geological database for territorial planning and management	Geological surveys conducted in the 1990s	ISPRA[a] CARG Project—geologic and geo-thematic cartography Marche Region geologic database Umbria Region geologic database

[a] *ISPRA* Institute for Environmental Protection and Research

Table 2 Number and total area of ELIM landslide types

	Fall		Flow		Slide-flow		Slide		Total	
	Count	Area (m^2)	Count	Area (m^2)	Count	Area (m^2)	Count	Area (m^2)	Count	Area (m^2)
Rock	18	5100	–	–	–	–	6	6900	24	12,000
Debris	–		304	600,000	132	190,000	232	110,000	668	900,000
Earth	–		65	22,000	88	49,000	842	140,000	995	210,000
Total	18	5100	369	622,000	220	239,000	1080	256,900	1687	1,122,000

Table 3 Number and total area of IFFI landslide types

	Fall topple	Roto/ translational slide	Slow earth flow	Debris flow	Complex	DSGSD	undetermined	Widespr. landslide area	Widespr. fall landslide area	Total
Count	30	1008	904	46	284	14	99	110	28	2523
Area (m^2)	703,404	3.16×10^7	1.9×10^7	3.06×10^5	9.3×10^6	5.76×10^6	5.6×10^5	6.6×10^6	2.6×10^6	7.6×10^7

Iadanza 2018). To date, in Italy, the recorded landslides are 634,716. The IFFI landslides in the study area are more than 2500, of which 2400 were mapped as polygons, the smaller of which is about 226 m^2, and 123 were mapped as points due to their too-small area for the project survey scale (Table 3).

In this study, both E-LIM and IFFI landslides mapped as polygons are spatially compared and analysed from the point of view of the relationships with the outcropping lithologies and the respective slope aspect patterns. Due to the lack of the area and slope aspect values for the point IFFI landslides, areal comparisons with the E-LIM point landslides were not possible.

3 Results and Discussion

Through the field surveys, the state of the places was verified in detail, deducing the post-event dangerous conditions and producing a rapid and timely assessment of the residual risk as a product of immediate use for the management of the terminal phases of the emergency. Concerning the observed areas, it was possible to identify the following geo-hydrological effects on the ground as direct consequences of the rainfall event:

- *fast/very fast and well-localized landslides*.
  - Landslides whose dynamics are connected to high water content as triggers and sometimes transport mechanisms (fall, flow, slides). Despite the abundant soil on which the vegetation has established itself, the landslides have also affected the underlying rock levels, and therefore, the coarse debris is predominant.

Some mass movements can be defined as "complex" because they change in behaviour during the movement, showing a combination of several types of movements in a temporal sequence. Thanks to the high quantity of circulating water over widespread weathered rocks and soils, the most common combination was a slide of unconsolidated material followed by a flow at high energy along different types of slopes.

- *Soil washout*:
  - surface or channelled erosion (often on the same deposits accumulated after the gravitational event as a prolonged consequence of less intense rainfall in the hours following the precipitation peak)
- *Riverbed dynamics in extraordinary flood conditions with turbulent high-energy flows*:
  - riverbank erosion
  - undermining of hydraulic protection works, road infrastructures (bridges and roads) and various types of human artefacts in the riverbed or facing it
  - lateral overflows
  - collapse of soil banks due to undermining actions at the base by turbulent high water levels during floods (landslides typical of very high banks).

Actions in the latter category were associated with a localised vertical bed incision in areas with mobile riverbeds by the contingent river dynamics and by high sediment transport due to solid material transport by river or the multiple lateral contributions of landslide phenomena, as well as slope erosion.

From the reconstruction of the overall evolutionary framework of the landslide areas through terrain clues, it emerged that the slope phenomena, which resulted more significant for its impact on the territory, occurred as rapid flows in rather narrow impluvium and very steep slopes in the medium-high part of them (rarely involving the summit) (Fig. 2).

Fig. 2 (**a**) Debris slide-flow that hit a tractor; (**b**) House devastated and damaged by a landslide

Landscape-wise, they appeared similar to deep scratches on the surface of mountain areas, with highly evident visual aspects in wooded areas. The evolutionary dynamics have sometimes significantly influenced each other in cases where multiple events have come together in approaching the valley floor.

Furthermore, some landslide-type situations were exhausted in themselves, having transported all the material towards the lower areas. Still, in other cases, where multiple events interacted or the event itself encountered a strong morphologic interference (anthropic or natural), part of the removed material was accumulated along the slopes or in dynamically active areas, ready to be remobilised at later times. In any case, they always present a potential for reactivation at the head with retrogressive phenomena or lateral widening due to their position. However, the new flow-type events may have come to partially share the same path as previous events in the lower parts of the slope if the morphology has induced a single channelling solution.

The event-related landslides (E-LIM by Santangelo et al. 2023a) were analysed from the point of view of their spatial distribution relative to the main 24-hour cumulative rainfall ranges registered in the AOI and defined as follows: 45–125 mm; 125–205 mm; 205–285 mm; 285–365 mm; 365–419 mm. The distribution is divided into five classes, each of 80 mm, except for the highest, which does not reach this range, allowing a not-so-high number of rainfall ranges with which to compare the landslides.

The highest value is the peak value of 419 mm in 9 h recorded by the rain gauge of Cantiano. The range's spatial distribution corresponds to the areas outlined in Fig. 3.

In the E-LIM landslide inventory, debris-material landslides (Debris flow/slide/slide-flow) are the most significant landslide types across all 24 h-cumulative rainfall-rate classes expressed as area percentage compared to the other landslide types. Debris flow type, in particular, is the most frequent in the 365–419 mm rainfall-rate class (Fig. 4). Its occurrence progressively decreases from the 285–365 to the 125–205 mm rainfall rate range. This can be related to the prevalence of carbonate lithologies in areas with higher cumulative rainfall rates. At the same time, the modal value in the lowest class can be associated with the widespread presence of Quaternary slope debris in the corresponding area. Earth-material landslides (Earth flow/slide/slide flow) follow the distribution of the siliciclastic lithologies spatially decreasing from the lowest 24 h-cumulative rainfall rate areas to the highest ones.

The IFFI landslide inventory, representing all the mapped landslides throughout Italy before the event with every type of trigger, considers 11 types. This classification is based mainly on schemes by Varnes (1978) and Cruden and Varnes (1996), and its definitions, based mainly on the description of movement, are not fully comparable with those followed by E-LIM. The *Complex* type of this classification is not included in that by Hungr et al. (2014), followed by E-LIM, because almost every landslide is complex to a degree (Hungr et al. 2014). The *Deep-seated gravitational slope deformation* (DSGSD) type is also not included among E-LIM landslide types. The other nine landslide types cannot be directly compared to the E-LIM types because they lack references to landslide materials. Here, the *Rapid flow* type is considered the same as a debris flow type due to their polygons' shape, their location along narrow impluvium and carbonate lithology or debris able to trigger this landslide movement type.

The statistical IFFI landslide-type distribution shows that Roto/translational slide and Slow earth flow are the significant landslide types across all 24 h-cumulative rainfall-rate classes expressed as area percentage compared to the other landslide types (Fig. 5). They also affect all lithology outcroppings in the study area.

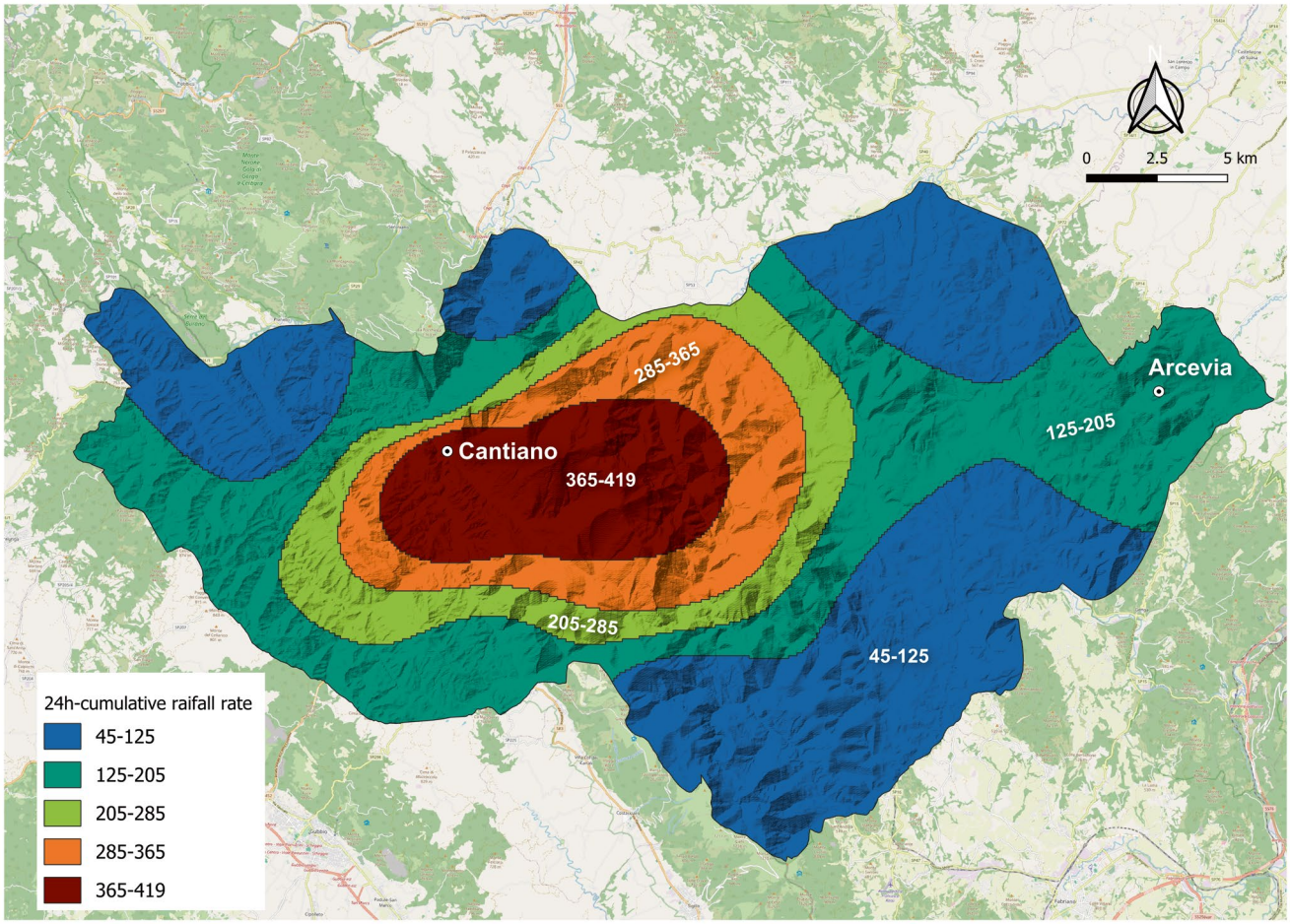

Fig. 3 Map of the 24 h-cumulative rainfall rate areas

26% of E-LIM landslides overlap IFFI landslides due to reactivation or new landslides triggered upslope of pre-existing landslides, which involved the latter in their movement. 80% of the E-LIM Debris flow overlaps with Roto/translational slide and slow earth flow from the IFFI inventory. These are followed by the percentages of the landslide types not found in the E-LIM inventory as *Complex* and *Widespread landslide areas* overlapped, respectively, with less than 2% and 3% of the E-LIM landslides.

An attempt was made to verify whether the landslides triggered during the extreme rainfall event developed predominantly on slopes facing the direction of precipitation (from WSW to ENE) by comparing them with the aspect of the slopes of pre-existing landslides. More parameters affect the slope stability conditions together aspect, which cannot be considered alone in assessing the landslide susceptibility (Cellek 2021; Morelli et al. 2018). However, the slope aspect indirectly influences landslides, determining the magnitude of the effect of the intense climate conditions (Cellek 2021; Liu et al. 2013). In the study area, the most frequent slope directions of the relief are to East and to West-NorthWest. The prevailing atmospheric humid currents are westerly, and the pre-existing landslides predominantly developed on slopes facing, in order of frequency, to East, to West, and secondly to SE, South, and SW (Fig. 6). The post-event predominant landslide type developed on slopes with a similar pattern of aspect but with the SE as the predominant slope direction and a reversal of the East and West aspect frequencies (Fig. 7). There is no significant difference in the distribution of slope aspect values between the two datasets that could be related to the impact of the extreme rainfalls received by slopes. We retain that the regional morpho-structural setting of the mountains has exerted a significant influence on generating landslides during the 2022 extreme event, just as for the past landslide.

4 Conclusions

The 2022 rainfall event that occurred in the Marche region (Italy) was extremely intense. Based on rainfall data collected from the Cantiano rain gauge, it was calculated that

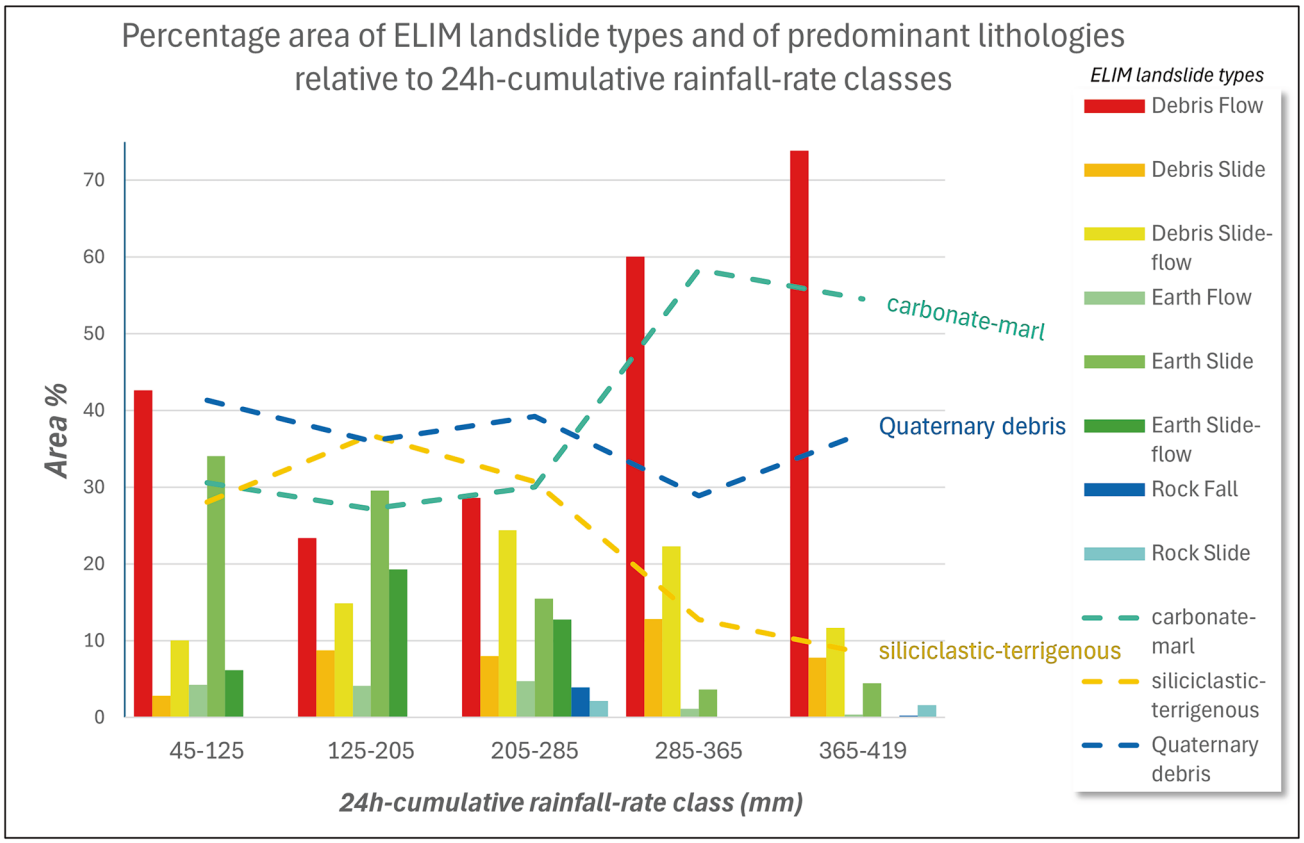

Fig. 4 Distribution of E-LIM landslide-type area percentages relative to the landslide areas in the main 24-h cumulative rainfall ranges

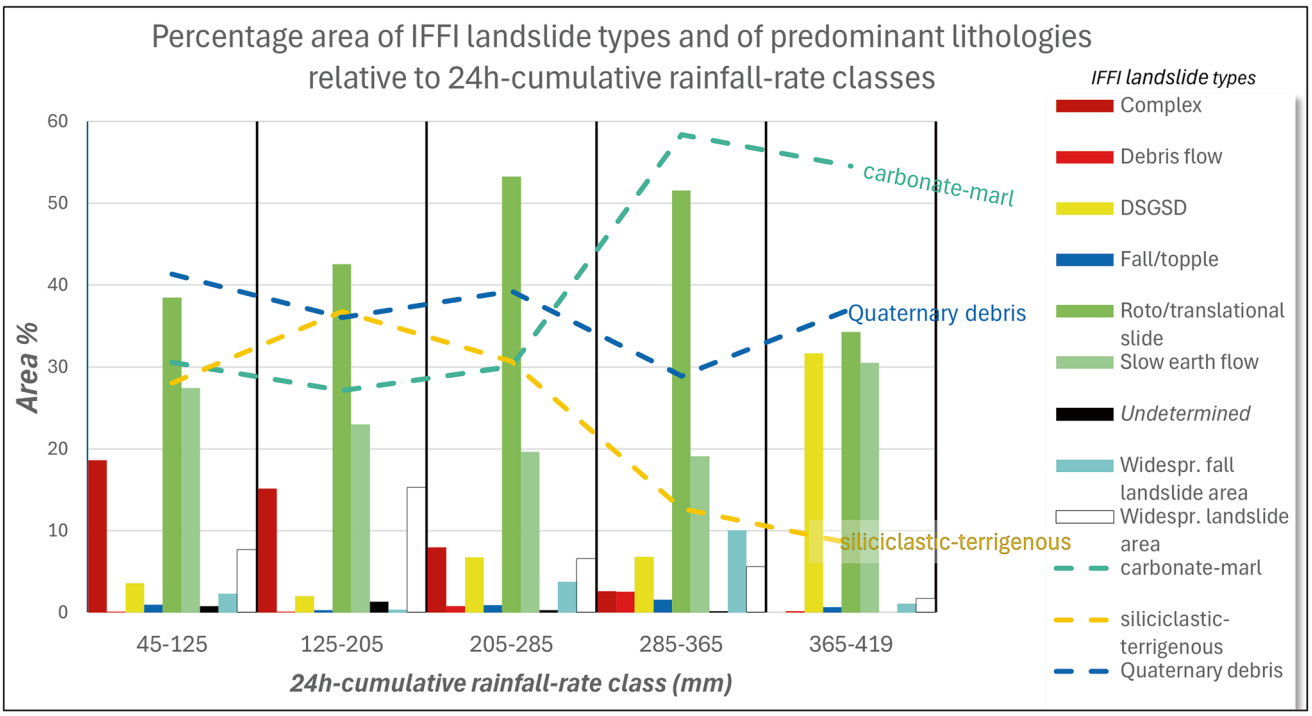

Fig. 5 Distribution of IFFI landslide-type area percentages relative to the landslide areas in the main 24-hour cumulative rainfall ranges

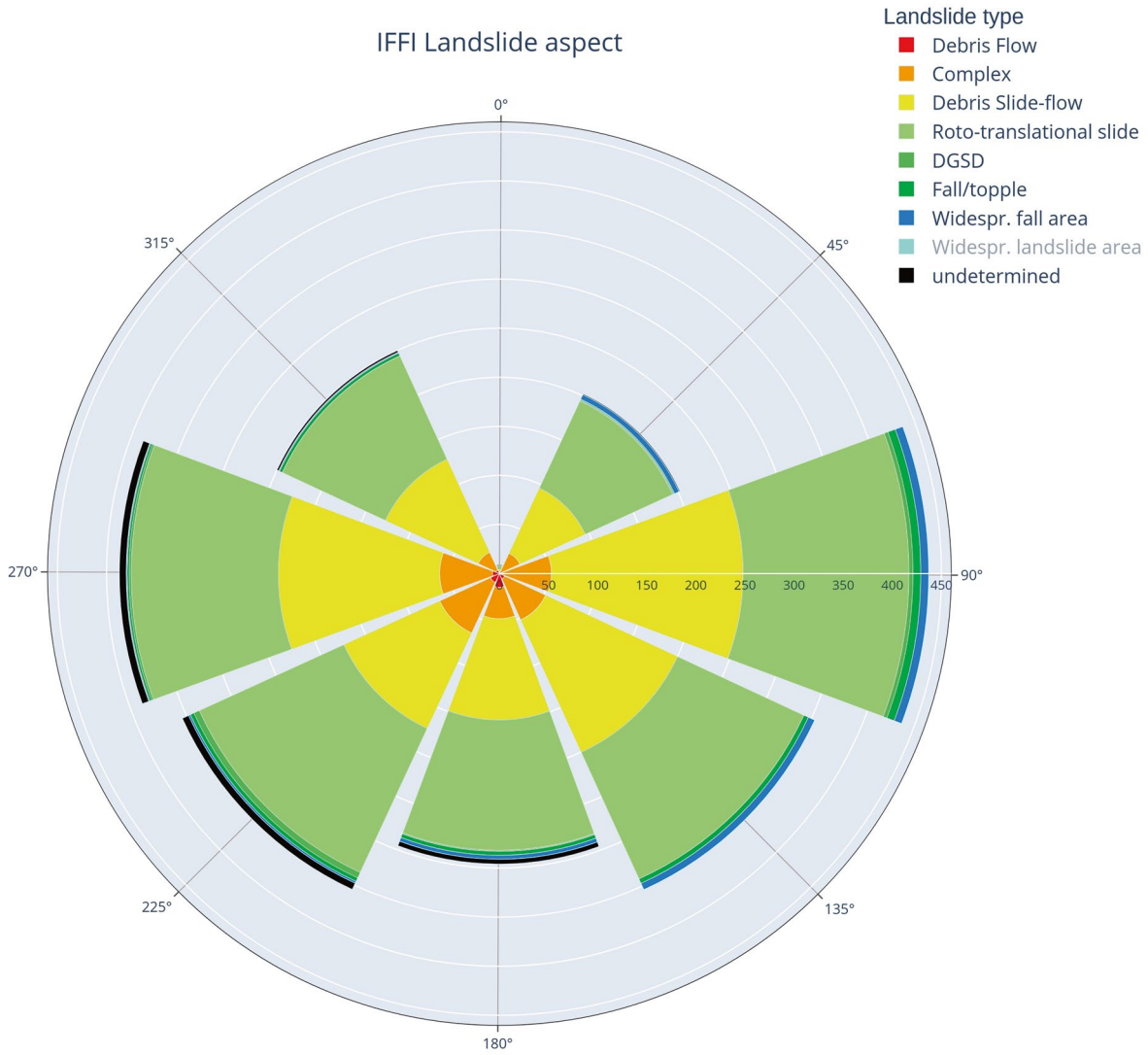

Fig. 6 Aspect frequency of event pre-existing landslides

the amount of precipitation corresponds to over 30% of the annual average (i.e., 1279 mm in the period 1951–2024 available by the Weather-Hydro-Pluviometric Regional Information System (SIRMIP); Marche Region (2024)), thus representing a particularly anomalous meteorological phenomenon for this geographical area. The 3-, 6-, 12-, 24-h cumulative rainfall rates have been well above the maximum values recorded since the 1920s (Report SNPA 2023), with 257 mm in 3 h, for example. Furthermore, based on 24-h rainfall data, extreme precipitations with 100 years as a return period can reach 140 to 180 mm in the study area (Gentilucci et al. 2019). During the event, the territory was devastated by several geo-hydrological hazards on the slopes and the valley floor, leaving the territory seriously injured.

During the event, landslides (1687, mapped by Santangelo et al. 2023a, b) occurred in greater numbers in areas where rainfall ranges from 285 to 365 mm and from 365 to 419 mm (the latter value being the peak) in the considered 24-h cumulative rainfall ranges. However, more than expected, the lowest precipitation class has a rather high number of landslides. In the first case, the high values can be associated with the prevalence of carbonate lithologies, while the high values of the last class are due to the predominant occurrence of Quaternary slope debris. The field surveys carried out in the days following the thunderstorm confirm this distribution.

From the comparison between a post-event mapping (E-LIM inventory) and a pre-existing national inventory (IFFI Inventory) emerges that:

- The post-event landslides are numerically and, by extension, predominantly constituted by detrital material (Debris flow/slide/slide flow) in the whole studied area, while the pre-existing mapping reports here the predomi-

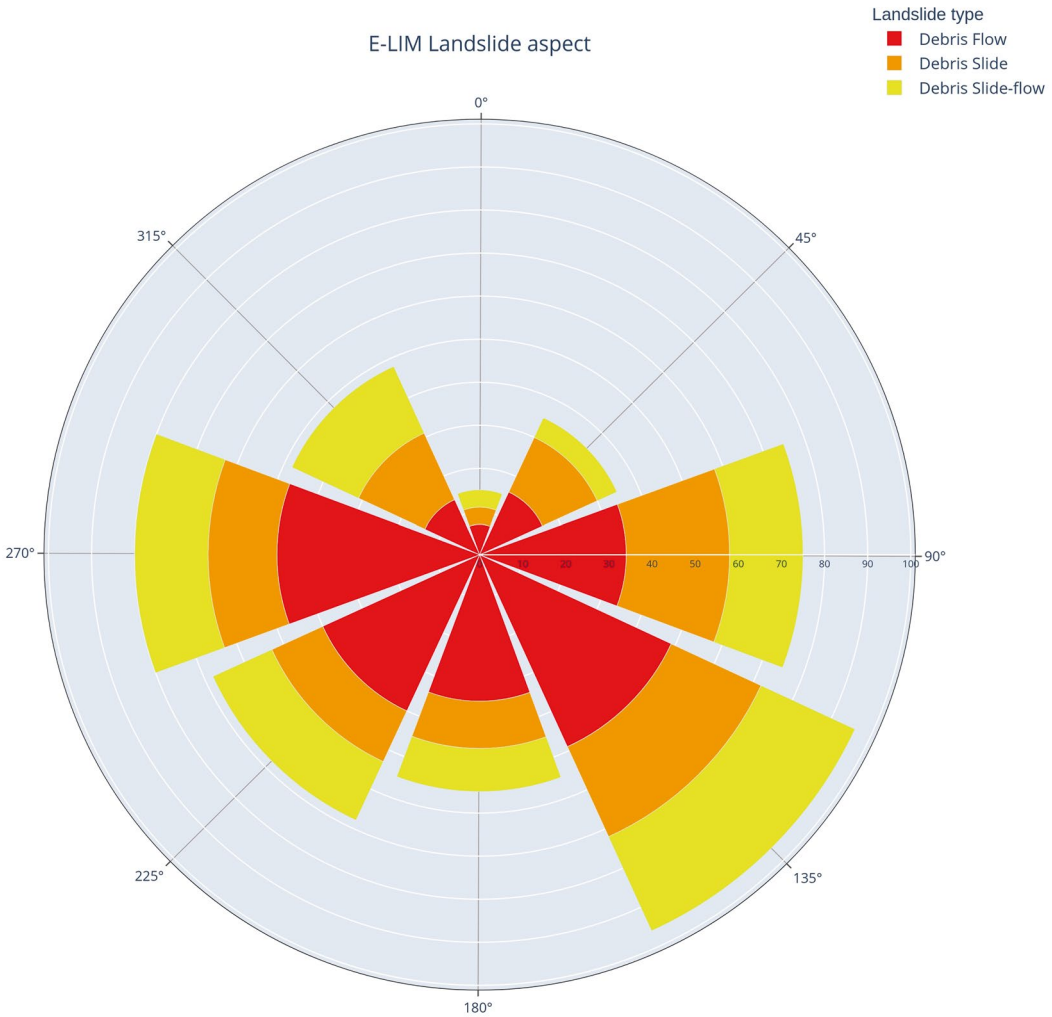

Fig. 7 Aspect frequency of post-extreme event landslide slopes showing the highest frequency of the debris-material landslide slopes in the SE category

nant presence of slides and earth flows without reference to the material.

- 74% of E-LIM landslides are new events triggered externally to those already mapped over the years, and only 26% of E-LIM landslides overlap IFFI landslides (either arising inside them or triggering externally but extending to involve them).
- Despite the difficulties of typological comparison, 80% of the E-LIM debris flow overlaps with Roto/translational slide and slow earth flow from the IFFI inventory, but it is probable that a new reclassification of the IFFI inventory could increase the number (especially considering the landslides classified as *Complex* and *Widespread landslides*).
- Considering the slope orientation with respect to the location of the landslides, there is no significant difference in the distribution of movements along the slopes between the two datasets, despite the strict directionality of the event that persisted in the atmospheric dynamics from WSW to ENE for many hours. We can affirm that the regional geology and the morpho-structural setting of the mountain chain have played a major role in generating landslide occurrences during the extreme event of 2022, as well as in all previous landslide occurrences.

From the overall analysed scenario, it emerges that the mapping currently used for territorial planning may be ineffective when faced with considerations that are based on the occurrence of extreme events under climate changes, and therefore, new analytical paradigms will have to be considered in the future.

References

Allen MR, Dube OP, Solecki W, Aragón-Durand F, Cramer W, Humphreys S, Kainuma M, Kala J, Mahowald N, Mulugetta Y, Perez R, Wairiu M, Zickfeld K (2018) Framing and context. In: Masson-Delmotte A et al (eds) Global warming of 1.5 °C. Cambridge University Press, Cambridge, pp 49–92. https://doi.org/10.1017/9781009157940.003

Calamita F, Centamore E, Deiana G, Micarelli A (1986) Evoluzione Tettonico-Sedimentaria Dell'area Umbro-Marchigiana Dal Trias Al Pleistocene, La Geologia Delle Marche. In: Centamore E, Deiana G (eds) Studi Geologici Camerti: Special number of 73rd Congresso della Società Geologica Italiana. Società Geologica Italiana, Roma

Cellek S (2021) The effect of aspect on landslide and its relationship with other parameters. In: Landslides. IntechOpen, London. https://doi.org/10.5772/intechopen.99389

Corti M, Francioni M, Abbate A, Papini M, Longoni L (2024) Analysis and modelling of the September 2022 flooding event in the Misa Basin. Italian J Eng Geol Environ 1(1):69–76

Cruden DM, Varnes DJ (1996) Landslide types and processes. In: Turner AK, Schuster RL (eds) Landslides investigation and mitigation. US National Research Council, Washington, pp 36–75

Diakakis M, Mavroulis S, Filis C, Lozios S, Vassilakis E, Naoum G et al (2023) Impacts of Medicanes on geomorphology and infrastructure in the eastern mediterranean, the case of Medicane ianos and the Ionian islands in Western Greece. Water 15(6):1026. https://doi.org/10.3390/w15061026

Donnini M, Santangelo M, Gariano SL, Bucci F, Peruccacci S, Alvioli M, Althuwaynee O, Ardizzone F, Bianchi C, Bornaetxea T, Brunetti MT, Cardinali M, Esposito G, Grita S, Marchesini I, Melillo M, Salvati P, Yazdani M, Fiorucci F (2023) Landslides triggered by an extraordinary rainfall event in Central Italy on September 15, 2022. Landslides 20(10):2199–2211. https://doi.org/10.1007/s10346-023-02109-4

Gentilucci M, Barbieri M, Lee HS, Zardi D (2019) Analysis of rainfall trends and extreme precipitation in the middle Adriatic side, Marche Region (Central Italy). Water 11(9):1948. https://doi.org/10.3390/w11091948

Guzzetti F, Mondini AC, Cardinali M, Fiorucci F, Santangelo M, Chang KT (2012) Landslide inventory maps: new tools for an old problem. Earth Sci Rev 112(1):42–66. https://doi.org/10.1016/j.earscirev.2012.02.001

Hungr O, Leroueil S, Picarelli L (2014) The Varnes classification of landslide types, an update. Landslides 11(2):167–194. https://doi.org/10.1007/s10346-013-0436-y

Kabir M, Habiba UE, Khan W, Shah A, Rahim S, Patricio R, Farooqi Z, Ali L, Shafiq M (2023) Climate change due to increasing concentration of carbon dioxide and its impacts on environment in 21st century; a mini review. J King Saud Univ Sci 35(5):102693

Kushabaha A, Scardino G, Sabato G, Miglietta MM, Flaounas E, Monforte P et al (2024) ARCHIMEDE—an innovative web-GIS platform for the study of medicanes. Remote Sens 16(14):2552

Liu C, Li W, Wu H, Lu P, Sang K et al (2013) Susceptibility evaluation and mapping of China's landslides based on multi-source data. Nat Hazards 69:1477–1495

Marche Region (2024) Sistema Informativo Regionale Meteo-Idro-Pluviometrico (SIRMIP) (Weather-Hydro-Pluviometric Regional Information System). http://app.protezionecivile.marche.it/sol/indexjs.sol?lang=it. Accessed 12 July 2024

Montanari A, Farley K, Coccioni R, Sabatino N, Bice D, Yesko M, Sinnesael M, de Winter N (2023) Cosmogenic 3He anomaly K1 vs. The early Campanian isotopic event (ECE) as recorded in pelagic limestones of the Umbria-Marche succession (Italy). GSA Bull 136(3–4):1753–1767. https://doi.org/10.1130/B36952.1

Morelli S, Pazzi V, Frodella W, Fanti R (2018) Kinematic reconstruction of a deep-seated gravitational slope deformation by geomorphic analyses. Geosciences 8(1):26. https://doi.org/10.3390/geosciences8010026

Morelli S, Bonì R, Guidi E, De Donatis M, Pappafico G, Francioni M (2023) L'alluvione delle Marche del 15 settembre 2022, cause e conseguenze. Cult Territ Linguaggi 24:136–147

Pierantoni P, Deiana G, Galdenzi S (2013) Stratigraphic and structural features of the Sibillini Mountains (Umbria-Marche Apennines, Italy). Ital J Geosci 132(3):497–520. https://doi.org/10.3301/IJG.2013.08

Report SNPA (2023) "Il clima in Italia nel 2022"; SNPA-Sistema Nazionale per la Protezione dell'Ambiente. https://www.snpambiente.it/temi/report-intertematici/cambiamenti-climatici/il-clima-in-italia-nel-2022/. Accessed 14 November 2024

Santangelo M, Althuwaynee O, Alvioli M, Ardizzone F, Bianchi C, Bornaetxea T, Brunetti MT, Bucci F, Cardinali M, Donnini M, Esposito G, Gariano SL, Grita S, Marchesini I, Melillo M, Peruccacci S, Salvati P, Yazdani M, Fiorucci F (2023a) Inventory of landslides triggered by an extreme rainfall event in Marche-Umbria, Italy, on 15 September 2022. Sci Data 10:427. https://doi.org/10.1038/s41597-023-02336-3

Santangelo M, Althuwaynee O, Alvioli M, Ardizzone F, Bianchi C, Bornaetxea T, Brunetti MT, Bucci F, Cardinali M, Donnini M, Esposito G, Gariano SL, Grita S, Marchesini I, Melillo M, Peruccacci S, Salvati P, Yazdani M, Fiorucci F (2023b) Inventory of landslides triggered by an extreme rainfall event in Marche-Umbria, Italy, on 15 September 2022. Dataset. https://doi.org/10.6084/m9.figshare.21981842.v1

Tarquini S, Isola I, Favalli M, Mazzarini F, Bisson M, Pareschi MT, Boschi E (2007) TINITALY/01: a new Triangular Irregular Network of Italy. Ann Geophys 50(3):407–425

Tarquini S, Isola I, Favalli M, Battistini A, Dotta G (2023) TINITALY, a digital elevation model of Italy with a 10 meters cell size (version 1.1). Istituto Nazionale di Geofisica e Vulcanologia (INGV), Rome. https://doi.org/10.13127/tinitaly/1.1

Trigila A, Iadanza C (2008) Landslides in Italy, Special Report. Italian National Institute for Environmental Protection and Re-774 search-Geological Survey of Italy/Land Protection and Georesources Department: Rome, Italy

Trigila A, Iadanza C (2018) Landslides and floods in Italy: hazard and risk indicators – summary report 2018. Institute for Environmental Protection and Research (ISPRA), Roma, p 30. https://www.isprambiente.gov.it/en/publications/reports/landslides-and-floods-in-italy-hazard-and-risk-indicators-2013-summary-report-2018

Trigila A, Iadanza C, Guerrieri L (2007) The IFFI project (Italian Landslide Inventory): methodology and results. In: Hervás J (ed) Proceedings 772 of the guidelines for mapping areas at risk of landslides in Europe. ISPRA, Roma, p 60

Trigila A, Iadanza C, Spizzichino D (2010) Quality assessment of the Italian landslide inventory using GIS processing. Landslides 7:455–470. https://doi.org/10.1007/s10346-010-0213-0

Trigila A, Iadanza C, Lastoria B, Bussettini M, Barbano A (2021) Dissesto idrogeologico in Italia: pericolosità e indicatori di rischio. ISPRA, Roma

Varnes DJ (1978) Slope movement types and processes. In: Schuster RL, Krizek RJ (eds) Landslides, analysis and control, special report 176: transportation research board. National Academy of Sciences, Washington, pp 11–33

The Khanh Waterfall Landslide in Hoa Binh Province, Vietnam: An Extraordinary Disaster and Hazard Assessment of Potential Landslides

Ngoc Ha Do, Huy Loi Doan, Satoshi Goto, Shinro Abe, Kim Thanh Nguyen, and Kazunori Hayashi

Abstract

Landslides represent a significant geological hazard in Vietnam, affecting various regions and posing threats to human lives, property, and the environment. On October 12, 2017, a massive landslide struck Khanh Village, Hoa Binh Province, Vietnam, resulting in 18 fatalities and the destruction of five houses. The event highlighted the vulnerability of limestone regions in Vietnam to landslides, particularly during periods of heavy rainfall. This paper first provides preliminary survey results to examine the cause and mechanism of the landslide. The results show that heavy rain was triggering factor in the 2017 Khanh waterfall landslide. Using the LS-RAPID computational model, we reproduce the 2017 event and assess the risk of future landslides from the remaining steep slope of the Khanh waterfall area. The findings provide valuable data to assist authorities in enhancing landslide hazard assessment, as the remaining steep slope poses a significant risk of future landslide occurrence.

Keywords

Khanh waterfall landslide · Hoa Binh Province · Limestone · UAV · LS-RAPID

N. H. Do (✉)
VNU Vietnam Japan University, Hanoi, Vietnam
e-mail: dn.ha@vju.ac.vn

H. L. Doan
International Consortium on Landslides (ICL), Kyoto, Japan

Institute of Transport Science and Technology, Hanoi, Vietnam

S. Goto
Faculty of Engineering, Graduate Faculty of Interdisciplinary Research, University of Yamanashi, Yamanashi, Japan
e-mail: goto@yamanashi.ac.jp

S. Abe · K. Hayashi
Okuyama Boring Co., Ltd, Akita, Japan
e-mail: abe@okuyama.co.jp; k.hayashi@okuyama.co.jp

K. T. Nguyen
Institute of Transport Science and Technology, Hanoi, Vietnam

1 Introduction

Vietnam, particularly the mountainous regions, faces a significant risk of landslides during the rainy season (May to October) (Bui et al. 2013; Loi et al. 2017). For example, in September 2024, following supper typhoon Yagi, thousands of landslides occurred in northern Vietnam, causing more than 300 deaths or missing (Thanien Media 2024). Figure 1a shows hundreds of landslides occurred in the mountainous areas of the Bat Xat district in Lao Cai province. In Fig. 1b, a landslide damaged 18 houses in A Mú Sung Village, Bat Xat district, Lao Cai province. Among thousands of landslides triggered by typhoon Yagi, the notable and worst was a rapid and long-travelling landslide that occurred in Lang Nu hamlet, Phuc Khanh commune, Bao Yen district, Lao Cai province, Vietnam, at 6:00 AM (GMT + 7) on 10 September 2024. The Lang Nu landslide is about 370 m long, 190 m wide and 45 m thick and the volume is approximately 1.1×10^6 m^3 (Fig. 2) (Tien et al. 2025).

In addition to recent events, historical landslides in Vietnam provide critical insights into the behavior of such disasters. Figure 2b shows a catastrophic landslide disaster on October 18, 2020, in Cop hamlet, Huong Phung commune, Huong Hoa district, Quang Tri Province. This event resulted in the loss of 22 soldiers in the barracks, completely burying four buildings and partially damaging three buildings (Tien et al. 2021). Another catastrophic event was a landslide that occurred at Khanh waterfall, Phu Cuong commune, Tan Lac district, Hoa Binh province, on 12 October 2017 (Fig. 3). The landslide caused significant damage to people and houses on the hill opposite the waterfall. The locals reported witnessing some small slopes collapsing at Khanh waterfall one month before the disaster. Landslides have not been documented in the Khanh waterfall area, and no landslide warning information has been announced. Consequently, residents did not evacuate to safer locations before the catastrophic disaster. The Khanh waterfall land-

B. Abolmasov et al. (eds.), *Progress in Landslide Research and Technology, Volume 4 Issue 1, 2025*, Progress in Landslide Research and Technology, https://doi.org/10.1007/978-3-031-89836-5_20

Fig. 1 Landslides triggered by Typhon Yagi: (**a**) hundreds of landslides occurred in the mountainous areas of the Bat Xat district in Lao Cai province (**b**) A landslide destroyed 18 houses in A Mú Sung Village, Bat Xat district, Lao Cai province (Thanien Media 2024)

slide of 2017 is a notable example of a catastrophic landslide in the limestone area and is a crucial case study for understanding landslide hazards in karst terrains.

This colossal landslide occurred at night (around 01:00) while the community was asleep. A massive amount of soil and rock cascaded down, surging over the river and the opposite hill, causing widespread damage to people and houses. The Khanh waterfall landslide, associated with the existing waterfall on the right bank of the Kem River, was triggered by 2 days of intense rainfall totaling 394.8 mm. The landslide, which had a volume of about 700,000 m^3, crossed the Kem River, rose 30 m overtop the opposite hill (left bank), and finally reached the rice fields. The devastating movement of the landslide destroyed five houses and the loss of 18 lives. It is believed that the collapsed rock and the sediment at the bottom slid down the same slope and crossed the river.

The site surveys and rainfall data collection were conducted to investigate the underlying factors that led to the landslide. To examine the failure mechanism and kinetic feature of the 2017 event, computer simulations using LS-RAPID were conducted. LS-RAPID is an integrated model that can simulate the initiation and motion of land-

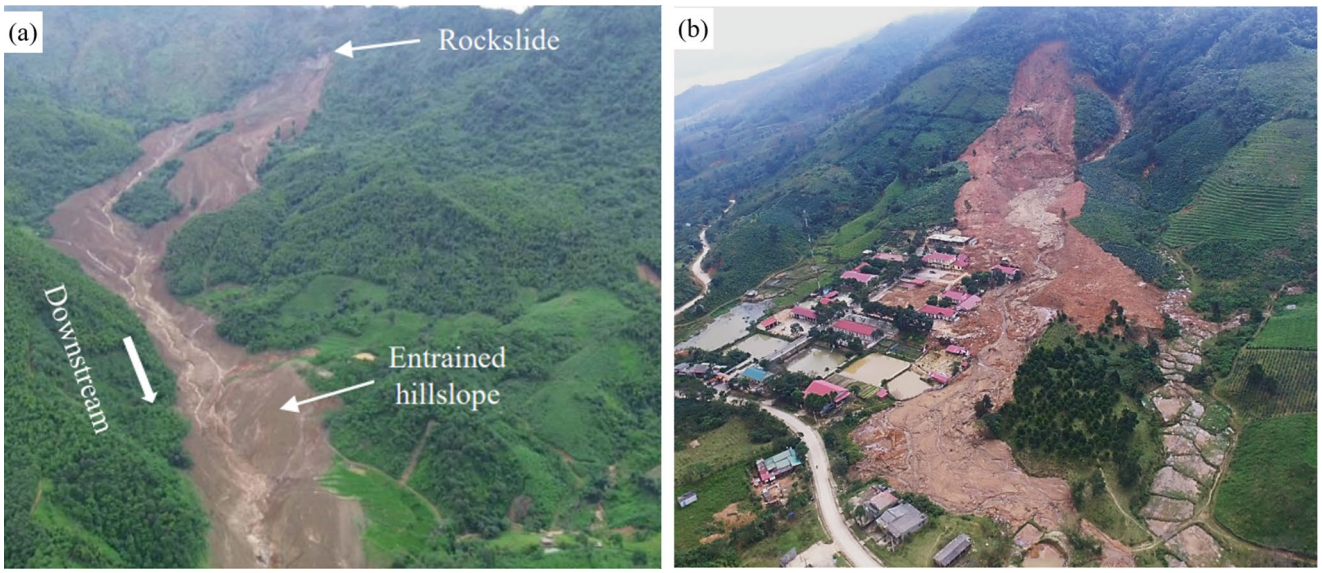

Fig. 2 Catastrophic landslides in Vietnam (**a**) a long travelling landslide in Lang Nu hamlet, Phuc Khanh commune, Bao Yen district, Lao Cai province (Photo taken by Hoang Chien) (Tien et al. 2025), (**b**) rainfall-induced landslide in Quang Tri Province: the deadliest single landslide event in Vietnam in 2020 (Tien et al. 2021)

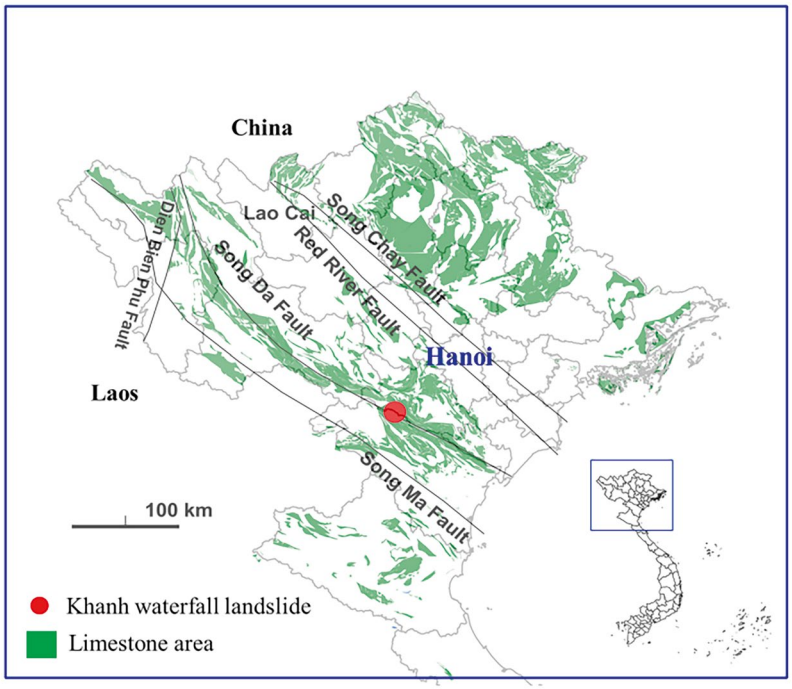

Fig. 3 Limestone distribution and location of Khanh waterfall landslide in Vietnam (Modified from Do et al. 2022)

slides triggered by rainfall and earthquakes (Sassa et al. 2010). Finally, achieved parameters from back analysis and the 2024 Digital Surface Model (DSM) were input to the LS-RAPID model to access the potential rainfall-induced landslides from the remaining body of the Khanh waterfall slope.

2 The 2017 Khanh Waterfall Landslide

2.1 Characteristics of Khanh Waterfall Landslide

Figure 4a shows an overview of the Khanh waterfall landslide. The photo was taken by Tuoi Tre Media soon after the disaster. The maximum width of the landslide at the toe of the slope was about 200 m. The landslide height was about 120 m. There are two close waterfalls, Khanh waterfall 1 and Khanh waterfall 2. During the heavy rain in October 2017, Khanh waterfall 1 failed, while the other was stable. Figure 4b shows the orthophoto of landslides made from UAV. A landslide dam was formed when material blocked the Kem River. The displaced landslide mass carries numerous stalactites, with sizes of 2–3 m, which have been dispersed across the river.

Figure 4c illustrates the A–A′ cross-section. The slope on which the landslide occurred was extremely steep, with an inclination of approximately 49.2°. The landslide moved a significant distance of over 350 m to the opposite hill. To determine its mobility, the apparent angle was calculated from the line connecting the head scar to the toe of the landslide. According to the calculations, the apparent friction angle was 11.9°, which is relatively high mobility.

Figure 5a shows the relationship between coefficient of the apparent friction angle and landslide volume. Fathani et al. (2017) collected the data for 26 cases of landslides and 6 cases of debris flows. For the Khanh waterfall landslide, the coefficient of apparent friction angle and landslide volume are 0.21 and 700,000 m^3, respectively.

Figure 5b indicates the relation between the ratio between height (H) and horizontal distance (L) from the top of the landslide to the toe landslide at deposition. Wu et al. (2024) collected the data from Hunter and Fell (2003), Whittall et al. (2016) for rockslides and Crosta et al. (2017) for Chalk flows. The authors added the Khanh waterfall landslide in this figure. With the same slope angle, the ratio H/L of the Khanh waterfall landslide is smaller than in other cases.

2.2 Contributing Factors to the 2017 Khanh Waterfall Landslide

2.3 Unexpected Heavy Rainfall

The Mai Chau rainfall station, which is the closest station to the landslide site (about 12 km west of the landslide site), was selected for our analysis. A 58-year rainfall data analysis covering the years between 1961 and 2018 revealed that the rainy season in the region lasts from May to October (Fig. 6). The highest monthly average rainfall, as per the data, occurs in August, with an average of 344.3 mm. However, in the year 2017, October witnessed the highest monthly rainfall of the year, with a total of 448.8 mm. The average rainfall in October was 170.4 mm, equaling about 38% of the 2017 value.

The landslide occurred at around 01: 00 (UTC +7) on 12 October, just after a daily rainfall of 251.8 mm on 11 October. The prolonged rainfall lasting 11 days was 439.9 mm (Fig. 7).

Figure 8 shows the hourly rainfall from 10 to 12 October 2017. The maximum hourly rainfall was 44.1 mm at 04:00 on 11 October 2017. The 48-h cumulative precipitation (10–11 October) was 394.8 mm. It is important to note that 10 h before the disaster, only light rain or no rain was recorded in this area.

2.4 Geology Setting

The Khanh waterfall landslide is situated in Hoa Binh Province, a mountainous territory in northern Vietnam. This region is characterized by fault systems, such as the Chay River Fault, Red River Fault, Da River Fault, and Ma River Fault, as reported by Nguyen (2014). The Khanh waterfall landslide is located on the Song Da fault (as depicted in Fig. 3), where many other landslides have also been documented (Tung et al. 2021).

Figure 9a shows the geological cross-section through the Khanh waterfall landslide. The area's geological structure primarily comprises shale and limestone from the Triassic of the late Paleozoic. The strike of the geological layer is identified as N40–50°W, and the dip is observed to be 70–80°W.

Most landslides in northern Vietnam occur in weathered layers of granitic rocks, mudstone, marl, and shale, and some small landslides occur in limestone areas (Tung et al. 2021). Large-scale landslides had not been reported in in limestone formations before 2017.

The Khanh waterfall area characterized by a small fault inclined at 45°E, plays a significant role in shaping the unique geological features. The Kem River flowing along the strike direction of the geological layer is believed to correspond to that fault. The limestone is predominantly found on the right riverbank in the steep terrain, while the shale is mainly distributed on the left riverbank.

Figure 9b shows the photos at the different locations along section A–A′. Many cracks were found in the limestone layer (Photo A). The evidence of the fault is present in Photo B. The fault is located between the limestone and shale layers. Photos C and D show the limestone in the landslide travelling route.

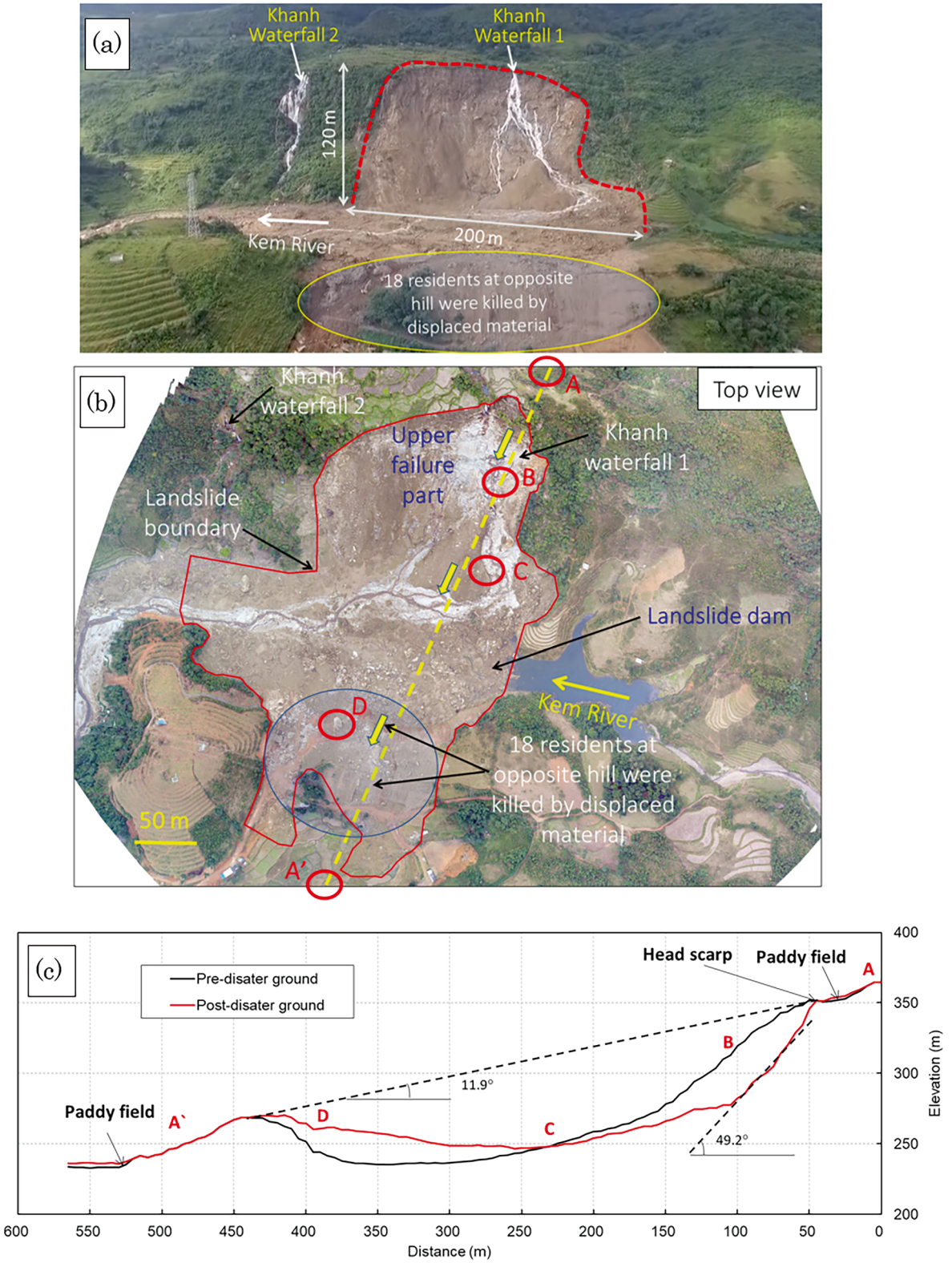

Fig. 4 Characteristics of Khanh waterfall landslide (**a**) overview of the landslide (The photo was extracted from a video published by Tuoi Tre Media in 2017), (**b**) UAV orthophoto of landslide (Modified from Do et al. 2022), (**c**) A–A′ cross-section

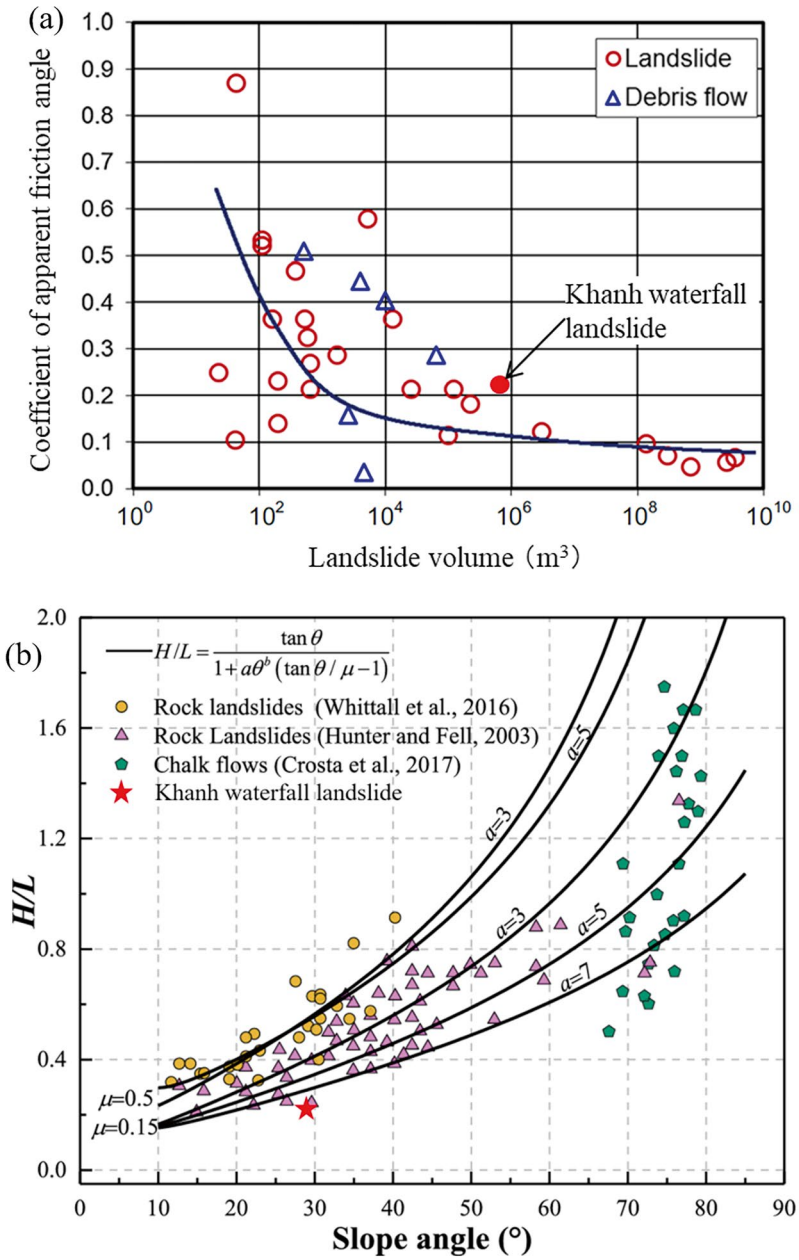

Fig. 5 (**a**) Relationship between coefficient of apparent friction angle and landslide volume (updated from Fathani et al. 2017), (**b**) Relationship between H/L and slope angle (updated from Wu et al. 2024), where H and L are runout height and distance, respectively

2.5 Simulation of 2017 Khanh Waterfall Landslide Using LS-RAPID

LS-RAPID is a commercial model developed and improved by Sassa et al. (2010) to investigate the failure mechanism and kinetic characteristics of rapid landslides. To quickly and efficiently use the program, Ajimera et al. (2023) published a detailed LS-RAPID manual with video tutorials. The LS-RAPID model is widely used with 48 case studies in eleven countries: Canada, China, Croatia, India, Indonesia, Italy, Japan, Korea, Philippines, Sri Lanka, and Vietnam. Recently, Loi et al. (2024), Kim and Jun (2024), and Zhang et al. (2024) published their research using the LS-RAPID model to reproduce various geohazards, including the 2024 earthquake-triggered landslides in the Noto Peninsula, Japan, the August 2020 debris flow in Gokseong County, Korea, and the 1946 landslide-induced tsunami in the Aleutian Islands, USA. Figure 10 shows the three main functions of the LS-RAPID model. Most of the applications reproduce past disasters. There are some publications on risk assessment of potential landslides using LS-RAPID, e.g. the landslide susceptibility analyses in Istra, Croatia (Jovančević et al. 2013), susceptibility assessment of the precursor stage of a landslide threatening Haivan Railway Station, Vietnam (Quang et al. 2018), analysis of potential landslide in Salem District, Brebes Regency, Central Java of Indonesia

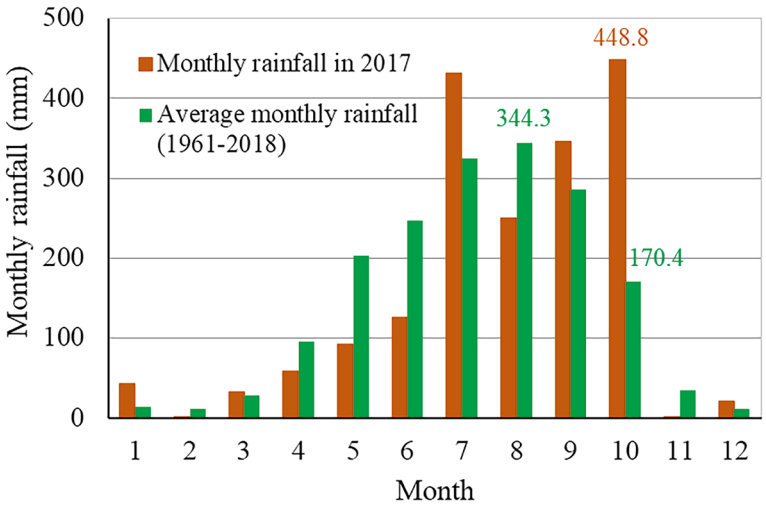

Fig. 6 Monthly rainfall in 2017 and average monthly rainfall for 58 years (1961–2018) (Data was provided by Vietnam Meteorological and Hydrological Administration 2019)

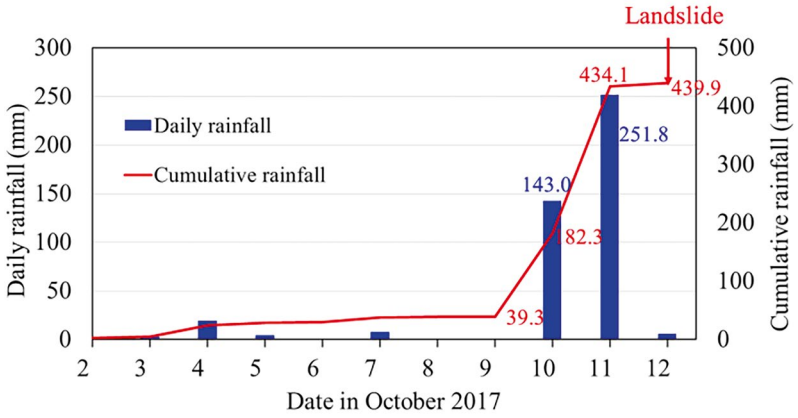

Fig. 7 Daily rainfall in October 2017 (Data was provided by Vietnam Meteorological and Hydrological Administration 2019)

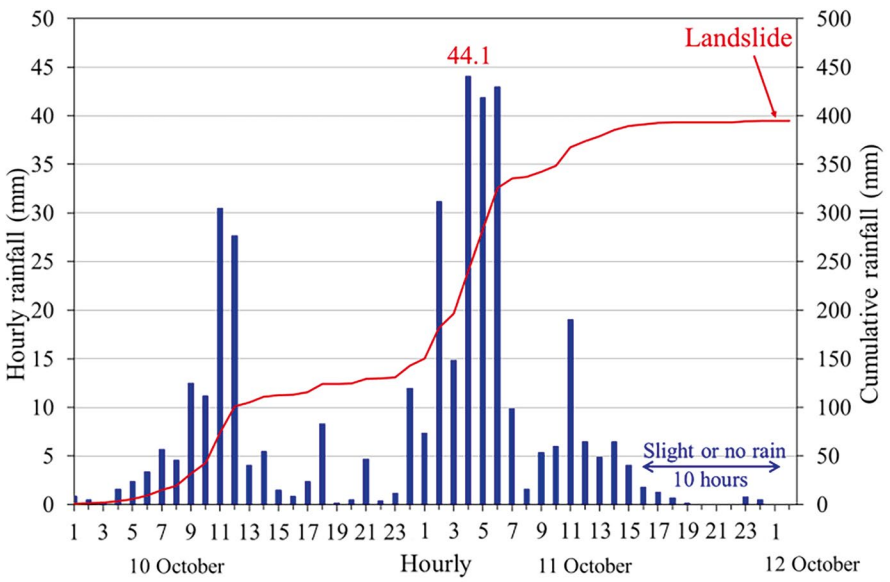

Fig. 8 Hourly rainfall from 10 to 12 October 2017 (Data was provided by Vietnam Meteorological and Hydrological Administration 2019)

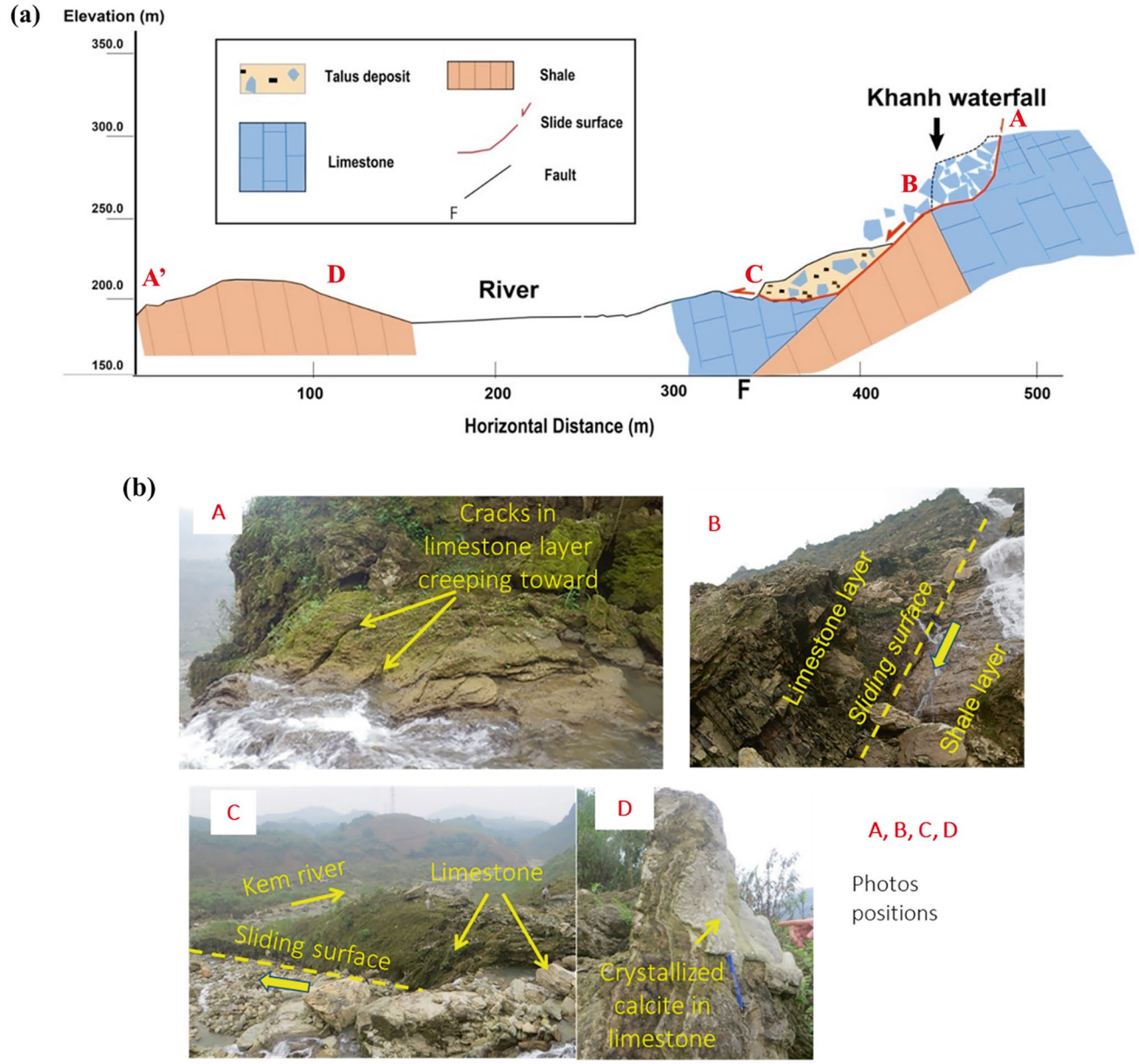

Fig. 9 (**a**) Geological cross-section, (**b**) photos at the different locations at Khanh waterfall landslide (Modified from Do et al. 2022)

(Setiawan et al. 2019), landslide hazard zoning in Yagi, Hiroshima, Japan (Loi et al. 2021), hazard assessment of Hakha slope in Myanmar (Dang et al. 2021) landslide risk evaluation by Aranayake, Sri Lanka by post-rainfall earthquakes (Sassa and Dang 2018) and assessing the potential landslides in Athwelthota, Sri Lanka (Weerasinghe et al. 2024).

In this paper, we first used the LS-RAPID model to reproduce the 2017 Khanh waterfall landslide and then analyzed the potential landslide on the Khanh waterfall slope. The post-disaster DSM derived from the UAV data conducted in January 2018 and ALOS Global Digital Surface Model "ALOS World 3D—30m (AW3D30)". The pre-DSM was estimated based on field survey and post-DSM. The pre-and post-disaster DSMs with 5 m resolution were input to the LS-RAPID model. Ring shear tests were not carried out for the Khanh waterfall landslide. Consequently, the approximation of soil parameters was determined within a range (Sassa and Dang 2018) as outlined in Table 1.

Figure 11 shows the simulation results of the 2017 Khanh waterfall landslide. The background image is the UAV photo taken in January 2018; the balls are moving part of when the landslide occurred. We initially increased the pore water pressure Ru from 0 to 0.5 to determine the critical pore water pres-

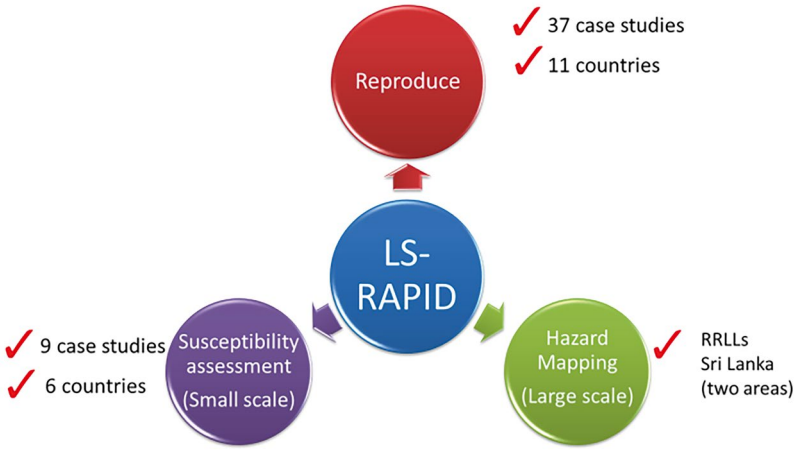

Fig. 10 Three functions of LS-RAPID (Updated from Loi et al. 2024)

Table 1 Soil parameters used in the LS-RAPID model

Soil parameters	Lower-upper case	Khanh waterfall landslide	Source
Total unit weight of the soil mass (γ_t, kN/m^3)		20	Estimated
Unit weight of water (γ_w, kN/m^3)		9.81	Normal value
Pore pressure generation rate (B_{ss})	0.1–0.99	0.9–0.99	Estimated
Lateral pressure ratio ($k = \sigma_h/\sigma_v$)	0.0–1.0	0.5–0.8	Estimated
Friction angle during motion (φ_m, °)	25–35	30.9	Estimated
Peak friction angle (φ_p, °)	33–45	45	Estimated
Peak cohesion at sliding surface (c_p, kPa)	2–200	100	Estimated
Steady-state shear resistance (τ_{ss}, kPa)	5–50	12–50	Estimated
Shear displacement at the start of strength reduction (D_L, mm)	5–100	5	Estimated
Shear displacement at the end of strength reduction (D_U, mm)	100–5000	200	Estimated

sure. For the Khanh waterfall landslide, the critical Ru is 0.25. To investigate the landslide motion, the pore water pressure was increased from 0 to 0.25 in 30 s and then kept constant.

At 30.5 s, failure occurred in the middle part of the Khanh waterfall slope and expanded to the adjacent area.
At 40 s, almost Khanh waterfall landslide body was formed and moved to the residence area.
At 50 s, the displaced landslide mass rose overtop the opposite hill.
At 80 s, the landslide mass stops moving.

Figure 12 presents the time-series data of average simulated velocities, with each step representing 0.5 s. From 0 s to 30 s, the average velocity is 0. Then the local failure occurs and expands in the slope, increasing the landslide mass and acceleration velocity. The peak of average velocity is about 13 m/s at 42 s. After the peak, the velocity shows deceleration.

3 Hazard Assessment of Potential Landslides in Khanh Waterfall

3.1 Landslides Following Landslides

Identifying the location of the landslide is an essential task in assessing the risk of a landslide disaster. This section introduces the example and mechanism of landslides following landslides. The aim of examining the example in the Kii Peninsula, Japan, is to underscore the necessity of assessing potential landslides in the past landslide area like Khanh waterfall. Landslides often occur in areas that have experienced previous landslides (Samia et al. 2017; Temme et al. 2020). Miyagi and Loi (2024) compared the locations of 54 large-scale landslides in the Kii Peninsula, Japan, in 2011 with previously mapped landslides. They found that 36 large-scale landslides took place in the former landslide areas. Figure 13 shows an example of the new landslide occurring in the past landslide terrain. The Kuridaira landslide, which

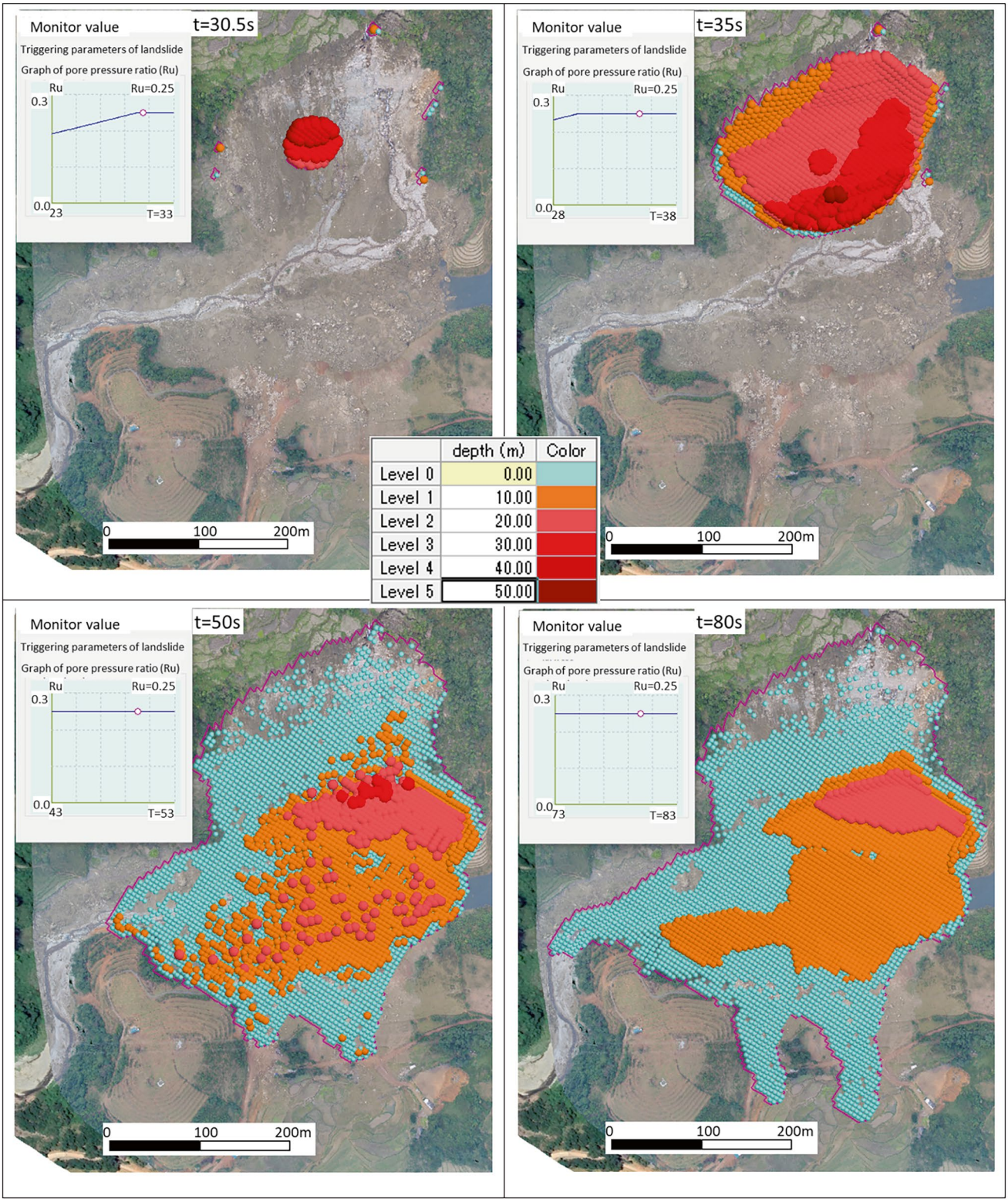

Fig. 11 Simulation result of the 2017 Khanh waterfall landslide using LS-RAPID. Pink zone is the calculated mass distribution area. The ball color presents the landslide thickness

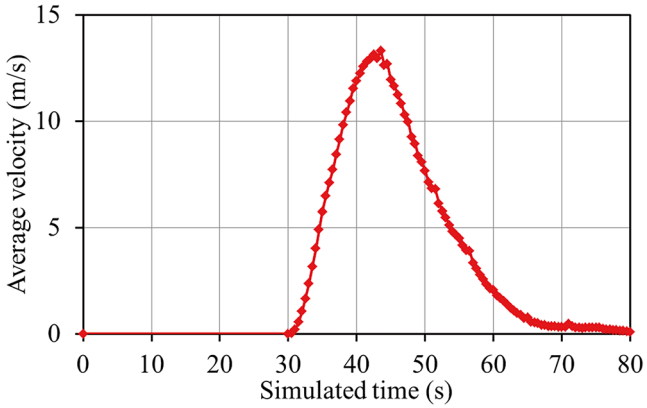

Fig. 12 Time-varying average simulated velocity of Khanh waterfall landslide

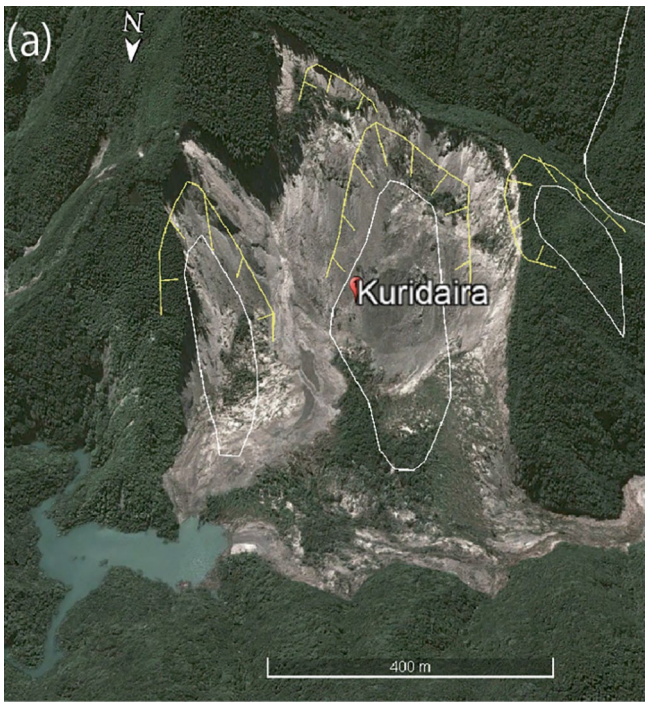

Fig. 13 Overview of the 2011 Kuridaira landslide (Miyagi and Loi 2024). Landslide distribution was published in 2005 by the National Research Institute for Earth Science and Disaster Prevention (NIED) (n.d.). The yellow line indicates the head scarp, while the white polygon represents the landslide body. The Google Earth images were captured in September 2011

occurred on the Kii Peninsula in Japan, was the largest landslide recorded in the area in 2011. It is located at 34.075°N, 135.837°E and measures approximately 680 m in length, 600 m in width, and 74 m in thickness, with a volume of about 14 million m^3 (Chigira et al. 2013). The mass of the landslide moved toward the river, creating a landslide dam that reached heights of up to 100 m (Tien et al. 2018). The Kuridaira landslide took place in an area previously affected by two other landslides. On the left side, the head scarp corresponds to the mapped landslide, while the right side is located higher than the mapped landslide. Figure 13 clearly shows that the largest landslide event in 2011 has been identified before its occurrence.

Understanding the recurrence of landslides in these specific areas can help assess risks and implement effective prevention and mitigation strategies. Figure 14 illustrates a model of retrogressive landslides. In the initial stage, a landslide occurs at the lower section of the slope (see Fig. 14a or a′). Subsequently, after the first landslide has taken place, an additional landslide occurs further upslope (refer to Fig. 14b, b′). There are two cases in landslide mass moving on the preexisting deposits. Case 1 (Fig. 14c, d) is the case where landslide mass moving together with the torrent deposit. The sliding mass moves downhill, exerting a load on torrent deposits at the foot of the slope. Some deposits are saturated due to surface water or groundwater flow. The torrent deposits are sheared under undrained loading and transported downstream along with the sliding mass. This model was used to explain many landslide triggered debris flow in Japan such as the 1984 Ontake debris flow (Sassa et al. 1988), the 2003 Minamata debris flow (Sassa et al. 2007) the 1997 Harihara River debris flow (Takahashi 2007). Case 2 (Fig. 14c′, d′) is where the entrainment does not occur. The total landslide volume is smaller than in case 1, and the landslide travels a shorter distance.

3.2 Hazard Assessment of Potential Landslides in Khanh Waterfall Using LS-RAPID

After the 2017 disaster, the uppermost part of the slope was steepened to between 75° and vertical. Figure 15 shows the high-resolution aerial images of Khanh waterfall captured in January 2018. The water flows along the faults and cracks. It is assumed that the potential sliding block (red dashed line) is bounded by two stream flows (which are two cracks systems). To evaluate the current condition of Khanh waterfall, especially after the prolonged rainfall in 2024, UAV and site investigation were conducted in October 2024. Figure 16 shows the 3D views of the Khanh waterfall generated by QGIS 3.40 using the DSM data and the orthomosaic of the terrain.

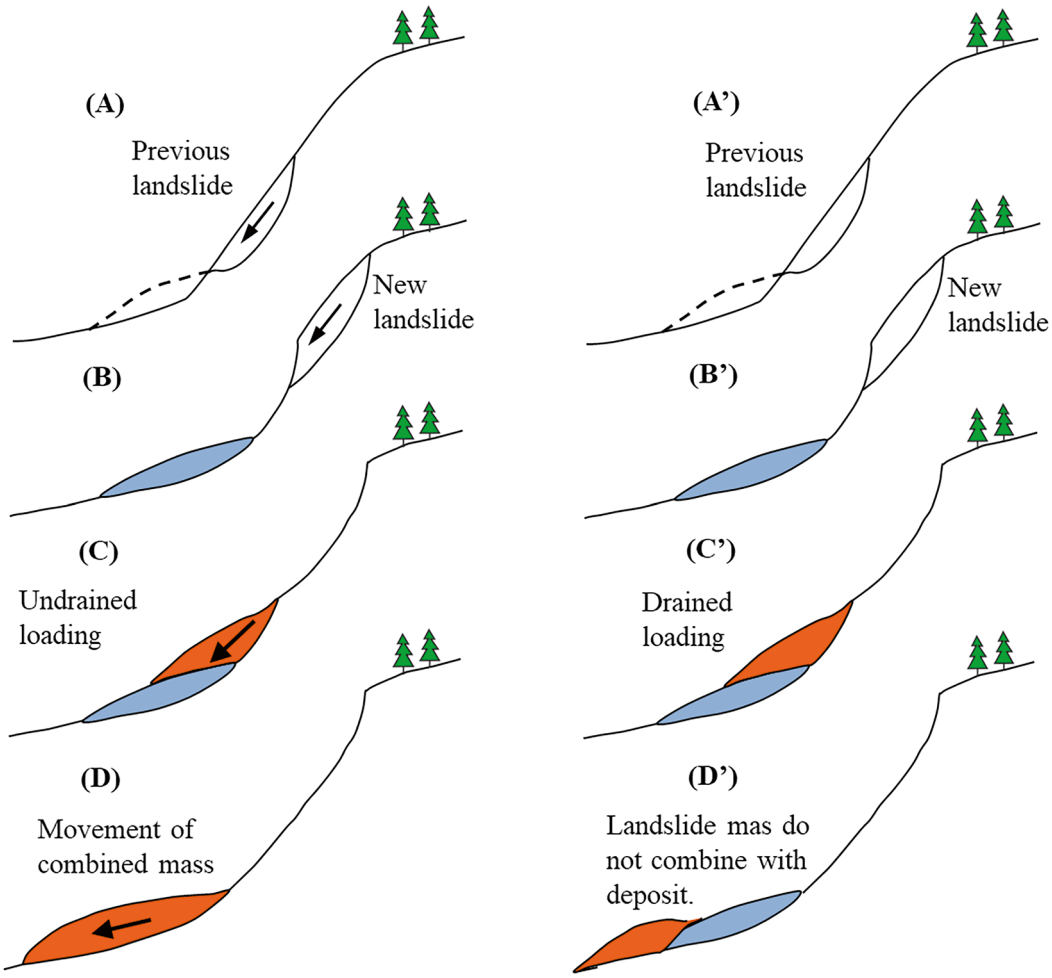

Fig. 14 Process model of retrogressing landslide for potential landslide in Khanh waterfall (based on a concept of landslide-triggered debris flow from Sassa et al. (2007) and Takahashi (2007)

3.2.1 The Hypothetical Landslide

Estimating the exact dimensions of future landslides is challenging. Therefore, we will assess the worst-case scenario in which the landslide depth is similar to the 2017 event and the landslide area is bounded by two waterfalls (Fig. 15).

In the simulation of the potential future landslide, the sliding surface was determined using an advanced ellipsoidal method, as illustrated in Fig. 17. This approach required the careful selection of specific cross-sectional and longitudinal profiles that accurately depict the expected path of failure. To achieve this, parameters such as the centroid of the sliding surface, the lengths of both the major and minor axes and the depth were meticulously defined.

The model's calculations estimated the landslide's dimensions to be approximately 260 m in length, 175 m in width, and 50 m deep. Furthermore, the total volume of the landslide was calculated to be around 1,176,000 m^3, which is 1.68 times greater than the 2017 event.

3.2.2 Modelling Cases

Based on the model in Fig. 14, the hazard assessment included two cases.

Case 1: Assuming the 0.5 m torrent deposit moving together with landslide mass.
Case 2: In the absence of entrainment occurring.

3.2.3 Simulation Result

The simulation result suggested that landslides reach residential areas in both cases, as shown in Fig. 18. The mass of the landslide in case 1 traveled longer and wider than in case 2.

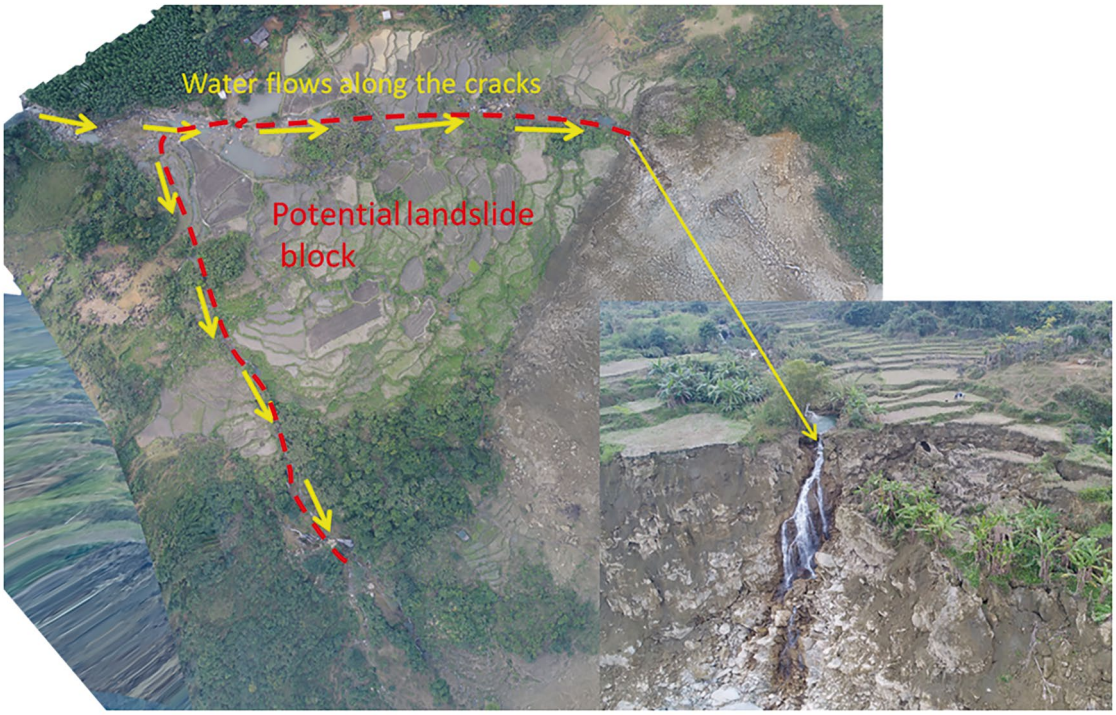

Fig. 15 Aerial images of Khanh waterfall captured in January 2018

Fig. 16 3D view of Khanh water fall landslide in 2024

3.3 Conclusion

The Khanh waterfall landslide is a stark reminder of the dangers posed by landslides in limestone areas in Vietnam, particularly during periods of heavy rainfall.

From the geological and rainfall analysis, the mechanism of the Khanh waterfall landslide can be summarized as follows.

1. The main triggering factor of the Khanh waterfall landslide was torrential rainfall, 394.8 mm in 48 h. A large amount of groundwater flowed down to the caves and cracks, increasing the pore water pressure in the sliding surface and causing slope failure.
2. The sliding surface was between the limestone and shale layers and overlapped with a minor fault. The numerous cracks in the limestone layer also contributed to the slope's instability.
3. The integrated simulation model (LS-RAPID) was employed to replicate the 2017 Khanh waterfall landslide. The simulation results were validated using UAV imagery and site investigations.
4. The current slope is extremely steep. These conditions may cause a landslide in the future. The hazard assessment results of the potential landslide in Khanh waterfall may effectively inform the local government authorities in Hoa Binh. When heavy rain comes, they need to request the local people to evacuate to safe places.Understanding the event's causes and devastating impact is vital for informing future disaster preparedness and mitigation efforts.

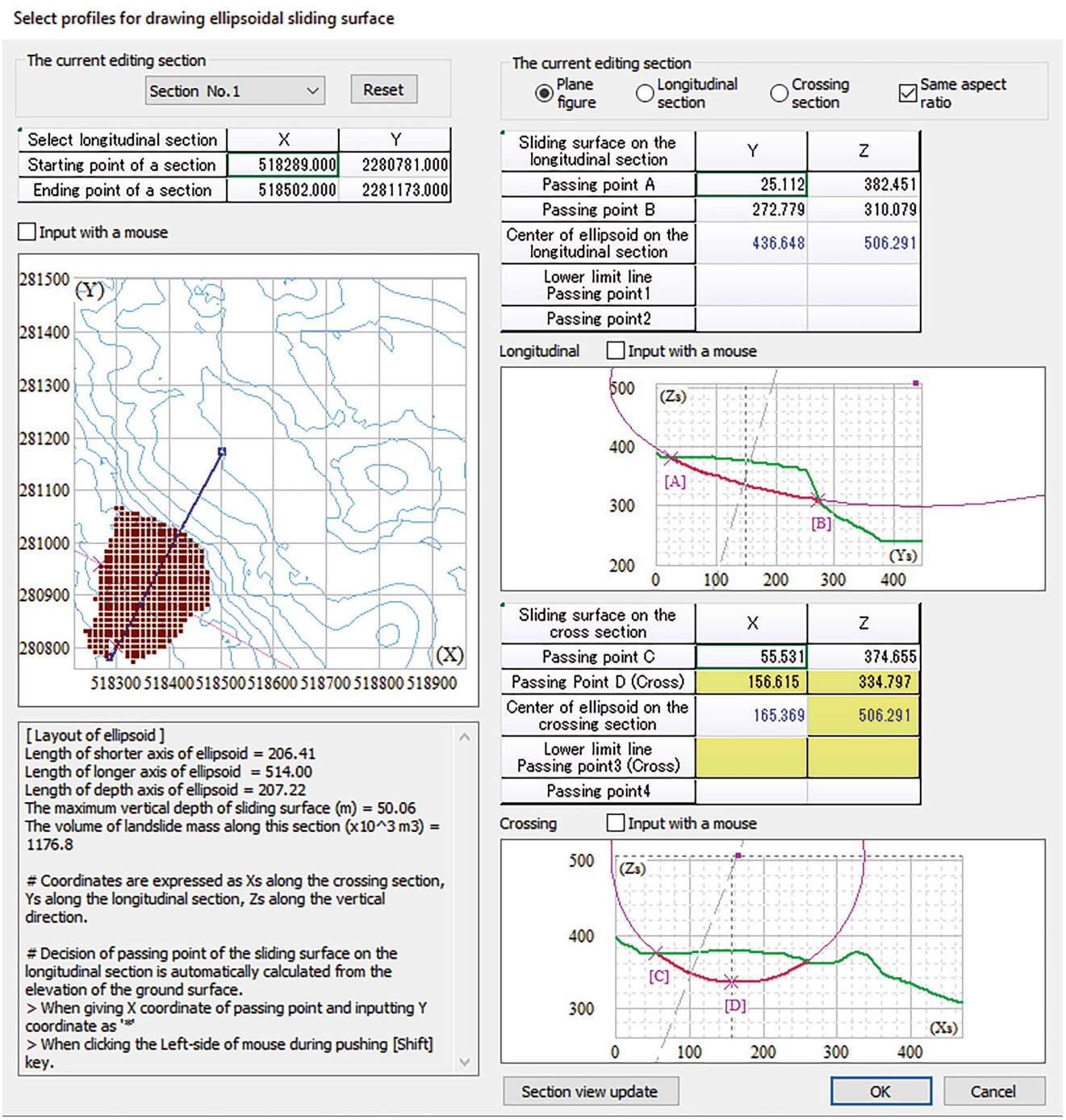

Fig. 17 Ellipsoidal sliding surface for hypothetical landslide at Khanh waterfall

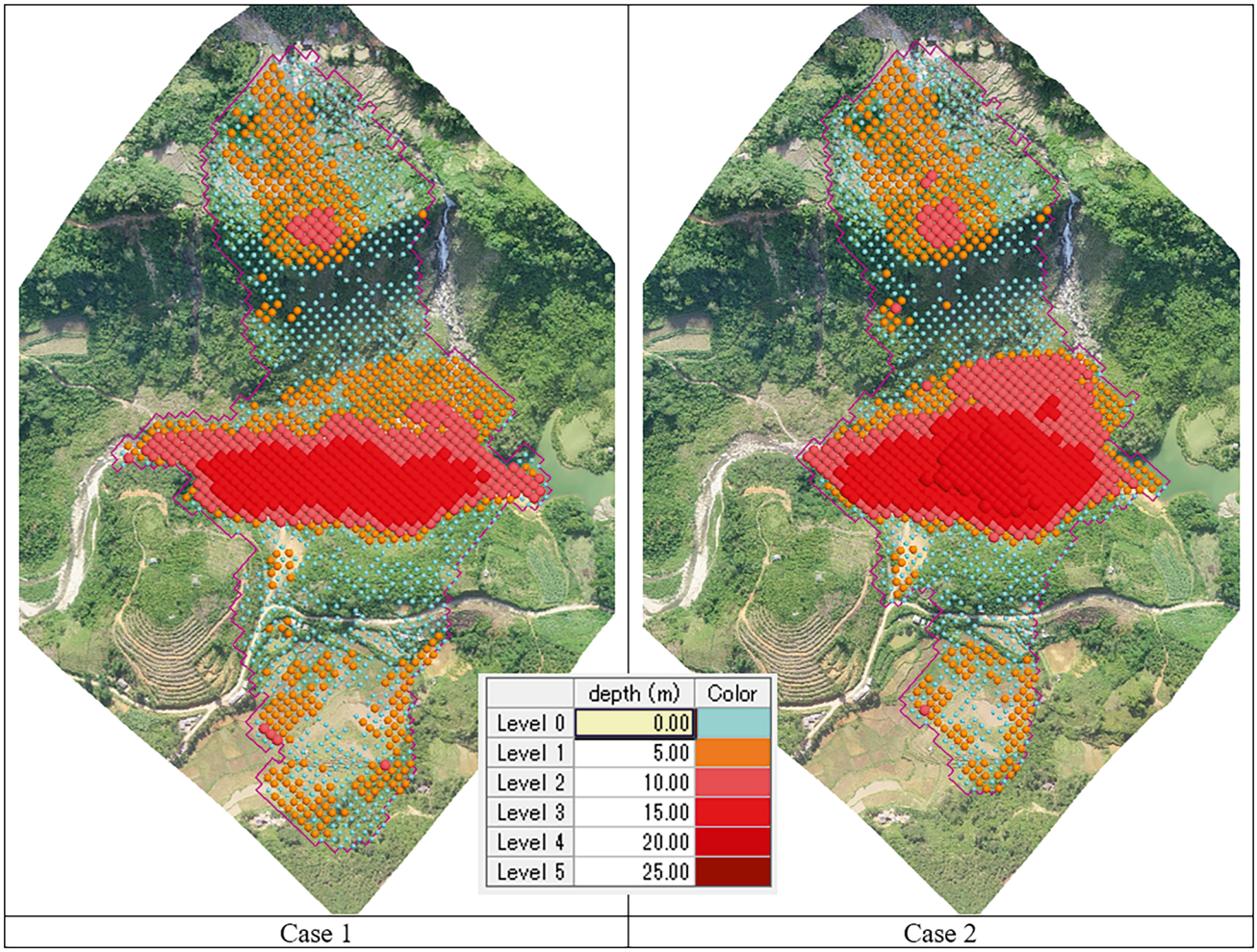

Fig. 18 Landslide mass distribution area of case 1 (left side) and case 2 (right side)

Acknowledgements The authors express our gratitude to Dr. Satoshi Suzuki and Mr. Huu Thang Nguyen of Okuyama Boring Co., Ltd., Japan; Dr. Osamu Watanabe of Suimonkikaku LLC, Miyagi, Japan; Prof. Toyohiko Miyagi, Professor Emeritus at Tohoku Gakuin University, Japan; Dr. Hong Luong Le, Dr. Thanh Binh Huynh, and Mr. Van Chuong Phan of the Institute of Transport Science and Technology, Vietnam for their invaluable support during the course of this study.

References

Ajimera B, Ahari HE, Loi DH, Setiawan H, Dang K, Sassa K (2023) LS-RAPID manual with video tutorials. Prog Landslide Res Technol 1(1):343–406. https://doi.org/10.1007/978-3-031-16898-7_26

Bui DT, Pradhan B, Lofman O, Revhaug I, Dick OB (2013) Regional prediction of landslide hazard using probability analysis of intense rainfall in the Hoa Binh province, Vietnam. Nat Hazards 66:707–730. https://doi.org/10.1007/s11069-012-0510-0

Chigira M, Tsou C-Y, Matsushi Y, Hiraishi N, Matsuzawa M (2013) Topographic precursors and geological structures of deep-seated catastrophic landslides caused by typhoon Talas. Geomorphology 201:479–493

Crosta GB, Blasio FVD, Caro MD, Volpi G, Imposimato S, Roddeman D (2017) Modes of propagation and deposition of granular flows onto an erodible substrate: experimental, analytical, and numerical study. Landslides 14:47–68. https://doi.org/10.1007/s10346-016-0697-3

Dang K, Loi DH, Sassa K, Duc DM, Ha ND (2021) Hazard assessment of a rainfall-induced deep-seated landslide in Hakha City, Myanmar. In: Tiwari B, Sassa K, Bobrowsky PT, Takara K (eds) Understanding and reducing landslide disaster risk. Springer, Cham. https://doi.org/10.1007/978-3-030-60706-7_23

Do NH, Goto S, Abe S, Nguyen KT, Miyagi T, Hayashi K, Watanabe O (2022) Torrent rainfall-induced large-scale karst limestone slope col-

lapse at Khanh waterfall, Hoa Binh Province, Vietnam. Geoenviron Disasters 9(4):1–20. https://doi.org/10.1186/s40677-022-00206-5

Fathani TF, Legono D, Karnawati D (2017) A Numerical model for the analysis of rapid landslide motion. Geotech Geol Eng 35:2253–2268. https://doi.org/10.1007/s10706-017-0241-9

Hunter G, Fell R (2003) Travel distance angle for "rapid" landslides in constructed and natural soil slopes. Can Geotech J 40:1123–1141. https://doi.org/10.1139/t03-06

Jovančević, S. D., Nagai, O., Sassa, K., & Arbanas, Ž. (2013). Deterministic landslide susceptibility analyses using LS-Rapid software. I*n The first regional symposium on landslides in Adrian-Balkan Region* (pp. 73–77)

Kim N, Jun B (2024) Enhancing debris flow simulation accuracy through high-resolution terrain information: a case study utilizing LS-RAPID and UAV-derived models. Landslides 21:2249–2260. https://doi.org/10.1007/s10346-024-02290-0

Loi DH, Quang LH, Sassa K, Takara K, Dang K, Thanh NK, Tien PV (2017) The 28 July 2015 rapid landslide at Ha Long City, Quang Ninh, Vietnam. Landslides 14:1207–1215. https://doi.org/10.1007/s10346-017-0814-y

Loi DH, Sassa K, Dang K, Luong LH (2021) Landslide hazard zoning based on the integrated simulation model (LS-rapid). In: Tiwari B, Sassa K, Bobrowsky PT, Takara K (eds) Understanding and reducing landslide disaster risk. Springer, Cham. https://doi.org/10.1007/978-3-030-60706-7_24

Loi DH, Jayakody S, Sassa K, Konagai K, Hirota K, Ôn A, Takanaka T, Oki T, Minamitani T (2024) Landslides triggered by the 2024 Noto Peninsula earthquake. Landslides. https://doi.org/10.1007/s10346-024-02333-6

Miyagi T, Loi DH (2024) How to detect the previous large-scale landslide: source of future landslides by interpretation of ground topography from digital maps. In: Abolmasov B et al (eds) Progress in landslide research and technology. Springer, Cham

National Research Institute for Earth Science and Disaster Prevention (NIED) (n.d.) Landslide topography distribution map. https://dil-opac.bosai.go.jp/publication/nied_tech_note/landslidemap/gis.html. Accessed 10 April 2024

Nguyen DA (2014) Tectonic deformation and earthquake hazard in Northwestern Vietnam inferred from GPS observations. Nagoya University, Nagoya

Quang, L. H., Loi, D. H., Sassa, K., Takara, K., Ochiai, H., Dang, K., ... & Ha, D. N. (2018). Susceptibility assessment of the precursor stage of a landslide threatening Haivan Railway Station, *Vietnam. Landslides*, 15(2):309–325

Samia J, Temme A, Bregt A, Wallinga J, Guzzetti F, Ardizzone F, Rossi M (2017) Do landslides follow landslides? Insights in path dependency from a multi-temporal landslide inventory. Landslides 14:547–558. https://doi.org/10.1007/s10346-016-0739-x

Sassa K, Dang K (2018) Txt-tool 0.081-1.1: landslide dynamics for risk assessment. In: Sassa K, Tiwari B, Liu K-F, McSaveney M, Strom A, Setiawan H (eds) Landslide dynamics: Isdr-icl landslide interactive teaching tools: volume 2: testing, risk management and country practices. Springer, Cham, pp 1–79

Sassa K, Fukuoka H, Wang G, Wang F (2007) Undrained stress-controlled dynamic-loading ring-shear test to simulate initiation and post-failure motion of landslides. In: Sassa K, Fukuoka H, Wang F, Wang G (eds) Progress in landslide science. Springer, Berlin. https://doi.org/10.1007/978-3-540-70965-7_6

Sassa K, Nagai O, Solidum R, Yamazaki Y, Ohta H (2010) An integrated model simulating the initiation and motion of earthquake and rain-induced rapid landslides and its application to the 2006 Leyte landslide. Landslides 7(3):219–236. https://doi.org/10.1007/s10346-010-0230-z

Setiawan H, Fathani TF, Wilopo W, Karnawati D (2019) Analysis of potential landslide and its motion behaviour in Salem District, Brebes Regency, Central Java of Indonesia by using the LS-RAPID numerical simulation. In: Proceedings international conference on landslide and slope stability SLOPE 2019a. Bali, Indonesia, pp 1–12

Takahashi T (2007) Progress in debris flow modeling. In: Sassa K, Fukuoka H, Wang F, Wang G (eds) Progress in landslide science. Springer, Berlin. https://doi.org/10.1007/978-3-540-70965-7_5

Temme A, Guzzetti F, Samia J, Mirus BB (2020) The future of landslides' past—a framework for assessing consecutive landsliding systems. Landslides 17:1519–1528. https://doi.org/10.1007/s10346-020-01405-7

Thanien Media (2024). https://thanhnien.vn/am-anh-hang-nghin-vet-cao-cua-thien-tai-tan-pha-tinh-lao-cai-185241007021219701.htm

Tien PV, Sassa K, Takara K, Fukuoka H, Khang D, Shibasaki T, Setiawan H, Ha ND, Loi DH (2018) Formation process of two massive dams following rainfall-induced deep-seated rapid landslide failures in the Kii Peninsula of Japan. Landslides 15(9):1761–1778

Tien PV, Luong LH, Duc DM, Trinh PT, Quynh DT, Lan NC, Thuy DT, Phi NQ, Cuong TQ, Khang D, Loi DH (2021) Rainfall-induced catastrophic landslide in Quang Tri Province: the deadliest single landslide event in Vietnam in 2020. Landslides 18:2323–2327. https://doi.org/10.1007/s10346-021-01664-y

Tien PV, Minh VC, Duc DM, Luong LH, Nam DH, Hieu TT (2025) Rainfall-induced catastrophic rapid and long-traveling landslide in Lang Nu hamlet: the worts natural landslide disaster in Vietnam. Landslides 22:1761–1767

Tung BD, Do NH, Thanh NK, Luong LH, Watanabe O, Hayashi K, Wakai A, Abe S (2021) Geometry and the mechanism of landslide occurrence in a limestone area – case examples of landslides in Vietnam and from Europe, China, and Japan. J Disaster Res 16(4):646–657

Tuoi Tre Media (2017) Khanh waterfall before and after a serious landslide caused 18 people to be buried. YouTube. https://www.youtube.com/watch?v=B6iU3eYA7_Q. Accessed Dec 2019 (in Vietnamese)

Vietnam Meteorological and Hydrological Administration (2019) Accessed Dec 2019

Weerasinghe AR, Jayakody SH, Amali NP, Maduranga HR, Loi DH (2024) Assessing the potential rapid and long travelling landslides in Sri Lanka: a case study of Athwelthota landslide. In: Abolmasov B et al (eds) Progress in landslide research and technology. Springer, Cham. https://doi.org/10.1007/978-3-031-55120-8_27

Whittall J, Eberhardt E, McDougall S (2016) Runout analysis and mobility observations for large open pit slope failures. Can Geotech J 54:373–391. https://doi.org/10.1139/cgj-2016-0255

Wu YB, Duan Z, Peng JB, Zhang Q (2024) Implications of sand grains' mobility and inundating area to landslides at different slope angles. Granul Matter 26:18. https://doi.org/10.1007/s10035-023-01387-y

Zhang W, Lu W, Wang L, Ma Y, Tan Q, Meng X, Liu S (2024) Landslide-induced tsunami simulation based on progressive landslide-shallow water equation coupling model: 1946 Aleutian tsunami case. Landslides 21:1719–1733. https://doi.org/10.1007/s10346-024-02241-9

KLC2020 Official Promoters

The Kyoto Landslide Commitment 2020 (KLC2020)

Kyoto 2020 Commitment for Global Promotion of Understanding and Reducing Landslide Disaster Risk

A Commitment to the Sendai Landslide Partnerships 2015–2025, the Sendai Framework for Disaster Risk Reduction 2015–2030, the 2030 Agenda Sustainable Development Goals, the New Urban Agenda and the Paris Climate Agreement-

KLC2020 Official promoters are public and private organizations who promote the Kyoto Landslide Commitment 2020 and provide financial support for the implementation of the KLC2020 activities including the Open Access Book Series "Progress in Landslide Research and Technology."

Host organization

International Consortium on Landslides (ICL)/Željko Arbanas.

Public sectors: KLC2020 Official Promoters-public

International Unions/Associations, Governmental organizations, Universities and Research institutes

- The International Union of Geological Sciences (IUGS)/Hassina Mouri
- The International Union of Geodesy and Geophysics (IUGG)/Chris Rizos
- The International Association for the Engineering Geology and the Environment/Vassilis Marinos
- International Geosynthetics Society (IGS)/John Kraus
- Geological Survey of Canada, Natural Resources Canada, Canada/Sonia Talwar
- Faculty of Civil and Geodetic Engineering, University of Ljubljana, Slovenia/Matjaž Mikoš
- China University of Geosciences, Wuhan, China/Huiming Tang
- The State Key Laboratory of Geohazard Prevention and Geoenvironment Protection, Chengdu University of Technology, Sichuan, China/Qiang Xu
- Department of Civil Engineering, National Taiwan University, Chinese Taipei/Louis Ge
- Institute of Rock Structure and Mechanics, the Czech Academy of Sciences/Josef Stemberk
- Institute of Cold Regions Science and Engineering, Northeast Forestry University/Wei shan.

Private sectors: KLC2020 Official Promoters-private

Companies and corporation.

- Marui & Co. Ltd, Japan
- Nippon Koei Co., Ltd, Japan
- Ellegi srl, Italy
- IDS GeoRadar s.r.l., Italy
- Chuo Kaihatsu Corporation, Japan
- Godai Kaihatsu Corporation, Japan
- Kiso-Jiban Consultants Co., Ltd, Japan
- Kokusai Kogyo Co., Ltd., Japan
- OSASI Technos, Inc., Japan.

B. Abolmasov et al. (eds.), *Progress in Landslide Research and Technology, Volume 4 Issue 1, 2025*, Progress in Landslide Research and Technology, https://doi.org/10.1007/978-3-031-89836-5

Geological Survey of Canada, Natural Resources Canada

GSC-Pacific Division

Geological Survey of Canada: Who We Are

The Geological Survey of Canada (GSC) is part of the Earth Sciences Sector of Natural Resources Canada. The GSC is Canada's oldest scientific agency and one of its first government organizations. It was founded in 1842 to help develop a viable Canadian mineral industry by establishing the general geological base on which the industry could plan detailed investigations. Throughout its long and colourful history, the GSC has played a leading role in exploring the nation.

Today, the GSC is Canada's national organization for geoscientific information and research. Its world-class expertise focuses on the sustainable development of Canada's mineral, energy and water resources; stewardship of Canada's environment; management of natural geological and related hazards; and technology innovation (Fig. A.1).

The GSC celebrated its 175th anniversary in 2017 which coincided with Canada's 150th anniversary of Confederation. The GSC co-leads the Canada-Nunavut Geoscience Office and works with dozens of universities and research institutes, industry organizations, other federal departments, provinces, territories and municipalities in Canada and across the world. In particular, we work closely with other geological survey organizations in Canada through the unique Intergovernmental Geoscience Accord.

Every year, we publish hundreds of maps, Open Files, peer-reviewed papers and other reports. Our scientists are recognized worldwide and sought after for their expert advice on locating mineral, energy and groundwater resources, reducing risk from natural hazards and reviewing environmental assessments.

Fig. A.1 Paleotsunami investigations in order to understand regional earthquake cycles and submarine landslide hazards

Strategic Priorities

The GSC has attempted to plot a course through this changing, uncertain world.

First, we identify three core areas of persistent scientific endeavour, which reflect stable, long-term needs of society:

- **Geological knowledge for Canada's onshore and offshore lands**
- **Geoscience for sustainable development**
- **Geoscience for keeping Canada safe.**

Next, we outline a new, fourth area of endeavour, Geoscience for society, which is the need to address the uncertainties of the changing world by expanding the reach and impact of geoscience knowledge in land-use decision making and in efforts to reduce the risk of disasters.

Finally, we recognize that our strength lies in a fifth area of endeavour, Our people, Our science, which we need to nurture to maintain a high-performing workforce capable of world leading innovative geoscience for the benefit of Canada.

G.-P. Division
GSC-Pacific Division, Vancouver, BC, Canada
e-mail: David.Huntley@nrcan-rncan.gc.ca

B. Abolmasov et al. (eds.), *Progress in Landslide Research and Technology, Volume 4 Issue 1, 2025*, Progress in Landslide Research and Technology, https://doi.org/10.1007/978-3-031-89836-5

(a) **Geological knowledge for Canada's onshore and offshore lands**

Geoscientific knowledge is fundamental to managing our onshore and offshore lands and their abundant resources. With its 10 million km^2 of onshore land and an additional 7 million km^2 of ocean estate, Canada is a vast country and a core mission of the GSC is to map and understand the land and its resources. Our Geo-mapping for Energy and Minerals (GEM) program continues to advance our knowledge of the North and by 2020 will complete a first mapping of surface geology at a coarse scale.

In the offshore lands, our geoscience knowledge also serves to confirm the farthest extents of the Canadian territory. Our joint program with Global Affairs Canada and Fisheries and Oceans Canada to delineate the outer limits of the continental shelf in the Atlantic and Arctic Oceans will reach a critical milestone in 2019. The program will file its Arctic submission under the United Nations Convention on the Law of the Sea (UNCLOS) (Fig. A.2).

(b) **Geoscience for sustainable development**

Finding new resources remains a major challenge. Many near-surface deposits have been discovered in Canada, but significant mineral resources remain to be found in less accessible regions and at depths below the surface. Finding new resources requires systematic, intensive and innovative methods to assess the mineral potential in remote locations.

It requires searching beneath overburden cover, imaging the 3-D structure of the earth and understanding the geological processes that lead to concentration of minerals in certain locations (Fig. A.3).

For the Energy sector, the greatest challenge is in the transition to a low-carbon economy. Although global fossil fuel use is likely to continue to grow over the foreseeable future, the trend will likely be at a decreasing rate. Canada has an abundant supply of conventional and unconventional (oil sands and shale) oil and gas, so development in frontier areas is likely to be slow. In addition, the government has placed a moratorium on exploration activity in the Arctic offshore lands.

Fig. A.2 The GSC studies the sea floor of the Arctic to understand its geology and geohazards. Here a small craft surveys the bottom of Southwind Fjord (Baffin Island, N Nunavut)

Fig. A.3 GSC geologists near the Heiberg Formation in northern Ellesmere Island (NU) as part of the geo-mapping for energy and minerals program. This formation is the primary host of major gas accumulations in the Canadian High Arctic

Fig. A.4 The GSC conducts climate change studies, here documenting the effects of fast melting permafrost leading to extreme coastal erosion on Pelly Island, NT

(c) **Geoscience for keeping Canada safe**

The GSC will continue to work on understanding how landscapes will change, how infrastructure will be affected and how resilience to climate change can be built into new infrastructure. Climate change will likely have a significant impact on the water cycle. GSC research will shed light on the risk to potable water supplies, hydroelectric power generation, and hazards from floods and drought (Fig. A.4).

Fig. A.5 The GSC conducts geohazard studies to reduce risks to people and infrastructure, here installing equipment to monitor landslide activity above a critical railway corridor in central BC

(d) **Geoscience for society**

The scientific knowledge required to assess cumulative effects is broad. The complex interactions between land use, water management and waste management require an integrated approach at a landscape scale. The GSC is a national provider of information on both land (surficial and solid geology) and water, including the integration of surface water and groundwater into the complete water cycle (Fig. A.5).

The GSC recognizes that this area of endeavour involves inherent complexities and that our goals in this area will be to some degree aspirational. However, we will investigate new ways of planning our programs, undertaking our fieldwork, interacting with key stakeholders, and communicating our expert knowledge in ways that contribute positively to decision making about resource development.

(e) **Our people, Our science**

As a science organization within the federal government, the GSC's mandate is to conduct world-class science to inform public decision making. The Canadian government has articulated and adopted the principle of evidence-based decision making and reaffirmed the need for government science to be objective and non-partisan.

To remain at the leading edge, our scientists need to work with a variety of partners. We need to reinforce the central role that the GSC plays in the Canadian geoscience community by building networks of collaboration, fully participating in national geoscience initiatives, and advocating for Canadian geoscience at the international level (Fig. A.6).

Fig. A.6 Among many celebratory activities for the GSC's 175th anniversary in 2017, the GSC held a Rock and Fossil Exhibit, at its site at the Bedford Institute of Oceanography (Dartmouth, NS), as part of a two-day open-house event, where more than 20,000 visitors participated

Moving Forward

Some of the objectives and goals that the GSC has set represent familiar territory for a national geoscience organization, but many others will pull us out of our comfort zone. We will take the time to better understand the challenges of delivering objective, nonpartisan science to support evidence-based decision making in Canada at a time of great technological and social change.

We will not be able to do this alone, so we look forward to strengthening our ties to other federal departments, provinces and territories, universities, Indigenous organizations, the private sector and civil society as a whole.

We ask all our stakeholders to contact us, to challenge us and, most importantly, to join with us to assure the future of Canada through thoughtful, respectful dialogue about the land we live on, its resources and its future (Fig. A.7).

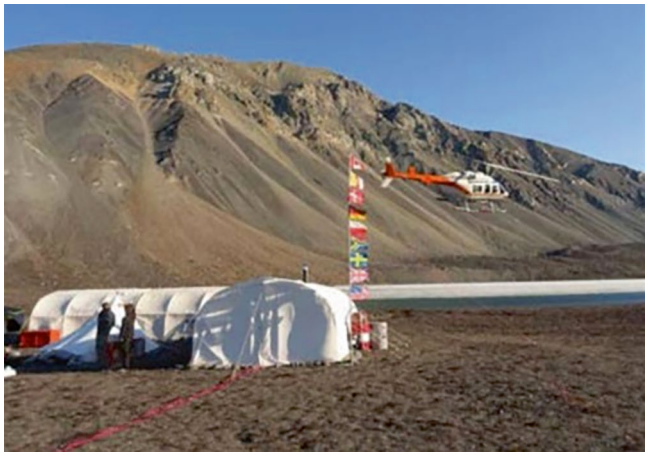

Fig. A.7 Joint Canadian/German (GSC/BGR) field mapping camp on northern Ellesmere Island, looking west as the fog covered sea ice of Yelverton Inlet, 2017

Exploring Canada

Through its history, the GSC has been responsible for mapping the land mass of Canada, which supported the integration of the western provinces and northern territories into the country that we have today. The limit of Canada's offshore territory is still being extended today though surveys conducted by the GSC and the Canadian Hydrographic Service.

In more recent years, the GSC helped find the first economic diamond deposit in the Northwest Territories, leading to the expansion of diamond mining in Canada. These are only a few of the key GSC achievements that have built our knowledge of Canada's lands and provided the building blocks of its natural resource economy.

Today, exploration of this vast land is still reaping its natural resource rewards. The search for natural resources is difficult, akin to looking for a needle in a haystack.

The GSC's GEM program is exploring vast tracts of Canada's North, a land mass roughly equivalent to the combined areas of Quebec, Ontario and Manitoba, to find the "haystacks" with resource potential. This information is shared with the provinces and territories, as well as the private sector, so that the search for the "needles" can continue. The information is also critical to inform land-use planning.

In November 2016, the Royal Canadian Geographical Society (RCGS) awarded its prestigious Gold Medal to the GSC in recognition of the Survey's outstanding contribution to the development of Canada on the occasion of it's 175th anniversary.

Faculty of Civil and Geodetic Engineering, University of Ljubljana

Matjaž Mikoš

Summary

The Faculty of Civil and Geodetic Engineering of the University of Ljubljana (UL FGG) covering engineering disciplines, including water science and technology, has been involved in landslide risk reduction activities at the national level in Slovenia (former Yugoslavia, until 1991) for decades. In 2008, UL FGG became an ICL Full Member and has gradually developed its ICL engagement. UL FGG has been awarded the title of the World Centre of Excellence (WCoE) in Landslide Risk Reduction for 5 consecutive periods (2008–2011, 2011–2014, 2014–2017, 2017–2020, 2020–2023). Together with the Geological Survey of Slovenia, UL FGG hosted in 2017 the 4th World Landslide Forum in Ljubljana, Slovenia.

UL FGG strongly supports diverse activities of the International Consortium on Landslides, Kyoto, Japan, and thus contributes to the 2030 Agenda for Sustainable Development, as well as to the Sendai Framework for Disaster Risk Reduction 2015–2030 (SF DDR). UL FGG was a signatory of the Sendai Landslide Partnerships 2015–2030, and is a dedicated official promoter of the Kyoto Landslide Commitment 2020, a SF DRR voluntary commitment by ICL.

In 2016, UL FGG started to host the University of Ljubljana UNESCO Chair on Water-related Disaster Risk Reduction (WRDRR), being still the only UNESCO Chair at this university, and one of a few in Slovenia. Among different activities, in 2022 the WRDRR Chair supported the launching of the regional platform called Resili- Enhance for enhancing the resilience to disasters for sustainable development. UL FGG also supports activities of the Slovenian National Committee for UNESCO Intergovernmental Hydrological Programme (IHP), now working on the IHP-IX programme (2022–2029).

UL FGG is actively involved in numerous international (bilateral) and national research projects in the field of hydrology and hydraulic engineering, including topics such as landslide research, landslide risk mitigation, natural risk dialogue, and capacity building for society resilience.

In the field of capacity building, UL FGG offers several courses for graduate and postgraduate students in landslide mechanics and dynamics, landslide stabilization and landslide risk mitigation. In this article, a short overview of the past and current activities of UL FGG as ICL Full Member and KLC2020 Official Promoter is shown.

World Centre of Excellence on Landslide

Risk Reduction and IPL projects

WCoE activities

The title of World Centre of Excellence (WCoE) on Landslide Risk Reduction is given to a governmental or non-governmental entity, which contributes to the landslide disaster risk reduction at a regional and/or global level in a specific unique field of expertise, as well as helps promoting International Programme on Landslides (IPL) and landslide research intellectually, practically and financially (https://www.landslides.org/ipl-info/world-centre-of-excellence/). UL FGG was granted the title of WCoE five consecutive times:

- WCoE 2008–2011 and 2011–2014: Mechanisms of landslides in over -consolidated clays and flysch.
- WCoE 2014–2017: Mechanisms of landslides and creep in over-consolidated clays and flysch.

M. Mikoš
Faculty of Civil and Geodetic Engineering, University of Ljubljana, Ljubljana, Slovenia
e-mail: matjaz.mikos@fgg.uni-lj.si

B. Abolmasov et al. (eds.), *Progress in Landslide Research and Technology, Volume 4 Issue 1, 2025*, Progress in Landslide Research and Technology, https://doi.org/10.1007/978-3-031-89836-5

- WCoE 2017–2020: Landslides in Weathered Flysch: from activation to deposition.
- WCoE 2020–2023: Landslides in Weathered Heterogenous Sedimentary Rock Masses such as Flysch.

The research efforts at UL FGG were focused on:

- Mechanisms of triggering such landslides (mud flows), estimation of debris-flow magnitudes triggered as shallow or deep-seated landslides (debris slides), and triggering of shallow rainfall-induced landslides using advanced statistical methods.
- Field and laboratory investigations of suction in over-consolidated clays and flysch, such as to improve the understanding of softening in stiff over–consolidated clays and marls, using soil matrix suction as an indicator for mudflow occurrence, and executing suction long-term monitoring of the Slano Blato landslide.
- Laboratory investigations of coarse debris-flow rheological parameters and soil–water characteristic curve of residual soil from a flysch rock mass.
- Mathematical modelling of debris flows (hazard assessment in deposition areas), using different numerical models and different digital terrain models.

The WCoE activities were financially supported by the Slovenian Research Agency through the Research Programme P2-0180 “Water Science and Technology, and Geotechnical Engineering: Tools and Methods for Process Analyses and Simulations, and Development of Technologies,” as well as by several national (Fig. A.8) and international (bilateral) research projects.

UL FGG and the Geological Survey of Slovenia jointly organized 4th World Landslide Forum (WLF4), in Ljubljana between May 29 and June 2, 2017. With over 600 participants from 49 countries and 5 international organizations, WLF4 was promoting the culture of living with natural hazards.

IPL projects

An important ICL activity is IPL projects (https://www.landslides.org/projects/ipl-projects/). The IPL Evaluation Committee examines the submitted proposals of ICL members by carefully reading the written proposals and by listening to their presentations at annual ICL conferences. The initially accepted proposals by the IPL Evaluation Committee are discussed and then approved at the annual Board of Representatives meeting of ICL members (Annual Assembly). Finally, the IPL projects are approved annually by the Global Promotion Committee IPL-KLC. UL FGG has

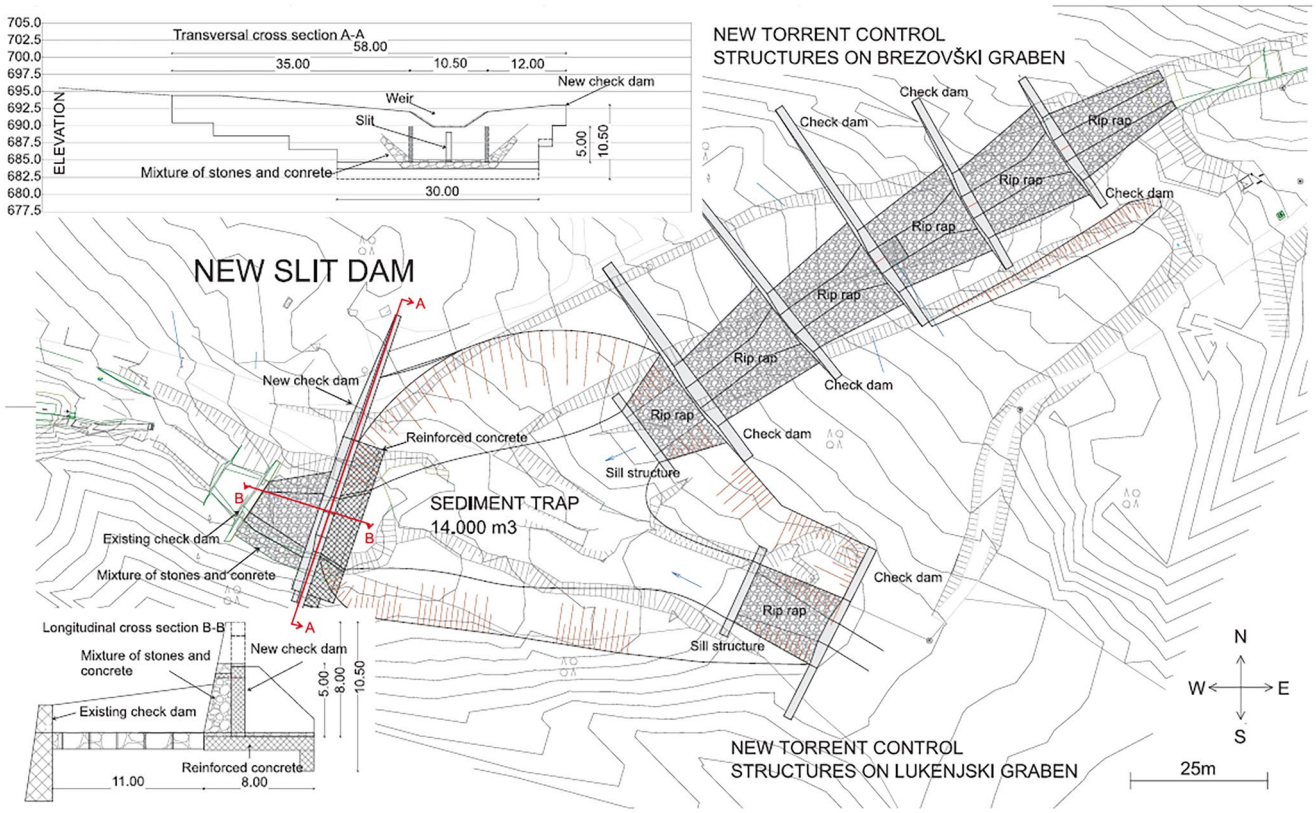

Fig. A.8 Technical countermeasures for future debris floods threatening the cabin station of the Krvavec ski area in N Slovenia. An extreme May 2018 debris flood case study in northern Slovenia: analysis, modelling, and mitigation. Landslides 17: 2373-2383, https://doi.org/10.1007/s10346-019-01325-1)

successfully submitted several proposals for IPL projects and has been so far actively involved in the following ones:

- IPL-151 Soil matrix suction in active landslides in flysch - the Slano Blato landslide case (2010–2012).
- IPL-225 Recognition of potentially hazardous torrential fans using geomorphometric methods and simulating fan formation (2017–2020).
- IPL-226 Studying landslide movements from source areas to the zone of deposition using a deterministic approach (2017–2020)—coordinated by the Geological Survey of Slovenia.
- IPL-261 World-wide-web-based Landslide Observatory (W3bLO) (2022-2024)

ICL Thematic and Regional Networks

Following the ICL Strategic Plan 2012–2021, several thematic networks and regional networks have been established (for an overview, see https://www.landslides.org/projects/icl-networks/).

Landslide Monitoring and Warning Thematic Network—LaMaWaTheN

In 2012, UL FGG proposed the ICL landslide monitoring and warning thematic network—almost 10 ICL members joined the initiative. The general objective of the proposed network was to compare experiences in the field of landslide monitoring and installed early warning systems for active landslides in various regions of the world. Lately, we contributed to the network activities by preparing practice guidelines on monitoring and warning technology for debris flows.

The idea of the network was partially taken over by the web database ICL World Report on Landslides (https://www.landslides.org/projects/world-report-on-landslides/), created to be a platform to share landslide case studies among the global landslide community, with monitoring and warning systems being a part of the platform.

ICL Adriatic-Balkan Network—ICL ABN

Jointly with other ICL members from Croatia and Serbia, in 2013, UL FGG proposed to establish an ICL Adriatic-Balkan Regional Network. Various network activities were proposed, the most active being the organization of biennial regional symposia on landslide risk reduction in the Adriatic-Balkan Region (called ReSyLAB). UL FGG supported the 1st Symposium in Zagreb (Croatia, 2013), 2nd in Belgrade (Serbia, 2015), 3rd in Ljubljana (Slovenia, 2017), 4th (Sarajevo, 2019), and 5th in Rijeka (Croatia, 2022).

In the last decade, UL FGG has signed bilateral research projects with the ICL members in the region: "Adriatic-Balkan Regional Network: Landslide Risk Mitigation for Society and Environment" (2012–2013 with University of Belgrade, Serbia), "Study of landslides in flysch deposits: sliding mechanisms and geotechnical properties for landslide modelling and landslide mitigation SoLiFlyD" (2014–2015 with University of Rijeka, Croatia), and "Laboratory investigations and numerical modelling of landslides in flysch deposits in Croatia and Slovenia" (2016–2017 with the University of Rijeka, Croatia). This joint research has helped strengthen regional cooperation within the ICL ABN regional network.

Other ICL-Related International Activities

UL FGG served the ICL by taking different leading roles in the Consortium, i. e. UL FGG member served as Chair of IPL Evaluation Committee, twice as ICL Vice President, and was elected to Co-Chair and in 2021 to Chair of the IPL-KLC (https://www.landslides.org/ipl-info/ipl-klc-globalpromotion-committee/).

UL FGG has been strongly supporting the journal Landslides: Journal of the International Consortium on Landslides, published by Springer Nature (https://link.springer.com/journal/10346) since its launch in 2004. UL FGG works for the journal in the roles of reviewers and an associate editor, and regularly publishes its top research results in the journal, as well as disseminates information important for capacity building in landslide risk reduction—such as results of bibliometric studies on the journal Landslides and ICL books.

UL FGG also contributed to the two-volume set of Landslide Dynamics: ISDR-ICL Landslide Interactive Teaching Tools (LITT), namely to Vol. 1: Fundamentals, Mapping and Monitoring by practice guidelines on monitoring and warning technology for debris flows (https://www.springer.com/gp/book/9783319577739), and to Vol. 2: Testing, Risk Management and Country Practices (https://www.springer.com/gp/book/9783319577760) by a state-of-the-art overview on landslide disaster risk reduction in Slovenia, a study on two-dimensional debris-flow modelling and topographic data, and by study on intensity duration frequency curves for rainfall-induced shallow landslides and debris flows using copula functions.

UL FGG also contributed to the open-access book series "Progress in Landslide Research and Technology" Vol. 1 by a review article on the history of the International Programme on Landslides (IPL) (https://doi.org/10.1007/978-3-031-16898-7_3), an original article on the natural-hazard-related web observatory as a sustainable development tool (https://doi.org/10.1007/978-3-031-16898-7_5), and an original article on landslide research and technology in patent documents (https://doi.org/10.1007/978-3-031-18471-0_3).

University of Ljubljana UNESCO Chair on Water-related Disaster Risk Reduction (2016–2020 and 2020–2024)

Experiences and knowledge accumulated in the past decades at the Chair on Hydrology and Hydraulic Engineering at UL FGG in the field of (applied) hydrology in experimental basins, hydraulic engineering, landslide research, landslide risk reduction, and flood risk management, culminated in 2016 in the establishment of the UNESCO Chair on Water-related Disaster Risk Reduction (WRDRR Chair; www.unesco-floods.eu) at the University of Ljubljana. The UNESCO WRDRR Chair was positively evaluated by UNESCO in 2020 and prolonged for another 4 years (2020–2024). The Chair is associated to the university twinning and networking UNITWIN UNESCO—Kyoto University—ICL on "Landslide and Water-Related Disaster Risk Management".

The UNESCO WRDRR Chair is involved into numerous international (bilateral) and national research projects. Their results are timely reported in scientific literature (https://www.unesco-floods.eu/category/publications/).

In 2022, the UNESCO Chair supported launching of the ResiliEnhance Program for enhancing the resilience to disasters for sustainable development (https://unescochair-sprint.uniud.it/en/resilienhance-program/). The program is at the moment focused to Central and Eastern Europe, and supported by the Central Europe Initiative (CEI).

In 2022, the UNESCO Chair started to lead the University of Ljubljana project on Sustainable Development (2022–2025; www.unesco-floods.eu/ultra-pilot-projects/) to modernize university professional study programmes, especially in civil engineering, to increase students' competences for sustainable development, including disaster risk reduction and resilience building.

UL FGG supports activities of the Slovenian National Committee for UNESCO Intergovernmental Hydrological Programme (www.ncihp.si)—focus of the activities is the development of the IHP-IX Programme (2022–2029).

Conclusions

UL FGG as one of World Centres of Excellence in Landslide Risk Reduction, hosts the UNESCO Chair on Water-related Disaster Risk Reduction. UL FGG strongly supports ISDR-ICL Sendai Partnerships 2015–2025 for global promotion of understanding and reducing landslide disaster risk, and its extension to 2030 and beyond: the Kyoto 2020 Commitment for Global Promotion of Understanding and Reducing Landslide Disaster Risk that that was signed in November 2020. UL FGG is proud to be its Official Promoter, and will specifically work for its Actions 2, 5, 6, 9 and 10.

This review article is intentionally written without a list of references to described activities. For this purpose, listed websites and links may be used.

The author wants to thank colleagues from UL FGG and University of Ljubljana, and from the ICL community for the past and long-lasting excellent cooperation with a joint vision to reduce landslide disaster risk.

China University of Geosciences, Wuhan

Huiming Tang, Changdong Li, and Qinwen Tan

Introduction

China University of Geosciences, Wuhan (CUG), founded in 1952, is a key national university affiliated with the Ministry of Education. It is also listed in the National "211 Project", the "985 Innovation Platform for Advantageous Disciplines," and the "Double First-class Plan". CUG, featuring geosciences, is a comprehensive university that also offers a variety of degree programs in science, engineering, literature, management, economics, law, education, and arts. Its Geology and Geological Resources and Engineering have both been ranked as the national number one disciplines.

CUG has two campuses in Wuhan. The main campus is the Nanwang Mountain Campus, located in the heart of the Wuhan East Lake National Innovation Demonstration Zone, which is popularly known as China Optics Valley. The Future City Campus is located in the east of Wuhan and is 27 km from the main campus. These two picturesque campuses cover a combined area of 1,474,353 m^2. They are ideal places to study, work, and enjoy life. CUG owns a 4A-Level tourist attraction—the Yifu Museum. CUG also boasts four field training centers: Zhoukoudian in Beijing, Beidaihe in Hebei Province, Zigui in Hubei Province, and Badong in Hubei Province.

CUG has established a complete education system. As of December 2020, 30,239 full-time students, including 18,080 undergraduate students, 9302 master's students, 1916 doctoral students, and 941 international students, have enrolled in its subsidiary 23 schools and 86 research institutes. CUG currently has a faculty of 1858 full-time teachers, among which there are 539 professors (11 of which are members of the Chinese Academy of Sciences) and 984 associate professors.

CUG is focused on fostering high-quality talent. Among its over 300,000 graduates, many have gone on to become scientific and technological elites, statesmen, business leaders and athletes. And they have made great contributions to the nation and society, represented by former Premier WEN Jiabao and 39 members of the Chinese Academy of Sciences and Chinese Academy of Engineering.

CUG has strengthened exchanges and cooperation with international universities. It has signed friendly cooperation agreements with more than 100 universities from the United States, France, Australia, Russia, and other countries. CUG has actively carried out academic, scientific, and cultural exchanges with universities around the world. There are about 1000 international students from more than 100 countries studying at CUG. It also sponsors more than 900 teachers and students to study abroad or conduct international exchanges and invites more than 400 international experts to visit, lecture, and teach at CUG every year. In 2012, CUG initiated and co-established the International University Consortium in Earth Science (IUCES) with 11 other world-renowned universities. IUCES is committed to promoting the common development of geosciences education and scientific research through resource sharing, exchange, and cooperation among its member institutions. In addition, CUG has partnered with Bryant University from the USA, Alfred University from the USA, and Veliko Turnovo University from Bulgaria in establishing three Confucius institutes on their campuses (Fig. A.9).

H. Tang
C. Li · Q. Tan
China University of Geosciences, Wuhan, P.R. China
e-mail: tanghm@cug.edu.cn

B. Abolmasov et al. (eds.), *Progress in Landslide Research and Technology, Volume 4 Issue 1, 2025*, Progress in Landslide Research and Technology, https://doi.org/10.1007/978-3-031-89836-5

Fig. A.9 Strategic plan of building a world-renowned research university in earth science

Strategic Plan of Building a World-Renowned Research University in Earth Sciences: A Beautiful China and a Habitable Earth—Towards 2030

CUG reviewed and approved Strategic Plan of Building a World-Renowned Research University in Earth Sciences on December 25 of 2019.

Themed "A Beautiful China & A Habitable Earth", the Plan depicts the blueprint of the second goal of the "three-step strategic goals", which is to build a world-renowned research university in Earth Sciences by 2030 based on the attained goal of developing CUG into a "high-level university with first-class Earth Sciences and coordinated development of multi-disciplines".

According to the Plan, our education missions are: Remaining true to CUG's core value of "seeking harmonious development between man and nature" we are committed to cultivating innovative talents who have lofty morality, solid foundation, and profound expertise and who pursue the unity of knowing and doing. We should provide personnel support and endeavor to innovate, apply and spread knowledge in order to provide theories, technologies, and approaches for the construction of a Beautiful China and a Habitable Earth. We should strive to optimize governance, reform culture, and fully invigorate the vitality of running a university. We should provide our service to the construction of an innovative country and to the promotion of a harmonious co-existence between man and nature. We should provide our service to the people and the governance of China. We should provide our service to the consolidation and development of the system of socialism with Chinese characteristics. We should provide our service to the reform and opening up and to the construction of socialist modernization.

According to the Plan, our endeavoring goals are: By 2030, we will have built a world-renowned research university in Earth Sciences, whose main indexes will have reached or nearly reached the level of other world-class universities. To upgrade CUG into a world-class university, we will endeavor to make the discipline of Earth Sciences rank top in the world and forge boldly ahead in competition to improve the quality of other disciplines of CUG. We will assemble a contingent of teachers and researchers with international competitiveness and influences to build a university with Chinese characteristics and superiority. We will build a world-class university that will be fully engaged in international exchange and cooperation and that will achieve educational, academic, cultural, and administrative excellence.

Outstanding Recent Achievements

In recent years, CUG has achieved significant progress in the research fields of geohazards, water resource, geochemistry, paleontology, geodetic surveying and lunar exploration program, etc. To keep to the theme of KLC2020, recent achievements on geohazards researches of CUG are focused and introduced.

(a) **Approval of National Observation and Research Station for Geohazards in the Three Gorges Reservoir Area, Hubei**

CUG was newly approved **National Observation and Research Station for Geohazards in the Three Gorges Reservoir Area, Hubei**. This station, founded and administrated by Prof. Huiming Tang, is responsible to carry out field observations and scientific research on geohazards in condition of reservoir operation.

The central site of the station is located in Badong County of the Three Gorges Reservoir area (hereinafter abbreviated as the TGR area), and a larger monitoring network of multiple sites has been established, including the geohazard field test site for the Majiagou landslide, Zigui County, and systematic geophysical monitoring station for the whole TGR area, etc.

The Badong field site (also named Badong in-situ large-scale experimental station) is located in the Huangtupo landslide area, which has been recognized the

largest reservoir landslide by volume in the TGR area. The field site consists of a tunnel complex and a series of monitoring systems (Fig. A.10). The tunnel complex, built in the Huangtupo riverside sliding mass #1, consists of a main tunnel with a length of 908 m and a width of 5 m, five branch tunnels (5–145 m long, 3.5 m wide), two test tunnels, and 35 observation windows. The test tunnels exposed the sliding zones of the landslide, facilitating their direct observation and the execution of scientific experiments, such as large-scale in-situ mechanical tests and deep deformation monitoring. The monitoring systems measure deformation as well as hydrologic, meteorological and hydro-chemical variables. The deformation system is composed of a slope surface displacement measurement unit and an underground displacement measurement unit. The slope surface displacement unit includes a number of GPS (Global Positioning System) and BDS (BeiDou Navigation Satellite System) measurement points, as well as an IBIS-FL (Interferometric Radar) monitoring system (Fig. A.12). The underground displacement unit includes nine deep inclinometer boreholes, a number of crack meters installed on the ground and the walls of tunnels, and many hydrostatic level gauges that measure the settlement of the tunnels in the sliding mass. The hydrologic system includes a number of devices that allow for observation of the water level of the Yangtze River, the ground water level and water discharge of the tunnels (Fig. A.12). A small meteorological station is located on the landslide and provides rainfall data. So far, multiple and massive data have been collected for the landslide area since the year 2012, when the field site was constructed; over 10,000 people with a variety of geology-related backgrounds from >20 countries have visited this experimental station.

(b) **Approval of the Basic research on the prediction and forecasting of major landslides program supported by the Major Program of NSFC**

CUG was approved the **Basic research on the prediction and forecasting of major landslides program** (2021–2025), supported by the Major Program of the National Natural Science Foundation of China. The program was designed for the prediction and forecasting of major landslides, with the concentration on the core scientific problems of landslide evolution process and physical-mechanical mechanism. Three key scientific problems, including correlation mechanism for landslide initiation, physical-mechanical mechanism for landslide initiation, and prediction and forecasting theory based on landslide evolution were proposed.

Five topics were set up to achieving those objectives. Topic 1 was proposing the initiation classification of major landslides based on large field test platform, with the adoption of field prototype test and other technical means. Topics 2–4 aimed to reveal the physical and mechanical mechanism of locked-segment dominated landslide, static liquefaction loess landslide and hydrodynamic pressure-driven landslide, and to establish the corresponding landslide initiation criteria, respectively. Topic 5 was responsible to established the prediction mode and real-time forecasting system. Ultimately, the landslide prediction and forecasting theory based on the evolution process and physical-mechanical mechanism would be put forward. The scientific thought for the implement of research is exhibited in Fig. A.11.

The implementation of the research is respected to lay the geological, mechanical and physical foundation for the above three types of landslide prediction, and to substantially promote the research on landslide prediction.

Figure A.12 shows the old Badong county, situated in the Huangtupo landslide area, and the exposures of the main rupture zones are now more than 50 m below the water surface of the Three Gorges Reservoir (Tang et al. 2015a). During the second relocation from 1982 to 2003, the county moved from Xinling town to the Huangtupo landslide area (Gong et al. 2021). A series of investigations were conducted during that period, and the new county area was further confirmed to be on the site of an ancient landslide then (Gong et al. 2021). Huangtupo landslide is developed in the Middle Triassic Badong Formation strata, within which interbedded strata structures are often observed, and many geohazards developed. The material composition of the Huangtupo landslide includes mudstone, pelitic siltstone, and argillaceous limestone (Tang et al. 2015b). Multiple slumps formed the complex mass at least 4000 years ago (Tang et al. 2015b). The elevation of the crown of the landslide is about 600 m asl., while its toe varies from 50 to 90 m, submerged in the Yangtze River. The composite landslide covers an area of 1.35 km^2, and its volume of nearly 70 million m^3 makes it the largest reservoir landslide in China (Tang et al. 2015b). Considering the risk of landslide reactivation by long-term reservoir operation and human activities, the drainage system and the anchored defense structures along its leading edge were constructed to control the landslide. Huangtupo demonstration base was designed and constructed in 2012, during the third relocation period from 2007 to 2017 (Gong et al. 2021). At that time, some Badong county residents still lived in the Huangtupo area, facing the unsure threat. The old giant landslide is in need of further research to ensure its safety as well as provide access for landslide hazard study. The demonstration base was in great request. With the building and development of the demonstration base, Over 10,000 people with various geology-related backgrounds from more than 20 countries have visited. A national observation station was also settled rely on the base in 2020.

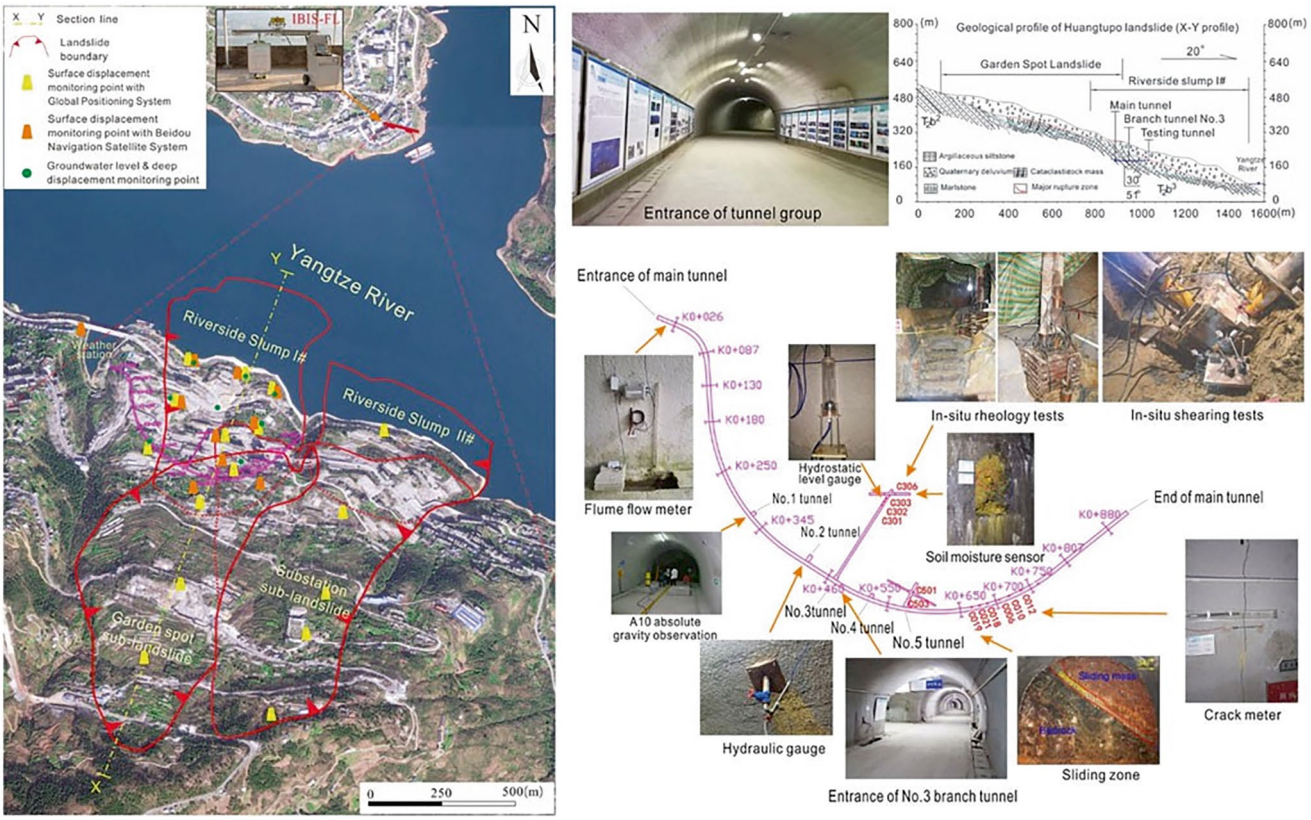

Fig. A.10 Badong in-situ large-scale experimental station of the National Observation and Research Station for Geohazards in the Three Gorges Reservoir Area, Hubei

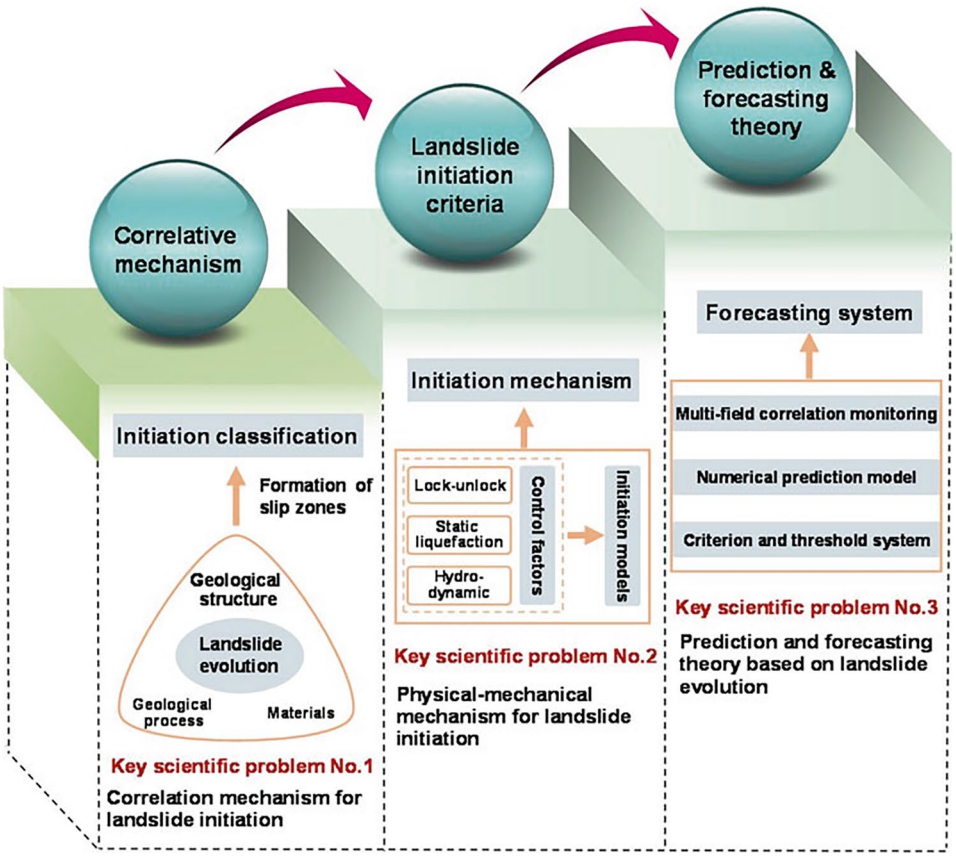

Fig. A.11 Scientific thought for the implement of research

Fig. A.12 Photo of old Badong County, showing the populated area built on the Huangtupo landslide (Tang et al. 2015a)

References

Tang H, Li C, Hu X, Wang L, Criss, R, Su A, Wu Y, Xiong, C (2015a) Deformation response of the Huangtupo landslide to rainfall and the changing levels of the Three Gorges Reservoir. Bull Eng Geol Environ 74(3):933–942.

Tang H, Li C, Hu X, Su A, Wang L, Wu Y, Criss R, Xiong C, Li Y (2015b) Evolution characteristics of the Huangtupo landslide based on in situ tunneling and monitoring. Landslides 12(3):511–521.

Gong W, Juang CH, Wasowski J (2021) Geohazards and human settlements: lessons learned from multiple relocation events in Badong, China—engineering geologist's perspective. Eng Geol 285:106051.

The State Key Laboratory of Geohazard Prevention and Geoenvironment Protection

The State Key Laboratory of Geohazard Prevention and Geoenvironment Protection

Introduction

The State Key Laboratory of Geohazard Prevention and Geoenvironment Protection (herein abbreviated as SKLGP) (Chengdu University of Technology), Chengdu, Sichuan Province, China, is dedicated to the applied basic research on geohazard prevention and geoenvironment protection. Committed to meeting the needs of territorial disaster prevention and mitigation, to safeguarding the national major construction projects, SKLGP focuses on the research of generation background, formation mechanism, early identification, monitoring and warning of geohazards which are either induced by nature or human activities, as well as the theories and methods of project management, thereby forming a world-class research center, which combines the applied fundamental research, the development and promotion of advanced technologies, the education of high-caliber talents with international communication and cooperation, SKLGP provides support in a comprehensive way to achieve the national targets of geohazard prevention and geoenvironment protection.

With a unique system of academic thoughts and technical methods, SKLGP focuses on geology and combines the theoretical basis of geology with modern earth science, key zone theory and engineering. By doing so, SKLGP has developed a featured academic thought system with "geological process mechanism analysis - quantitative evaluation" and "system engineering geology". SKLGP has built a whole set of theories and methods, from field investigation, rock mass parameterization, simulation, and evaluation to early identification of potential risk, monitoring and early warning, risk prevention and mitigation, design and construction of projects, which is applicable, complete and targeted for geohazard prevention and geoenvironment protection, equipped with auxiliary facilities and software analysis system in addition.

The State Key Laboratory of Geohazard Prevention and Geoenvironment Protection
The State Key Laboratory of Geohazard Prevention and Geoenvironment Protection,
Chengdu City, Sichuan Province, P.R. China
e-mail: sklgp_cdut@126.com

B. Abolmasov et al. (eds.), *Progress in Landslide Research and Technology, Volume 4 Issue 1, 2025*, Progress in Landslide Research and Technology, https://doi.org/10.1007/978-3-031-89836-5

The State Key Laboratory of Geohazard Prevention and Geoenvironment Protection, Chengdu University of Technology

Geotechnical Centrifuge Laboratory and Shaking Table Apparatus

We Are HIRING
SKLGP Positions Available!
Join the world first-class laboratory for geohazards!
It is more than a career.
Position:

- Scientific researcher
- Post doctor
- Professors, Associate Professors, Assistant Professors.
- Science Fund Program for Excellent Young Scientists (Overseas)
- National High-level Talent Recruitment Programs

Subjects: Geotechnical, Geology Engineering, Civil engineering, Geoscience, Remote sensing/GIS and all related subjects.

Basic Salary: 180,000-800,000 RMB per year

Additional benefits: settling-in allowance (150,000–500,000 RMB), research start-up funds (80,000–500,000 RMB), exceeding Expectations Bonus (depend on the research achievement, publications and etc.), national funding application (100,000–3,000,000 RMB), free accommodation

Research areas:

1. Evaluation and Prevention of Major Geohazards
2. Interaction between Human Activities and Geoenvironment and Disaster Mitigation
3. Regional Geoenvironment Evaluation and Protection
4. Geohazard Monitoring and Early Warning and Information Technology

How to apply:

The application should include:

1. A long-term CV that includes publications and research achievements,
2. 1–2 pages statement summarizing your expertise and present/future career goals,
3. Names and contact details of two references.

The full application package should be sent electronically as a PDF document to:

Email: sklgp_cdut@126.com

Address: State Key laboratory of Geohazard Prevention and Geo-environment Protection, Sichuan, China

Don't hesitate to contact us for more details!

Tel: +86 84073193

Email: sklgp_cdut@126.com

iRALL School 2024

13 October to 27 October, 2024

"iRALL" The International Research Association on Large Landslides, is an international non-governmental, non-political, non-profit-making and unaffiliated institution for the promotion of knowledge about large landslides founded on 11 November 2015. The scientific committee consists of international experts in the field of large landslides. The secretariat of iRALL is located at the State Key Laboratory of Geohazard Prevention and Geoenvironment Protection (SKLGP), Chengdu University of Technology, Chengdu, China.

The objectives of iRALL are to promote:

- Cooperation and exchange of knowledge among scientists and engineers working on large landslides
- The dissemination of scientific knowledge of large landslides
- The mitigation of risks associated with large landslides and their consequences

Courses in the iRALL School 2024:

Module 1: Occurrence and mechanism of large landslides
Module 2: Field investigation and geophysical survey of large landslides
Module 3: Remote sensing and AI technology application of large landslides
Module 4: Numerical modelling of large landslide
Module 5: Risk analysis, prevention and mitigation for large landslides
Module 6: Co-seismic landslides and hazard-chain Field excursion

Application and registration

The iRALL School is opened for 20 PhD students and for a maximum of 10 doctors/postdocs who have obtained their PhD degree not earlier than 2019.

Please click the following linkage to apply online. http://irall.sklgp.cdut.edu.cn/Application.htm

The deadline for applications is July 31, 2024 and selection of participants will be announced by August 20, 2024.

2023 iRALL School 2023

The 1st International Conference on Smart Informatics and Multi-hazard Reduction (SIMR 2024)

We are pleased to announce that the First International Conference of the Global Partnership for Smart Informatics and Multi-hazard Reduction (SIMR 2024) **will be held at Loughborough University, the United Kingdom, September 15–19, 2024.**

SIMR 2024 will create a multi-disciplinary forum for academic researchers and professionals to share research and practical experiences in developing and implementing multi-faceted approaches to address the global challenges created by increasing multi-hazard risk and climate change in a fast-changing world. It aims to foster international and interdisciplinary collaboration to advance scientific research and practice in harnessing data and informatics technologies to understand, assess and manage hazard risk for disaster risk reduction to achieve long-term resilience. This First SIMR conference will not only provide a platform for networking, skill development and information exchange, but more importantly, act as a catalyst for shaping the further development of smart informatics and multi-hazard risk reduction. Contributions from all relevant science, engineering, social and humanity disciplines are welcome.

In addition to scientific sessions, SIMR 2024 will offer training courses where participants can learn the latest high-performance hazard modelling and risk assessment skills. The conference will also include a field trip to the Peak District and enjoy the English countryside scenery.

15 Sep	16 Sep	17 Sep	18 Sep	19 Sep
Registration and training courses	Opening ceremony and sessions	Sessions and conference dinner	Sessions	Field trip

Organizers

- UNESCO Chair in Informatics and Multi-hazard Risk Reduction (IMRR), Loughborough University, UK
- State Key Laboratory of Geohazard Prevention and Geoenvironment Protection, Chengdu University of Technology, China
- School of Water Conservancy and Transportation, Zhengzhou University, China

GEODATA and AI an up-coming high-impact Journal by Elsevier Affiliated with The State Key Laboratory of Geohazard Prevention and Geoenvironment Protection (SKLGP)

Editor-in-chief	Kok-Kwang Phoon
Editors	Jianye Ching & Xuanmei Fan
Special editor	Limin Zhang
Managing editors	Zi-Jun Cao & Chong Tang

Aims and Scope:

Geodata and AI is an international journal that is focused on the development of machine learning and artificial intelligence for scientific discovery in geo-disciplines (research) and creation of novel digital service over the life cycle of natural or engineered geo-systems (practice). Geo-disciplines include geotechnical engineering, rock engineering, earthquake engineering, engineering geology, mining, geophysics, and geo-hazard. Geodata can be broadly defined as data produced by the characterization of the constituent ground and observation of the processes emerging from these disciplines. The heterogeneous spatial/temporal features and complex sampling characteristics (multi-source, uncertain, sparse, incomplete, potentially corrupted) of geodata are common in these disciplines with potential for data fusion. They are pivotal to the training of machine learning and artificial intelligence that are transformative business drivers when combined with other digital technologies.

The objectives of this international journal are to advance geodata science to address the challenges posed by geodata intrinsic and sampled features, to promote the compilation and sharing of geo-databases, to develop novel machine

learning and artificial intelligence methods that are of significant value or even indispensable to actual projects, to establish benchmarks for competitive evaluation of algorithms, and to solve complex challenges such as risk and resilience related to geo-disciplines. All aspects of a geodata-centric agenda that can transform research and/or practice are of interest:

- Geodata science
- Geo-databases
- Data fusion
- Physics-informed machine learning
- Data-driven site characterization
- Machine learning guided observational method
- Benchmarking
- Data-informed risk and resilience
- Trustworthy/explainable/interpretable AI
- Human-machine teaming
- Autonomous construction
- Smart infrastructure
- Building Information Modelling/Digital twin
- Privacy enhancing technologies

Timeline for Vol. 1, Issue 1

Submission of full paper: 1 Sep 2024

Final decision: 1 Feb 2025

Publication: Mar 2025

Please submit by email to Prof. Zijun Cao (zijuncao@swjtu.edu.cn) or Chong Tang (ceetc@dlut.edu.cn)

For more information, please contact the same email address.

Department of Civil Engineering, National Taiwan University

Department of Civil Engineering, National Taiwan University

Introduction

National Taiwan University (NTU) was originally established in 1928, when Taiwan was under Japanese rule, as Taihoku Imperial University. The current name dates back to 1945. As Taiwan's oldest and most prestigious university, we are also the largest comprehensive higher education institution (HEI) in the country. The academic freedom that we cherish and our excellent faculties attract both domestic and international students. Throughout our 90-year history, we have nurtured many talents, including leading academics and leaders in the public and private sectors. Our campus is vast, and spans across multiple locations, including Taipei, Yilan, Hsinchu, Yunlin, and mountainous areas in central Taiwan—accounting for nearly 1% of Taiwan's total land area. This provides teachers and students with an environment rich in biological and ecological diversity.

As the leading university in Taiwan, we are strongly committed to social responsibility as we strive to drive sustainable development and influence positive change in society. This was also reflected in the first University Impact Rankings launched in 2019 by Times Higher Education (THE), which measure the contributions of HEIs to the United Nations' Sustainable Development Goals (SDGs). We were ranked 70th in the world overall, and 1st in the world for SDG16: Peace, Justice, and Strong Institutions. Starting from creating a sustainable culture on campus, we aim awareness about sustainability throughout the university, through innovative teaching and research, environmental protection and recycling efforts, and a school administration that supports equality and wellbeing. Our sustainability efforts extend beyond our campus through industry-academia collaborations and service teams deployed to remote areas. In the near future, we will continue to reinforce the spirit of innovation and sustainability thinking among all faculty members and students. We will also continue our efforts to address economic, environmental, and social challenges through interdisciplinary collaboration, as we create connections between the local and the international community. The Department of Civil Engineering (Fig. A.13) can be regarded as the root of The College of Engineering. The early civil engineering education covers a wide range of professions. With the development and differentiation of various social industries, some fields have gradually separated and established specialized departments. We have also moved on, combining different fields and top-notch technology to remain as the leader of the tide.

Civil engineering is inseparable from the development of human civilization. From the beginning of civilization, all man-made structures have enchased and highlighted the value of civil engineering. NTU Civil Engineering is no exception. From the Department of Civil Engineering of the Imperial College of Taipei to the National Taiwan University Department of Civil Engineering today, the majority of Taiwan's significant constructions is and will always be our finest gallery.

In National Taiwan University, you will obtain high-quality guidance in and out of the classroom. Academic resources in the classroom and sports culture clubs, various student activities throughout the year, will bind you together with peers of the same dream. These friends may also be partners that can help you in future careers. If you are willing to take civil engineering as a career and take on the challenges and step forward as a team, then listen to your inner call, join us, and let us stride ahead hand in hand (Fig. A.14).

Department of Civil Engineering, National Taiwan University
Department of Civil Engineering, National Taiwan University, Taipei, Taiwan
e-mail: louisge@ntu.edu.tw

B. Abolmasov et al. (eds.), *Progress in Landslide Research and Technology, Volume 4 Issue 1, 2025*, Progress in Landslide Research and Technology, https://doi.org/10.1007/978-3-031-89836-5

Fig. A.13 Quick facts of the Department of Civil Engineering

Fig. A.14 Life beyond classroom

Fig. A.15 Taiwan Earthquake Loss Estimation System (TELES)

Outstanding Recent Achievements

Mitigating the Impacts of Natural Disasters via Cutting Edge Technology

Taiwan is located in the Circum-Pacific seismic belt, with many active faults and frequent typhoons. Due to the effects of climate change, extreme rainfall events that used to occur once in a century are now becoming more frequent, exacerbating the threat of landslides and debris flows. The prevention and mitigation of natural disasters such as earthquakes and flooding have therefore become a priority for the twenty-first century.

(a) **Earthquake Early Warning Systems: gain valuable response time**

For most natural disasters, potential losses to life and property can be mitigated through early warning and prevention. After the earthquake disaster of September 21, 1999, building safety inspections needed to be conducted all across Taiwan. Our faculty and students with expertise in civil engineering and geology were quick to respond to this urgency, working closely with the National Center for Research on Earthquake Engineering to help the government improve the earthquake resistance standards and test specifications. Moreover, they proposed a more elaborate system for earthquake damage and liquefaction assessment, and conducted a complete review and classification of the earthquake risk tolerance for all areas in Taiwan. The team also developed new disaster prevention technologies. One of the most significant contributions was to assist the public high (vocational) schools around Taiwan with assessments of the earthquake resistance and reinforcement needs of old buildings. In the numerous earthquakes that have since occurred, the effect of these reinforcements has become apparent. The stronger earthquake resistance of these buildings has improved safety for 2.65 million teachers and students around Taiwan (Fig. A.15).

Our school has also developed technology to monitor the status of bridges with high traffic volumes. This optical fiber monitoring system will emit a warning whenever poor conditions are recorded, prompting an early

response from management that can prevent a disaster from happening. When bridges in remote areas are damaged, a lightweight bridge developed by NTU out of composite materials can be assembled by residents in short time. In this way, access to affected areas can be quickly restored, and disaster relief provided more efficiently. In the event of an earthquake, Taiwan's citizens will immediately receive an emergency alert by text message. This warning system, which was developed by Professor Wu, Yih-Min at our Department of Geosciences, analyzes the properties of a P-wave within three seconds after detecting the wave so that it can issue an alert to citizens more than 10 seconds before the S-wave, which is most likely to cause damage arrives. This early warning system is accurate and fast, giving people valuable seconds to escape to safety. Because it is also much cheaper to manufacture network of multiple sites has been established, including the geohazard field test site for the Majiagou landslide, Zigui County, and systematic geophysical monitoring station for the whole TGR area, etc. than previous seismographs, it could be rapidly rolled out to several hundred elementary and junior high schools, ensuring better protection of our country's younger generation. Moreover, this system has been successfully introduced in other earthquake-threatened countries, such as Indonesia, India, Vietnam, Nepal, and Mexico.

(b) **After the Flood: Rapid Mobilization and Improved Ability to Provide Relief**

Another critical area is flood disaster prevention. Also here, our faculty and students are actively involved in key activities ranging from early warning and response during the disaster, to raising the awareness of, and capability for, disaster prevention among citizens more generally. Our Center for Weather Climate and Disaster Research comprises experts in meteorology, hydrology, bioenvironmental engineering, and geology etc. This center helped New Taipei City and Keelung City establish an extreme weather and flood monitoring & warning system. Other projects include combining advanced deep learning with the analysis of radar data, which allows for closer monitoring of rainfall data in hydrologically sensitive areas. The improvement of flood models increases the accuracy of flood warnings and pro- vides disaster prevention units with valuable information for them to rapidly formulate response strategies. From past experiences outside of Taiwan, we know that self-help and mutual support account for the largest share of the relief effort (90%) in the event of a disaster. In other words, even if flood warnings are effective, people in the affected area still need to be able to take own measures to protect themselves. At NTU, we actively participate in the community-level disaster relief preparations around the country, as well as in the training of disaster relief officers. Our experts provide citizens with the most up-to-date knowledge in disaster prevention, operate independent disaster relief systems, and evaluate the safety of shelters. These efforts contribute to the resilience and ability of local communities to mitigate impact, helping them recover more quickly. A plan for how to improve the disaster relief ability in the country proposed by our experts is another example of how we help make sure that the best disaster response capacity is in place. After improving the ability to respond to disasters, NTU's team also contributed to disaster prevention infrastructure around Taiwan, such as seismic isolation technology for buildings and equipment, or detention ponds in communities at risk. Our work and efforts in these areas help protect lives and property. As climate change continues to impact the world, we hope to leverage our technologies and expertise in these domains even further, and help strengthen the capacity to prevent and withstand natural disasters throughout the world.

Institute of Cold Regions Science and Engineering, Northeast Forestry University

Wei Shan and Ying Guo

Introduction

Institute of Cold Regions Science and Engineering of Northeast Forestry University (ICRSE-NEFU) is committed to the environmental geology and engineering geology of high latitude permafrost region and deep seasonal frozen area under the background of climate change, and attaches importance to the combination of basic research and applied research. With undergraduate, master, doctor, postdoctoral professional training system and standards, ICRSE-NEFU initiated "Geological environment risk research plan for permafrost degraded areas in Northeast China (GERRP)". With the support of the Chinese government, "Field scientific observation and research station of the Ministry of Education—Geological environment system of permafrost area in Northeast China (FSSE-PFNEC)" was established. Its observation stations cover all kinds of permafrost areas in Northeast China. At the same time, in order to develop and transfer technologies related to environmental governance and infrastructure construction in permafrost regions, "Provincial Collaborative Innovation Centre, Environment and road construction & maintenance in permafrost area of Northeast China (PCIC-PFER)" was established. Over the years, ICRSE-NEFU have continuously established cooperation with academic institutions and organizations at home and abroad, held various academic exchanges and regularly held "Academic Seminar on Engineering Geology and Environmental Geology in the Permafrost Along the Sino-Russian-Mongolian Economic Corridor", edited and published research cases of geoenvironmental disasters in permafrost regions in Northeast China, and shared the research results of GERRP. At present, the research results of GERRP are gradually enriched, some of them have highly academic value, and have been put into engineering practice. ICRSE-NEFU has gradually shown its unique research charm since it became an ICL member in 2002. In 2012, ICRSE-NEFU established a landslide research net- work in cold regions (ICL-CRLN), and then Research Center of Cold Regions Landslide was built.

Permafrost as one of the elements of the cryosphere, the change of thermodynamic stability of permafrost will directly affect the changes of hydrosphere, biosphere and lithosphere. Under the trend of global warming, the frequency and intensity of environmental and engineering geological disasters caused by permafrost degradation are getting higher and higher (Figs. A.16 and A.17). Taking the cold area in the southern boundary of the permafrost zone in Northeast China as study area, disasters such as ground subsidence, slope icing, landslides and other disasters caused by permafrost melting were studied. At the same time, we found melting permafrost also leads to seasonally high concentrations of greenhouse gases, triggering wildfires that may further accelerate permafrost degradation and environ- mental changes of terrestrial ecosystems and roads.

W. Shan · Y. Guo
Institute of Cold Regions Science and Engineering Northeast Forestry University, Harbin, China
e-mail: shanwei456@163.com

B. Abolmasov et al. (eds.), *Progress in Landslide Research and Technology, Volume 4 Issue 1, 2025*, Progress in Landslide Research and Technology, https://doi.org/10.1007/978-3-031-89836-5

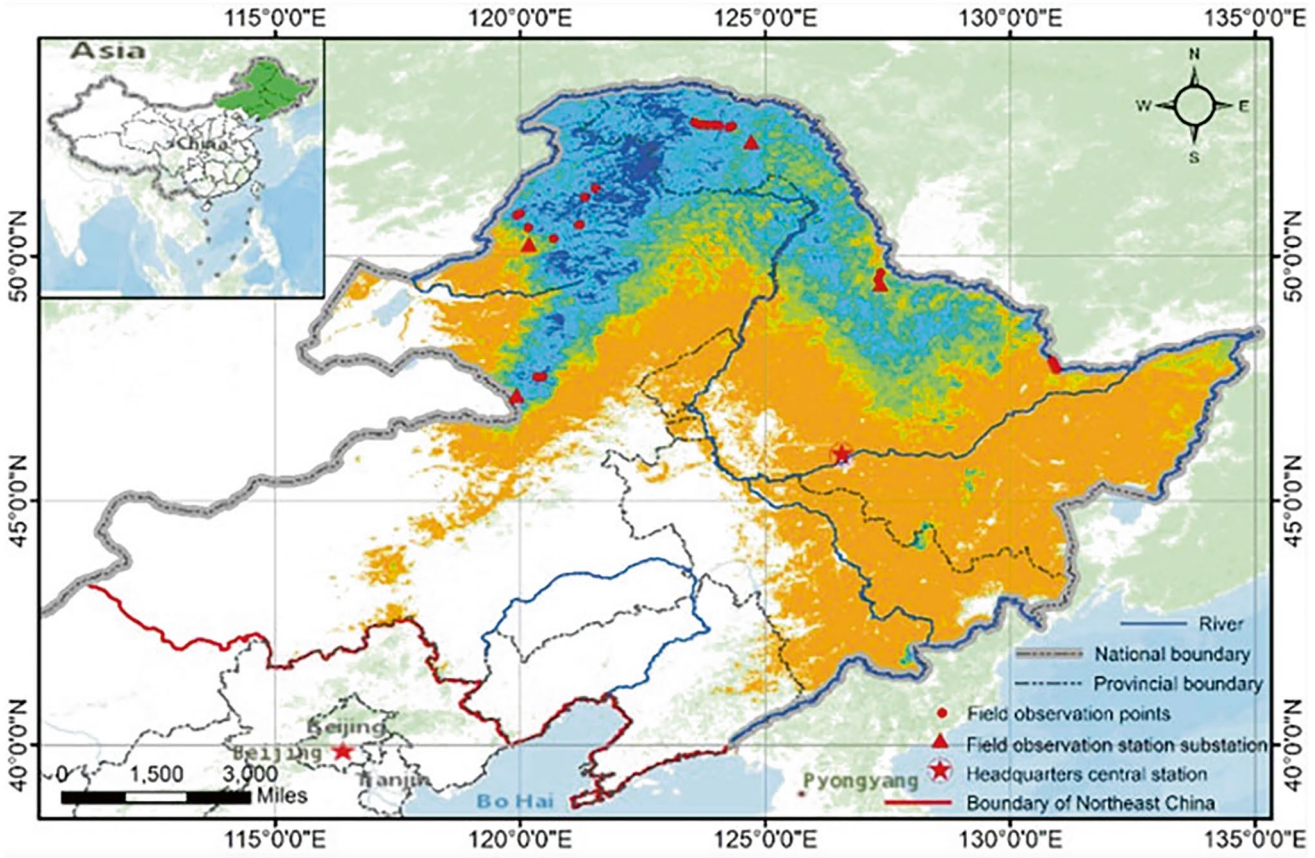

Fig. A.16 Permafrost distribution in NE of China (2014–2019)

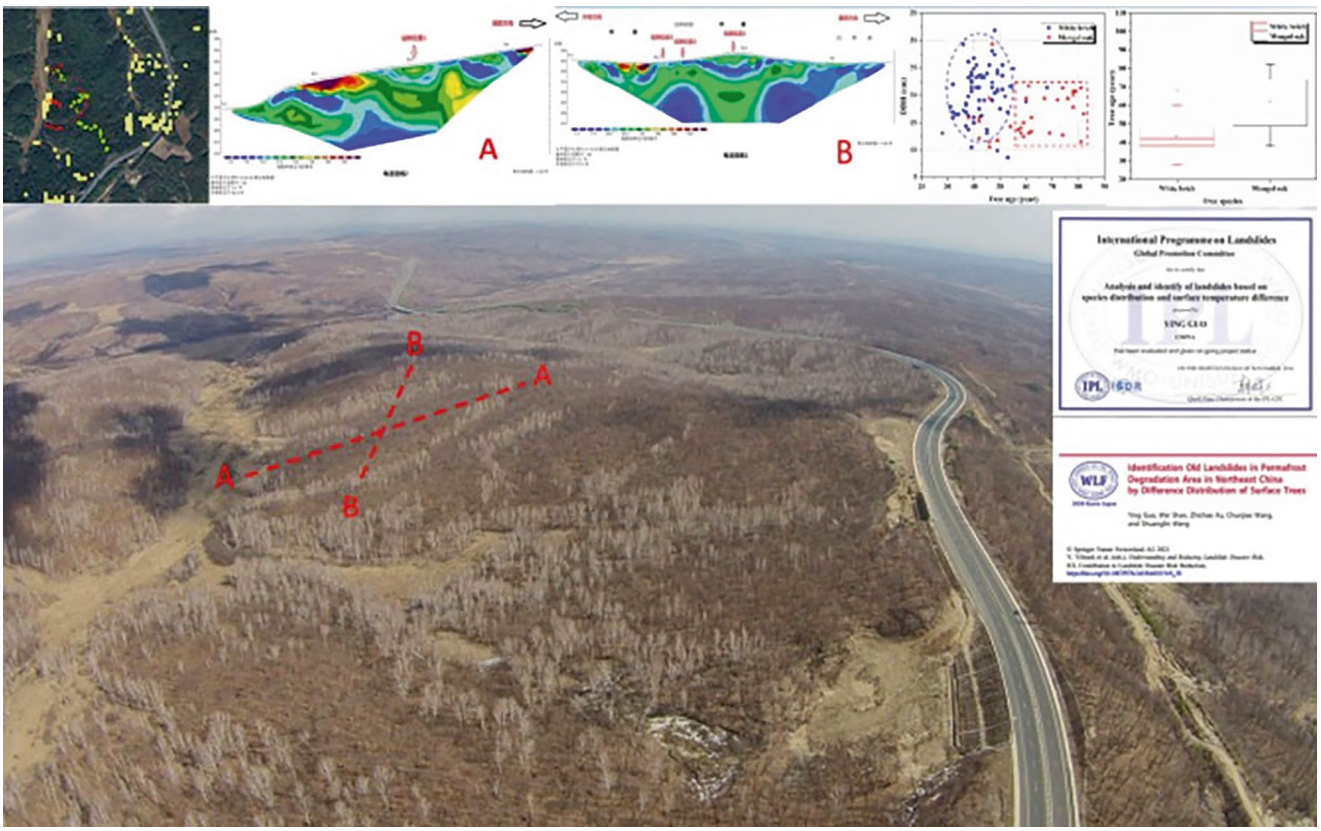

Fig. A.17 Different tree species and ages in the landslide area caused by permafrost degradation

Marui & Co. Ltd.

Taketoshi Marui and Yuji Ikari

Introduction

Marui & Co. Ltd. celebrated its 100th anniversary in 2020. Marui, as one of the leading manufacturers of testing apparatuses in Japan, has constantly been striving further to improve its service since its foundation in 1920, thus contributing to the sustainable development of our nation and society. Our main products cover various destructive and non-destructive testing apparatuses in geotechnical engineering, concrete engineering (mortar, aggregates, etc.), and ceramic engineering (Fig. A.18). Of particular note is that Marui has been helping manufacture ring-shear apparatuses (Fig. A.19) for the past half-century based on the leading-edge idea of Dr. Kyoji Sassa, Professor Emeritus at Kyoto University. Marui has delivered seven ring-shear apparatuses to the Disaster Prevention Research Institute, Kyoto University, and two to the International Consortium on Landslides. Also, the apparatuses were exported to the United States of America, China, Croatia, and Vietnam.

Since 2002, Marui has been a supporter of the International Consortium on Landslides (ICL) and has gradually been intensifying its contribution to the ICL's worldwide efforts for landslide risk reduction and international promotion of landslide research. According to NASA, more frequent and intense rainfall events due to climate change have been causing frequent landslides, particularly in mountains of Asian regions, including Japan, where waters can be stored in various ways. Summer monsoon rains, snow and glacier melt waters can destabilize steep mountainsides, triggering landslides, which are down-slope movements of rocks, soils, water, trees, etc. Marui, as an engineering supporter, com-

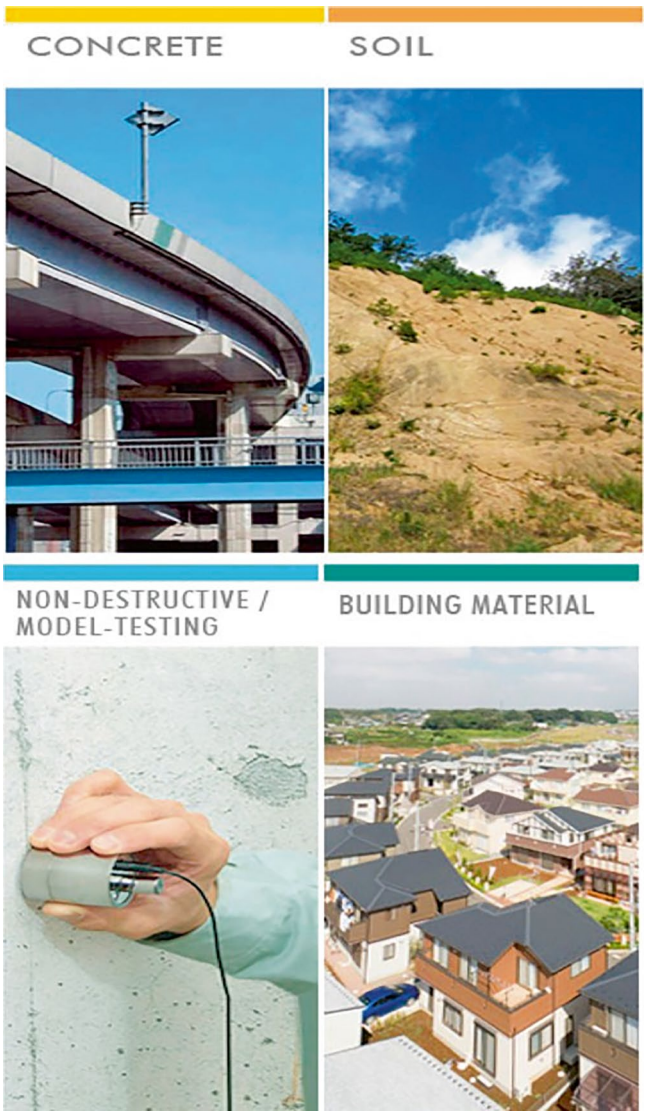

Fig. A.18 Products of testing apparatus such as non-destructive/model-testing for measuring intensity, physical property, durability, etc. for concrete, soil, building material, etc.

T. Marui · Y. Ikari
Marui & Co. Ltd., Osaka, Japan
e-mail: hp-mail@marui-group.co.jp; http://marui-group.co.jp/en/index.html

B. Abolmasov et al. (eds.), *Progress in Landslide Research and Technology, Volume 4 Issue 1, 2025*, Progress in Landslide Research and Technology, https://doi.org/10.1007/978-3-031-89836-5

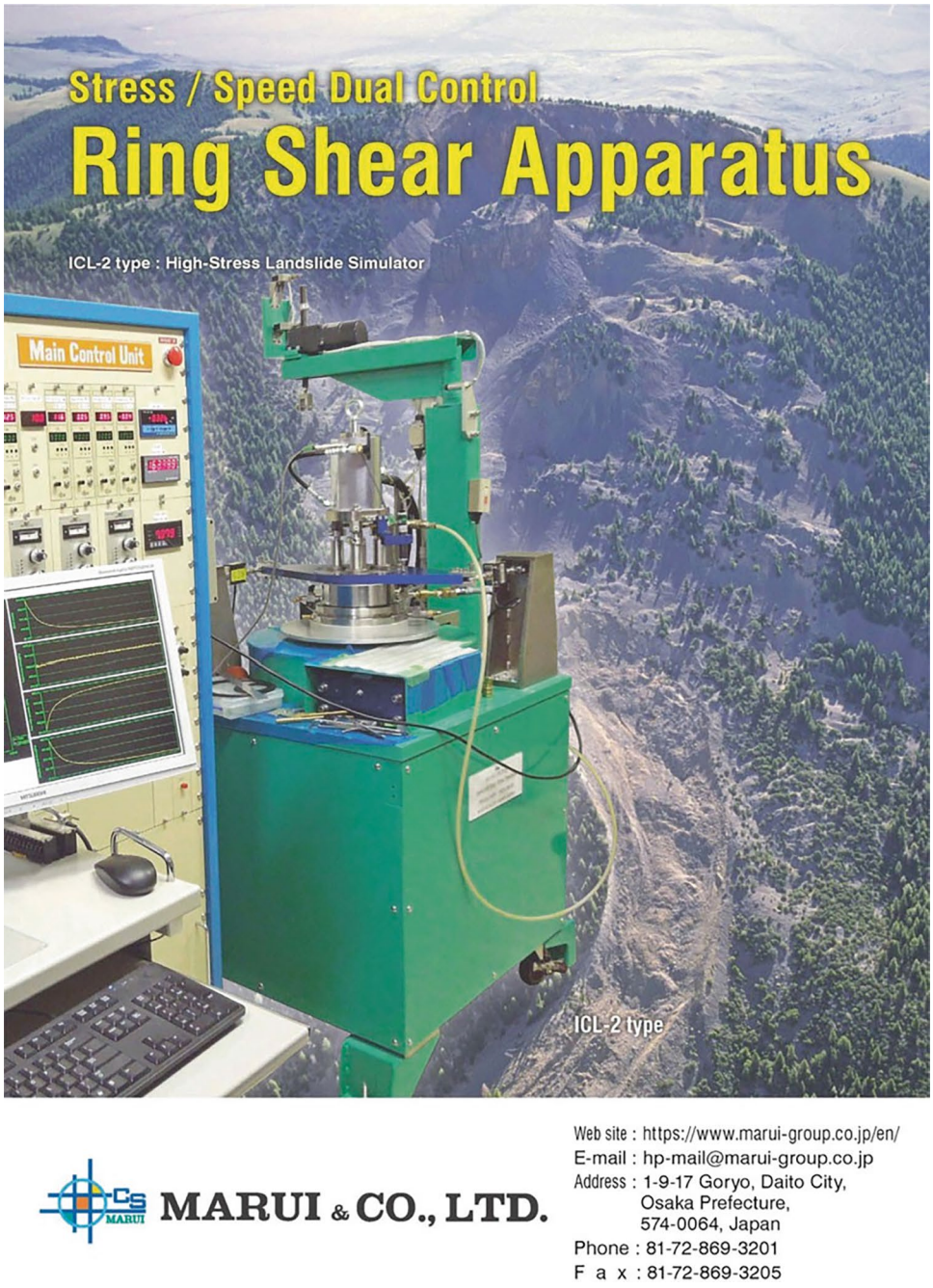

Fig. A.19 High-stress landslide simulator

mits deeply to various activities of research, particularly on triggering mechanisms of landslides.

In addition to the ring-shear apparatuses mentioned above, our company develops and sells soil and ground testing equipment. For example, our standard cyclic triaxial testing machine (Fig. A.20) is used by geological consultants, research laboratories, and educational institutions such as universities and technical colleges. Ground destruction phenomena, which often occur concurrently with earthquakes, significantly affect the seismic resistance of superstructures. Cyclic triaxial tests are used to determine the constants required to judge the liquefaction potential and to determine the cyclic deformation characteristics of the ground required for seismic response analysis.

This equipment can perform not only liquefaction and deformation tests, but also static triaxial tests, isotropic consolidation tests, and anisotropic consolidation tests.

In addition, control and data recording can be processed entirely on a personal computer.

Marui & Co. Ltd. takes great pleasure in developing, manufacturing, and providing new products of high value, sharing the sense of s achievement with our customers and

Fig. A.20 Cyclic triaxial testing machine

thus contributing to social development. The entire staff of Marui is determined to devote ceaseless effort to keep its organization optimized for its speedy and high-quality services, by the motto "Creativity and Revolution," and strive hard to take a step further as a leading manufacturer of testing apparatuses, to answer our customer's expectations for the twenty-second century to come.

Marui continuously contributes to the 2030 Agenda for Sustainable Development and the Sendai Framework for Disaster Risk Reduction 2015–2030. In line with this, Marui signed KLC2020 in 2019 and will strongly support its actions, especially KCL2020 Actions 3, 4, 5, and 9.

Nippon Koei Co., Ltd., Geohazard Management Division

Hiroaki Tauchi

Introduction

The Nippon Koei Group (NK) has been a leading international consultant providing engineering consulting services to over 5500 multi-disciplinary infrastructure and development projects in 160 countries worldwide. The landslide prevention specialist team (now called Geohazard Management Division) was established in 1966 to provide countermeasures against sediment disasters. Over the last 50 years, we have significantly improved the capacity of countries to respond and reduce risk from debris flows, slope instabilities, landslides, avalanches, and rock falls due to torrential rains, large-scale earthquakes, and volcanic eruptions that threaten a country's vital economic infrastructure lifelines, especially the road networks. At present, approximately 160 engineers provide a variety of technical consulting services to protect communities from disasters, as shown in Fig. A.21.

During disasters, we utilize remote sensing technologies such as 3D point clouds and interferometric SAR to create 3D models and gather surface and damage information to conduct a broad area survey, as shown in Fig. A.22. Based on this information, we provide experienced professional engineers to assess risk quickly and promptly respond with engineering design analyses and emergency and permanent measures based on our extensive experience and know-how. In order to efficiently plan and design disaster countermeasure works, we have implemented the automated design using visual programming. This automated design enables us to perform the 3D design of countermeasures quickly and calculate project costs, streamlining the overall process. Organizing design and construction information in 3D facilitates the construction process and allows for permanent maintenance by passing it on to the maintenance management phase as BIM (Building Information Modeling). As a result, the information necessary for effective maintenance is readily available and can be utilized throughout the project's lifespan.

To maximize the effectiveness of infrastructures, we address efficient countermeasure plans, design, and research regarding cost reduction and cost-effectiveness using various numerical analyses such as the finite element method (FEM) and discrete element method (DEM), etc.

With climate change, the scale of disasters is enlarged and the frequency of disasters is increasing. This has resulted in more severe damage in more widespread and more urbanized areas, and more diverse and higher risks of disasters. In addition, in response to the SDG concept of "leaving no one behind," developing countries are lagging behind in hazard zoning and other efforts, which must be resolved. For this reason, NKG believes that it is important to assume that multiple types of disasters, such as floods, landslides and tsunamis, occur at the same time and in the same place. NKG provides risk mapping services using multi-hazard analysis as shown in Fig. A.23.

In Japan, we have worked hard to restore and recover from sediment-related disasters caused by earthquakes and heavy rainfalls that have frequently occurred in recent years (the 2011 Great East Japan Earthquake, the Northern Kyushu Flood in 2017, etc.). We have received letters of appreciation from national and local governments for our efforts.

Our major international projects include "The Project for Countermeasure Construction Against the Landslides on Sindhuli Road Section II, Nepal," "The project for the rehabilitation of Sindhuli road affected by the 2015 Gorkha

H. Tauchi
Geohazard Management Division, Nippon Koei Co., Ltd.,
Tokyo, Japan

B. Abolmasov et al. (eds.), *Progress in Landslide Research and Technology, Volume 4 Issue 1, 2025*, Progress in Landslide Research and Technology, https://doi.org/10.1007/978-3-031-89836-5

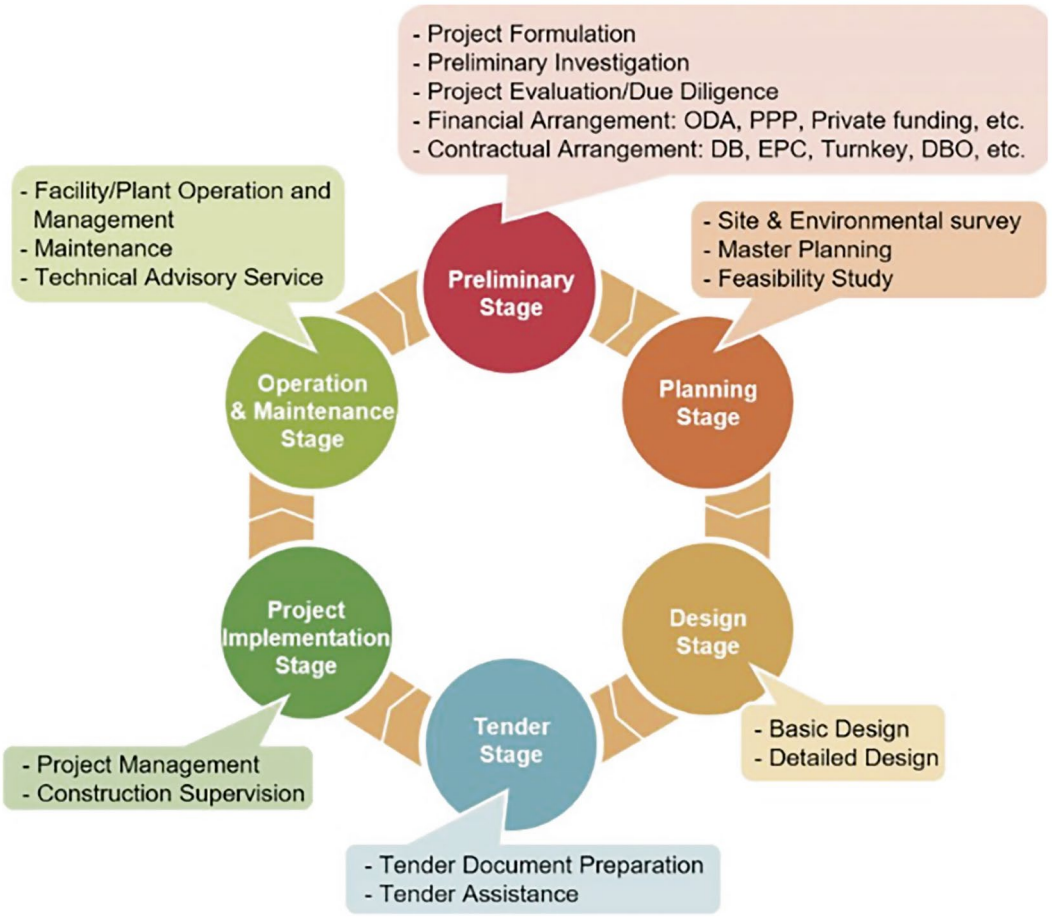

Fig. A.21 Our service for geohazard management

Fig. A.22 (left) A landslide site, (right) 3D point clouds

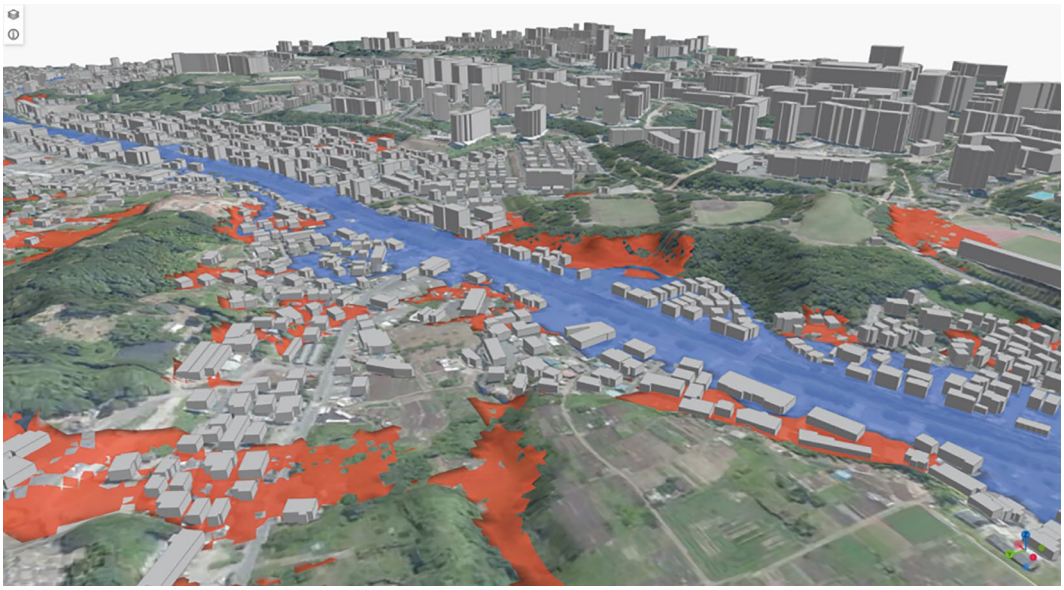

Fig. A.23 Visual programming and Automated design

Earthquake, Nepal," and "The project for landslide prevention for National Road 6 in Honduras"; all funded by the Japan International Cooperation Agency (JICA) grantsin-aid. Through these projects, we are contributing to the socio-economic development of each country by improving vulnerable locations in road networks against sediment disasters, promoting traffic safety, and providing logistics assistance for road users. In particular, the 1st of the three NK's projects mentioned above won the "3rd JAPAN Construction International Award" from the Ministry of Land, Infrastructure, Transport and Tourism as the project that has realized "high-quality infrastructures" through its excellent know-how, technical capabilities, and project management capabilities.

NK is an ICL member using its technology to reduce geohazard risk. Through various projects, NK continuously contributes to the 2030 Agenda for Sustainable Development and the Sendai Framework for Disaster Reduction 2015–2030. Using our full capability with abundant experiences in Japan and Asia prone to natural disasters, we hope to contribute much more to reducing global sediment disasters, including landslides (Fig. A.24). In line with this, NK has signed the KLC 2020 and will strongly support its actions.

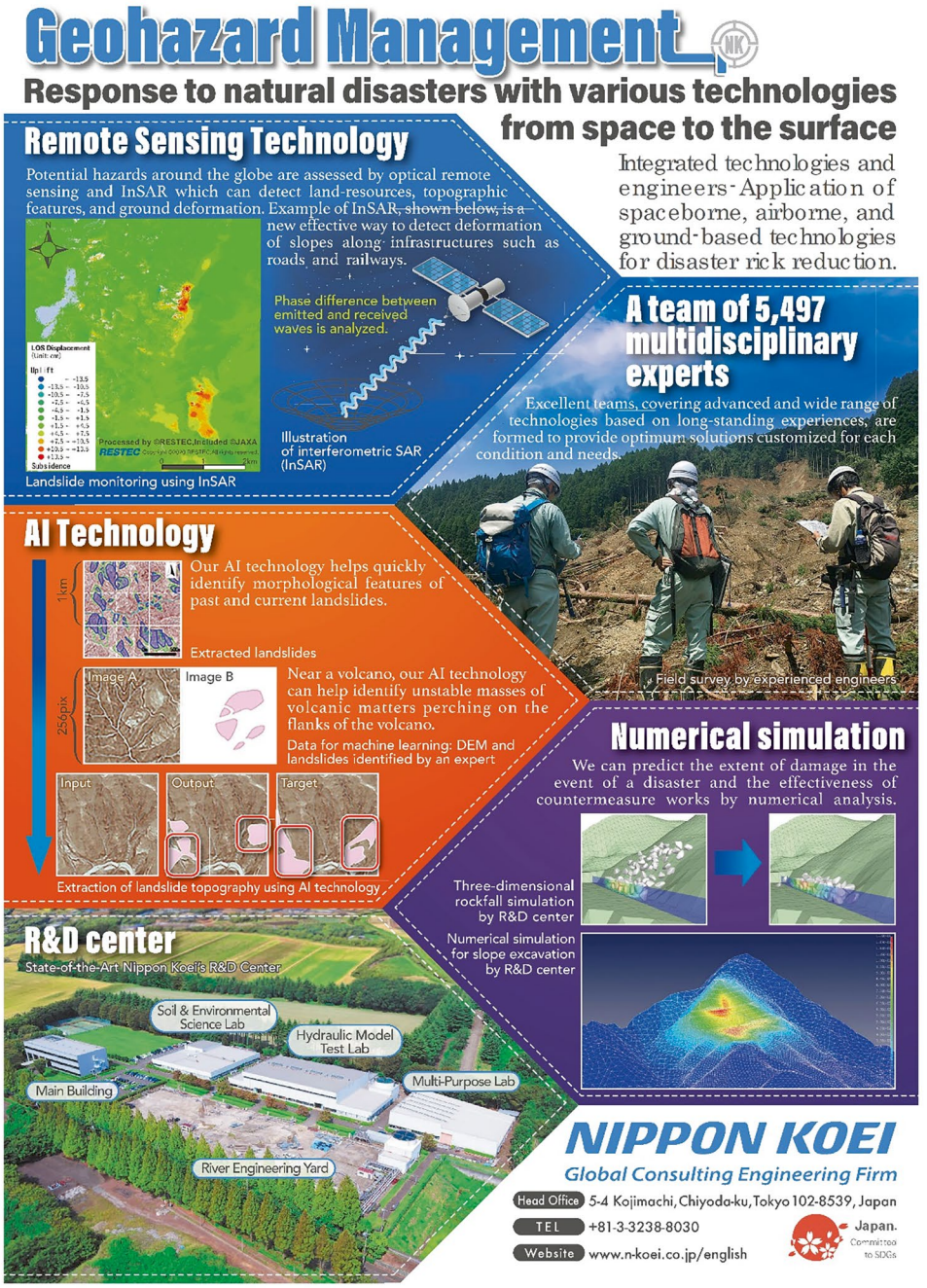

Fig. A.24 Introduction of our survey analysis technology for geohazard

Ellegi Srl

Ellegi Srl

Introduction

Ellegi srl provides worldwide monitoring services and produces Ground Based synthetic aperture radar (GBInsAR) for remote measurement of displacements and deformations on natural hazards and manmade buildings using its own designed and patented LiSALab system.

Its activities started in 2003 as a spin off project to exploit commercially the Ground Based Linear Synthetic Aperture Radars technology developed by European Commission's Ispra Joint Research Centre and based on the results of more than 10 years of research. Since then, Ellegi has industrialized and developed the core technology of the LiSALab system and latest LiSAmobile system represents the 5th generation of development.

In 2003 it was the first commercial company in the world to provide GBInSAR measurements of natural hazards and structure (Figs. A.25 and A.26).

Ellegi srl offers:

- Displacement fields measurement, control and monitoring of the deformation caused by natural hazards, like landslides, rockslides, sinkhole, volcanic deformation in every operative condition, including emergencies,
- Structural strain fields measurement, control, monitoring and diagnosis of the deformation affecting buildings, bridges, viaducts, dams.

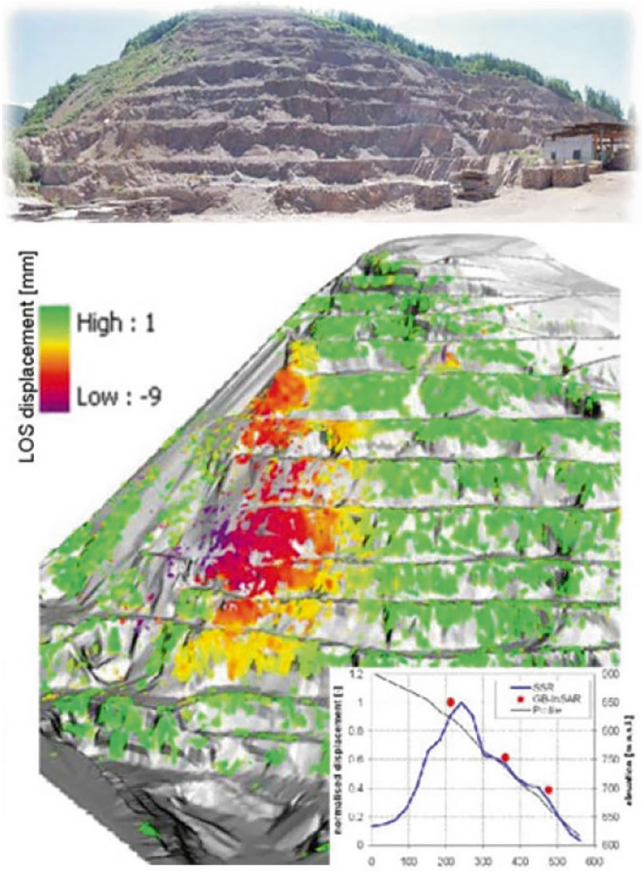

Fig. A.25 GBInSAR LiSALab technology quarry monitoring example and displacements' field comparison between the GBInSAR measurement and FEM model results

Ellegi Srl
Ellegi Srl, Como, Italy

B. Abolmasov et al. (eds.), *Progress in Landslide Research and Technology, Volume 4 Issue 1, 2025*, Progress in Landslide Research and Technology, https://doi.org/10.1007/978-3-031-89836-5

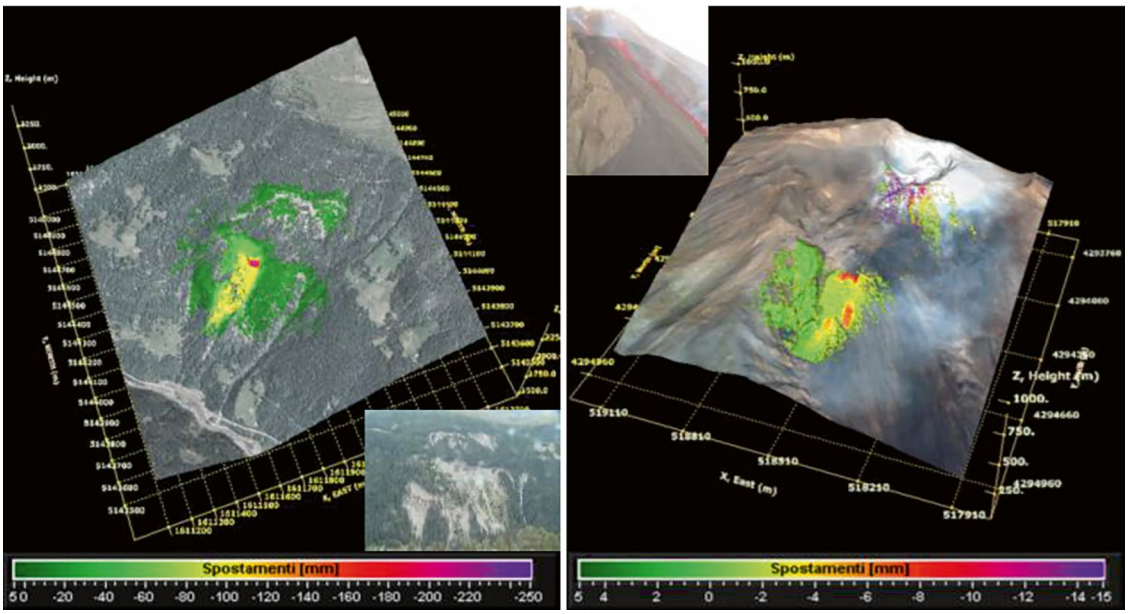

Fig. A.26 GBInSAR LiSALab technology result in monitoring a slope affected by a landslide (left) and a volcanic slope affected by deformation (right). Landslide or moving area mapping and boundaries identification is made easy by GBInSAR LiSALab technology

- GBInSAR monitoring systems, installation, management and maintenance in order to provide information about natural hazards or anthropic activity, that can generate or cause slopes failures or buildings instabilities.

In all the above-mentioned activities Ellegi srl uses the GBInSAR LiSALab technology that represents a real "break-through".

IDS GeoRadar s.r.l.

IDS GeoRadar s.r.l.

Introduction

IDS GeoRadar, part of Hexagon, provides products and solutions, based on radar technology, for monitoring applications including landslides, rockfalls, complex structures, mining and civil engineering. The company is a leading provider of Ground Penetrating Radar (GPR) and Interferometric Radar solutions worldwide.

IDS GeoRadar is committed to delivering best-in-class performance solutions and to the pursuit of product excellence, through the creation of application-specific, innovative and cost-efficient systems for a wide range of applications:

- Utility mapping and detection
- Civil engineering
- Railway and road engineering
- Geology and environment management
- Archaelogy
- Forensics
- Landslide monitoring
- Mining safety

Natural Hazard Monitoring Solution

The use of slope monitoring radar is now the standard practice for the active monitoring of slope in open pit mines and for safety critical landslide monitoring with the aim of providing alerts in the event of progressive movements which could potentially lead to slope failure and assessing worker safety. The unique IBIS-FM EVO radar system accurately monitors multiple scales of displacements in real time, from early detection of slow movements to fast accelerations associated with slope collapse. The great operative range, up to 5000 m, allows to safely deploying the system in comfortably accessible areas, without exposing people and equipment to hazardous zones.

IDS GeoRadar cooperate with TRE ALTAMIRA, the worldwide leader in ground monitoring services using satellite InSAR offer a comprehensive solution—InSAR Service—to fulfill all mine stability needs, ranging from monitoring large-scale mining operations over hundreds of square kilometers, to specific movements at the pit scale. With the large spatial coverage of satellite data, mining engineers can identify unstable areas over wide areas, also with the ability to extend the analysis of deformation back in time. All mining assets can be monitored regularly and precisely for deformation (Figs. A.27 and A.28).

IDS GeoRadar s.r.l.
IDS GeoRadar s.r.l., Pisa, Italy

B. Abolmasov et al. (eds.), *Progress in Landslide Research and Technology, Volume 4 Issue 1, 2025*, Progress in Landslide Research and Technology, https://doi.org/10.1007/978-3-031-89836-5

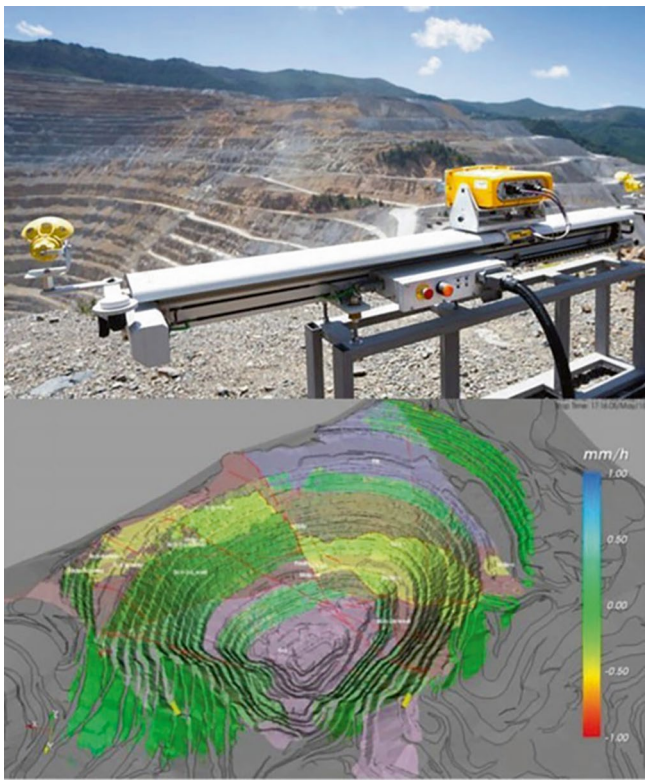

Fig. A.27 IDS GeoRadar: innovative interferometric radar for mining, environmental and civil engineering

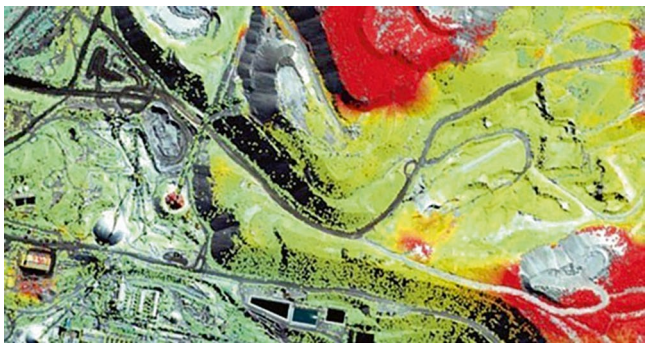

Fig. A.28 InSAR service—ground motion monitoring for mining operations

Chuo Kaihatsu Corporation

Lin Wang

wang@ckcnet.co.jphttps://www.ckcnet.co.jp/global-
https://www.ckcnet.co.jp/contactus/

Introduction

Chuo Kaihatsu Corporation (CKC) was founded in 1946, and has been aiming to become the "Only One" consultant for our customers. We engage in the hands-on work that will "Remain with the earth, Remain in people's hearts, and Lead to a prosperous future". We focus on road, river and dam engineering to flesh out industrial infrastructures specifically by means of geophysical/geotechnical/geological investigations, civil engineering surveys and project implementations. In recent years, we make significant efforts on earthquake disaster mitigation, sediment disaster prevention/mitigation and ICT information services. Many achievements of ours have already contributed to the mitigation of natural disasters such as landslides, earthquakes and slope failures in Japan, Asia and the Pacific Region. We aim to provide technological contributions so that a sustainable society will continue to develop in the future (Figs. A.29, A.30, A.31 and A.32).

Fig. A.29 Design for various structures

B. Abolmasov et al. (eds.), *Progress in Landslide Research and Technology, Volume 4 Issue 1, 2025*, Progress in Landslide Research and Technology, https://doi.org/10.1007/978-3-031-89836-5

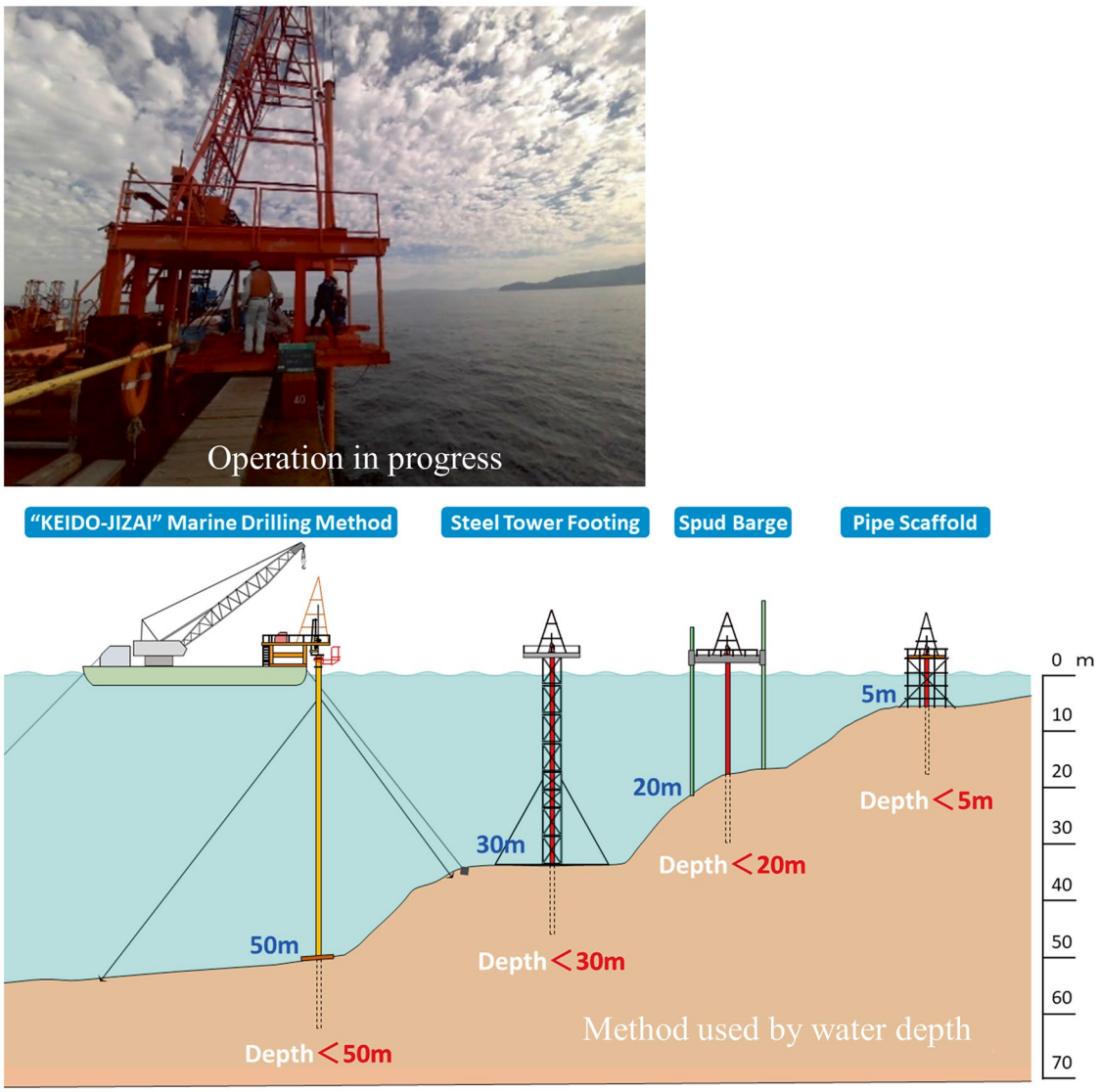

Fig. A.30 Deepwater drilling surveys

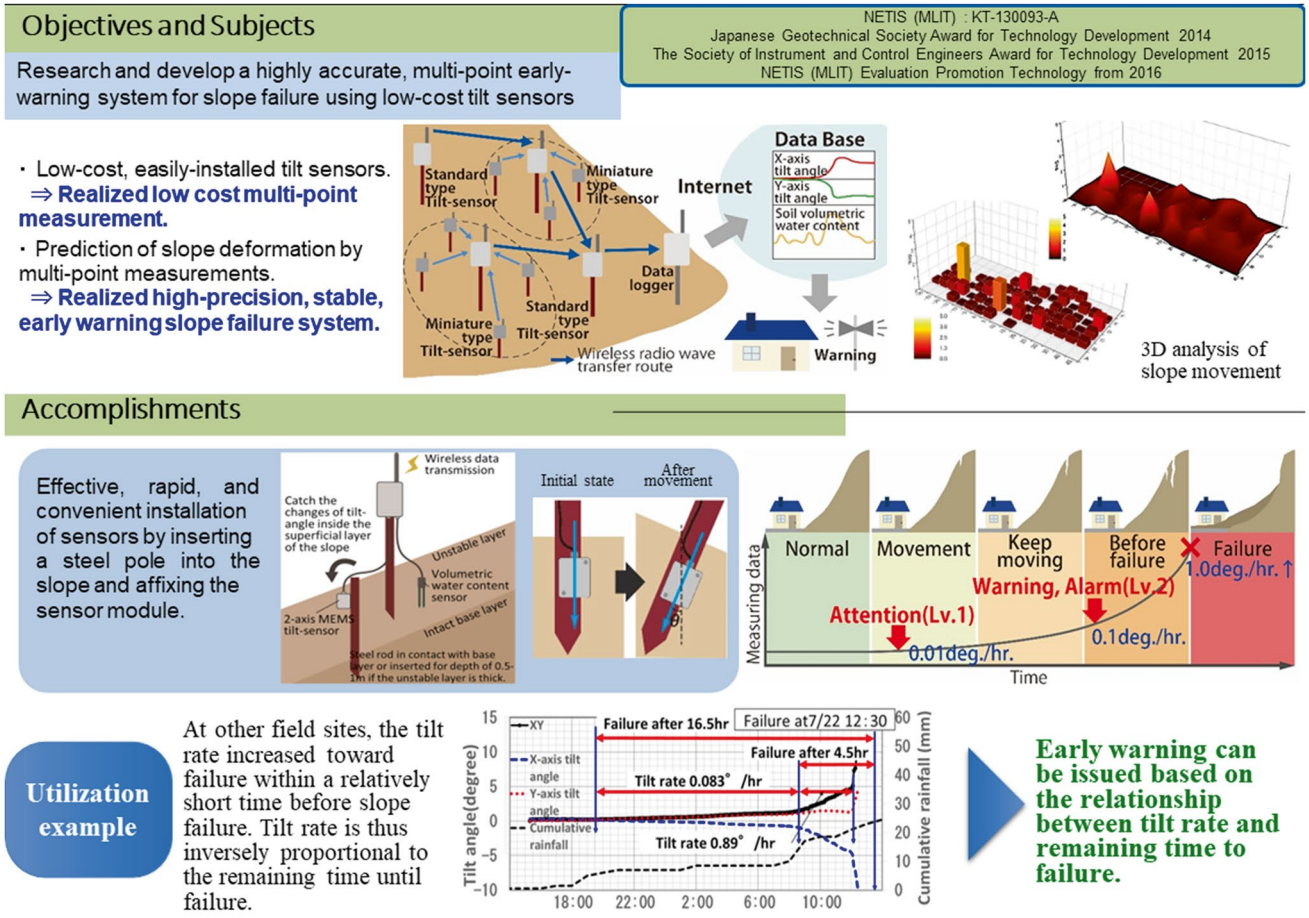

Fig. A.31 The early warning monitoring system of slope failure using multi-point tilt change and volumetric water content

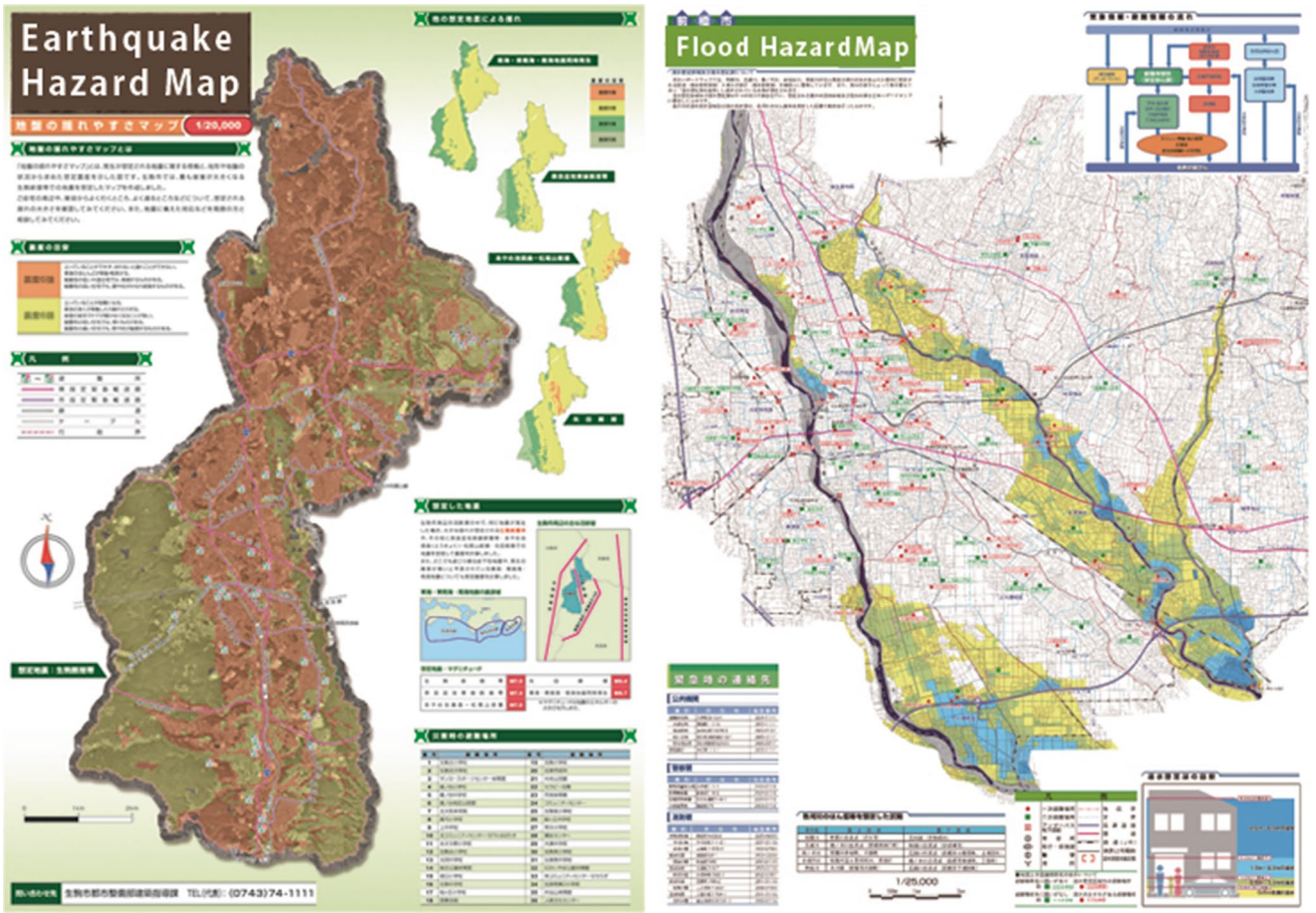

Fig. A.32 Making hazard map for sediment disaster, tsunami, flood, earthquake, liquefaction, etc.…

Godai Kaihatsu Corporation

Godai Kaihatsu Corporation

Introduction

Ever since its foundation in 1965, Godai Kaihatsu Co. Ltd. a civil engineering consulting firm, has long been providing a variety of software and measures particularly for natural disaster mitigation. With its rich expertise in both civil engineering and information technology (IT), the company has its primary goal to address real-world needs of disaster mitigation. All the staff of Godai Kaihatsu Co. Ltd. feels it more than happy that their cutting-edge technologies help mitigate natural disasters (Figs. A.33, A.34, A.35 and A.36).

Godai Kaihatsu Corporation
Godai Kaihatsu Corporation, Kanazawa, Ishikawa, Japan
e-mail: pp-sales@godai.co.jp; https://soft.godai.co.jp/soft/

B. Abolmasov et al. (eds.), *Progress in Landslide Research and Technology, Volume 4 Issue 1, 2025*, Progress in Landslide Research and Technology, https://doi.org/10.1007/978-3-031-89836-5

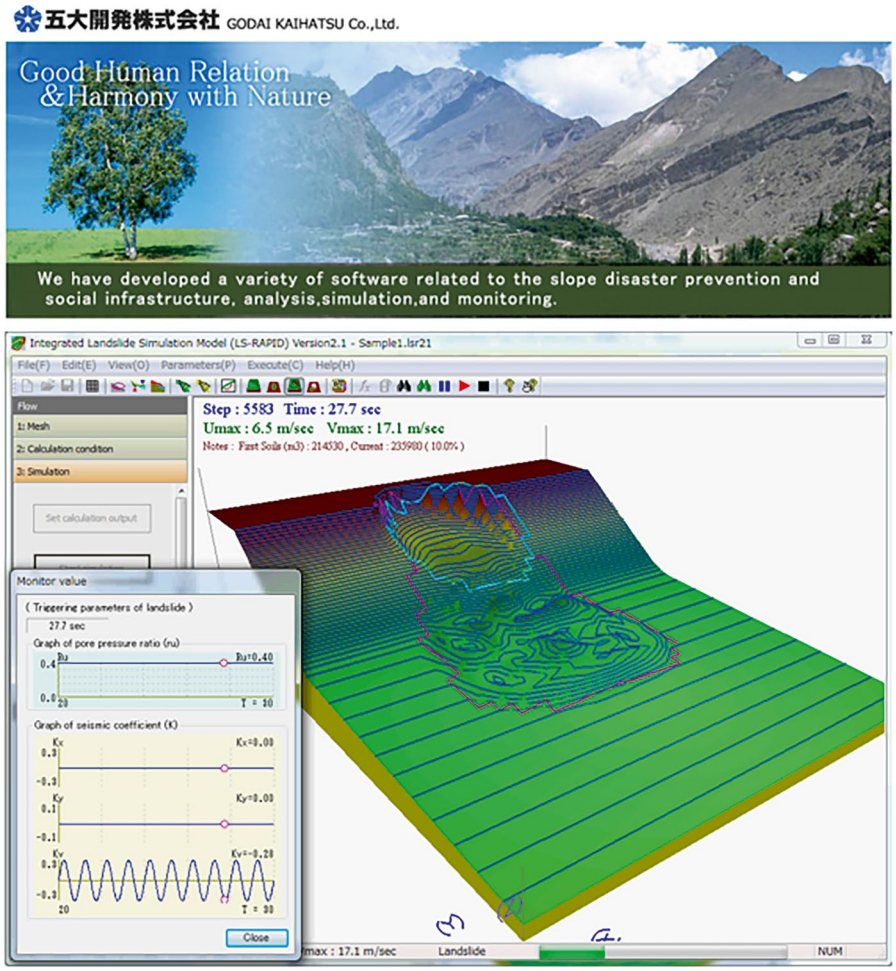

Fig. A.33 Integrated model simulating of earthquake and rain induced rapid landslides (LS-RAPID)

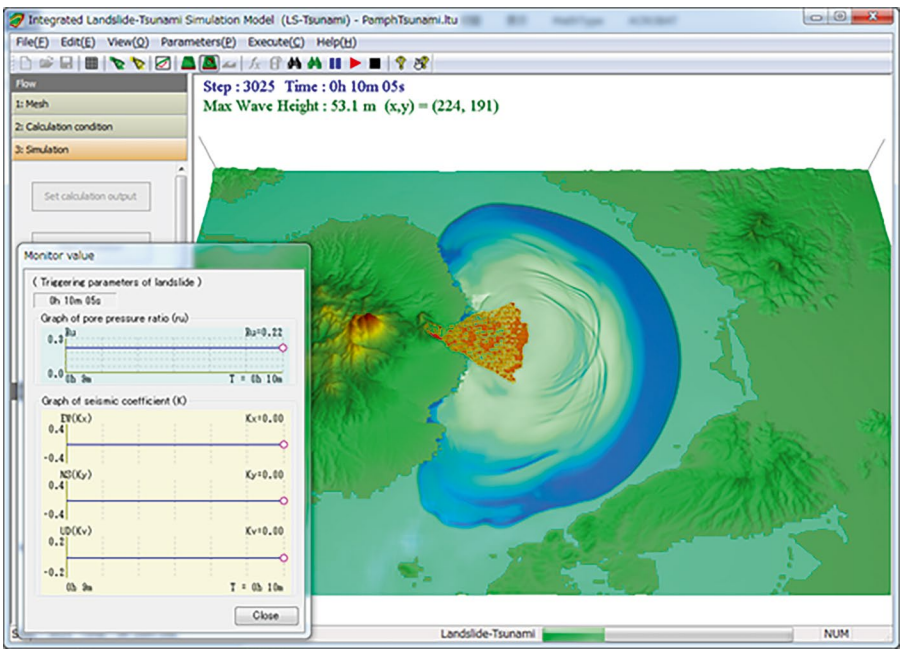

Fig. A.34 Tsunami model (LS-Tsunami)

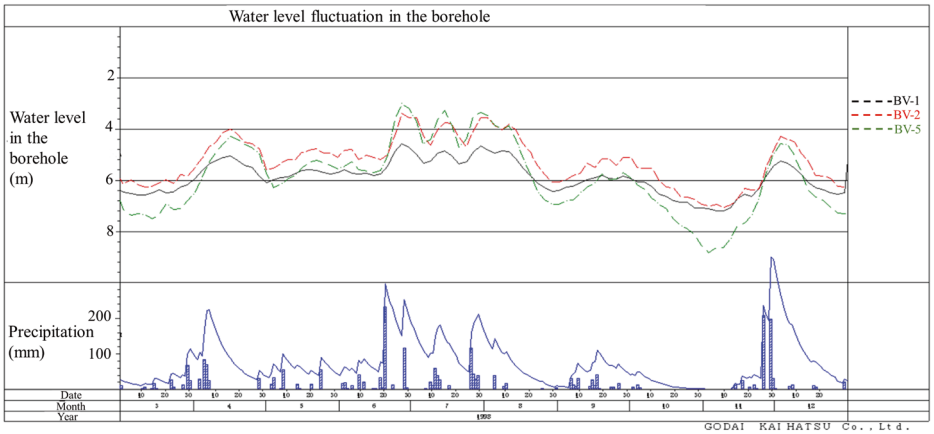

Water level data in the borehole is reflected in the analysis cross section. Calculate safety factor for each observation date.

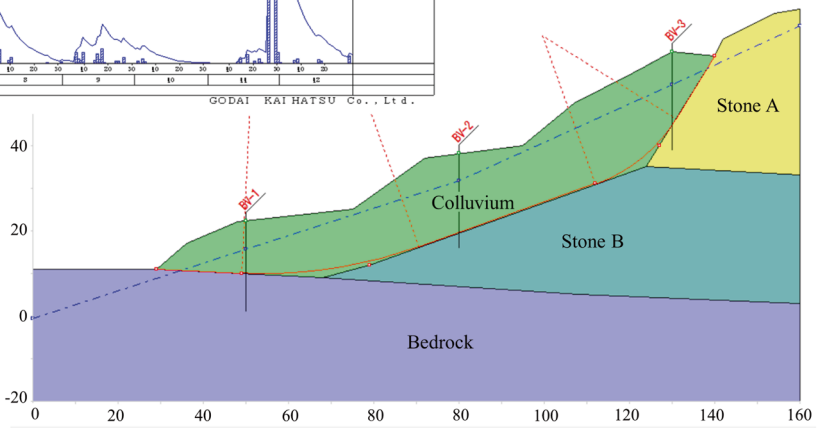

Fig. A.35 Power SSA PRO-Two-dimensional slope stability calculation of earthquake and rain induced landslide

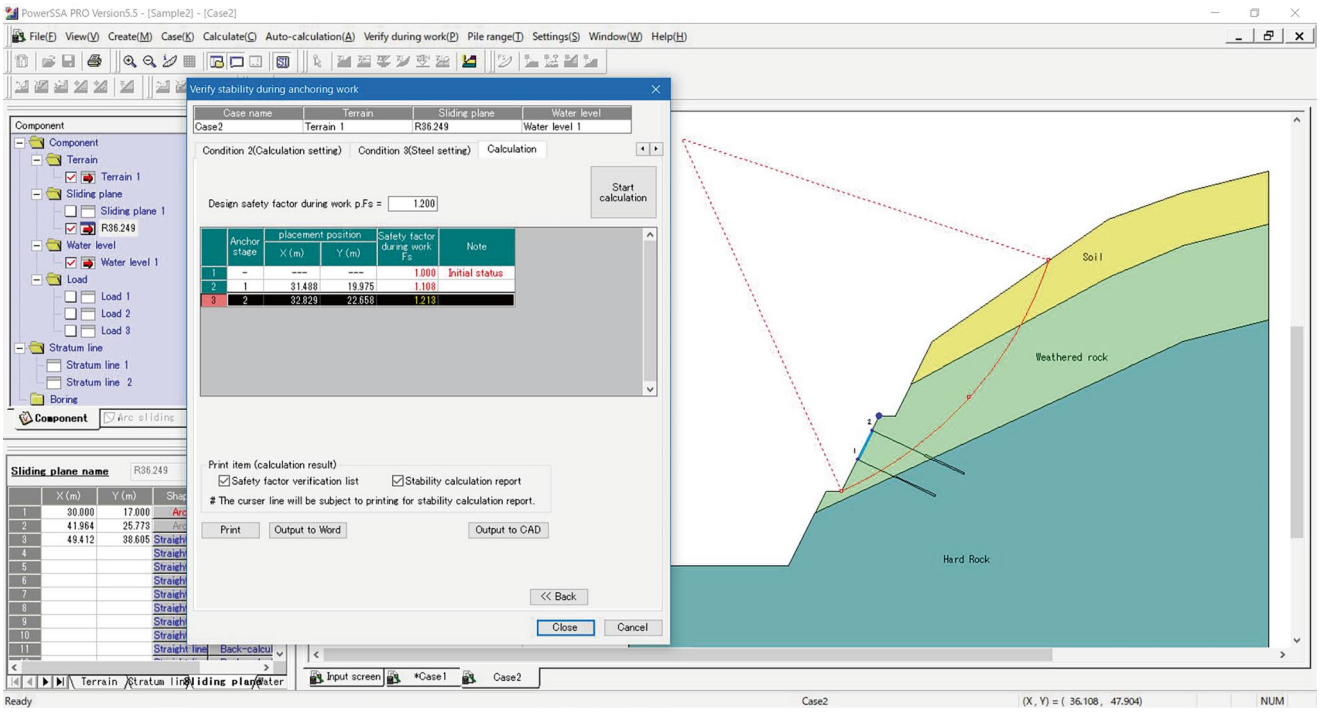

Fig. A.36 Anchor software-slope stability analysis for ground ancho

Kiso-Jiban Consultants Co. Ltd

Kaoru Hanai and Junichiro Odaka

Introduction

Since its establishment in 1953, Kiso-Jiban has been contributing on the development of social infrastructure as a "comprehensive construction consultant with strong geotechnical capabilities" in various situations, such as ground investigation, laboratory testing, analysis, civil structure design, etc. Kiso-Jiban has been working on the technological development for disaster prevention and mitigation against the recent exacerbation of natural disasters.

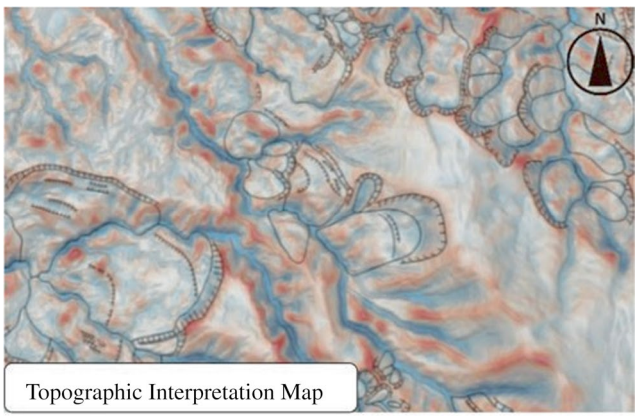

Topographic Interpretation Map

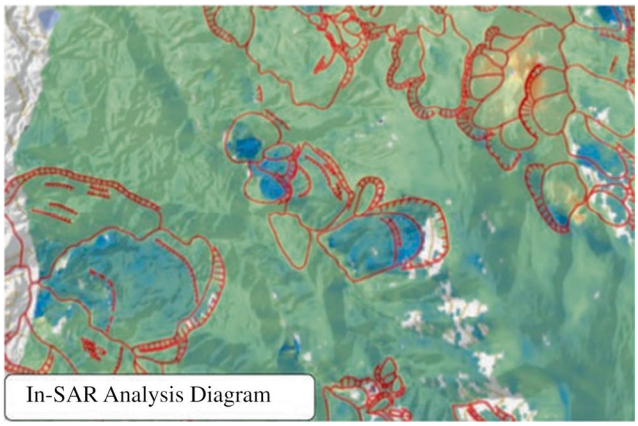
In-SAR Analysis Diagram

InSAR (Interferometric Synthetic Aperture Radar)

SAR is a technique that utilizes interference of radio waves for precise determination of distance. Kiso-Jiban has succeeded in estimation of both extent and rate of landslide movements by combining the topography interpretation and InSAR analysis.

K. Hanai · J. Odaka
Kiso-Jiban Consultants Co. Ltd., Tokyo, Japan
e-mail: kisojiban-contactus@kiso.co.jp; https://www.kisojiban.com

B. Abolmasov et al. (eds.), *Progress in Landslide Research and Technology, Volume 4 Issue 1, 2025*, Progress in Landslide Research and Technology, https://doi.org/10.1007/978-3-031-89836-5

GP (Gel-Push) Sampling

GP Sampling can collect gravelly soil, etc., which is difficult to be collected by conventional samplers, by using a highly-concentrated water-soluble polymeric gel. GP Sampling was introduced in ISO 22475-1: 2021 revised in October 2021 as Category A, which provides the highest quality soil samples.

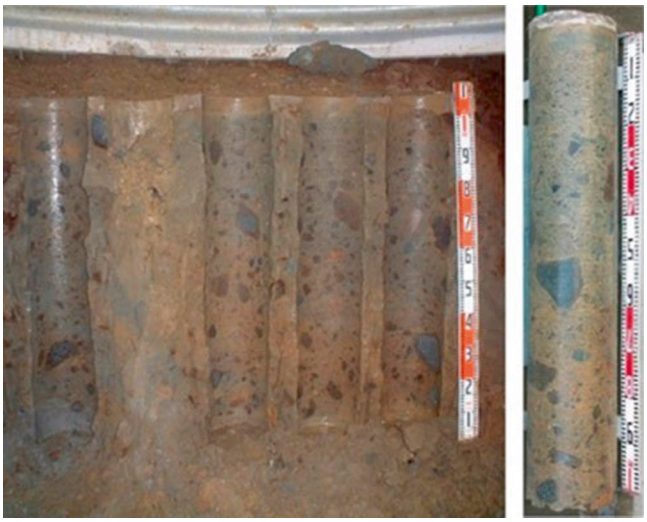

GP Sampling was performed in the disturbed soil mass right above the landslide surface (left) and the soil sample collected (right)

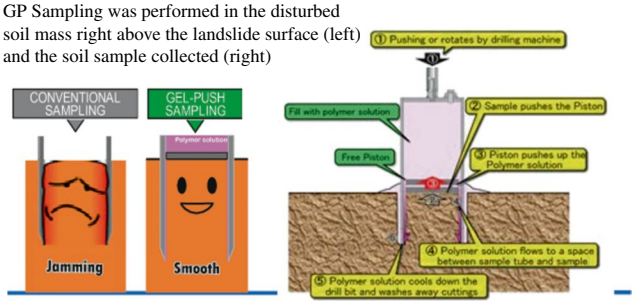

Inspection Technique for Disaster Danger Spots Using Mixed Reality (MR) Technology

MR (Mixed reality) is a technology that blends physical and digital worlds by superimposing 3D data and digital information on the real world as computer graphics.

Dangerous slopes with rockfall sources are spots where many unstable bedrocks and floating rocks exist. In many cases, approaching the inspection point on an outcrop is a difficult and dangerous task for investigators. Using MR technology makes it possible to realistically reproduce the outcrop situation at the site as a hologram. The outcrop situation can be safely inspected and confirmed without going to the site.

Slope Stability Analysis and Evaluation

Kiso-Jiban provides a wide range of numerical analyses related to slope stability evaluation. We have a wide range of analysis methods, from general two-dimensional limit equilibrium analysis to finite element analysis and analysis of rock masses with discontinuities, and we are challenging on the analysis that considers variability of ground and modelling uncertainty.

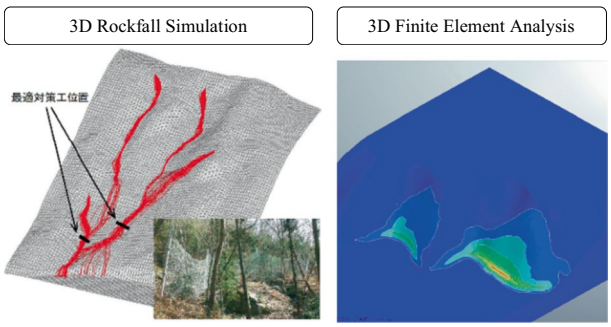

Kokusai Kogyo Co. Ltd

Kokusai Kogyo Co. Ltd.

Introduction

Kokusai Kogyo Co. Ltd. as a leading company of geospatial information technologies has long been providing public services with its comprehensive expertise to address real-world needs and cutting-edge measurement technologies. Kokusai Kogyo Co. Ltd. helps rebuild "Green Communities," which has been of our great concern in terms of "environment and energy," "disaster risk reduction" and "asset management". Kokusai Kogyo Co. Ltd. offers advanced and comprehensive analyses of geospatial information for developing new government policies, maintaining and operating social infrastructures safe and secure, and implementing low-carbon measures in cities. Influenced by the recent global climate change, extreme rainfall events have become more frequent worldwide and resultant hydro-meteorological hazards are creating more deaths and devastations particularly in many developing countries where effective advanced countermeasures are not readily available. Kokusai Kogyo Co. Ltd. is proud of its achievements in establishing resilient infrastructure systems and implementing effective monitoring/early warning systems in developing countries, which have long been helping reduce the risks from natural hazards (Figs. A.37, A.38, A.39 and A.40).

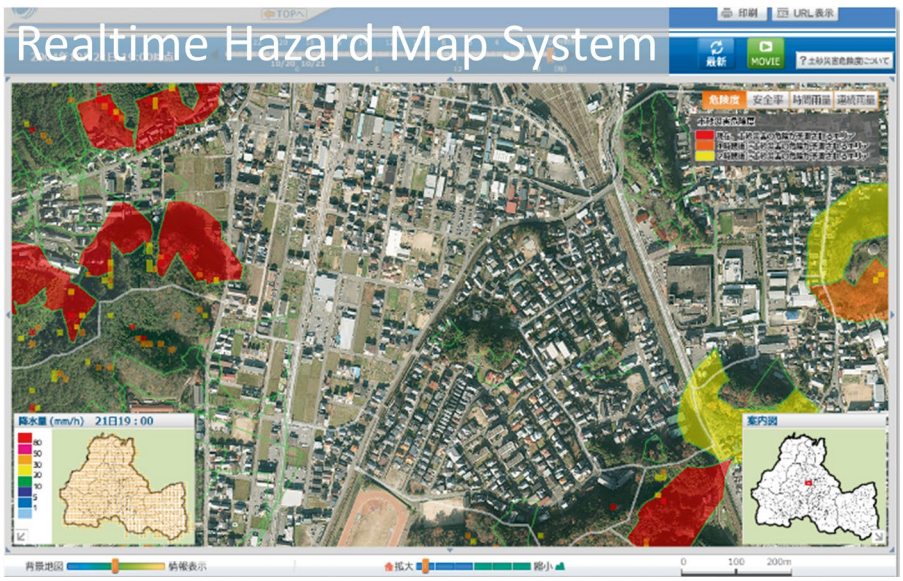

Fig. A.37 Our realtime hazard map reflects up-to-date information of soil natures and precipitations at landslide hazard sites, etc. that can constantly be changing, and evaluates area-wide hazard risk in real-time

B. Abolmasov et al. (eds.), *Progress in Landslide Research and Technology, Volume 4 Issue 1, 2025*, Progress in Landslide Research and Technology, https://doi.org/10.1007/978-3-031-89836-5

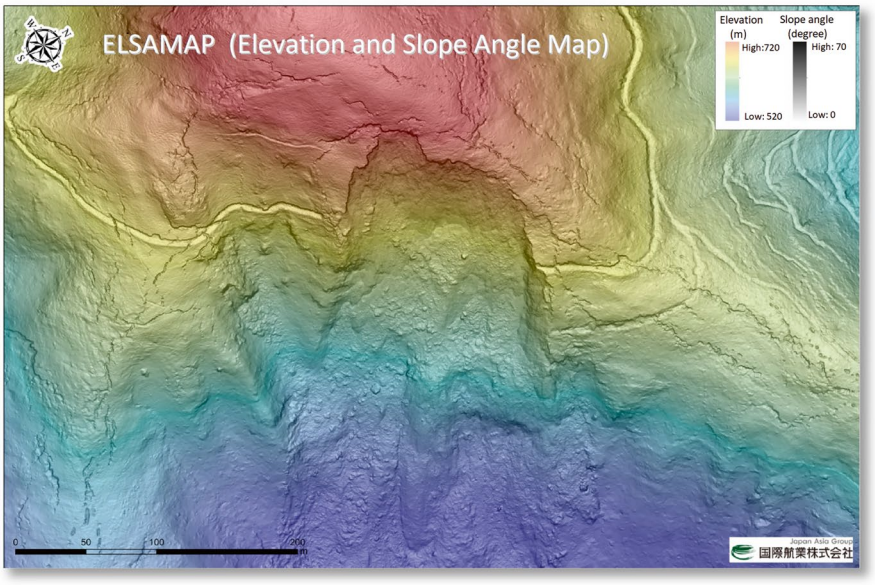

Fig. A.38 ELSAMAP is our cutting-edge 3D terrain visualization method allowing great geomorphological details to be visualized in one glance with gray-scaled slope inclinations and colored altitudes. ELSAMAP has been used to interpret micro-topographies, landslides and some other things

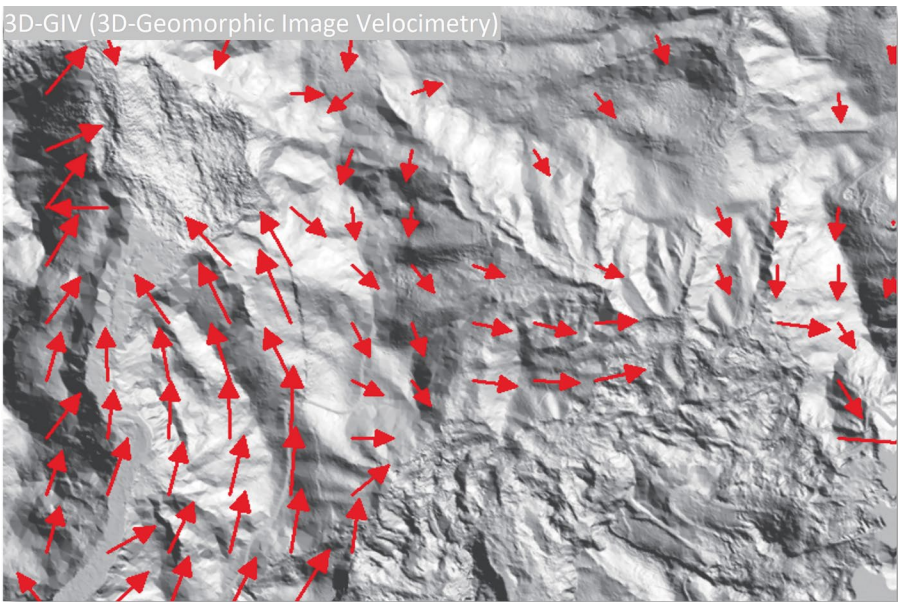

Fig. A.39 3D-GIV can help grasp the ground surface displacement caused by natural phenomena such as landslide by analyzing differences between digital geomorphic images obtained through ad hoc Airborne Laser Surveys

Fig. A.40 "Shamen-net" is a total monitoring system integrating GNSS and other monitoring device (Measurement precision: ±mm, on a real time basis)

OSASI Technos, Inc.

OSASI Technos, Inc.

Introduction

OSASI Technos, Inc. has been making its best efforts to develop its cutting-edge technologies for landslide early warning. Its unique compact and lightweight sensors making up the Landslide Early Warning System enable long-term monitoring of unstable landslide mass movements, precipitations, porewater pressure buildups, etc. in a remote mountainous area where commercial power is often unavailable. OSASI Technos, Inc. is also proud of its advanced technology to transfer observed data even in areas with poor telecom environments as proven in the successful implementations in South Asia. All staff members of OSASI Technos work together for mitigation of landslide disasters worldwide (Figs. A.41, A.42, and A.43).

OSASI Technos, Inc.
OSASI Technos, Inc., Kochi, Japan

B. Abolmasov et al. (eds.), *Progress in Landslide Research and Technology, Volume 4 Issue 1, 2025*, Progress in Landslide Research and Technology, https://doi.org/10.1007/978-3-031-89836-5

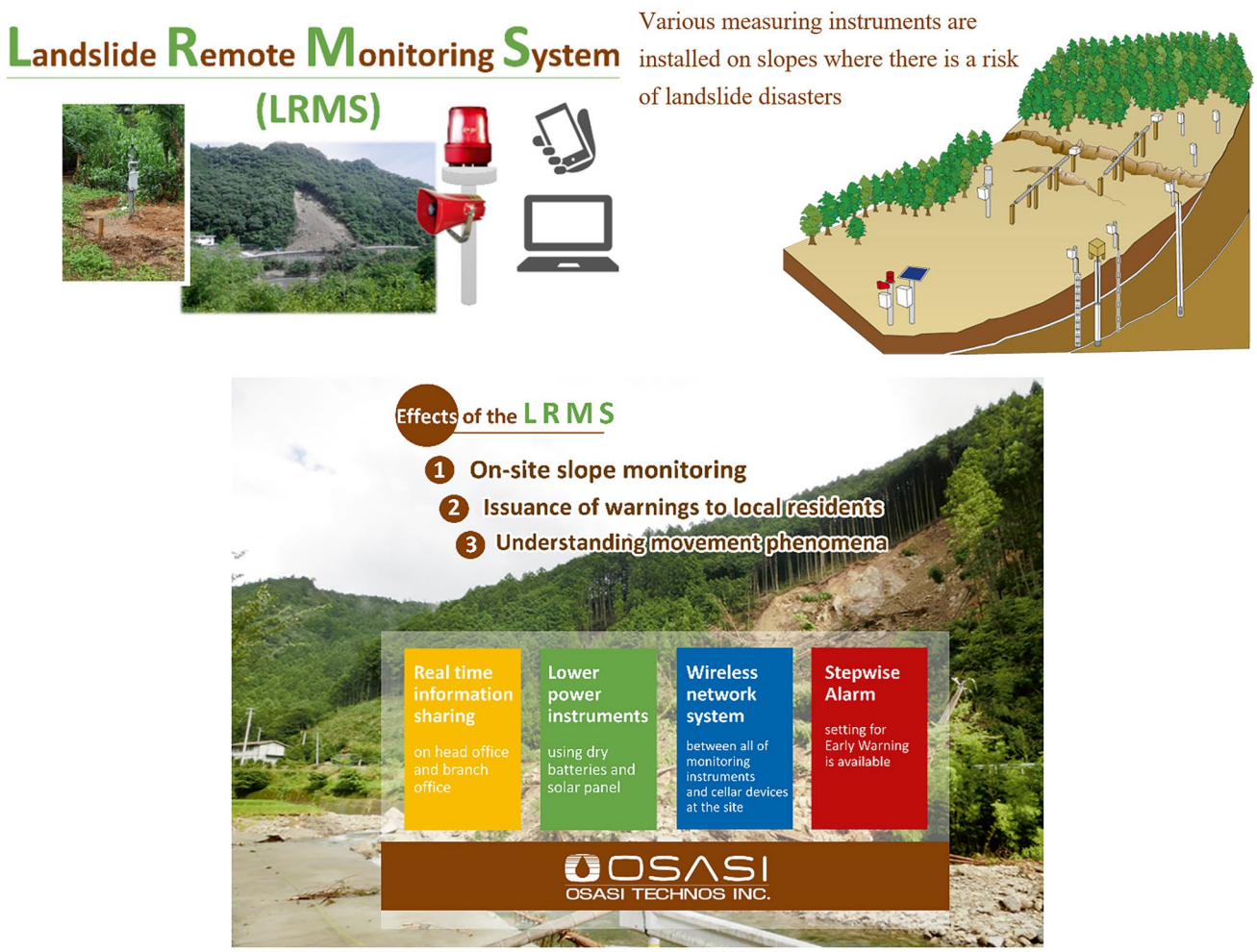

Fig. A.41 Landslide remote monitoring system

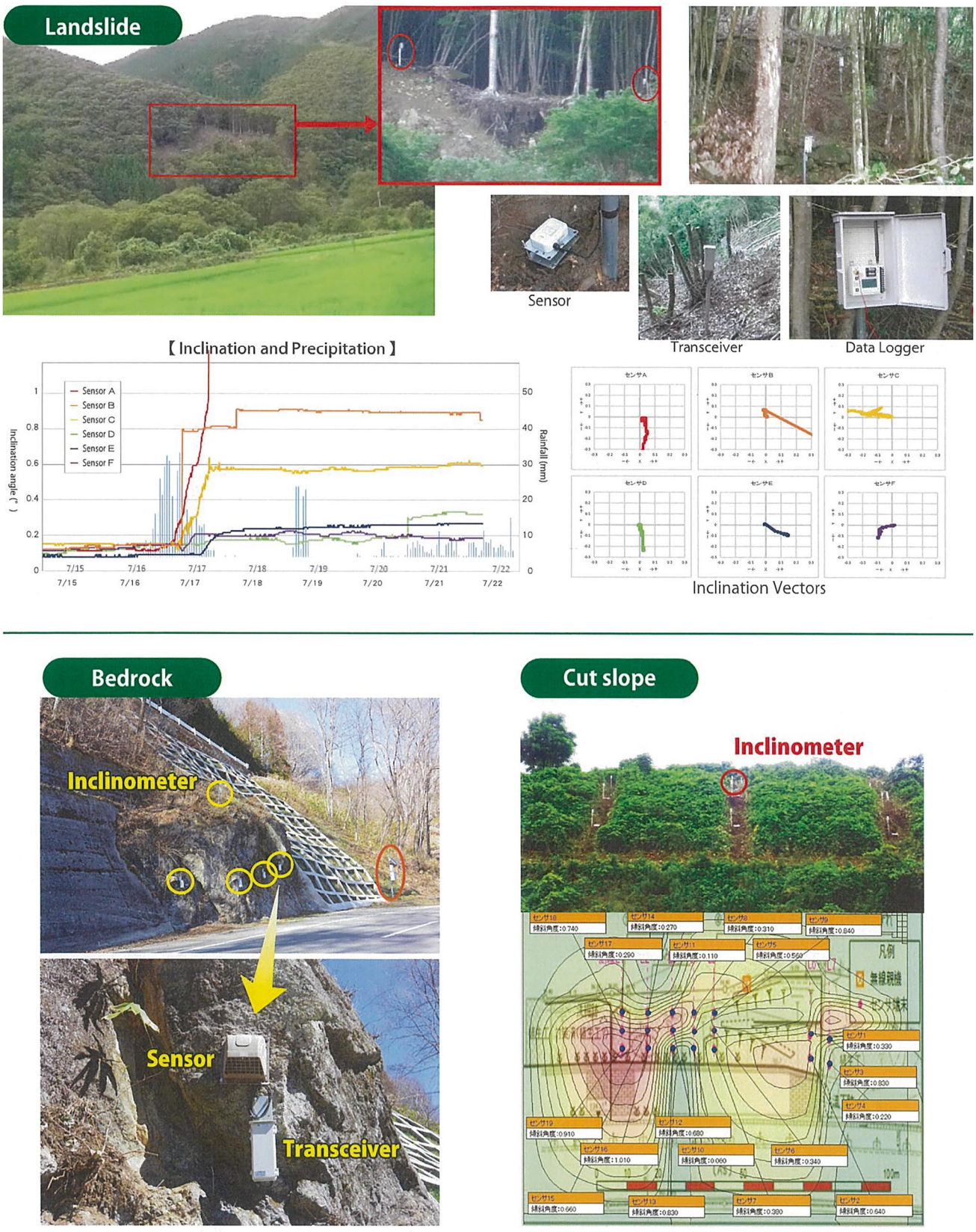

Fig. A.42 Inclination measure technology that enables surface deformation monitoring of slopes and bedrocks

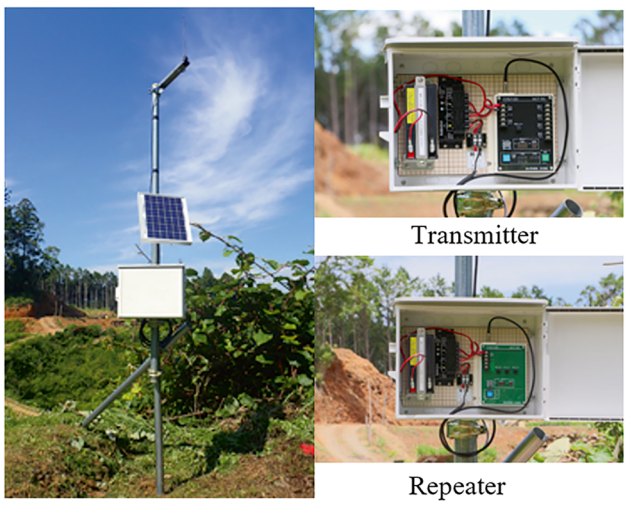

Wireless communication device for transmitting contact signals

Wireless communication device for receiving contact signals

Features

- No need for cable wiring
- Compact and lightweight equipment for easy installation
- Regular monitoring of communication status (with retransmission)
- Transmitter operates for over 1 year on batteries
- Communication range of over 1000m (with clear line of sight)

Fig. A.43 An alarm wireless transmitter to prevent secondary disasters after landslides. This device transmits contact signals detected from debris flow sensors, extensometers, etc. using 429 MHz wireless communication

List of ICL Members

International Consortium on Landslides
An international non-government and non-profit scientific organization promoting landslide research and capacity building for the benefit of society and the environment.
President: Željko Arbanas (University of Rijeka, Croatia)
Vice Presidents: Nicola Casagi (University of Florence, Italy), Faisal Fathani (Gadjah Mada University, Indonesia), David Huntley (Geological Survey of Canada, Canada), Biljana Abolmasov (University of Belgrade, Serbia), Giovanna Capparelli (University of Calabria, Italy), Maneesha V. Ramesh (Amrita University, India) Executive Director: Kaoru Takara (National Research Institute for Earth Science and Disaster Resilience, Japan), Treasurer: Kyoji Sassa (Prof. Emeritus, Kyoto University, Japan)

Country/Region	ICL Full member
Bosnia and Herzegovina	The Geotechnical Society of Bosnia and Herzegovina
Brazil	Center for Scientific Support in Disasters—Federal University of Parana
Canada	Geological Survey of Canada
	University of Alberta
China	Northeast Forestry University, Institute of Cold Regions Science and Engineering
	China University of Geosciences
	Chinese Academy of Sciences, Institute of Mountain Hazards and Environment
	Tongji University
	Shanghai Jiao Tong University
	Tsinghua University
	The State Key Laboratory of Geohazard Prevention and Geoenvironment Protection (SKLGP), Chengdu University of Technology
	Civil Engineering and Development Department, Geotechnical Engineering Office, Hong Kong
	The Hong Kong University of Science and Technology
Colombia	Universidad Nacional de Colombia
Croatia	Croatian Landslide Group from Faculty of Civil Engineering University of Rijeka and Faculty of Mining, Geology and Petroleum University of Zagreb
Czech Republic	Charles University, Faculty of Science
Egypt	The American University in Cairo
Germany	Technische Universitat Darmstadt, Institute and Laboratory of Geotechnics
Georgia	Department of Geology of National Environmental Agency of Georgia
India	Amrita Vishwa Vidyapeetham, Amrita University
	National Institute of Disaster Management, New Delhi
	Geological Survey of India
	Vellore Institute of Technology
Indonesia	Gadjah Mada University, Center for Disaster Mitigation and Technological Innovation (GAMA-InaTEK)
	Parahyangan Catholic University
	Agency for Meteorology, Climatology, and Geophysics of the Republic of Indonesia (BMKG Indonesia)
Italy	UNESCO Chair for the prevention and the sustainable management of geo-hydrological hazards - University of Florence
	ISPRA-Italian Institute form Environmental Protection and Research
	University of Calabria, DIMES, CAMILAB
	Istituto di Ricerca per la Protezione Idrogeologica (IRPI), of the Italian National Research Council (CNR)
	Centro di Ricerca CERI—Sapienza Università di Roma
	National Institute of Oceanography and Applied Geophysics—OGS, Italy
	Department of Earth and Environmental Sciences, University Aldo Moro

B. Abolmasov et al. (eds.), *Progress in Landslide Research and Technology, Volume 4 Issue 1, 2025*, Progress in Landslide Research and Technology, https://doi.org/10.1007/978-3-031-89836-5

Japan	Kyoto University, Disaster Prevention Research Institute
	Japan Landslide Society
	National Research Institute for Earth Science and Disaster Resilience
Korea	Korean Society of Forest Engineering
	National Institute of Forest Science
	Korea Authority of Land and Infrastructure Safety
	Korea Institute of Civil Engineering and Building Technology
Mexico	Institute of Geography, National Autonomous University of Mexico (UNAM)
Russia	Moscow State University, Department of Engineering and Ecological Geology
	JSC "Hydroproject Institute"
Serbia	University of Belgrade, Faculty of Mining and Geology
Slovakia	Comenius University, Faculty of Natural Sciences, Department of Engineering Geology
Slovenia	University of Ljubljana, Faculty of Civil and Geodetic Engineering (ULFGG)
	Geological Survey of Slovenia
Sri Lanka	Central Engineering Consultancy Bureau (CECB)
	National Building Research Organization
	Engineering Geology Research Group (EGRG), Department of Geology, University of Peradeniya
Chinese Taipei	Landslide group in National Central University from Graduate Institute of Applied Geology, Department of Civil Engineering, Center for Environmental Studies
	National Taiwan University, Department of Civil Engineering
Thailand	Ministry of Agriculture and Cooperatives, Land Development Department
	Asian Disaster Preparedness Center (ADPC)
Ukraine	Institute of Telecommunication and Global Information Space
United Kingdom	British Geological Survey
USA and Nepal	California State University, Fullerton and Tribhuvan University, Institute of Engineering
Viet Nam	Institute of Transport Science and Technology
	Vietnam Institute of Geosciences and Mineral Resources (VIGMR)
Country/Region	**ICL Associate member**
Belgium	Liege University, Georisk and Environment (G&E) group
China	State Key Laboratory of Plateau Ecology and Agriculture (Qinghai University)
	China Three Gorges University
	Xi 'an Geological Environment Monitoring Station
	The University of Hong Kong
Czech Republic	Czech Geological Survey
	Institute of Rock Structure and Mechanics, Department of Engineering Geology
India	Centre of Excellence in Disaster Mitigation and Management (CoEDMM) Indian Institute of Technology Roorkee
Italy	University of Sannio, Department of Sciences and Technologies
	Geotechnical Engineering Group (GEG), University of Salerno
	Department of Earth and Environmental Sciences—University of Pavia
	University of Chieti-Pescara, Department of Engineering and Geology
	Federico II University of Naples, Department of Earth, Environmental and Resource Sciences
	DIA – Università degli Studi di Parma
	University of Urbino "Carlo Bo", Department of Pure and Applied Sciences
	University of Turin
Japan	Ehime University, Center for Disaster Management Informatics Research
	Kochi University
	National Institute of Maritime, Port and Aviation Technology
North Macedonia	Macedonian Association for Geotechnics
Russia	Russian State Geological Prospecting University n.a. Sergo Ordzhonikidze (MGRI-RSGPU)
Slovenia	University of Ljubljana, Faculty of Natural Sciences and Engineering (UL NTF)
Switzerland	Institute of Earth Sciences, Faculty of Geoscience and Environment/ University of Lausanne

USA	Iowa State University	
Country/Region	**ICL Supporter**	
China	Beijing Brilliant Sun Technology Co., Ltd	
Italy	IDS GeoRadar s.r.l.	
Japan	Marui & Co., Ltd., Osaka	Okuyama Boring Co., Ltd., Yokote
	Ohta Geo-Research Co., Ltd., Nishinomiya	Japan Conservation Engineers Co., Ltd., Tokyo
	Sabo Technical Center, Tokyo	GODAI Kaihatsu Corp., Kanazawa
	OYO Corporation, Tokyo	Kokusai Kogyo Co., Ltd., Tokyo
	OSASI Technos Inc., Kochi	NIPPON KOEI CO., LTD.
	Geosystem Co., Ltd., Osaka	

ICL Secretariat
Secretary General: Kyoji Sassa
International Consortium on Landslides, 138-1 Tanaka Asukai-cho, Sakyo-ku, Kyoto, 606-8226, Japan
Web: https://www.landslides.org/, E-mail: secretariat@landslides.org
Tel: +81 (75) 723 0640, Fax: +81(75) 950 0910

Index

B. Abolmasov et al. (eds.), *Progress in Landslide Research and Technology, Volume 4 Issue 1, 2025*, Progress in Landslide Research and Technology, https://doi.org/10.1007/978-3-031-89836-5